Université de Montréal

Asteroseismological Studies of Long- and Short-Period Variable Subdwarf B Stars

par

Suzanna Randall

Département de physique

Faculté des arts et des sciences

Thèse présentée à la Faculté des études supérieures

en vue de l'obtention du grade de

Philosophiæ Doctor (Ph.D.)

en physique

Novembre, 2005

Université de Montréal

Faculté des études supérieures

Cette thèse intitulée:

Asteroseismological Studies of Long- and Short-Period Variable Subdwarf B Stars

présentée par:

Suzanna Randall

a été évaluée par un jury composé des personnes suivantes:

Pierre Bergeron,	président-rapporteur
Gilles Fontaine,	directeur de recherche
Pierre Brassard,	membre du jury
Tony Lynas-Gray,	examinateur externe

Thèse acceptée le: 05/01/04

Sommaire

Le principal but de cette thèse est d'établir les bases observationnelles et théoriques nécessaires à l'interprétation astéroséismologique des étoiles sous-naines de type B (sdB) variant sur de longues périodes, qui n'ont été que récemment découvertes. La présente étude nous permet également d'améliorer notre connaissance des sdBs pulsantes de courtes périodes et de développer une méthode de vérification des analyses effectuées jusqu'à maintenant pour ces objets.

Après avoir décrit la classe des étoiles sous-naines chaudes et la théorie des pulsations, nous effectuons une analyse astéroséismologique de l'étoile pulsante de courtes périodes EC 20117−4014. Ensuite, nous explorons, d'une manière théorique, le potentiel que comporte la photométrie multi-filtre pour l'identification partielle des modes observés dans les deux types de variables sdB. Pour les pulsateurs rapides, les outils développés devraient être utiles pour vérifier l'identification des modes obtenus à partir de l'astéroséismologie, tandis que pour les oscillateurs lents, ils fourniront les contraintes requises pour entreprendre des analyses quantitatives. La partie restante de cette thèse est constituée d'une étude ambitieuse qui a pour but d'extraire et d'interpréter quantitativement les pulsations observées chez les sdBs variables de longues périodes. Notre analyse est fondée sur une moyenne de 350 heures de photométrie rapide obtenue pour chacune des trois cibles représentatives : PG 1627+017, PG 1338+481 et PG 0101+039. Si, d'une part, les propriétés oscillatoires de ces étoiles concordent bien avec les prévisions de façon relative, nous constatons qu'elles s'accordent mal à celles prédites par les modèles stellaires sur un plan absolu. En particulier, la valeur observée pour la limite bleue des étoiles pulsantes pourrait dépasser, jusqu'à un maximum de 8000 K, la valeur prédite, indiquant quelques inexactitudes dans les modèles utilisés présentement. D'autre part, il est

possible d'interpréter les distributions de périodes d'une façon quantitative pour deux des étoiles observées. Ces analyses indiquent que les modes sont, de préférence, excités dans des intervalles de fréquence bien précis, suggérant ainsi la présence d'un mécanisme de sélection d'énergie inconnu. La sous-abondance résultante des périodes observées comparées à celles prédites par les modèles, ajoutée au fait que les modes démontrent un comportement quasi-asymptotique, compliquent les analyses astéroséismologiques tentées. Néanmoins, les résultats obtenus se révèlent très prometteurs et, nous l'espérons, permettront éventuellement l'étude astéroséismologique complète des sous-naines de type B variables de longues périodes.

Mots clefs:

étoiles: intérieurs, étoiles: oscillations, étoiles: astéroséismologie, étoiles: branche horizontale, étoiles: individuelles: EC 20117−4014, étoiles: individuelles: PG 1627+017, étoiles: individuelles: PG 1338+481, étoiles: individuelles: PG 0101+039

Abstract

The thesis presented here lays the observational and theoretical foundations for the asteroseismological interpretation of the newly discovered class of long-period variable subdwarf B stars. In addition, we further our understanding of the short-period variable subdwarf B stars and develop a method of verifying the analyses achieved for these more extensively studied objects.

After summarising the status quo on hot subdwarfs and introducing basic pulsation theory, we carry out an asteroseismological analysis of the rapid oscillator EC 20117−4014. We then describe a theoretical exploration into the potential of multi-colour photometry for partial mode identification in both the short- and the long-period variables. In the case of the former, the tools developed should provide a means of verifying the mode identification inferred from asteroseismology for a number of objects, while for the latter they provide necessary a priori constraints. The remainder of the thesis is devoted to a pioneering study aimed at quantitatively extracting and interpreting the oscillations exhibited by long-period variable subdwarf B stars. Our analysis is based on between 300 and 400 hours of time-series photometry obtained for each of three representative targets: PG 1627+017, PG 1338+481 and PG 0101+039. We find that their oscillatory properties are in agreement with predictions from non-adiabatic pulsation calculations at the relative but not the absolute level. In particular, the experimental blue edge of the instability strip exceeds that predicted by up to 8000 K, indicating that the subdwarf B star models currently used are subject to deficiencies. Quantitative interpretations of the period spectra uncovered were possible for two of the targets and indicate the preferential excitation of modes in well-defined frequency ranges, attributed to an unknown energy channelling mechanism. The ensuing underabundance of observed pulsations compared

to those predicted together with the near-asymptotic behaviour of the modes greatly complicates the asteroseismological exercises attempted. Nevertheless, the results achieved are very promising and will in all likelihood pave the way for future studies of long-period variable subdwarf B stars.

Subject headings:

stars: interiors, stars: oscillations, stars: asteroseismology, stars: horizontal-branch, stars: individual: EC 20117-4014, stars: individual: PG 1627+017, stars: individual: PG 1338+481, stars: individual: PG 0101+039

Table of Contents

List of Figures

List of Tables

Acknowledgements

First and foremost thanks go to my supervisor Gilles Fontaine for everything, from taking me on because a student from England seemed exotic at the time to reassuring me that writing up a thesis is a mind game for the best of us. I'd like to express my gratitude also for all the things in between: taking me along for an amazing observing experience in Hawaii, stoically defying the antics of the Mt. Lemmon 60" telescope, actively encouraging me to make the most of conferences in every way, and understanding my compulsive and frequent need for holidays in far-away places. Last but by no means least, I am thankful for the academic support and motivation I received during my time as a PhD student.

I also thank Pierre Brassard for developing and patiently teaching me how to use a number of programs, and coming to my technical rescue on more than one occasion. I am indebted to Betsy Green, who first discovered the Betsy stars and later showed me how to observe them. Further thanks go to the members of the "groupe dégénéré", notably Patrick, Mathieu, Caroline, Alex, Agis, P.-O. and Jean-Philippe for advice, comments and lively discussions on subjects ranging from supermongo to vegetarianism. I would also like to thank my lovely flatmates Caroline and Tassia for unforgettable moments, deep psychological insights, and the extensive broadening of my Québecois vocabulary, not always in the most academic direction.

Finally, my heartfelt appreciation to Stuart, who has been incredibly motivating and patient all this time. For their long-term support, encouragement, and the good times spent together I am grateful to my family and friends, in particular Julia, Katrin, Dad, Chrissi, Sam, Ben, Dan and Jerry.

To my mother.

Chapter 1

INTRODUCTION

1.1 INTRODUCTION TO SUBDWARF B STARS

1.1.1 What Are Subdwarf B Stars?

Subdwarf B (sdB) stars are evolved, low mass, compact objects, that lie on the Extreme Horizontal Branch (EHB) and post-EHB of the Hertzsprung-Russell diagram (Greenstein & Sargent 1974). They have effective temperatures between $\sim$ 22,000 and 42,000 K and high surface gravities in the $5.0 \lesssim \log g \lesssim 6.2$ range (Saffer et al. 1994). First discovered in the 1950's (Humason & Zwicky 1947; Iriarte & Chavira 1957; Chavira, 1958; Feige 1958), they were later spectroscopically classified as blue objects with anomalously broad Balmer lines, a consequence of their elevated surface gravity compared to main sequence stars (Greenstein 1960; Berger 1963; Greenstein 1966). The latter implies a comparatively small radius and a low luminosity, placing them between the main sequence and the white dwarf graveyard in terms of physical parameters.

The chemical composition of subdwarf B stars is characterised by a helium-burning core surrounded by a very thin hydrogen-rich envelope. The dominant nuclear process taking place in the core is the conversion of helium to carbon and oxygen via the triple-alpha chain. Due to the high temperature dependence ($\propto T^{32}$) of the nuclear reaction rate, the hottest innermost regions of the star are subject to convection. Moving towards the surface and lower temperatures, the nuclear reaction rate decreases quickly, giving rise to first a thin

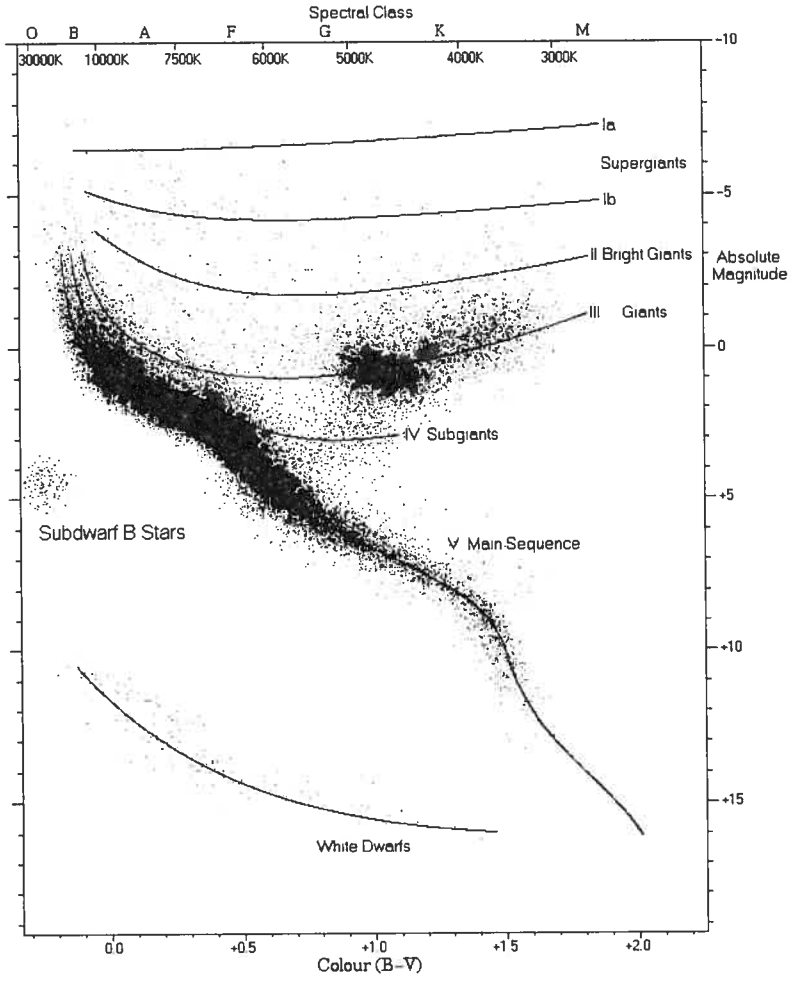

FIGURE 1.1 – Location of subdwarf B stars on the H-R diagram

semi-convection zone and then a radiative outer core composed almost entirely of helium. In contrast, the heavier end-products of nuclear burning, carbon and oxygen, are concentrated in the inner core. The hydrogen-rich shell surrounding the core is thought to have a mass of between 0.0001 and 0.0050 solar masses, depending on the effective temperature of the star in question. Since the inert envelope acts as an isolator for the heat generated by the nuclear reactions in the core, sdBs with higher effective temperatures should be associated with thinner hydrogen shells than their cooler counterparts (Dorman et al. 1993). All subdwarf B stars display chemically peculiar atmospheres made up of nearly pure hydrogen, helium typically being underabundant by more than one order of magnitude compared to solar. Heavy elements such as C, N and Si also show abundance anomalies that can be quite large (Heber 1991).

These are believed to be the result of diffusion processes, in particular gravitational settling and radiative levitation, operating in competition with weak stellar winds (Michaud et al. 1985). It is thought that these processes result in the formation of large inhomogeneities in the stars' atmospheres, an important point that will be revisited below.

Subdwarf B stars correspond to an advanced phase of stellar evolution and are believed to be the immediate progenitors of low-mass white dwarfs (e.g. de Kool et al. 1993). There is however some debate as to their exact formation process, for which a number of theories have been proposed. The simplest of these is based on the idea that the (single) subdwarf B star progenitor experiences heavy mass loss near the tip of the first giant branch (FGB), at which the core attains the mass required for the helium flash ($M \sim 0.48\ M_{\odot}$; see e.g. Faulkner 1972; Dorman et al. 1993; Castellani et al. 1995; Dorman et al. 1996 for details on this evolutionary theory). Assuming that the red giant is stripped of a significant amount of mass but stops just short of losing its entire envelope, helium ignition can nevertheless occur and the star settles on to the hot end of the horizontal branch on the zero-age extreme horizontal branch. This core helium-burning phase is identified with subdwarf B star evolution and lasts around 10^8 years. Due to the thinness of the hydrogen shell the majority of the star's luminosity originates from the nuclear reactions taking place in the core, and hydrogen shell burning is insignificant. After core helium exhaustion, the star has insufficient hydrogen energy to force a supergiant style envelope and ascend the asymptotic giant branch (AGB). Instead, the ignition of the outer layers of helium leads to post-EHB evolution along the so-called "AGB-Manqué" track (Greggio and Renzini 1990) for a time comparable to the equivalent early AGB phase. The helium-shell burning phase is identified with subdwarf O stars, which have temperatures around 45,000 K and surface gravities of $\log g \sim 5.5$. Finally, the star joins the white dwarf cooling track at $T_{\rm eff} \sim 80{,}000$ K and collapses as a low-mass white dwarf (Bergeron et al. 1994). This evolutionary scenario produces single core helium burning EHB stars with tightly constrained total masses of around 0.48 $M_{\odot}$ and helium envelope masses $M_{env} \leq 0.02\ M_{\odot}$. Historically, the main problem with the theory has been the necessity of "fine-tuning" the mass loss in order to produce subdwarf B stars, however recent simulations have shown that the significant mass loss occurring in the red giant phase may well lead to

extreme horizontal branch evolution quite naturally (D'Cruz et al. 1996, Sweigart 1997).

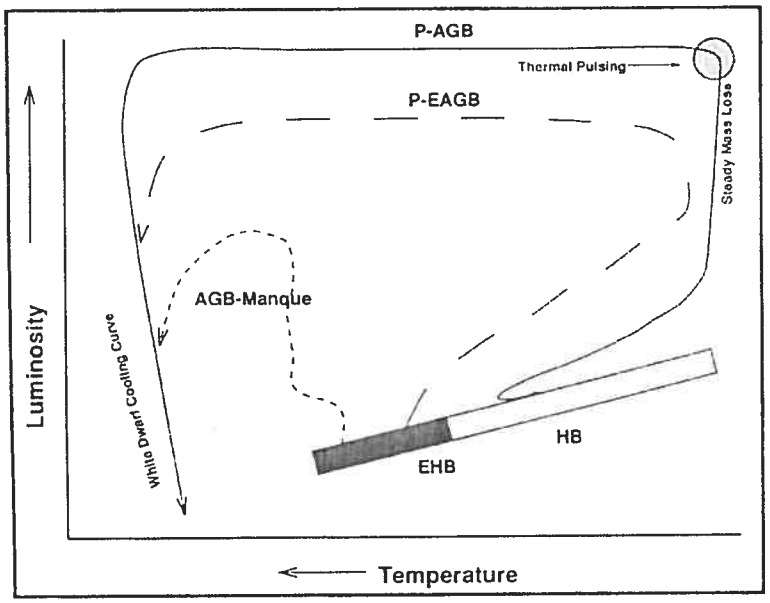

FIGURE 1.2 – Schematic representation of post-AGB, post-EAGB and EHB evolution. In the first case, the sdB progenitor has sufficient envelope mass ($M_{env} \gtrsim 0.02\ M_{\odot}$) to follow the classical AGB and post-AGB (P-AGB) track. In the remaining two cases, the hydrogen shell is too thin ($M_{env} \lesssim 0.02\ M_{\odot}$) for thermal pulsing to take place at the tip of the AGB; the star thus settles on the EHB. If the envelope mass is sufficiently high, the star is able to develop a convective envelope, placing it on the AGB for a while. However, envelope convection cannot be sustained until the tip of the AGB, and the star instead follows the P-EAGB ("Post-Early AGB") track to the white dwarf cooling sequence. If the hydrogen envelope is particularly thin, the star becomes a subdwarf and spends its post-EHB evolution in the AGB-Manqué phase. From Dorman et al. (1993).

Another evolutionary channel potentially capable of producing single subdwarf B stars is the merger of two helium white dwarfs in a close binary. In this scenario, the two primaries are driven together by orbital angular momentum loss due to gravitational wave radiation, and the merged object ignites helium to produce an EHB star (Webbink 1984; Iben & Tutukov 1986; Han 1998). According to simulations by Han et al. (2002), subdwarfs formed on the basis of two white dwarfs will have a relatively wide mass distribution ($0.4-0.65\ M_{\odot}$) peaked at $\sim 0.51\ M_{\odot}$. Their envelope masses are expected to be extremely thin, since any residual hydrogen present in the white dwarfs' atmospheres will be buried deep within the star and mixed with helium during the merger process, thus igniting violently and being consumed quickly. The birth rates calculated indicate that a significant fraction of sdB stars may form

this way, which could help explain some of the observed sdB stars that appear to be more massive than $\sim 0.5\ M_{\odot}$, provided that these are single objects.

The recent identification of many subdwarf B stars as both short- and long-period binaries (e.g. Allard et al. 1994; Maxted et al. 2001) raised the need for evolutionary scenarios that were able to produce sdBs with companions. Such systems start out as close binaries in which the red giant primary loses most of its envelope to the secondary star through mass transfer before igniting helium and settling on the EHB. While this idea had first been proposed by Mengel, Norris, & Gross (1976), their treatment was not complete from a binary evolution point of view since it did not distinguish between dynamically stable and unstable mass transfer (i.e. Roche lobe overflow vs. common envelope phase). The creation of binary subdwarfs was thus re-examined in detail by Han et al. (2002; see also Han et al. 2003), who proposed two distinct formation channels giving rise to sdB binary systems with different orbital characteristics. In both cases, the subdwarf's red giant progenitor starts to fill its Roche lobe when it is relatively close to the tip of the first red giant branch. If the radius of the mass-losing star increases more quickly than its Roche lobe, mass transfer will be dynamically unstable and lead to the formation of a common envelope where the envelope of the red giant engulfs both its degenerate core and the companion star. Friction between the orbiting components will then cause them to loose angular momentum and spiral in towards each other. Assuming this releases enough energy for the common envelope to be ejected, we are left with a very close binary system containing a helium core stripped of most of its hydrogen. The latter may still ignite helium if it was close enough to the red giant tip before the mass transfer, and thus evolve into a subdwarf B star. In the second scenario, mass transfer is dynamically stable and occurs via Roche lobe overflow, stopping when the primary's radius (and hydrogen envelope) has decreased sufficiently. If the degenerate core mass is large enough, helium will ignite, producing a subdwarf B star in a fairly wide binary. Both the common envelope ejection (CE) channel and the Roche lobe overflow (RLOF) channel can be divided into sub-channels depending on the nature of the binary companion. If the latter is a main sequence star, the CE channel is most likely to form sdB stars with a mass distribution sharply peaked at around $0.46\ M_{\odot}$ and short binary periods between 0.05 d and $\gtrsim$ 40 d. In comparison, CE ejection

with a white dwarf companion typically yields lower mass subdwarfs ($M \sim 0.35\ M_{\odot}$) and a slightly wider distribution of orbital periods. The creation of a subdwarf via the RLOF channel is much more likely on the basis of a main sequence rather than a white dwarf companion, since the secondary must be relatively massive for stable RLOF to occur. Subdwarfs produced in this scenario can have masses in a very wide range between 0.33 and 1.1 $M_{\odot}$, although the more massive sdBs are unlikely and the mass distribution again peaks sharply at around 0.46 $M_{\odot}$.

While all four of the evolutionary scenarios detailed present plausible explanations for the existence of subdwarf B stars, the different theories have yet to be tested observationally. It would be particularly interesting to examine which combinations of the stellar mass, the thickness of the hydrogen envelope and the binary characteristics occur in nature, and whether these are in accordance with those predicted from the formation channels. This would lead to a more mature understanding of the creation of subdwarf B stars, one of the last great mysteries in stellar evolution theory.

1.1.2 Why Are Subdwarf B Stars Worth Studying?

Subdwarf B stars are currently a hot research topic in stellar astronomy. Many specialists in the field of evolved stars have recently directed their attention towards these small, seemingly insignificant objects and the summer of 2003 saw the first of a series of conferences devoted solely to EHB stars. But what makes sdB's so special and worth studying?

One of the reasons subdwarf B stars are important is their sheer abundance. Shallow photographic surveys such as the Palomar-Green (Villeneuve et al. 1995), Montreal-Cambridge-Tololo (Lamontagne et al. 2000) and Edinburgh-Cape (Stobie et al. 1995) survey have shown that they dominate the Galactic population of blue objects more luminous than 16th magnitude in the visible. The Palomar-Green survey alone found over 300 sdB stars with magnitudes brighter than V $\sim$ 14.3. A kinematical analysis of a sample of 110 subdwarf B stars (Altman et al. 2001) revealed that the majority belong to our Galaxy's disc and the halo population forms a minority. This means that the kinematical history of sdBs is different from that of cooler A-type horizontal branch (HBA) stars, which mainly occur in the halo. In fact, when

considering sdB, HBB and HBA stars, their spatial behaviour seems to be related to their location on the horizontal branch. The bluer species are normally not found in the halo, the redder ones preferably there. A better understanding of horizontal branch and extreme horizontal branch stars could perhaps shed some light on this and provide us with a firmer grasp on the structure and evolution of our Galaxy.

Subdwarf B stars are also useful for constraining the ages of the oldest galaxies and hence cosmological models. Giant elliptical galaxies have been observed to exhibit an increasing flux with decreasing wavelength in the ultra-violet (1000−2500 Å), thought to be largely due to the radiation of HB and EHB stars (e.g. Yi, Demarque & Oemler 1997). This so-called "UV upturn" can be used as an age indicator for the galaxy using population synthesis models, providing that certain input parameters are known (Yi et al. 1999). One of the most important of these is the metallicity of the dominant UV sources, since the "metal-poor HB hypothesis" and the "metal-rich HB hypothesis" predict significantly different ages for the same nearby elliptical galaxies. In the former scenario, giant ellipticals are similar in age or even younger than old Galactic globular clusters, while in the latter they are about 30 % older than the old halo populations in the Milky Way. The inferred age further depends on the mass loss of the HB and EHB stars; if the mass-loss efficiency correlates positively with metallicity, nearby giant ellipticals may only be 60−70 % as old as our Galaxy. Therefore, placing constraints on the structure and evolution of HB and EHB stars is imperative to the precise determination of these galaxies' ages.

Perhaps the most important reason for studying subdwarf B stars is their intrinsic interest as exotic objects because of their extremely thin hydrogen shell. As was discussed in the previous section, we do not yet fully understand their formation process, in particular the details surrounding the mass loss near the tip of the first red giant branch. While this in its own right warrants the closer investigation of sdB's, the information gained from any such study has wide-ranging implications for stellar and binary evolution scenarios. Effectively constituting the bare helium core remnant of red giants, subdwarf B stars can be used as laboratories to test theories of core he-burning and post-red giant evolution. This renders them of fundamental interest to stellar astrophysics as well as the understanding of nuclear

reaction processes.

1.1.3 Subdwarf B Stars as Asteroseismic Probes

The popularity of subdwarf B stars received a sudden boost when it was discovered that some of them show multi-periodic brightness variations, also known as pulsations or oscillations. As variable stars, sdBs join the likes of classical Cepheids, RR Lyrae, δ Scuti or ZZ Ceti white dwarfs, to name only a few. In the simplest case (that of radial pulsations), the brightness variations observed from Earth are caused by the regular expansion and contraction of the star, similar to that of the human lung as air is inhaled and exhaled. The timescale on which this occurs depends on the physical parameters of the star, such as its mass, radius and internal composition. Therefore, oscillations can be used to probe the stellar interior, much in the same way as seismic waves are employed to infer the inner structure of the Earth. This field of study is called asteroseismology, and is thought to hold the key to a more mature understanding of subdwarf B stars. In particular, it is hoped that asteroseismology can constrain the thickness of these stars' hydrogen shells and the extent of their convective core, parameters which cannot be deduced any other way but are of paramount importance for evolutionary scenarios.

Short-period Variable Subdwarf B Stars (EC 14026 Stars)

The first class of pulsating subdwarf B star was discovered at the South African Astronomical Observatory only relatively recently (Kilkenny et al. 1997; see also Koen et al. 1997; O'Donoghue et al. 1997; Stobie et al. 1997). Named EC 14026 stars after the prototype, these oscillators exhibit multi-periodic luminosity variations with short periods between 80−500 s and low amplitudes of a few mmags (typical amplitudes lie below 5−10 mmags, however amplitudes as high as 60 mmags have been detected in certain objects). They correspond to the hotter and more compact sdB stars at 28,000 K $\lesssim T_{\rm eff} \lesssim$ 37,000 K and 5.25 $\lesssim \log g \lesssim$ 6.00.

Interestingly, short-period variations in subdwarf B stars were predicted nearly simultaneously to their discovery by an independent group here in Montréal (Charpinet et al. 1996),

an extremely rare occurrence in stellar pulsation study. It is believed that the oscillations in EC 14026 stars are caused by an opacity mechanism associated with a local overabundance of iron (see section 1.2.4), and that a good understanding of the driving process has been reached. Indeed, all 34 EC 14026 stars detected to date fall into the instability strip predicted by theory (see Charpinet et al. 2001 for a review). Moreover, it has been possible to quantitatively match the periods of oscillation observed to those predicted for four targets (see section 1.3), allowing the tools of asteroseismology to be applied. Since the oscillations in EC 14026 stars are sensitive mostly to the structure of the outer layers, this resulted in the accurate determination of the hydrogen shell thickness as well as the total mass. The values derived so far indicate the correlation between the envelope mass and effective temperature predicted from theory, as well as the expected stellar masses around $0.46-0.48\ M_{\odot}$ (Charpinet et al. 2005). While it is too early to speak of definite constraints on sdB formation theories, it is clear that the study of EC 14026 stars is beginning to bear fruit from an evolutionary point of view.

Despite the success of pulsation theory in explaining the fast pulsators' observed properties, certain challenges remain. One of these is the fact that short-period variable subdwarf B stars co-exist in the same region of the H-R diagram as their non-pulsating counterparts (see Figure 1.3), when according to predictions all stars in the instability strip should pulsate. Although the reason for this is still open to debate, a currently favoured theory (Fontaine & Chayer 1997; Chayer et al. 2004) proposes that weak stellar winds could be to blame. It is suggested that these would, over time, empty out the iron reservoir in the envelope layers of the star and cause the opacity mechanism driving the oscillations to cease. In this scenario, non-pulsating subdwarf B stars would either suffer a higher mass loss rate than the oscillators, or be significantly older. Evolutionary calculations have shown that stars with similar values of $T_{\rm eff}$ and $\log g$ can have different ages depending on the mass of the stellar core, that of its envelope, its helium abundance and metallicity (e.g. Dorman et al. 1993). Furthermore, exploratory modelling (Fontaine et al. 2005) of a weak stellar wind's effect on the iron abundance profile in sdB envelopes found that a depletion does occur in the layers critical to driving within the He-core burning timescale. Unfortunately from an observational point of view the iron

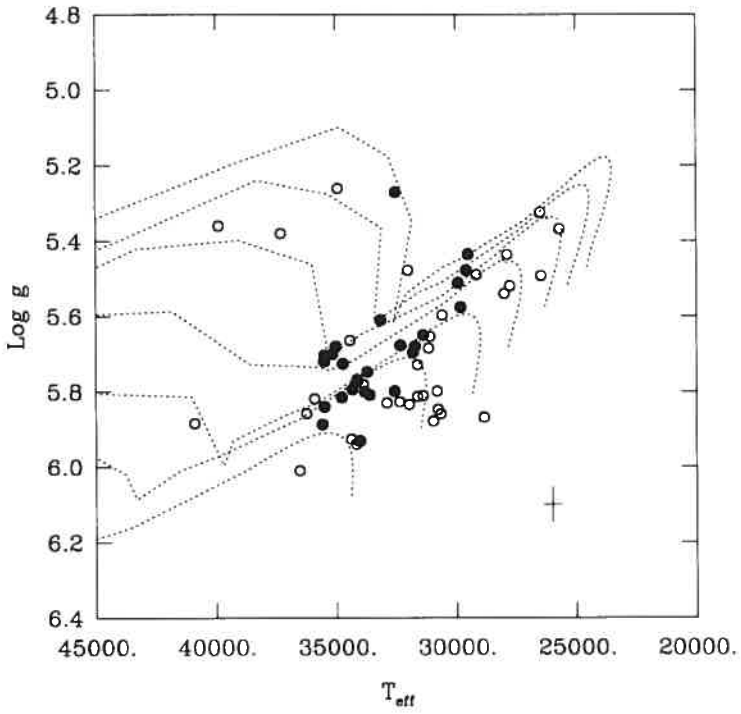

FIGURE 1.3 – Distribution of EC 14026 stars (filled black circles) and constant sdB stars (open circles) in the $\log g - T_{\rm eff}$ plane. The spectroscopic estimates of the stars' atmospheric parameters are those of Green, Fontaine, & Chayer (in preparation), typical uncertainties on which are indicated by the cross. Also shown are some of Ben Dorman's evolutionary tracks for models with a range of hydrogen shell masses (dotted lines). From Fontaine et al. (2005).

abundance decreases in the driving region before any significant change registers at the stellar surface. Therefore, it is quite possible that two targets with the same atmospheric metallicity experience very different conditions in the layers contributing to pulsational instability, causing one of them to oscillate while the other does not. This may help explain recent negative results reported from searches for a spectroscopic signature of pulsating subdwarf B stars (e.g. Blanchette et al. 2005).

Long-Period Variable Subdwarf B Stars (PG 1716 Stars or Betsy Stars)

Just as the subdwarf B community felt that they were beginning to achieve an understanding of the pulsations in the EC 14026 stars, Betsy Green announced the discovery of yet another class of pulsating subdwarf B star (Green et al. 2003). The new oscillators appear to

be multi-mode pulsators with long periods of the order of one to two hours and very small pulsational amplitudes of $\lesssim 5$ mmags. Commonly referred to as PG 1716 stars after the prototype PG 1716+426, some of the Montréal group prefer to call them "Betsy stars" in honour of their discoverer. I will use this name throughout the non-article part of my thesis.

The reason it took five years to discover the Betsy stars, despite the search for pulsating sdBs being on since the discovery of the EC 14026 prototype, is that their periods are a factor of ten longer, and their amplitudes of pulsation are generally lower than in the case of the EC 14026 stars. When testing a subdwarf for pulsations it was usually declared constant if no relative amplitude variations greater than ~0.05 % were detected on a timescale of 1-2 hours (see Billères et al. 2002), which automatically led to an oversight of the slow pulsators. They were eventually discovered in the course of an sdB monitoring campaign searching for reflection effects and eclipses in close binary systems, features of a similar timescale and amplitude level as the pulsations uncovered. In order to illustrate the challenges faced in the search for Betsy stars compared to the EC 14026 stars, Figure 1.4 shows typical light curves for these two types of object on the same amplitude scale.

In addition to their differing pulsation properties, the two classes of subdwarf B pulsators can also be distinguished by their atmospheric parameters, the typical Betsy star being distinctly cooler and less compact ($T_{\rm eff} \sim 27{,}000$ K; $\log g \sim 5.4$) than the average EC 14026 star ($T_{\rm eff} \sim 33{,}000$ K; $\log g \sim 5.7$, see Figure 1.5 for details). However, their domains of instability seem to touch, as was confirmed by the detection of two hybrid objects that exhibit both long- and short-period luminosity variations (Schuh et al. 2005; Oreiro et al. 2005). While it is difficult to establish a precise temperature scale towards the cooler end of the subdwarf B star domain, Betsy stars can be described as lying between roughly 20,000 and 29,000 K. It is believed that, as a result of their lower temperatures, the outer hydrogen shell is thicker than in the rapid pulsators, extending to 0.003 - 0.004 $M_{\odot}$ in the coolest objects. Another noteworthy fact is that the slow oscillators are surprisingly common. Whereas less than 5 % of subdwarf B stars are identified with the rapid pulsators, Betsy stars make up 25-30 % of the sdB population, and it is indeed possible that all cool subdwarfs are slowly oscillating at some amplitude level.

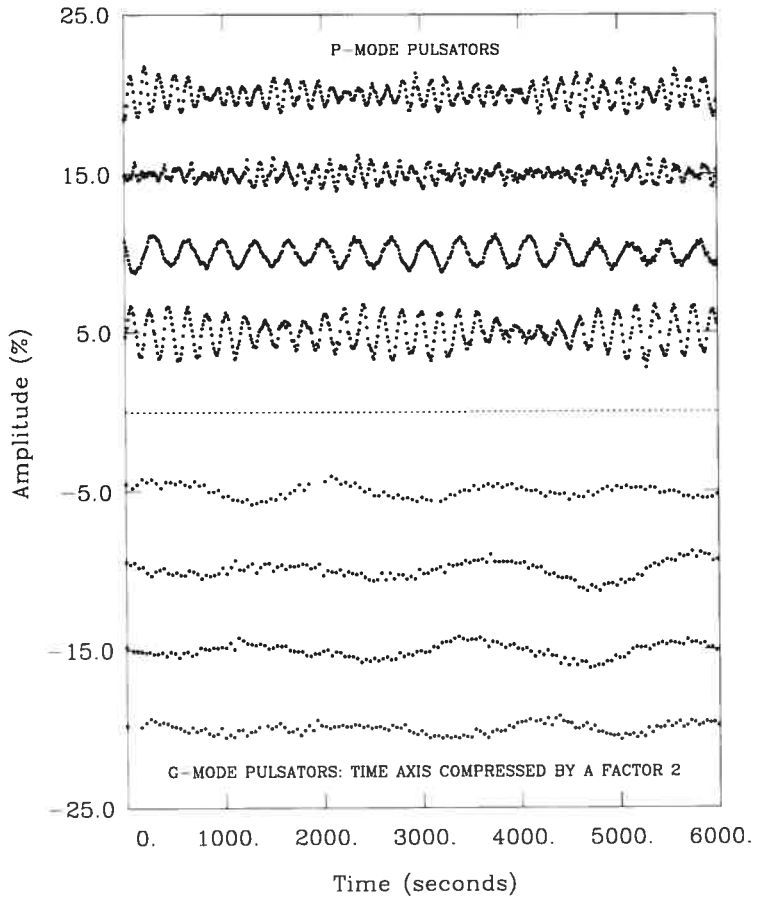

FIGURE 1.4 – Representative light curves of short-period and long-period variable subdwarf B stars. Note that the time-axis refers to the top half of the figure; the light curves in the bottom half have been compressed by a factor of 2. From Fontaine et al. (2003).

The most obvious challenge following the surprising discovery of these new variables was explaining their instability. Following several unfruitful attempts, Fontaine et al. (2003) succeeded in computationally exciting bands of periods in a range comparable to those observed by invoking the same iron opacity mechanism responsible for the EC 14026 instability region (see section 1.2.5). In contrast to the case of the fast pulsators, the oscillations observed in the Betsy stars are sensitive to the inner layers, and thus have the potential to constrain the extent of the convective core. However, our understanding of the slow pulsators is still relatively limited, and it remains to be seen whether asteroseismology will be possible in the

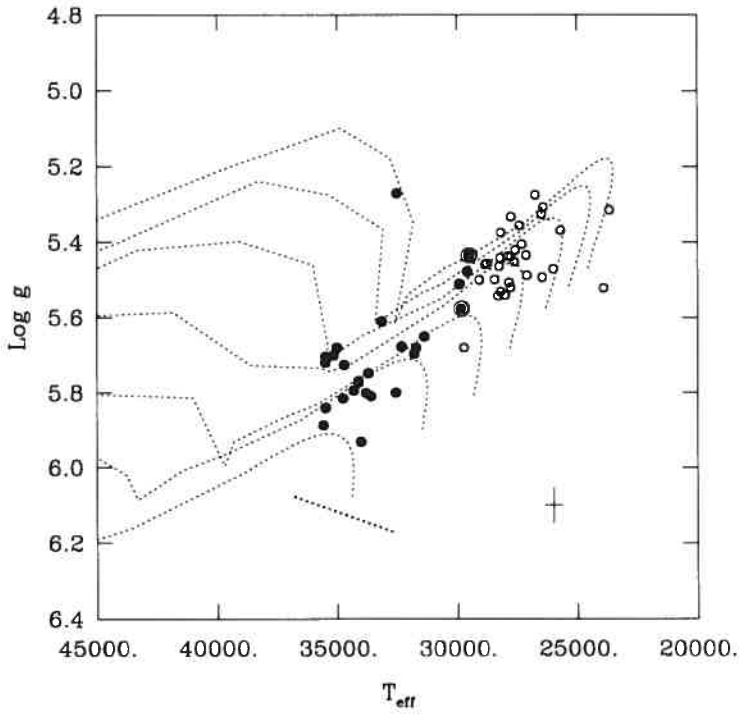

FIGURE 1.5 – Distribution of 26 EC 14026 stars (filled black circles) and 30 Betsy stars (open circles) on the H-R diagram. The two circled black points refer to hybrid objects that exhibit both short- and long-period variations. Shown are all pulsators for which we have consistent atmospheric parameters derived from MMT spectra. The thin dotted lines show some of Ben Dorman's evolutionary tracks for models with a range of H envelope masses. The thick dotted line represents the zero-age He-burning main sequence for masses between 0.3–0.6 $M_{\odot}$. From Fontaine et al. (2005).

future.

1.2 THEORY OF PULSATING SUBDWARFS

1.2.1 Basic Properties of Non-Radial Modes of Oscillation

The oscillations found in subdwarf B stars are non-radial, which by definition means that during a pulsation cycle the star deviates from its spherical shape rather than oscillating around its equilibrium figure as is the case for radial pulsations. However, it should be noted that in subdwarf B stars the pulsations manifest themselves not so much in the physical displacement of material but rather in the form of surface temperature perturbations, which

give rise to the observed luminosity variations. The reason for this is that the stars' high surface gravity hinders any appreciable radial outward displacement, instead directing the available energy into heating the corresponding region.

Non-radial oscillations are conventionally described by three spherical harmonic coordinates, k, l and m. The radial order k corresponds to the shell number n in quantum physics, and in a stellar oscillation model represents the number of nodes in the radial component of the displacement from the centre to the surface. The harmonic degree l refers to the number of nodal lines that divide the stellar surface into regions oscillating in opposite phase to each other, while the azimuthal quantum number m (where $m = -l, -l+1, ..., l-1, l$) corresponds to the number of those that cross the equator. The effects of changing l and m on the surface of a stellar model are illustrated in Figure 1.6. Radial modes (not illustrated) are nothing more than special cases of non-radial modes, namely those with $l = 0$. It is evident from Figure 1.6 that the value of l plays a critical part in the amplitude of the brightness variation as observed from Earth. Since stellar disks (with the exception of that of the Sun) are generally not resolvable and we can thus not make out the spherical harmonic patterns as depicted in Figure 1.6, all we see is the brightness variation of the integrated disk. Assuming the same intrinsic amplitude, it is obvious that the overall brightness variation of the visible disk during a pulsational cycle will decrease as the value of l increases. It is for this reason that observations claiming to have detected modes with $l \geq 3$ are received with scepticism.

In a given spherical equilibrium model, a mode's eigenfrequency σ is a function of k and l, while both the frequency and the eigenfunction are independent of m, exhibiting a $(2l+1)$-fold degeneracy. This degeneracy is due to the symmetry of the equilibrium structure around an arbitrary axis and can hence be lifted by introducing rotation, resulting, to first order, in equally spaced frequency splittings corresponding to the rotational frequency. Therefore, analysing the frequency spectrum of an oscillating star not only yields information on the pulsations themselves but can also render the star's rotational period.

Non-radial pulsations can be divided into two distinct types owing to the existence of two restoring forces, pressure and gravity. They occupy different period domains, which are divided by two characteristic frequencies describing the local vibrational property of the star.

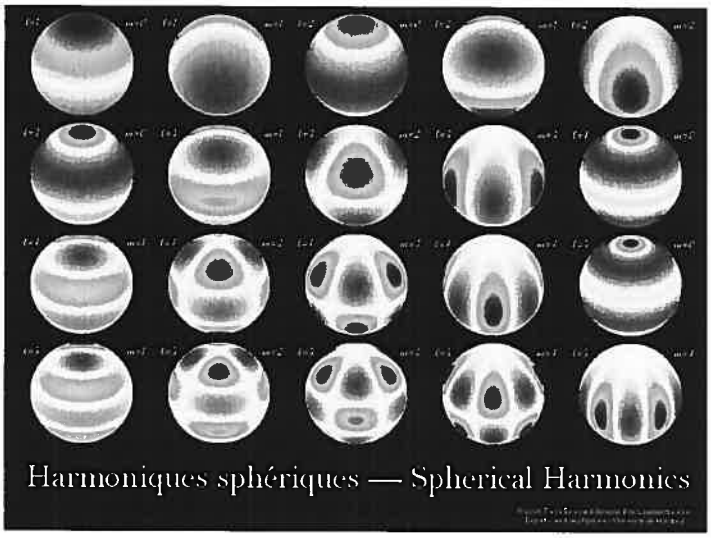

FIGURE 1.6 – Illustration of spherical harmonics in a spherical stellar model. The dark and light coloured regions refer to areas of maximum temperature variation (i.e. hot and cold patches) and those where the temperature stays at its equilibrium value (i.e. nodal lines) respectively. From Pierre Brassard (private communication).

The first of these is called the Lamb frequency and corresponds to the reciprocal of the time scale of one horizontal wavelength divided by the local sound speed. The latter quantity is given by $c^2 = (d\ln P/d\ln\rho)_{ad}(P_0/\rho_0)$ where P_0 and ρ_0 are the pressure and density of the unperturbed state respectively. The horizontal wavelength can be expressed in terms of the horizontal wave number $k_h = [l(l+1)]^{1/2}/r \sim l/r$, yielding $\lambda_h = 2\pi/k_h \sim 2\pi r/l$. Since this wavelength is travelled horizontally by a sound wave in a period $\lambda_h/2\pi c$, the Lamb frequency is given by

$$L_l^2 = (k_h c)^2 = \frac{l(l+1)c^2}{r^2}. \tag{1.1}$$

The second characteristic frequency describes the vertical oscillation of a bubble of gas around its equilibrium position under gravity and is called the Brunt-Väisälä frequency (N^2). It can be expressed as

$$N^2 = g\left(\frac{1}{\left(\frac{d\ln P}{d\ln\rho}\right)_{ad}}\frac{d\ln P_0}{dr} - \frac{d\ln\rho_0}{dr}\right), \tag{1.2}$$

where g is the local gravitational acceleration.

In the case of high-frequency oscillations where $\sigma^2 > L_l^2, N^2$, the relative radial displacement is dominated by the relative Eulerian pressure perturbation, implying that the restoring

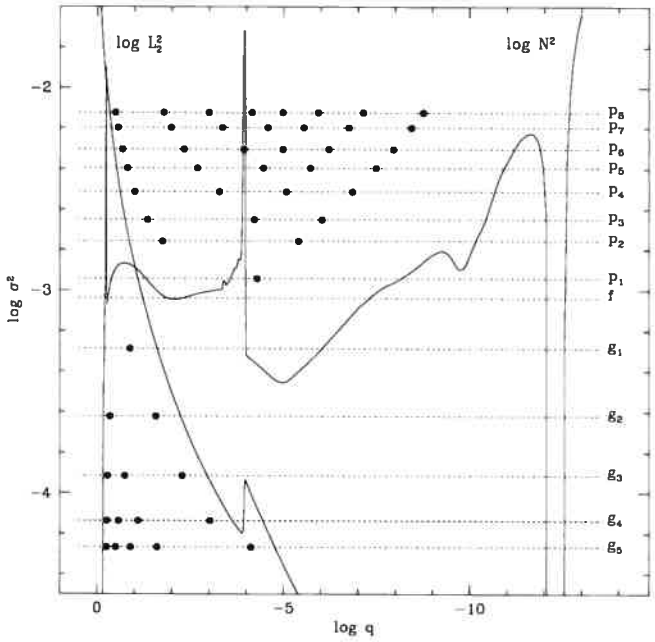

FIGURE 1.7 – Propagation diagram for a representative subdwarf B model illustrating the regions of propagation for p- and g-modes as a function of logarithmic depth $\log q \equiv \log(1 - M(r)/M_*)$, where $M(r)$ is the stellar mass within a spherical volume of radius r and M_* is the total mass of the star. Note that in this notation $\log q = 0$ corresponds to the centre of the star and the surface lies at $\log q \sim$ - 15. The eigenfrequencies σ^2 of the p-modes are shown up to $k = 8$ (p8), while those of the g-modes are given up to $k = 5$ (g5). The fundamental mode, as well as the Lamb and Brunt-Väisälä frequency are also indicated. Each black point refers to a node of the mode's eigenfunction. From Charpinet (1998).

force is caused mostly by excess pressure. The high-frequency modes are consequently named p-modes and show the characteristics of acoustic waves, such as a decrease in period as the radial order k increases. It can be seen from Figure 1.7 that p-modes propagate mostly in the outer layers of the star (note the logarithmic depth scale), and thus constitute shallow envelope modes. For low-frequency perturbations with $\sigma^2 < L_l^2, N^2$ the restoring force is mainly due to buoyancy. These oscillations behave like gravity waves (such as those found in the oceans), in that their period increases with k and are thus called g-modes. In contrast to the p-modes, their nodes are confined to the inner regions of the star; they thus probe deep within the stellar interior. In between the two frequency domains (i.e. for $L_l^2 > \sigma^2 > N^2$ or $L_l^2 < \sigma^2 < N^2$) is an evanescent zone where the eigenfunction exponentially decays with the distance from the wave propagation region. This region acts as a "tunnel" that, if it is thick

enough, completely separates the p- and g-modes, leaving them trapped in the star's P or G zone respectively. Between the P and G domains is the so-called fundamental mode (f-mode), which has a hybrid status and exhibits both p- and g-mode characteristics.

1.2.2 Determining a Stellar Model's Adiabatic Periods

In this section, I will give a very brief overview of how the pulsational periods characteristic of a given stellar model are obtained. This is meant to provide the reader with some basic understanding of the concepts involved; it does by no means constitute an exhaustive mathematical treatment of pulsation theory. More details can be found in the textbook *Nonradial Pulsations of Stars* by Unno et al. (1989) as well as in *Theory of Stellar Pulsations* by Cox (1980).

A star can be described as a closed system governed by thermodynamic and fluid dynamic laws. Neglecting complicating factors such as rotation, convection and the effects of a magnetic field, the system can be fully described by the following six equations:

mass conservation

$$\frac{\partial \rho}{\partial t} + \vec{\nabla} \cdot (\rho \vec{v}) = 0, \tag{1.3}$$

energy conservation

$$\rho T \left(\frac{\partial}{\partial t} + \vec{v} \cdot \vec{\nabla} \right) S = \rho \epsilon_N - \vec{\nabla} \cdot \vec{F}_R, \tag{1.4}$$

the Navier-Stokes relation (Newtonian fluid mechanics)

$$\rho \left(\frac{\partial}{\partial t} + \vec{v} \cdot \vec{\nabla} \right) \vec{v} = -\vec{\nabla} P - \rho \vec{\nabla} \Phi, \tag{1.5}$$

Poisson's equation (which describes the distribution of matter in a gravitational field)

$$\vec{\nabla}^2 \Phi = 4\pi G \rho, \tag{1.6}$$

the equation of state, which normally takes a numerical form, and the equation of energy transfer. In an optically thick medium (such as the stellar interior) we can make the assumption

that energy is transferred by diffusion and write

$$\vec{F_R} = -K\vec{\nabla}T \qquad \text{where} \qquad K = \frac{4ac}{3\kappa\rho}T^3. \tag{1.7}$$

The symbols used in these equations have their conventional meaning as follows: ρ is the density, T is the temperature, S is the entropy, P is the pressure, ϵ_N is the nuclear energy production rate, F_R is the radiative flux, Φ is the gravitational potential, $\vec{v}$ is the velocity vector of the fluid, and κ is the opacity.

If the star is in hydrostatic equilibrium (i.e. not pulsating), its structural quantities are time-independent and all time derivatives as well as the velocity vector can be set to zero. The equation of mass conservation then annihilates, while the remaining four analytical expressions can be written as

$$\rho_0\epsilon_{N,0} - \vec{\nabla}\cdot\vec{F_0} = 0 \tag{1.8}$$

$$-\vec{\nabla}P_0 - \rho_0\vec{\nabla}\Phi_0 = \vec{0} \tag{1.9}$$

$$\vec{\nabla}^2\Phi_0 - 4\pi G\rho_0 = 0 \tag{1.10}$$

$$\vec{F_0} + K_0\vec{\nabla}T_0 = \vec{0}, \tag{1.11}$$

where the subscript "0" indicates an unperturbed value. Things can be further simplified by replacing the parameter gradients by simple derivatives with respect to the distance from the stellar center r in the approximation of spherical symmetry, yielding

$$\frac{dL}{dr} = 4\pi r^2\rho\epsilon_N \qquad \text{where} \qquad L = 4\pi r^2 F_R \tag{1.12}$$

$$\frac{dP}{dr} = -\rho g \qquad \text{where} \qquad g = \vec{\nabla}\Phi = \frac{d\Phi_0}{dr} = \frac{GM}{r^2} \tag{1.13}$$

$$\frac{dM}{dr} = 4\pi r^2\rho \tag{1.14}$$

$$\frac{dT}{dr} = -\frac{3\kappa\rho}{4acT^3}\frac{L}{4\pi r^2} \tag{1.15}$$

It is this system of linear differential equations that is numerically solved, for each of a number

of layers characterised by r, when an unperturbed stellar model is calculated. The resulting physical quantities and their local dependence on r are subsequently used in the computation of the model's pulsational properties.

Since stellar oscillations rarely reach large amplitudes compared to the overall structure of the star, they can be treated as small perturbations to its equilibrium state. These perturbations can be described mathematically in two ways. In the Eulerian formalism the point of reference is fixed to a physical location $\vec{r}$ at which the parameters of stellar structure change during a pulsation cycle. The time-dependence of a given quantity f can then be expressed as

$$f(\vec{r},t) = f_0(\vec{r}) + f'(\vec{r},t), \tag{1.16}$$

where $f_0(\vec{r})$ is the unperturbed value of f at a location $\vec{r}$ and $f'(\vec{r},t)$ is its Eulerian perturbation at time t. In contrast, the Lagrangian approach monitors the physical displacement of a given fluid element characterised by a particular value of f, yielding

$$f(\vec{r},t) = f_0(\vec{r_0}) + \delta f(\vec{r},t). \tag{1.17}$$

Here, $\vec{r_0}$ is the equilibrium position of the element and $\vec{r}$ is its perturbed location. As the latter is time-dependent, it is useful to introduce the Lagrangian displacement vector $\vec{\xi} \equiv \delta\vec{r} = \vec{r} - \vec{r_0}$.

The perturbations are introduced into the previously static system by replacing each of the structural quantities in equations 1.3−1.6 by their time-dependent equivalent in either the Eulerian or Lagrangian formalism (equation 1.16 or 1.17). Since the perturbations are assumed to be small, only the first order terms in f' and δf are kept by (linearisation). Terms consisting of unperturbed quantities only can be eliminated by applying the condition of hydrostatic equilibrium (equations 1.8−1.11), leaving a set of linear differential equations with the perturbed quantities as variables. Their coefficients are functions of the non-perturbed quantities, which depend only on the radial coordinate r, and are calculated during the model building process. The perturbed quantities on the other hand depend on the three spherical coordinates r (the radial coordinate already introduced), θ (the angular altitude, corresponding to latitude on Earth) and ϕ (the angular azimuth, corresponding to longitude on Earth)

as well as on the time t. Consequently, a given perturbed quantity $f'(r,\theta,\phi,t)$ can be expressed in terms of a product of functions, each depending on only one or two coordinates (separation of variables). Individual solutions to the set of linear differential equations (also called the *eigenmodes* of the system) then take the form

$$f'_{k,l,m}(r,\theta,\phi,t) = f'_{k,l}(r)Y^l_m(\theta,\phi)e^{i\sigma_{kl}t} \qquad \text{or} \qquad \delta f_{klm}(r,\theta,\phi,t) = \delta f_{kl}(r)\, Y^l_m(\theta,\phi)e^{i\sigma_{kl}t} \tag{1.18}$$

in the Eulerian and Lagrangian formalism respectively. Here, σ_{kl} is an eigenfrequency of the system, $f'_{kl}(r)$ or $\delta f_{kl}(r)$ is the corresponding eigenfunction, and $Y^l_m(\theta,\phi)$ is the (numerically known) spherical harmonic associated with the geometry of an l,m oscillation (see previous section for the significance of k,l and m). The general solution to the set of equations is a linear combination of many eigenmodes, given by

$$f'(r,\theta,\phi,t) = \sum_{k,l,m} \alpha_{klm} f'_{kl}(r)Y^l_m(\theta,\phi)e^{i\sigma_{kl}t}, \tag{1.19}$$

where α_{klm} is an arbitrary coefficient corresponding to the intrinsic amplitude of the mode that cannot be determined from linear theory.

The eigenfrequencies and eigenfunctions of eigenmodes are computed by solving the complex system of six linearised and variable separated equations of oscillation, which are given by

$$\frac{1}{\rho}\frac{dP'}{dr} + \frac{g}{\rho c_s^2}P' + (N^2-\sigma^2)\xi_r + \frac{d\Phi'}{dr} = g\nabla_{ad}\frac{\rho T}{P}\delta S \tag{1.20}$$

$$\frac{1}{r^2}\frac{d}{dr}\left(r^2\xi_r\right) + \frac{1}{\Gamma_1}\frac{d\ln P}{dr}\xi_r + \left(1-\frac{L_l^2}{\sigma^2}\right)\frac{P'}{\rho c_S^2} - \frac{l(l+1)}{\sigma^2 r^2}\Phi' = \nabla_{ad}\frac{\rho T}{P}\delta S \tag{1.21}$$

$$\frac{1}{r^2}\frac{d}{dr}\left(r^2\frac{d\Phi'}{dr}\right) - \frac{l(l+1)}{r^2}\Phi' - 4\pi G\rho\left(\frac{P'}{\rho c_s^2} + \frac{N^2}{g}\xi_r\right) = -4\pi G\nabla_{ad}\frac{\rho^2 T}{P}\delta S \tag{1.22}$$

$$K\frac{dT'}{dr} = -F'_R - K'\frac{dT}{dr} \tag{1.23}$$

$$i\sigma\rho T\delta S = (\rho\epsilon_N)' - \frac{1}{r^2}\frac{d}{dr}(r^2F'_R) - \frac{l(l+1)}{r^2}KT' \tag{1.24}$$

$$\frac{\delta T}{T} = \frac{\Gamma_2 - 1}{\Gamma_2}\frac{\delta P}{P} + \frac{\delta S}{C_p}. \tag{1.25}$$

The thermodynamic quantities Γ_1, Γ_2 and ∇_{ad} have their usual meaning, while $F_r'(r)$ is the radial component of the radiative flux perturbation, ξ_r is the radial component of the Lagrangian displacement vector, and c_S is the local sound speed. N^2 and L_l^2 correspond, respectively, to the Brunt-Väisälä and the Lamb frequency defined in the previous section.

If information on the excitation of the eigenmodes is not an issue, the system of equations given above can be simplified considerably using what is commonly known as the *adiabatic approximation.* In this approach it is assumed that no energy transfer takes place between the internal energy of the gas and the kinetic energy of the oscillations. As a consequence, the perturbation in entropy $\delta S = 0$. The six complex equations of oscillation (they are complex on account of the imaginary term in equation 1.24) can then be summarised in two first order and one second order equations corresponding to equations 1.20−1.22, which contain real components only, as

$$\frac{1}{\rho}\frac{dP'}{dr} + \frac{g}{\rho c_S^2}P' + (N^2 - \sigma^2)\xi_r = -\frac{d\Phi'}{dr} \tag{1.26}$$

$$\frac{1}{r^2}\frac{d}{dr}\left(r^2\xi_r\right) - \frac{g}{c_S^2}\xi_r + \left(1 - \frac{L_l^2}{\sigma^2}\right)\frac{P'}{\rho c_S^2} = \frac{l(l+1)}{\sigma^2 r^2}\Phi' \tag{1.27}$$

$$\frac{1}{r^2}\frac{d}{dr}\left(r^2\frac{d\Phi'}{dr}\right) - \frac{l(l+1)}{r^2}\Phi' = 4\pi G\rho\left(\frac{P'}{\rho c_S^2} + \frac{N^2}{g}\xi_r\right). \tag{1.28}$$

Complemented by four boundary conditions (two at the centre and two at the surface of the star), this system of equations is reduced to an eigenvalue problem that yields a set of discrete eigenfrequencies σ_{kl}^2 and their associated eigenfunctions. Since these cannot be determined analytically, Pierre Brassard developed a designated numerical code perfectly suited to their evaluation (see Brassard et al. 1992 for details). It is this code that is used to compute the adiabatic period spectra of both the long-and short period variables discussed in the remainder of this thesis.

1.2.3 Determining Pulsational Stability from Non-Adiabatic Calculations

The properties of non-radial pulsations in stars are often studied in the adiabatic approximation because this is less involved than solving all six of the complex equations describing stellar oscillations (equations 1.20−1.25). Nevertheless, full non-adiabatic calculations are of

paramount importance when attempting to determine the stability of a given mode. Since the set of equations solved is complex rather than real, the resulting eigenfrequencies and eigenfunctions are also complex quantities and as such consist of real and imaginary components. The eigenfrequency can then be written

$$\sigma = \sigma_R + i\sigma_I, \tag{1.29}$$

where σ_R and σ_I are real numbers. Consequently, the time dependence of an eigenmode (cf. equation 1.18) is of the form

$$\exp(i\sigma t) = \exp[i(\sigma_R + i\sigma_I)t] = \exp(i\sigma_R t)\exp(-\sigma_I t). \tag{1.30}$$

The first component on the right hand side of the equation describes the oscillatory behaviour of a mode with frequency $\sigma_R (= 2\pi/P)$, while the second part indicates the damping or growth of the pulsation with time. This latter term does not exist in adiabatic theory as the imaginary part of the eigenfrequency σ_I is not computed. It is the sign of σ_I that is decisive: if it is positive, the oscillation will be damped over time; it is thus stable. If on the other hand σ_I is negative, the amplitude of the pulsation will experience an exponential growth and the mode will be unstable to oscillations. In practical terms this occurs if an excitation mechanism is operative in a region of the star where the amplitude of its eigenfunction is large. I will briefly discuss the reason for stellar instability and the underlying driving mechanism for sdB stars in what follows.

The reason stars pulsate is because they are not in hydrostatic equilibrium and the force of gravity acting on the outer mass of the star is not quite balanced by the interior pressure. As a result of this, when a star expands due to increased gas pressure, its density decreases to the point of hydrostatic equilibrium and overshoots it, before gravity dominates and the star begins to contract again. The momentum of the in-falling material carries the contraction and the pressure beyond the equilibrium point, starting the process all over again. Because energy is lost during such pulsations they are normally damped, resulting in the star's overall stability. However, observations show that this is not always the case. On the contrary, we

now know of a number of families of oscillating stars, most of which pulsate with very regular periods. This implies that the dissipated energy must be replaced by some form of excitation mechanism.

A star's stability is the result of the competition between the excitation and damping mechanisms, which respectively supply and dissipate energy in certain regions of a star. The energy theorem is given by

$$\frac{dE}{dt} = \int_0^M \left(\varepsilon_N - \frac{1}{\rho}\nabla \cdot \vec{F}\right) dM_r - \int_{r=R} P\vec{v} \cdot dS, \tag{1.31}$$

where the total energy E of the star consists of the kinetic, potential and internal energies and can be written as

$$E = \int_0^M \left(\frac{1}{2}\vec{v}^2 + \frac{1}{2}\Phi + U\right) dM_r. \tag{1.32}$$

Here Φ is the gravitational potential, U is the specific internal energy M is the total mass of the star, ε_N is the nuclear energy generation rate, ρ is the density, $\vec{F}$ is the total energy flux, P is the pressure and $\vec{v}$ is the velocity vector. Put into words, the energy theorem states that change in the total energy of a system is caused by either nuclear energy generation ε_N in the interior, loss of radiative flux $\vec{F}$ at the surface or the outgoing waveflux $P\vec{v}$ if no work is done from the outside. Since stability is the problem of the exchange from one type of energy to another in a given system, at least one form of energy must increase or decrease monotonically for instability to be achieved. Considering this, it is useful to introduce the work function W corresponding to the total increase in energy over one period of oscillation. W can be derived from the first term on the right hand side of equation 1.31 if the pressure goes to zero at the surface, and is given by

$$W = \oint \frac{dE}{dt} dt = \oint dt \int_0^M \frac{\delta T}{T} \delta \left(\varepsilon_N - \frac{1}{\rho}\nabla \cdot \vec{F}\right) dM_r \tag{1.33}$$

The star will pulsate in the case where $W > 0$, i.e. when a net energy increase is taking place. This energy increase originates from nuclear reactions in the core, which release photon energy that is efficiently converted to kinetic energy through some kind of driving mechanism.

In the case of subdwarf B stars, this mechanism is the κ-mechanism. The κ-mechanism contributes to the driving of an oscillation if

$$\frac{d}{dr}\left(\kappa_T + \frac{\kappa_\rho}{\Gamma_3 - 1}\right) > 0, \tag{1.34}$$

where $\kappa_T = \left(\frac{\partial \ln \kappa}{\partial \ln T}\right)_\rho$ is the temperature dependence of opacity with constant density, $\kappa_\rho = \left(\frac{\partial \ln \kappa}{\partial \ln \rho}\right)_T$ is the density dependence of opacity with constant temperature and $\Gamma_3 - 1$ is an adiabatic exponent defined by

$$\Gamma_3 - 1 = \left(\frac{\partial \ln T}{\partial \ln \rho}\right)_S, \tag{1.35}$$

where S refers to entropy. If this inequality is satisfied by a particular region in the stellar envelope, the radiative flux from the stellar interior is blocked by the effect of the temperature and density dependence of opacity. Analogous to the concept of a dam blocking water from a river and thereby creating a reservoir, this opaque layer in the stellar envelope causes the radiative energy to build up. The blocked energy is subsequently converted to kinetic energy and hence used to drive the oscillations. Local enhancement of opacity is generally due to the presence of a partial ionisation zone, such as the region where singly ionised helium absorbs ultraviolet radiation to become doubly ionized. Since the value of κ_T increases in the inner part of an ionisation zone and decreases in the outer layers, the excitation and damping zones are located in the inner and outer zones of the ionisation zone respectively. The application of the κ-mechanism to subdwarf B stars will be discussed in more detail in the following paragraph.

1.2.4 Pulsations in EC 14026 Stars

Uncovering the Driving Mechanism

As models of subdwarf B stars are characterized by the presence of a He II/He III convection zone where He II is ionized, it seemed natural to investigate whether it could serve as a driving mechanism for pulsations. However, early modelling (Charpinet et al. 1996) showed that, in fact, the He II/He III partial ionization zone was located too high in the envelope, in a region that contained too little mass for driving to be significant. On the other hand, there

was another maximum in the opacity, this time due to heavy-metal ionization, that seemed to lie at just the right envelope depth for pulsations to be driven efficiently (see Figure 1.8 for details). Furthermore, this newly found opacity bump (referred to as the Z-bump) was strongly dependent on the metallicity of the uniform model; whereas employing solar metal abundances (Z $\sim$ 0.02) resulted in an opacity too weak to drive pulsations, increasing the metallicity of the model to beyond Z $\sim$ 0.04 produced excited modes. The modes excited were found to be non-radial low-order p-modes whose excitation depended on the model's surface gravity $\log g$ and, to a lesser extent on the effective temperature $T_{\rm eff}$, as well as on the metallicity Z.

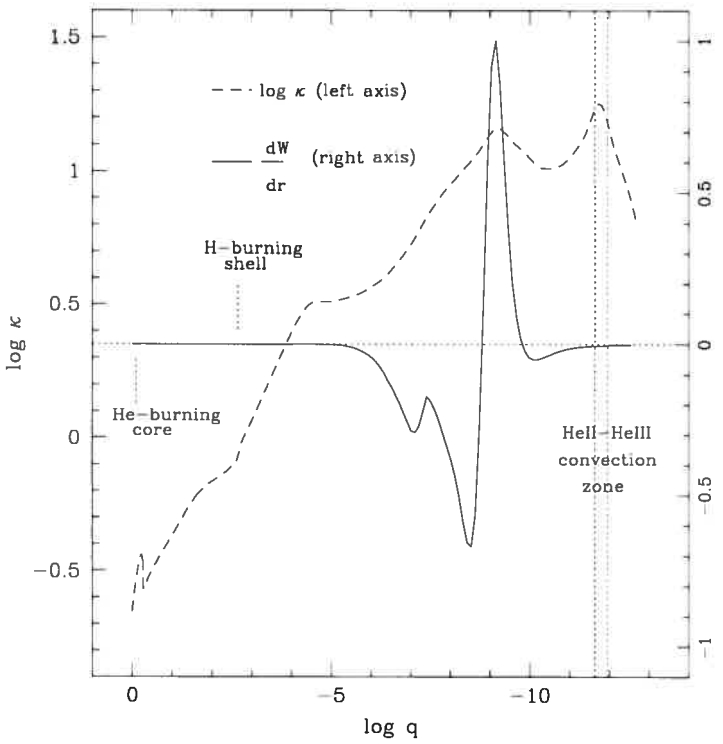

FIGURE 1.8 – Of interest here is the derivative of the work function dW/dr (solid line) as well as the Rosseland mean opacity profile (dotted line) as a function of depth. The quantity dW/dr gives the net amount of energy gained (or lost) by the displaced material during a cycle of pulsation. Where it is positive, the corresponding region transfers energy INTO the mode, thereby exciting it. It can be seen that while dW/dr is essentially zero at the depth of the HeII/HeIII convection zone, it has a peak at the same depth as the secondary bump in the Rosseland mean opacity profile due to the ionization of heavy elements, in particular iron. This enables the driving of pulsations. From Charpinet et al. (1996).

It is however improbable that subdwarfs, as old evolved stars, contain a high proportion of metals as assumed in the successful models. Hence it has to be stressed that, for driving to be successful, the high metallicity proposed does not have to be uniformly present in the whole envelope. It is sufficient to locally enhance the metal abundance in the driving region only, leaving the rest of the atmosphere metal-poor and thus keeping the overall metallicity solar. As all subdwarf B stars show peculiar surface abundances, local enrichments and depletions are not only plausible, but expected. It is believed that the abundance anomalies seen are due to diffusion, the competition between gravitational settling and radiative levitation. As the name implies, gravitational settling forces particles to sink under gravity, heavier ones more so than light species. Radiative levitation has the opposite effect, propelling particles outwards. The degree of this depends on the atomic structure of the particles, and favours elements that can absorb a large number of photons from the radiation field (such as iron). The two key stellar parameters involved in the diffusion process are hence the effective temperature and the surface gravity. The effective temperature controls the intensity of the photon field which produces radiative levitation, while the surface gravity directly influences the strength of the gravitational settling. A recent investigation (Chayer et al. 1996) found that metals, and in particular iron, do indeed levitate in the envelopes of these stars, resulting in local metal overabundances of more than one order of magnitude.

To account for these local abundance anomalies, more sophisticated "second generation models" (Charpinet et al. 1997) were based on the assumption that an equilibrium had been reached between gravitational settling and radiative levitation. This seemed justified because, according to Fontaine & Chayer (1997), the equilibrium state is reached on a timescale much shorter than the typical evolutionary lifetime of a subdwarf B star. The result is a non-uniform distribution of heavy elements as a function of depth in the envelope. To simplify matters, the envelope model was constructed using only iron in a bed of hydrogen, resulting in the plot of iron as a function of depth shown in Figure 1.9.

The solid curves in the figure show the iron abundance as a function of fractional mass depth in the outer envelopes of representative models of sdB stars with $M = 0.48\ M_{\odot}$, $\log g = 5.8$ and various effective temperatures ranging from $\sim$ 22,000 K to $\sim$ 42,000 K. The

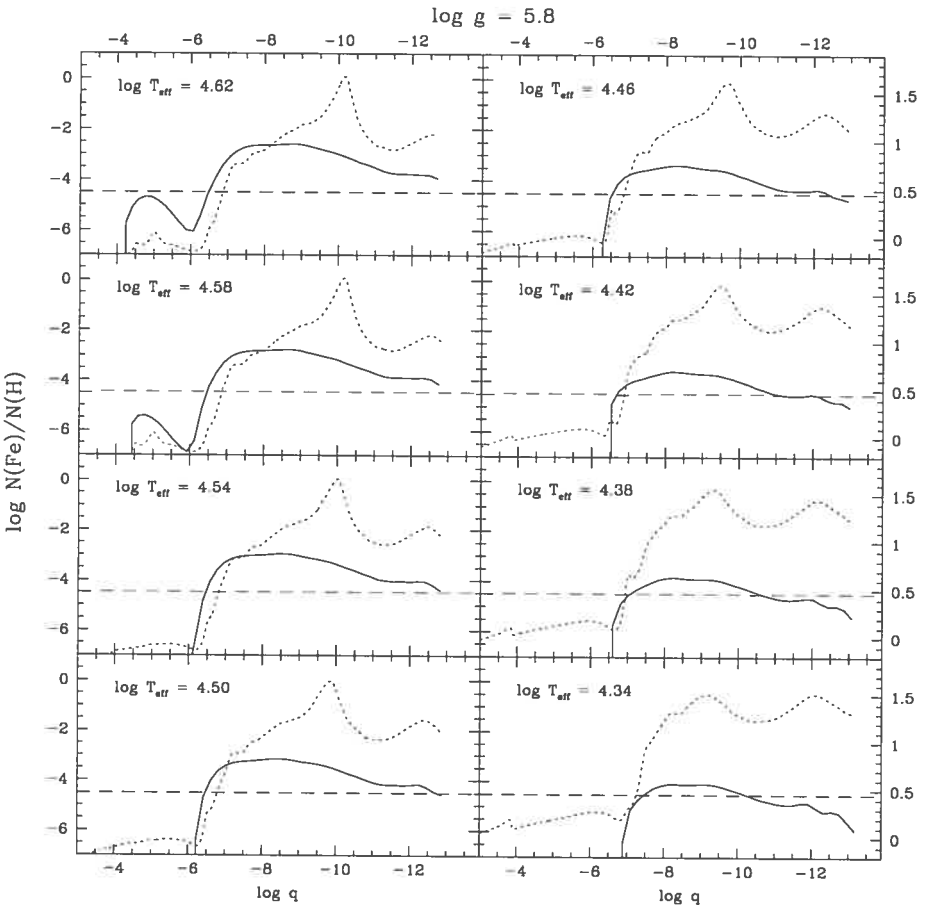

FIGURE 1.9 – Equilibrium abundance of iron (solid curve) as a function of fractional mass depth for a series of representative sdB models with $\log T_{\rm eff}$ from 4.34 (bottom right) to 4.62 (top left) in steps of 0.04. Also shown are the Rosseland mean opacity (dotted curve) and the mean fractional iron abundance (dashed line). From Charpinet et al. (1997).

radiative support increases monotonically with increasing effective temperature, and supports large local overabundances of iron, particularly in the hotter models (upper left-hand panels). The dotted curves represent the Rosseland mean opacity, a quantity associated with the non-uniform iron abundance profile. It can be seen that the opacity profile features two bumps, the one nearer the stellar surface being due to the hydrogen ionization zone mentioned earlier, and the deeper one arising from the ionization of the K-shell of iron. The location and shape of the second bump are critical factors in the efficiency of the driving mechanism. It is clear from the figure that at low effective temperatures, radiative levitation does not support enough iron, resulting in a broad opacity peak too deep in the envelope to make driving possible.

As the effective temperature increases, the peak becomes sharper, thus boosting the opacity derivatives, and moves towards the surface, reaching the critical region for efficient excitation. However, at even higher effective temperatures, the peak has migrated too close to the stellar surface to contain enough mass to drive pulsations. This results in the formation of a broad instability strip in the H-R diagram between Teff $\sim$ 27,000 and 39,000 K.

The Theoretical Period Spectrum

The pulsation properties of the sdB models developed by Pierre Brassard (details on these models can be found in e.g. Charpinet (1998) and in the following chapters) are calculated using adapted versions of the adiabatic and non-adiabatic pulsation codes described in Brassard et al. (1992) and Fontaine et al. (1994). After the unperturbed stellar parameters have been computed for each of a number of layers making up the model (usually around 1600$-$1700) in a first step, they are submitted to adiabatic pulsation calculations numerically solving the 4 adiabatic oscillation equations detailed earlier (equations 1.26$-$1.28). This yields the values of the eigenfrequencies, which are used as a best estimate in the subsequent non-adiabatic computations solving the full 6 complex oscillation equations (equations 1.20$-$1.25). In addition to rendering slightly adjusted periods and eigenfunctions, these predict whether or not the mode is unstable from the imaginary part of the eigenfrequency (see above). The stellar models, and consequently the period spectra predicted, are dependent on 4 input parameters: the surface gravity, $\log g$, the effective temperature, $T_{\rm eff}$, the total mass of the model, M_*, and the logarithmic depth of the transition zone between the hydrogen-rich envelope and the helium core, $\log q(\mathrm{H}) \equiv \log (M_{env}/M_*)$.

Figure 1.10 shows the dependence of the periods on effective temperature, while the other three parameters are kept constant at typical values. Values of $l = 0$, 1, 2, 3 are considered in the period window from 80 to 280 s. The solid curves represent the fundamental modes that divide the diagram into two regions: the domain of the p-modes (below the curve), and that of the g-modes (above the curve). We find that, while the p-modes are found to be unstable within the instability strip mentioned earlier, none of the g-modes are excited. Apart from the fundamental modes, the p-modes are not very sensitive to the effective temperature. However,

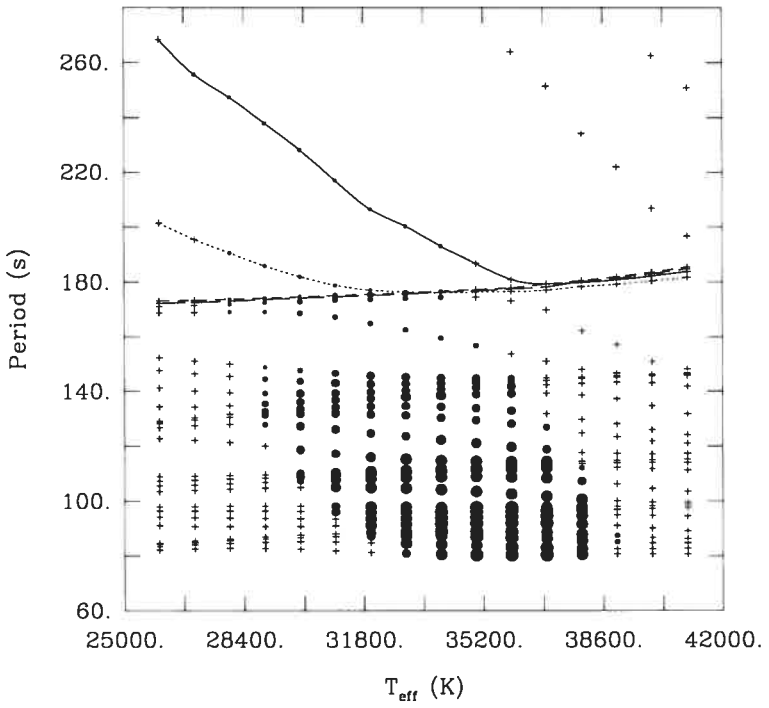

FIGURE 1.10 – Period spectrum as a function of effective temperature for representative sdB models with $M = 0.48\ M_{\odot}$, $\log g = 5.8$ and a H-rich outer layer extending to a depth $\log q(\mathrm{H})$ = -3.70. A stable mode is represented by a small cross, while an excited mode is indicated by a filled circle. The bigger the circle, the more unstable the mode. The curves join together the fundamental modes and separate the p-modes from the g-modes. From Fontaine et al. (1998).

while at the low-temperature end of the instability strip only low-order (long period) p-modes are excited, it is the high-order (short period) modes that are unstable at the high-temperature end. From this we can deduce that the higher a star's temperature, the shorter its excited periods will be. In addition to this, maximum driving is found between $T_{\mathrm{eff}} \sim$ 33,000-36,000, which means we would expect to find the majority of EC 14026 stars to be clustered around these values.

The variation of the period with surface gravity is illustrated in Figure 1.11 (the other three parameters are once again kept constant). Apart from the odd g-mode in the lowest gravity models, we again find that it is only the low-order p- and f-modes that are excited. This can be attributed to the fact that p-modes in subdwarf B models are shallow envelope modes, while g-modes are core modes, with significant amplitudes located far below the driving region. It

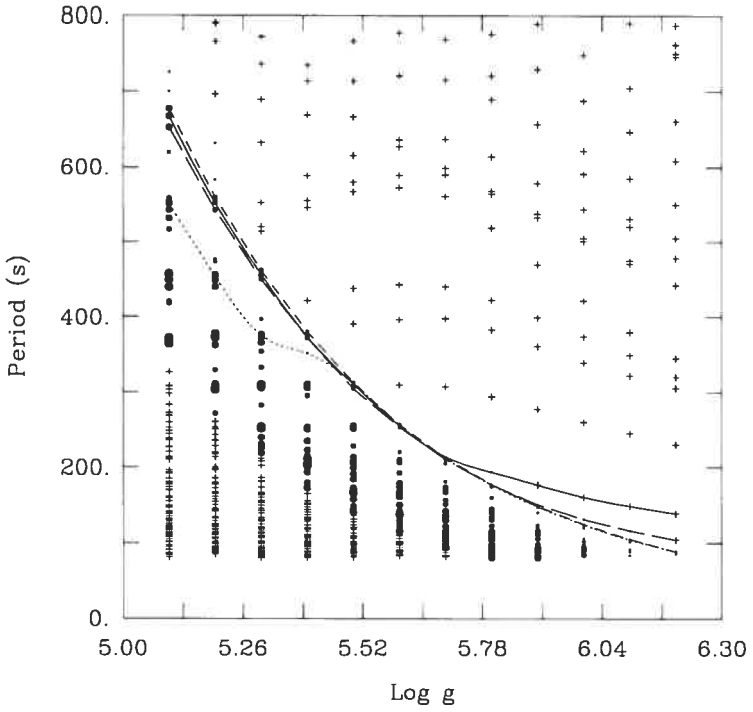

FIGURE 1.11 – Period spectrum as a function of surface gravity for representative sdB models with $M = 0.48\ M_{\odot}$, $\log g = 5.8$ and a H-rich outer layer extending to a depth $\log q(\mathrm{H}) =$ -3.70. For further details, please see Figure 1.10. From Fontaine et al. (1998).

can be seen that a change in surface gravity has a much larger effect on predicted periods than was the case for the temperature. The period of a given mode will decrease substantially with decreasing surface gravity, implying that lower gravity sdBs should show the longer periods. In addition, the most unstable modes (indicated by the largest filled circles in the diagram) occur for the lowest gravity models, which suggests that lower gravity subdwarfs should pulsate at larger amplitudes. As for the other two free parameters, M_* and $\log q(\mathrm{H})$, it has been calculated (Charpinet et al. 2002) that the former has only a slight, though noticeable, impact on the periods, which tend to increase slightly with total stellar mass. On the other hand, the mass of the hydrogen-rich envelope has a strong influence on the periods. Rather than affecting all modes more or less systematically like the other three parameters, a change in envelope mass alters the spacing between periods. For p-modes, this is due to the so-called micro-trapping effect, which is caused by the He/H chemical transition zone between the H-rich envelope and

the He-rich core generating perturbations in the acoustic mode spectrum.

A more recent study (Charpinet et al. 2002b) also investigated the effects of stellar evolution on the pulsational modes, focusing primarily on the evolution of the pulsation periods and the rates of period change, both of which are observable quantities. It was found that p-modes respond mainly to the secular variation of the surface gravity and their evolution is dominated by two principal phases. The first, longer phase is identified with a period in the life of an sdB when the surface gravity decreases as the star moves slowly away from the ZAEHB on the H-R diagram and corresponds to a monotonic and regular increase of the periods. The second phase starts about 90 Myr after the ZAEHB and lasts until helium-shell burning begins ($\sim$ 110 Myrs after the ZAEHB) and involves a contraction of the model. This means that both $\log g$ and $T_{\rm eff}$ increase rapidly, which manifests itself in an important systematic decrease of the periods.

1.2.5 Pulsations in Betsy Stars

Uncovering the driving mechanism

Unlike in the case of the EC 14026 stars, where instabilities were computationally predicted and observationally detected completely independently and nearly simultaneously, the pulsations in Betsy stars were a puzzle to the scientific community in the years following their discovery. The long periods observed automatically implied the excitation of high radial order g-modes rather than the low radial order p-modes found in the EC 14026 stars. One thing that seemed certain was that whatever was driving the instabilities, it was not the same κ-mechanism that worked so well for the rapid pulsators. Underlying this conclusion was the assumption that only modes with the lowest possible values of the degree index for g-modes, $l = 1$ and 2 would be observable, higher degree order modes being undetectable due to cancellation effects when integrating over the visible disk of the star. Unpublished calculations by Charpinet (1998) had already established that low-degree, high-order g-modes cannot be driven in typical subdwarf B star models. Beyond this, it was shown in the previous section that the efficiency of the κ driving mechanism reaches a maximum at $\sim$ 33,500 K and falls to zero for the much lower temperatures ($\sim$ 27,000 K) attributed to Betsy stars.

Consequently, the search was on for other possible driving mechanisms. One of these was the excitation of high-order gravity modes by dynamic tides (Fontaine et al. 2003a). Given that about half of all known sdB stars belong to close binary systems, it seemed likely that at least *some* of the Betsy stars could be driven into pulsation by dynamic interactions with their companion. Detailed calculations showed that, unlike in solar-type stars, the ratio of the work done by the tidal force (which implements itself in form of an oscillation mode) to the kinetic energy of that mode increases with increasing radial order. Because the amplitude of a resonantly excited mode is proportional (among other things) to that ratio, this implies that the probability of tidal coupling increases with increasing radial order, and hence with increasing periods (as a higher radial order signifies a longer period for a g-mode). Thus the probability that the low-frequency modes observed in Betsy stars could be excited by dynamic tides is relatively high. The major problem with this theory is that, while it may be able to explain the oscillations observed in close binaries, it offers no explanation for the pulsations discovered in single or long-period binary Betsy stars.

Attention returned to the κ-mechanism as a possible pulsation driver when it was realised that a very strong qualitative resemblance exists between the two families of sdB oscillators on the EHB and two neighbouring groups of pulsating B stars on the main sequence. In the case of the main sequence pulsators, the hotter β Cep stars oscillate rapidly with low-degree p- and g-modes, while the cooler slowly pulsating B-type (SPB) stars excite long-period high-order g-modes. Both classes of pulsator were shown to be excited by the same driving engine, a κ-mechanism dependent on the Z-bump associated with the ionization of iron (Dziembowski & Pamyatnykh 1993; Dziembowski, Moskalik, & Pamyatnykh 1993). It was found that, in the β Cep models, non-observable high-degree ($l \geq 6$), high-order g-modes were excited simultaneously with the visible low-degree ($l = 1, 2$) low-order modes. Owing to the different physical conditions in the SPBs, the instability domain of high-order g-modes in the β Ceps shifted to low-degree modes in the cooler stars, rendering them observable. This constituted a natural explanation for the close proximity on the H-R diagram of two groups of oscillators with very different pulsational characteristics on the basis of a single driving mechanism. Since the analogy between these two families of main sequence pulsators and

the two types of variable sdBs was so strong, it was considered worthwhile to investigate a possible variant of this effect for the EC 14026−Betsy star scenario. As was pointed out above, the excitation of g-modes with $l = 1$ and 2 is not possible in current sdB models, therefore particular attention was paid to including higher degree index modes in the new instability calculations.

To this end, Fontaine et al. (2003) built a series of equilibrium models spanning the range of effective temperature from $T_{\rm eff}$ = 22,000 K to 38,000 K using the same numerical tools as previously outlined for the EC 14026 stars (Charpinet et al. 1997). The only change made to the "second generation" models was a uniform decrease of the iron abundance by a factor of three. As the non-uniform equilibrium abundance of iron in the "second generation" models is calculated assuming radiative levitation in a pure H background, the effects of other species are not taken into account. They would most likely absorb a fraction of the available photons, thus reducing the radiative levitation of iron by an estimated factor as large as two to four. Numerical experiments showed that reducing the variable abundance profile of iron by a factor of three in fact shrinks the theoretical EC 14026 instability strip, which was originally too broad, to fit the observations almost exactly. Hence, this admittedly rather crude, but effective, modification was kept by in the new extended instability calculations.

In addition to recovering the well-established EC 14026 instability region, the stability survey (Fontaine et al. 2003) also uncovered a new island of instability at lower temperatures, roughly corresponding to the $T_{\rm eff}$ domain of the Betsy stars. However, the modes driven have unusually high degree indices of $l \geq 3$, apart from in the very coolest model at 22,000 K, where $l = 2$ modes are also excited. As mentioned before, this is in conflict with canonical wisdom, which suggests that high degree modes should have amplitudes too small to be observable due to cancellation effects when integrating over the visible disk of the star. On the other hand, high degree modes could offer a natural explanation for the very small pulsational amplitudes observed in the long-period variables. Figure 1.12 shows all the high-order excited g-modes up to a degree value of $l = 8$ as a function of the effective temperature of the model. We can see that the periods excited lie in the $\sim$ 2500 to $\sim$ 7000 s range for degree indices up to 4 (i.e. for modes that have the potential of being observable), which is in rough agreement with the

periods observed.

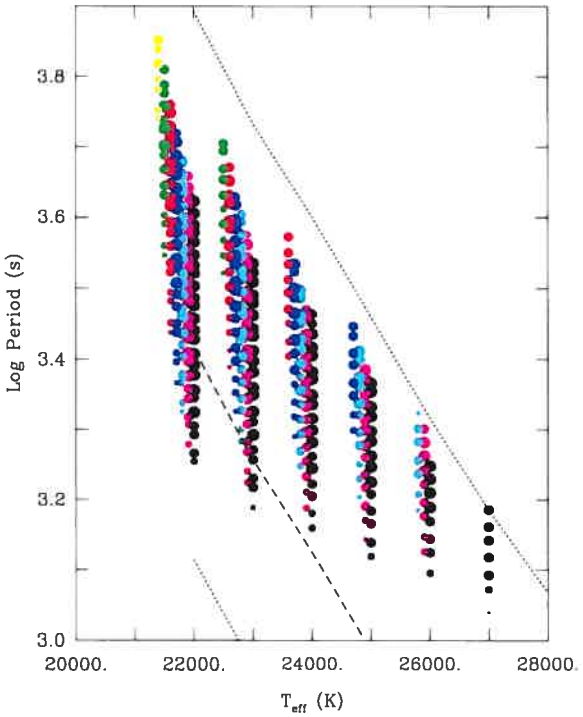

FIGURE 1.12 – High-order g-mode periodicities predicted to be unstable for a representative sequence of Betsy stars. The sizes of the points provide a logarithmic measure of the modulus of the imaginary part of the eigenfrequency, while the colour code distinguishes modes with $l = 2$ (yellow), $l = 3$ (green), $l = 4$ (red), $l = 5$ (blue), $l = 6$ (cyan), $l = 7$ (magenta), and $l = 8$ (black). The columns of circles for individual models are slightly dispersed in $T_{\rm eff}$ to facilitate viewing. The dashed curve shows the value of the thermal timescale in the driving region, whereas the dotted curves correspond to 0.5 and 3 times that value. From Fontaine et al. (2003).

As with the EC 14026 stars, the band of excited periods is sensitive to the effective temperature and the surface gravity. Note that, in Figure 1.12, $\log g$ is not kept constant with temperature because the models were chosen so as to be parallel to the ZAEHB, resulting in an increase of the surface gravity with temperature. Keeping this in mind, we find that the cooler, low-gravity models exhibit the longest periods at the highest amplitudes and also span the widest period range, a scenario somewhat similar to the case of the short period pulsators.

Why does the Kappa mechanism excite g-modes in Betsy stars?

There are two important criteria that must be fulfilled for pulsational driving to be possible through the Kappa mechanism. Firstly, as was outlined in Section 1.2.3, the Kappa mechanism can only potentially excite modes in those regions of the stellar envelope where the derivative of the work function dW/dr is positive. Secondly, the period of an excited mode should be of the same order of magnitude as the thermal timescale in the driving region, a quantity that varies with the iron opacity peak and hence from model to model.

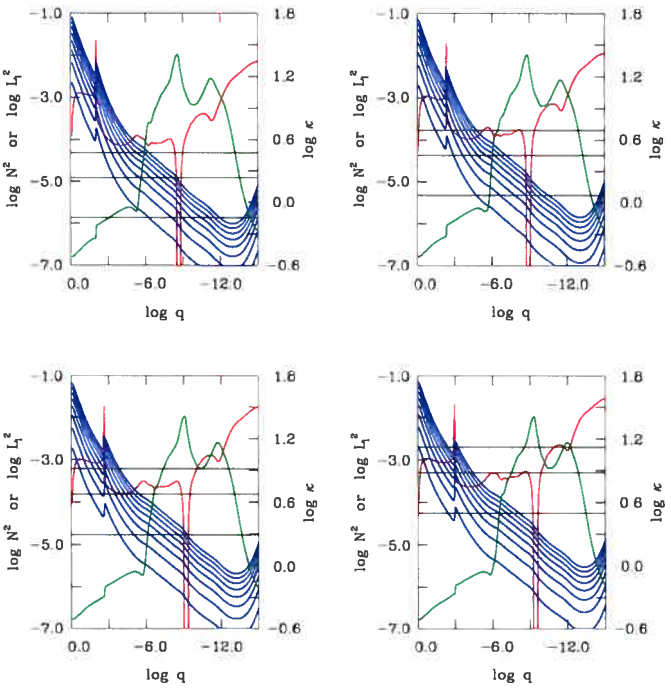

FIGURE 1.13 – Illustration of the driving/damping process for four $l = 4$ modes from a typical reference model with $T_{\rm eff}$ = 24,000, $\log g$ = 5.25, M_* = 0.48 $M_\odot$ and $\log q(H)$ = -1.97. In each plot, the red curve represents the derivative of the work integral with respect to depth $dW/d\log q$, while the green graph refers to the running (from left to right) work integral W. Both quantities are normalised to an extremum value of either +1 or -1. The blue curve shows the combination of the eigenfunctions $y_1^2 + y_2^2$ and the black curve illustrates the run of the Rosseland mean opacity. A feature that should be noted is the tight correlation between the maximum in the opacity profile and the maximum in $dW/d\log q$. Finally, the vertical line indicates the location of a local thermal timescale equal to the period of the mode in the model. From Fontaine et al. (2003).

The driving/damping process is illustrated in Figure 1.13, which shows four representative

high-order g-modes found in a typical Betsy star, each identified by its k and l values and its period P. The red curve in each panel indicates the derivative of the work function, the same quantity used to explain the EC 14026 driving, which is positive in regions that contribute to instability and negative in those where damping occurs. The sum of all local contributions is given by the running work integral W, represented by the green curve. If its value is positive at the surface, the mode is globally excited, if it is negative the mode is stable. Hence, the upper LHS panel shows a g-mode that is globally stable, with a period smaller than the shortest period found in the band of excited modes. Although there are two regions of instability at $\log q \sim$ -7.2 and $\log q \sim$ -8.5, they are overcome by two damping domains, especially the one extending from $\log q \sim$ -5.3 to $\log q \sim$ -6.7, which is mainly responsible for the global stability of the mode. With increasing radial order, the oscillatory region of the eigenfunctions $y_1 + y_2$ (represented by the blue curve) migrates towards the surface, neutralizing the damping region in the process. As a result of this, the modes pictured in the upper RHS panel and the lower LHS panel are globally driven by the κ-mechanism, which in turn is reliant on the iron opacity peak at $\log q \sim$ -8.7. However, at higher radial orders still, the amplitude of the damping region has become comparable to that of the driving region, and the mode in the lower RHS panel becomes globally stable, as do modes with higher radial orders still. This indicates why the κ-mechanism gives rise to a *band* of globally unstable g-modes in Betsy stars.

It was pointed out earlier that, in the majority of the models computed, only modes with $l \geq 3$ can be driven, an effect that can be explained by invoking the timescale criterion as well as a positive derivative of the work function. Figure 1.14 shows the propagation diagram for a model with $T_{\rm eff} = 24{,}000$, where only modes with $l \geq 4$ are excited. The solid curve represents the run of the logarithm of the square of the Brunt-Väisälä frequency (N^2) as a function of fractional mass depth, the well in which corresponds to a narrow convection zone carrying virtually no flux. The runs of the logarithm of the Lamb frequency (L_l^2) for non-radial modes with $l = 1$ to $l = 4$ from bottom to top are given by the dotted lines and the Rosseland mean opacity κ is represented by the stroked curve. It has been established that a g-mode of degree l can show oscillatory behaviour only in regions where $\sigma_r^2 (= 2\pi/P)$ is smaller than both N^2 and L_l^2. This implies that, on the left, the propagation zone of a g-mode is constrained by the

dropping off of N^2 towards the centre, and that on the right it is limited by the outwardly decreasing value of L_l^2, which depends on the l-index of the mode.

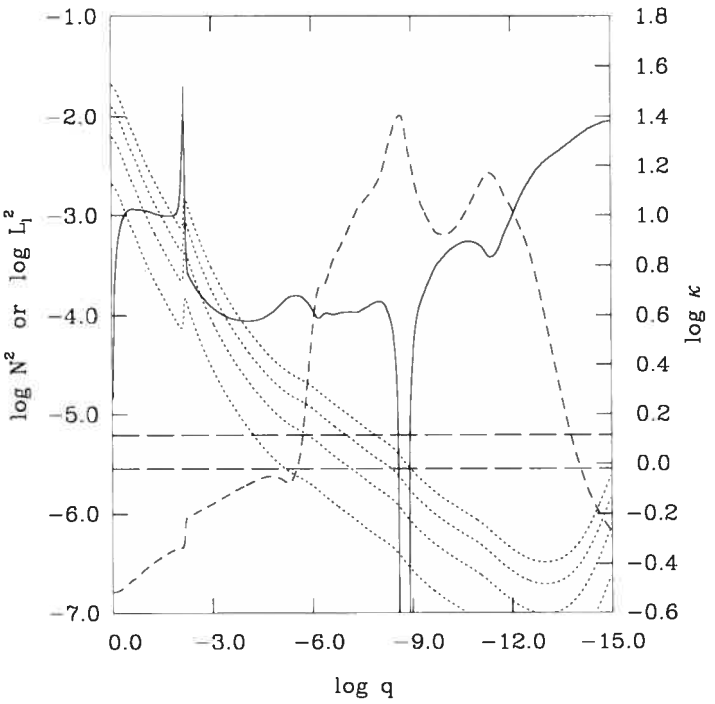

FIGURE 1.14 – Propagation diagram for the same typical Betsy star reference model as detailed in Figure 1.13. The solid curve depicts the profile of the square of the Brunt-Väisälä frequency N^2 from the centre to the surface of the model (from $\log q = 0$ to -15). Also shown are the runs of the square of the Lamb frequency L_l^2 (dotted curves) for modes with $l = 1$ to $l = 4$ from bottom to top. The dashed curve illustrates the Rosseland mean opacity profile and the two horizontal long-dashed lines indicate the band of excited periods (in σ^2 units) found in the model. From Fontaine et al. (2003).

Taking into account only the criterion that driving becomes possible when the outer boundary of the oscillatory region of a mode reaches out from below into the driving/damping region would imply that even modes with $l = 1$ and 2 should be excited, as their propagation zones do reach the instability region roughly corresponding to the peak in the Rosseland mean opacity. However, we also need to consider the second condition, which limits the periods excited to the same order of magnitude as the thermal timescale in the driving region. The range in which unstable periods were found in the survey lies between 0.5 and 3 times the value of the thermal timescale in the driving region $\tau_{th}(\kappa_{max})$ and is indicated by the stroked

horizontal lines in the propagation diagram. Hence we can see that while the propagation zone for modes with $l = 4$ just reaches into the driving region at the same time as their periods fall into the horizontal instability strip, the modes with lower degree values cannot reach the driving region and fulfil the timescale criterion simultaneously. Thus, in this model it is only modes with $l \geq 4$ that are excited.

1.3 OBSERVATIONS OF PULSATING SUBDWARF B STARS

1.3.1 Observational Goals and Techniques

The ultimate goal when observing pulsating subdwarf B stars is, as almost always in astronomy, to compare the observational data with theoretically predicted values and thus gain a deeper understanding of the object studied. In the case of the sdB pulsators this ideally means extracting the periods of pulsation from observations, assigning them to pulsational modes predicted from models, and using this information as an asteroseismological tool to deduce fundamental stellar parameters. For the p-modes found in EC 14026 stars, the most interesting of these is the thickness of the hydrogen shell, firstly because it cannot be measured otherwise, and secondly because knowing the mass of the shell is important for restricting the amount of mass-loss these stars must have experienced in their past. The study of g-modes has even more potential. In addition to holding information on the location of the transition zone between the helium core and the hydrogen shell, these modes are also affected by the extent of the inner CO core, a parameter fundamental to constraining evolutionary scenarios.

The first step when observing a potentially pulsating subdwarf is obviously to determine its variability. For EC 14026 star candidates this is done by obtaining a high-speed photometric time-series of the order of a few hours, reducing the data to obtain a light curve corrected for atmospheric variations and computing the Fourier Transform. For Betsy stars the same technique applies, but a much longer light curve is needed, and matters are further complicated by daily aliasing and differential extinction, as we will see later. The Fourier Transform converts a curve taken in the time domain into a spectrum in the frequency domain, with the periods of pulsation standing out as peaks. Using this technique may well yield pulsational periods even

if the star's variability is not obvious from the light curve itself. The next step is to extract the star's pulsational properties. The periods can be deduced directly from the Fourier Transform and are used as fixed variables in a least-squares fitting procedure to determine each pulsation's amplitude and phase. The computed sinusoids (or peaks in the Fourier domain) are then subtracted from the original light curve in a technique called pre-whitening until the residual light curve is consistent with noise. We now know the combination of sinusoidal waves that best matches our observations, and can compare their periods to the values predicted by theoretical models. Unfortunately, the linear oscillation equations discussed earlier cannot predict the pulsations' amplitudes; to do this we would need non-linear calculations that are beyond the scope of current computational facilities.

Considering the fact that the theoretical period spectrum of a given stellar structure depends on 4 free parameters, it is not trivial to find the model that matches the observed periods best (the so-called "optimal model"). Fortunately, this difficulty was overcome by the recent development of a designated code (Brassard et al. 2001). Using a grid of models as input, the program determines the theoretical modes that fit those observed most closely for each combination of $\log g$, $T_{\rm eff}$, M_*, and $\log q(\mathrm{H})$. The quality of the match is then quantified by the goodness-of-fit merit function χ^2 at each gridpoint, smaller values of χ^2 indicating a better fit. Consequently, the model associated with the smallest value of χ^2 corresponds to the "optimal model", which however at this point is not necessarily meaningful. The quantitative match to the observed period spectrum may for example not be acceptable, or the parameter hyperspace may exhibit a large number of models with similarly good fits (this is often the case if there are not enough observed periods available). It is only when the "optimal model" is well constrained and can quantitatively reproduce the experimental period spectrum that its parameters can be assigned to the target with some certainty.

This so-called forward approach in asteroseismology has so far been used to successfully analyse the observed period spectrum of four EC 14026 stars: PG 0014+067 (Brassard et al. 2001), PG 1047+003 (Charpinet et al. 2003), PG 1219+534 (Charpinet et al. 2005a) and Feige 48 (Charpinet et al. 2005b). In each case, the authors found just one or two well-defined regions of χ^2 minima in parameter space, which could conclusively be discriminated

between on the basis of constraints on $\log g$ and $T_{\rm eff}$ from spectroscopy. However, for the majority of known subdwarf B stars we have not observed a sufficient number of periods (this is sometimes due to observational restrictions, other times the star may simply not pulsate in enough frequencies) or else the period spectrum is too rich and/or distorted by rotation to enable an easy interpretation.

1.3.2 Observations of EC 14026 Stars

Since the discovery of the first short-period variable subdwarf B star, EC 14026-2647 (Kilkenny et al. 1997), the total number of known EC 14026 stars has risen to 34 thanks to further efforts by the South African team (see Kilkenny (2002) for a recent review), the Montréal group (see Billères et al. 2002 for details on their survey) and a Norwegian-German-Italian collaboration (Silvotti et al. 2002a; 2002b), among others. Remarkably, they all fall into the p-mode instability strip predicted by invoking the κ-mechanism in correlation with a local overabundance of iron (see e.g. Charpinet et al. 2001). As expected, the fast oscillators tend to cluster around $\sim$ 33,000 K and the lower gravity pulsators generally exhibit higher amplitudes than their more compact counterparts. Moreover, the periods observed fall into the theoretically unstable range for almost all of the targets, as can be seen in Figure 1.15. Indeed, it seems that non-adiabatic theory is able to account for the EC 14026 phenomenon exceedingly well at the qualitative level. Beyond this, the successful asteroseismology of the four pulsators mentioned earlier clearly shows that attempts at interpreting the period spectra of EC 14026 stars on a more quantitative basis are beginning to bear fruit. As noted by Charpinet et al. (2005b), the acceptable reproduction of the observed frequencies depends on the incorporation of radiative levitation, models assuming a uniform metallicity generally not being able to explain all the frequencies observed.

While the asteroseismological inference of key stellar parameters such as the total mass and the thickness of the hydrogen shell in EC 14026 stars is beginning to indicate evolutionary tendencies (see Charpinet et al. 2005 for a recent review), it is clear that asteroseismology will have to be achieved for a much larger proportion of subdwarfs if convincing constraints are to be placed on their formation. In the case of the EC 14026 stars, the main challenge is

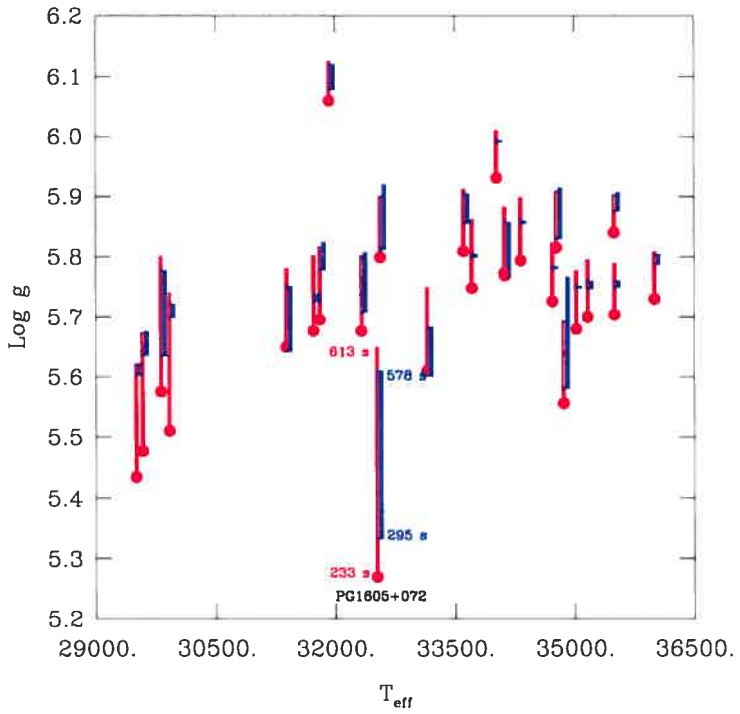

FIGURE 1.15 – Ranges of periods observed (blue) for 26 EC 14026 stars compared to those computed (red) from models with appropriate atmospheric parameters. For each target, the observed period range is scaled to that predicted, as illustrated for the example of PG 1605+072. The values of $\log g$ and $T_{\rm eff}$ are those of Green, Fontaine, & Chayer (in preparation).

detecting a sufficient number of time-resolved harmonic oscillations. One way to achieve this is by organising large-scale multi-site campaigns on the basis of small telescopes, such as the Whole Earth Telescope (WET) collaboration (see e.g. Kilkenny et al. 2003). The resulting data often boast a high duty cycle and frequency resolution, however the fact that the telescopes involved are normally in the 0.5 to 2-m range introduces a significant level of noise. More sensitive frequency measurements can be obtained with mid-size telescopes, although the time baseline and duty cycle generally suffer due to telescope allocation constraints. All of the convincing asteroseismological fits achieved to date are based on just a few nights of data obtained at the 3.6-m Canada-France-Hawaii telescope (CFHT) with the portable Montréal 3-channel photometer *LAPOUNE*. While these are not subject to much noise and therefore allow the extraction of low-amplitude pulsations, individual periodicities can only be resolved

if the peaks are relatively widely spaced.

Observational challenges aside, the interpretation of EC 14026 stars' period spectra can also be hampered by complicating factors intrinsic to the object, such as a fast rotation rate (e.g. PG 1605+072; Koen et al. 1998), a close binary status (e.g. KPD 1930+2752; Billères et al. 2000) or very high amplitude pulsations (e.g. Balloon 090100001; Oreiro et al. 2004). The first of these results in rotational splitting to the extent where it is difficult to distinguish $m \neq 0$ components (that are not predicted in the standard static models used) from independent pulsations and is closely linked to the second factor. Indeed, sdB stars in short-period binaries are predicted to exhibit a rotation rate on the same timescale as their binary period. High amplitude pulsations on the other hand induce a multitude of peaks corresponding to harmonics of the real periodicities, which again can be difficult to discriminate against in the data. Therefore, the extraction of a very rich frequency spectrum is not necessarily more advantageous to asteroseismology than that of only a handful of periodicities.

In what follows, I will present some of the EC 14026 stars observed in more detail. It is far beyond the scope of this introduction to do this for all 34 fast pulsators, thus I will focus only on some particularly interesting targets.

PG 1605+072: A Class of its Own

The variability of PG 1605+072 was first discovered by Koen et al. (1998) at the South African Astronomical Observatory (SAAO). Having uncovered relatively simple period spectra for all previously observed EC 14026 stars, the authors were astounded to find of order 30 pulsational frequencies, most of whose periods exceeded 300 s and were spread over a range of 400 s, much larger than had been found for any other rapid pulsator at the time. The dominant period at $\sim$ 480 s also had the highest amplitude (64 mmags) detected in a subdwarf until that point. Both the uncharacteristically long periods and the high amplitudes were attributed to the extremely low surface gravity, determined spectroscopically to be $\log g = 5.27 \pm 0.03$ (Green, Fontaine, & Chayer, in preparation). The low surface gravity is probably due to PG 1605+072 being significantly older than the other EC 14026 stars and having already evolved

away from the core helium-burning horizontal branch. Another fact of interest is that PG 1605+072 was the first EC 14026 star to be discovered without a detectable binary companion; if there was to be a secondary, it would have to be a main sequence star of type K0 or later. As this new sdB star left much open to speculation, a multi-site campaign was launched a little later (Kilkenny et al. 1999), resulting in 180 h of useful data being accumulated from telescopes around the world. The new data revealed of order 55 frequencies, five of which dominated the others by at least an order of magnitude (see Figure 1.16, top panel). Some of the peaks were very closely spaced, and had varied substantially in amplitude compared to the light curves obtained in 1998. Model periods calculated in the range of the observed periods showed modes of mixed character, which were g-modes in the deep interior and p-modes in the envelope. The model suggested that mode trapping by the hydrogen/helium transition "selects" the large amplitude modes, which would correspond to the five high-amplitude modes observed. The authors also noted that, because the evolution of horizontal branch stars is slow in the vicinity of the ZAHB but accelerates as the star exhausts its core helium, there should not be many objects like PG 1605+072 compared to the number of "normal" rapid oscillators. To date, this is consistent with observations: PG 1605+072 is the only known EC 14026 pulsator with a surface gravity below $\log g \sim 5.35$. Therefore, this star should evolve extremely rapidly, rendering it one of the best candidates to search for evolutionary changes over the next few decades.

PG 0014+067: The first success story of sdB asteroseismology

As described in the previous section, the ultimate goal when observing a pulsating star is to successfully fit the periods observed to those predicted by theory. PG 0014+067 is the first, and to date one of only four, EC 14026 stars for which this has been achieved.

Brassard et al. (2001) found PG 0014+067 to pulsate with 13 distinct oscillations in the period range 80−170 s, some of them showing the lowest intrinsic amplitudes detected so far. Of the 13 frequencies found, 3 are in fact doublets, which, if interpreted as being due to rotational splitting, imply a relatively slow rotation period of $\sim$ 29 hours. The Fourier spectrum also featured five high-frequency peaks thought to be the harmonics of the basic

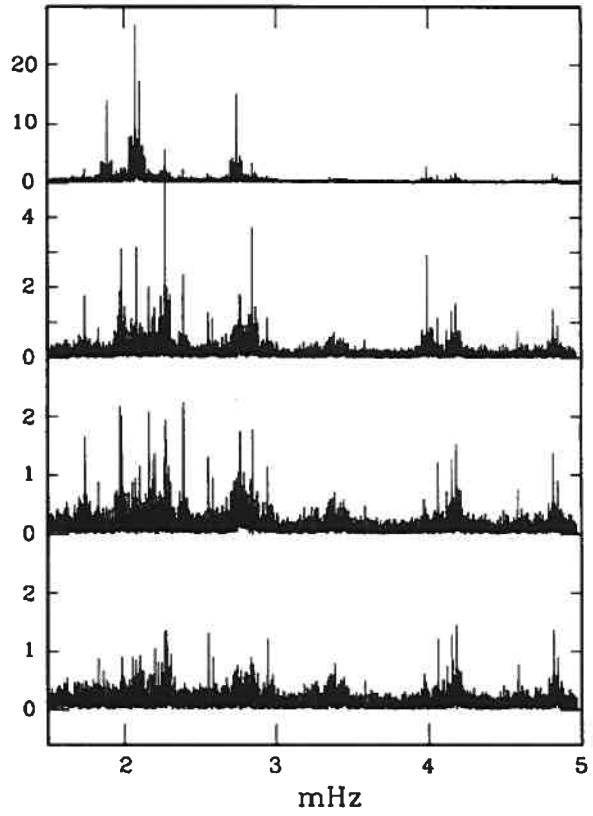

FIGURE 1.16 – Periodograms for the multi-site campaign conducted by Kilkenny et al. (1999). The top panel is the Fourier spectrum for the campaign data, the second panel that for the data pre-whitened by the first 35 frequencies, and the bottom panel that for the data pre-whitened by all 55 frequencies found. Note the changes in the scale of the ordinate axes.

oscillations.

The number of frequencies uncovered seemed just right for an in-depth analysis, being enough to have something to work with but not too large as to make matters confusing (as was the case for PG 1605+072). Hence the authors attempted mode identification of the periods observed employing the χ^2 minimisation technique. They found that the optimal model selected by the code was able to account for the 13 observed periods remarkably well, as can be seen in Figure 1.17. In addition, the model predicted the existence of another 10 frequencies, which were successfully matched up with lower amplitude peaks in the observed spectrum, bringing the total number of oscillations up to 23. As predicted, all these periods correspond to low-order p-modes with adjacent values of k and $l = 0$, 1, 2 and 3, defining a band of unstable modes. Finally, the optimal model used values of $\log g$ and $T_{\rm eff}$ that are in line

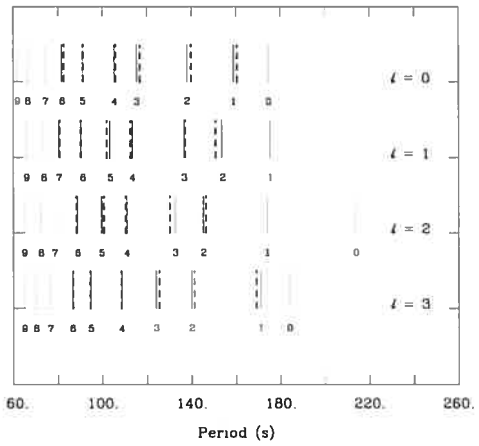

FIGURE 1.17 – Comparison of the observed period spectrum of PG 0014+067 (thick dashed lines) with the theoretical period spectrum of the optimal model. For the latter, the solid lines indicate excited modes, while the dotted ones correspond to stable modes. The values of the radial order index k are also illustrated. From Brassard et al. (2001).

with those derived for the star from spectroscopy, an important consistency check. Reassured by this, the authors found the mass of PG 0014+067 to be $M_* = 0.49 \pm 0.02\ M\odot$, and for the first time in subdwarf B history determined the fractional envelope mass to be $\log(M(H)/M) = -4.31 \pm 0.22$. A more recent study of PG 0014+067 (Charpinet et al. 2005c) based on a different set of data yielded very similar stellar parameters, thus confirming the validity of the original analysis. It is in principle possible to test the mode identification postulated from asteroseismology through the exploitation of multi-colour photometry, which can be used to constrain the degree index l (see chapter 3). This was attempted for PG 0014+067 (Jeffery et al. 2005), however the results were rather inconclusive due to the observational error and could neither convincingly verify nor refute the mode identification achieved.

PG 1336−018: A pulsating subdwarf B star in an eclipsing binary

PG 1336−018 is part of a very short-period ($\sim$ 0.1 days) detached binary system that is so far unique in exhibiting beautiful eclipses as well as the short-period oscillations characteristic of EC 14026 stars. Keeping in mind that a pulsation's surface geometry changes with its degree index l, it makes sense that analysing the lightcurve during primary eclipse (i.e. when the companion passes in front of the subdwarf) could help constrain mode identification.

From that point of view, PG 1336-018 presents a very interesting target for asteroseismology. Following its discovery and approximate frequency analysis (Kilkenny et al. 1998), the star was recently re-observed in an involved multi-site campaign (Kilkenny et al. 2003). This uncovered approximately 20 periodicities in the 90−180 s range, however it was not clear which of these were intrinsic oscillations and which were due to rotational splitting. Unfortunately, the amount of photometry gathered during primary eclipse was not sufficient to resolve any periodicities, never mind place any constraints on mode identification.

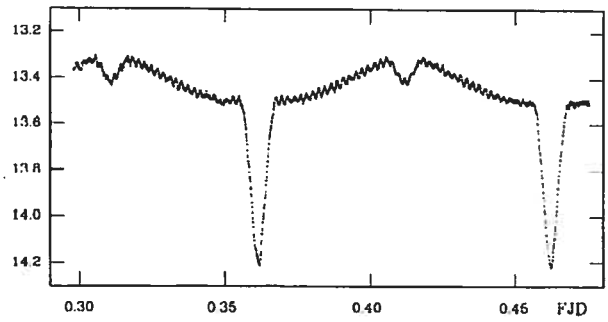

FIGURE 1.18 – The discovery lightcurve for the eclipsing EC 14026 star nature of PG 1336−018 plotted in V-magnitude as a function of fractional Julian Date. From Kilkenny et al. (1998).

Considering that the binary period of PG 1336-018 is among the shortest known for any detached system, it may be possible to detect a change in its orbit within the next few years. A very similar binary system, HW Vir, has already been shown to have a diminishing period (Kilkenny et al. 1994; the subdwarf component of that system however does not pulsate). The cause of the period decrease is not certain, but the most likely explanation is angular momentum loss due to magnetic breaking in a weak stellar wind. While the authors were not at all sure what could cause such an unusually close binary system, it seemed clear that the two stars must have undergone a common-envelope phase. However, more examples of binaries such as PG 1336-018 and HW Vir are needed for a conclusive analysis.

KPD 1930+2752: P-Mode Pulsations Superposed on Ellipsoidal Luminosity Variations

The fast pulsator KPD 1930+2752 (Billères et al. 2000), at $T_{\rm eff} \sim 33{,}800$ K and $\log g \sim 5.61$, is a completely normal EC 14026 star in terms of atmospheric parameters. Its light curve however, reveals something special, as it is completely dominated by a nearly sinusoidal

variation with a period of $\sim$ 4109 s (see Figure 1.19).

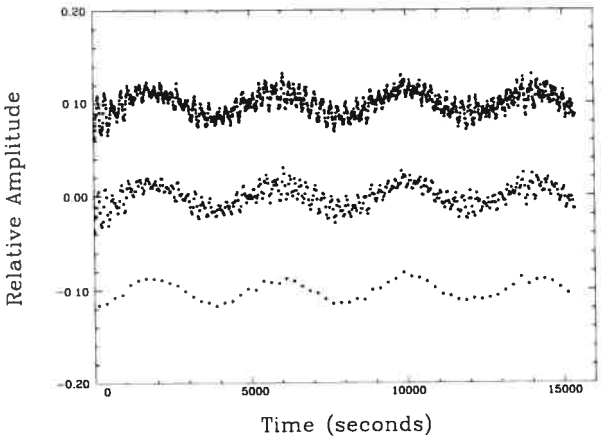

FIGURE 1.19 – Lightcurve of KPD 1930+2752, expressed in terms of residual amplitude relative to the mean brightness of the star. The upper curve is the original lightcurve, with each plotted point representing a sampling time of 10 s. The middle curve is a binned version of the top one with a sampling time of 30 s and the points of the lower curve correspond to a sampling time of 250 s. From Billères et al. (2000).

In addition, KPD 1930+2752 shows at least 44 harmonic oscillations in the range 145−332 s at low to medium amplitudes. This is one of the richest period spectra uncovered for an EC 14026 star, comparable to that of PG 1605+072. However, unlike in the case of the latter, the large number of oscillations cannot be explained by low surface gravity. Modelling reveals that the period range 145−332 s harbours only 20 theoretical pulsation modes, as opposed to 44+ observed periodicities. This probably implies that KPD 1930+2752 is not perfectly spherically symmetric (as assumed in most models), which lifts the $2l$+1 period degeneracy associated with each pulsation mode in a spherical model and renders more than enough theoretical modes to account for those observed. Considering the long-period variations found in the light curve, the most natural explanation for this would be an ellipsoidal deformation of the sdB star in a close but detached binary system containing a faint, invisible companion such as a white dwarf. Indeed, it is possible to explain the dense observed period spectrum in terms of a p-mode spectrum rotationally split in a star spinning on its axis with a period of $\sim$ 8218 s, the period expected from the ellipsoidal pattern in the light curve. This hypothesis was only recently confirmed by a high time-resolution radial velocity study (Woolf et al. 2002)

determining an orbital period in line with the ellipsoidal brightness variation.

HS 0702+6043 and Balloon 090100001: EC 14026 / Betsy star hybrids

As mentioned earlier, we know of two subdwarfs that exhibit both the short-period pulsations typical of the EC 14026 oscillators and the long-period variations found in the Betsy stars. As these objects lie in between the two regimes on the H-R diagram, it seems not only plausible but natural that they constitute hybrids of the p and g-mode oscillators. This could prove invaluable for evolutionary theory in the future, since the two types of modes probe the envelope and inner layers of the star respectively.

The first simultaneous p- and g-mode sdB pulsator to be discovered was HS 0702+6043. It had initially been labelled a simple EC 14026 pulsator with a relatively high-amplitude (29 mmag) periodicity at 363 s and a weaker (A = 3.8 mmag) peak at 382 s (Dreizler et al. 2002). Long-period variability on a time-scale of one hour (P = 3690 s) was hinted at when subsequently testing a new set of time-series analysis tools, and later confirmed by follow-up observations (Schuh et al. 2005; see also Schuh et al. 2005b). While at first it was not clear whether the long-period luminosity variation could be explained by a harmonic of the rapid oscillations, this was later excluded by higher resolution observations (Schuh et al. 2006). An intrinsic gravity-mode pulsation as those uncovered in many of the only slightly cooler sdBs remained the most logical explanation.

The credibility of the EC 14026 / Betsy star hybrid hypothesis was greatly boosted by the discovery of another such object. Similarly to the case of HS 0702+6043, Balloon 090100001 was initially labelled an EC 14026 star with a very strong (A = 59 mmag) dominant peak at $\sim$ 356 s and at least one other independent periodicity (Oreiro et al. 2004). It was subsequently re-visited and observed to a higher frequency resolution by Baran et al. (2005), who uncovered 13 short-period ($P \sim 200-360$ s) as well as 9 long-period ($P \sim 2700-5000$ s) pulsations. However, a quantitative interpretation of the frequency spectrum was complicated by the presence of innumerable harmonics of the highest amplitude peaks and rotational splitting. Observational multi-site efforts are currently underway to shed more light on this EC 14026 / Betsy star hybrid.

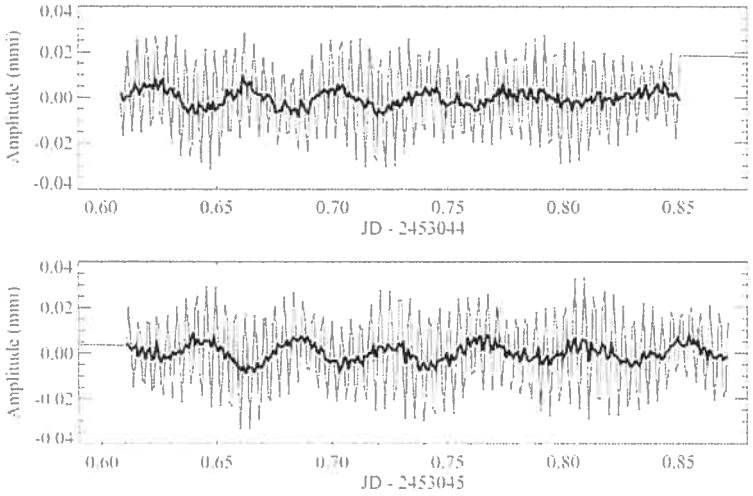

FIGURE 1.20 – Lightcurve of HS 0702+6043. Shown are the original data points (joined by lines) and the residuals after pre-whitening of the short-period oscillations (thick line). The latter are characteristic of the brightness variations observed in Betsy stars. From Schuh et al. 2005b.

1.3.3 Observations of Betsy Stars

Since the serendipitous discovery of the Betsy star prototype, PG 1716+426 (Green et al. 2003), the total number of known long-period variables has risen to 31 (Green et al. in preparation; Kilkenny 2005; see also Fontaine et al. 2005). However, unlike in the case of the fast pulsators, where period determination is generally possible after only a few nights of high quality observations, the slow oscillators require hundreds of hours of monitoring before any quantitative statements are possible. This implies that is not feasible to follow up on one of these objects immediately after variability has been established, as this requires thorough planning, the allocation of vast amounts of observing time and usually setting up a multi-site collaboration. Consequently, the photometry data for the majority of Betsy stars is limited to the discovery lightcurve and perhaps a few nights of follow-up observations confirming variability.

At the time of starting my PhD, the only long-period variable subdwarf B star that had been monitored in any detail was the class prototype, PG 1716+426 (Green et al. 2003b; Reed et al. 2004). This object happened to be in a post-common envelope binary with an orbital period of $\sim$ 1.8 days, which is why it was included in a pilot program to monitor the

light curves of 15 binary systems. During this study, variability was detected and confirmed in a later multi-site campaign yielding 81 hours of photometric monitoring. A preliminary analysis of the data indicated the presence of at least 3−5 pulsation modes in the 0.8−1.4 hour range. Unfortunately, the number of pulsational cycles accumulated was not sufficient for detailed analysis, and no definite quantitative statements were possible, raising the need for more in-depth investigations of selected Betsy stars. This constituted a large part of my PhD project, as will be discussed in the following section.

1.4 MY PHD PROJECT

The thesis presented here is made up of 5 articles that can be divided into three categories: the observation and analysis of an EC 14026 star (Chapter 2), the development of a method to constrain the identification of observed periodicities for both short- and long-period variable subdwarf B stars (Chapter 3), and the observation and analysis of three Betsy stars (Chapters 4−6). The first of these projects is based on time-series photometry gathered at the South African Astronomical Observatory prior to starting my PhD, however the vast majority of the analysis and modeling was achieved during my time in Montréal and would in fact not have been possible without the models developed here. As it was, we were able to constrain the mass and hydrogen shell thickness of the fast pulsator EC 20117-4014 quite reliably, although some uncertainties remain due to the fact that its period spectrum exhibits only 3 independent modes.

The second paper included in my thesis constitutes a largely theoretical study on the potential of multi-colour photometry for mode identification in subdwarf B stars. Since the wavelength dependence of an oscillation's amplitude as observed across the integrated disk of the star is a strong function of its degree index l, the latter can theoretically be determined from the ratio of amplitudes as measured in different band passes. In the case of the EC 14026 stars, the resulting partial mode identification could provide a much needed consistency check for asteroseismology. As for the Betsy stars, the exploitation of multi-colour photometry may well hold the key to unambiguously matching observational frequencies to those predicted. Taking into account all low-degree modes, the theoretical period spectrum is much denser

than that extracted from photometry in the slow pulsators monitored to date. Therefore, it is impossible to find a meaningful optimal model if no a priori assumptions are made regarding the degree indices of the oscillations. We developed the necessary theoretical tools to achieve just that, and current efforts to observationally exploit the knowledge gained are ongoing.

The remainder of my thesis is devoted to the detailed observation and analysis of three representative Betsy stars: PG 1627+017, PG 1338+481 and PG 0101+039. The former two were observed during dedicated long-term multi-site campaigns while the latter was monitored by the Canadian space telescope *MOST*. As part of a short-period binary system and one of the coolest subdwarf B stars known, PG 1627+017 exhibited a rather complicated period spectrum that was difficult to interpret. Consequently, we chose PG 1338+481, a cooler single star as our second target. Following the development of the colour-amplitude theory outlined above, we deemed it would be worthwhile to conduct the observations in two wavebands simultaneously. This provided, together with other factors, some constraint on the degree index of the oscillations detected, leading to a more fruitful asteroseismological interpretation than was possible for the previous target. Nevertheless, one of the main conclusions reached from the quality of the data was that the extraction of periodicities would be much facilitated by space-based observations. Due to fortunate circumstances, I was able to persuade Jaymie Matthews, the mission scientist of the *MOST* satellite, to select the long-period variable subdwarf PG 0101+039 as a target during the instrument's commissioning phase. While it was not clear from the outset that the 0.15-m telescope would be able to achieve the required sensitivity for the comparatively faint subdwarf, the observations proved a success and will hopefully pave the way for future space-based campaigns on Betsy stars.

Chapter 2

FURTHER OBSERVATIONS AND ANALYSIS OF THE RAPIDLY PULSATING SUBDWARF B STAR EC 20117−4014

S.K. Randall[1] , G. Fontaine[1], S. Charpinet[2] , A.E. Lynas-Gray[3] , I.P. Lopes[3], S.J. O'Toole[4], and P. Brassard[1]

To be submitted to *The Astrophysical Journal*

[1]Département de Physique, Université de Montréal, C.P. 6128, Succ. Centre-Ville, Montréal, Québec, H3C 3J7, Canada; [redacted]

[2]UMR 5572, Université Paul Sabatier et CNRS, Observatoire Midi-Pyrénées, 14 Av. Edouard Belin, 31400 Toulouse, France; [redacted]

[3]University of Oxford, Astrophysics, Keble Road, Oxford, OX1 3RH, England; [redacted]

[4]Dr. Remeis Sternwarte, Astronomisches Institut der Universität Erlangen-Nürnberg, Sternwartstr. 7, 96049 Bamberg, Germany; [redacted]

2.1 ABSTRACT

We present the results of further observations and the subsequent analysis of the rapidly pulsating subdwarf B star EC 20117−4014. Due to bad weather during much of our observing runs, the only pulsations detected were those already reported by O'Donoghue et al. (1997) at 137.3, 142.1 and 157.4 s. All three oscillations exhibit a systematic frequency change over a time-scale of a few months, most likely due to binary motion with a period in the $\sim$ 20−350 day range. Attempts at asteroseismology using the well-known forward approach are complicated by the low number of observed periods available, requiring the effective temperature to be held fixed at the spectroscopic value during the exploration of model parameter space. Under this approximation we are able to isolate just two potential families of optimal models, one of which is to be preferred on the basis of the period fit achieved and the surface gravity inferred. The corresponding optimal model has $T_{\rm eff}$ = 34,800 $\pm$ 1000 K (the spectroscopic value), $\log g$ = 5.859 $\pm$ 0.006, M_* = 0.54 $\pm$ 0.02 $M_\odot$, and $\log\,(M_{env}/M_\odot)$ = −4.15 $\pm$ 0.05. While the stellar mass determined is significantly higher than the canonical value predicted from evolutionary scenarios, it may be lowered substantially if the effective temperature adopted is found to be too high. The uncertainties asssumed for the spectroscopic parameters are typical of the realistic errors estimated for other EC 14026 stars, however the values obtained for EC 20117−4014 are expected to be relatively poorly constrained due to the contamination of the spectra by the main sequence companion. Consequently, the structural parameters inferred for this target from asteroseismology are less accurate than has been the case for previous studies of EC 14026 stars.

2.2 INTRODUCTION

Rapidly pulsating subdwarf B (sdB) stars form a relatively new class of variable star that exhibits low-amplitude, multi-periodic luminosity variations with a typical period range of 100−200 s. They make up only a small fraction (5−10 %) of the known subdwarf B stars, which are low-mass ($\sim$ 0.5 $M_\odot$) extended horizontal branch (EHB) objects characterised by a helium-burning core surrounded by a thin hydrogen-rich envelope. Evolutionary models

predict that this envelope is too thin to sustain hydrogen-shell burning during helium core burning on the zero-age EHB (ZAEHB), which means that instead of ascending the asymptotic giant branch (AGB) these objects evolve off the EHB, turn left on the HR diagram, and join the white dwarf cooling track near $T_{\rm eff} \sim 80{,}000$ K, ultimately becoming low-gravity DAO white dwarfs (Bergeron et al. 1994). The core helium burning phase is identified with subdwarf B stars and lasts around 10^8 years. Although the basic course of these stars' evolution is well understood, the question that remains is what caused their hydrogen envelopes to become so thin. It is obvious that sdBs must have lost a large fraction of their envelope mass at the time of the helium flash, but the details of this mass loss are unclear. Theories involving strong stellar winds and various binary evolution scenarios have been brought forward, but still await observational confirmation (e.g., D'Cruz et al. 1996; Sweigart 1997; Han et al. 2002; Han et al. 2003). It is hoped that this can be achieved on the basis of asteroseismology, the quantitative interpretation of the period spectra uncovered in variable stars.

The idea of pulsating subdwarf B stars was first brought forth by Charpinet et al. (1996), who calculated that radial and non-radial pulsations could be excited by an opacity mechanism associated with the presence of iron in the stars' envelopes. At roughly the same time, an independent group of astronomers at the South African Astronomical Observatory (SAAO) discovered the first real sdB pulsator (Kilkenny et al. 1997) and three others followed shortly (Koen et al. 1997; Stobie et al. 1997; O'Donoghue et al. 1997). Since then, the number of so-called EC 14026 stars (named after the prototype, EC 14026−2647) has risen to 34 thanks to the efforts of the South African astronomers (e.g., Kilkenny 2002), a Norwegian-German-Italian team (e.g., Silvotti et al. 2002), and a survey carried out by the Montréal group (e.g., Billères et al. 2002), among others. All of the EC 14026 stars discovered to date fall into the well-defined instability strip predicted by theory, most of them clustering around $\log g \sim 5.7$ and $T_{\rm eff} \sim 33{,}000$ K (see Fontaine et al. 2005 for a recent review). Subdwarf B stars in this region of the H-R diagram attain a balance between gravitational settling and radiative levitation that creates a local overabundance of iron in the driving region of the κ-mechanism, which results in short-period, pressure-mode (p-mode) pulsations. However, not all the stars in the instability strip pulsate. Although the reason for this is not entirely clear, it has been

suggested that the presence of stellar winds could have caused a varying degree of mass-loss in different stars (Fontaine & Chayer 1997, see also Chayer et al. 2004). Hence, those objects subject to a stronger stellar wind may have lost too much of their iron reservoir to sustain the opacity bump crucial to the driving mechanism. Likewise, it is possible that the constant sdB stars are simply older and have lost their envelope iron over time (Fontaine et al. 2005).

The rapid pulsators must be distinguished from the more recently discovered long-period variable subdwarf B stars (Green et al. 2003), which oscillate on timescales of the order of one hour. These significantly longer periods automatically imply high radial order gravity modes, believed to be excited by the same mechanism that drives pressure modes in the fast pulsators (Fontaine et al. 2003). Distinctly cooler than the EC 14026 stars, the slow variables are also more common, accounting for $\gtrsim$ 75 % of the cool subdwarf B star population (Green et al. 2003b).

As the driving mechanism of the instabilities in EC 14026 stars appears to be well understood, stellar modelling can be used to predict the theoretical periods of unstable modes (see Charpinet et al. 2000). As pointed out by Charpinet et al. (2001), the EC 14026 stars tend to exhibit a fair number ($\gtrsim 7-8$) of pulsations when observed at higher sensitivity than that characteristic of discovery runs. The latter have typically led to the uncovering of 2−4 pulsation modes, generally deemed too few to lead to useful asteroseismological constraints (but see below). Observations with higher sensitivity open up the exciting possibility of employing asteroseismological analyses to derive basic stellar parameters such as effective temperature, surface gravity, stellar mass and, most interestingly, the mass fraction of the hydrogen envelope. Asteroseismological analyses have in fact been completed successfully for four short-period variable subdwarf B stars: PG 0014+067 (Brassard et al. 2001), PG 1047+003 (Charpinet et al. 2003), PG 1219+534 (Charpinet et al. 2005a), and Feige 48 (Charpinet et al. 2005b). In each of these cases, the observed periodicities could be reproduced accurately by just one or two families of models, which were then further constrained on the basis of spectroscopic estimates of the atmospheric parameters. The resulting determination of the total and envelope masses for the four targets is beginning to indicate tendencies that may have a bearing on evolutionary scenarios (see Charpinet et al. 2005), however it is clear that more EC 14026

stars need to be analysed for these to become statistically significant.

In this paper, we present further observations and a quantitative analysis of the period spectrum of the fast pulsator EC 20117−4014 (O'Donoghue et al. 1997, hereafter DOD97). We review the work already done on this star before presenting an account of our observations and the oscillations extracted from the lightcurves. We then use these for an exploration into the binary nature of the target. Finally, we describe the results of our asteroseismological analysis and discuss their implications for evolutionary theory.

2.3 EC 20117−4014

EC 20117−4014 was first identified as a bright ultraviolet-rich star in the Edinburgh-Cape (EC) Blue Object Survey (e.g., Stobie et al. 1992) at a position of $\alpha(1950.0) = 20^h11^m43.8^s$ and $\delta(1950.0) = -40°14'55"$ with a magnitude of $V = 12.47\pm0.01$ (Kilkenny et al. 1997b). Spectra taken at SAAO indicated a binary system consisting of a subdwarf B primary and a F or G main sequence companion (see DOD97 for details).

In 1997, it was reported that rapid multi-periodic pulsations had been detected in EC 20117−4014, thus making it the 4th member of the then brand new class of EC 14026 stars. In the discovery paper (DOD97) three pulsation periods were identified from nine nights of high-speed photometry gathered over a period of eleven months (34.4 h of observations altogether): one prominent main oscillation frequency at $f_1 = 7.285$ mHZ (137.3 s) with an amplitude of 3.5 mmag, as well as two lower-amplitude ($\sim$ 1 mmag) pulsations at $f_2 = 7.043$ mHz (142.0 s) and $f_3 = 6.350$ mHz (157.5 s). While the amplitude of the main pulsation frequency remained approximately constant, those of the two secondary periods showed some night-to-night variation. The authors also uncovered a real change in the main oscillation period at 137.3 s on a timescale of three months, an effect potentially attributable to the star's motion around the binary system's centre of gravity. Finally, there was tentative evidence for a fourth pulsation at 3.58 mHz (279 s).

DOD97 also obtained spectroscopic measurements of EC 20117−4014 and modelled the spectra as a combination of a subdwarf B primary and a late F main sequence companion. Depending on the assumptions made as to the exact nature of the latter, this yielded three

sets of estimates for the atmospheric parameters of EC 20117−4014. Those are: $\log g = 5.87 \pm 0.07$ and $T_{\rm eff} = 34{,}800 \pm 300$ K, $\log g = 5.82 \pm 0.17$ and $T_{\rm eff} = 34{,}400 \pm 700$ K, and $\log g = 6.19 \pm 0.17$ and $T_{\rm eff} = 36{,}000 \pm 800$ K. It is the first pair of atmospheric parameters that is thought to be the most reliable, since it was obtained on the basis of a far greater number of higher resolution spectra than the latter two (35 spectra with 1.1 Å resolution obtained over four consecutive nights compared to just two measurements at 3.5 Å). And indeed, the last set of spectroscopic values can be excluded from the outset on the basis of non-adiabatic pulsation calculations, which predict oscillations to be damped in targets more compact than $\log g \sim 6$. We thus consider EC 20117−4014's atmospheric parameters to correspond most closely to those given by the first pair of estimates, although it should be kept in mind that as formal errors the uncertainties are most likely severely underestimated. For the purpose of the asteroseismological analysis attempted below, we therefore adopt slightly less tightly constrained values of $T_{\rm eff} = 34{,}800 \pm 1000$ K and $\log g = 5.87 \pm 0.10$. The errors listed are typical of the uncertainties considered realistic for EC 14026 stars on the basis of model atmosphere fits to the high S/N MMT spectra obtained as part of a long-term radial velocities/atmospheric parameters survey (see Green, Fontaine, & Chayer, in preparation). However, given the fact that the spectra for EC 20117−4014 are contaminated by the flux contribution of its main sequence companion, the errors on the atmospheric values computed are in all likelihood significantly larger than those adopted. While this will need to be investigated in more detail in future spectroscopic studies, we would like to emphasise that the uncertainties assumed constitute lower limits with respect to the constraints we can realistically hope to place on the atmospheric parameters of EC 20117−4014.

2.4 OBSERVATIONS

The results presented in this paper are based on high-speed photometry data obtained with the 0.75-m telescope at SAAO in 2001 and 2002. The observing time allocated consisted of two weeks in early July 2001 and another two weeks of follow-up time in mid July 2002. As our observations were planned entirely around EC 20117−4014, we were able to schedule them according to its best position in the sky, which meant that, theoretically, we could track

the star for nearly 12 hours on a clear night. Unfortunately, our original hope of gathering data sets with a markedly improved sensitivity over the original 1997 observations was stifled by poor weather conditions. Indeed, due to highly variable weather during both of the runs, we were able to obtain useful data sets on only five nights in 2001 and on four nights in 2002. Due to passing cirrus clouds and technical problems some of these data sets show gaps lasting from a couple of minutes to nearly one hour.

The data gathered at SAAO are supplemented by independent observations carried out on the 1.54-m Danish telescope at La Silla, Chile during six nights in June 2002. Consisting of three shorter runs obtained towards the end of each night, the number of pulsational cycles accumulated is clearly smaller than in the case of the SAAO data, however the resulting loss of sensitivity is greatly compensated for by the size of the telescope as well as excellent weather conditions.

A log of the observing runs can be found in Table 2.1. In 2001, we gathered 36.0 h of useful high-speed photometric data over five nights. This corresponds to a duty cycle of 17.9% and to a temporal resolution of 1.38 μHz. The following year at SAAO, we obtained 27.4 h of data over four nights, corresponding to a duty cycle of 13.6% and to the same resolution of 1.38 μHz. At La Silla, we secured 9.9 hours of photometry, achieving a duty cycle of 8.1% and a temporal resolution of 2.27 μHz.

The SAAO photometry of EC 20117−4014 was obtained with the University of Cape Town (UCT) high speed photometer, a Wright Instruments Peltier-cooled camera with a 576 × 420 thinned, back-illuminated EEV CCD. One of the features of the UCT CCD is that it can be set to run on frame transfer mode, which means that only one half of the chip is exposed while the other is kept permanently masked off for readout. This implies that there is in effect no readout time, a factor critical to monitoring short-period pulsations. The sampling time at SAAO was hence equal to the exposure time of 10 s throughout all our runs, while at La Silla the use of a standard 2k × 4k CCD resulted in an effective sampling time of approximately 23 s compared to an exposure time of 5 s.

In order to account for atmospheric variations, differential photometry was performed at both sites using the only comparison star on the CCD chip, GSC 07952−01358 (Lasker et al.

1990), a star of roughly the same magnitude as EC 20117−4014. Observations taken on the 0.5-m telescope during the 2001 run at SAAO gave the following magnitude and colours: $V = 12.12$, $B-V = 0.88$, $U-B = 0.46$, $V-R = 0.48$, $V-I = 0.98$. Comparing these colours with the calibration of MK spectral types in *Allen's Astrophysical Quantities* leads us to believe that GSC 07952−01358 is a main sequence K-type star. In order to be able to use this red star as a comparison star for the very blue subdwarf, all observations were obtained with a B filter of the Johnson and Bessel variety at SAAO and La Silla respectively. The two filters were deemed to lie close enough in wavelength so as not to leave their mark on the amplitudes of pulsation.

The SAAO photometry was reduced using DuPhot, a version of the point-spread function fitting program DoPhot (Schechter et al. 1993) modified for use on the SAAO 0.75-m telescope by Darragh O'Donoghue. DoPhot is designed to search bias subtracted and flat-fielded digital sky images for any objects above an imposed noise threshold, fit them to a Gaussian and thus yield their relative magnitudes. The data obtained at La Silla were treated using standard IRAF bias subtraction, flat-fielding and aperture photometry routines. All flat fields were exposed on the twilight sky. Following the initial reduction, the data were fed into OSCAR, a special data reduction program developed by one of us (P.B.) and described in detail by Billères et al (2002). Employing OSCAR allowed us to eliminate low-frequency variations caused by atmospheric effects and differential extinction by subtracting low order spline functions from the nightly data sets.

However, despite careful data reduction, the variable weather encountered at SAAO left its mark on the quality of the light curves. Detecting rapid luminosity variations of the order of 1 mmag in a $\sim$ 12.5 magnitude star was always going to be a challenge on a 0.75-m telescope, but observing them through passing cirrus was nearly impossible. Figure 2.1 shows one of the best segments of the light curve of EC 20117−4014 that we obtained in South Africa. Although the main oscillation of $\sim$137 s can be seen easily in the figure, it is not as clear as in the lowest panel of Figure 2 of DOD97, for example. While the light curves from La Silla are of higher quality, this is outweighed by their low duty cycle and temporal resolution. Hence, our data sets are subject to significant levels of noise.

2.5 ANALYSIS OF THE LIGHT CURVES

The time-series photometry gathered for EC 20117−4014 was analysed in a standard fashion using a combination of Fourier analysis, least-squares fits to the light curve and pre-whitening techniques. Since this method has been used for the period determination in numerous EC 14026 stars, we refer the interested reader to a previous paper (Billères et al. 2000) containing a detailed description of the procedure followed.

Fourier Transforms (FTs) were calculated for each of the runs listed in Table 2.1, as well as for the combination of all the nightly light curves obtained in 2001 (SAAO), June 2002 (La Silla) and July 2002 (SAAO) respectively. Attempts to combine runs from different seasons and subsequently compute a "grand" FT were unfruitful and hence abandoned. Figure 2.2 shows one of the best Fourier spectra resulting from a single night's data in the 0−15 mHz band pass. The part of the spectrum extending beyond 15 mHz and up to the Nyquist limit of 50 mHz is consistent with noise, and thus not illustrated here. We can easily identify the three pulsation periods discovered by DOD97. Together with a few spurious low-frequency (< 1 mHz) peaks arising from atmospheric variations, they correspond to the only oscillations with amplitudes above the detection threshold, indicated by the horizontal dotted line. The detection threshold was set to three times the mean noise level, a practice which has proven reliable both empirically and statistically. Note that in all SAAO periodograms shown the effects of the 119.7-s drive error inherent to the 0.75-m telescope have been removed using pre-whitening techniques.

The combined spectra for the 2001 and 2002 runs at SAAO are depicted in the two lower panels of Figure 2.3. While the 2002 data in particular are rather noisy, we can nevertheless recover the three basic periods mentioned above in both Fourier transforms. Moreover, the fact that the two sets of data have exactly the same temporal resolution can be exploited to derive a meaningful average spectrum, which is shown in the top panel of Figure 2.3. The basic idea behind this procedure is that periodicities present in both data sets will stand out more strongly in the mean Fourier transform, while any spurious peaks as well as the noise level should diminish. Indeed, in the resulting periodogram the three previously identified periods stand out more clearly above the noise, leaving no doubt as to their tangibility.

We show the period spectrum computed from the complete lightcurve obtained at La Silla in Figure 2.4. Since the frequency resolution for this run is poorer than for the two sets of SAAO data, it would be imprudent to add the data to the average spectrum calculated earlier. We thus exploit it completely independently, with the aim of later comparing the periodicities extracted to those found at SAAO. Looking at the spectrum, we find that just two of the three known periods lie above the detection threshold, namely those at $\sim$ 137.3 s and at $\sim$ 142.1 s. It is only by probing below the detection limit that we can also recover the third previously identified period at $\sim$ 157.4 s. There seems to be no clear evidence for any further oscillations in the light curve.

In order to correctly identify all oscillations present in the light curves, each of the Fourier spectra shown were subjected to pre-whitening, a method where any frequencies present in the transform are identified and then subtracted from the lightcurve one by one. The results of this exercise are illustrated in Figure 2.5 for the SAAO 2001 run. The upper Fourier transform is that of the original lightcurve and corresponds to the spectrum shown in the middle panel of Figure 2.3, zoomed in on the region of interest from 6.15-7.50 mHz. Plotted upside down is the model spectrum, constructed on the basis of the three basic periods rising above the threshold in the original transform. The bottom curve illustrates the residual amplitude based on a point-by-point subtraction of the first two spectra in the Fourier domain. Although the latter is relatively flat and no significant peaks remain, the noise level and low-level fluctuations are too significant for us to exclude the possibility of EC 20117−4014 harbouring more low-level peaks. Judging by the fair number ($\gtrsim$ 7−8) of oscillations discovered in other EC 14026 stars when working at higher sensitivity, it seems unlikely that we extracted all the periodicities present. However, the elevated noise level of our spectra prevents us from probing any deeper, leaving only three definite oscillations, the characteristics of which are summarised in Table 2.2 for all three seasons. We list the frequencies and periods extracted from each of the combined Fourier transforms together with their amplitudes and phases. Note that while the amplitudes and phases are derived from least-squares fits to the light curve and are hence associated with formal errors, the frequencies are not. This is due to the fact that they are extracted directly from the period spectrum, without any form of fitting procedure taking

place. We can, however, estimate the probable accuracy of the frequencies to be of the order of 1/10 of the formal resolution (Billères et al. 2000), and it is these values that are given in the table. In the case of the data from La Silla, the periodicity at 157.4 s was identified only after conducting a targeted search below the detection threshold. The characteristics of this oscillation are thus given in brackets and are ignored in all further analyses.

Comparing the frequencies lifted from the light curves obtained in different seasons reveals a systematic variation for all three harmonic oscillations on a scale larger than the estimated measurement errors. Initially considering only the higher resolution SAAO data, we find that for each of the periodicities the frequency measured in 2002 is an average of 0.6±0.1 μHz higher than that identified in 2001. The two frequencies detected at La Silla, though subject to a larger uncertainty, lie in between the corresponding SAAO 2001 and 2002 values. Supplementary evidence for variability in the prominent frequency was produced in an (O-C) analysis, where we compared the times of maxima of the oscillation during one season to those expected from the best linear ephemeris derived from another season. In all cases, we encountered discrepancies of the same order of magnitude as the period itself, implying a significant frequency change over time. This finding is in accordance with previous results (DOD97), which reported a frequency change of 1.7±0.5 μHz in the prominent oscillation over a period of three months.

In summary, we detected three harmonic oscillations in the lightcurve of EC 20117−4014, the frequencies of which seem to vary systematically beyond the estimated measurement errors from one season to the next. It is somewhat disappointing that the oscillations extracted from our three independent sets of data are the same as those already found by DOD97. Moreover, we find no indication of their tentatively identified peak at $\sim$ 279 s. This may not be surprising from a strictly theoretical point of view, since modelling predicts that EC 20117−4014, as a rapid pulsator with relatively high values of $\log g \sim 5.8-5.9$, should excite modes in the $\sim$ 60−160 s period range only (Charpinet et al. 2001). Unfortunately, it also means that the asteroseismological analysis we attempt below is based on only three oscillations, rendering the exercise rather challenging.

2.6 EVIDENCE FOR BINARY MOTION FROM FREQUENCY VARIATION

We believe that the frequency shifts detected in the previous section are a result of EC 20117−4014's binary motion. This conclusion rests on two observations: Firstly, the frequency variations detected are systematic for all three harmonic oscillations found, implying a global stellar origin rather than localised stochastic effects. Secondly, if we take into account the frequencies of the main oscillation measured by DOD97 at 7.28668±0.00014 mHz in May 1995 and at 7.28668±0.00002 mHz in August 1995 and compare these to the corresponding values in Table 2.2, we find that the frequency variation is not monotonic with time, but instead has exhibited non-linear changes since the initial measurement. It is thus unlikely to be due to evolutionary processes, since in acoustic modes these would produce either a monotonic and regular increase of the periods in the first phase of the subdwarf's evolution off the ZAEHB, or an important and systematic decrease in the second phase until the onset of helium shell burning (Charpinet et al. 2002). The former phase lasts around 90 Myr and is identified with a period in an sdB's life where the surface gravity decreases as the star slowly moves away from the ZAEHB. Following this, the star begins to contract in order to compensate for the rarefaction of thermonuclear fuel (helium) at the centre, incurring an increase in both $\log g$ and $T_{\rm eff}$ until the onset of helium shell burning approximately 20 Myr later. As the frequencies of p-modes depend sensitively on the model's surface gravity, we would expect to observe the two stages of systematic period change outlined above given a long enough timeline. However, in consideration of the non-linear behaviour of the frequency variation measured as well as its very short time scale, we can definitely exclude evolutionary changes as a possible culprit.

Instead, we favour an explanation in terms of the subdwarf's binary motion. The basic idea behind this is that the light travel time from the star to Earth varies as the oscillator orbits the barycentre of the binary system. When the sdB is moving away from the observer, the brightness maxima of a given oscillation will be spaced further apart in time than when it is stationary, giving rise to slightly longer oscillation periods. The reverse will be the case

when the star moves towards Earth. Assuming a circular orbit, the frequency variation of any one pulsational mode with time should describe a perfect sine wave with a period equal to that of the binary system. According to DOD97, the semi-amplitude of the orbital radial velocity curve is given by

$$K = 210 \frac{q'}{(1+q')} \left(\frac{M}{P_{orb}} \right)^{1/3} \sin i \qquad \text{km/s}, \tag{2.1}$$

where q' is the mass ratio M_l/M_{sdB} (where l refers to EC 20117−4014's late-type main sequence companion), M is the total mass of the binary system, P_{orb} is the orbital period in days, and i is the inclination angle. Adopting representative values of $M_{sdB} = 0.5\ M_\odot$ and $M_l = 1\ M_\odot$ and dividing by the speed of light to convert radial velocity into Doppler shift, $\Delta f/f$, yields the relative amplitude of the frequency variation expected

$$A(\Delta f/f_0) = \frac{9.3398 \times 10^{-4}}{f_0} \left(\frac{1.5}{P_{orb}} \right)^{1/3} \sin i, \tag{2.2}$$

where f_0 is the mean (stationary) frequency of the oscillation in question. It is evident from the equation that the amplitude of the frequency variation predicted depends on both the orbital period and the system inclination; in particular, it systematically decreases with increasing period. Given that $\sin i \leq 1$, we can therefore use the maximum frequency variation observed to place an upper limit on the system's orbital period. Likewise, the inclination i can be constrained if the minimum possible orbital period is known.

In order to exploit this, we attempted to model the frequency variation observed for the dominant oscillation uncovered at ~ 7.286 mHz (137.3 s) on the basis of a sinusoid with an amplitude given by equation 2.2. We used the Levenberg-Marquardt algorithm for non-linear least-squares fitting (Press et al. 1986) to determine values of the four free parameters P_{orb}, i, f_0 and phase ϕ that provide a good match to the three frequency values determined from our data (see Table 2.2) as well as the two measured by DOD97. Note that for the latter, we increased the published errors to conform to the standards adopted for our own uncertainty estimates, i.e., that they be around 1/10th of the formal frequency resolution. The unknown parameters were assumed to lie in the ranges $0° \leq i \leq 90°$, $7.28 \leq f_0 \leq 7.29$ mHz, $0 \leq \phi \leq 2\pi$

and 8 days $\leq P_{orb} \leq$ 2000 days. While these cover all physically viable values in the case of the first three variables, the orbital period was constrained at the outset from evolutionary scenarios as well as the absence of rotational splitting in our data. Considering the 1.38 μHz frequency resolution achieved for both the 2001 and 2002 SAAO photometry, stellar rotation should have left a detectable imprint on the Fourier transform if it occurred on a timescale of less than $\sim$ 8.4 days. Since subdwarf B stars in short-period binary systems are expected to be tidally locked, the absence of a rotational signature automatically implies a relatively long orbital period. The upper limit set for P_{orb} is based on an evolutionary scenario in which the sdB loses a significant proportion of its envelope mass to a main sequence companion via stable Roche lobe overflow (Han et al. 2003). Being the formation channel which produces the widest binaries, this results in orbital periods of up to $\sim$ 2000 days.

Owing to the limited number of sparsely sampled data points, it was not possible to unambiguously fit the four input parameters discussed. Instead, we found a large number of acceptable matches to the observed frequency shifts, especially at relatively short orbital periods ($<$ 100 days). A small selection of these is illustrated in Figure 2.6 for visualisation purposes. We have also listed, in Table 2.3, a number of combinations of the orbital period and system inclination that (with optimised values of f_0 and ϕ) minimise the goodness-of-fit merit function χ^2. Both the shortest and longest orbital periods resulting in an acceptable fit to the data ($\sim$ 18 and $\sim$ 340 days respectively) are included. It is obvious from the values found that there is a strong correlation between P_{orb} and i, the latter in effect limiting the maximum binary period due to the amplitude of the frequency changes detected (see equation 2.2). Orbital periods longer than 340 days would require $\sin i > 1$ in order to account for the frequency shifts measured, and can therefore be excluded. Likewise, a system inclination of much less than 26° can be ruled out on the basis of a minimum period of 18 days. While the uncertainties on these values are difficult to quantify and depend on the accuracy of the errors on the oscillation frequencies observed, we can conclude that EC 20117−4014 forms part of a binary with a relatively long orbital period in the $\sim$ 20−350 day range and a system inclination of $\gtrsim$ 25°. The former constraint strongly points towards an sdB evolutionary channel involving stable Roche lobe overflow (already suggested by DOD97), however more measurements are

needed to infer the binary period with any precision.

2.7 ASTEROSEISMOLOGY

2.7.1 Initial Considerations

The ultimate aim of this study is a quantitative asteroseismological analysis of EC 20117−4014 using the "forward approach" pioneered by Brassard et al. (2001) for the rapid pulsator PG 0014+067. In their paper, the authors used 13 observed harmonic oscillations as a basis for finding an optimal model that was capable of reproducing the observed period spectrum surprisingly accurately, as well as predicting another 10 frequencies which were subsequently found in the period spectrum at amplitudes below the detection threshold. Remarkably, the average relative dispersion between the 23 observed periods and those of the corresponding theoretical modes was only 0.8 %. Very similar results were obtained for the next two pulsators to be submitted to asteroseismology, PG 1047+003 and PG 1219+534, where 19 and 9 observed periods were fit to predicted modes with an average dispersion of 0.75 % and 0.6 % respectively (Charpinet et al. 2003; Charpinet et al. 2005a). In contrast, the analysis of the most recent target, Feige 48 (Charpinet et al. 2005b), was carried out on the basis of only four observed oscillations. Since this corresponds to the number of parameters characterising a model (see below), it was reasoned that keeping all of these as free variables would lead to strong degeneracies in the fit. Therefore, the effective temperature was held fixed at the spectroscopic value throughout the model-finding procedure. This yielded two families of models that adequately reproduced the periods observed, one of which could be discriminated against on the basis of spectroscopy as well as the quality of the period match. Note that each of these families was strongly degenerate, i.e., a change in one of the input parameters was entirely compensated for by varying another in terms of the theoretical period spectrum. It was only by imposing the spectroscopic uncertainties on $\log g$ and $T_{\rm eff}$ that the remaining parameters (these being the total stellar mass and the thickness of the hydrogen envelope) could be constrained.

Our attempt at quantitatively interpreting the period spectrum uncovered for our target

EC 20117−4014 is similar to the analysis of Feige 48 in that we do not have a large number of observational frequencies available. In fact, the outlook is slightly bleaker than for the previous case, as in theory fitting only 3 experimental periodicities should induce strong degeneracies when attempting to find the same number of free parameters. In practice however, the stellar parameters specified are not completely independent of each other and a meaningful fit may nonetheless be achieved. Fortunately for our purposes, EC 20117−4014 is one of the rapid pulsators with the highest surface gravities at $\log g \sim 5.87$. In such cases, the density of theoretical modes in a given period window is relatively low. Moreover, according to radiative levitation theory, the high gravity causes the partial draining of the iron reservoir in the driving region, leaving a weakened opacity mechanism able to drive fewer modes with smaller amplitudes than in less compact EC 14026 pulsators (Fontaine et al. 1998). The number of modes excited (and the density of the period spectrum in general) is therefore relatively low, enabling the determination of a unique solution on the basis of fewer observational periods than was the case for previous asteroseismic targets.

2.7.2 Methodology

Our approach to asteroseismology consists of searching for theoretical models whose period spectra can closely reproduce the pulsation properties observed in EC 20117−4014. These are found in a double-optimisation procedure that simultaneously considers the period matching and model parameter space domains. The first optimisation determines the mode identification that yields the best global match between the periods observed and those calculated for a particular model, and quantifies the fit in terms of the merit function

$$\chi^2 = \sum_{i=1}^{N_0} \left(\frac{P^i_{obs} - P^i_{theo}}{\sigma^i} \right)^2 \tag{2.3}$$

where P^i_{obs} is the ith of N_0 observed periods, P^i_{theo} represents the theoretical value assigned to that period, and σ^i is an optional weight function that can be employed to counteract the tendency for denser theoretical period spectra to be assigned lower values of χ^2 (setting $\sigma^i = 1$ as in the present exercise gives equal weight to all models). Note that, at this point, the

period match quantified by χ^2 does not necessarily have to be good; the latter simply indicates the best fit that can be achieved to the observed periods on the basis of a given model. It is the goal of the second optimisation to determine which model (or models) in parameter space minimises the merit function and as such optimally reproduces the observed periods.

We currently possess two independent sets of numerical tools that are able to carry out the double optimisation procedure described. The first of these was developed in Montréal, and corresponds to an updated version of the code employed by Brassard et al. (2001) in their pioneering asteroseismological analysis of PG 0014+067. The second double optimisation package is operational in Toulouse and was used for the analysis of PG 1219+543 and Feige 48 (see Charpinet et al. 2005a, 2005b). Although the two double optimisation packages are numerically independent, they are based on the same theoretical period spectra and yield compatible fits to the observed periods (see, e.g., Charpinet et al. 2005c for a re-analysis of PG 0014+067 with the Toulouse algorithm). The computation of the period spectra to be matched to the observations involves three codes, starting with the equilibrium model building algorithm first written by Brassard and Fontaine (1994) for white dwarfs, and later adapted for sdB stars (see, e.g., Charpinet et al 1997, 2001). These so-called "second generation" stellar models require four input parameters: the effective temperature, $T_{\rm eff}$, the logarithm of the surface gravity, $\log g$, the total mass of the model, M_*, and the logarithmic depth of the transition between the hydrogen-rich envelope and the helium core $\log q(\mathrm{H}) = \log[M(\mathrm{H})/M_*]$. They constitute spherical static structures, where the central nucleus (comprising around 10 % of the star's mass) has been replaced with a "hard ball". Since the p-mode periods that we are interested in correspond to shallow envelope modes and are completely insensitive to the structure of the nucleus, this is a reasonable approximation to make. Another noteworthy characteristic of the models is that they feature non-uniform iron abundance profile as a function of depth. The latter is the result of the competing action between radiative levitation and gravitational settling and is characterised by a local enhancement of iron in the driving region. It is this so-called Z-bump that provides the necessary opacity for the κ-mechanism to operate, thus leading to the excitation of the oscillations observed. Hot subdwarf models must therefore include diffusion if any predictions are to be made as to the stability of modes.

Moreover, it was shown by Charpinet et al. (2005b) that the chemical composition of a model affects its eigenfrequencies at the quantitative level, rendering an accurate description of utmost importance when attempting asteroseismology.

In the second step of the period computation process, the equilibrium models are subjected to adiabatic pulsation calculations with the aid of an updated version of the finite-element code described by Brassard et al. (1992). Numerically solving the four adiabatic oscillation equations given, for example, by Unno et al. (1989), the program provides necessary estimates of the eigenmodes that are subsequently used as first guesses for the solutions of the six complex equations describing non-adiabatic non-radial oscillations. The latter are fully solved by an improved version of the non-adiabatic code briefly described by Fontaine et al. (1994). In addition to improved frequencies, the non-adiabatic code provides information on the stability of an eigenmode, which is of great importance for the comparison with observations. A typical output from the program is illustrated in Table 2.4. While it refers specifically to the optimal model (see below), we would like to simply illustrate the pulsational properties generated by the code at this point. For each mode identified in a selected period range, Table 2.4 lists the degree index l (the values of l considered are also specified by the user), the radial order k, the period P_{th} ($= 2\pi/\sigma_R$, where σ_R is the real part of the complex eigenfrequency), the stability coefficient σ_I (the imaginary part of the eigenfrequency), the logarithm of the kinetic energy of the mode $\log E$, and the dimensionless first-order rotation coefficient C_{kl}. As is standard, our equilibrium models are perfectly spherical and each mode specified by (k, l) is $2l + 1$ fold degenerate in eigenfrequency.

In the context of asteroseismology and mode identification, the most important parameters computed by the pulsation code are evidently the periods (or frequencies) of the modes determined. Since these are dependent on the four input parameters detailed earlier, their comparison with the oscillations observed can be used to infer the physical properties of the target. Further information is provided by the stability coefficient, the sign of which determines whether or not a given mode is expected to be excited. While a positive value of σ_I signifies that the mode is damped, a negative value implies instability, i.e., that the mode may reach observable amplitudes. Excited modes in EC 14026 stars are predicted to fall into

designated unstable period bands, which generally completely overlap with the oscillations detected. We therefore expect all the periods observed for EC 20117−4014 to fall within the theoretical instability range, and can use this as a cross-check for the viability of any optimal model identified. In comparison, the remaining pulsation parameters are of secondary importance for practical applications. The kinetic energy gives a measure of the energy required to excite a mode to a given amplitude at the surface and provides some indication as to where in the star it is primarily formed, while the rotation coefficient is useful for interpreting the fine frequency structure caused by the lifting of the $2l + 1$-fold degeneracy in a non-spherical star (generally a fast rotator). The latter is however of no immediate interest in the present case, since no rotational splitting was detected in the Fourier transform of the EC 20117−4014 light curves.

2.7.3 Finding the Optimal Model for EC 20117−4014

We searched the four-dimensional $T_{\rm eff} - \log g - M_* - \log q({\rm H})$ parameter space for the solution (or solutions) that could optimally re-produce the three oscillations observed for EC 20117−4014 using the Toulouse numerical package briefly mentioned above. As for the case of Feige 48 (see Charpinet et al. 2005b), the effective temperature was held fixed at the spectroscopic value of $T_{\rm eff} = 34{,}800$ K to prevent excessive degeneracies in the goodness-of-fit. The resulting dependence of the optimal model(s) on spectroscopy is unfortunate in that the temperature estimate at least cannot be used as an independent cross-check of its physical viability, however the periods of pressure modes are not particularly sensitive to $T_{\rm eff}$ and the latter is generally determined more accurately from spectroscopy than asteroseismology. During the model finding exercise it is thus preferable to fix the temperature rather than the surface gravity, which influences the period spectrum much more strongly. Once regions of minimum χ^2 have been identified, the impact of varying $T_{\rm eff}$ over the measurement uncertainty on the theoretical periods and other input parameters can be investigated, and errors on the asteroseismic properties adjusted accordingly.

The boundaries of the search domain for the remaining 3 free parameters were set as follows: $5.70 \leq \log g \leq 6.40$, $0.43 \leq M_*/M_\odot \leq 0.60$ and $-5.20 \leq \log q({\rm H}) \leq -2.10$. While

the range of the surface gravity was loosely based on the spectroscopic estimates of DOD97, possible values of the other two unknowns rely on stellar evolution theory. According to the evolutionary models of Dorman et al. (1993), the masses of subdwarf B stars are confined to the narrow range $0.40 - 0.43 \lesssim M_*/M_\odot \lesssim 0.53$, however more recent predictions by Han et al. (2002, 2003) suggest a somewhat larger mass distribution. Depending on the formation channel, the total mass of a sdB can then be as low as $\sim 0.3\ M_\odot$ or as high as $\sim 0.7\ M_\odot$, although the distributions are nevertheless peaked around the canonical value of $\sim 0.47\ M_\odot$. In the case of EC 20117−4014, its wide binary status implies an evolution via the stable Roche lobe overflow channel, which is associated with sdB masses concentrated towards the higher end of the possible range (peaking at $\sim 0.51\ M_\odot$, slightly higher than for the other evolutionary scenarios). We thus kept the lower limit of $0.43\ M_\odot$ suggested by Dorman et al. (1993), while extending the upper boundary to $0.60\ M_\odot$. Finally, the constraints on $\log q(\mathrm{H})$ were chosen so as to fully map the region of the $\log g - T_{\mathrm{eff}}$ plane where sdB stars are found.

For the pulsation calculation step, we considered all (p, f, or g-) modes in the 50−500 s range, thus amply sandwiching the periods observed for EC 20117−4014. Our calculations were limited to low degree modes with $l = 0$ and 1 since these are sufficient to reproduce the low density frequency spectrum measured. Due to cancellation effects when integrating over the (non-resolved) visible disk of the star, the observed amplitudes of oscillation drastically decrease with increasing degree index assuming equivalent intrinsic amplitudes. Unless the period distribution detected requires the inclusion of higher degree modes, it is therefore common to limit the latter to the canonical values $l = 0$, 1 and 2. In the present case, we restrict our period matching exercise even further to degree indices of 0 and 1. Remarkably, a subsequently verification of the solutions invoking modes with $l = 0$, 1 and 2 yielded exactly the same mode identification, thus confirming the robustness of our approach.

The exploration of parameter space uncovered two distinct families of models that both very accurately reproduce the periods observed and lie at surface gravities consistent with spectroscopic estimates. They are centred at $T_{\mathrm{eff}} = 34{,}800$ K (the spectroscopic value), $\log g = 5.86$, $M_*/M_\odot = 0.54$, $\log q(\mathrm{H}) = -4.15$ and $T_{\mathrm{eff}} = 34{,}800$ K (again, the value from spectroscopy), $\log g = 5.77$, $M_*/M_\odot = 0.56$, $\log q(\mathrm{H}) = -3.59$. While either of these could cor-

respond to the "true" optimal model, we favour the first (higher gravity) solution for two reasons. Firstly, the associated value of χ^2 is a factor of ~ 10 smaller compared to that of the lower gravity model ($\chi^2 = 1.75\times10^{-7}$ compared to $\chi^2 = 1.06\times10^{-6}$ for the second solution). Secondly, and more importantly considering the essentially perfect fits provided by both of the models, the second family has a surface gravity just below the range predicted from the best spectroscopic estimate of DOD97. Although the value is consistent with spectroscopy within the more conservative uncertainties adopted, we find it indicative that the best fit solution falls very close to the first estimate, and therefore designate it the "optimal" model over the lower gravity solution. The χ^2 hypersurface in the vicinity of the optimal model is shown in Figures 2.7 and 2.8, which respectively illustrate slices of the $\log g - T_{\rm eff}$ and the $M_* - \log q(\mathrm{H})$ planes with the other two parameters fixed at their optimal values. Regions of hyperspace identified with the best fits (lowest values of χ^2) appear in dark blue, while areas corresponding to the worst matches to the observed periods are indicated in red. Bearing in mind the logarithmic scale of the contours, it is obvious that the families of χ^2 minima are well defined and recreate the measured frequency spectrum far better than an average model.

Although the plots are designed to highlight the best fit solution, structures associated with the secondary solution discussed above can nevertheless be discerned in both plots. While the low χ^2 valley at $\log g \sim 5.79$ in the $\log g - T_{\rm eff}$ slice does not reveal the true secondary minimum (which is associated with a value of $\log q(\mathrm{H})$ quite different to that illustrated), it is related to the latter through the $T_{\rm eff} - \log q(\mathrm{H})$ degeneracy that exists for p-modes in subdwarf B stars. In essence, the relative variation in the period spectrum arising from a change in effective temperature is almost exactly compensated for by a shift in $\log q(\mathrm{H})$. This gives rise to the degeneracy valleys shown in Figure 2.9, where the minima predicted for the different values of $\log q(\mathrm{H})$ indicated on the horizontal white axis (with M_* kept constant at its optimal value) are superposed in the $\log g - T_{\rm eff}$ plane. There is a clear trend whereby the location of minimum χ^2 shifts from higher effective temperatures (e.g., $T_{\rm eff} \sim 37{,}200$ K for $\log q(\mathrm{H}) = -4.275$) to lower $T_{\rm eff}$ ($\sim 30{,}100$ K for $\log q(\mathrm{H}) = -3.950$) as the mass of the hydrogen shell increases. The value of the surface gravity on the other hand remains virtually unaffected. This behaviour is similar to that encountered for Feige 48 (Charpinet et a. 2005b)

in that there is no discernable degradation in the fit (i.e., the value of χ^2 does not grow noticeably) along the degeneracy valley, due of course to the low number of observed periods. Therefore, our ability to constrain $\log q(\mathrm{H})$ depends on the spectroscopic measurement of $T_{\rm eff}$.

We find a similar χ^2 degeneracy for the total stellar mass, as is illustrated in Figure 2.10. This time, both the effective temperature and the surface gravity of the optimal model are affected. In particular, the location of minimum χ^2 shifts from lower $T_{\rm eff}$ and $\log g$ (e.g., $T_{\rm eff} \sim$ 31,400 K, $\log g \sim 5.852$ for $M_* = 0.4750$) to higher temperatures and surface gravities (e.g., $T_{\rm eff} \sim$ 37,400 K, $\log g \sim 5.875$ for $M_* = 0.5975$) as the mass increases. Once again, the quality of the fit remains the same over the entire minimum χ^2 valley, implying that the stellar mass parameter must also be constrained on the basis of the spectroscopic temperature estimate.

2.7.4 Period Fit and Mode Identification

The pulsational properties of the optimal model are listed in Table 2.4 together with the observed periods used in the search (also see Figure 2.11 for a graphical illustration). We can see that the match achieved is essentially perfect, there being no residuals in the fit at the accuracy of the observational errors. This is in line with the finding of Charpinet et al. (2005b) that the average relative dispersion achieved from the asteroseismology of EC 14026 stars increases with the number of pulsations detected, pointing to slight inaccuracies in the models that have yet to be resolved. Nevertheless, we believe the fact that our second generation structures have so far been able to recreate the period spectra detected for 5 short-period variables to an average accuracy of typically $\lesssim 1$ % indicates that the basic input physics is correct. At the non-adiabatic level we should note that the longest observed period at 157.4 s falls just outside the band of instability predicted. This is almost certainly due to the effective temperature having been fixed at slightly too high a value. Indeed, test calculations for which we decreased $T_{\rm eff}$ by just 100 K (well within the spectroscopic uncertainty) resulted in an excited period range encompassing the 157.4 s oscillation, while changing the theoretical periods by only ~ 0.02 s. Hence, we do not believe that the slight discrepancy encountered between the predicted and observed unstable period ranges points to problems with our models or the non-adiabatic code used. On the contrary, the fact that we are able to reproduce the

band of instability detected on the basis of a model with atmospheric parameters in line with those predicted from spectroscopy confirms the validity of our approach.

In the mode identification achieved, the observed oscillations correspond to low-order p-modes with degree indices of $l = 0$ and 1. Whereas the latter is a result of the limitations imposed at the outset, it was not clear that the periodicities detected would cluster at the low radial order (or high period) end of the instability strip. Incidentally, this is precisely what was found for the other EC 14026 stars analysed to date. A possible explanation is that, within the band of excited periods, the energy driving the pulsations may preferentially be distributed among modes of low radial order (Charpinet et al. 2005a). The latter would then reach observable amplitudes more easily, and therefore be detected more readily. However, lacking non-linear pulsation theory, it is not clear why certain parts of the unstable period range should be excited to a greater extent than others. In this context it is interesting to note that a similar effect has been observed for some of the long-period variable subdwarf B stars (see e.g., Randall et al. 2006). Although in their case non-adiabatic computations are unable to quantitatively account for the ranges of periods observed, the fact that the oscillations are thought to be driven by the same κ-mechanism as the EC 14026 stars would lead us to expect *bands* of excited periods, within which all modes should be unstable. These are indeed detected over some of the observed period range, however we have found significant gaps in the period distribution, which points towards some kind of mode selection taking place. It therefore seems that the channelling of energy into specific frequency bands is intrinsic to both types of pulsating subdwarf, an idea that should be investigated in more detail in the future.

We should mention that the mode identification postulated here can in principle be tested using an independent means. One promising avenue is the exploitation of a mode's colour-amplitude dependence on its degree index through multi-colour photometry (see, e.g., Randall et al. 2005). Some very encouraging applications of this technique have been published by Jeffery et al. (2004, 2005), suggesting the presence of $l = 4$ modes in two EC 14026 pulsators. Unfortunately, the colour-amplitude behaviour predicted for modes with $l = 0$, 1 and 2 is extremely similar, making it very challenging to discriminate between the lowest degree (and thus

presumably most visible) modes. Indeed, the preliminary analysis of high-quality multi-colour photometry obtained at the Canada-France-Hawaii telescope for PG 1219+534 indicates that the quality of the data will have to be improved upon markedly if we are to convincingly discriminate between low-degree modes in the EC 14026 stars. Other ways of restricting the l-value for modes observed include the exploitation of rotational splitting (see, e.g., Charpinet et al. 2005b) and line-profile variations (see, e.g., Schoenaers & Lynas-Gray 2005). However, the former is applicable only in the case of sufficiently rapidly rotating pulsators, and the latter has not yet been tested observationally. Thus, for the time being, the analysis of multi-colour photometry seems to constitute the most promising method of verifying the accuracy of the asteroseismological analyses achieved.

2.7.5 Structural Parameters of EC 20117−4014

The optimal model identified is characterised by the values of its input parameters $T_{\rm eff}$, $\log g$, M_* and $\log q({\rm H}) = \log M_{env}/M_*$ given in Table 2.5. From these, we can derive a plethora of secondary quantities: the radius R (as a function of M_* and g), the luminosity L (as a function of $T_{\rm eff}$ and R), the absolute magnitude M_V (as a function of g, $T_{\rm eff}$ and M_* in conjunction with the use of detailed model atmospheres), and the distance from Earth d (as a function of V and M_V, where we adopt $V = 13.55$ as derived from the spectroscopy presented by O'Donoghue et al. 1997). Given the parameter degeneracies discussed above, the errors listed for M_* and $\log q({\rm H})$ are derived using the constraints on the effective temperature from spectroscopy, similarly to the case of Feige 48 (Charpinet et al. 2005b). A close examination of the projection maps of the merit function illustrated in Figures 2.9 and 2.10 yields, at the 68.3 % confidence level, the uncertainty estimates given in Table 2.5. The uncertainty on $\log g$ is set to the typical value derived from previous asteroseismological studies, since we do not have enough observed periods available to apply the method developed by Brassard et al. (2001). Errors on the secondary quantities are then easily derived from those of the primary parameters.

We find that the value of $\log g$ derived from asteroseismology is remarkably consistent with that expected from spectroscopy. Of course, this is partly due to the fact that we selected the

χ^2 minimum closest to the spectroscopic gravity to correspond to the optimal model. On the other hand, the model chosen did present the best overall fit to the periodicities observed, a result that was by no means guaranteed from the outset. Assuming that the valley picked is the "correct" one, the surface gravity of EC 20117−4014 is much more tightly constrained (by an order of magnitude) on the basis of asteroseismology than from spectroscopy. This is due to the strong dependence of the p-mode periodicities on the gas density, which is mainly influenced by the $\log g$ parameter. In comparison, the temperature plays a much less important role, and is generally determined more accurately from spectroscopy. The total mass inferred for EC 20117−4014 is noticeably higher than those found for the other rapidly pulsating subdwarfs analysed to date, which tend to cluster around the canonically expected value of $\sim$ 0.47 $M_{\odot}$ (see Charpinet et al. 2005). While this is somewhat surprising, it is not completely incomprehensible from an evolutionary scenario point of view. According to the work of Han et al. (2002, 2003), a subdwarf in a wide binary such as EC 20117−4014 should have formed via stable Roche lobe overflow. Assuming that the companion is a main sequence star (as is very strongly suggested from spectroscopy for EC 20117−4014), this evolutionary channel can produce sdB stars with masses up to 1.1 $M_{\odot}$, although the more massive stars are thought to be less likely and the distribution still sharply peaks at $\sim$ 0.46 $M_{\odot}$. It is clear that the matter remains to be investigated in more detail, particularly considering the uncertainties surrounding the error estimates for the spectroscopy and hence those of the asteroseismological quantities inferred. However, for the moment the result obtained for EC 20117−4014 seems to point towards an evolutionary history slightly different from that encountered for the single and short-period binary pulsators analysed previously. The inferred hydrogen shell thickness on the other hand is very similar to that obtained for the hot EC 14026 stars PG 0014+067 and PG 1219+534, and significantly smaller than that computed for the cooler pulsator Feige 48 (see Charpinet et al. 2005). This is in line with predictions that subdwarfs with lower effective temperatures should have thicker envelopes, since the latter acts as an isolating layer between the helium core and the stellar surface.

Of all the secondary quantities inferred, only the distance of EC 20117−4014 has previously been estimated. Using the ratio of a stellar radius derived from the spectroscopic value of

$\log g$ and an assumed mass of 0.5 $M_\odot$, as well an apparent angular radius determined from the continuum level of their spectra, DOD97 computed the distance of EC 20117−4014 to be $d = 680$ pc. This is in reasonable agreement with the asteroseismological value of $d \sim 647$ pc (see Table 2.5) and as such provides a nice confirmation of the validity of the parameters inferred.

2.8 CONCLUSION

In this study, we obtained further observations of the rapidly pulsating subdwarf B star EC 20117−4014 with the aim of improving on the quality of previous data. Unfortunately, poor weather conditions during both of the main runs prohibited the detection of any as yet unknown pulsation periods. We did however succeed in measuring a systematic frequency variation over a time-scale of a few months, which is most likely due to binary motion. From the constraints posed by the amplitude of the frequency shifts and the lack of rotational splitting in the photometry, we were able to restrict the binary period of the system to between ~ 20 and 350 days. According to theoretical evolution calculations, this points to a formation of the subdwarf via stable Roche lobe overflow.

In principle, the evolution of a subdwarf can be constrained from its internal parameters, obtainable through asteroseismological means. We therefore attempted an in-depth analysis of EC 20117−4014 on the basis of the three periods detected. Fixing the effective temperature to the spectroscopic value, we searched for the model in $\log g - M_* - \log q(\mathrm{H})$ space that could optimally reproduce the observed periods. This led to two possible solutions, one of which had to be preferred on the basis of the fit achieved and the surface gravity inferred. The corresponding optimal model has $T_{\mathrm{eff}} = 34{,}800 \pm 1000$ K (the spectroscopic value), $\log g = 5.859 \pm 0.006$, $M_* = 0.54 \pm 0.02\ M_\odot$ and $\log q(\mathrm{H}) = -4.15 \pm 0.05$. Note that the value of $\log g$ is determined to an accuracy of about a factor of 10 higher than is currently possible from spectroscopy. In addition, asteroseismology allows the estimation of the two structural parameters M_* and $\log q(\mathrm{H})$, which can normally not be inferred any other way. In exceptional cases, the mass can be constrained from radial velocity observations in a binary system, however the resulting uncertainties are typically very large. The determination of the

envelope thickness for its part is a pure product of asteroseismology. We find that our optimal model has a relatively thin hydrogen shell typical of the hotter EC 14026 pulsators so far analysed, in line with the theory that the cooler subdwarfs should be associated with the thickest envelopes. On the other hand, the mass inferred is surprisingly high. While this could be a result of EC 20117−4014's evolutionary history, it should be kept in mind that the errors on the asteroseismological parameters may well be larger than assumed, since they are derived from the spectroscopic uncertainties. Although these were chosen so as to be representative of the realistic errors obtained for other EC 14026 stars, the fact that the spectrum of EC 20117−4014 is contaminated by its main sequence companion will lead to larger uncertainties than those typical of single targets or those with an invisible secondary. Consequently, the temperature error could easily be of the order of 2000−3000 K, which would imply at least twice the mass uncertainty assumed. The total mass of the star could then be as low as $\sim$ 0.48 $M_{\odot}$, a value very similar to that found for the other asteroseismic targets.

The optimal model found accounts for the pulsations observed in terms of low degree modes that cluster at the low radial order end of the theoretical unstable frequency band. Given that a similar effect was encountered for the other sdB pulsators monitored to date, this points to some kind of mode selection mechanism, whereby the available pulsation energy is preferentially channelled into the excitation of modes in certain frequency ranges. Unfortunately, current pulsation computations are based on linear theory and are not able to predict the amplitudes of oscillations, leaving us with no means of verifying the theory of selective mode driving. These limitations notwithstanding, the results obtained for EC 20117−4014 show that our second generation models are capable of accurately reproducing the periods observed in terms of a model consistent with spectroscopic estimates and non-adiabatic theory (within the formal temperature uncertainties). We consider this as proof that the basic input physics of the models is sound, especially bearing in mind that EC 20117−4014 constitutes the fifth EC 14026 pulsator for which asteroseismology has been successfully achieved.

Given the very limited number of observed periods available, the outstanding result of our study is not so much the fact that we managed to find such a close theoretical match to the measured periods, but rather that we were able to isolate a small number of χ^2 minima in

the parameter range specified by spectroscopy. The fact that it was feasible to isolate just one plausible family of optimal models on the basis of only three observed periods opens up the exciting possibility of deriving the asteroseismological parameters for many more known EC 14026 stars without obtaining extra data at higher sensitivity. It had previously been assumed that the 2−3 oscillations detected in the majority of known EC 14026 stars were completely useless in terms of quantitative asteroseismology. However, it should be kept in mind that the principal reason this exercise was so enlightening for EC 20117−4014 is its relatively high surface gravity, which implies the theoretical excitation of a relatively sparse period spectrum compared to an average, less compact sdB model. Hence, while asteroseismology on the basis of very few observed frequencies may work well for the odd high-gravity fast pulsator, the majority of these objects will require follow-up monitoring on mid-size telescopes. Nonetheless, our results underline the vast potential of the forward approach in asteroseismology as well as the validity of the iron bump opacity mechanism as the instability driver in EC 14026 stars (Charpinet et al. 1997). Ultimately, we hope asteroseismological quantities will be derived for the greater part of all pulsating subdwarf B stars, thus leading to a mature understanding of their evolutionary status.

S.K.R. would like to thank Prof. Allan Willis for generously funding the SAAO 2000 observing run. This work was also supported in part by the Natural Sciences and Engineering Research Council of Canada and by the Fonds de recherche sur la nature et les technologies (Québec). G.F. also acknowledges the contribution of the Canada Research Chair Program.

2.9 TABLES

TABLE 2.1 – Observing Log for EC 20117−4014

Run	Date UT	Start of Run (UT)	Sampling Time (s)	Total Number of Data Points
saao−001	06/07/2001	19:17	10	2635
saao−002	10/07/2001	18:52	10	2081
saao−003	11/07/2001	19:14	10	2315
saao−004	13/07/2001	19:14	10	3152
saao−005	14/07/2001	19:19	10	2774
lasilla−001	18/06/2002	07:23	23	499
lasilla−002	21/06/2002	07:04	23	540
lasilla−003	23/06/2002	06:56	23	426
saao−006	17/07/2002	18:00	10	897
saao−007	20/07/2002	19:30	10	3087
saao−008	21/07/2002	17:07	10	2706
saao−009	25/07/2002	17:11	10	3168

TABLE 2.2 – Harmonic Oscillations Detected in the Light Curve of EC 20117−4014

Season	Frequency (mHz)	Period (s)	Amplitude (%)	Phase (s)
2001	7.28440±0.00014	137.2797±0.0026	0.332±0.011	45.64±0.73
2002 (June)	7.28475±0.00023	137.2731±0.0043	0.313±0.015	100.25±1.05
2002 (July)	7.28515±0.00014	137.2656±0.0026	0.374±0.015	40.22±0.87
2001	7.03472±0.00014	142.1521±0.0028	0.094±0.011	79.38±2.66
2002 (June)	7.03522±0.00023	142.1419±0.0046	0.092±0.015	101.76±3.76
2002 (July)	7.03526±0.00014	142.1411±0.0028	0.117±0.015	70.72±2.90
2001	6.35136±0.00014	157.4466±0.0034	0.073±0.011	48.63±3.79
2002 (June)	(6.35100±0.00023)	(157.4555±0.0056)	(0.064±0.015)	(151.77±5.96)
2002 (July)	6.35186±0.00014	157.4342±0.0034	0.088±0.015	74.00±4.25

TABLE 2.3 – Posssible Orbital Periods and System Inclination Angles for EC 20117−4014

Period (days)	Angle (degrees)
18	26
49	39
120	52
302	79
340	90

TABLE 2.4 – Pulsation Characteristics of the Optimal Model and Mode Identification

l	k	P_{obs} (s)	P_{th} (s)	σ_I (rad/s)	$\log E$ (ergs)	C_{kl}
0	10	...	50.487843194	$8.650196357\times10^{-04}$	38.48382	...
0	9	...	54.231364208	$3.721194710\times10^{-04}$	39.34537	...
0	8	...	58.796345272	$2.569028190\times10^{-04}$	39.50131	...
0	7	...	65.812107465	$2.901415294\times10^{-05}$	39.84345	...
0	6	...	71.817445283	$-2.793901469\times10^{-05}$	40.23871	...
0	5	...	80.593402443	$-6.744653007\times10^{-05}$	40.26244	...
0	4	...	92.731393526	$-3.382933111\times10^{-05}$	40.64702	...
0	3	...	101.978153372	$-1.165968812\times10^{-05}$	41.06321	...
0	2	...	122.121247256	$-4.230331260\times10^{-06}$	41.26701	...
0	1	142.1	142.099946612	$-8.604996056\times10^{-08}$	42.46366	...
0	0	...	158.146125265	$3.460642996\times10^{-09}$	42.56275	...
1	10	...	50.251008192	$8.387120244\times10^{-04}$	38.85325	0.0029283
1	9	...	53.717767452	$4.081409801\times10^{-04}$	39.29281	0.0036589
1	8	...	58.467637599	$2.811299678\times10^{-04}$	39.46817	0.0035716
1	7	...	65.251235793	$3.683519764\times10^{-05}$	39.85436	0.0050753
1	6	...	70.787648835	$-2.549477448\times10^{-05}$	40.16206	0.0065600
1	5	...	80.011117875	$-6.800222939\times10^{-05}$	40.24479	0.0062957
1	4	...	91.213111248	$-3.168998281\times10^{-05}$	40.66765	0.0111621
1	3	...	100.131027561	$-1.689746239\times10^{-05}$	40.91531	0.0117782
1	3	...	121.255856201	$-4.432109769\times10^{-06}$	41.25727	0.0126393
1	2	137.3	137.300376336	$-1.768263676\times10^{-07}$	42.28933	0.0269348
1	1	157.4	157.400175012	$1.104609172\times10^{-09}$	42.50726	0.0175613

TABLE 2.5 – Inferred Properties of EC 20117−4014

Quantity	Values from Asteroseismology
$\log g$	5.859 ± 0.006
$T_{\rm eff}$ (K)	34,800 ± 1000 (spectroscopy)
$M_*/\,{\rm M}_\odot$	0.54 ± 0.02
$\log\,(M_{env}/M_*)$	−4.15 ± 0.05
$R/R_\odot(M_*, g)$	0.143 ± 0.005
$L/L_\odot(T_{\rm eff}, R)$	26.6 ± 3.6
$M_V(g, T_{\rm eff}, M_*)$	4.50 ± 0.11
$d(V, M_V)$	646.8 pc

2.10 REFERENCES

Bergeron, P., Wesemael, F., Beauchamp, A., Wood, M.A., Lamontagne, R., Fontaine, G., & Liebert, J. 1994, ApJ, 432, 305

Billères, M., Fontaine, G., Brassard, P., Charpinet, S., Liebert, J., & Saffer, R.A. 2000, ApJ, 530, 441

Billères, M., Fontaine, G., Brassard, P., & Liebert, J. 2002, ApJ, 578, 515B

Brassard, P., Fontaine, G., Billères, M., Charpinet, S., Liebert, J., & Saffer, R.A. 2001, ApJ, 563, 1013

Brassard, P., & Fontaine, G. 1994, in IAU Colloq. 147, The Equation of state in Astrophysics, ed. G. Chabrier and E. Schatzman (Cambridge Univ. Press), 560

Brassard, P., Pelletier, C., Fontaine, G., & Wesemael, F. 1992, ApJS, 80, 725

Charpinet, S., Fontaine, G., Brassard, P., Chayer, P., & Green, E.M. 2005, Baltic Astronomy, in press

Charpinet, S., Fontaine, G., Brassard, P., Green, E.M., & Chayer, P. 2005a, A&A, 437, 575

Charpinet, S., Fontaine, G., Brassard, P., Billères, M., Green, E.M., & Chayer, P. 2005b, A&A, in press

Charpinet, S., Fontaine, G., Brassard, P., Billères, M., Green, E.M., & Chayer, P. 2005c, 14th European Workshop on White Dwarfs, ASP Conf. Series, Vol. 334. Proceedings of a meeting held at Kiel, July 19-23 2004, ed. D. Koester and S. Moehler. San Francisco: ASP 2005, p. 619

Charpinet, S., Fontaine, G., & Brassard, P. 2003, in White Dwarfs, proceedings of the conference held at the Astronomical Observatory of Capodimonte, Napoli, Italy. Ed. D. de Martino, R. Silvotti, J.-E. Solheim and R. Kalytis, Kluwer Academic Publishers. NATO Science Series II - Mathematics, Physics and Chemistry, Vol. 105, p. 69

Charpinet, S., Fontaine, G., Brassard, P., & Dorman, B. 2002, ApJS, 140, 469

Charpinet, S, Fontaine, G., & Brassard, P. 2001, PASP, 113, 785

Charpinet, S., Fontaine, G., Brassard, P., & Dorman, B. 2000, ApJS, 131, 223

Charpinet, S., Fontaine, G., Brassard, P., Chayer, P., Rogers, F.J., Iglesias, C.A., & Dorman, B. 1997, ApJ, 483, L123

Charpinet, S., Fontaine, G., Brassard, P., & Dorman, B, 1996, ApJ, 471, L103

Chayer, P., Fontaine, G., Fontaine, M., Lamontagne, R., Wesemael, F., Dupuis, J., Heber, U., Napiwotzki, R., & Moehler, S. 2004, Ap&SS, 291, 359

D'Cruz, N.L., Dorman, B., Rood, R.T., & O'Connell, R.W. 1996, ApJ, 466, 359

Dorman, B., Rood, R.T., & O'Connell, R.W. 1993, ApJ, 419, 596

Fontaine, G., Green, E.M., Chayer, P., Brassard, P., Charpinet, S., & Randall, S.K. 2005, Baltic Astronomy

Fontaine, G., Brassard, P., Charpinet, S., Green, E.M., Chayer, P., Billères, M., & Randall, S.K., 2003, ApJ, 597, 518

Fontaine, G., Charpinet, S., Brassard, P., Chayer, P., Rogers, F.J., Iglesias, C.A., & Dorman, B. 1998, in IAU Symposium 185, New Eyes inside the Sun and Stars, ed. F. Deubner & D.W. Kurtz (Dordretch: Kluwer), 367

Fontaine, G., & Chayer, P., 1997, The third conference on faint blue stars, edited by A.G.D. Philip, J. Liebert, R. Saffer and D.S. Hayes, published by L. Davis Press, p.169

Fontaine, G., Brassard, P., Wesemael, F., & Tassoul, M. 1994, ApJ, 428, L61

Green, E.M., Fontaine, G., Reed, M.D., Callerame, K., Seitenzahl, I.R., White, B.A., Hyde, E.A., Ostensen, R., Cordes, O., Brassard, P., Falter, S., Jeffery, E.J., Dreizler, S., Schuh, S.L., Giovanni, M., Edelmann, H., Rigby, J., & Bronowska, A. 2003, ApJ, 583, L31

Han, Z., Podsiadlowski, P., Maxted, P.F.L., & Marsh, T.R. 2003, MNRAS, 341, 669

Han, Z., Podsialowski, Ph., Maxted, P.F.L, Marsh, T.R., & Ivanova, N. 2002, MNRAS, 336, 449

Jeffery, C.S., Aerts, C., Dhillon, V.S., Marsh, T.R., & Gänsicke, B.T. 2005, MNRAS, 362, 66

Jeffery, C.S., Dhillon, V., Marsh, T., & Ramachandran, B. 2004, MNRAS, 352, 699

Kilkenny, D. 2002, in ASP Conference Proceedings, Vol. 259

Kilkenny, D., Koen, C., O'Donoghue, D., & Stobie, R.S. 1997, MNRAS, 285, 640-644

Kilkenny, D., O'Donoghue, D., Koen, C., Stobie, R.S., & Chen, A. 1997b, MNRAS, 287, 867

Koen, C., Kilkenny, D., O'Donoghue, D., Van Wyk, F., & Stobie, R.S., 1997, MNRAS, 285, 645-650

Lasker, B, Sturch, C., McLean, B., Russel, J., Jenkner, H., & Shara, M. 1990, ApJ, 99, 2019

O'Donoghue, D., Lynas-Gray, A.E., Kilkenny, D., Stobie, R.S., & Koen, C. 1997, MNRAS, 285, 657-672

Press, W.H., Teukolsky, S.A., Vetterling, W.T., & Flannery, B.P. 1986, Numerical Recipes, Second Edition, Cambridge University Press

Randall, S.K., Fontaine, G., Green, E.M., Brassard, P., Kilkenny, D., Crause, L., Terndrup, D.M., Daane, A., Kiss, L.L., Jacob, A.P., Bedding, T.R., For, B.-Q., & Quirion, P.-O. 2006, ApJ, submitted

Randall, S.K., Fontaine, G., Brassard, P., & Bergeron, P. 2005, ApJS, in press

Schechter, P.L., Mateo, M., & Saha, A. 1993, PASP, 105, 693

Schoenaers, C., & Lynas-Gray, A.E. 2005, Baltic Astronomy, in press

Sweigart, A.V. 1997, ApJ, 474, L74

Silvotti, R., Ostensen, R., Heber, U., Solheim, J.-E., Dreizler, S., & Altmann, M. 2002, A&A, 383, 239

Stobie, R.S., Chen, A., O'Donoghue, D., & Kilkenny, D. 1992, in Warner B., ed., ASP Conference Series 30, Variable stars and Galaxies, Astron. Soc. Pac., San Francisco, p. 87

Stobie, R.S., Kawaler, S.D., Kilkenny, D., O'Donoghue, D., & Koen, C. 1997, MNRAS, 285, 651

Unno, W., Osaki, Y., Ando, H., Saio, H., & Shibahashi, H. (1989). *Non-radial Oscillations of Stars"*. University of Tokyo Press.

2.11 FIGURES

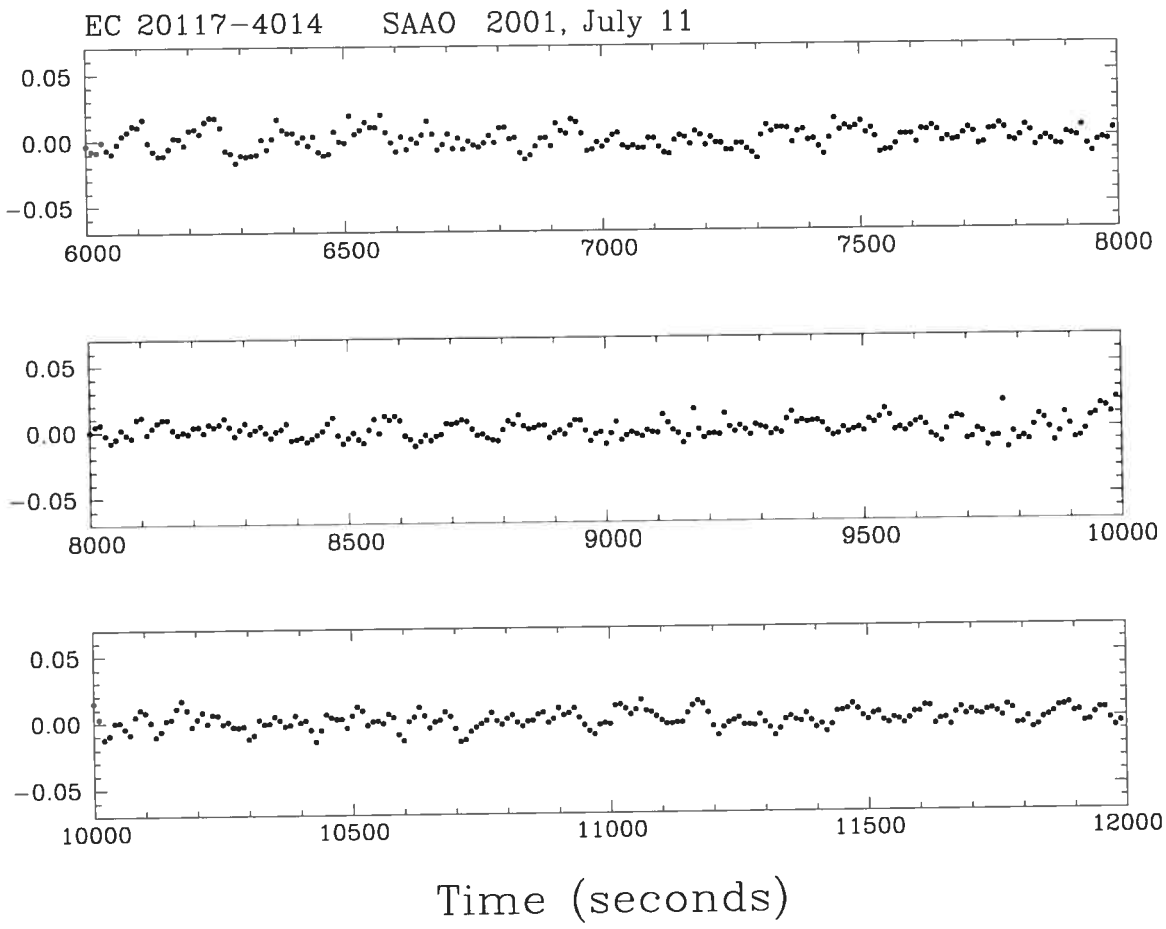

FIGURE 2.1 – Segment of the light curve of EC 20117−4014 from run saao−003, obtained on the 11/07/2001, expressed in terms of the residual percentage amplitude relative to the mean brightness of the star. Each plotted point represents a sampling time of 10 s.

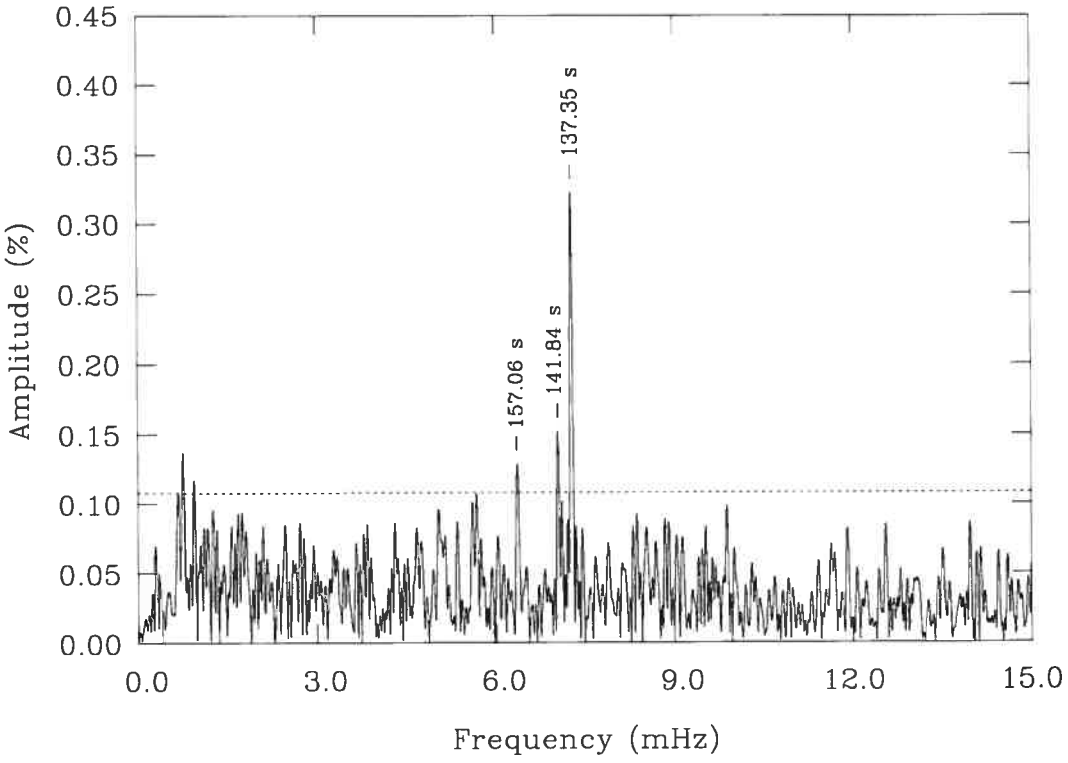

FIGURE 2.2 – The 0−15 mHz bandwidth Fourier amplitude spectrum of the light curve of EC 20117−4014 obtained during run saao−003. The amplitude axis is expressed in terms of the percentage variations about the mean brightness of the star. The positions of the three harmonic oscillations that we identified in the light curve are indicated by short solid line segments. The horizontal dotted line gives the value of three times the mean noise level in the bandwidth after removing the three harmonic signals through pre-whitening techniques.

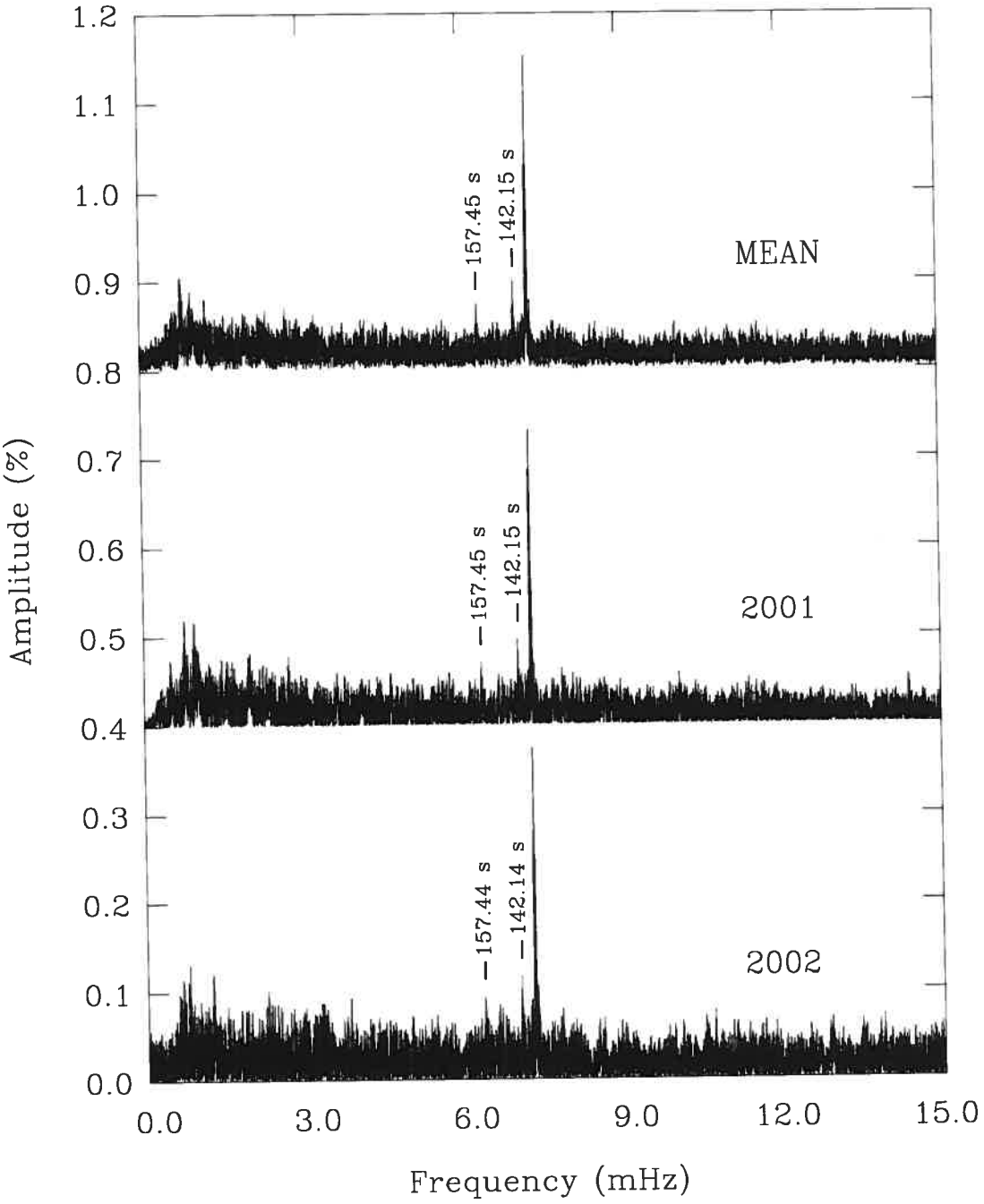

FIGURE 2.3 – Fourier amplitude spectrum (0–15 mHz band pass) of the complete light curve of EC 20117–4014 obtained during the 2002 season (lower panel) and during the July 2001 season (middle panel) at SAAO. Some 200,000 frequency points were used in the calculations of these Fourier transforms. The straight mean of those two spectra is shown in the upper panel. Except for arbitrary vertical shifts for the 2002 and mean spectra, the format is the same as that in Figure 2.2.

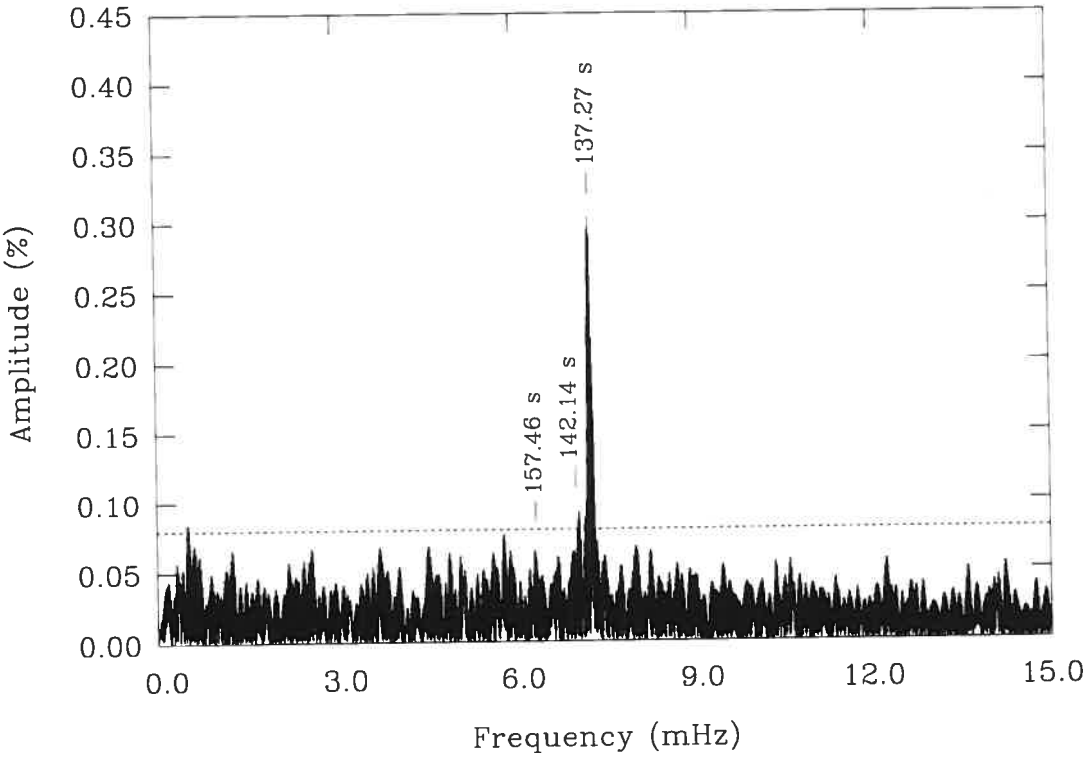

FIGURE 2.4 – Fourier amplitude spectrum (0-15 mHz band pass) of the complete light curve of EC 20117−4014 obtained during June 2002 at La Silla. The two harmonic oscillations extracted from the data, as well as the third basic frequency identified from the SAAO data are indicated by short solid line segments. The format is the same as in Figure 2.2.

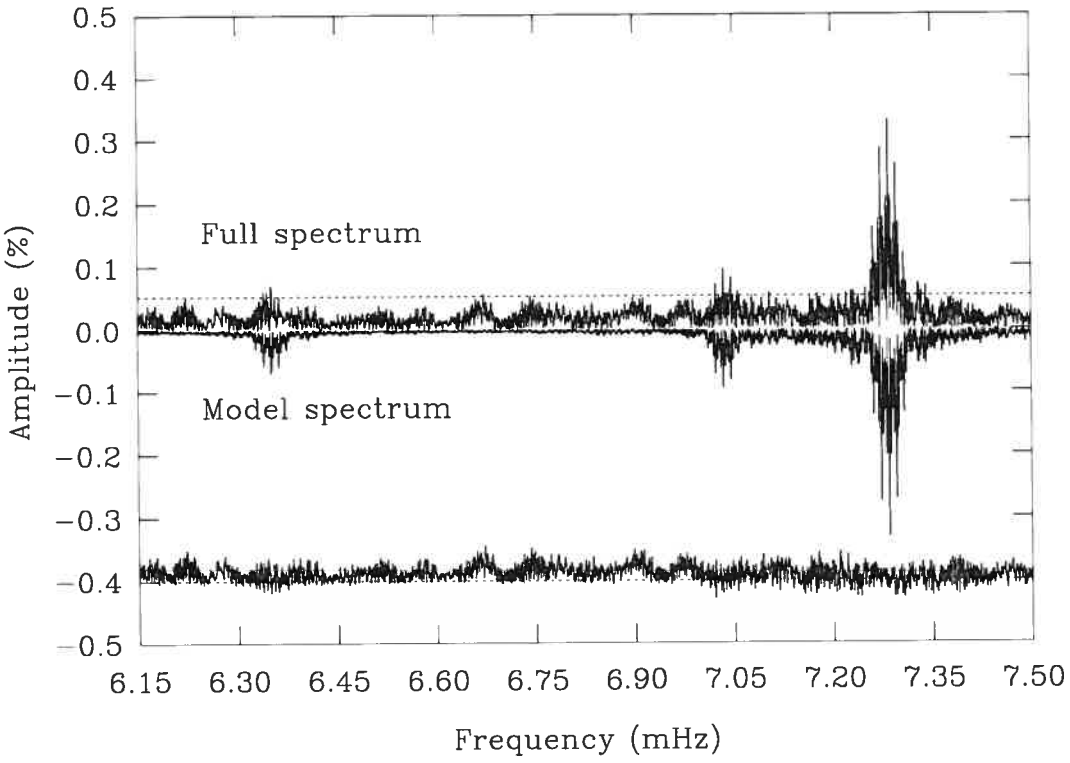

FIGURE 2.5 – Upper half: Fourier amplitude spectrum of the complete 2001 light curve of EC 20117−4014 in the 6.15−7.50 mHz bandwidth obtained on the basis of 40,000 frequency points. The dotted horizontal line shows the value of three times the mean noise level in the band pass after the pre-whitening removal of the three dominant harmonic oscillations. Lower half: Fourier amplitude spectrum (plotted upside down) of the noiseless light curve reconstructed on the basis of the three harmonic oscillations listed in Table 2.2. We also show the point-by-point frequency difference between the "observed" Fourier spectrum and the "computed" spectrum, but shifted downward by 0.4 %.

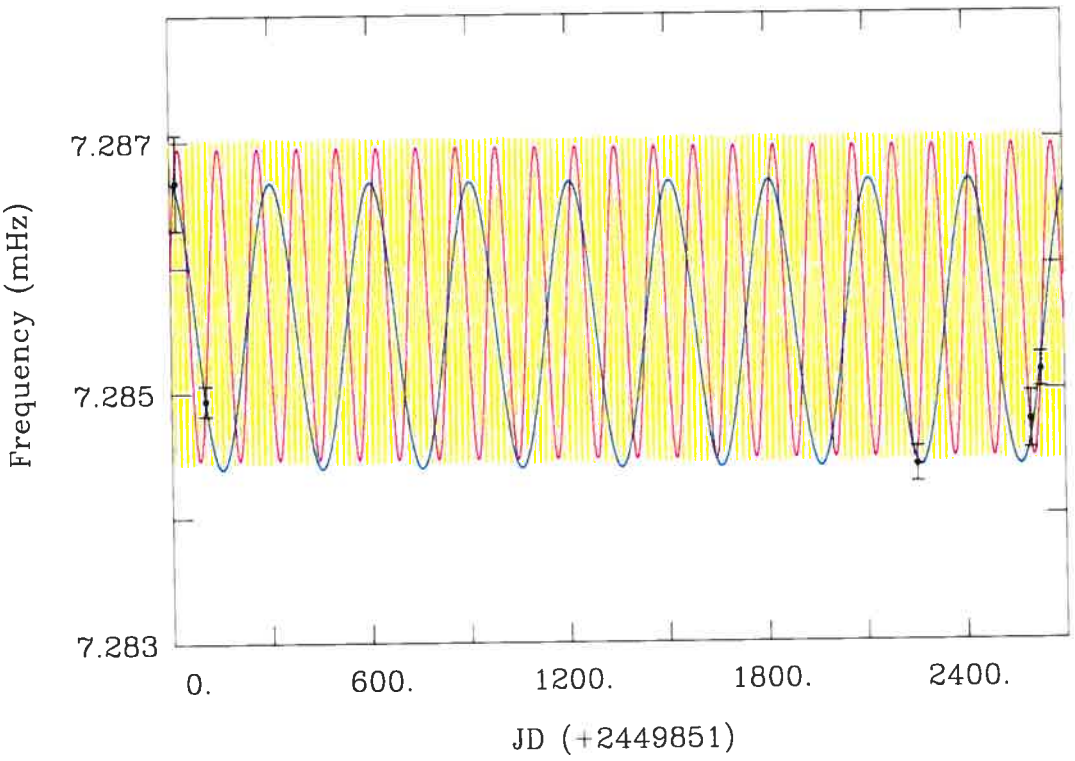

FIGURE 2.6 – Variation in frequency of EC 20117−4014's dominant oscillation as caused by three potential binary orbit scenarios. The yellow curve refers to the shortest plausible orbital period found at 18 days (system inclination: 26°), the magenta line indicates the change in frequency arising from a period of 120 days (system inclination: 52°), and the blue sinusoid indicates an orbit of 301 days (system inclination: 79°). All three curves provide good fits to the observed frequencies of the strongest periodicity (black points).

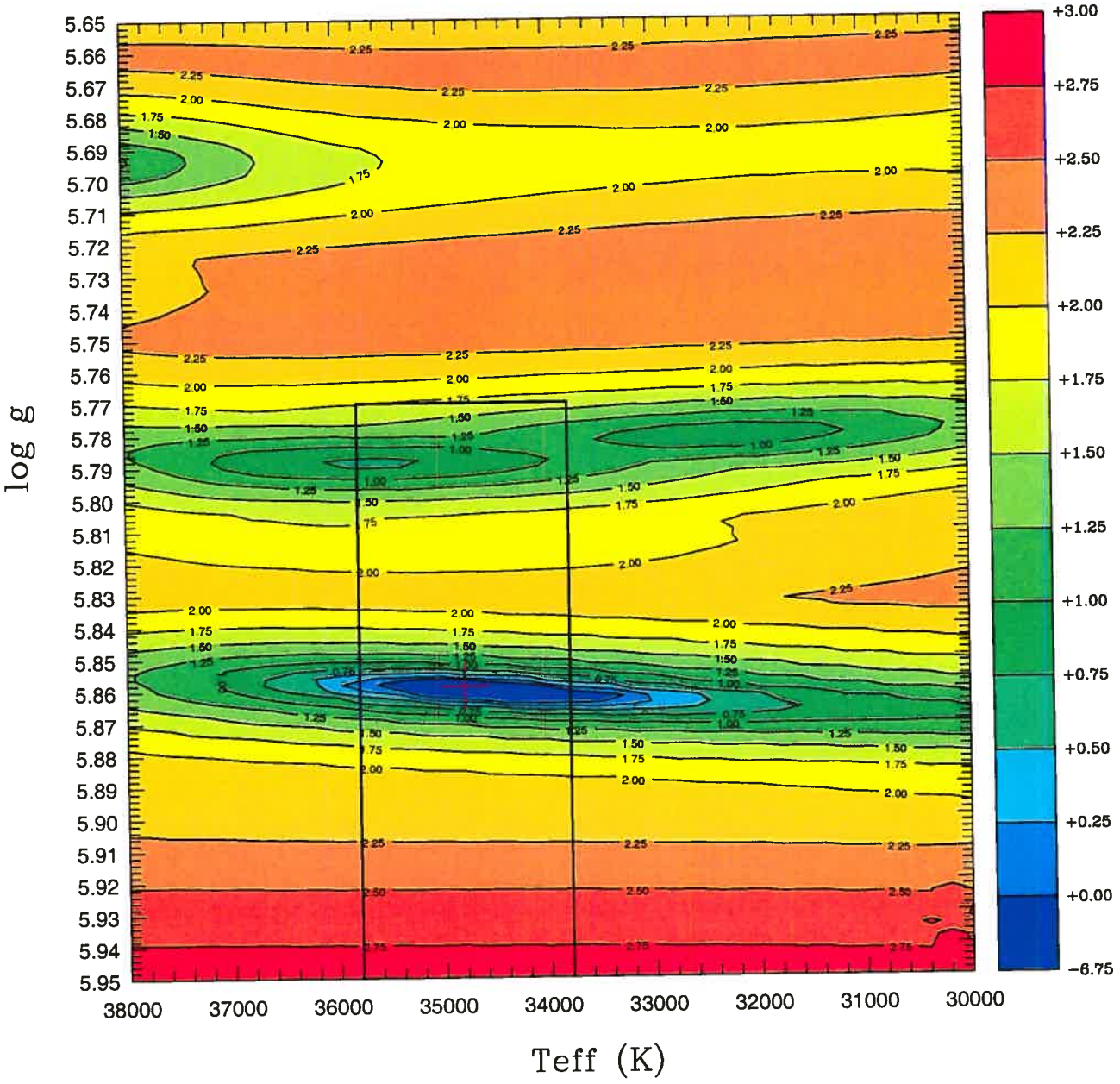

FIGURE 2.7 – Slice of the χ^2 function (in logarithmic units) along the $\log g - T_{\rm eff}$ plane with the remaining two parameters set to their optimal values ($M_* = 0.54$ and $\log q(\mathrm{H}) = -4.15$). The red cross indicates the location of the best fit solution, while the rectangle shows the uncertainties on the spectroscopic estimates of $\log g$ and $T_{\rm eff}$.

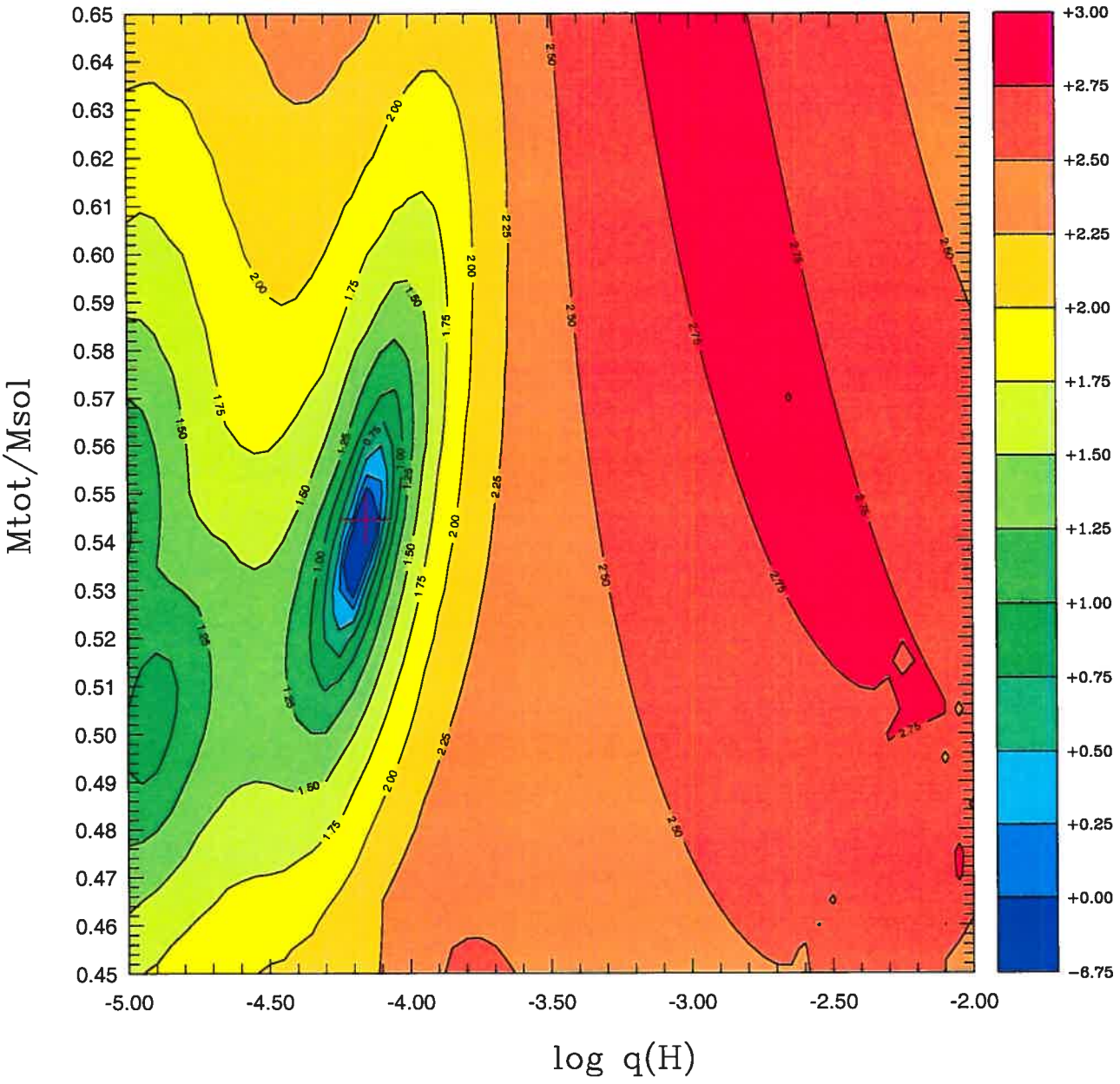

FIGURE 2.8 – Slice of the χ^2 function (in logarithmic units) along the $M_* - \log q(\mathrm{H})$ plane with the remaining two parameters set to their optimal values ($T_{\mathrm{eff}} = 34{,}800$ K and $\log g = 5.86$). The red cross indicates the location of the best fit solution.

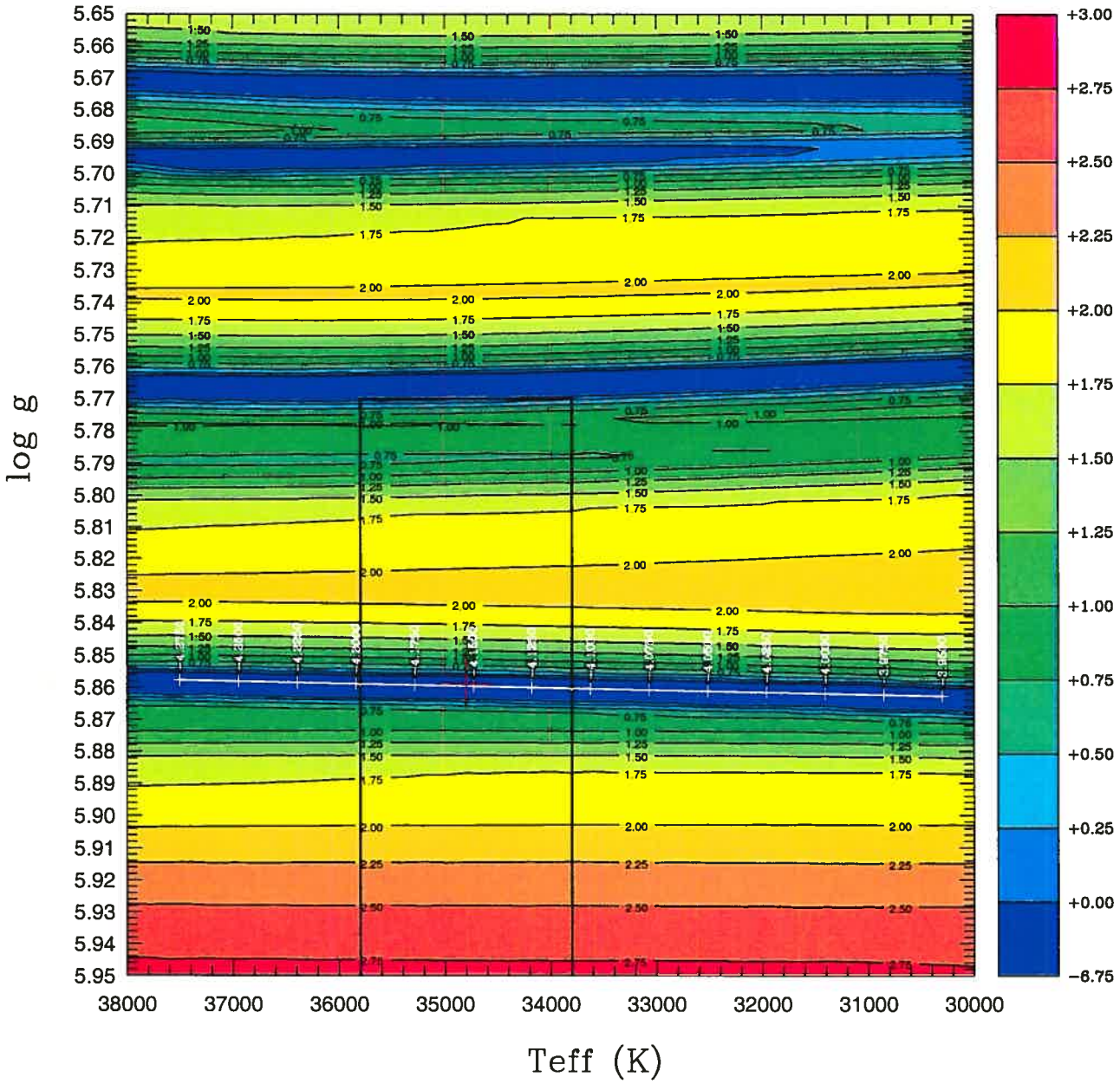

FIGURE 2.9 – Slice of the "projected" χ^2 function (in logarithmic units) along the $\log g - T_{\rm eff}$ plane with M_* set to its optimal value ($M_* = 0.54\ M_\odot$). The projected $\log q$(H) parameter was varied from -4.275 to -3.950, as indicated by the labels on the white projection axis. The latter give the location of the χ^2 minimum in the $\log g - T_{\rm eff}$ plane as a function of the hydrogen shell thickness. The rectangle shows the uncertainty box associated with the spectroscopic estimates of $\log g$ and $T_{\rm eff}$.

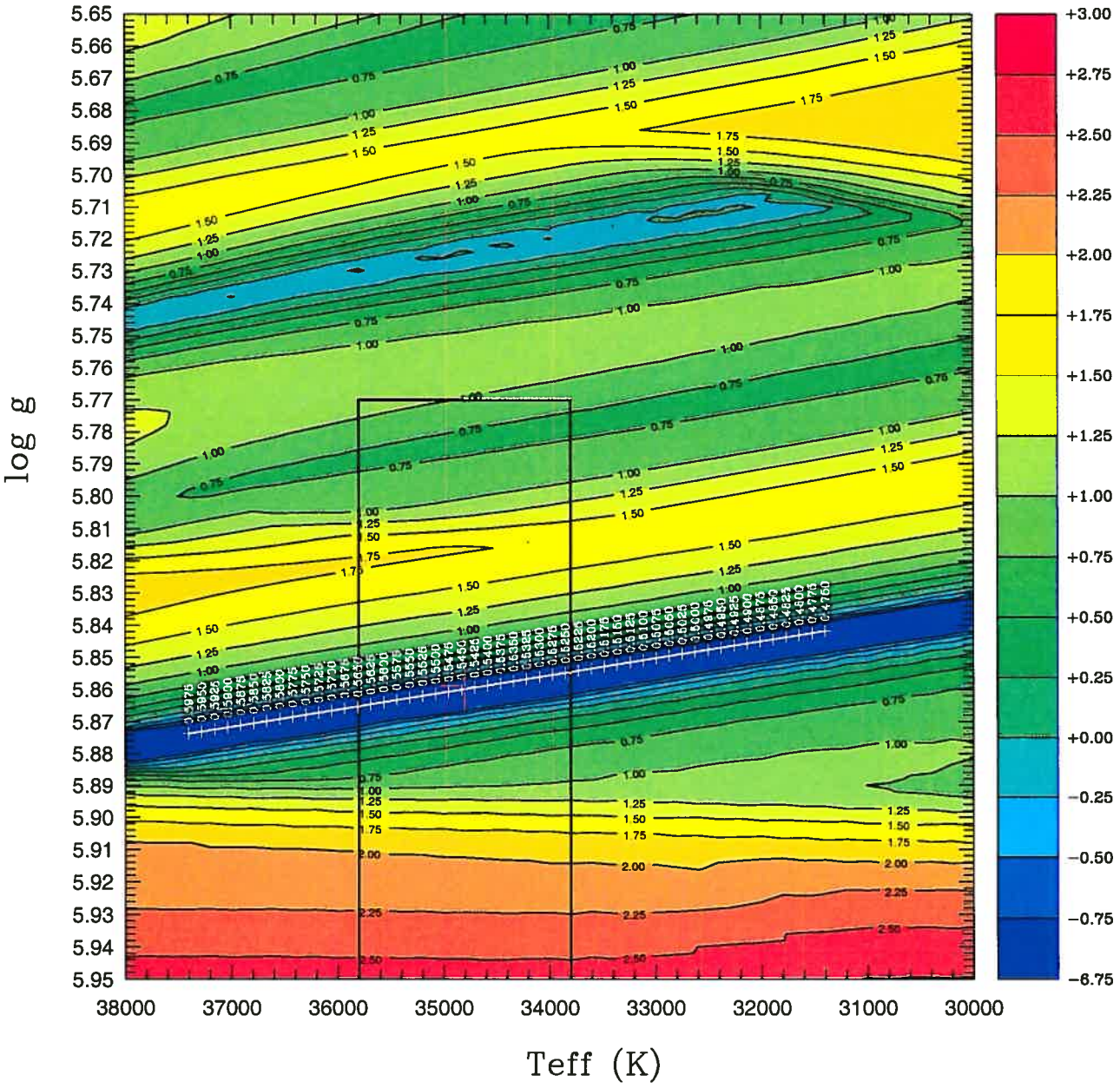

FIGURE 2.10 – Slice of the "projected" χ^2 function (in logarithmic units) along the $\log g - T_{\rm eff}$ plane with $\log q({\rm H})$ set to its optimal value ($\log q({\rm H}) = -4.15$). The projected M_* parameter was varied from 0.4750 to 0.5975, as indicated by the labels on the white projection axis. The latter give the location of the χ^2 minimum in the $\log g - T_{\rm eff}$ plane as a function of the hydrogen shell thickness. The rectangle shows the uncertainty box associated with the spectroscopic estimates of $\log g$ and $T_{\rm eff}$.

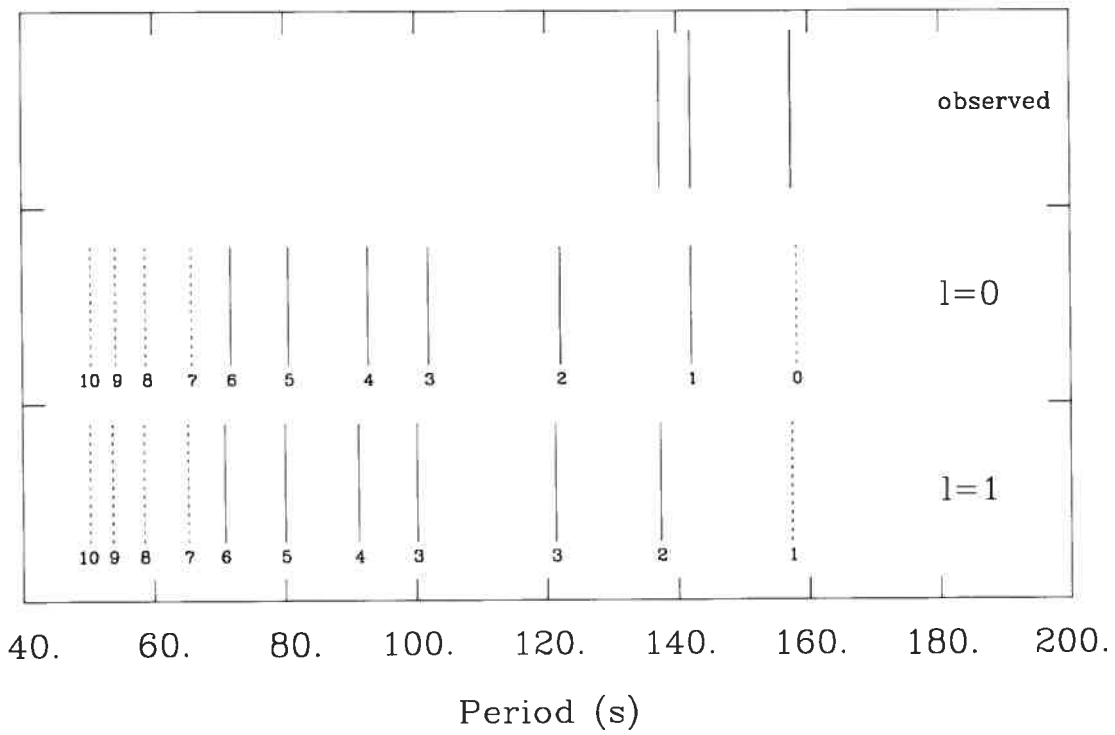

FIGURE 2.11 – Comparison of the observed period spectrum for EC 20117−4014 with the theoretical pulsation spectrum of the optimal model in the 50−200 s period range for degree indices $l = 0$ and 1. Solid line segments indicate modes predicted to be excited, while dotted line segments refer to stable modes. The radial indices k of the predicted modes are also given.

Chapter 3

THE POTENTIAL OF MULTI-COLOUR PHOTOMETRY FOR PULSATING SUBDWARF B STARS

S.K. Randall, G. Fontaine, P. Brassard, and P. Bergeron

Département de Physique, Université de Montréal, C.P. 6128, Succ. Centre-Ville, Montréal, Québec, Canada H3C 3J7

randall@astro.umontreal.ca, fontaine@astro.umontreal.ca, brassard@astro.umontreal.ca, bergeron@astro.umontreal.ca

Received 2005 March 22; accepted 2005 July 13

To be published in *The Astrophysical Journal (Supplement Series)*, 2005 December

3.1 ABSTRACT

We investigate the potential of multi-colour photometry for partial mode identification in both long- and short-period variable subdwarf B stars. The technique presented is based on the fact that the frequency dependence of an oscillation's amplitude and phase bears the signature of the mode's degree index l, among other things. Unknown contributing factors can be eliminated through the evaluation of the amplitude ratios and phase differences arising from the brightness variation in different wavebands, theoretically enabling the inference of the degree index from observations in two or more band passes. Employing a designated model atmosphere code, we calculate the brightness variation expected across the visible disk during a pulsation cycle in terms of temperature, radius, and surface gravity perturbations to the emergent flux for representative EC 14026 and PG 1716 star models. Non-adiabatic effects are considered in detail and found to be significant from non-adiabatic pulsation calculations applied to our state-of-the-art models of subdwarf B stars. Our results indicate that the brightness variations observed in subdwarf B stars are caused primarily by changes in temperature and radius, with surface gravity perturbations playing a small role. For PG 1716 stars, temperature effects dominate in the limit of long periods with the result that the oscillatory amplitudes and phases loose their period dependence and non-adiabatic effects become unimportant. Outside this regime however, their values are strongly influenced by both factors. We find that the phase shifts between brightness variations in different wavebands are generally small, but may lie above the experimental detection threshold in certain cases. The prospect of mode discrimination seems much more promising on the basis of the corresponding amplitude ratios. While in EC 14026 stars the amplitude ratios predicted are very similar for modes with $l = 0$, 1 or 2, they are well separated from those of modes with $l = 3$, $l = 5$, and $l = 4$ or 6, each of which form a distinct group. For the case of the PG 1716 stars it should be possible to discriminate between modes with $l = 1$, 2 , 4 or 6 and those of degree indices $l = 3$ and $l = 5$. Identifying modes within a given group is challenging for both types of pulsator and requires multi-colour photometry of extremely high quality. Nevertheless, we demonstrate that it is feasible using the example of the largest amplitude peak detected for the fast pulsator KPD 2109+4401 by Jeffery et al. (2004).

3.2 INTRODUCTION

Subdwarf B (sdB) stars are evolved extreme horizontal branch stars with effective temperatures in the range 20,000−42,000 K and low masses of around 0.5 $M_{\odot}$ (e.g., Saffer et al. 1994). They are believed to be composed of a helium-burning core surrounded by a hydrogen envelope too thin for them to ascend the Asymptotic Giant Branch after core helium exhaustion (Heber 1986; Dorman 1995). Instead, they evolve off and along the horizontal branch and eventually end their lives as low-mass white dwarfs (Bergeron et al. 1994). The discovery of pulsators among subdwarf B stars (Kilkenny et al. 1997) has opened them up to asteroseismological probing, an important tool for understanding the internal structure of these interesting objects. Pulsating subdwarfs can be divided into two categories: the rapidly pulsating EC 14026 stars and the slowly oscillating long-period variable subdwarf B stars (or PG 1716 stars for short).

The first EC 14026 stars were discovered to be pulsating multi-periodically with typical periods in the range 100-200 s in 1997 (Kilkenny et al. 1997; Koen et al. 1997; Stobie et al. 1997; O'Donoghue et al. 1997). At about the same time and completely independently, Charpinet et al. (1996, 1997) predicted the existence of pressure mode (p-mode) instabilities in these stars caused by a classical kappa mechanism associated with the iron opacity peak in the subdwarfs' envelopes. This opacity peak in turn is dependent on a local overabundance of iron, which is achieved by the competitive action of gravitational settling and radiative levitation. As the relative contributions of these two processes are determined by the surface gravity and the effective temperature of the star, all pulsating subdwarfs should lie in a designated instability strip on the $\log g - T_{\rm eff}$ diagram. To date, the number of known EC 14026 stars has risen to 33 (see Kilkenny 2002, Silvotti et al. 2002, Billères et al. 2002, and Fontaine et al. 2004 for a recent census), all of which fall into the theoretically predicted instability strip, clustering around $\log g \sim 5.75$ and $T_{\rm eff} \sim 33{,}000$. Since theoretical and observed pulsational properties are in good agreement, it is believed that a qualitative understanding of the pulsation mechanism has been reached. Beyond this, detailed quantitative interpretations of observed period spectra have been possible in a few instances (Brassard et al. 2001; Charpinet et al. 2003, 2005), allowing the identification of the modes excited through the so-called forward method. Being the ultimate

goal in asteroseismology, this led to the determination of the stars' fundamental parameters, including the mass fraction of the thin hydrogen shell which cannot be deduced otherwise. It goes without saying that independent observational tests of these mode identifications would be most welcome. In particular, the dense period spectra detected in certain EC 14026 pulsators force the controversial inclusion of modes with $l = 3$ and 4 in the asteroseismological process, since there are not enough theoretical modes with $l = 0$, 1, and 2 to account for the mode density observed.

Long-period variables constitute a newer, less extensively studied class of subdwarf B pulsator. Their variability was first announced by Betsy Green at the "Asteroseismology across the H-R diagram" conference held in Porto in July 2002 (Green et al. 2003a; see also Green et al. 2003b). Slowly pulsating sdB stars are distinctly cooler than their short period counterparts and show multi-periodic, low-amplitude ($\sim$ 1 milli-magnitude) luminosity variations with typical periods between 0.8 and 1.6 hours. These are about a factor of 30 longer than those of the EC 14026 stars, and automatically imply high radial order gravity modes (g-modes). Early ideas on a possible excitation mechanism for this new class of star included tidal excitation in a close binary system (Fontaine et al. 2003a) and a mechanism involving a slow reviving of the hydrogen shell (Green et al. 2003a), but proved unfruitful. A much more promising mechanism capable of qualitatively explaining the observed periods was brought forward more recently (Fontaine et al. 2003b) and involves the same driving process that so successfully explains the instabilities in the EC 14026 stars. The excitation by the κ mechanism of two neighbouring classes of pulsator on the H-R diagram is analogous to the case of the β Cep/slowly pulsating B stars on the main sequence (Dziembowski & Pamyatnykh 1993; Dziembowski, Moskalik, & Pamyatnykh 1993; Gautschy & Saio 1993).

In their paper describing the excitation mechanism in the slow pulsators, Fontaine et al. (2003b) built a series of representative models of subdwarf B stars along the Extreme Horizontal Branch and computed their non-adiabatic pulsation properties in a wide range of periods for modes with $l = 0$ to $l = 8$. This uncovered two distinct "islands" of instability in the pulsational period vs $T_{\rm eff}$ diagram (as can be seen in their Figure 4). The first of these is clustered around $T_{\rm eff} \sim 31,000$ K and corresponds to the short period, low-order p-modes

typical of the EC 14026 stars, where modes with degree values of $l = 0$ and upward are driven. The second region of instability, attributed to the long period pulsators, lies at lower temperatures between 22,000 and 26,000 K and features g-modes with long periods similar to those observed in the slow oscillators. However, in the majority of models only modes with degree indices of $l = 3$ and higher can currently be excited, which would imply that the long-period luminosity variations observed in the cooler subdwarfs correspond to modes with $l = 3$, 4, and 5. This is in conflict with canonical wisdom, which suggests that modes with $l \geq 3$ should generally not be observable due to cancellation effects when integrating over the visible disk of the star. While Fontaine et al. (2003b) argue that the low amplitudes of the variations observed point to modes of relatively high degree indices, they concede that the instability calculations are subject to a real blue-edge problem. In particular, we now know of long-period pulsators with effective temperatures as high as $\sim 28,000$ K, which according to current theory should excite only modes with $l \geq 8$. As it does not seem feasible that these could be observed even in the best of circumstances, it is clear that we face major challenges as far as mode identification for the slow pulsators is concerned. However, there is scope for improvement on the theoretical side. Following a suggestion of Hideyuki Saio, we are currently developing more realistic subdwarf B star models that incorporate the presence of helium in the iron radiative levitation calculations, rather than adopting the pure hydrogen background assumed by Fontaine et al. (2003b). While this may well lead to a better description of the PG 1716 stars' blue edge, we nevertheless feel it would be highly beneficial if the degree indices of the periods observed could be determined using a method completely independent of the instability calculations.

The best way of achieving this is to exploit the wavelength dependence of a mode's pulsational amplitude, which depends on l as well as on other parameters such as the viewing angle and the intrinsic amplitude of the oscillation in question. By calculating the ratio of amplitudes in different wavebands, the latter unknown quantities can be eliminated, leaving (to a first approximation) a dependence only on l and the atmospheric parameters of the star. The theoretical colour-amplitude ratios can thus be computed for a given target and compared to pulsational amplitudes from multi-colour photometry in order to determine the

modes' degree indices. Likewise, phase shifts between oscillations in different wavebands may be exploited in certain cases. This method is by no means revolutionary and has been applied to many different types of pulsating star, such as δ Scuti stars (Garrido, García-Lobo, & Rodriguez 1990), β Cepheids (Cugier, Dziembowski, & Pamyatnykh 1994), ZZ Ceti white dwarfs (Robinson et al. 1995; Fontaine et al. 1996), and γ Doradus stars (Breger et al. 1997), to name just a few. Attempts to understand the observed period spectrum on the basis of multi-colour photometry have also been made for EC 14026 stars, first by Koen (1998) and more recently by Jeffery et al. (2004). The former study gives a qualitative interpretation of the periods observed for KPD 2109+4401 based on the theory of Watson (1988), while the latter asserts to have provisionally identified the modes detected for the fast oscillators KPD 2109+4401 and HS 0039+4302. In this case, the identification is based on amplitude ratios computed by Ramachandran, Jeffery, & Townsend (2004) as well as on comparisons with the pulsational properties of the evolutionary sequences published by Charpinet et al. (2002).

In the present study, we assess the potential of multi-colour photometry for pulsating sdB stars in some detail. Using a grid of specially designed model atmospheres, we are able to compute vital quantities such as the emergent specific intensities and their derivatives with respect to effective temperature and surface gravity to high accuracies. Moreover, we carry out full non-adiabatic pulsation calculations in order to obtain eigenfunctions that are as realistic as possible, an aspect that was not studied by Ramachandran et al. (2004). In the next section, we briefly review the theory of colour-amplitude variations in pulsating stars. We then describe our computations for subdwarf B stars, and present results for a representative EC 14026 and PG 1716 model before examining the influence of the atmospheric parameters of the model in question. We end with a discussion of the practical applications of the tools developed.

3.3 BASIC THEORY

The theoretical foundations for the modelling of light curves of a star undergoing non-radial pulsations in the linear regime were laid by the pioneering calculations of Osaki (1971), Dziembowski (1977), Balona & Stobie (1979), and Buta & Smith (1979). Based on the Baade-

Wesselink technique, their work exploited the wavelength dependence of a pulsational mode's amplitude and phase and enabled the inference of its degree index l based on light and radial velocity observations. The equations were reformulated by Stamford & Watson (1981) and Watson (1988) for use with multi-colour photometric data alone. Their approach proved very convenient for practical purposes, and has been applied to many types of non-radially pulsating stars by a host of different authors. More recent versions, comparable in scope to the Watson method, have been presented by Cugier, Dziembowski, & Pamyatnykh (1994), Heynderickx, Waelkens, & Smeyers (1994), Balona & Evers (1999), Cugier & Daszyńska (2001), and Townsend (2002). The latest advancement was proposed by Dupret et al. (2003) and consists of including a detailed discussion of non-adiabatic effects in the optically-thin atmospheric layers. All of the above treatments model the light curves of non-radially pulsating stars in terms of perturbations to the photospheric pressure or surface gravity, the effective temperature and the stellar radius. For cases where temperature effects completely dominate the brightness variations – in pulsating white dwarfs for instance – a simpler approach is possible, as was first discussed by Robinson, Kepler and Nather (1982) and later exploited for ZZ Ceti white dwarfs by Brassard, Fontaine, & Wesemael (1995, hereafter BFW95). For our application to pulsating sdB stars below, we mostly follow the presentations of Cugier and Daszyńska (2001) and Townsend (2002), but adopt a notation closer to that of BFW95.

The Lagrangian perturbations to the stellar radius R, the effective temperature $T_{\rm eff}$, and surface gravity g_s caused by a single non-radial pulsation may be expressed as

$$\frac{\delta R}{R}(\theta,\phi,t) = \Re\left[\frac{\delta r}{r^0}Y_l^m(\theta,\phi)e^{i\omega t}\right], \tag{3.1}$$

$$\frac{\delta T_{\rm eff}}{T_{\rm eff}}(\theta,\phi,t) = \Re\left[\frac{\delta T}{T^0}Y_l^m(\theta,\phi)e^{i\omega t}\right], \tag{3.2}$$

$$\frac{\delta g_s}{g_s}(\theta,\phi,t) = \Re\left[\frac{\delta g}{g^0}Y_l^m(\theta,\phi)e^{i\omega t}\right], \tag{3.3}$$

where $\Re[...]$ denotes the real part of a complex quantity, ω is the complex angular eigenfrequency of the mode (we define $\omega_{nlm} \equiv \Re[\omega] = 2\pi/P_{nlm}$, where P_{nlm} is the pulsation period of a mode of radial order n, harmonic degree l and azimuthal order m), t is the time coordinate, $Y_l^m(\theta,\phi)$ is the usual spherical harmonic function describing the angular dependence of the

mode, and $\frac{\delta r}{r^0}$, $\frac{\delta T}{T^0}$ and $\frac{\delta g}{g^0}$ are the radial components of the complex eigenfunctions. We define the spherical harmonics in terms of the polar angle θ and the azimuthal angle ϕ using the nomenclature of Jackson (1975) as

$$Y_l^m(\theta,\phi) = \sqrt{\frac{2l+1}{4\pi}\frac{(l-m)!}{(l+m)!}} P_l^m(\cos\theta) e^{im\phi}, \tag{3.4}$$

where the associated Legendre functions P_l^m can be generated by the equation

$$P_l^m(x) = \frac{(-1)^m}{2^l l!}(1-x^2)^{m/2}\frac{d^{l+m}}{dx^{l+m}}(x^2-1)^l. \tag{3.5}$$

With this definition, we may introduce the real quantity

$$\bar{Y}_l^m(\theta) \equiv Y_l^m(\theta,\phi)e^{-im\phi}, \tag{3.6}$$

which will be useful below and is described in more detail by BFW95. The radial components of the complex eigenfunctions may be written as

$$\frac{\delta r}{r^0} = \left|\frac{\delta r}{r^0}\right| e^{i\phi_r} \equiv \epsilon_r e^{i\phi_r}, \tag{3.7}$$

$$\frac{\delta T}{T^0} = \left|\frac{\delta T}{T^0}\right| e^{i\phi_T} \equiv \epsilon_T e^{i\phi_T}, \tag{3.8}$$

$$\frac{\delta g}{g^0} = \left|\frac{\delta g}{g^0}\right| e^{i\phi_g} \equiv \epsilon_g e^{i\phi_g}, \tag{3.9}$$

where we have introduced the dimensionless amplitudes (moduli) ϵ_r, ϵ_T and ϵ_g of the complex radial eigenfunctions, as well as their phases ϕ_r, ϕ_T and ϕ_g with respect to some arbitrary value, which by convention is set to $\phi_r = 0$. Note that the upper script " ^{0} " indicates the unperturbed value of the variable of interest in the atmospheric layers.

In the Watson approach, the brightness variation of a non-radially pulsating star is calculated by assuming a dependence of the local flux on the local instantaneous effective temperature and surface gravity, and then integrating over the observed disk taking into account the geometry of the mode and the radial distortions involved. As implemented by Townsend (2002), the first order perturbation to the emergent Eddington flux of a star undergoing a single

non-radial pulsation can thus be written in terms of the radial components of the complex eigenfunctions detailed in equations 3.7−3.9 as

$$\frac{H_\nu^1}{H_\nu^0} = \Re\Bigg[\Bigg(\left\{(2+l)(1-l)\frac{\delta r}{r^0}\frac{I_{l\nu}^0}{I_{0\nu}^0}\right\} + \left\{\frac{\delta T}{T^0}\frac{1}{I_{0\nu}^0}\frac{\partial I_{l\nu}^0}{\partial \ln T^0}\right\} + \\ + \left\{\frac{\delta g}{g^0}\frac{1}{I_{0\nu}^0}\frac{\partial I_{l\nu}^0}{\partial \ln g^0}\right\}\Bigg) Y_l^m(\theta_0,\phi_0)e^{i\omega t}\Bigg]. \tag{3.10}$$

Keeping with the notation of BFW95, H_ν^0 is the unperturbed emergent monochromatic Eddington flux, H_ν^1 is its first-order perturbation, and $I_{l\nu}^0$ is the angle-integrated unperturbed emergent monochromatic specific intensity

$$I_{l\nu}^0 = \int_0^1 I_\nu^0(\mu) P_l(\mu)\mu d\mu, \tag{3.11}$$

with a weight function given by a Legendre polynomial $P_l(\mu)$. The angles (θ_0, ϕ_0) are the angular coordinates of the observer in the spherical coordinate system of the star. The quantity $I_{0\nu}^0$ refers to the specific case of $I_{l\nu}^0$ where the degree index $l = 0$. It is also understood that the derivative of $I_{l\nu}^0$ with respect to the effective temperature T^0 (surface gravity g^0) is taken at constant surface gravity (effective temperature).

In order to simplify equation (3.10) and to enable the eventual elimination of the intrinsic amplitude of the oscillation by taking flux ratios obtained at different wavelengths, it is necessary to link the radial components of the three eigenfunctions. By convention, we express the surface gravity and temperature perturbations in terms of the radius eigenfunction. Regarding the former, Cugier and Daszyńska (2001; see also Dupret et al. 2003) have argued that one may approximate

$$\frac{\delta g}{g^0} \simeq -(2+\sigma_{nlm}^2)\frac{\delta r}{r^0} \equiv -D_{nlm}\frac{\delta r}{r^0} \tag{3.12}$$

in the limit where the radial gradient of the amplitude of the pressure perturbation ($|\delta P/P^0|$) is small. The real dimensionless quantity σ_{nlm} is given by

$$\sigma_{nlm} \equiv \omega_{nlm}\sqrt{\frac{R}{g_s}}, \tag{3.13}$$

where R is the stellar radius and g_s is the surface gravity. Given the definition of $\delta r/r^0$ and $\delta g/g^0$ in equations (3.7) and (3.9), the relationship implies that the radius and surface gravity variations occur in phase, i.e., $\phi_g = \phi_r$ (=0, by convention). It must be mentioned that equation (3.12) differs from the more standard expression employed in the Watson approach (see, e.g., equation (11) of Cugier et al. (1994)), which suggests

$$\frac{\delta g}{g^0} \simeq -\left(4 + \sigma_{nlm}^2 - \frac{l(l+1)}{\sigma_{nlm}^2}\right)\frac{\delta r}{r^0} \equiv -C_{nlm}\frac{\delta r}{r^0}. \tag{3.14}$$

In the original theory outlined by Stamford and Watson (1981) and Watson (1988), the coefficient C_{nlm} is multiplied by an additional term of order unity denoted by $P^*(\equiv \partial \log g^0/\partial \log P^0|_{\tau=1})$ when used in the context of equation (3.14). There has been some debate as to the proper value to adopt for P^*, with some authors (e.g., Cugier et al. 1994, Balona & Evers 1999, Townsend 2002) arguing that it should be taken strictly at unity, while most others employ grids of model atmospheres to compute precise values. Regardless of whether or not the P^* quantity is included in equation (3.14), the expression remains considerably different from that recommended by Cugier and Daszyńska (2001; our equation (3.12)), particularly when considering long period modes. The latter is deemed more physical, as it is more consistent with the outer boundary conditions employed during pulsation calculations for a stellar model. We thus adopt the result of Cugier and Daszyńska (2001) after verifying that we do indeed find $|\delta P/P^0|$ to be mostly flat in the atmospheric layers of our subdwarf B star models (as discussed below).

The radial component of the temperature eigenfunction for its part may be related to the radius perturbation by the expression

$$\frac{\delta T}{T^0} = \frac{\left|\frac{\delta T}{T^0}\right|}{\left|\frac{\delta r}{r^0}\right|} e^{i(\phi_T - \phi_r)}\frac{\delta r}{r^0} \equiv \frac{\epsilon_T}{\epsilon_r} e^{i\psi_T}\frac{\delta r}{r^0}, \tag{3.15}$$

where we have introduced ψ_T as the phase lag between the temperature and the radius perturbation. In the adiabatic approximation, we set $\psi_T = \pi$, since maximum temperature occurs at minimum radius for p-modes. In the non-adiabatic case, the phase lag can be evaluated

using

$$\psi_T = \tan^{-1}\left(\frac{\Im\left[\frac{\delta T}{T^0}\right]}{\Re\left[\frac{\delta T}{T^0}\right]}\right) - \tan^{-1}\left(\frac{\Im\left[\frac{\delta r}{r^0}\right]}{\Re\left[\frac{\delta r}{r^0}\right]}\right), \tag{3.16}$$

where $\Im[...]$ indicates the imaginary part, and $\Re[...]$ denotes the real part of a complex quantity. We will apply this relation to detailed non-adiabatic calculations with the aim of modelling ψ_T as a function of depth, period, and degree index l below.

In the standard Watson approach, it is customary to introduce a second dimensionless real parameter R, which measures the departure from adiabacity of the amplitude factor in equation (3.15), and can hence be defined as

$$R \equiv \frac{\epsilon_T/\epsilon_r}{\left|\left(\frac{\delta T}{T^0}\right)_{ad}\right| / \left|\left(\frac{\delta r}{r^0}\right)_{ad}\right|}. \tag{3.17}$$

It is obvious that, in the adiabatic limit, R=1. As for the non-adiabatic case, many authors seem to believe that physically acceptable values of R are confined to the range $0 \leq R \leq 1$. We beg to differ, since we see no physical reason for R not to exceed 1 and, indeed, find no justification for the constraint in the literature. As far as we can see, it arose primarily from the fact that observations of certain types of pulsating stars (such as the β Cephei, δ Scuti and short-period Cepheids mentioned by Stamford & Watson 1981) indicated $0.25 \leq R \leq 1$. While similar values have been recovered computationally for other classes of pulsator (see, e.g., Townsend 2002 describing slowly pulsating B stars), predictions for white dwarfs have yielded R values greater than 1 in some cases (Robinson, Kepler, & Nather, 1982). This is also what our pulsation calculations indicate for the slowly pulsating subdwarf B stars, as will be decribed in the next section.

The quantities appearing in the denominator of equation (3.17) can be described by recalling a well-known expression relating the moduli of the temperature perturbation and the radius perturbation under the assumption of adiabacity and the Cowling approximation, namely

$$\left|\left(\frac{\delta T}{T^0}\right)_{ad}\right| = -\nabla_{ad} C_{nlm} \left|\left(\frac{\delta r}{r^0}\right)_{ad}\right|, \tag{3.18}$$

where $\nabla_{ad}(= 1 - \Gamma_2^{-1})$ is the usual adiabatic temperature gradient and C_{nlm} is the same

coefficient as introduced in equation (3.14). Here the eigenfunctions $(\delta T/T^0)_{ad}$ and $(\delta r/r^0)_{ad}$ are real quantities, and the minus sign corresponds to a phase shift of $\psi_T = \pi$. Using this relation together with the definition of R, we can reformulate equation (3.15) to yield

$$\frac{\delta T}{T^0} = R\nabla_{ad} C_{nlm} e^{i\psi_T} \frac{\delta r}{r^0}. \tag{3.19}$$

Note that, in practice, the most direct way of computing the relationship between $\delta T/T^0$ and $\delta r/r^0$ is to use equation (3.15), calculating their relative phase ψ_T from equation (3.16), and evaluating their amplitude ratio using

$$\frac{\epsilon_T}{\epsilon_r} = \frac{\left\{\left(\Re\left[\frac{\delta T}{T^0}\right]\right)^2 + \left(\Im\left[\frac{\delta T}{T^0}\right]\right)^2\right\}^{1/2}}{\left\{\left(\Re\left[\frac{\delta r}{r^0}\right]\right)^2 + \left(\Im\left[\frac{\delta r}{r^0}\right]\right)^2\right\}^{1/2}}. \tag{3.20}$$

In addition, we then explicitly evaluate the adiabacity parameter R using equation (3.19). This will prove useful in numerical experiments aimed at assessing the impact of non-adiabatic effects on the predicted pulsational amplitudes and phases in different filters, as ψ_T and R can be input directly and set to the adiabatic values for instance.

Returning to equation (3.10), the expression describing the perturbation to the emergent Eddington flux, we now seek to reformulate the intensity terms and link them to both the BFW95 and the standard Watson (1988) notation. It can be shown that the specific intensity term appearing in the temperature perturbation can be related to the monochromatic quantity $A_{l\nu}$ defined by BFW95 by the expression

$$\frac{1}{I^0_{0\nu}} \frac{\partial I^0_{l\nu}}{\partial \ln T^0} = \frac{T^0 A_{l\nu}}{H^0_\nu}, \tag{3.21}$$

where, according to equation (17) of BFW95,

$$A_{l\nu} = \frac{1}{2}\int_0^1 \frac{\partial I^0_\nu}{\partial T^0} P_l(\mu)\mu d\mu. \tag{3.22}$$

By following the steps described in Appendix B of BFW95, we can re-write equation (3.21)

using the notion of the limb-darkening law $h_\nu(\mu)$ as

$$\frac{1}{I^0_{0\nu}}\frac{\partial I^0_{l\nu}}{\partial \ln T^0} = \alpha_{T\nu} b_{l\nu} + \frac{\partial b_{l\nu}}{\partial \ln T^0}, \tag{3.23}$$

where

$$\alpha_{T\nu} \equiv \frac{\partial \ln H^0_\nu}{\partial \ln T^0}, \tag{3.24}$$

and

$$b_{l\nu} \equiv \frac{\int_0^1 h_\nu(\mu) P_l(\mu) \mu d\mu}{\int_0^1 h_\nu(\mu) \mu d\mu}. \tag{3.25}$$

The two last quantities (the logarithmic derivative of the emergent flux with respect to the effective temperature, and the weighted monochromatic limb darkening integral) are familiar notions in the Watson model. It can be seen that, when expressing the intensity term of the temperature perturbation, one has the choice of using a single expression such as the left-hand side of equation (3.23) employed by BFW95 or Townsend (2002), or the split terms on the right hand side of the equation favoured in the more traditional implementations of the Watson model. We choose to adopt the latter here in order to facilitate comparisons with the Watson approach.

Clearly, the specific intensity component of the gravity perturbation in equation (3.10) can be expressed in an equivalent way, yielding

$$\frac{1}{I^0_{0\nu}}\frac{\partial I^0_{l\nu}}{\partial \ln g^0} = \alpha_{g\nu} b_{l\nu} + \frac{\partial b_{l\nu}}{\partial \ln g^0}, \tag{3.26}$$

with

$$\alpha_{g\nu} \equiv \frac{\partial \ln H^0_\nu}{\partial \ln g^0}. \tag{3.27}$$

Finally, we use the fact that

$$I^0_\nu(\mu) = I^0_\nu(0) h_\nu(\mu) \tag{3.28}$$

together with the definition of $I^0_{l\nu}$ (equation (3.11)) and equation (3.25) to reformulate the

specific intensity coefficient in the radius term of equation (3.10) as

$$\frac{I^0_{l\nu}}{I^0_{0\nu}} = b_{l\nu}. \tag{3.29}$$

We can now re-write the perturbation to the relative instantaneous emergent monochromatic Eddington flux of equation (3.10), using equations (3.12), (3.19), (3.23), (3.26) and (3.29), as

$$\begin{aligned}\frac{H^1_\nu}{H^0_\nu} = \epsilon_r \bar{Y}^m_l(i)\Bigg[& \left\{(2+l)(1-l)b_{l\nu} - D_{nlm} b_{l\nu}\alpha_{g\nu} - D_{nlm}\frac{\partial b_{l\nu}}{\partial \ln g^0}\right\} \\ & \times \cos(m\phi_0 + \omega_{nlm}t) + \\ & + \left\{R\nabla_{ad}C_{nlm}b_{l\nu}\alpha_{T\nu} + R\nabla_{ad}C_{nlm}\frac{\partial b_{l\nu}}{\partial \ln T^0}\right\} \\ & \times \cos(m\phi_0 + \omega_{nlm}t + \psi_T)\Bigg],\end{aligned} \tag{3.30}$$

where we used the fact that $\theta_0 = i$, the inclination angle, in $\bar{Y}^m_l(i)$, the real function giving the viewing aspect (see BFW95 for details).

In practice, the last equation will be applied to broadband, rather than monochromatic photometry, so it is necessary to express it in terms of frequency-integrated quantities. We thus introduce

$$b_{lx} \equiv \frac{\int_0^\infty W^x_\nu b_{l\nu} d\nu}{\int_0^\infty W^x_\nu d\nu}, \tag{3.31}$$

$$\alpha_{Tx} \equiv \frac{\int_0^\infty W^x_\nu \alpha_{T\nu} d\nu}{\int_0^\infty W^x_\nu d\nu}, \tag{3.32}$$

$$\alpha_{gx} \equiv \frac{\int_0^\infty W^x_\nu \alpha_{g\nu} d\nu}{\int_0^\infty W^x_\nu d\nu}, \tag{3.33}$$

where W^x_ν represents the transmission function for filter x, convolved, in principle, with the response of the telescope/detector combination and the atmospheric extinction curve at a given site.

We can now regroup the various components of equation (3.30) into five terms analogous to those employed in the traditional Watson model. We thus introduce the following short-hand

notation:

$$T_1 \equiv R\nabla_{ad} C_{nlm} b_{lx} \alpha_{Tx}, \tag{3.34}$$

$$T_2 \equiv R\nabla_{ad} C_{nlm} \frac{\partial b_{lx}}{\partial \ln T^0}, \tag{3.35}$$

$$T_3 \equiv (2+l)(1-l) b_{lx}, \tag{3.36}$$

$$T_4 \equiv -D_{nlm} b_{lx} \alpha_{gx}, \tag{3.37}$$

$$T_5 \equiv -D_{nlm} \frac{\partial b_{lx}}{\partial \ln g^0}. \tag{3.38}$$

We finally follow Koen (1998) and define

$$\gamma_1 \equiv T_1 + T_2, \tag{3.39}$$

$$\gamma_2 \equiv T_3 + T_4 + T_5, \tag{3.40}$$

which represent the effects on the brightness variation during a pulsation cycle due to effective temperature (γ_1) and radius/gravity perturbations (γ_2) respectively. Using a trigonometric identity we may then obtain our final expression for the relative flux in a photometric band pass x arising from the excitation of a single pulsation mode

$$\frac{H_x^1}{H_x^0} = \epsilon_r \bar{Y}_l^m(i) A_{nlm}^x \cos(m\phi_0 + \omega_{nlm} t + \phi_{nlm}^x), \tag{3.41}$$

with the wavelength-dependent amplitude given by

$$A_{nlm}^x = (\gamma_1^2 + \gamma_2^2 + 2\gamma_1\gamma_2 \cos\psi_T)^{1/2}, \tag{3.42}$$

and the wavelength-dependent phase given by

$$\phi_{nlm}^x = \tan^{-1}\left(\frac{\gamma_1 \sin\psi_T}{\gamma_1 \cos\psi_T + \gamma_2}\right). \tag{3.43}$$

Strictly speaking, this expression is valid only for non-rotating stars where the amplitude and phase depend on the radial order n and the degree index l, but not the azimuthal order

m. However, Cugier & Daszyńska (2001) have argued that it may also be applied to slowly rotating stars, loosely defined as those with a spin parameter $S = 2\Omega/\omega_{nlm} < 0.5$ (where Ω is the rotation frequency). In this case, the $\omega_{nlm}t$ term in the cosine function of equation (3.41) is replaced by $(\omega_{nlm} - m\Omega)t$. The amplitude and phase also become sensitive to the azimuthal index m, but only through the period dependence of an m component in a rotationally split $(2l+1)$ multiplet. For fast rotators with higher values of S, things become more complicated and a rigorous treatment such as the one developed by Townsend (2003) becomes necessary.

In practice, equation (3.41) is not used directly since it depends on the unknown factor $\epsilon_r \bar{Y}_l^m(i)$. Instead, we take advantage of the wavelength independence of the latter and eliminate it by calculating the amplitude ratios A^x_{nlm}/A^y_{nlm} and phase differences $\phi^x_{nlm} - \phi^y_{nlm}$ arising from the light curves for two different band passes x and y. Mode discrimination can then proceed by exploiting the fact that the wavelength dependence of an oscillation's amplitude and phase may depend strongly on its degree index l, and that observational amplitude ratios and phase differences are readily obtainable from multi-colour photometry.

We note that if non-adiabatic effects are neglected in the calculations of the theoretical quantities, then $\psi_T = \pi$, the phase ϕ_{nlm} calculated from equation (3.43) will always be zero, and no phase shifts will be predicted between different band passes. However, a small or negligible observed phase shift does not necessarily imply the absence of non-adiabatic effects, and one may well encounter situations where the expected phase shifts remain quite small despite important deviations of the adiabacity parameter R from its adiabatic value of $R = 1$. This is the case for our model of a typical EC 14026 star discussed below. On the other hand, the observed phase shifts will be expected to be negligible if effective temperature perturbations completely dominate the brightness variation and radius/surface gravity effects can safely be ignored ($\gamma_2 = 0$ in the limiting case). In that instance, equation (3.43) immediately infers $\phi^x_{nlm} = \psi_T$ irrespective of the band pass in question. Moreover, the period dependence of the T_1 and T_2 terms through their common factor RC_{nlm} cancels out in the calculation of the amplitude ratios, with the result that the latter bear the signature only of the degree index l and not the period dependent radial order n. By the same logic, the amplitude ratios are no longer affected by non-adiabatic effects, a point on which we concur with Ramachandran et

al. (2004). In retrospect, this alleviates the worry expressed by Robinson et al. (1982) about the legitimacy of using the adiabatic relationship between $\delta T/T^0$ and $\delta r/r^0$ in their discussion of colour variations in pulsating white dwarfs (see also BFW95). When considering the pulsations of white dwarfs in the linear regime, the brightness variations are completely dominated by temperature effects, which implies an absence of phase shifts between the light curves of different colours, as well as amplitude ratios insensitive to non-adiabatic effects and the period of the mode in question. The latter then depend only on the degree index l, a situation also encountered for high-order g-modes in our typical PG 1716 star model discussed below.

3.4 MODEL ATMOSPHERES AND MONOCHROMATIC QUANTITIES

The quantities required in the theoretical framework discussed above can broadly be divided into three groups: those that can be inferred observationally, those that must be computed on the basis of full stellar models, and finally those that are derived from model atmospheres. In this section we focus on the latter group, which includes the monochromatic quantities $\alpha_{T\nu}$, $\alpha_{g\nu}$, $b_{l\nu}$, $b_{l\nu,T} \equiv \partial b_{l\nu}/\partial \ln T^0$, and $b_{l\nu,g} \equiv \partial b_{l\nu}/\partial \ln g^0$. Since their computation involves not only the standard specific intensities, but also the corresponding derivatives with respect to effective temperature and surface gravity across the visible disk, we needed to modify our model atmosphere code (a continuously evolving LTE code developed and maintained by Pierre Bergeron) for subdwarf B stars in order to carry out the task efficiently and accurately. We constructed a grid of model atmospheres defined at 9 gravity points ($\log g$ = 4.8 to 6.4 in steps of 0.2 dex) and 11 temperature points ($T_{\rm eff}$ = 20,000 to 40,000 K in steps of 2000 K) representative of the distribution of sdB stars in the $\log g - T_{\rm eff}$ plane. Detailed interpolation within this grid enables the calculation of the desired quantities for any given $\log g - T_{\rm eff}$ combination. The model atmospheres are computed under the assumption of LTE and uniform composition specified by $\log N(He)/N(H) = -2.0$, a typical value for sdBs. Metals were not included, since subdwarf B stars are known to be chemically peculiar, and metal abundances vary from one target to the next. While it could prove interesting to incorporate representative

metal abundances and thus assess the importance of metals in this kind of calculation in the future, our H/He LTE model grid is quite sufficient for the purposes of this study.

As mentioned above, the colour-amplitude technique is usually applied to broadband photometry, but we find it instructive to first examine the behaviour of the key monochromatic quantities. We begin with the unperturbed emergent Eddington flux, which is shown in the top panel of Figure 3.1 in the optical domain for a model with $T_{\rm eff} = 33{,}000$ K and $\log g = 5.75$. These are also the atmospheric parameters we adopt for our representative EC 14026 star model in the next section, where more details are provided. As is typical for the observed optical spectra of sdB stars, the Eddington flux is characterized by the presence of broad hydrogen Balmer lines and several weak and narrow helium lines. For comparison, the middle panel illustrates the predicted first-order perturbation to the emergent Eddington flux assuming a nonradial pulsation with a period of 150 s (a typical low-order p-mode in an EC 14026 star) and six values of the degree index from $l = 0$ (top curve) to $l = 5$ (bottom curve). Note that here, H_ν^1 is divided by the unknown factor $\epsilon_r \bar{Y}_l^m(i)$. It is evident that the pulsational amplitude rapidly decreases with increasing l, which is a direct manifestation of the well-known geometric cancellation effects associated with an increasing number of nodal lines crisscrossing the visible disk. For values of $l > 2$, the decrease of the amplitude with increasing l at a given frequency is no longer monotonic, but also depends on the limb-darkening law of the model atmosphere in question in quite a complex way. The amplitude of the $l = 4$ curve for instance is higher than that of the $l = 3$ curve in the optical domain shown, and the latter dips below the $l = 5$ curve above ~ 4000 Å. By dividing the curves by the unperturbed flux H_ν^0, one obtains the *relative* monochromatic amplitude of the assumed mode (again to within the unknown parameter $\epsilon_r \bar{Y}_l^m(i)$), as indicated in the bottom panel of the figure. It is the latter quantity that forms the basis of the colour-amplitude technique, which relies on comparing the relative amplitude at two wavelengths in order to eliminate the unknown factor.

The result of such an operation is illustrated in Figure 3.2, where we have divided the relative monochromatic amplitude curves for each l by the corresponding relative amplitude at an (arbitrary) frequency point in the continuum with $\lambda = 3650$ Å. In this particular example, there is little difference between curves with $l = 0$, 1, and 2, however those with $l = 3$, 4, and

5 bear a stronger and more distinct signature of their degree index. Along with the amplitude ratios, the phase differences between the brightness variations at different wavelengths may also be used to infer the degree l of a pulsation mode. This is shown in Figure 3.3, where we plot the monochromatic phase difference with respect to the spectral point at 3650 Å for the same assumed pulsation mode with a period of 150 s and l values from 0 to 5 as indicated. In our example, the phase shifts remain relatively small (less than a few degrees) over the optical domain. This implies that, in practice, mode discrimination will be difficult to achieve on the basis of phase differences alone.

The amplitude ratios and phase shifts discussed in the following sections are simply frequency-integrated counterparts to the monochromatic curves pictured in the last two figures. In this context it should be noted that the spikes associated with the central cores of the absorption lines, and in particular those related to the narrow helium lines, do not significantly contribute to the band pass integrated quantities. We would once again like to emphasise that the behaviour of the amplitude ratios and phase shifts with wavelength depends not only on the degree index l, but also on the period of the mode and, of course, on the atmospheric parameters of the model in question.

3.5 NONADIABATIC EFFECTS IN REPRESENTATIVE MODELS OF PULSATING SDB STARS

We now evaluate the quantities R and ψ_T through the use of full non-adiabatic pulsation calculations. To do this, we use the same numerical tools employed earlier by Charpinet et al. (1997; see also Fontaine et al. 1998, Charpinet et al. 2001, and Fontaine et al. 2003b) to construct their second-generation stellar models. These are characterized by four free parameters, the effective temperature $T_{\rm eff}$, the surface gravity $\log g$, the fractional mass contained in the H-rich envelope $M(H)/M_*$, and the total mass M_*. The models feature an opacity profile that largely depends on the non-uniform distribution of iron as a function of depth. This distribution results from the competition between gravitational settling and radiative levitation and has been shown to be responsible for the excitation of low-order p-modes in

models of EC 14026 stars as well as high-order g-modes in models of PG 1716 stars (Fontaine et al. 2003b) through the κ-mechanism. Note that, according to the same authors, standard models of sdB stars with uniform metallicity are unable to excite pulsation modes.

In this section we will focus on a representative model of an EC 14026 star and a PG 1716 pulsator respectively. According to Figure 1 of Fontaine et al. (2004), which summarizes the location of subdwarf B stars on the H-R diagram, a typical EC 14026 star has $\log g \simeq 5.75$ and $T_{\rm eff} \simeq 33{,}000$ K, which implies that it is significantly denser and hotter than its typical PG 1716 counterpart at $\log g \simeq 5.40$ and $T_{\rm eff} \simeq 27{,}000$ K. We adopt these values, and list some of the models' other characteristics, including the two defining variables $M(H)/M_*$ and M_* in Table 3.1. We explicitly give the value of the total radius as well as that of the adiabatic temperature gradient averaged over the atmospheric layers (see below), as both of these quantities enter into our equations. For completeness, we also provide the value of the quantity P^* evaluated from our model atmosphere grid at the appropriate values of $T_{\rm eff}$ and $\log g$, despite the fact that we do not use that variable in our calculations, since we choose to relate the surface gravity and radius perturbation via the expression developed by Cugier & Daszyńska (2001).

Taking into account the range of periods observed in typical EC 14026 stars, we compute all modes with periods in the range 80−300 s and with values of l from 0 to 5 for our representative short-period pulsator model. For the case of our PG 1716 star model, we calculate modes with periods in the range 2000−6000 s and with values of $l = 1$, 2, and 3. The first results are illustrated in Figures 3.4 and 3.5, where we show the modulus of the radial component of each mode's non-adiabatic pressure eigenfunction as a function of depth in the outermost layers for the EC 14026 and PG 1716 model respectively. We define the "atmospheric layers of interest" as those lying between the optical depths $\tau = 0.1$ and $\tau = 10.0$. It can be seen that about half of the modes considered in the EC 14026 model show small gradients across these layers as is required in the Cugier & Daszyńska (2001) expression connecting the surface gravity perturbation to the total radius perturbation. The other modes, which systematically correspond to those with shorter periods, do not strictly pass this test but, lacking a more generally applicable relation, there is little we can do to remedy this shortcoming. The

situation is better for the PG 1716 model, where the vast majority of the modes considered show very small $|\delta P/P|$ gradients across the atmospheric layers, with the exception of the few modes with the longest periods. As it turns out, we will find out below that surface gravity perturbations contribute very little to the brightness variations in pulsating sdB stars, which is lucky in the context of our present "problems", as any inaccuracies in the surface gravity perturbations will have little impact on the final results.

Figures 3.6a and 3.6b show the behaviour of the adiabaticity parameter R in the atmospheric layers of our EC 14026 model for all modes of interest. Figures 3.7a and 3.7b illustrate similar results for the phase lag ψ_T. The figures give the distinct impression that both R and ψ_T depend primarily on the period and very little on the degree index l. This can, in fact, be confirmed quantitatively by computing an "average" atmospheric value of both quantities for each mode, and plotting them as functions of the mode's period as shown in Figure 3.8. The averaging process used is a simple unweighted integration over all atmospheric layers between $\tau = 0.1$ and $\tau = 10.0$. We believe that this approach is slightly more rigorous than simply taking the local values at the photosphere itself ($\tau = 2/3$). Figure 3.8 highlights the almost perfect one-to-one relationship that exists between the value of $< R >$ and the period of the mode for the range of interest. A similar situation is encountered for the averaged quantity $< \psi_T >$. In both cases there is very little, if any, dependence on the degree index l, allowing us to model $< R >$ and $< \psi_T >$ as functions of the period P in a simple and accurate way (we drop the subscript "nlm" in what follows for a more concise notation). While this is not necessary when examining a specific equilibrium model for which individual values can be obtained for each mode (e.g., the small circles in Figure 3.8), the procedure will prove useful in our applications below, where we want to treat the pulsation period as a free continuous variable rather than a discrete eigenvalue. Values of R and ψ_T sufficiently accurate for our needs were obtained by least squares χ^2-fitting the data points in Figure 3.8 to cubic curves as illustrated. The cubic solutions are given by

$$< R >= 0.3459 - 3.031 \times 10^{-4} P + 1.784 \times 10^{-5} P^2 - 3.040 \times 10^{-8} P^3, \qquad (3.44)$$

and

$$< \psi_T >= \pi + 1.1010 - 1.415 \times 10^{-2} P + 3.702 \times 10^{-5} P^2 - 2.122 \times 10^{-8} P^3, \qquad (3.45)$$

which are formally valid in the period range 80−300 s and for values of the degree index in the range $l = 0$−5. Figure 3.8 reaffirms the well-known fact that non-adiabatic effects are never negligible in stellar atmospheres, but it is the particular dependence of $< R >$ (and $< \psi_T >$) on the period that is of central interest here and that cannot be ignored in the computations. In future studies, the accuracy of the estimates for R and ψ_T could be further improved by examining the non-adiabatic pulsation equations in the presence of optically thin layers more closely, for example by following the theory of Dupret (2001) and Dupret et al. (2003).

The situation is slightly more complicated for the high-order g-modes in our representative PG 1716 model, where R and ψ_T depend on both the period P and the index l as is illustrated in Figures 3.9 and 3.10. The presence of a few trapped modes (trapped above the H-rich envelope/He core interface) renders things somewhat more challenging in terms of defining an "average" behaviour for a pulsation mode. Furthermore, while $< \psi_T >$ depends monotonically on the period for a given l (at least in the period range of interest), this is not the case for $< R >$, making it ever more tedious to acceptably fit the data points. As illustrated in Figure 3.11, we were finally able to find fits to $< R >$ and $< \psi_T >$ sufficiently accurate for our present needs by using the following analytic relationships

$$< R > l^{0.13} = 0.5817 + 6.399 \times 10^{-4} (Pl^{0.38}) - 1.164 \times 10^{-7} (Pl^{0.38})^2 + 6.082 \times 10^{-12} (Pl^{0.38})^3, \qquad (3.46)$$

and

$$< \psi_T >= \pi - 2.30 e^{(Pl^{0.38}/1800)}. \qquad (3.47)$$

Figure 3.11 clearly indicates that non-adiabatic effects are important in the atmospheres of PG 1716 stars, and should not be neglected in the computations. As mentioned in the theory section, the adiabaticity parameter $< R >$ may become larger than 1 for the long period g-modes characteristic of these objects. However, as we will see below, temperature

variations increasingly dominate the brightness variations in the limit of long periods, causing the *observable* effects of a departure from adiabaticity to disappear.

3.6 APPLICATION TO UBVRI PHOTOMETRY

As a representative application, we consider multi-colour photometry in the standard Johnson-Cousins system $UBVRI$. For each reference model (specified by a value of $T_{\rm eff}$ and a value of $\log g$ for the model atmosphere calculations), we computed the frequency-integrated quantities α_{Tx}, α_{gx}, b_{lx}, $b_{lx,T} \equiv \partial b_{lx}/\partial \ln T^0$, and $b_{lx,g} \equiv \partial b_{lx}/\partial \ln g^0$, where the subscript "$x$" denotes one of the wavebands. In our modelling of the effective response curves W_ν^x, we convolved the standard Johnson-Cousins $UBVRI$ transmission curves from Bessell (1990) with the extinction curve of Kitt Peak National Observatory (representative of sites with 2000−2500 m altitudes). We also assumed a grey response for the instrument/telescope combination. Our values for the frequency-integrated quantities are given in Table 3.2 (Table 3.3) for our reference EC 14026 (PG 1716) star model. For the former model, we list the values for modes with degree indices in the range $l = 0{-}5$, while for the latter they are provided for modes with l between 1 and 6 since the case $l = 0$ is of no interest for the long-period variables (as a rule, the p-branch period spectra of sdB stars do not reach into the range of the long periods observed in PG 1716 stars).

We draw attention to the fact that in both Table 3.2 and Table 3.3 $\alpha_{gx} << \alpha_{Tx}$ and $b_{lx,g} << b_{lx,T}$ with only very few exceptions. This means that the T_4 and T_5 terms will generally be very small compared to the T_1 and T_2 terms in the equations discussed in Section 3.2, implying that in sdB stars the contributions to the brightness variations due to surface gravity perturbations are small compared to the effects of effective temperature perturbations (T_1 and T_2) and radius changes (T_3). Thus, the exact expression used to relate the surface gravity perturbation to the radius perturbation (see our discussion of the Cugier & Daszyńska 2001 method versus the more traditional one in Section 3.2) is of minor importance for sdB stars.

Employing the data listed in Tables 3.1, 3.2, and 3.3 as well as our polynomial models for R and ψ_T given by equations (3.44) through (3.47), we computed amplitudes and phases for

a number of modes according to our equations (3.42) and (3.43). The period was treated as a free parameter, which enabled a detailed examination of its influence on the final results. Keeping with tradition, the amplitudes ratios and phase shifts were calculated with respect to the bluest filter, in this case the U band pass. The results for our representative EC 14026 star model and those for our PG 1716 model are discussed separately in the following subsections.

3.6.1 Results for our representative EC 14026 star model

We first show, in Figure 3.12, the ratio $|\gamma_1/\gamma_2|$ as a function of effective wavelength in the five filters considered for three representative periods spanning the range of those observed in a typical EC 14026 pulsator. All the modes illustrated are associated with degree indices $l = 0{-}5$ and correspond to low-order p-modes. Excepting the modes with $l = 1$, for which T_3 is always equal to 0 (see our equation (3.36)), as well as the $l = 3$ modes in the I band pass, for which the contributions of the effective temperature perturbations are particularly small, the figure infers that both effects (i.e., temperature and radius changes) contribute to the brightness variations in a non-negligible way. Unlike for white dwarfs, it is thus not appropriate to assume that temperature effects completely dominate in EC 14026 stars. While we already mentioned that the T_4 and T_5 terms usually remain quite small, it is the T_3 term, whose numerical value dominates γ_2, that becomes appreciable compared to γ_1 $(= T_1 + T_2)$.

In order to assess the importance of non-adiabatic effects, we repeated the calculation of $|\gamma_1/\gamma_2|$, this time imposing the adiabatic values $R = 1$ and $\psi_T = \pi$ for all modes considered. The results are represented by the dotted lines in Figure 3.12. Keeping in mind the logarithmic scale of the ordinate axis, it is obvious that non-adiabatic effects are significant in the composition of brightness variations in EC 14026 pulsators.

Figure 3.13 shows the expected phase shifts for the same set of modes. It can be seen that, in the optical domain, the phase shifts depend on the period quite sensitively, while remaining relatively small and reaching a maximum of a few degrees at the most in the period range of interest. In the adiabatic approximation we expect no phase shifts at all. This means that, in practice, it will be very difficult to exploit the (weak) l dependence of such phase shifts. The situation seems more promising for the amplitude ratios illustrated in

Figure 3.14. However, while the modes with $l = 3$, 4, and 5 bear distinct signatures of their degree index, the capacity to discriminate between modes with $l = 0$, 1, and 2 on the basis of optical photometry appears much more limited. Observational amplitude measurements for such modes will have to be unusually precise if they are to be used as mode discriminators in EC 14026 stars. We would like to point out that non-adiabatic effects on the amplitude ratios are generally non-negligible, as can be deduced by comparing the continuous lines (non-adiabatic results) to the dotted lines (adiabatic values) in Figure 3.14. It may also be worth mentioning that the results depicted in the middle panels of Figures 3.13 and 3.14 (the case with $P = 150$ s) are consistent with the monochromatic results illustrated in Figures 3.2 and 3.3, as is to be expected.

In Figures 3.15a and 3.15b (separated for visualization purposes), we plot the expected amplitude ratios for modes with $P = 100$ s (dotted lines), 150 s (dashed lines), and 200 s (long-dashed lines), with the aim of emphasizing their strong period dependence. In order to compare the results to corresponding period-independent values, we also include amplitude ratios (solid lines) obtained by postulating that effective temperature perturbations completely dominate the brightness variations (i.e. by setting $\gamma_2 = 0$ in the calculations). As suggested above, it becomes evident that this not a good working assumption for the EC 14026 stars.

Finally, in Figure 3.16, we show the results of a numerical experiment in which we explicitly adopt $T_3 = 0$ in order to assess the relative impact of the T_4 and T_5 terms on the amplitude ratios. The resulting period-dependent ratios are indicated by the dotted lines and contrast with the continuous lines corresponding to the period-independent limiting case in which $\gamma_2 = 0$. While we previously argued that the contributions of the T_4 and T_5 terms are generally quite small in pulsating sdB stars, the figure reveals that non-negligible effects remain for certain cases, especially in the B band. We thus recommend that these terms be kept in the calculations, particularly since they are readily computable.

3.6.2 Results for our representative PG 1716 star model

The computations for our reference PG 1716 model uncover two distinct regimes as far as the relative importance of the temperature perturbation is concerned. At the lower end

of the period range of interest, contributions from both the γ_1 and γ_2 terms are significant, whereas the brightness variations are dominated by temperature changes for the longer periods involved. This can be seen from Figures 3.17a and 3.17b, where we show the ratio $|\gamma_1/\gamma_2|$ as a function of effective wavelength in a format similar to that of Figure 3.12. In these and the following figures, we illustrate our results for six different periods between P= 2400 s and P = 6000 s. Comparing Figures 3.17a and 3.17b clearly reveals that the ratio $|\gamma_1/\gamma_2|$ monotonically increases with period for all filters and degree indices l. This is a direct consequence of the the γ_1 term increasing in absolute value with period via the period-dependent coefficient C_{nlm} for the long periods considered, while T_3 remains constant for a given filter and degree index. We recall that modes with $l = 1$ represent a special case, since $T_3 = 0$ in that instance.

This transition from one regime to the other strongly influences the phase shifts and amplitude ratios calculated. The former are depicted in Figures 3.18a and 3.18b for the same set of modes as considered above. For the shorter periods we predict significant phases shifts, which reach more than 10 degrees for the 2400 s period. Unlike the much smaller phase shifts expected for the EC 14026 stars, this is well within achievable measurement accuracy. At the same time, we find the magnitude of the expected phase shifts to drop very rapidly with increasing period in PG 1716 stars (note, in particular, the change of the ordinate scale between Fig. 3.18a and Fig. 3.18b), to the point where they would not be detected with any confidence for the longer period modes.

The expected amplitude ratios are shown in Figures 3.19a and 3.19b. Once again, the transition from the period-dependent regime, where γ_1 and γ_2 are of similar importance, to the period-independent case dominated by effective temperature perturbations is striking. The plots also emphasize the diminishing importance of non-adiabatic effects with increasing period, as can be seen from the convergence of the dotted (adiabatic) and continuous (non-adiabatic) lines. Thus, in our PG 1716 model non-adiabatic effects range from extremely significant for $P = 2400$ s to practically negligible for $P = 6000$ s.

In Figures 3.20a and 3.20b (separated for visualization purposes), we compare the expected amplitude ratios for modes with $P = 3000$ s (dotted lines), 4000 s (dashed lines), 5000 s (long-dashed lines), 6000 s (dot-dashed lines), 7000 s (dot-long-dashed lines), and 8000 s (dashed-

long-dashed lines), again with the aim of highlighting the period dependence of the results. The convergence of the ratios to the period-independent values (solid lines) in the limiting case of long periods is recovered nicely. As before, the period-independent ratios are obtained by assuming that effective temperature perturbations completely dominate the brightness variations (i.e., by setting $\gamma_2 = 0$ in the calculations).

Analogously to the case presented in Figure 3.16 for our EC 14026 model, we carry out supplementary calculations where we explicitly set $T_3 = 0$ in order to assess the relative impact of the T_4 and T_5 terms on the amplitude ratios. The results of this numerical experiment are shown in Figure 3.21. As in Figure 3.16, the resulting period-dependent ratios are indicated by dotted lines and are compared to the solid lines representing the period-independent limiting case for which $\gamma_2 = 0$. In contrast to the previous plot, the contributions of the T_4 and T_5 terms are essentially negligible in PG 1716 stars, apart for in the very shortest periods. For the three longest periods (not illustrated) the two curves are not distinguishable.

Having discussed the signature of the period and the degree index, as well as that of the different terms contributing to the brightness variations on band pass-integrated wavelength, we now focus specifically on results expected from the $U - I$ filter combination (which corresponds to the longest wavelength base in the system used here). Figure 3.22 shows the I to U amplitude ratio as a function of the degree index l on the basis of calculations extending to $l = 8$. From bottom to top, the various curves correspond to periods with $P = 2400$, 3000, 4000, 5000, 6000, 7000 and 8000 s respectively. The top curve represents an infinite period, to which the finite period curves converge in the limiting case. While evident from previous figures, the peculiar behaviour of the l=3 and 5 modes is particularly striking here. In practice, these are the modes most likely to be identified from multi-colour photometry, since the amplitude ratios of the remaining modes may not differ enough to the extent where they can be resolved observationally.

Finally, Figure 3.23 and 3.24 respectively show the I/U amplitude ratio and the $I - U$ phase shift expected for our PG 1716 model as a function of period for modes with l=1 (black), 2 (grey), 3 (blue), 4 (cyan), 5 (green) and 6 (red). Note that here, the periods illustrated were not considered as free parameters, but are the solution of the eigenvalue problem. Once again,

the convergence of values to the period-independent value in the limiting case of long periods is evident. Interestingly, in Figure 3.23 the results for the very shortest periods break with the systematic decrease in amplitude ratio with period, and slightly increase instead. These same periods are associated with particularly large (potentially detectable) phase shifts in Figure 3.24, however it should be noted that these are shorter than the periods so far observed in PG 1716 stars and of primarily theoretical interest.

3.6.3 Results for other models: Dependence on $T_{\rm eff}$ and log g

In this section, we go beyond the two representative subdwarf B star models explored above and discuss the dependence of amplitude ratios and phase differences on the atmospheric parameters $\log g$ and $T_{\rm eff}$. To this end, we constructed a sequence of subdwarf B star models parallel to the zero-age extreme horizontal branch, the vital parameters of which are detailed in Table 3.4. Note that the surface gravity increases with effective temperature, while the thickness of the hydrogen-rich outer layer decreases. The division between the PG 1716 and EC 14026 regime is based on spectroscopically determined values of $\log g$ and $T_{\rm eff}$ for the two types of pulsator, such as those illustrated in Figure 1 of Fontaine et al. (2004). In addition to the fundamental parameters, Table 3.4 also gives the approximate period range in which modes are believed to be excited for each model. For the EC 14026 stars, these correspond to modes that are found to be unstable from our non-adiabatic pulsation calculations, since the latter have been shown to predict the observed period ranges very accurately. Note that we have uniformly decreased the iron abundance in our models by a factor of 3 compared to the original "second-generation" models, as suggested by Fontaine et al. (2003b). In the case of the PG 1716 stars the situation is more complicated due to the discrepancies that still exist between modelled and observed instability regions (see our discussion in the Introduction). We can however constrain the unstable period ranges for the PG 1716 models in our sequence on the basis of the frequencies extracted from long-period variable subdwarfs observed. To date, a quantitative analysis of the period spectrum has been possible for three targets spanning the range of PG 1716 stars in effective temperature: PG 1627+017 at $T_{\rm eff} \sim$ 23,000 K (Randall et al. 2004a), PG 1338+481 at $T_{\rm eff} \sim$ 26,000 K (Randall et al. 2004b) and PG 0101+039 at $T_{\rm eff} \sim$ 28,000 K

(Randall et al. 2005). The study of these objects revealed that the width and mode density of the excited period range, as well as the numerical values of the periods themselves, decrease systematically with increasing temperature, enabling us to infer approximate instability bands for all models in our sequence by interpolation of the observed values. It is these estimated period ranges, rather than precisely modelled quantities, that are given in Table 3.4.

For each model in the sequence, we computed the necessary model atmosphere parameters in the same band passes as used for the representative models for modes with $l = 0 - 6$ according to their specific $\log g - T_{\rm eff}$ combination. The stellar radius was likewise determined for every model on the basis of its mass and surface gravity, and its characteristic periods were evaluated from pulsation theory in the range of interest. On the other hand, the remaining three quantities derived from the full stellar models and non-adiabatic pulsation calculations were approximated to the values determined for the appropriate representative model. Thus the values of $< \nabla_{ad} >$ were taken from Table 3.1, while $< R >$ and $< \psi_T >$ were computed using equations (3.44) and (3.45) or expressions (3.46) and (3.47) for the EC 14026 and PG 1716 models respectively. The resulting accuracy of $< R >$ and $< \psi_T >$ is deemed sufficient for the illustrative purposes sought here, however it is understood that for quantitative analyses of observed multi-colour photometry the fitting process outlined in section 4 will have to be repeated for the designated object.

Figures 3.25 and 3.26 respectively show the phase shifts and amplitude ratios predicted for our sequence of subdwarf B star models from the $I - U$ band pass combination. They are illustrated for modes with $l = 0$ (yellow, EC 14026 stars only), $l = 1$ (black), $l = 2$ (grey), $l = 3$ (blue), $l = 4$ (cyan), $l = 5$ (green) and $l = 6$ (red). Points of different colour are shifted slightly in effective temperature for a given model in order to facilitate viewing and the PG 1716 and EC 14026 domains are separated by the vertical dotted line. From Figure 3.25 we find that the phase shifts predicted are small (less than 5 degrees) for the majority of modes in both EC 14026 and PG 1716 stars, and would most likely lie below the detection threshold of multi-colour observations. Larger phase shifts of up to $\sim$ 10 degrees are expected for the very shortest periods in the hotter PG 1716 variables, as well as for the $l = 3$ modes at the higher end of the period range excited in the hotter EC 14026 stars. While it seems plausible

that the latter could be detected observationally, the potential for mode discrimination in subdwarf B stars clearly lies with the amplitude ratios depicted in Figure 3.26. In the case of the PG 1716 stars, the values for modes with $l = 1$, 2, 4 or 6 are very similar, but can easily be distinguished from those of $l = 3$ or $l = 5$ modes. Even though the three regimes slowly approach each other with increasing temperature, they remain well separated irrespective of the model in question. In the case of the EC 14026 stars, we identify four distinct groups of modes with $l = 0$, 1 or 2, $l = 3$, $l = 5$ and $l = 4$ or 6. Again, the influence of the model parameters is relatively small compared to the separation between the domains and becomes vital only when attempting to discriminate between the modes of a given group.

It should be kept in mind that the results depicted in Figures 3.25 and 3.26 depend not only on the atmospheric parameters of the models in question, but also on the period range excited in each case. As such, they represent the phase shifts and amplitude ratios predicted in real subdwarf B stars and give a good indication of what would be expected from multi-colour photometry. However, in terms of a purely theoretical exploration we find it instructive to examine the impact of both the surface gravity and the effective temperature on the amplitude ratios individually. To this end, we repeated the computation process detailed above for both EC 14026 and PG 1716 stars, keeping the effective temperature (surface gravity) constant at the representative value from Table 3.1, and varying the surface gravity (effective temperature) within the ranges found in the sequences of Table 3.4. We imposed a representative period of $P = 150$ s for the EC 14026 star domain and $P = 4500$ s for the PG 1716 star regime. The variation of the amplitude ratio with effective temperature is illustrated in Figures 3.27a and 3.27b for short- and long-period variable subdwarf B stars respectively (see the figure captions for more detail). For both types of oscillator, the curves are reminiscent of the amplitude ratios found for our sequence of subdwarf B stars presented in Figure 3.26, and change gradually and monotonically with temperature. The situation is more interesting for the variation with surface gravity, depicted in Figure 3.28a (3.28b) for EC 14026 (PG 1716) models. In the case of the fast oscillators, the amplitude ratios for most of the modes move in the opposite direction compared to Figure 3.26, and the closely spaced $l = 0$, 1, 2 graphs seem to diverge from the (constant) $l = 1$ value as the surface gravity increases. For the PG 1716 models,

curves representing modes of different degree indices overlap in several instances, giving rise to a behaviour similar to that encountered as a function of period (see Figure 3.23).

3.7 FEASIBILITY OF APPLICATION TO MULTI-COLOUR DATA

In this section we demonstrate the potential of the method developed by applying it to published multi-colour photometry. To date, the only sets of multi-colour observations that exist for pulsating subdwarf B stars are those of Koen (1998), Falter et al. (2003), Jeffery et al. (2004), and Oreiro et al. (2005). Among these, the Jeffery et al. (2004) data for the fast pulsator KPD 2109+4401 yielded the most accurate amplitude estimates. Based on three nights of Sloan filter u'g'r' photometry with ULTRACAM (Dhillon et al., in preparation) mounted on the 4.2-m William Herschel Telescope, the authors were able to extract seven periodicities in the 180−200 s range. For the purposes of our brief feasibility study, we attempt to determine the degree index of the highest amplitude mode at 182.4 s only.

The first step towards finding the theoretical amplitudes in different wavebands is the calculation of the monochromatic model atmosphere quantities $\alpha_{T\nu}$, $\alpha_{g\nu}$, $b_{l\nu}$, $b_{l\nu,T}$ and $b_{l\nu,g}$ described in Section 3.3. Since these depend quite sensitively on the atmospheric parameters of the target, they need to be computed for KPD 2109+4401 specifically. We adopt $T_{\rm eff}$=31,380 K and $\log g$=5.65 as derived from our model atmosphere fit to the hydrogen Balmer and helium lines present in the time-averaged high-resolution MMT spectrum obtained by Betsy Green (private communication). These values are part of an ongoing program designed to provide homogeneous estimates of the atmospheric parameters of a large sample of subdwarf B stars, and we refer the interested reader to the forthcoming Paper by Green, Fontaine, & Chayer (in preparation) for more information. The monochromatic quantities are then integrated over the effective u'g'r' wavebands, computed by convolving the Sloan band passes with the quantum efficiency curves of the ULTRACAM CCD chips (Vik Dhillon, private communication) and the atmospheric transparency curve of a representative observing site at 2000−3000 m altitude (in this case Kitt Peak National Observatory). Next, we derive the

curves representing modes of different degree indices overlap in several instances, giving rise to a behaviour similar to that encountered as a function of period (see Figure 3.23).

3.7 FEASIBILITY OF APPLICATION TO MULTI-COLOUR DATA

In this section we demonstrate the potential of the method developed by applying it to published multi-colour photometry. To date, the only sets of multi-colour observations that exist for pulsating subdwarf B stars are those of Koen (1998), Falter et al. (2003), Jeffery et al. (2004), and Oreiro et al. (2005). Among these, the Jeffery et al. (2004) data for the fast pulsator KPD 2109+4401 yielded the most accurate amplitude estimates. Based on three nights of Sloan filter u'g'r' photometry with ULTRACAM (Dhillon et al., in preparation) mounted on the 4.2-m William Herschel Telescope, the authors were able to extract seven periodicities in the 180−200 s range. For the purposes of our brief feasibility study, we attempt to determine the degree index of the highest amplitude mode at 182.4 s only.

The first step towards finding the theoretical amplitudes in different wavebands is the calculation of the monochromatic model atmosphere quantities $\alpha_{T\nu}$, $\alpha_{g\nu}$, $b_{l\nu}$, $b_{l\nu,T}$ and $b_{l\nu,g}$ described in Section 3.3. Since these depend quite sensitively on the atmospheric parameters of the target, they need to be computed for KPD 2109+4401 specifically. We adopt $T_{\rm eff}$=31,380 K and $\log g$=5.65 as derived from our model atmosphere fit to the hydrogen Balmer and helium lines present in the time-averaged high-resolution MMT spectrum obtained by Betsy Green (private communication). These values are part of an ongoing program designed to provide homogeneous estimates of the atmospheric parameters of a large sample of subdwarf B stars, and we refer the interested reader to the forthcoming paper by Green, Fontaine, & Chayer (in preparation) for more information. The monochromatic quantities are then integrated over the effective u'g'r' wavebands, computed by convolving the Sloan band passes with the quantum efficiency curves of the ULTRACAM CCD chips (Vik Dhillon, private communication) and the atmospheric transparency curve of a representative observing site at 2000−3000 m altitude (in this case Kitt Peak National Observatory). Next, we derive the

adiabacity parameters R and Ψ_T (Section 3.4) for a period of 182.4 s from the non-adiabatic eigenfunctions of an envelope model characterised by the atmospheric parameters given above as well as representative values of M_*=0.48 $M_\odot$ and $\log q(H)$=−4.0. We finally calculate the pulsational amplitudes expected from the u', g', and r' photometry for degree indices from l=0 to l=5 using the equations given in Section 3.2.

The predicted multi-colour amplitudes are fit to those observed using a χ^2 minimisation routine following Fontaine et al. (1986). Compared to the standard normalisation of all amplitudes to one particular waveband this is a more objective way of determining the quality of a match, since the data from all band passes are weighted evenly. For every degree index l the theoretical amplitudes a_{theo} in each of the three band passes i are multiplied by a scale factor f_l, chosen in such a way as to minimise

$$\chi^2 = \sum_{i=1}^{3} \left(\frac{f_l a^i_{theo} - a^i_{obs}}{\sigma^i} \right)^2, \tag{3.48}$$

where a^i_{obs} is the amplitude observed in a given waveband and σ^i is the error on the measurement. The results of this operation for the 182.4-s mode of KPD 2109+4401 detected by Jeffery et al. (2004) are illustrated in Figure 3.29, and the corresponding χ^2 and quality-of-fit (Q) values are listed in Table 3.5. It is immediately obvious that the data are matched well by the predictions for an l=0 mode, the theoretical values falling within the (very small) error bars in all band passes. The next best fit is that of the l=1 mode, however the associated χ^2 residuals are a factor of 30 larger than those for l=0. In fact, if we adopt the canonical notion that a fit cannot be considered convincing unless the quality-of-fit $Q > 0.001$ (see, e.g., Press et al. 1986), the theoretical l=0 mode is the *only* one that can reproduce the observed amplitudes in a satisfactory manner. While this implies an unambiguous identification of the mode's degree index, it should be kept in mind that the estimated χ^2 and Q values are sensitive to the formal uncertainties on the observed amplitudes, which may well have been underestimated. Assuming, in an extreme case scenario, that the true errors are twice as large as those calculated by Jeffery et al. (2004), both l=0 and l=1 would provide acceptable fits. Nevertheless, the match for l=0 remains far superior, and we believe that our identification

of the degree index is sound.

We would like to point out that this is the first partial mode identification in a subdwarf B star on the basis of its amplitude-wavelength dependence alone. While the net result – the mode has a degree index of l=0 – is the same as that of Jeffery et al. (2004), we were not forced to invoke additional constraints to distinguish modes with l=0, 1, and 2. The greater accuracy achieved is undoubtedly due to the fact that we were able to compute a detailed model atmosphere characteristic of KPD 2109+4401 specifically, and could incorporate non-adiabatic effects from realistic envelope models.

3.8 CONCLUSION

We have modelled the brightness variations expected across the visible disk during a pulsation cycle for both short- and long-period variable subdwarf B stars taking into account the effects of temperature, radius, and surface gravity perturbations. The quantities related to the emergent intensity and its derivatives with respect to effective temperature and surface gravity were computed with the aid of a full model atmosphere code specifically modified for this purpose. Employing full model atmospheres has led to a degree of self-consistency not often achieved in this kind of calculation for other types of pulsating stars. For instance, in the case of pulsators near the main sequence most researchers use the Kurucz (1993) model atmospheres (or their equivalent) to compute α_{Tx} and α_{gx}. However, since these data do not treat limb darkening, the same authors are forced to turn elsewhere, in particular to the popular tables of Wade & Rucinski (1985), for limb darkening coefficients that allow them to approximately estimate the quantities b_{lx}, $b_{lx,T}$, and $b_{lx,g}$. Notwithstanding the fact that sdB stars are not main sequence stars, our approach alleviates the uncertainties associated with this mixed procedure.

In contrast to previous studies concerning the potential of multi-colour photometry for mode identification in sdB stars, we were able to model non-adiabatic effects in some detail. Applying full non-adiabatic pulsation calculations to representative EC 14026 and PG 1716 star models showed that these are by no means negligible. In EC 14026 stars, the two parameters measuring the departure from adiabacity of the eigenfunctions in the atmospheric layers

of interest ($< R >$ and $< \psi_T >$) vary systematically with period, but are independent of the degree index l. This is fortunate as it implies that $< R >$ and $< \psi_T >$ can be accurately computed for observed periodicities without assuming any prior knowledge of l. We should mention here that, while we use the fits to $< R >$ and $< \psi_T >$ obtained from our representative model throughout this explorative study, the latter are sensitive to the atmospheric parameters of the model in question. As such, they must be computed individually according to the specifications of each target if a quantitative interpretation of the observational data is to be achieved. For the PG 1716 stars, the situation is more complicated as the departure from adiabacity depends on l as well as on the period. The values of $< R >$ and $< \psi_T >$ attributed to oscillations observed will therefore constitute only rough estimates, introducing inaccuracies into the amplitude ratios and phase shifts computed. Fortunately, measurements of the longer periods excited in these stars are insensitive to non-adiabatic effects since they are dominated by temperature perturbations and $< R >, < \psi_T >$ cancel out in the amplitude ratios and phase shifts. It is of interest to note that our computations return $R > 1$ for the majority of modes believed to be excited in long-period variable subdwarf B stars. Although this is in conflict with the prevailing sentiment that R must lie in the range $0 < R < 1$ (see e.g., Balona & Evers 1999), we find no physical justification for this and believe our results to be accurate.

According to our computations, the brightness variations observed in subdwarf B stars are caused primarily by temperature and radius perturbations, the contribution of surface gravity changes being small in EC 14026 stars and negligible in PG 1716 stars. For the latter, temperature effects alone dominate the flux changes in the limit of long periods. In this regime, non-adiabatic effects loose their influence on the amplitude ratios and phase shifts, and the period of the mode is no longer an issue. The adiabatic approximation is thus valid in this particular case, which immediately implies that oscillations should occur in phase at all wavelengths. Note however that conversely a lack of observed phase shifts does not automatically justify use of the adiabatic approximation. Even outside the temperature dominated regime, phase shifts are generally predicted to be small, although they may reach up to $\sim$ 10 degrees for the shortest periods in PG 1716 stars and certain l=3 modes in EC

14026 stars. Whereas this may be large enough for an observational detection, it is clear that mode discrimination will occur primarily on the basis of the amplitude ratios. We note that for main sequence g-mode oscillators (e.g., Aerts et al. 2004 or De Cat et al. 2005) as well as for white dwarfs (e.g., Robinson et al. 1982) the measured phase shifts are negligible.

In the case of the EC 14026 stars, it should be relatively straightforward to distinguish modes with $l = 0$, 1, or 2 from those with $l = 3$, $l = 4$ or 6 and $l = 5$. This could well prove invaluable as a consistency check for the "forward approach" in asteroseismology, which has been used to claim mode identification in a number of short period variables through the inference of modes with $l = 0$, 1, 2 and 3/4 (e.g., Charpinet et al. 2005). It is interesting to note, in this connection, that the visibility of the $l = 3$ modes in the optical domain is less than that of the $l = 4$ modes (see Fig. 3.1), very much like the situation in main sequence p-mode pulsators (e.g., Heyndericks et al. 1994), and this should be taken into account in future asteroseismological exercises of the sort. Discrimination between modes with $l = 0$, 1, or 2 is much more challenging and requires multi-colour photometry of unprecedented quality as well as accurate spectroscopic estimates of the atmospheric parameters for the target observed. Nevertheless, we have demonstrated that it is feasible using the highest amplitude mode detected for KPD 2109+4401 (Jeffery et al. 2004) as an example. It is not yet clear whether similar results can be achieved on the basis of other published datasets, or even for the lower-amplitude modes detected in KPD 2109+4401. This can only be answered through detailed quantitative analyses, which we plan to carry out in the near future. It will be particularly interesting to see whether we can confirm the tentative mode identifications reported by Jeffery et al. (2004) for the remaining modes detected for KPD 2109+4401 and HS 0039+4302. Regardless of the outcome of this project, we feel confident that colour-amplitude ratios and phase shifts could be measured to sufficient accuracy from future observations provided that the targets are bright enough and light curves with well resolved frequency peaks in the Fourier domain are obtained. Several consecutive nights on a 4 m-class telescope, or even a single night on an 8 m telescope for a well-chosen "simple" pulsator such as PG 1219+534 (see Charpinet et al. 2005) would likely be adequate. Alternatively, simultaneous ground- and space-based observations would be useful insofar as the frequency baseline could

be extended to the UV, where the signature of the degree index on the pulsational amplitude is greater than in the visible domain. Given the observing time on the appropriate instrument, it would be interesting to monitor a target for which an asteroseismological analysis has already been completed, and compare the degree indices inferred from the two independent methods.

For the PG 1716 stars, discrimination on the basis of colour-amplitude ratios seems feasible between modes with degree indices $l = 1, 2, 4, 6$ and those with $l = 3$ and $l = 5$. To date, the only substantial set of multi-colour photometry for a long-period variable subdwarf consists of the $\sim$ 250 hours of simultaneous (Johnson-Cousins) U/R data obtained for PG 1338+481. While detailed results will be presented elsewhere, a preliminary analysis of the photometry indicates amplitude ratios consistent with those predicted for $l = 1, 2, 4$ or 6 rather than $l = 3$ or $l = 5$.[1] Compared to the study of EC 14026 stars, that of the PG 1716 stars is still in its infancy, which is partly due to deficiencies in the models, and partly a result of the considerable observational challenges presented by the low amplitudes and long periods of the pulsations. Unambiguous mode identification in these objects will likely be possible only by using a combination of the "forward approach" employed for the EC 14026 stars, and inference of the degree index from multi-colour photometry, which we have developed the tools for. In the immediate future we hope that restricting, if not identifying, the degree index will clarify the current discrepancies between predicted and observed instabilities and pave the way for a more mature understanding of these exciting objects.

This work was supported in part by the Natural Sciences and Engineering Research Council of Canada and by the Fonds de recherche sur la nature et les technologies (Québec). G.F. also acknowledges the contribution of the Canada Research Chair Program.

[1] We point out in this context that main sequence g-mode pulsators with good empirical mode identification all have $l = 1$.

3.9 TABLES

TABLE 3.1 – Basic properties of our representative sdB models

	EC 14026	PG 1716
$T_{\rm eff}$ (K)	33,000	27,000
$\log g$	5.75	5.40
$M_*/M_\odot$	0.48	0.48
$\log M(H)/M_*$	-4.0	-2.5
$R_*/R_\odot$	0.1528	0.2286
$< \nabla_{ad} >$	0.345	0.350
$(P*)$	(1.86)	(1.90)

TABLE 3.2 – Model atmosphere parameters for our reference EC 14026 star model

Filter	α_{Tx}	α_{gx}	b_{lx}	$b_{lx,T}$	$b_{lx,g}$
l=0					
U	2.92408e+00	−8.79918e−03	1.00000e+00	0.00000e+00	0.00000e+00
B	2.39047e+00	−1.03963e−02	1.00000e+00	0.00000e+00	0.00000e+00
V	2.22439e+00	−3.58973e−03	1.00000e+00	0.00000e+00	0.00000e+00
R	2.20732e+00	−4.44731e−03	1.00000e+00	0.00000e+00	0.00000e+00
I	2.16038e+00	−4.66709e−03	1.00000e+00	0.00000e+00	0.00000e+00
l=1					
U	2.92408e+00	−8.79918e−03	6.82603e−01	−8.27838e−02	1.50712e−04
B	2.39047e+00	−1.03963e−02	6.80962e−01	−7.07727e−02	−4.30909e−04
V	2.22439e+00	−3.58973e−03	6.79500e−01	−6.48752e−02	4.72654e−05
R	2.20732e+00	−4.44731e−03	6.77752e−01	−5.72272e−02	3.63862e−05
I	2.16038e+00	−4.66709e−03	6.75976e−01	−4.98751e−02	1.40290e−04
l=2					
U	2.92408e+00	−8.79918e−03	2.77831e−01	−1.45151e−01	2.72343e−04
B	2.39047e+00	−1.03963e−02	2.74875e−01	−1.23325e−01	−7.48759e−04
V	2.22439e+00	−3.58973e−03	2.72346e−01	−1.12924e−01	7.83689e−05
R	2.20732e+00	−4.44731e−03	2.69307e−01	−9.93220e−02	5.76610e−05
I	2.16038e+00	−4.66709e−03	2.66224e−01	−8.62079e−02	2.41525e−04
l=3					
U	2.92408e+00	−8.79918e−03	2.21585e−02	−1.13544e−01	2.28955e−04
B	2.39047e+00	−1.03963e−02	1.96901e−02	−9.49294e−02	−5.71154e−04
V	2.22439e+00	−3.58973e−03	1.77843e−02	−8.66973e−02	5.26364e−05
R	2.20732e+00	−4.44731e−03	1.54585e−02	−7.57038e−02	3.31297e−05
I	2.16038e+00	−4.66709e−03	1.31074e−02	−6.50246e−02	1.79893e−04
l=4					
U	2.92408e+00	−8.79918e−03	−3.37428e−02	−2.92580e−02	8.03034e−05
B	2.39047e+00	−1.03963e−02	−3.45850e−02	−2.23291e−02	−1.25024e−04
V	2.22439e+00	−3.58973e−03	−3.49776e−02	−2.01295e−02	2.41962e−06
R	2.20732e+00	−4.44731e−03	−3.55043e−02	−1.68782e−02	−7.22134e−06
I	2.16038e+00	−4.66709e−03	−3.60262e−02	−1.36059e−02	3.36702e−05
l=5					
U	2.92408e+00	−8.79918e−03	2.94649e−03	1.84351e−02	−1.87196e−05
B	2.39047e+00	−1.03963e−02	3.17349e−03	1.73638e−02	1.16289e−04
V	2.22439e+00	−3.58973e−03	3.57060e−03	1.60135e−02	−1.73842e−05
R	2.20732e+00	−4.44731e−03	4.01634e−03	1.44965e−02	−1.84547e−05
I	2.16038e+00	−4.66709e−03	4.47573e−03	1.31376e−02	−4.11307e−05

TABLE 3.3 – Model atmosphere parameters for our reference PG 1716 star model

Filter	α_{Tx}	α_{gx}	b_{lx}	$b_{lx,T}$	$b_{lx,g}$
l=1					
U	2.55827e+00	−9.44029e−03	6.86440e−01	−1.35877e−02	−2.13902e−04
B	2.02976e+00	−9.88741e−03	6.84945e−01	−1.93784e−02	−9.19858e−04
V	1.81454e+00	−4.38065e−04	6.82739e−01	−1.60495e−02	−1.91847e−04
R	1.71773e+00	−1.30255e−03	6.80274e−01	−9.93252e−03	−1.67575e−04
I	1.59319e+00	−2.00633e−03	6.77747e−01	−3.46771e−03	−3.34334e−05
l=2					
U	2.55827e+00	−9.44029e−03	2.84671e−01	−2.52137e−02	−3.57770e−04
B	2.02976e+00	−9.88741e−03	2.81883e−01	−3.41905e−02	−1.61503e−03
V	1.81454e+00	−4.38065e−04	2.78062e−01	−2.86214e−02	−3.41634e−04
R	1.71773e+00	−1.30255e−03	2.73758e−01	−1.81031e−02	−2.98321e−04
I	1.59319e+00	−2.00633e−03	2.69344e−01	−6.92282e−03	−5.62310e−05
l=3					
U	2.55827e+00	−9.44029e−03	2.77314e−02	−2.24244e−02	−2.45991e−04
B	2.02976e+00	−9.88741e−03	2.52149e−02	−2.70928e−02	−1.26624e−03
V	1.81454e+00	−4.38065e−04	2.23207e−02	−2.32581e−02	−2.77800e−04
R	1.71773e+00	−1.30255e−03	1.89973e−02	−1.54544e−02	−2.42536e−04
I	1.59319e+00	−2.00633e−03	1.55810e−02	−7.03719e−03	−3.96414e−05
l=4					
U	2.55827e+00	−9.44029e−03	−3.20092e−02	−9.31317e−03	−1.84146e−05
B	2.02976e+00	−9.88741e−03	−3.31155e−02	−7.28935e−03	−3.27026e−04
V	1.81454e+00	−4.38065e−04	−3.37299e−02	−6.98455e−03	−8.61390e−05
R	1.71773e+00	−1.30255e−03	−3.45198e−02	−5.57709e−03	−7.54679e−05
I	1.59319e+00	−2.00633e−03	−3.53407e−02	−3.89855e−03	−5.21899e−06
l=5					
U	2.55827e+00	−9.44029e−03	2.29813e−03	7.35094e−04	7.80329e−05
B	2.02976e+00	−9.88741e−03	2.29739e−03	4.39081e−03	2.10197e−04
V	1.81454e+00	−4.38065e−04	2.88750e−03	3.20848e−03	3.19444e−05
R	1.71773e+00	−1.30255e−03	3.49885e−03	1.36516e−03	2.70668e−05
I	1.59319e+00	−2.00633e−03	4.12129e−03	−5.06197e−04	9.33007e−06
l=6					
U	2.55827e+00	−9.44029e−03	2.84314e−02	1.14630e−03	7.21713e−06
B	2.02976e+00	−9.88741e−03	2.85101e−02	1.43976e−03	5.62154e−05
V	1.81454e+00	−4.38065e−04	2.86265e−02	1.36594e−03	9.79649e−06
R	1.71773e+00	−1.30255e−03	2.87730e−02	9.96041e−04	7.43661e−06
I	1.59319e+00	−2.00633e−03	2.89270e−02	5.57062e−04	−1.04396e−06

TABLE 3.4 – Equilibrium models for a sequence of subdwarf B stars with $M_*/M_\odot$=0.48

No.	$T_{\rm eff}$(K)	$\log g$	$\log q(H)$	ΔP (s)
PG 1716 stars				
1	22,000	5.13	−1.64	4500−9500
2	23,000	5.19	−1.81	4000−8000
3	24,000	5.25	−1.97	3500−6500
4	25,000	5.31	−2.13	3000−5700
5	26,000	5.37	−2.30	2500−5000
6	27,000	5.44	−2.46	2300−4000
7	28,000	5.50	−2.62	2000−3500
EC 14026 stars				
8	29,000	5.56	−2.79	220−450
9	30,000	5.62	−2.95	190−450
10	31,000	5.68	−3.12	170−360
11	32,000	5.75	−3.28	150−260
12	33,000	5.81	−3.44	110−200
13	34,000	5.87	−3.61	100−150
14	35,000	5.93	−3.77	95−110

TABLE 3.5 – Fit of predicted u'g'r' amplitudes to those observed for the 182.4-s mode of KPD 2109+4401 by Jeffery et al. (2004)

Degree index l	χ^2	Q
0	0.736	0.692
1	22.6	1.24×10^{-5}
2	96.0	1.43×10^{-24}
3	1470	0.00
4	1150	0.00
5	4860	0.00

3.10 REFERENCES

Aerts, C., Cuypers, J., De Cat, P., Dupret, M.-A., de Ridder, J., Eyer, L., Scuflaire, R., & Waelkens, C. 2004, A&A, 432, 1013

Balona, L.A., & Evers, E.A. 1999, MNRAS, 302, 349

Balona, L.A., & Stobie, R.S. 1979, MNRAS, 187, 217

Bergeron, P., Wesemael, F., Beauchamp, A., Wood, M.A., Lamontagne, R., Fontaine, G., & Liebert, J. 1994, ApJ, 432, 305

Bessel, M.S. 1990, PASP, 102, 1181

Billères, M., Fontaine, G., Brassard, P., & Liebert, J. 2002, ApJ, 578, 515

Brassard, P., Fontaine, G., Billères, M., Charpinet, S., Liebert, J., & Saffer, R.A. 2001, ApJ, 563, 1013

Brassard, P., Fontaine, G., & Wesemael, F. 1995, ApJS, 96, 545

Buta, R.J., & Smith, M.A. 1979, ApJ, 232, 213

Breger, M., Handler, G., Garrido, R., Audard, N., Beichbuchner, F., Zima, W., Paparo, M., Zhi-Ping, L., Shi-Yang, J., Zong-li, L., Ai-ying, Z., Pikall, H., Stankov, A., Guzik, J.A., Sperl, M., Krzesinski, J., Ogloza, W., Pajdosz, G., Zola, S., Serkowitsch, E., Reegen, P., Rumpf, T., & Schmalwieser, A. 1997, A&A, 324, 566

Charpinet, S., Fontaine, G., Brassard, P., Green, E.M., and Chayer, P. 2005, A&A, in press

Charpinet, S., Fontaine, G., & Brassard, P. 2003, in NATO ASIB Proc. 105: White Dwarfs, 69

Charpinet, S., Fontaine, G., Brassard, P., & Dorman, B. 2002, ApJS, 140, 469

Charpinet, S., Fontaine, G., & Brassard, P. 2001, PASP, 113, 785

Charpinet, S., Fontaine, G., Brassard, P., Chayer, P., Rogers, F.J., Iglesias, C.A., & Dorman, B. 1997, ApJ, 483, L123

Charpinet, S., Fontaine, G., Brassard, P., & Dorman, B. 1996, ApJ, 471, L103

Cugier, H., & Daszyńska, J. 2001, A&A, 377, 113

Cugier, H., Dziembowski, W., & Pamyatnykh, A.A. 1994, A&A, 291, 143

De Cat, P., Briquet, M., Daszyńska-Daskiewicz, J., Dupret, M.-A., de Ridder, J., Scuflaire, R., & Aerts, C. 2005, A&A, 432, 1013

Dorman, B. 1995, in Proc. 32d Liège Astrophys. Colloq., Stellar Evolution: What Should be Done?, ed. A. Noels, D. Fraipont-Caro, M. Gabriel, N. Grevesse, & P, Demarque (Liège: Institut d'Astrophysique), 291

Dupret, M.-A. 2001, A&A, 366, 166

Dupret, M.-A., De Ridder, J., De Cat, P., Aerts, C., Scufflaire, R., Noels, A., & Thoul, A. 2003, A&A, 398, 677

Dziembowski, W., 1977, Acta Astron. 27, 203

Dziembowski, W., & Pamyatnykh, A.A. 1993, MNRAS, 262, 204

Dziembowski, W., Moskalik, P., & Pamyatnykh, A.A. 1993, MNRAS, 265, 588

Falter, S., Heber, U., Dreizler, S., Schuch, S.L., Cordes, O., & Edelmann, H. 2003, A&A, 401, 289

Fontaine, G., Green, E.M., Brassard, P., Charpinet, S., Chayer, P., Billères, M., Randall, S.K., & Dorman, B. 2004, Ap&SS, 291, 379

Fontaine, G., Brassard, P., Charpinet, S., Green, E.M. and Willems, B., 2003a, Asteroseismology Across the HR Diagram. Proceedings of the Asteroseismology Workshop, Porto, Portugal, 1-5 July, 2002. Ed. M.J. Thompson, M.S. Cunha, M.J.P.F.G. Monteiro. Reprinted from Astrophysics & Space Science, Volume 284, No. 1, 2003. Kluwer Academic Publishers, Dordrecht., 517

Fontaine, G., Brassard, P., Charpinet, S., Green, E.M., Chayer, P., Billères, M., & Randall, S.K. 2003b, ApJ, 597, 518

Fontaine, G., Charpinet, S., Brassard, P., Chayer, P., Rogers, F.J., Iglesias, C.A., & Dorman, B. 1998, in IAU Symposium No. 185, New Eyes to See Inside the Sun and Stars, ed. F.-L. Deubner, J. Christensen-Dalsgaard and D. Kurtz, Kyoto, Japan, 18-22 August 1997, 367

Fontaine, G., Brassard, P., Bergeron, P., & Wesemael, F. 1996, ApJ, 469, 320

Gautschy, A., & Saio, H. 1993, MNRAS, 262, 213

Garrido, R., García-Lobo, E., & Rodriguez, E. 1990, A&A, 234, 262

Green, E.M., Callerame, K., Seitenzahl, I.R., White, B.A., Hyde, E.A., Giovanni, M., Reed, M., Fontaine, G., & Østensen, R. 2003a, Ap&SS, 284, 65

Green, E.M., Fontaine, G., Reed, M.D., Callerame, K., Seitenzahl, I.R., White, B.A., Hyde, E.A., Østensen, R., Cordes, O., Brassard, P., Falter, S., Jeffery, E.J., Dreizler, S., Schuh, S.L., Giovanni, M., Edelmann, H., J. Rigby, & Bronowska, A. 2003b, ApJ, 583, L31

Heber, U. 1986, A&A, 155, 33

Heynderickx, D., Waelkens, C., & Smeyers, P. 1994, A&A, 105, 447

Jackson, J.D. 1975, Classical Electrodynamics, 2nd ed. (New York: Wiley & Sons)

Jeffery, C.S., Dhillon, V., Marsh, T., & Ramachandran, B. 2004, MNRAS, 352, 699

Kilkenny, D., Billères, M., Stobie, R.S., Fontaine, G., Shobbrook, R.R., O'Donoghue, D., Brassard, P., Sullivan, D.J., Burleigh, M.R., & Barstow, M.A. 2002, MNRAS, 331, 399

Kilkenny, D., Koen, C., O'Donoghue, D., & Stobie, R.S. 1997, MNRAS, 285, 640

Koen, C., 1998 MNRAS, 300, 567

Koen, C., Kilkenny, D., O'Donoghue, D., Van Wyk, F., & Stobie, R.S. 1997, MNRAS, 285, 645

Kurucz, R.L. 1993, Atlas9 Stellar Atmosphere Programs, Kurucz CDROM No. 13

O'Donoghue, D., Lynas-Gray, A.E., Kilkenny, D., Stobie, R.S., & Koen, C. 1997, MNRAS, 285, 657

Osaki, Y., 1971, PASJ, 23, 485

Oreiro, R., Pérez Hernández, F., Ulla, A., Garrido, R., Østensen, R., & MacDonald, J. 2005, preprint

Press, W.H., Flannery, B.P., Teukolsky, S.A., & Vetterling, W.T. 1986, Numerical Recipes (Cambridge: Cambridge University Press)

Ramachandran, B., Jeffery, C.S., & Townsend, R.H.D. 2004, A&A, 428, 209

Randall, S., Fontaine, G., Green, E., Kilkenny, D., Crause, L., Cordes, O., O'Toole, S., Kiss, L., For, B.-Q., & Quirion, P.-O. 2004a, Ap&SS, 291, 465

Randall, S.K., Fontaine, G., Green, E.M., Brassard, P., & Terndrup, D.M. 2004b, Proceedings of the SOHO 14/GONG 2004 Workshop (ESA SP-559). "Helio- and Asteroseismology: Towards a Golden Future". 12-16 July 2004, New Haven, Connecticut, USA. Ed. D. Danesy, 119

Randall, S.K., Matthews, J.M., Fontaine, G., Rowe, J., Kuschnig, R., Green, E.M., Brassard, P., Chayer, P., Guenther, D.B., Moffat, A.F.J., Rucinski, S., Sasselov, D., Walker, G.A.H., & Weiss, W.W. 2005, ApJ, submitted

Robinson, E.L., Kepler, S.O., & Nather, R.E. 1982, ApJ, 259, 219

Saffer, R., Bergeron, P., Koester, D., & Liebert, J. 1994, ApJ, 432, 351

Silvotti, R., Østensen, R., Heber, U., Solheim, J.-E., Dreizler, S., & Altmann, M. 2002, A&A, 383, 239

Stamford, P.A., & Watson, R.D. 1981, Ap&SS, 77, 131

Stobie, R.S., Kawaler, S.D., Kilkenny, D., O'Donoghue, D., & Koen, C. 1997, MNRAS, 285, 651

Townsend, R.H.D. 2002, MNRAS, 330, 855

Townsend, R.H.D. 2003, MNRAS, 343, 125

Watson, R.D. 1988, Ap&SS, 140, 255

Wade, R.A., & Rucinski, S.M. 1985, A&AS, 60, 471

3.11 FIGURES

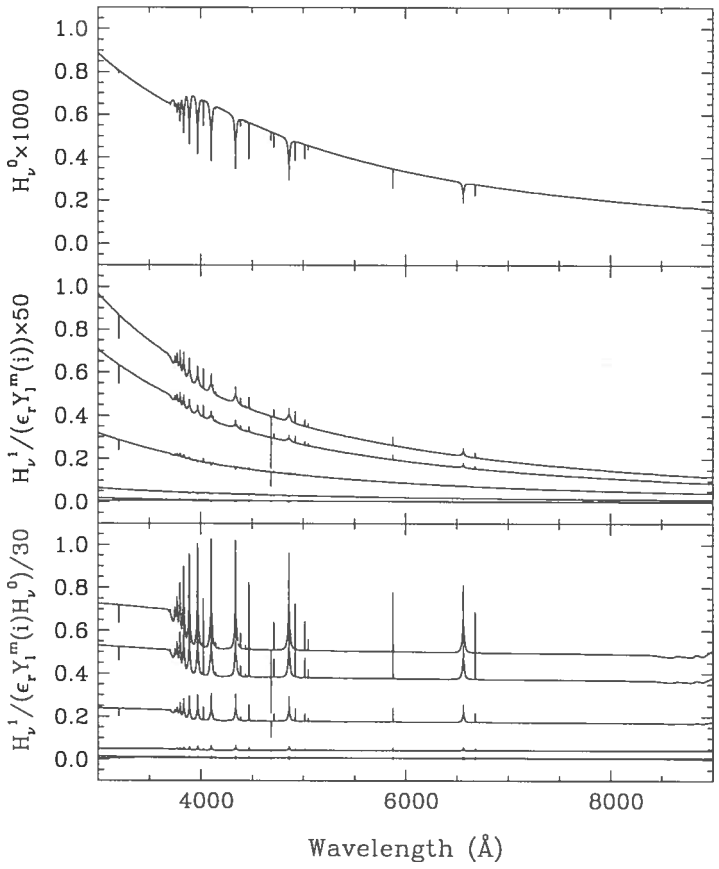

FIGURE 3.1 – Behavior of some key monochromatic quantities for our representative EC 14026 star model. The latter has $\log g = 5.75$ and $T_{\rm eff} = 33{,}000$ K. Top panel: Unperturbed emergent Eddington flux in the optical domain in units of erg/Hz/s/cm^2/steradian. Middle panel: First order perturbation to the flux caused by a nonradial pulsation with a period of 150 s (p-mode); at 3500 Å, from top to bottom, each curve is characterized by a value of the degree index l = 0, 1, 2, 4, 3, and 5. Bottom panel: Similar to the middle panel, but, this time, illustrating the *relative* amplitude of the perturbation.

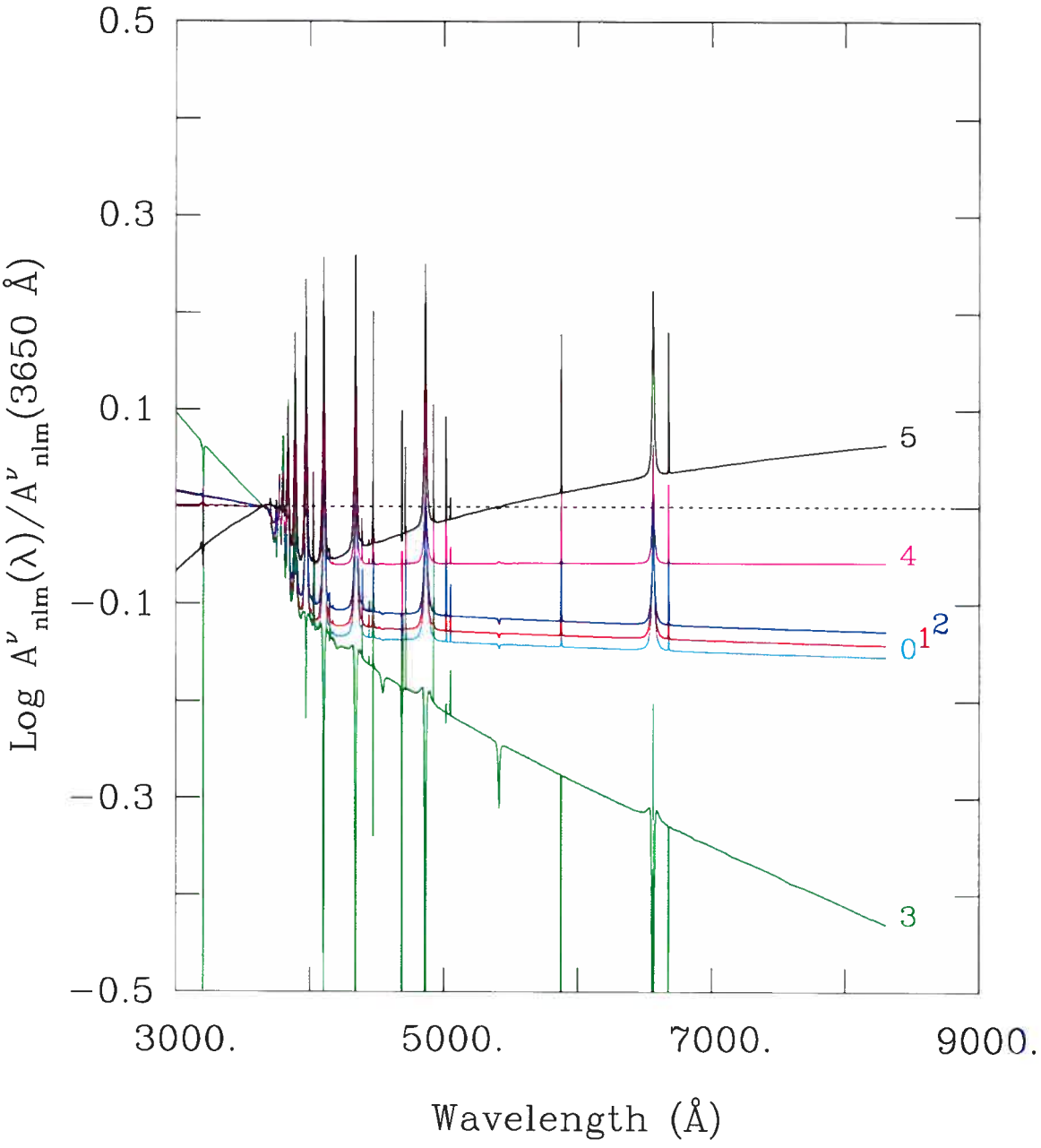

FIGURE 3.2 – Logarithm of monochromatic amplitude ratios with respect to an arbitrary spectral point at 3650 Å. This again refers to our representative EC 14026 star model and for a mode with a period of 150 s and degree index $l = 0$ (cyan), 1 (red), 2 (blue), 3 (green), 4 (magenta), and 5 (black).

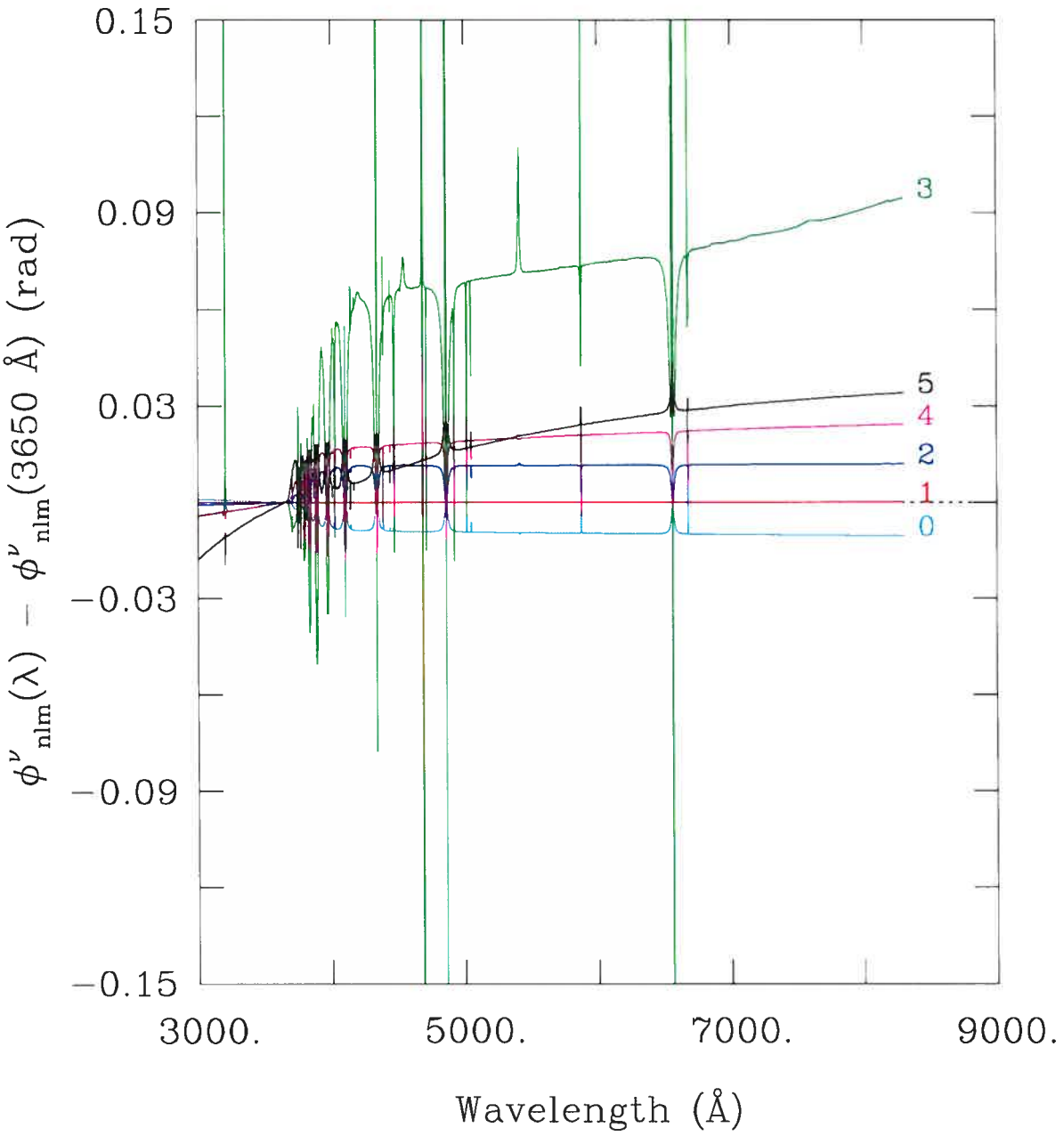

FIGURE 3.3 – Similar to Figure 3.2, but for monochromatic phase differences.

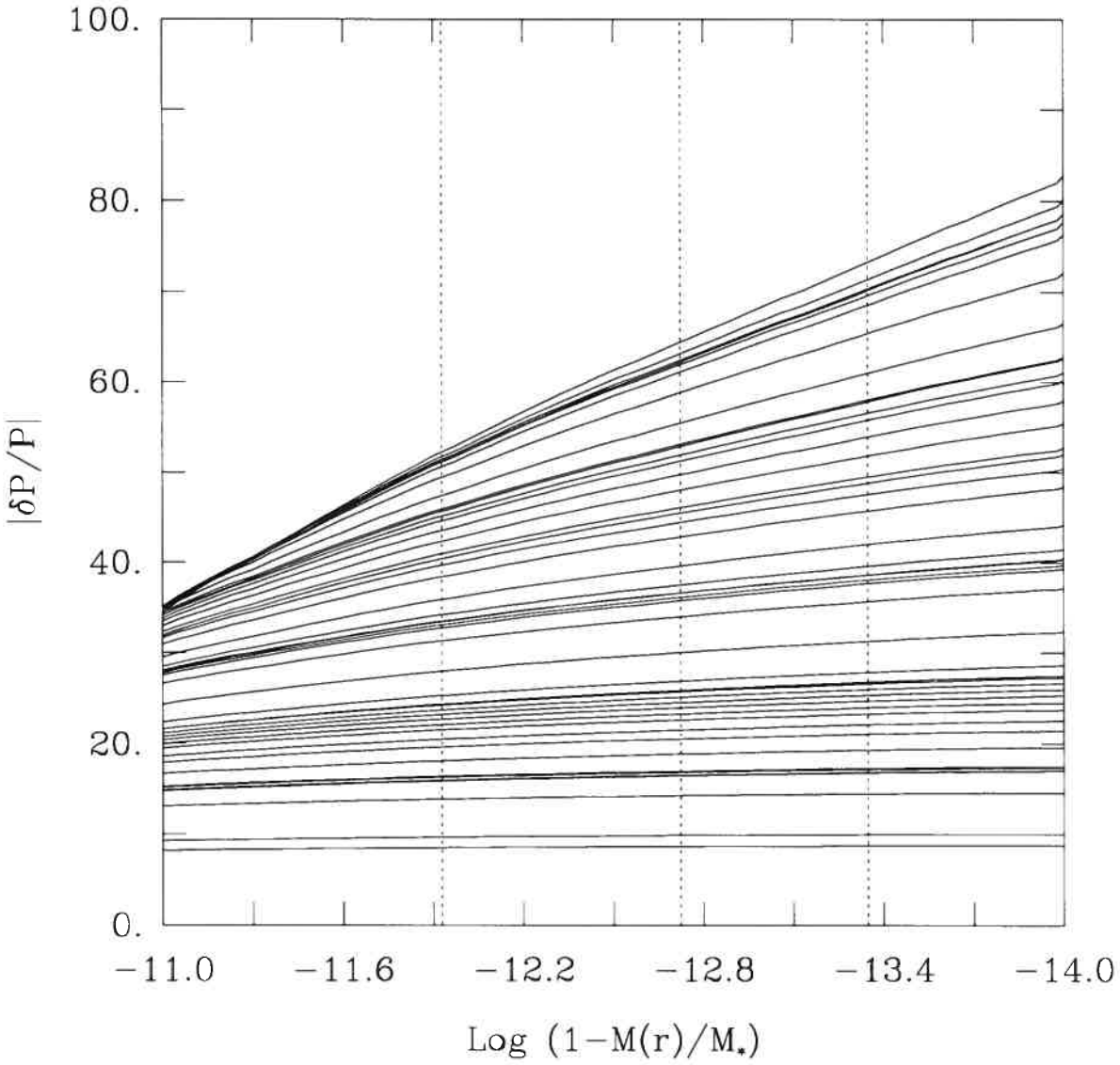

FIGURE 3.4 – Behaviour of the radial component of the pressure eigenfunction in the atmospheric layers of interest for our representative EC 14026 star model on the basis of modes with degree indices from $l = 0$ to 5 for all periods in the range 80−300 s. The illustrated function has been multiplied by an arbitrary factor for the creation of this plot, therefore no physical interpretation should be given to the actual values of $|\delta P/P|$. The vertical dotted lines correspond, from right to left, to Rosseland optical depths of $\tau = 0.1$, 1.0, and 10.0, respectively.

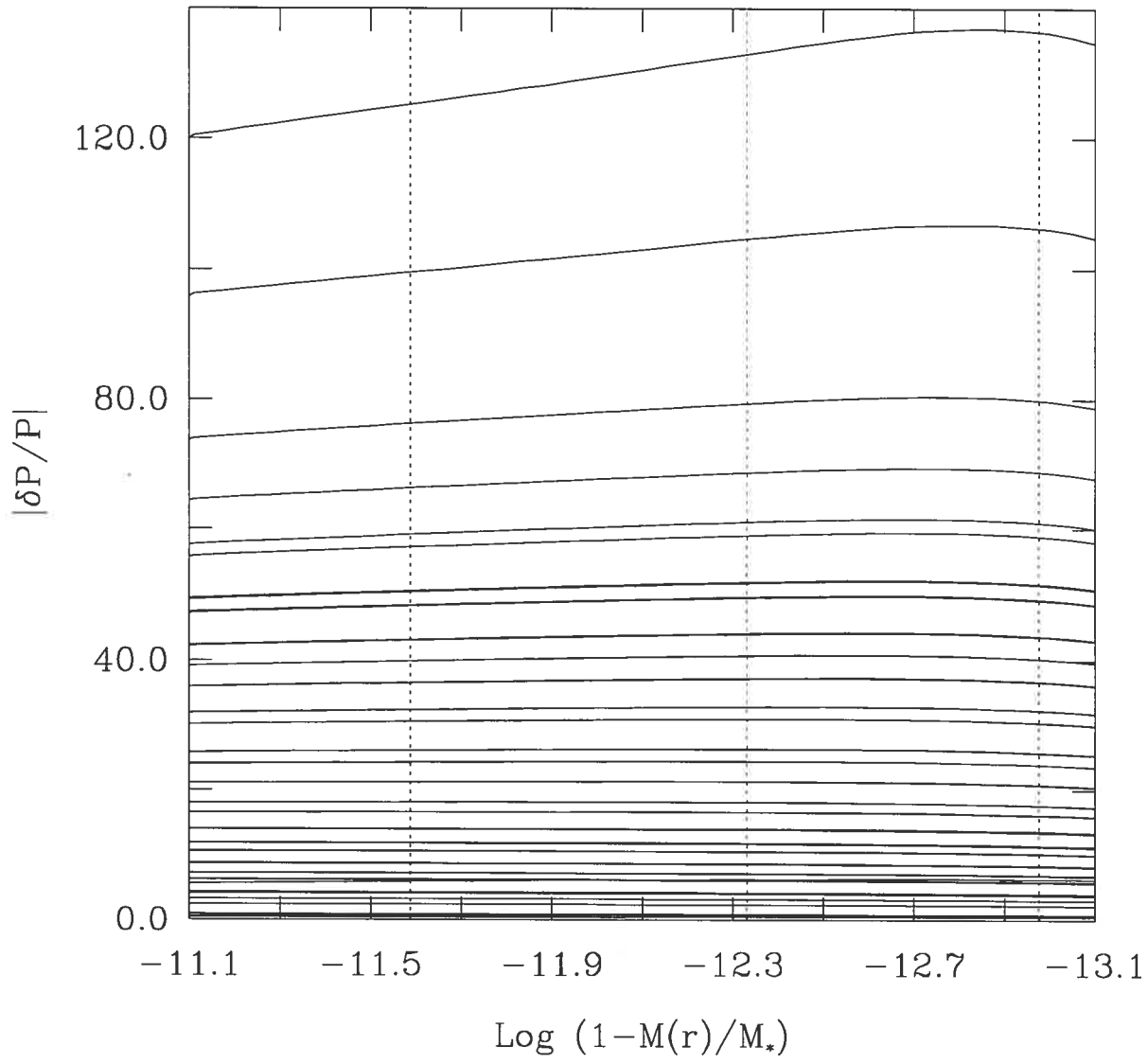

FIGURE 3.5 – Similar to Figure 3.4, but for our representative PG 1716 model and considering modes with l= 1, 2 and 3 in the period range 2000−6000 s.

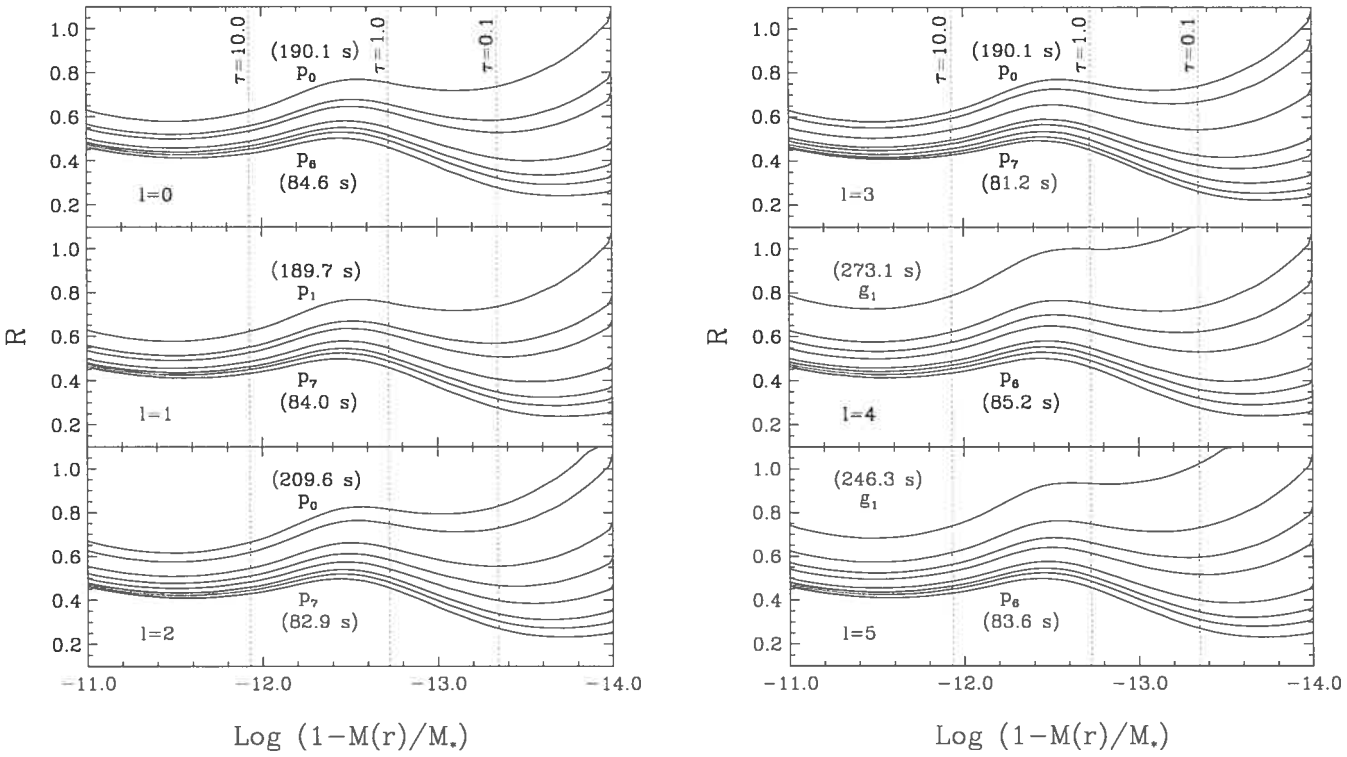

FIGURE 3.6 – R values for our representative EC 14026 model in the atmospheric layers of interest for periods in the range 80−300 s. The curves for different degree indices are illustrated separately as indicated. The type of mode (p or g) and its radial order k are indicated for the shortest and the longest period in each panel and can be used to infer the k-values of the intermittent modes.

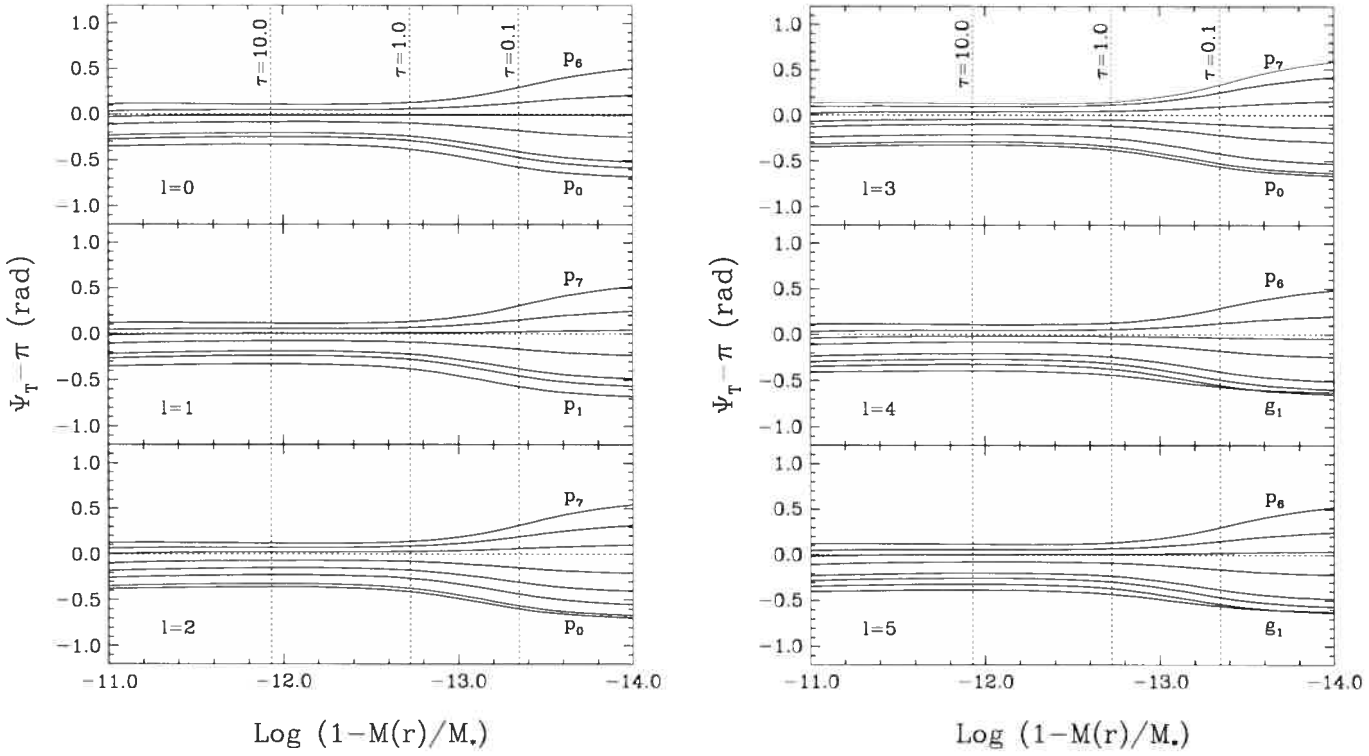

a) b)

FIGURE 3.7 – Similar to Figure 3.6, but for the quantity $\psi_T - \pi$.

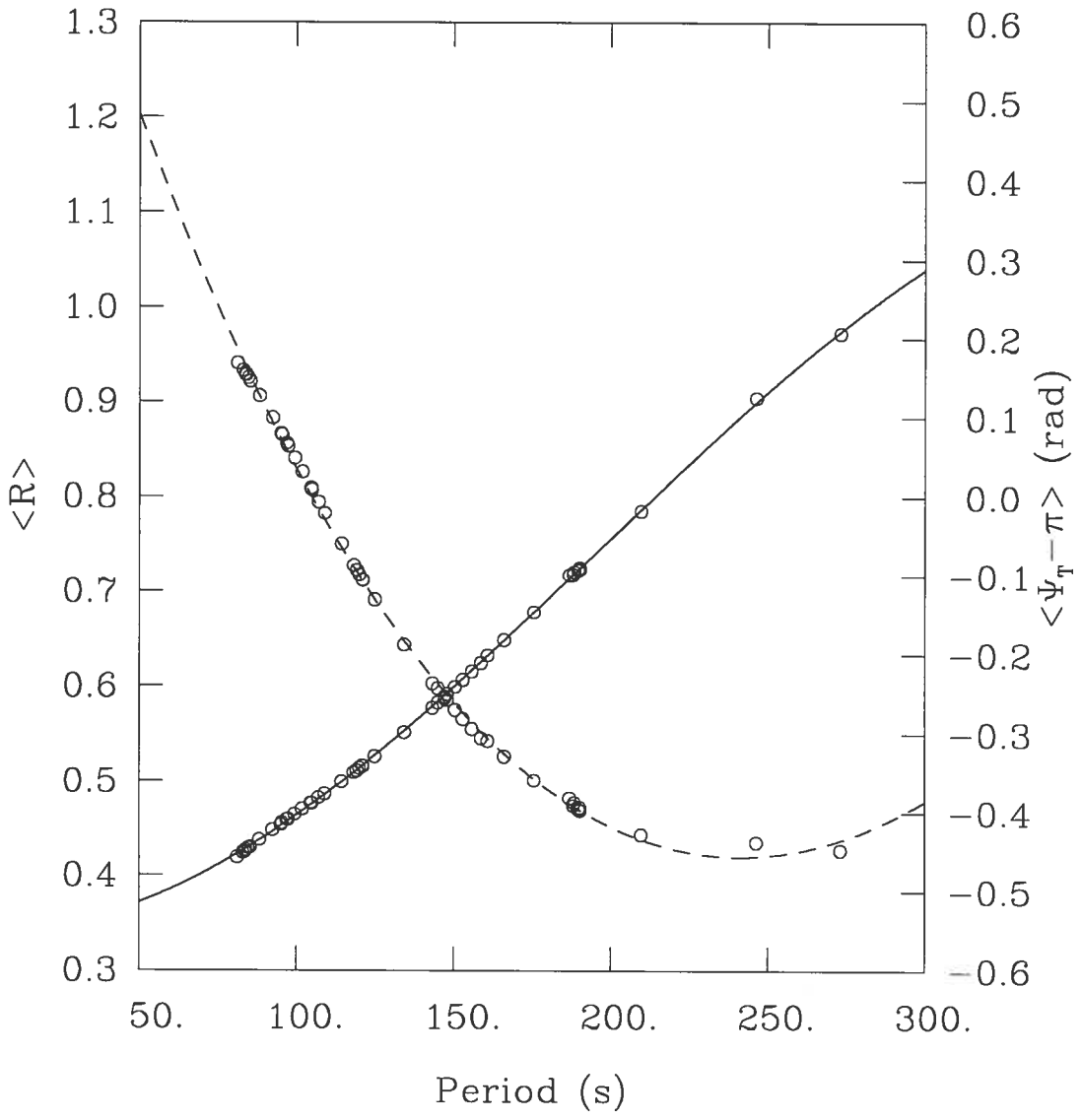

FIGURE 3.8 – Cubic fit to computed $< R >$ (continuous line) and $< \psi_T >$ (dashed line) values as a function of period for our representative EC 14026 star model. The cubic functions were generated using equations 3.44 and 3.45.

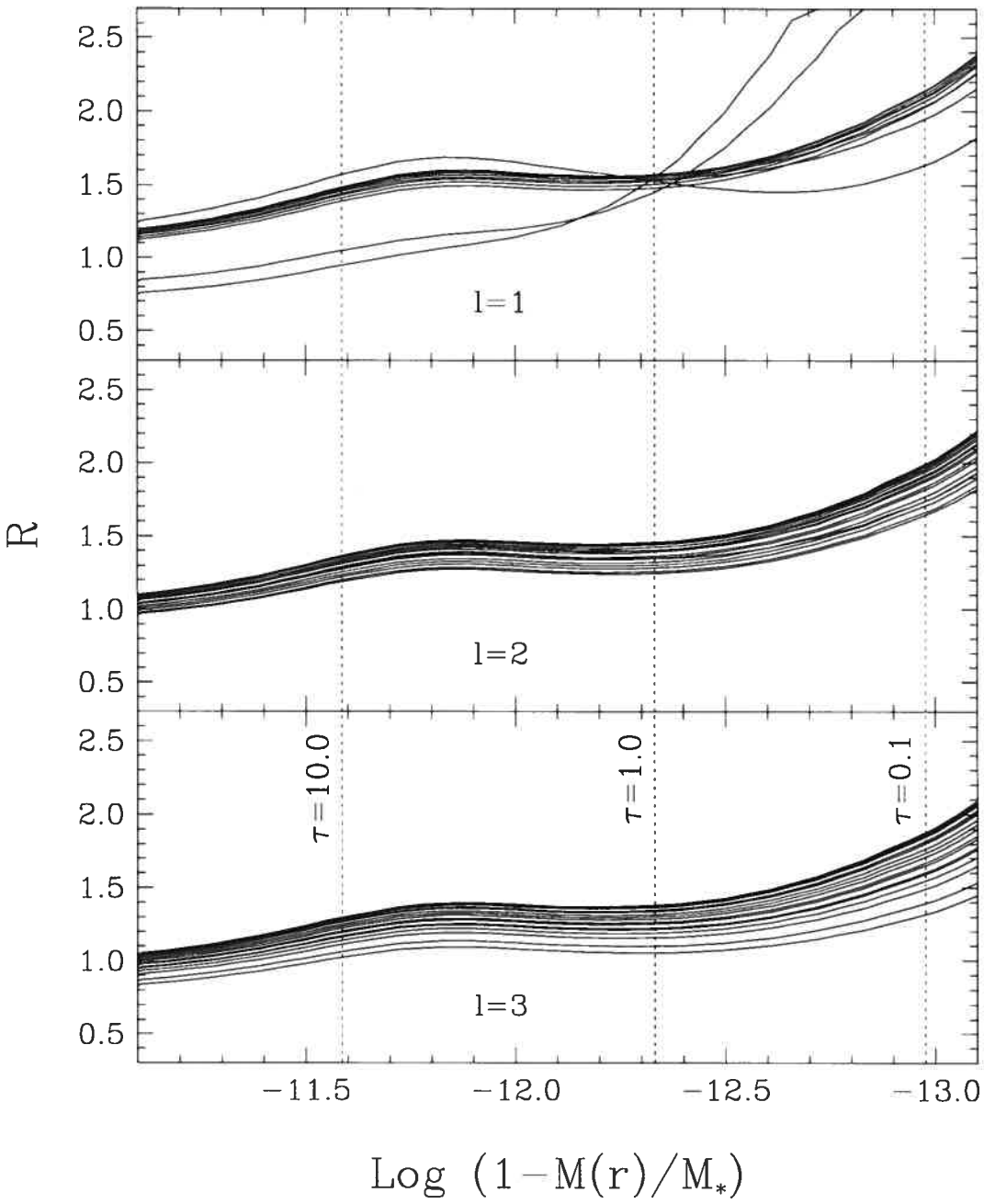

FIGURE 3.9 – R values for our representative PG 1716 model in the atmospheric layers of interest for periods in the range 2000−6000 s. The curves for different degree indices are illustrated separately as indicated.

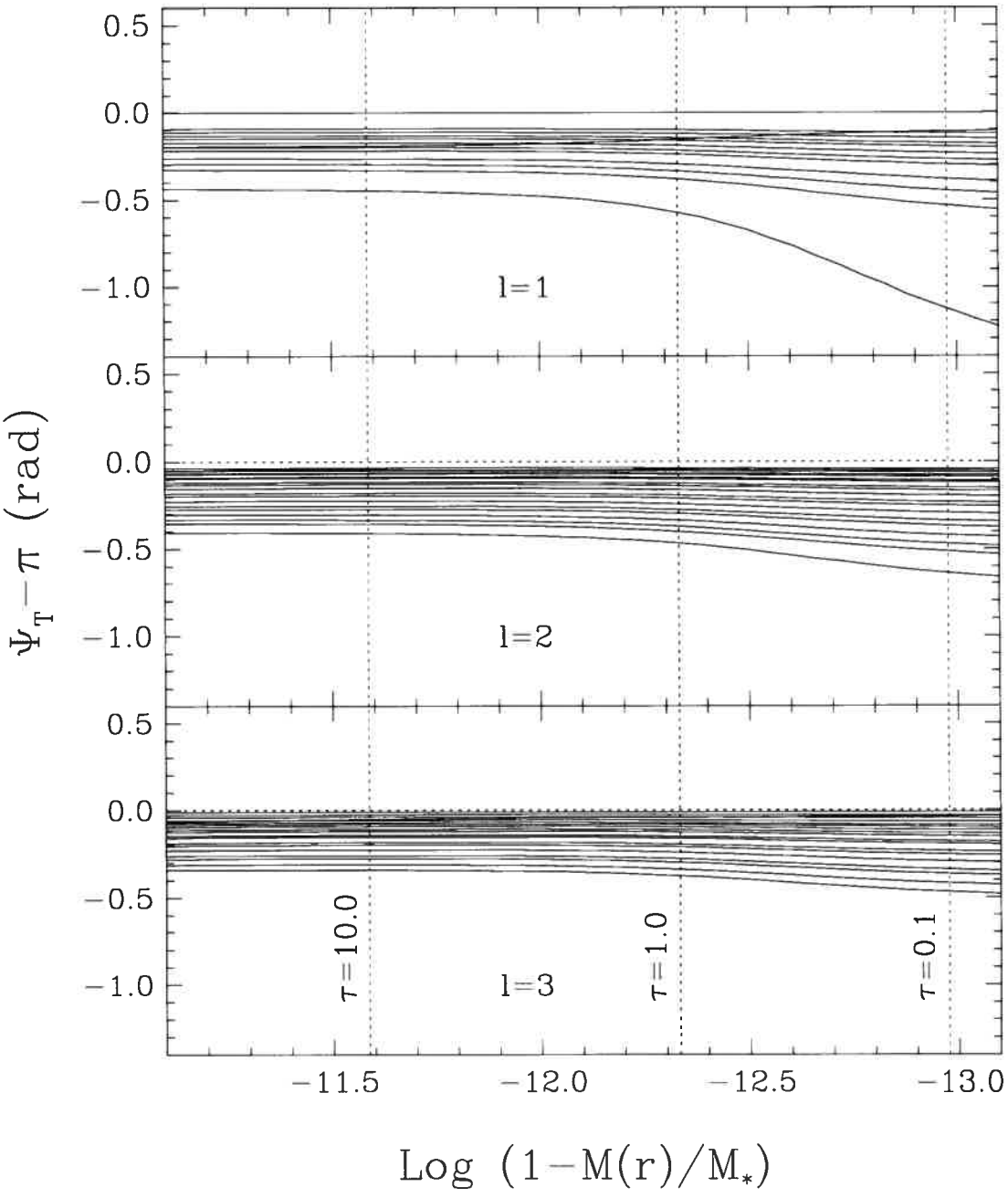

FIGURE 3.10 – Similar to Figure 3.9, but for the quantity $\psi_T - \pi$.

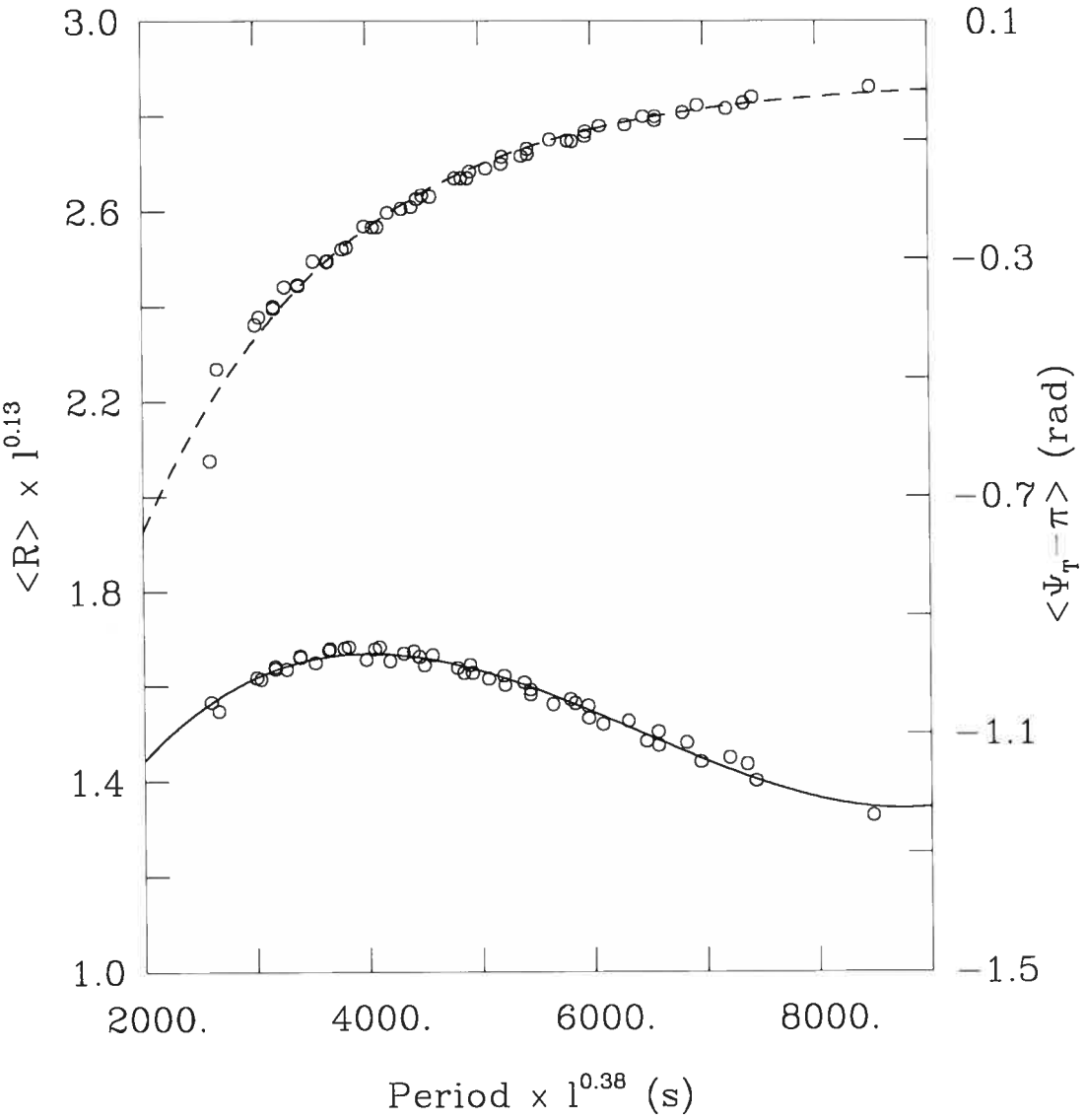

FIGURE 3.11 – Cubic fit to computed $< R >$ (continuous line) and $< \psi_T >$ (dashed line) values as a function of period and of degree index l for our representative PG 1716 star model. The cubic functions were generated using equations 3.46 and 3.47.

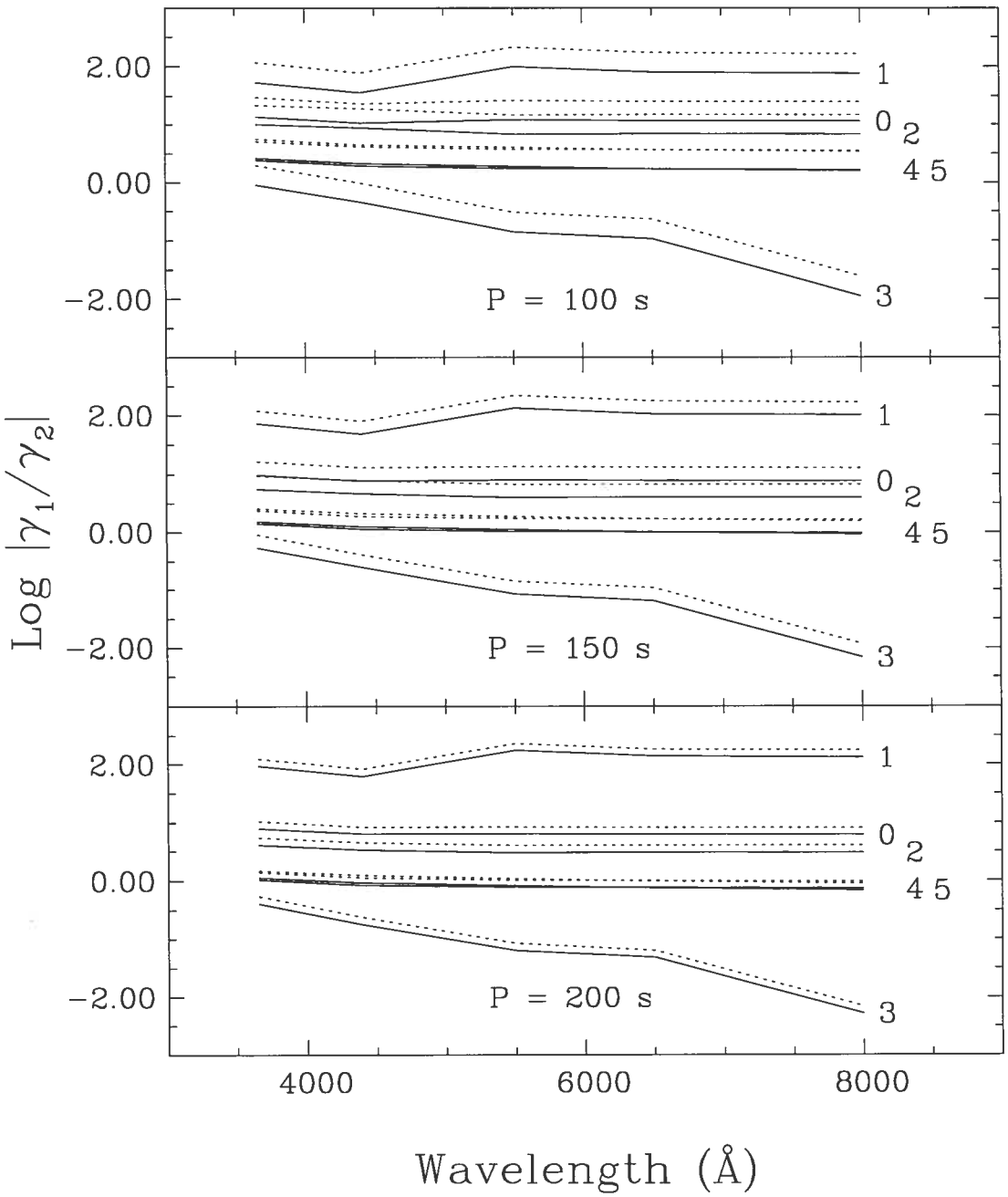

FIGURE 3.12 – Relative importance of the temperature terms (γ_1) compared to the radius and surface gravity terms (γ_2) for our representative EC 14026 star model in the *UBVRI* bandpasses. Continuous lines indicate the results obtained by fitting $< R >$ and $< \psi_T >$ according to equations (3.44) and (3.45) while dotted curves represent results obtained by setting the two parameters to their adiabatic values of $< R >= 1$ and $< \psi_T >= \pi$. Three typical periods (low-order p-modes) of 100, 150, and 200 s, as well as six values of the degree index, $l = 0$–5, are considered. The effective wavelengths of the various bandpasses are 3650 Å (U), 4400 Å (B), 5500 Å (V), 6500 Å (R), and 8000 Å (I).

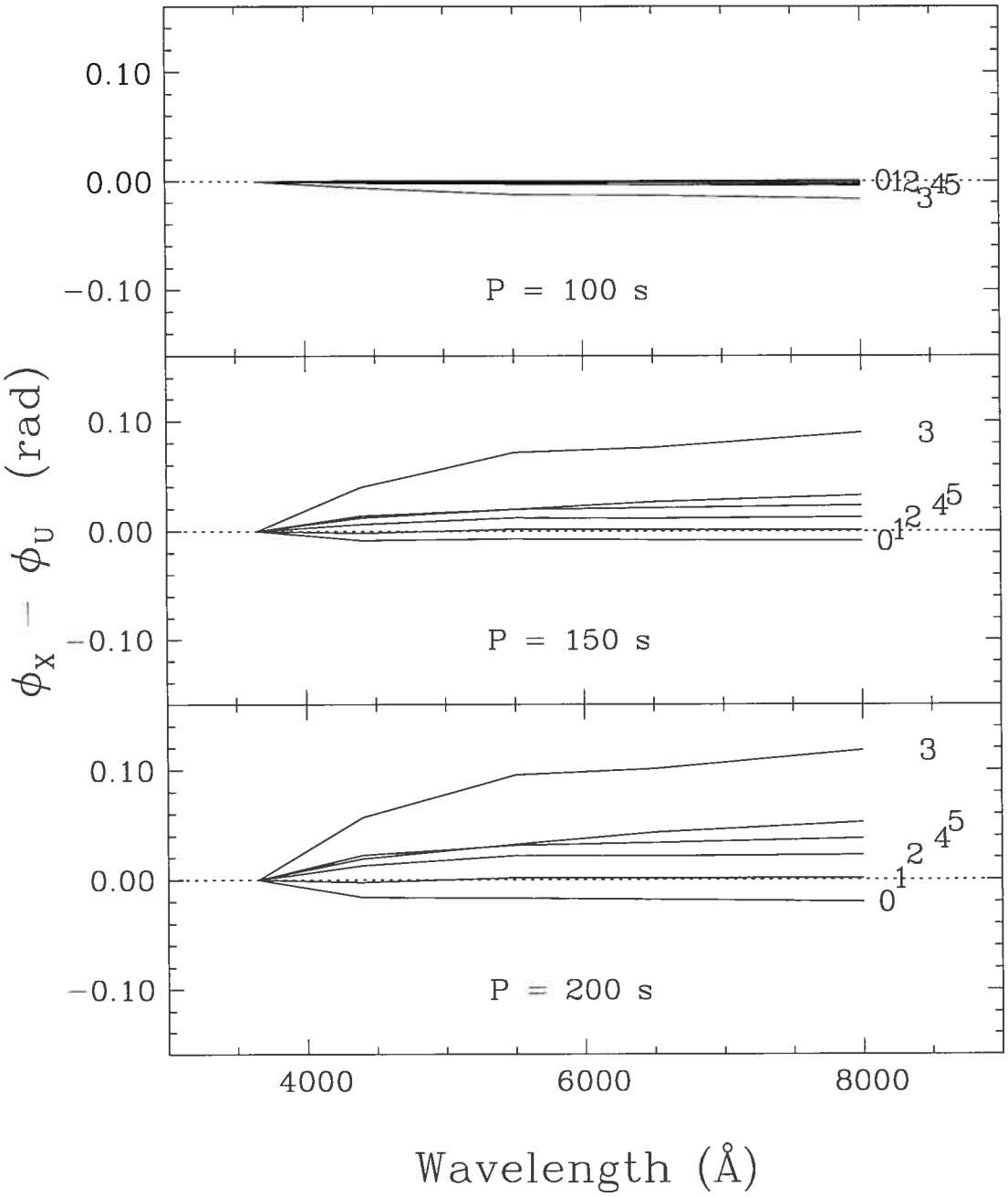

FIGURE 3.13 – Phase shifts relative to the U filter calculated for our EC 14026 star model for the $UBVRI$ bandpasses. Continuous lines represent full non-adiabatic results while the dashed curve indicates the adiabatic values (which are always equal to zero).

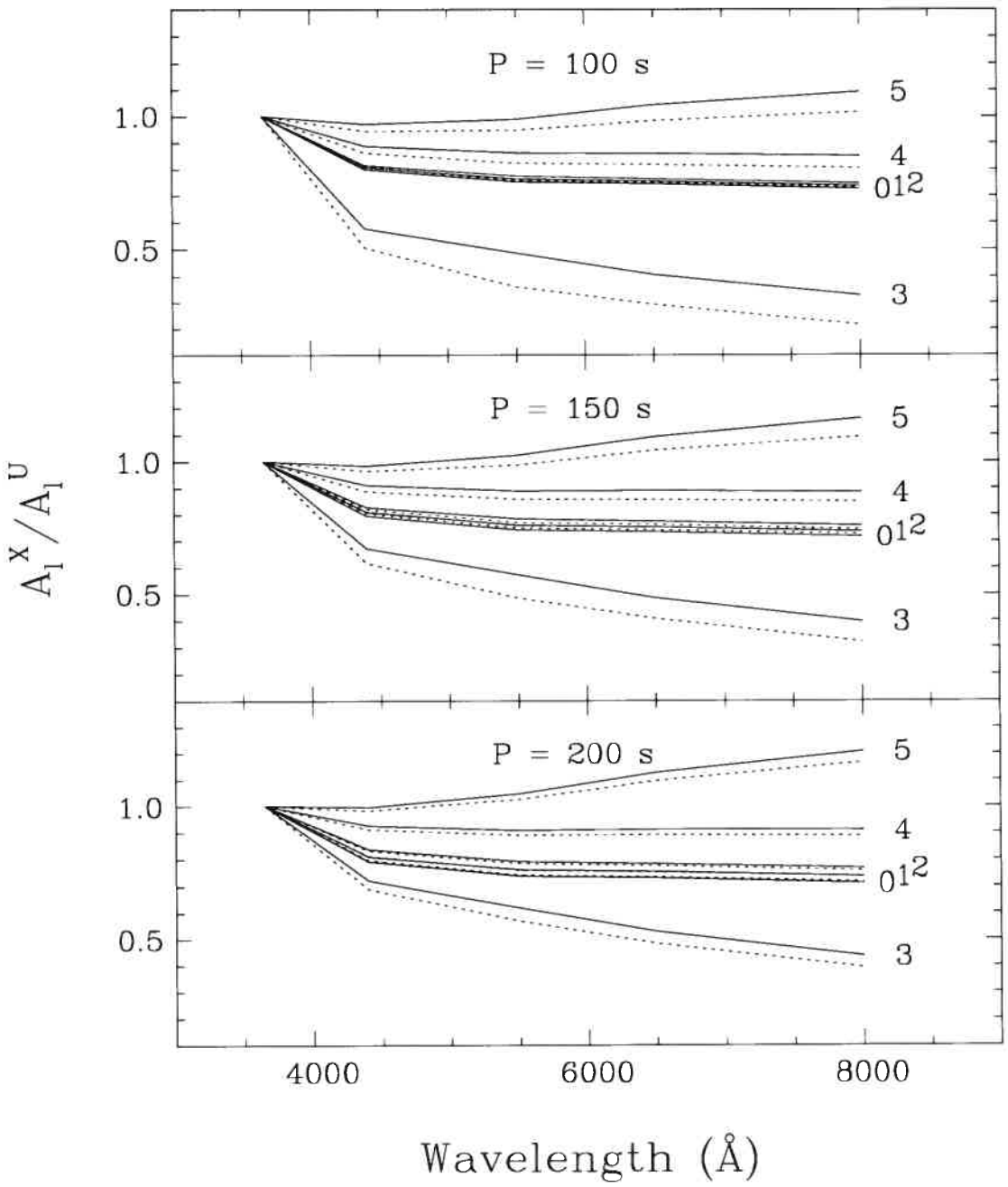

FIGURE 3.14 – Amplitude ratios relative to the U filter calculated for our EC 14026 star model for the $UBVRI$ bandpasses. Continuous lines represent full non-adiabatic results while the dashed curves indicates the adiabatic values obtained by forcing $< R >= 1$ and $< \psi_T >= \pi$.

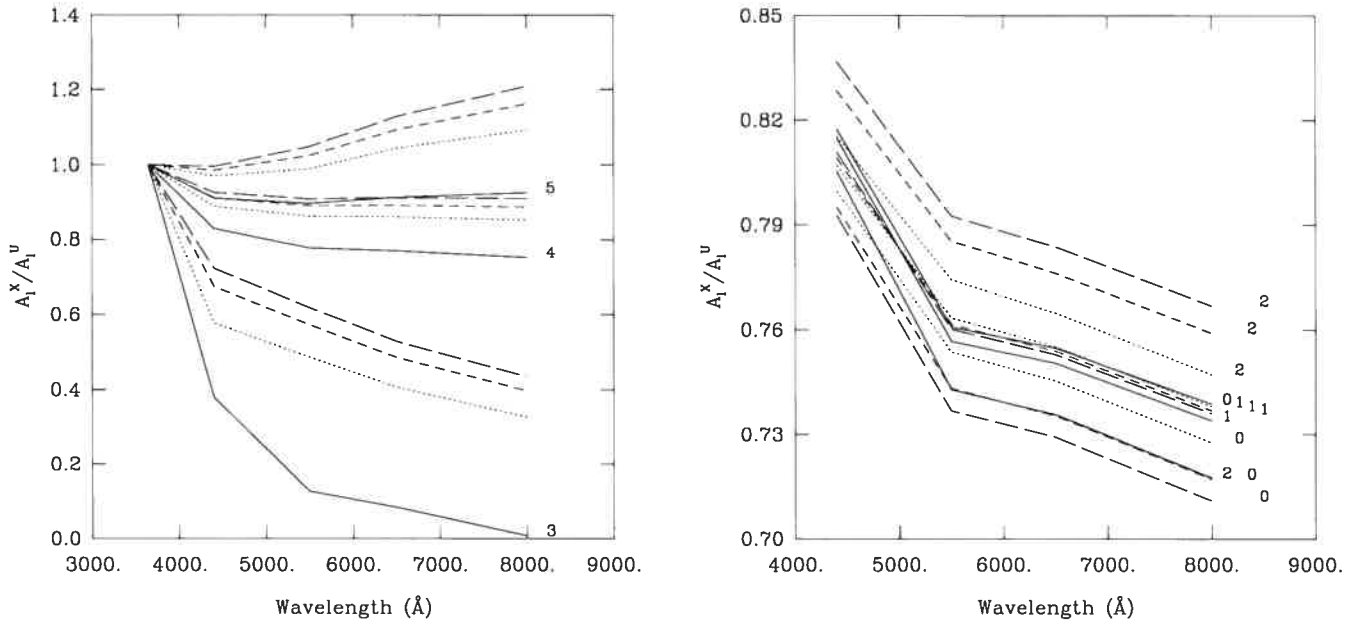

a) b)

FIGURE 3.15 – Amplitude ratios relative to the U filter calculated for our EC 14026 star model for the $UBVRI$ bandpasses. Ratios referring to l values of 3, 4 and 5 (panel a) have been separated from those for $l = 0$, 1 and 2 (panel b) for clarity. Dotted, dashed and long-dashed lines refer to periods with 100, 150 and 200 s respectively. They are compared to the amplitude ratios obtained in the limit where $\gamma_2 = 0$ (continuous curves).

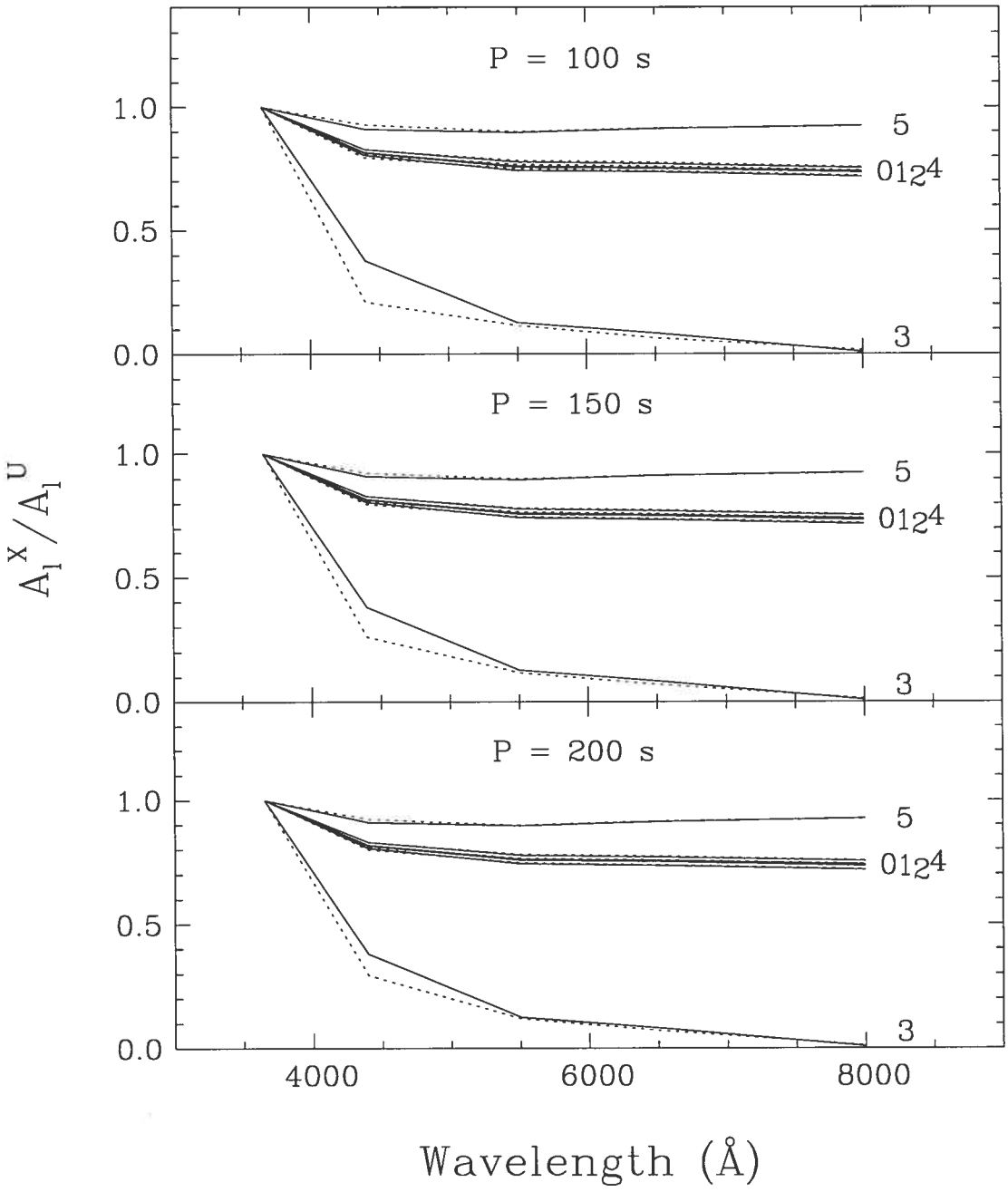

FIGURE 3.16 – Results of a numerical experiment in which the amplitude ratios relative to the U band were obtained by adopting $T_3 = 0$ (dotted lines) and by setting $\gamma_2 = 0$ (continuous lines).

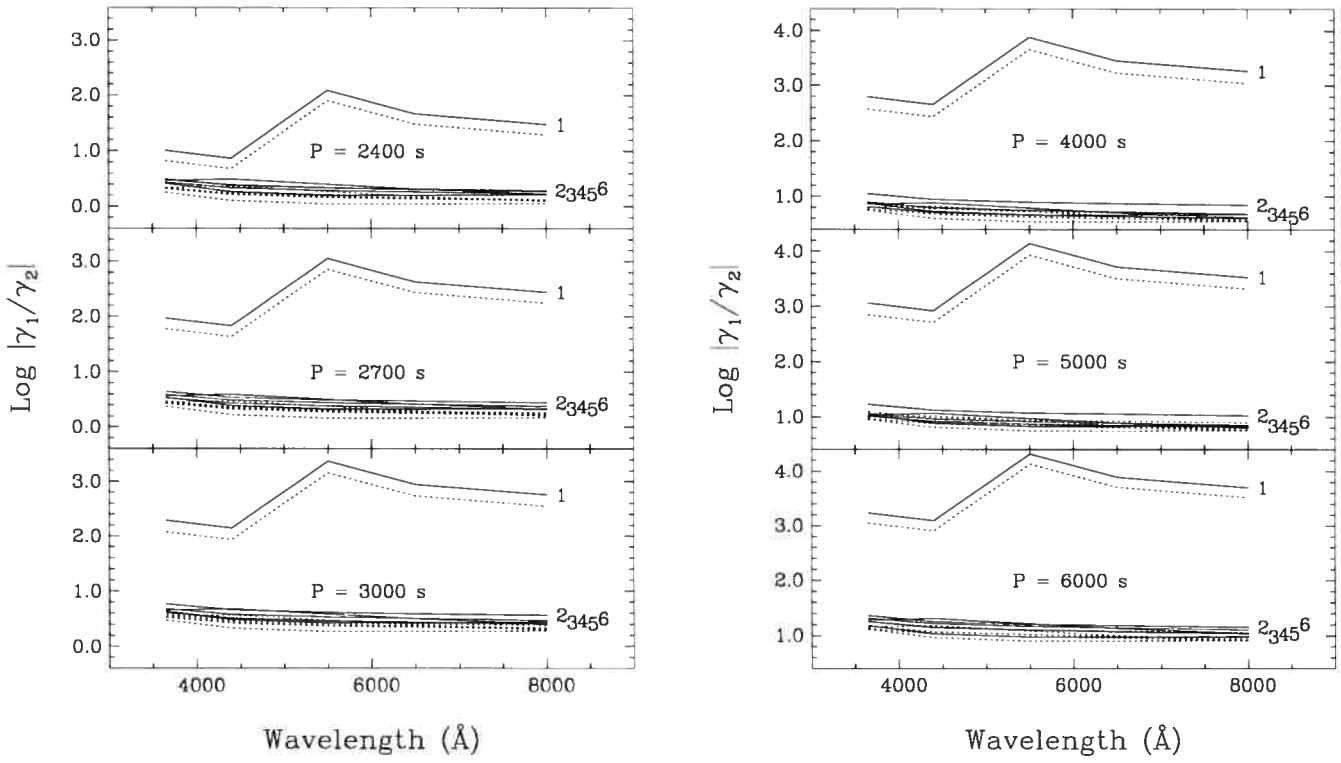

FIGURE 3.17 – Similar to Figure 3.12, but referring to our representative PG 1716 model. Six periods from 2400 s to 6000 s as well as six values of l from 1 to 6 are considered. For the continuous lines, $< R >$ and $< \psi_T >$ were derived from equations (3.46) and (3.47) while adiabatic values were imposed for the dotted lines.

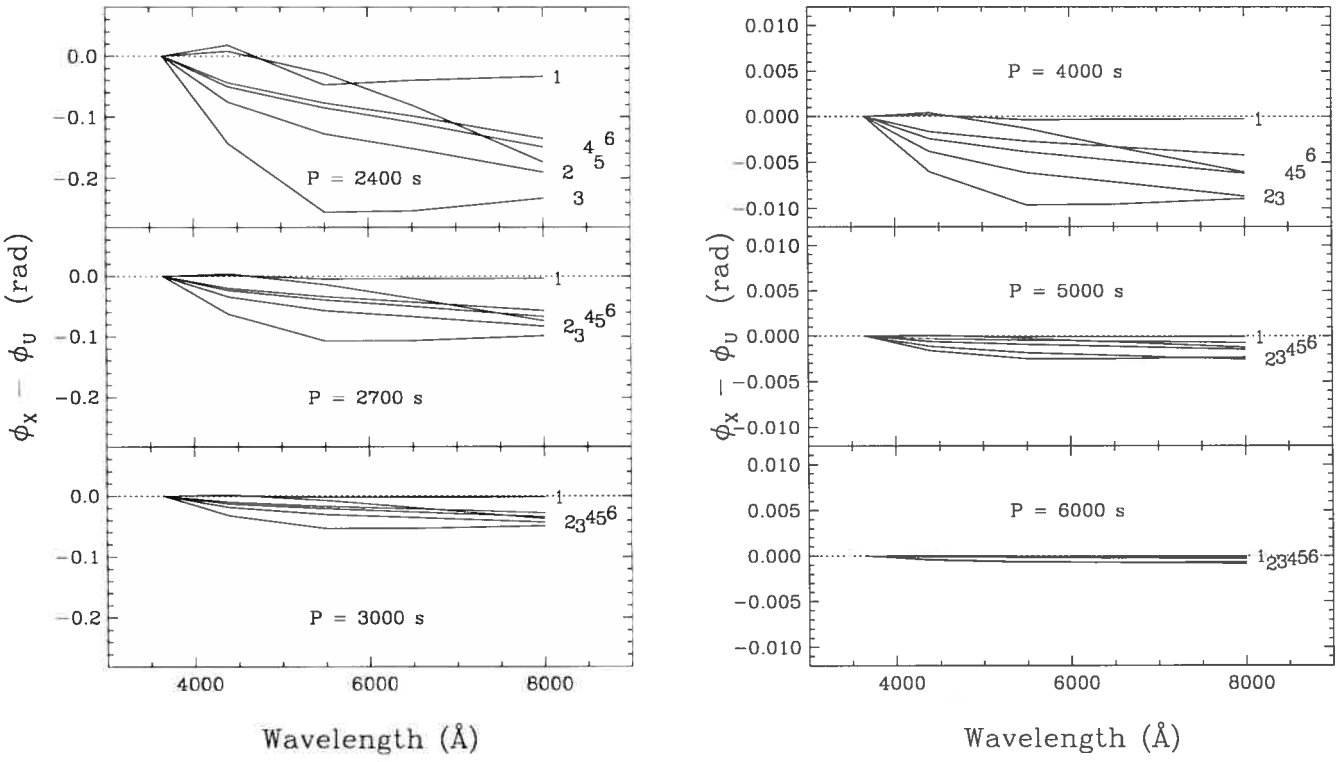

FIGURE 3.18 – Similar to Figure 3.13, but referring to our representative PG 1716 model. Note the change of ordinate scale between panel a) and panel b).

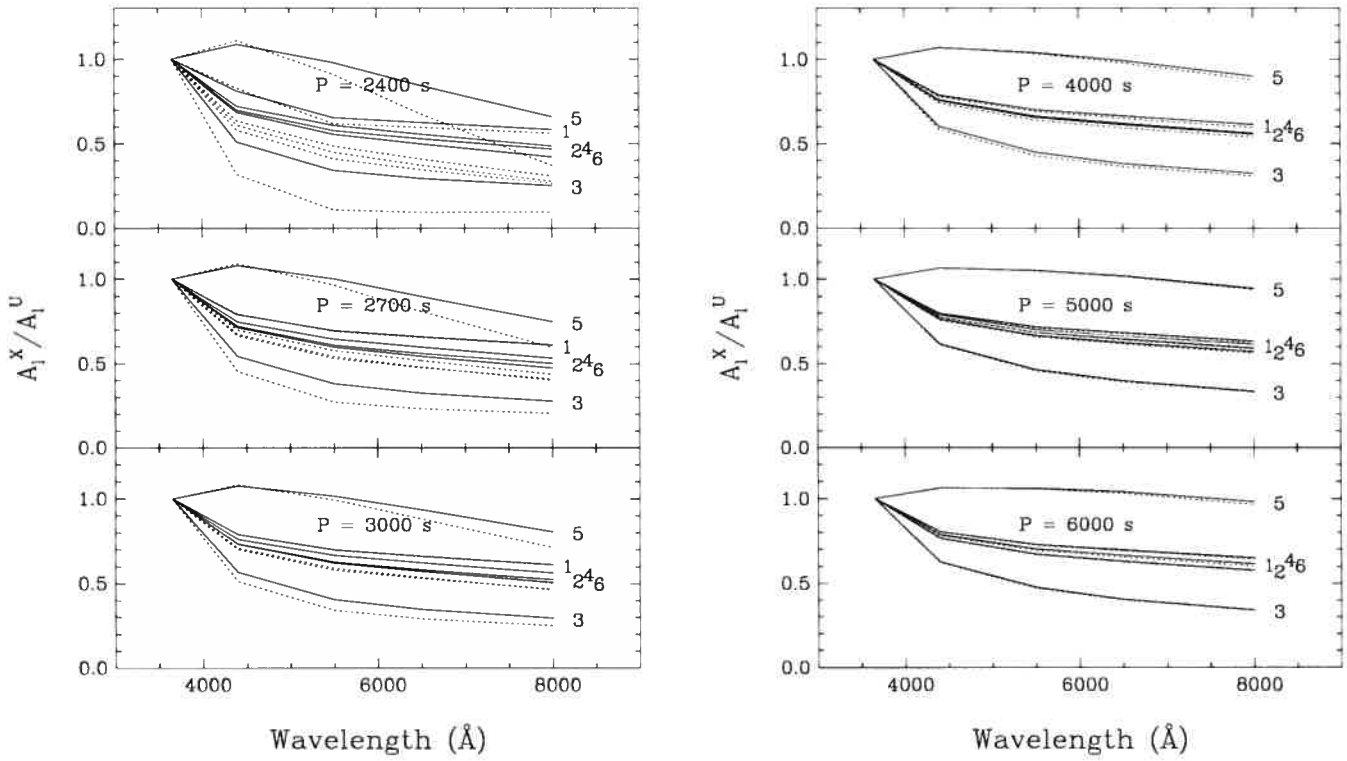

a) b)

FIGURE 3.19 – Similar to Figure 3.14, but referring to our representative PG 1716 model.

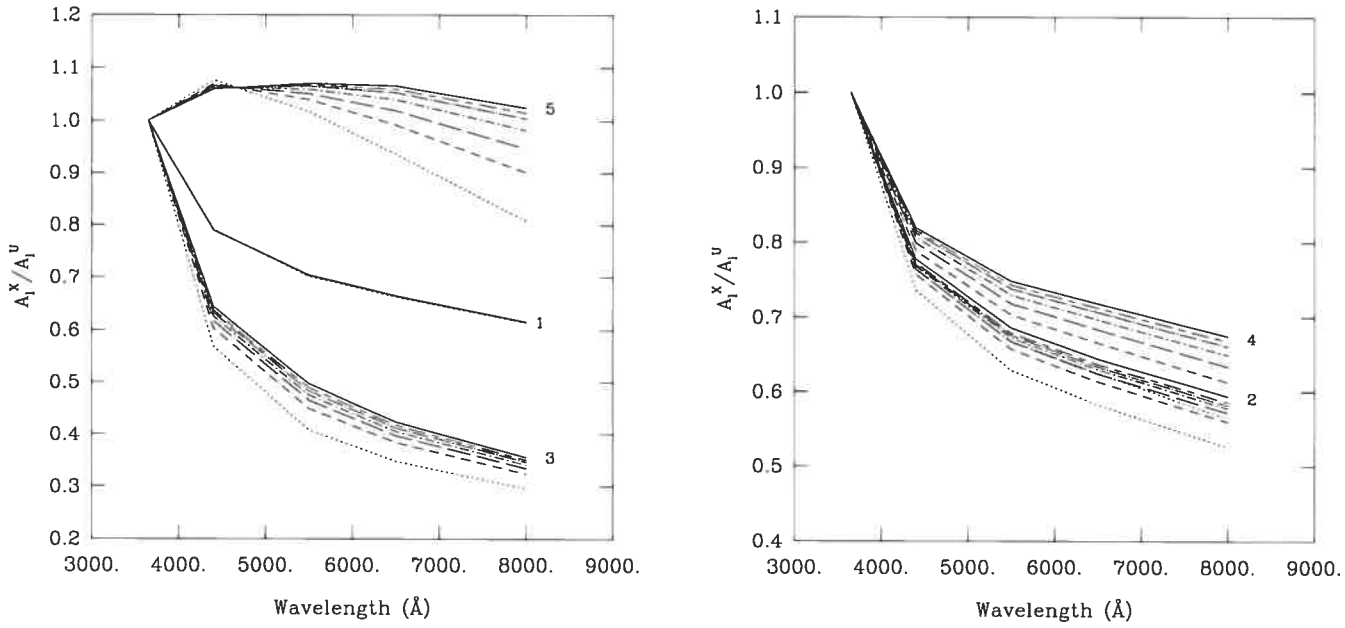

FIGURE 3.20 – Similar to Figure 3.15, but referring to our representative PG 1716 model. Amplitude ratios are illustrated for representative periods of $P = 3000$ s (dotted lines), 4000 s (dashed lines), 5000 s (long-dashed lines), 6000 s (dot-dashed lines), 7000 s (dot-long-dashed lines) and 8000 s (dashed-long-dashed lines). The continuous line refers to the case of $\gamma_2 = 0$.

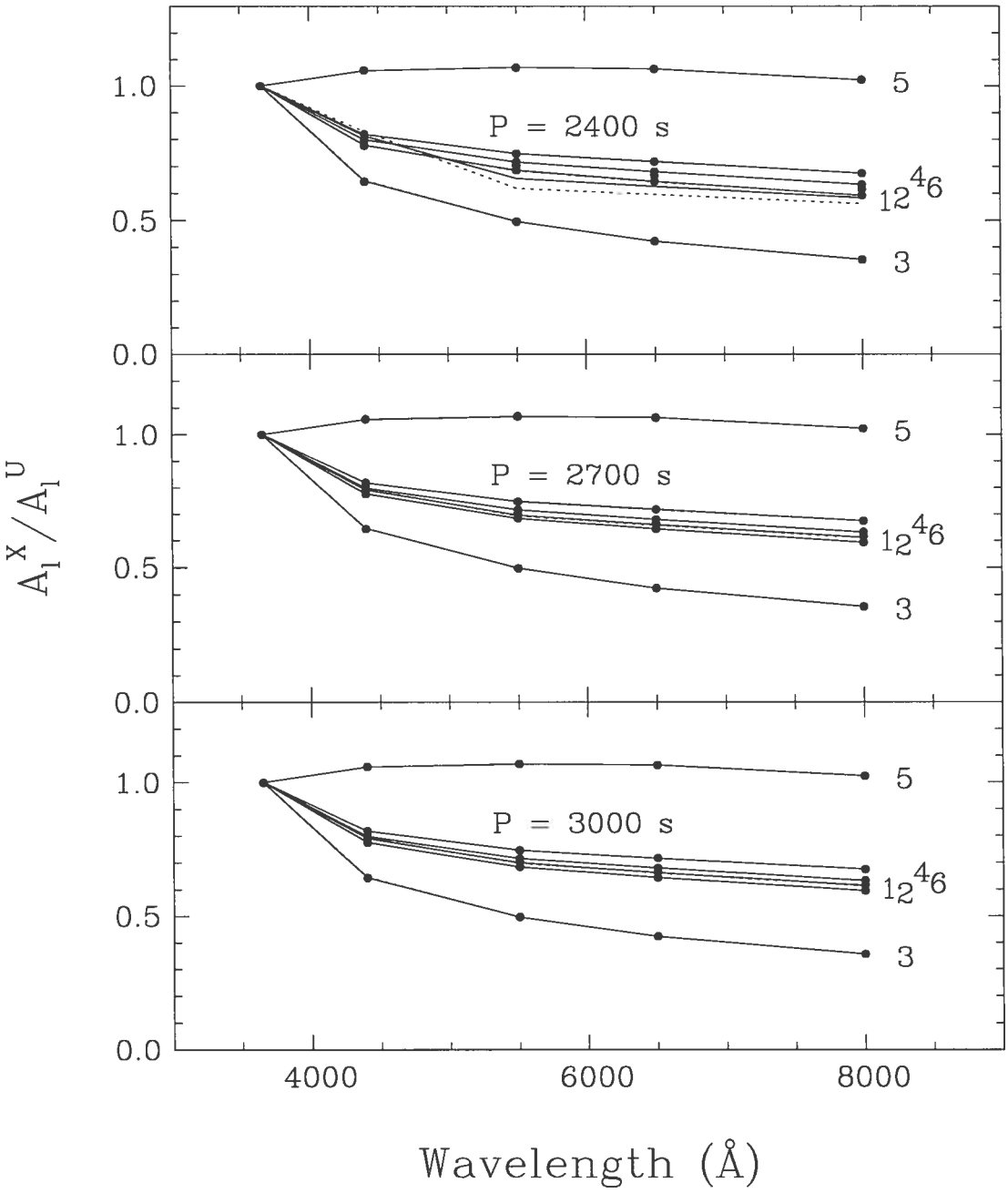

FIGURE 3.21 – Similar to Figure 3.16, but referring to our representative PG 1716 model.

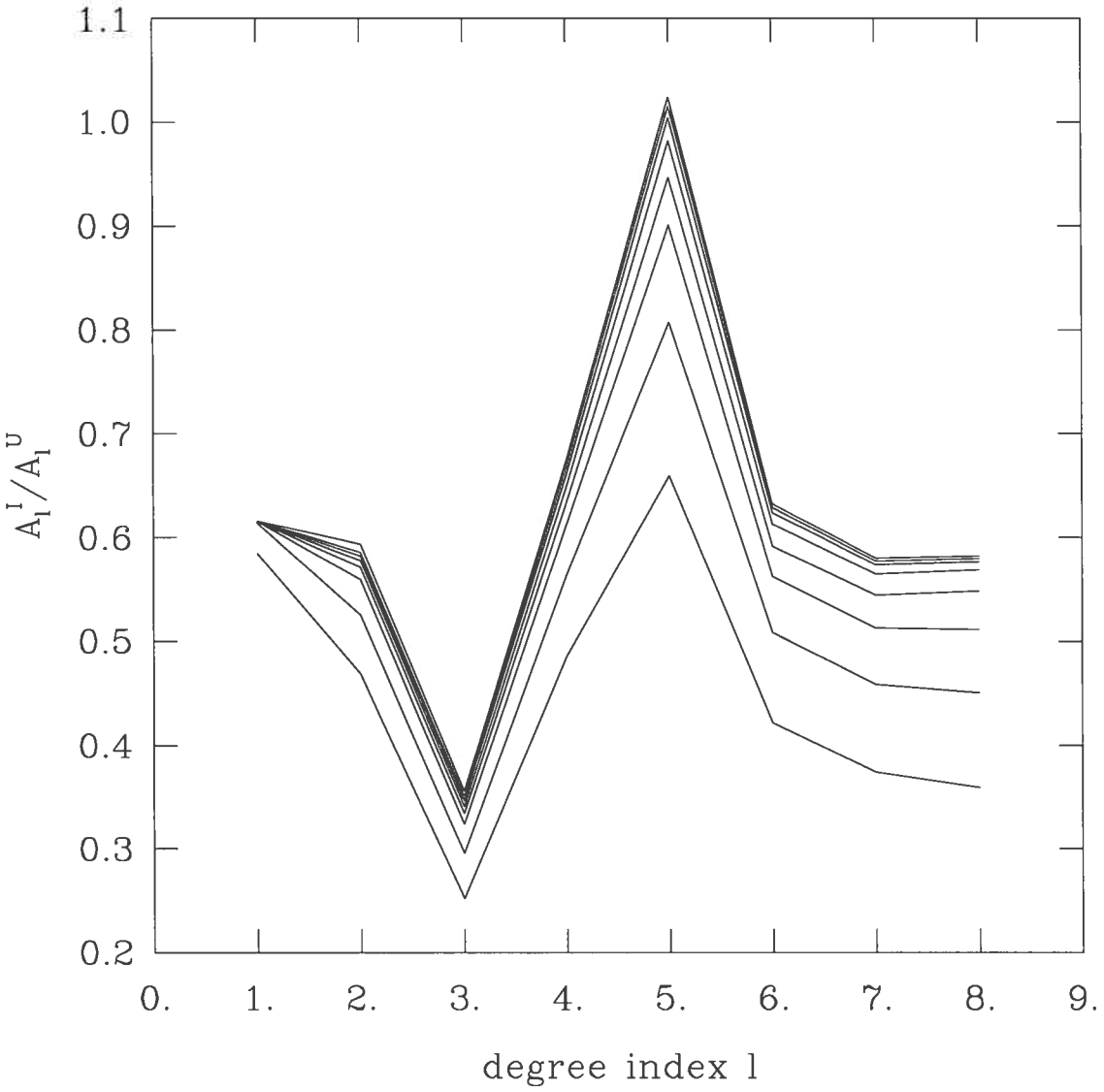

FIGURE 3.22 – I to U amplitude ratio as a function of degree index l on the basis of modes extending up to $l = 8$. From bottom to top, the various curves correspond to periods with P = 2400, 3000, 4000, 5000, 6000, 7000, 8000 s and an infinite period respectively.

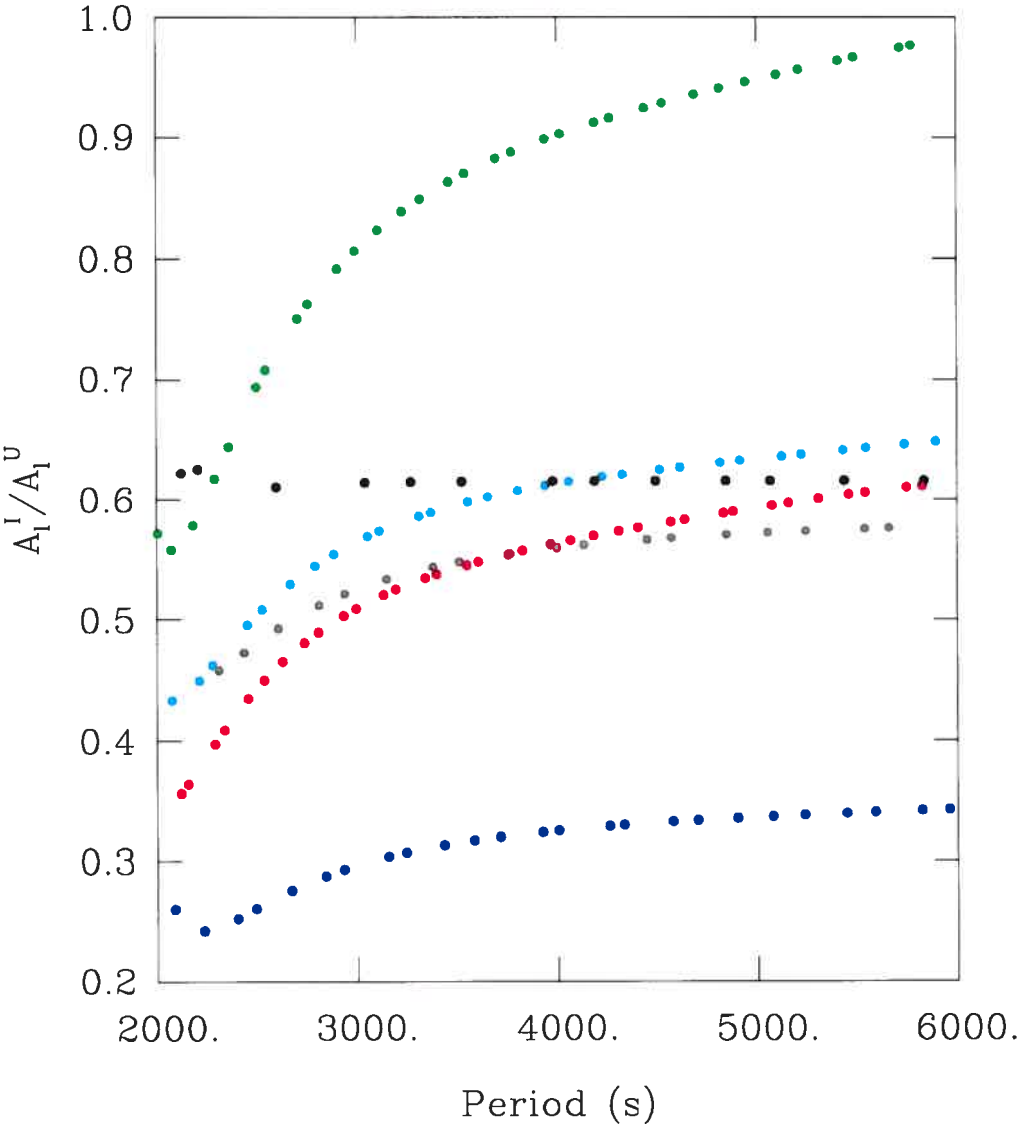

FIGURE 3.23 – Variation of the I/U amplitude ratio with period for our representative PG 1716 model. The values for different modes are indicated by points in black ($l = 1$), grey ($l = 2$), blue ($l = 3$), cyan ($l = 4$), green ($l = 5$) and red ($l = 6$).

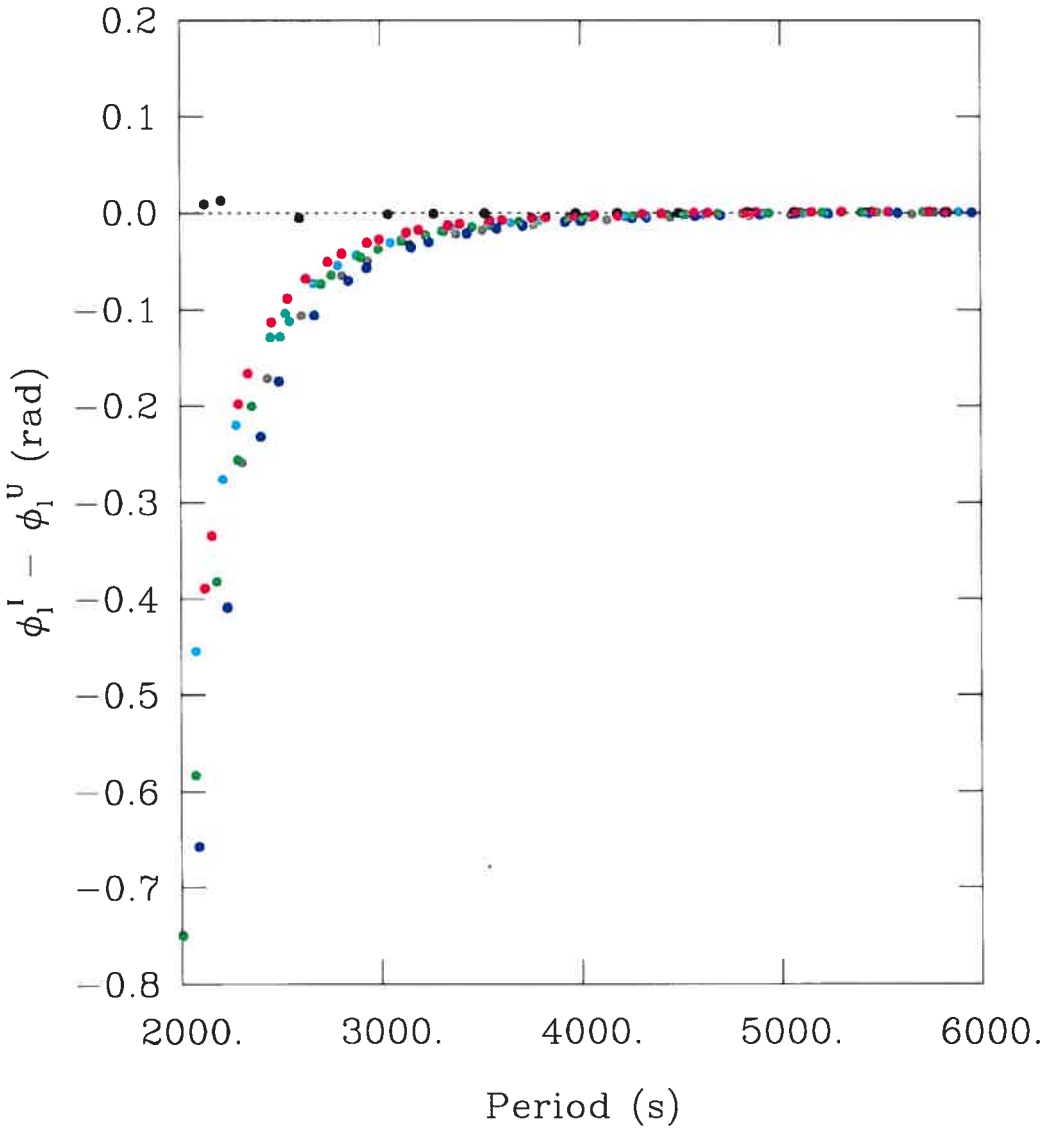

FIGURE 3.24 – Similar to Figure 3.23, but for phase differences between oscillations in the I and U bandpasses.

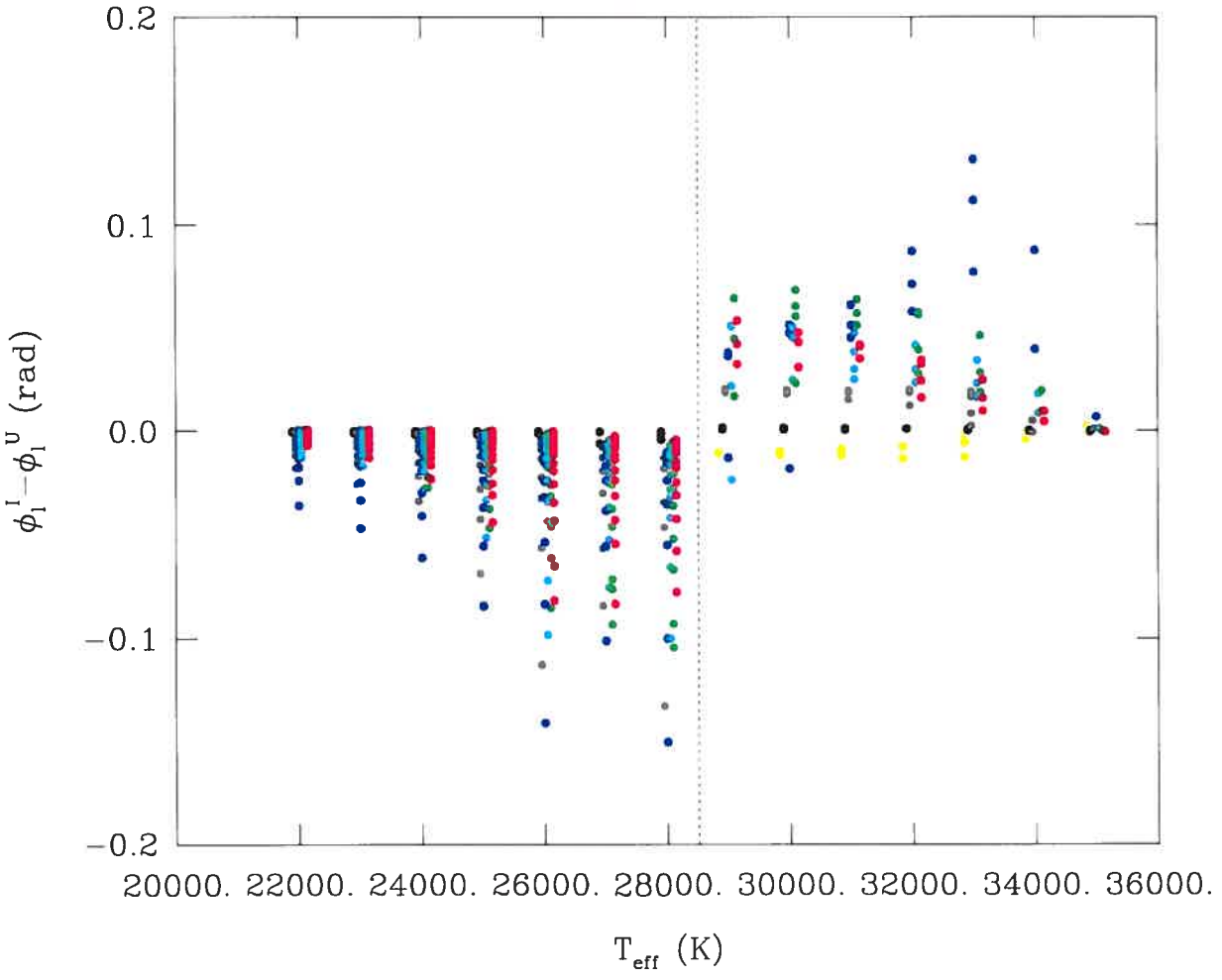

FIGURE 3.25 – Phase differences between oscillations in the I and U bandpasses for the sequence of subdwarf B star models listed in Table 3.4. The dotted vertical line divides the PG 1716 star models on the left from the EC 14026 models on the right. We illustrate modes with $l = 0$ (yellow, EC 14026 models only), $l = 1$ (black), $l = 2$ (grey), $l = 3$ (blue), $l = 4$ (cyan), $l = 5$ (green) and $l = 6$ (red).

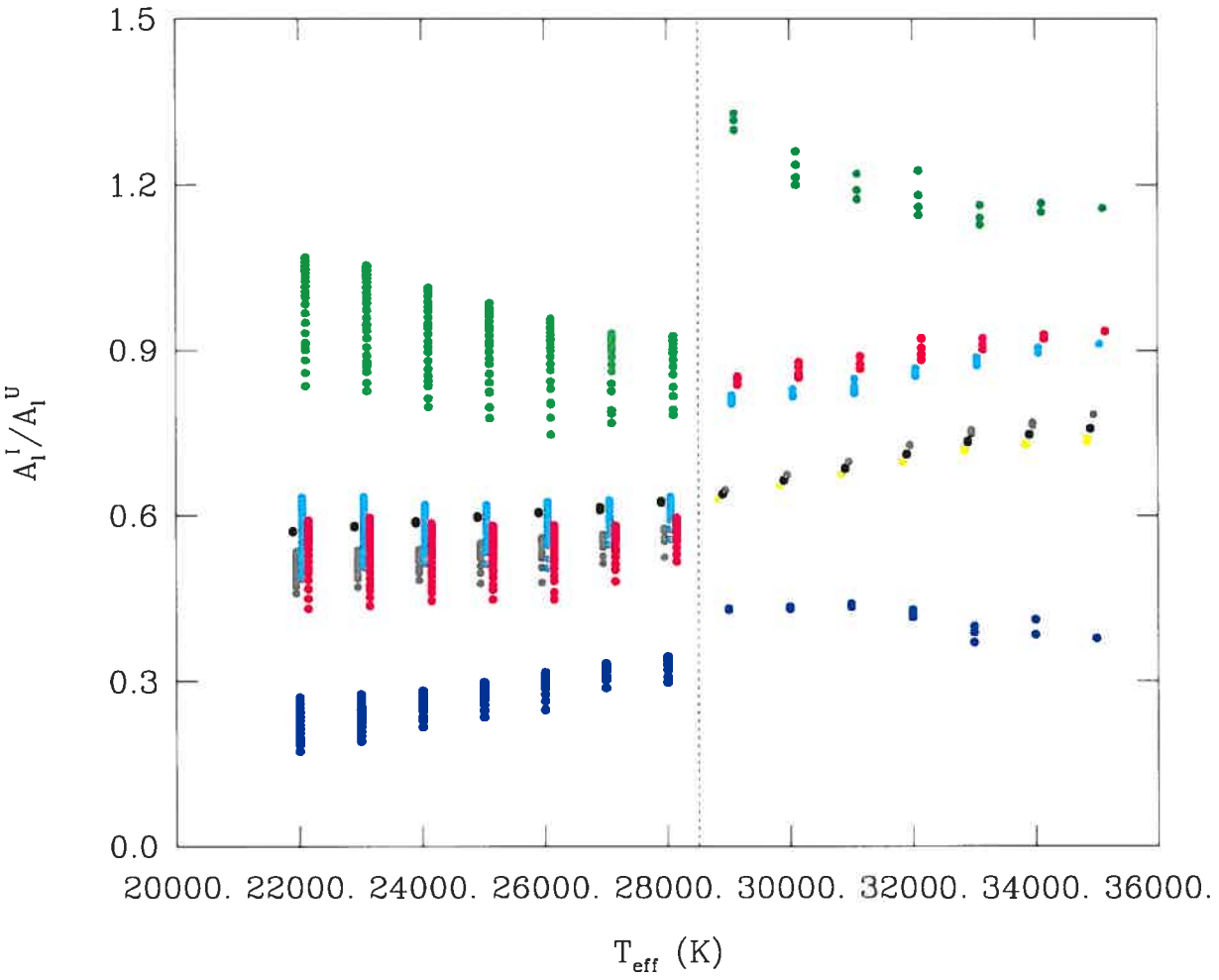

FIGURE 3.26 – Similar to Figure 3.25, but for I/U amplitude ratios.

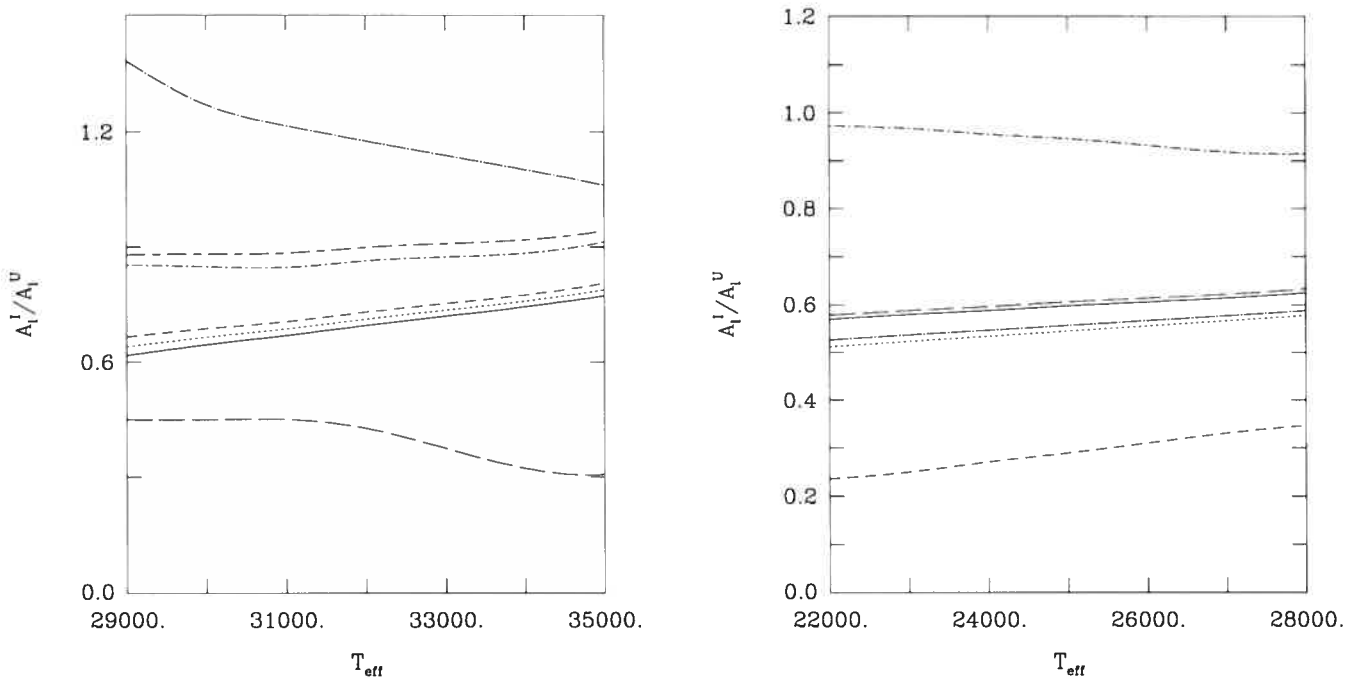

a) b)

FIGURE 3.27 – Behaviour of the I/U amplitude ratio with effective temperature of a model. (a) EC 14026 regime: the surface gravity was kept constant at $\log g = 5.75$, while $T_{\rm eff}$ was varied from 29,000 K – 35,000 K in increments of 1000 K. From top to bottom, the curves refer to modes with degree indices $l = 5$, 6, 4, 2, 1, 0 and 3. (b) PG 1716 regime: we adopted the representative value of $\log g = 5.40$ and varied the effective temperaure from 22,000 K – 28,000 K, again in steps of 1000 K. From top to bottom, the modes in question correspond to $l = 5$, 4, 1, 6, 2 and 3.

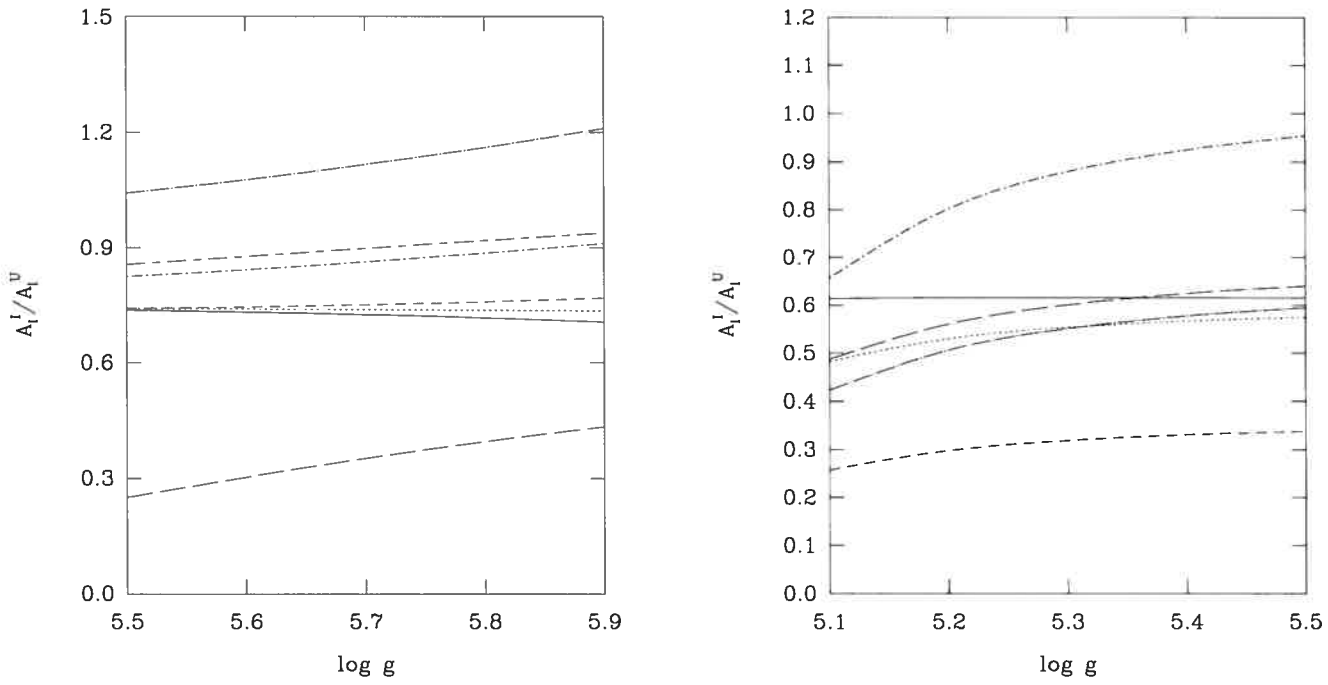

a) b)

FIGURE 3.28 – Behaviour of the I/U amplitude ratio with surface gravity. (a) EC 14026 regime: the effective temperature was kept constant at $T_{\rm eff} = 33,000$ K, while $\log g$ was varied from $5.5 - 5.9$ in increments of 0.1 dex. From top to bottom on the right hand side, the curves refer to modes with degree indices $l = 5$, 6, 4, 2, 1, 0 and 3. (b) PG 1716 regime: we adopted the representative value of $T_{\rm eff} = 27,000$ K and varied the surface gravity from 5.1 to 5.5, again in steps of 0.1 dex. From top to bottom on the right hand side, the modes in question correspond to $l = 5$, 4, 1, 6, 2 and 3.

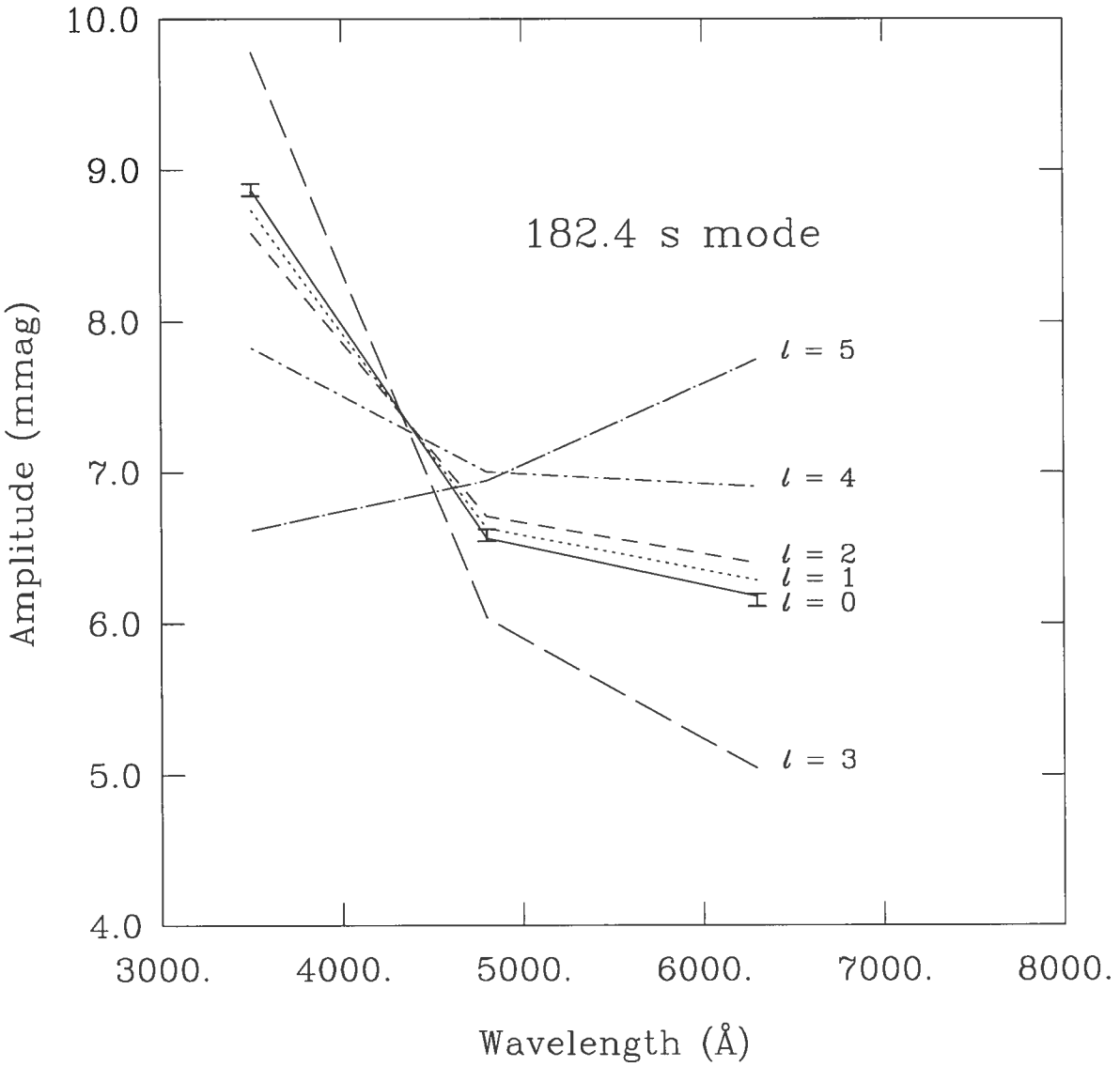

FIGURE 3.29 – Fit to the u', g' and r' pulsational amplitudes observed for the 182.4 s mode of KPD 2109+4401 by Jeffery et al. (2004). The predicted amplitude-wavelength behaviours of modes with l=0 to l=5 have been fit to the observed values using a least-squares procedure. Only the l=0 curve provides an acceptable fit.

Chapter 4

ASTEROSEISMOLOGICAL STUDIES OF LONG-PERIOD VARIABLE SUBDWARF B STARS - I. A MULTI-SITE CAMPAIGN ON PG 1627+017[1]

S.K. Randall[2] , G. Fontaine[2], E.M. Green[3] , P. Brassard[2], D. Kilkenny[4] , L. Crause[4], D.M. Terndrup[5] , A. Daane[5,6] , L.L. Kiss[7] , A.P. Jacob[7], T.R. Bedding[7], B.-Q. For[3], and P.-O. Quirion[2]

Submitted to *The Astrophysical Journal*

---

[1]Some of the observations reported here were obtained at the MMT Observatory, a joint facility of the University of Arizona and the Smithsonian Institution.

[2]Département de Physique, Université de Montréal, C.P. 6128, Succ. Centre-Ville, Montréal, Québec, Canada H3C 3J7; randall@astro.umontreal.ca, fontaine@astro.umontreal.ca, brassard@astro.umontreal.ca, quirion@astro.umontreal.ca

[3]Steward Observatory, University of Arizona, Tucson, AZ 85721; bgreen@as.arizona.edu, bfor@as.arizona.edu

[4]South African Astronomical Observatory, PO Box 9, Observatory 7935, Cape Town, South Africa; dmk@saao.ac.za, lisa@saao.ac.za

[5]Department of Astronomy, The Ohio State University, 140 West 18th Avenue, Columbus, OH 43210; terndrup@astronomy.ohio-state.edu

[6]Clemson University, 118 Kinard Laboratory, Clemson, SC 29634; abigaid@clemson.edu

[7]School of Physics, University of Sydney, Sydney 2006, Australia; laszlo@physics.usyd.edu.au, a.jacob@physics.usyd.edu.au, bedding@physics.usyd.edu.au

4.1 ABSTRACT

We present the results of an extensive multi-site campaign on the long-period variable subdwarf B star PG 1627+017. Gathering data at telescopes around the world over a period of three months yielded over 300 hours of useful R band and ~50 hours of simultaneous U/R differential photometry. From the R band data we were able to extract 23 periodicities in the 4500-9000 s range with amplitudes between 0.05 and 0.5 % of the star's mean brightness. The oscillations with the highest amplitudes cluster between 6300 and 7050 s and are thought to exhibit frequency splitting due to binary-synchronous stellar rotation. Interestingly, we find the observed period distribution to be extremely non-uniform, with dense frequency multiplets occurring in several narrow band passes. Though the reason for this is not clear, we suggest that it is related to either an unknown mode selection mechanism or the short-period binary nature of the target. In order to compare the observed period spectrum to theoretical predictions, we constructed a set of newly updated and improved subdwarf B star models. We find that, by invoking degree indices of $l = 2$, 3 and 4, non-adiabatic calculations can qualitatively reproduce the range of periodicities measured for PG 1627+017 if its atmospheric parameters are pushed to the lower end of their spectroscopic temperature uncertainties. However, the exploitation of rotational splitting and the U/R photometry, as well as the mean spacing between periodicities indicate that at least the four highest amplitude peaks probably correspond to modes with $l = 1$. While this points to deficiencies in our models at the non-adiabatic level, the resulting constraints on mode identification are invaluable to first attempts at asteroseismology. Indeed, we identify only a few families of models that can closely reproduce the main periodicities observed in terms of dipole modes. This leaves us hopeful that, given a larger number of partially identified observed frequencies, asteroseismology may be achieved for long-period variable subdwarf B stars.

4.2 INTRODUCTION

Subdwarf B (sdB) stars are evolved extreme horizontal branch (EHB) stars with atmospheric parameters in the range 20,000 $\lesssim T_{\rm eff} \lesssim$ 40,000 K and 5.0 $\lesssim \log g \lesssim$ 6.2 (Saffer et al.

1994). They are characterised by low masses of $M \sim 0.5\ M_{\odot}$ and are believed to be composed of a He-burning core surrounded by a very thin hydrogen shell, having lost most of the envelope near the first red giant tip (Heber 1986). The resulting hydrogen layer is too feeble to sustain significant H-shell burning during core He-evolution, preventing these stars from ascending the asymptotic giant branch. Instead, they evolve along and off the EHB to become subdwarf O stars (which typically have $T_{\rm eff} \sim 45,000$ K, $\log g \sim 5.5$ according to Dreizler 1993) and eventually end their lives as low-mass white dwarfs (Bergeron et al. 1994).

The interest in subdwarf B stars received a formidable boost when it was discovered that a small fraction of them show rapid multi-periodic luminosity variations. Following the discovery of the first short period pulsator at the South African Astronomical Observatory (Kilkenny et al. 1997), the number of known so-called EC 14026 stars has now risen to 34 (see Fontaine et al. 2005 for a recent review). Typical members of this class oscillate with periods in the range 100−200 s at relatively low amplitudes between 1 and 25 mmag and are clustered around atmospheric parameters of $T_{\rm eff} \sim 33,000$ K and $\log g \sim 5.7$. Interestingly, independent theoretical calculations (Charpinet et al. 1996, 1997) predicted luminosity variations in these objects at about the same time as the first observational discovery was made. The pressure mode (p-mode) instabilities detected in the models are caused by a classical κ-mechanism associated with the iron opacity peak in the stellar envelope. This opacity peak in turn requires a local overabundance of iron, which is achieved by the competitive action of gravitational settling and radiative levitation. As the relative contributions of these two processes are determined by the surface gravity and the effective temperature of the star, a theoretical instability strip is formed in the $\log g$ - $T_{\rm eff}$ plane, into which all observed EC 14026 stars fall. This, together with the fact that the predicted periods correlate well with those observed, leads us to believe that a good qualitative understanding of the driving mechanism has been reached. Beyond that, there have been four successful cases of a quantitative match between theoretically calculated and observed pulsation periods (Brassard et al. 2001; Charpinet et al. 2003; Charpinet et al. 2005a; Charpinet et al. 2005b), allowing the tools of asteroseismology to be applied. Being the ultimate goal in the study of sdB pulsations, the quantitative interpretation of the periodicities detected led to the determination of the stars' basic structural parameters including

1994). They are characterised by low masses of $M \sim 0.5\ M_{\odot}$ and are believed to be composed of a He-burning core surrounded by a very thin hydrogen shell, having lost most of the envelope near the first red giant tip (Heber 1986). The resulting hydrogen layer is too feeble to sustain significant H-shell burning during core He-burning, preventing these stars from ascending the asymptotic giant branch. Instead, they evolve along and off the EHB to become subdwarf O stars (which typically have $T_{\rm eff} \sim 45,000$ K, $\log g \sim 5.5$ according to Dreizler 1993) and eventually end their lives as low-mass white dwarfs (Bergeron et al. 1994).

The interest in subdwarf B stars received a formidable boost when it was discovered that a small fraction of them show rapid multi-periodic luminosity variations. Following the discovery of the first short period pulsator at the South African Astronomical Observatory (Kilkenny et al. 1997), the number of known so-called EC 14026 stars has now risen to 34 (see Fontaine et al. 2005 for a recent review). Typical members of this class oscillate with periods in the range 100−200 s at relatively low amplitudes between 1 and 25 mmag and are clustered around atmospheric parameters of $T_{\rm eff} \sim 33{,}000$ K and $\log g \sim 5.7$. Interestingly, independent theoretical calculations (Charpinet et al. 1996, 1997) predicted luminosity variations in these objects at about the same time as the first observational discovery was made. The pressure mode (p-mode) instabilities detected in the models are caused by a classical κ-mechanism associated with the iron opacity peak in the stellar envelope. This opacity peak in turn requires a local overabundance of iron, which is achieved by the competitive action of gravitational settling and radiative levitation. As the relative contributions of these two processes are determined by the surface gravity and the effective temperature of the star, a theoretical instability strip is formed in the $\log g$ - $T_{\rm eff}$ plane, into which all observed EC 14026 stars fall. This, together with the fact that the predicted periods correlate well with those observed, leads us to believe that a good qualitative understanding of the driving mechanism has been reached. Beyond that, there have been four successful cases of a quantitative match between theoretically calculated and observed pulsation periods (Brassard et al. 2001; Charpinet et al. 2003; Charpinet et al. 2005a; Charpinet et al. 2005b), allowing the tools of asteroseismology to be applied. Being the ultimate goal in the study of sdB pulsations, the quantitative interpretation of the periodicities detected led to the determination of the stars' basic structural parameters including

masses as well as the thickness of their hydrogen envelopes, parameters which can often not be deduced any other way.

However, the scientific community was presented with a further puzzle when the discovery of a second class of subdwarf B pulsators was announced by one of us (E.M.G.) at the "Asteroseismology across the H-R diagram" conference held in Porto in July 2002 (Green et al. 2003a). In contrast to the EC 14026 stars, the new pulsators oscillate slowly, and are hence referred to as long-period variable subdwarf B stars, or PG 1716 stars after the prototype PG 1716+426. They appear to be multi-mode pulsators with typical periods of around one hour or more, and very small pulsational amplitudes of 0.5−5 mmag. The long periods observed automatically imply the excitation of high radial order gravity (g-) modes, rather than p-modes as in the case of the EC 14026 stars. Another difference between the two types of pulsator is that the long-period variables are distinctly cooler, with effective temperatures between $\sim$ 21,000−27,000 K, and lie at lower surface gravities clustering around $\log g \simeq 5.4$. Helium core-burning models suggest that the lower temperatures encountered are a consequence of the hydrogen envelopes being somewhat thicker than in the EC 14026 pulsators, extending to masses of perhaps 0.003−0.004 $M_{\odot}$ in the coolest objects (Dorman et al. 1993). Another noteworthy fact is that the slow oscillators are surprisingly common. While EC 14026 stars make up less than 5 % of the subdwarf B population, the long-period variables account for 25−30 % of all sdBs, and for more than 75 % of those at temperatures below 30,000 K. Indeed, it is possible that all cool subdwarf B stars are slowly pulsating at some detectable amplitude level.

The most pressing question following the discovery of these new variables was that of their very existence. Early suggestions for a possible driving mechanism included a slow reviving of the hydrogen shell (Green et al. 2003b) and tidal excitation in a close binary system (Fontaine et al. 2003b), but were discarded. A much more promising idea was subsequently brought forward. Invoking the same κ-mechanism that so successfully explains the EC 14026 instability strip, Fontaine et al (2003a) were able to computationally excite bands of periods in the same range as those observed. In contrast to the EC 14026 stars, where we believe the p-modes to have low degree indices (l = 0, 1, 2, 3...), only g-modes with $l = 3$ or higher

could be excited in the majority of the PG 1716 star models computed. The one exception to this rule was the coolest model ($T_{\rm eff} = 22,000$ K), which also showed unstable $l = 2$ modes. Although canonical wisdom suggests that modes with $l \geq 3$ cannot be detected due to cancellation effects when integrating over the visible disk of the star, the authors argued that their calculations rule out the excitation of modes with smaller l-values and that in fact the higher degree indices of the modes could be the explanation for the very small pulsational amplitudes encountered.

The presence of observable $l = 3$ modes can in principle be determined by independent means. In a recent application of well-known theory to sdB stars, it was shown (Randall et al. 2005a) that the l-index of a given mode, together with the viewing aspect, leaves its mark on the relationship between the amplitude of the pulsation and the wavelength at which it is measured. The effects of the viewing aspect can be eliminated by considering the ratio of amplitudes at different wavelengths, or in more practical terms the amplitude ratio of periodicities obtained through different bandpasses. While the amplitudes are predicted to increase towards shorter wavelengths in the optical domain for all modes, the ratio of amplitudes in the blue to those in the red is significantly larger for modes with $l = 3$ than for modes with $l = 1$, 2 or 4. Hence the interpretation of multi-colour data of sufficient quality should enable the distinction of $l = 3$ modes from the canonically expected $l = 1$ and 2 modes.

Since the discovery of the first long-period variable, the total count has risen to 31 (Fontaine et al. 2005; Green et al. in preparation), a number which is roughly the same as for the fast pulsators. However, while many EC 14026 stars have been studied in detail, the photometry data on most of the new pulsators consists of only one or two nights of observations, which is generally enough to confirm variability, but far too little to determine the periods of pulsation. At the time of our observations, there was only one exception to this rule: the class prototype PG 1716+426, which was monitored for $\sim$ 81 hours in a multi-site campaign (Green et al. 2003b; Reed et al. 2004), revealing the presence of at least 3–5 modes with periods in the range 0.8 to 1.4 hours. Unfortunately, the baseline and duty cycle obtained were not sufficient for detailed analyses, and no convincing quantitative statements were possible.

In view of this, the next obvious step was an observational campaign on a larger scale, the

ultimate aim being an asteroseismological analysis similar to those accomplished for the four EC 14026 stars mentioned earlier. We believe the study of the long-period variables to be extremely useful to the understanding of the structure and evolution of subdwarf B stars for two different reasons. Firstly, being so much more common than their short-period counterparts, the slow pulsators offer many more potential targets for asteroseismology. Secondly, they are the only type of sdB to exhibit g-modes. In contrast to the EC 14026 stars' p-modes, which have significant amplitudes only in the shallow envelope region, g-modes are thought to probe much deeper into the stellar interior (Charpinet et al. 2001). Hence applying asteroseismological tools to the slow pulsators opens up the exciting possibility of determining the extent of the inner carbon-oxygen core, a parameter of fundamental importance for constraining evolutionary scenarios.

It was in this context that we undertook the first major multi-site campaign on a long-period variable subdwarf B star. Note that since then two other slow oscillators, PG 1338+481 (discussed in part II of these series; see also Randall et al. 2004b) and PG 0101+039 (Randall et al. 2005b) have been monitored to similar accuracy. Although we draw upon some preliminary conclusions from these campaigns for the present analysis, most of the pioneering work and background, both observational and theoretical, is detailed here. Our primary aim in this study is to quantitatively identify as many periods as possible from photometry observations and then qualitatively compare them to theoretical models. We devote the next part of this Paper to the organisation and outcome of the observational campaign, followed by a section on the analysis of the data and the periods extracted. We then outline the steps taken to model the star's behaviour and compare the resulting periods to the observations. Finally, we summarise our findings in the last section.

4.3 A MULTI-SITE CAMPAIGN

4.3.1 Initial Considerations

Before embarking on an observational campaign of any new type of star, it is vital to determine the most efficient methods and techniques to maximise the success of the observa-

tions. As long-period variable subdwarfs had never been observed long enough for quantitative period determination prior to this campaign, the guidelines for a suitable baseline and duty cycle were adapted from similar studies on EC 14026 stars. In addition, we drew on E.M.G.'s experience at obtaining high-quality light curves of small amplitude variations in binary subdwarfs.

Considering their very different pulsational properties, it is clear that the observation of PG 1716 stars presents different challenges to that of the rapid variables. Most importantly, the slow oscillators' much longer periods require a correspondingly increased baseline in order to secure a comparable number of pulsation cycles. While an average (clear) 8-hour night may yield 150−300 cycles for a typical EC 14026 star with 100−200 s periods, this same night would result in the accumulation of only 5−10 cycles for a long-period pulsator. Judging by the case of PG 0014+067, where five $\sim$ 2-hour chunks of data led to the identification of 13 periods and a subsequent asteroseismological analysis (Brassard et al. 2001), the lower useful limit on the number of pulsation cycles was estimated to lie between 150 and 350. For a slow oscillator with quasi-periods of around 1 hour this corresponds to a minimum of $\sim$ 35 eight-hour nights of observation. Acquiring a low number of cycles per night also manifests itself in the form of major aliasing problems. Thus it becomes increasingly important to achieve a high duty cycle by avoiding long daily gaps, making a multi-site campaign with a good longitudinal distribution the obvious choice.

Another difficulty when observing the slow variables is that, due to their extremely small pulsational amplitudes, atmospheric variations play a prominent role. This can be largely compensated for if the field of view includes a number of relatively close comparison stars of comparable magnitude positioned evenly around the target, enabling precise differential photometry. However, when observing slowly pulsating sdBs, even differential photometry still suffers from differential atmospheric extinction. Whereas observations of EC 14026 stars can easily be corrected for the resulting low-frequency artefacts by virtue of their pulsations' short timescales, the case is not as clear cut for the long-period variables. The problem is minimised by observing through an R filter rather than the historically more common B filter. Though this means that less flux is received from the target, the extinction on the blue

subdwarf compared to the generally much redder comparison stars is greatly reduced. An added bonus is that the Moon, being comparatively faint in the red region of the spectrum, leaves less of an imprint on the data, enabling fruitful observing during bright time.

In spite of the challenges outlined above, the observation of PG 1716 stars has some advantages over that of the fast pulsators. The slow oscillations only loosely constrain the maximum exposure times, enabling the effective use of small telescopes. This makes the long-period variables ideal targets for the multi-site campaigns required to achieve the necessary long baseline and high duty cycle. Moreover, it is not necessary to observe in frame transfer mode for faster readout, which yields a larger field of view and thus more potential comparison stars. In short, monitoring a long-period variable subdwarf can be just as rewarding as observing an EC 14026 star, though it does require more patience.

4.3.2 PG 1627+017

Our target for this campaign, PG 1627+017, was chosen on a number of different grounds. Firstly, with peak-to-peak luminosity variations in the lightcurve of up to $\sim$ 50 mmag, it exhibits by far the largest pulsational amplitudes of any of the known long-period oscillators, which facilitates the detection of the main periods and reduces the relative noise when observing. In addition to this, PG 1627+017 is one of the brightest long-period variables (V = 12.899 according to Allard et al. 1994) and is conveniently located in the direction of the Galactic Bulge, resulting in the presence of a large number of suitable comparison stars in a relatively modest field of view. Finally, its equatorial location renders it a suitable object for observations from either hemisphere.

PG 1627+017 forms one half of a close binary system with a period of $\sim$ 0.829226 days (Morales-Rueda et al. 2003; For et al. 2006). Its invisible companion is most likely a white dwarf, as can be deduced from the short binary period and the lack of observed eclipses. PG 1627+017 stands out as the coolest long-period pulsator known, and is in fact one of the coolest subdwarf B stars proper. However, estimates of its temperature vary. This is associated with current problems in establishing a homogeneous temperature scale for subdwarf B stars, particularly at the extreme hot and cool ends of the distribution. Spectroscopically

derived atmospheric parameters are only ever as reliable as the spectra obtained and the models used to fit them. While the quality of the spectra can be improved by increasing the signal-to-noise ratio, the case is not as clear cut from a modelling point of view. Ideally, one would construct models taking into account both non-LTE effects and atmospheric metals in abundances appropriate for the chemically peculiar subdwarf in question. Since this is both complicated and extremely time-consuming, current efforts concentrate either on including the main metals, albeit at solar abundances, under the LTE approximation or on computing full non-LTE models at zero metallicity. For the cooler subdwarfs, the values of $T_{\rm eff}$ and $\log g$ tend to be significantly lower if the former model atmospheres are used rather than the latter. In all probability the true values lie somewhere in between, however we will have to wait for more sophisticated models to be confident of this.

A quick search through recent literature clearly reveals the discrepancies that still exist between atmospheric parameters derived for an extremely cool subdwarf such as PG 1627+017. While the analysis of a time-averaged, high S/N MMT spectrum obtained suggests values of $T_{\rm eff} = 23{,}670 \pm 190$ K and $\log g = 5.32 \pm 0.02$ using NLTE models with no metals (Green, Fontaine, & Chayer, in preparation), a study by Maxted et al (2001) gives $T_{\rm eff} = 22{,}800$ K and $\log g = 5.27$, whereas a third estimate by Morales-Rueda et al (2003) yields $T_{\rm eff} = 21{,}600$ K and $\log g = 5.12$. As these parameters are all derived using different spectra as well as independent models, it is interesting to learn the outcome of an analysis employing the same technique for all three spectra. To this end, U. Heber (private communication) kindly provided us with the results of his re-analysis of the published spectra of PG 1627+017. Finding them to be consistent with each other, he judges the best estimate of the atmospheric parameters to be $T_{\rm eff} = 20{,}713 \pm 504$ K and $\log g = 5.04 \pm 0.059$ using LTE models with solar metal abundances. Since it is clear that the issue is not yet resolved, we conservatively consider the atmospheric parameters of PG 1627+017 to lie in the range $20{,}000 \lesssim T_{\rm eff} \lesssim 24{,}000$ K and $4.95 \lesssim \log g \lesssim 5.35$.

4.3.3 Observations

Our foremost objective when organising the campaign was the photometric accumulation of high quality light curves totalling a sufficient number of cycles to enable the extraction of pulsational periods, resulting in a qualitative understanding of the period spectrum and, ultimately, paving the way for asteroseismology. As outlined in Section 4.2.1, we deemed this could best be achieved with a minimum of ~ 35 nights of R band photometry, preferably obtained from locations well separated in longitude. Since the use of relatively small telescopes is not a drawback when observing the slow oscillators, we restricted our observing proposals to telescopes in the 1-m to 2.3-m range. Our applications being successful without exception, we were allocated 31 nights over a 34-night period at the campaign's lynchpin site, the Steward Observatory's 1.55-m telescope on Mt. Bigelow in Arizona, as well as 14 overlapping nights on the 1.0-m telescope at the South African Astronomical Observatory (SAAO) and 10 nights at the 2.3-m Siding Spring Observatory (SSO) in Australia. Whereas all the time at Mt. Bigelow (MB) and the SAAO 1.0-m was reserved for R band photometry, it was understood that observations at SSO would alternate between R band photometry and spectroscopy, depending on the weather conditions. In addition to this, we were granted ~ 20 extra nights (sometimes half-nights) at Mt. Bigelow in the 6 weeks leading up to and the 3 weeks after the termination of the main campaign, with the purpose of extending the time baseline and thus improving the temporal resolution.

While this accumulation of R band photometry constituted the bulk of the observations, the campaign on PG 1627+017 also incorporated two smaller, somewhat independent projects of significant interest. The first of these involved obtaining simultaneous time-series spectroscopy with the aim of confirming the principal photometrically deduced pulsation periods by measuring the line shifts, however the results of this are reported elsewhere (For et al. 2006). The second supplementary study is based on theoretical work linking the colour-amplitude ratio of a given pulsation to its degree index l (Randall et al. 2005a). It was suggested that, in principle, comparing the amplitudes of two modes in different wavebands could restrict the corresponding mode's l-value. Since the trace of the l-value is particularly strong in the blue and the difference between colour-amplitude ratios for different l increases with the separa-

tion in wavelength between the bandpasses considered, we decided simultaneous U/R band photometry would be the most effective option. Hence an effort was made to secure a week of U band data at the Steward Observatory's 1.52-m telescope on Mt. Lemmon, Arizona, at the same time as the R band data were being gathered for the main campaign. In addition, we were given the opportunity of obtaining 5 nights of simultaneous U/R photometry on the MDM 2.4-m telescope at Kitt Peak, Arizona, six weeks after the completion of the main campaign. Details of the observing time allocated for the entire campaign are summarised in Table 4.1, however only the outcome and results of the photometry will be discussed in the remainder of this Paper.

At the main campaign site on Mt. Bigelow, the existing red-sensitive facility 2KCCD was used to obtain images with a $5' \times 5'$ field of view, enabling the incorporation of 10 suitable comparison stars. The normal sampling time was 86.4 s, the sum of the 60 s exposure time and the overhead time. All images were reduced using standard IRAF[8] routines for debiasing, flat-fielding and aperture photometry. Correcting for first-order atmospheric variations using the weighted mean of the comparison stars and finally normalising the data to the mean intensity typically yielded light curves of similar quality to those depicted in Figure 4.1. The curves show the variation of the relative amplitude with time and each comprise $\sim$ 8 hours, but very clearly differ in the amplitudes of the pulsations. This effect is a result of destructive and constructive beating between different modes of pulsation, temporarily giving rise to unusually large or small observed amplitudes. Another noteworthy feature is that these 8-hour chunks of data sample only just over 4 pulsational cycles, less than the usual 5−10 expected for a typical long-period variable. Indeed, PG 1627+017 turns out to exhibit the longest periods of any known slowly oscillating sdB, a feature that is linked to its low temperature and surface gravity (see section 4).

Observations at SAAO were obtained using a CCD with a $5' \times 5'$ field of view employing anywhere between 5 and 7 comparison stars, depending on observing conditions. The sampling time was adjusted according to the prevailing sky conditions, ranging from $\sim$ 80 to $\sim$ 140 s

[8]The Image Reduction and Analysis Facility, a general purpose software package for astronomical data, is written and supported by the IRAF programming group of the National Optical Astronomy Observatories (NOAO) in Tucson, AZ.

with 22 s of this constituting readout time. The images were reduced using GoPhot, which cleans and flat-fields each frame before running DoPhot (Schechter et al. 1993) to produce differential aperture and profile fitted magnitudes. We generally used the less noisy aperture magnitude output to produce relative amplitude plots compatible with and similar to those illustrated for the Mt. Bigelow data.

At Siding Spring, the observations were carried out using a circular field of view with a diameter of $6'$ and a sampling time of $\sim$ 80 s. Things were greatly complicated by the fact that the telescope's imager is mounted at the Nasmyth focus, resulting in the circular motion of objects on the CCD chip in the course of the night. It is possible to correct for this by rotating the CCD accordingly, however for unknown reasons the flat-fields vary with the rotator angle, leaving persistent residual gradients of 1% in the reduced data. Of the three sets of photometry data obtained at SSO, one was taken with the rotator on and the remaining two were acquired without any rotational correction taking place. While we found the former set of data useless for the detection of pulsational brightness variations, we were able to reduce the latter two chunks with the aid of an IDL routine conceived specifically for this purpose. Using the relative positions of the two brightest stars on the chip as a guide, we were able to compensate for the apparent circular motion of the stars in the images and perform aperture photometry analogous to that of the Mt. Bigelow data, once again employing 10 comparison stars.

The R band photometry data obtained at each of the sites are summarised in Table 4.2. We obtained a total of 303 hours of useful data, 262 of which lie in the main campaign period 10th May to 12th June 2003, corresponding to a duty cycle of 33% over a 5-week period. Due to the atypically long quasi-periods found for PG 1627+017, the data acquired cover only $\sim$ 165 cycles, less than the anticipated minimum of $\sim$ 250. From this point of view, PG 1627+017 presents more of a challenge than the average long-period variable, though we believe that the low noise level of the data largely compensates for this shortcoming. Adding to this the relatively high frequency resolution of 0.15 μHz (which corresponds to $\sim$ 7 s for the dominant periods around 6500 s) renders us confident of the data's suitability for the quantitative extraction of pulsational periods.

Details of the simultaneous U/R band photometry obtained are listed in Table 4.3. The Mt. Lemmon (ML) U band data were acquired with the portable Montréal three channel photometer LAPOUNE, which uses three photomultiplier tubes as detectors to measure the counts coming from the target star, a sky patch and a (non-variable) comparison star. The sampling time was 10 s, however the data were later binned into points separated by 640 s with the aim of increasing the signal-to-noise ratio. The light curves were sky-subtracted, extinction corrected and cleaned using OSCAR, a special software program developed by one of us (P.B.). For further details on the data reduction process, see Billères et al. (2002). At the Kitt Peak MDM observatory, simultaneous U/R band photometry was gathered with exposure times between 30−75 s for the U band and 7−25 s for the R band. As with all the previous CCD data we employed differential photometry, using 7 comparison stars in the U, and the customary 10 in the R. The data were reduced using standard IRAF aperture photometry routines, after which they were corrected for atmospheric variations using the weighted mean of the comparison stars and normalised to the mean intensity.

In total, we managed to gather 52.5 hours of simultaneous U/R photometry, however the data is split into two $\sim$ 25-hour sets separated by more than five weeks and will thus have to be considered independently. For a slow pulsator such as PG 1627+017, a dataset of 25 hours duration is far from adequate for the determination of pulsation periods. Therefore, we plan to search the multi-colour data for the most prominent periodicities uncovered from the R band data and, if successful, determine their U/R amplitude ratio. Far from constituting an independent frequency analysis, it is hoped that the multi-colour data will shed light on the nature of some of the periods already found.

4.4 FREQUENCY ANALYSIS

4.4.1 The R band Data: Extracting the Pulsations

As outlined in the previous section, the reduced data from all three observatories were normalised to express the variation of relative intensity with time, eliminating any effects inherent to the telescope or instrument used on the amplitude of pulsation. We also ensu-

red that the shutter opening times were within 1 s of the corresponding UT time and that the time-line of all datasets was expressed in terms of the heliocentric Julian Date with the aim of preventing incorrect timing between the chunks of data. Thus rendering the various light curves compatible, the time-series data were combined for further analysis. After experimentation with different combinations of data chunks, such as taking only the high duty cycle data acquired during the main campaign period, using solely the Mt. Bigelow data or combining only high S/N light curves, it was found that the lowest noise level and the best resolution were obtained by simply pooling together all the available data. While this may seem counterintuitive, especially compared to studies of fast pulsators where a few nights of high quality data can yield far better results than a much larger number of noisy light curves, it should be kept in mind that we are dealing with very long periods. Since the 303 hours of photometry secured for PG 1627+017 covered only around 165 cycles, it makes sense that every extra cycle, even if it is noisy or well separated in time from the majority of the data, adds a non negligible amount of information.

The resulting combined lightcurve was analysed in a standard fashion, being subjected to a combination of Fourier analysis, least-squares fits to the lightcurve and pre-whitening techniques. Since this method has been used extensively for period determination in the case of EC 14026 stars, we will not dwell upon the finer details here, but refer the interested reader to a previous paper discussing the procedure (Billères et al. 2000). We would, however, like to demonstrate the necessity of establishing an adequate baseline, a goal that is easier to achieve for the EC 14026 stars due to their much shorter periods. To this end, Figure 4.2 illustrates the Fourier Transform (FT) obtained from a) a single, high-quality lightcurve of $\sim$ 8 hours length, b) the combination of 5 consecutive data sets and c) a time series consisting of 15 nights' observations. The improvement in quality from one FT to the next can be seen very clearly. While the top curve only suggests a possible agglomeration of peaks around 0.15 mHz, panel b) provides some resolution in the frequency domain, indicating the presence of 3–5 separate peaks in the 0.12–0.22 mHz range. The spectrum in panel c) enables a more precise determination of $\sim$ 3–5 periods between 0.14 and 0.17 mHz and clearly shows a single additional peak at $\sim$ 0.22 mHz. Finally, the FT's plotted in the top three panels should also

be compared to the complete spectrum illustrated in panel d).

Since the part of the Fourier spectrum extending beyond 0.3 mHz was found to be consistent with noise, we restricted our plots to the 0−0.3 mHz region, where all significant frequency peaks are to be found. The bottom panel in Figure 4.2 pictures the Fourier Transform resulting from all the data obtained as listed in Table 4.2. Though the clarity is greatly impaired by the window pattern (see Figure 4.3), an effect of the low number of cycles obtained in a given data set, we can easily identify the agglomeration of ~ 4 peaks in the centre of the spectrum, as well as a clearly separated frequency at ~ 0.22 mHz and some apparently spurious peaks at low frequencies. While we are confident that the higher frequency peaks are genuine indicators of pulsations taking place in the star itself, the peaks at extremely low frequencies are most likely due to atmospheric variation and differential extinction. As was discussed earlier, all the single-colour photometry was taken in the R band to minimise differential extinction, however it was not possible to eliminate the resulting low-frequency peaks altogether. Our original idea for dealing with these was to simply extract all the periods present in the data and to subsequently evaluate whether they were likely to be inherent to the star or caused by atmospheric effects. In the course of doing this, we found that virtually all the low-frequency power could be explained in terms of the harmonics of the 24-hour daily alias, implying a non-stellar origin. We also realised that, having appreciable amplitudes and being very close to the pulsational peaks in frequency space, the low-frequency peaks would most likely be associated with harmonics reaching into the domain of the pulsational peaks. Since such harmonics could easily be confused with stellar periods, we needed to find a way of eliminating them.

After experimenting with different techniques, we empirically found that the most efficient way of cleaning the Fourier spectrum was to take a night's lightcurve, subtract the 10 most prominent sinusoidal amplitude variations thought to be inherent to the star and then flatten the remaining slow variations using a spline function. This resulted in a relatively flat lightcurve, to which the 10 periods previously subtracted could be added, giving a "flattened" dataset. Applying the technique to each chunk of data in turn yielded the "flattened" Fourier Transform shown in the top panel of Figure 4.3, which constitutes a great improvement over

the original spectrum illustrated in the lowest panel of Figure 4.2. The one drawback to our method is that only datasets spanning around 3 hours or more were treated and thus incorporated into the final FT, as shorter data chunks could not be flattened without running the risk of eliminating real stellar pulsations.

The remaining panels of Figure 4.3 illustrate the process of pre-whitening, a technique used to unambiguously identify the periods present in the data one at a time. It should be noted that pre-whitening removes not only the clearly visible peak of a given period but also the corresponding window function (shown in the bottom panel), resulting in the disappearance of multiple "peaks" at a time. The second graph from the top shows the spectrum pre-whitened by the 4 strongest periods, removing much of the power. Moving downwards, the next plot depicts the spectrum after the pre-whitening by an additional 4, followed in panel d) by another 4 rather convincing pulsational periods, bringing the total number of frequencies extracted to 12. As there are clearly some potentially real periods left, we continue with the pre-whitening until the residual spectrum contains no more peaks above the imposed threshold of three times the noise level (0.042%). Finally, panel e) contains the original Fourier Transform pre-whitened by the 23 frequencies listed in Table 4.4. Though even this residual spectrum shows some low-amplitude structure, the remaining peaks are too weak compared to the noise level to be credible.

The details of the periodicities uncovered during the pre-whitening process are given in Table 4.4, which shows the frequency, period, amplitude, relative phase (with respect to an arbitrary point in time, which in practice is identified with the beginning of the first run in Table 4.2) and their respective errors for each mode. The quoted uncertainties were estimated from the recipes proposed by Montgomery & O'Donoghue (1999). We note that the uncertainties in amplitude and phase are about 3 times as large as the formal errors of the least-square fits used in the pre-whitening process. We note also that, on average, the uncertainty on the period is ~ 0.4 s, which corresponds to about 1/16 of the formal resolution at 6500 s. Table 4.4 lists all periods extracted from the data, regardless of whether they are believed to constitute discrete modes of pulsation or to be rotationally, or otherwise, split components. The probable nature of the frequencies found and their implications for our

understanding of PG 1627+017 will be further discussed in Section 4.4.

The quality of the results of the pre-whitening procedure is visualised in Figure 4.4. Here, the top spectrum corresponds to the original Fourier Transform, the very similar graph plotted upside down is the Fourier spectrum of the noiseless reconstructed lightcurve based on the 23 oscillations extracted, and the bottom curve illustrates the residual amplitude. The latter is given by the transform of

$$R(t) = I(t) - \sum_{i=1}^{23} a_i \cos[\frac{2\pi}{P_i}(t - \phi_i - \phi_0)], \tag{4.1}$$

where $R(t)$ and the original lightcurve $I(t)$ are expressed in percentage variations about the mean intensity of the star, and P_i, a_i and ϕ_i respectively correspond to the periods, amplitudes and relative phases of the oscillations detailed in Table 4.4. As mentioned before, we believe the residual spectrum to be harbouring more low-amplitude oscillations than detected, but feel we have reached the detection limit for credible periods. Using the average value of the Fourier amplitude of $R(t)$ in the frequency range of interest as a guide, we estimate the noise level to be 0.014 %. Comparison with more sophisticated methods such as false alarm probability confirms the validity of the rule-of-thumb used to determine the lower amplitude limit of credible periods, namely that it be three times the noise level. A more conservative approach would have been to adopt a 4σ selection criterion, thus eliminating the 5 modes with the lowest amplitudes (indicated by colons in the amplitude columns of the table) from Table 4.4. In light of this, we believe we have extracted all the oscillations that can be determined with any certainty from the available data.

To summarise, exploiting the lightcurve obtained for PG 1627+017 using standard Fourier and pre-whitening techniques yields 23 periodicities believed to be inherent to the star. The oscillations fall into the period range 4580 to 8901 s, with noticeable clustering occurring between 6299 and 7032 s. Their amplitudes lie between $\sim$ 0.04 and $\sim$ 0.5% of PG 1627+017's mean brightness, there being a large difference in amplitude between the dominant 4 peaks (between 0.321 and 0.479%) and the remaining periodicities (below 0.186%).

4.4.2 The Multi-Colour Data: Determining the Relative Amplitudes

As was outlined in Section 4.2.3, we obtained the main campaign photometry in the R band rather than in the B or even the U band for two important reasons: to minimise the effects of differential extinction and to reduce light contamination from the Moon. It hence came as no surprise that all the U band light curves obtained showed significant long-term variations with change in airmass and atmospheric conditions. In addition to this, the Mt. Lemmon data were gathered during bright time, which further degraded the quality of the light curves. The MDM run, by contrast, was scheduled during dark time. We had initially hoped that the R band method of pre-whitening the light curves of the dominant stellar pulsations before flattening them by self-calibration would yield similar results in the U, but were disappointed. Since the long-term variations were more prominent than the stellar pulsations, and the U band runs were generally shorter than those we were accustomed to from the main campaign at Mt. Bigelow, it was not possible to pre-whiten the data of the stellar pulsations without also including contributions from differential extinction.

In the case of the Mt. Lemmon data, the U light curves were particularly noisy because of the presence of the Moon, so we binned the data points to an effective sampling time of 640 s. The usual procedure for flattening the light curve consists in dividing it by the smoothed light curve of the comparison star, and then removing any residual trend (caused particularly by differential extinction) through spline fitting. This method works quite well if there are many pulsation cycles accumulated in one night, allowing the definition of several anchor points for the spline fitting. In the present case, we were forced to use only 4 anchor points for the full night because of the very long cycles involved and, thus, the flattening process was not perfect. The results are illustrated in Figure 4.5, where all five U/R light curves obtained during the main campaign are compared. While the frequency and phase coherence between the two light curves is evident, the amplitudes appear to differ somewhat. Indeed, if we compute the Fourier transforms of the two datasets, we find the amplitude in the U to be a factor of 1.5 to 2 larger than in the R (see Figure 4.6). This is in accordance with theoretical expectations, which predict the observed U/R amplitude ratio to lie between $\sim$ 1.5 and $\sim$ 4 for a long-period variable subdwarf B star such as PG 1627+017 (Randall et

al. 2005a). The precise value depends on the atmospheric parameters of the star, which are subject to some uncertainty, as well as on the l-value of the mode in question. Thus, in order to constrain a mode's degree index, we need to isolate the corresponding peaks in the two Fourier spectra before computing the colour-amplitude ratio. Due to the poor duty cycle and frequency resolution as well as the elevated noise level of the Mt. Lemmon data, this was possible for only the highest pair of peaks at 7056 s (A = 0.84 ± 0.33%) and 7038 s (A = 0.56 ± 0.06 %) in the U and the R respectively. As the estimated accuracy of these periods is 11 s, the two peaks can be associated with the same oscillation within the error limits. The U/R ratio calculated for this mode is then 1.5 ± 0.6. We also note that the measured phase shift $\phi(R) - \phi(U)$ for this mode is equal to 140 ± 435 s, which is consistent with the zero phase shift expected for such a long period g-mode regardless of its degree index l (see Randall et al. 2005a).

For the MDM run we made an effort to obtain calibration data in order to facilitate the subsequent flattening of the light curves. To this end, we monitored PG 1432+004, an essentially non-variable subdwarf B star, at intervals of approximately 1 hour. PG 1432+004 is situated 2 hours to the west of PG 1627+017, and its effective temperature and gravity are the same within the measurement errors. We then utilised the same IRAF data reduction procedure as for the PG 1627+017 data, including the incorporation of comparison stars to minimise atmospheric effects. The resulting lightcurve was used to estimate the apparent brightening/dimming as a function of airmass of the hot target subjected to differential photometry on the basis of much cooler comparison stars. Depending on weather conditions and the ensuing uncertainty on the data points, we were able to calculate a linear or second order polynomial correction of the relative amplitude as a function of air mass and apply it to the PG 1627+017 data. This flattened out the U/R light curves very efficiently, as can be seen in Figure 4.7. The subsequently computed U and R Fourier transforms of all MDM runs combined are depicted in Figure 4.8. Compared to the Mt. Lemmon/Mt. Bigelow amplitude spectrum, we find that the noise level in the U band is greatly reduced thanks to the more reliable flattening procedure and the absence of moonlight, while the R band FT is of similar quality for the two runs. From the MDM Fourier transforms, we succeeded in isolating two in-

dependent pairs of periods at 7011/7012 s (A = 0.79 ± 0.15 / 0.51 ± 0.12%) and at 6609/6611 s (A = 0.59 ± 0.12 / 0.41 ±0.12%) in the U/R data. In both pairs the two components are close enough in period to be unambiguously identified as the same oscillation. The amplitude ratios are thus 1.5 ± 0.5 for the 7012 s periodicity and 1.4 ± 0.5 for the 6610 s pulsation. Likewise, the measured $\phi(R) - \phi(U)$ phase shifts are, respectively, 322 ± 314 s and −259 ± 365 s, again consistent with the theoretical expectation of 0 s.

Comparing the oscillations and colour-amplitude ratios measured at Mt. Lemmon/Mt. Bigelow (ML/MB) and at MDM reveals some compatibility. If we take the ML/MB periodicity at ∼ 7045 s to represent the same mode as the MDM oscillation at 7012 s, the colour-amplitude ratios are in perfect agreement. In addition, both this ratio and that obtained for the 6610 s period lie in the range predicted by theory. As for matching up the multi-colour periods with the high-amplitude peaks determined from the full R band campaign, we believe the 7012 and 7045 s periodicities to correspond to the prominent 7032 peak in the campaign data. Similarly, the MDM 6610 s oscillation can be associated with the 6630 s periodicity measured at Mt. Bigelow. The couplings seem justified considering the high amplitudes of the MB peaks represented in the multi-colour data and the relative proximity of the periods matched, however due the elevated noise level and poor frequency resolution in both sets of simultaneous U/R data the periodicities and their amplitudes are not well constrained. It is thus with caution that we assign the two highest amplitude peaks found in the PG 1627+017 R band lightcurve at 6630 s and 7032 s the U/R amplitude ratios of 1.4 ± 0.5 and 1.5 ± 0.5 respectively.

Theoretical U/R colour-amplitude ratios for an sdB model with $T_{\rm eff} \sim$ 20,000−24,000 K and $\log g \sim 4.9-5.4$ calculated according to Randall et al. (2005a) predict values in different ranges depending on the degree index of the mode in question. Given periods in the 6500−7500 s range, the U/R ratio calculated for $l = 1$ lies between ∼ 1.5 and ∼ 1.6, for $l = 2$ the range is ∼ 1.7−2.0, for $l = 3$ we have $U/R \sim 2.8-4.2$ and for $l = 4$ it falls between ∼ 1.5 and 1.8. Comparing this to the observational values, we find that, due to the uncertainties associated with PG 1627+017's atmospheric parameters and the U/R amplitude ratios measured, we cannot unambiguously determine the two main periodicities' degree indices. While the mea-

surements lie closest to the predictions for $l = 1$, they could easily correspond to modes with $l = 2$ or 4. We can, however, be relatively confident that the peaks at 7032 s and 6630 s do not have degree indices $l = 3$, which may well prove to be of importance for the interpretation of the period spectrum.

4.5 INTERPRETATION OF THE RESULTS

4.5.1 A Brief Overview

Since we are, to our knowledge, proposing the first ever in-depth analysis of the pulsational properties of a long-period variable subdwarf B star, we feel it is appropriate to begin with a qualitative comparison to theoretical predictions before embarking on any more quantitative explorations. The theory outlined in this subsection constitutes a brief recap of the study by Fontaine et al (2003a) uncovering the driving mechanism responsible for the instabilities in these stars.

High radial order g-modes in slowly oscillating sdBs are thought to be excited through a classical κ-mechanism, which can be effective only if the driving region coincides with a local overabundance of iron. As this is achieved by the competitive actions of radiative levitation and gravitational settling, only stars with certain combinations of $\log g$ and $T_{\rm eff}$ may drive oscillations, giving rise to an instability strip in the $\log g - T_{\rm eff}$ plane, into which all pulsators should fall. Computing 17 equilibrium models parallel to the zero-age extreme horizontal branch (ZAEHB) in the range 22,000 K $\leq T_{\rm eff} \leq$ 38,000 K in steps of 1000 K and 5.13 $\leq \log g \leq 6.12$ in steps of 0.06 and calculating their pulsational properties for $l \leq 8$ uncovered a new instability strip between 22,000 and 27,000 K in addition to the well-established EC 14026 domain between 27,000 and 37,000 K. While the very coolest model at $T_{\rm eff} =$ 22,000 K was able to excite high radial order g-modes with $l \geq 2$, hotter models could only drive modes with an increasingly large minimum l-value. For instance, the next hottest model at $T_{\rm eff} =$ 23,000 K was able to drive $l \geq 3$ modes, but the 28,000 K model could only excite modes with $l \geq 8$ (see Figure 4.9 from Fontaine et al. 2003a), leading to the prediction that the cooler oscillators should exhibit larger pulsational amplitudes than hotter ones. Moreover,

the calculations showed that cooler (lower $\log g$) models drive longer periods in a wider band pass than their higher temperature counterparts. Qualitative comparisons with quasi-periods deduced from PG 1716 star light curves showed that the periods predicted were of the right order, leaving the authors confident of the validity of the mechanism.

A preliminary comparison between the range of periods extracted for PG 1627+017 and those predicted for the coolest model from Fontaine et al. 2003a ($T_{\rm eff} = 22{,}000$ K, $\log g = 5.13$) found them to be in rough agreement (Randall et al. 2004a). Taking into account only modes with $l = 2$ and 3 resulted in a theoretical band of unstable periods between ~ 3500 s and ~ 7500 s, which largely overlaps with the observed periods at $\sim 4600-8900$ s. In fact, the periods predicted are slightly too low to fit the observations, indicating the need for even cooler models in order to produce a period range more representative of PG 1627+017. This is in accordance with some recent spectroscopic estimates, which predict the star's effective temperature to be around 21,000 K (U. Heber, private communication). As the lowest temperature covered by the equilibrium models computed by Fontaine et al. (2003a) is 22,000 K, we needed to extend the model sequence towards the cool end to be able to compare the observed and predicted range of excited periods quantitatively.

4.5.2 Improved Static Models and their Pulsation Properties

The code used to compute the models in this study constitutes an updated and extended version of that employed by Fontaine et al. (2003a) in their identification of the pulsation mechanism in the long-period variable subdwarf B stars and corresponds to numerical tools similar to those used by Charpinet et al. (1997; see also Fontaine et al. 1998 and Charpinet et al. 2001) for the second-generation models used in their surveys explaining the EC 14026 instability region. Each model is characterised by four free parameters: the effective temperature $T_{\rm eff}$, the logarithm of the surface gravity $\log g$, the total mass $M/M_{\odot}$ and $\log q({\rm H})$, the logarithmic depth of the transition zone between the helium-rich core and the thin hydrogen envelope. The periods computed from the models are dependent on all four of these parameters and have been very successful in quantitatively reproducing the observed period spectra in EC 14026 stars, the fast p-mode pulsators. One potentially important limitation for

g-modes however is the fact that they represent *static* structures with central inert spheres, rather than full evolutionary models and thus lack a detailed treatment of the star's inner regions, in particular the helium-burning core. Since the p-modes found in EC 14026 stars constitute shallow envelope modes, this shortcoming has a negligible effect on the calculated period spectrum as demonstrated by Charpinet et al. (2000). For the g-modes observed in PG 1627+017 the situation is somewhat more complicated, as this type of mode propagates deep within the star and as such will be sensitive to its central structure. In order to obtain a more realistic quantitative estimate of the periods excited in long-period variable subdwarf B stars we have thus modified the existing models to include a second chemical transition zone, namely that between the central CO core and the outer He mantle. Since the inner part of the nucleus is dominated by nuclear fusion via the triple-alpha chain and thus contains significant levels of carbon and oxygen in addition to helium while the outer region of the core is composed almost exclusively of helium, we refer to this new feature as the CO/He transition zone. Hence, in addition to extending the model sequence to cooler temperatures, we introduce a fifth free parameter to characterise a sdB model: log q(He), the logarithmic depth of the transition zone between the He mantle and the CO core.

Extending the Temperature Sequence

As discussed in the previous section, the lowest temperature model that was computed before our effort was not cool enough to fully sandwich PG 1627+017 in parameter space. This limitation in temperature was due to the lack of data on the fractional iron abundance as a function of depth at lower temperatures, which had been computed by P. Chayer in the temperature range 22,000 K $\leq T_{\rm eff} \leq$ 39,000 K only. On our request, P. Chayer kindly performed the extensive radiative levitation calculations necessary to extend the temperature range towards the cool end and provided us with iron abundance profiles for models with effective temperatures down to 18,000 K. We are thus able to determine the theoretical period spectrum for models sandwiching PG 1627+017 in parameter space, an invaluable asset for both the qualitative and quantitative comprehension of the pulsations observed. As before, we analysed the pulsational stability of our models with the help of updated versions of the

Montréal adiabatic and non-adiabatic pulsation codes (Brassard et al. 1992; Fontaine et al. 1994).

The extended sequence of excited periods of the equilibrium models between 19,000 K and 24,000 K is shown in Figure 4.9. Models 4 (22,000 K), 5 (23,000 K) and 6 (24,000 K) correspond to Models 1, 2 and 3 from Fontaine et al (2003a) respectively, while the three cooler models were derived on the basis of the newly calculated iron abundance profiles. Their parameters were chosen so as to be parallel to the ZAEHB, and are listed in Table 4.5. None of the models considered here include the CO/He transition zone, but this does not affect the plot, which shows only the qualitative dependence of the band of excited g-modes on the temperature of the model. Every coloured point refers to the period of an unstable mode and is correlated in size with the modulus of the imaginary part of the complex eigenfrequency. This provides an estimate of the amplitude of the excitation, larger points denoting more unstable modes. It should be noted that, since we are ultimately aiming to compare our predictions to the periods observed, only modes with $l \leq 4$ are shown. Higher degree modes are likely to have integrated amplitudes too small for them to be observable and hence are of no practical interest here. The points denoting $l = 1$, 3 and 4 for a given model have been shifted slightly in the temperature domain to facilitate viewing. We can see from the figure that the number and length of the excited periods, as well as their range increases towards the cool end. These trends are well understood in terms of a thermal time scale argument (see Fontaine et al. 2003a). Interestingly, the two coolest models exhibit $l = 1$ modes with periods up to $\sim$ 15,000 s, a feature that can not be found in any of the hotter models.

The black box superposed on the bands of excited periods gives the temperature uncertainty on PG 1627+017 (see Section 4.2.2) in the horizontal direction and the range of periods observed in the vertical direction. It can be seen that the observed periods are accounted for by those predicted to be unstable if the atmospheric parameters of the target are pushed to the lower end of the spectroscopic errors. The oscillations extracted would then correspond to modes with $l = 2$, 3 and/or 4. Unfortunately, the overlap between the theoretical and experimental instability regions does not necessarily mean that our non-adiabatic calculations are accurate. Considering the current difficulties in determining the atmospheric parameters

of PG 1716 stars, the temperature of PG 1627+017 could well lie at the higher end of the uncertainty box, in which case the theoretically driven periods would no longer account for those observed. Apart from that, long-period variations have been detected in stars as hot as $\sim$ 27,000−28,500 K, which according to current models cannot drive modes with l lower than 7 or 8. In addition to the fact that these would probably not be observable due to cancellation effects when integrating over the visible disk, a quantitative frequency analysis of the hot long-period variable PG 0101+039 (Randall et al. 2005b) revealed that the measured periods are significantly longer than those calculated for an appropriate model. While this strongly indicates problems with the models at the non-adiabatic level, these are less pronounced for a cool object such as PG 1627+017 and will be discussed in more detail in Paper II of the series (Randall et al. in preparation). Considering the uncertainties surrounding the non-adiabatic calculations, we feel that it is appropriate to base the quantitative exploration of the period spectrum on adiabatic predictions only. In addition to employing the adiabatic pulsation code, this means that we do not favour the modes with high degree indices predicted to be excited, but instead consider all modes from $l = 1$ to 4.

Incorporating the CO/He transition zone

The other important modification made to the existing model building code is the incorporation of a second compositional transition zone between the inner CO nucleus and the He mantle in addition to the already present chemical discontinuity found at the base of the outer H-rich envelope. This second chemical transition zone, necessarily located much deeper than the first, could safely be ignored for the EC 14026 pulsators because their p-modes are formed in the star's shallow envelope region and are not noticeably affected by the composition of the core. Similarly, the core does not influence the *range* of periods excited, which is why Fontaine et al. (2003a) needed to include only the He/H compositional discontinuity in their instability survey. In this study however, we are aiming to quantitatively explain the periods found in a g-mode pulsator, making a more accurate description of the core necessary.

The effect that including the CO/He transition zone has on a given model is illustrated in Figure 4.10. The model represented has $T_{\rm eff} = 24{,}000$, $\log g = 5.25$, $M = 0.48\ M_{\odot}$, $\log q(\mathrm{H}) =$

-1.97 and $\log q(\mathrm{He}) = -0.24$ and, apart from the inclusion of the latter parameter, corresponds to model 3 shown in Figure 6 in Fontaine et al. (2003a). The depth of the CO/He transition zone was chosen from the evolutionary models presented by Charpinet et al. (2000) and corresponds to the extent of the inner convective core around halfway through the model's helium core burning phase. The diagram contains the full run of the logarithm of the square of the Brunt-Väisälä frequency (N^2, solid line) as well as the logarithm of the Rosseland mean opacity (κ, dotted line) as a function of fractional mass depth. The well in the former curve indicates a narrow convection zone in conjunction with the iron opacity peak, which however carries practically no flux. Both the curves illustrate two discontinuities caused by the change in chemical composition at the CO/He and the He/H transition zone respectively. These propagation discontinuities and their locations significantly influence the periods of the model's g-modes, as was demonstrated by Charpinet et al. (2000).

In Figure 4.11 we show the period distribution of this model for modes with degree indices $l = 1$, 2, 3 and 4 in the 4000−9000 s period range of practical interest for PG 1627+017. It can be seen that the period spacing of adjacent modes is relatively uniform compared to that calculated, for example, for the thin hydrogen-shell model ($\log q(\mathrm{H}) = -4.0$ compared to $\log q(\mathrm{H}) = -1.97$ used here) by Charpinet et al. (2000). We also find the average spacing between adjacent modes to be a lot smaller and to decrease with increasing l as expected from theory (see, e.g., Charpinet et al. 2002), giving rise to $\sim$ 100 low degree modes in the 4000−9000 s period range for our representative PG 1627+017 model. The $l = 1$ modes are spaced furthest apart with ΔP ranging from $\sim$ 150 to 450, while $l = 2$ modes lie closer together at $80 \lesssim \Delta P \lesssim 350$, and $l = 3$ and $l = 4$ modes are associated with $\Delta P \sim 80$−300 s and $\Delta P \sim 50$−250 s respectively. The influence of the CO/He boundary on the period spectrum is quantified by the dotted lines, which represent the period spacings calculated for a modified model 6 with no CO/He transition zone. We find that, while the inclusion of the latter parameter changes the modes' periods and spacings at the quantitative level, it does not noticeably affect the average period spacing or the amplitude of oscillation about it. This is not unexpected since the trapping/confinement behaviour due to the CO/He transition zone is weak compared to that of the H/He boundary. The reason for this is of course that the

CO/He discontinuity is located deep inside the model where the oscillatory amplitudes are far smaller than at the base of the H-envelope. Nevertheless, we believe its incorporation to be a vital step towards a better modelling and understanding of long-period variable subdwarf B stars.

4.5.3 Interpretation of the Observed Non-Uniform Period Distribution

When studying the frequencies extracted from the lightcurve of PG 1627+017 (see Table 4.4) it becomes apparent that the distribution of detected excited modes in frequency space is by no means uniform, with significant clustering occurring between $\sim$ 145 and $\sim$ 165 μHz. Moreover, the frequency spectrum is characterised by closely spaced doublets/triplets at 142.2/142.6/143.0 μHz, 150.1/150.8/151.1 μHz, 217.6/218.0/218.3 μHz and 158.3/158.8 μHz. It is this latter feature that is particularly intriguing. While the large-scale non-uniform period distribution observed may well be due to the presence of low-amplitude periodicities that are not detected, or explained in terms of the intrinsic pulsation spectrum, the closely spaced peaks elude easy interpretation. In what follows, we outline several possible ideas.

An established and frequently observed mechanism for producing approximately evenly spaced frequency splitting is stellar rotation. It is well known that rotation destroys a star's spherical symmetry, resulting in the lifting of the $(2l+1)$-fold degeneracy of non-radial modes with given degree index l and radial order k. Rigid rotation, treated as a first-order perturbation, will transform a mode described by the doublet of indices (k, l) in a spherical model into $2l + 1$ modes now specified by three indices (k, l, m), where m is the azimuthal index. The modes with adjacent values of m will then be separated by a frequency spacing

$$\Delta f = \frac{(1 - C_{kl})}{P_{rot}}, \tag{4.2}$$

where Δf is given in units of Hz, the rotation period $P_{\rm rot}$ is expressed in seconds and C_{kl} is the dimensionless first-order rotation coefficient, which depends on the original degenerate mode's k and l indices. In the case of p-modes, such as those present in EC 14026 stars, C_{kl} is usually small compared to 1 and can thus be ignored (see, e.g. Charpinet et al. 2000).

However, for the g-modes found in long-period variable subdwarf B stars, the situation is a little more complicated as C_{kl} is not necessarily negligible. Assuming k is large (which is strongly implied by the length of the periods observed) we can approximate

$$C_{kl} \sim \frac{1}{l(l+1)}. \tag{4.3}$$

Radial velocity measurements suggest that PG 1627+017 is part of a short-period binary system (Morales-Rueda et al. 2003; For et al. 2006). Since the time required for stellar rotation to adjust to orbital motion in a close binary is short compared to the lifetime of a subdwarf, evolutionary scenarios predict PG 1627+017's rotation to be binary synchronous. Hence, PG 1627+017 should be spinning about its own axis with a relatively short period of $P_{\rm rot}$ = 0.829226 days. Substituting the l-indices 1, 2, 3 and 4 into equation 4.3 yields values of $C_{kl} = 1/2, 1/6, 1/12$ and $1/20$ respectively, and subsequently postulates frequency spacings of Δf = 6.98 μHz for l = 1, 11.6 μHz for l = 2, 12.8 μHz for l = 3 and 13.3 μHz for l = 4. Comparing these frequency spacings to the puzzling $\sim$ 0.35 μHz splittings uncovered immediately crushes the hope of justifying them in terms of binary synchronous rotation. We are left with two possibilities: either PG 1627+017 is rotating much more slowly than expected (the 0.35 μHz splittings would indicate a rotational period $P_{\rm rot}$ between 19 and 31 days depending on l), or we are witness to a binary-synchronous rotation rate and the splittings are caused by some other effect. In the spirit of clarifying this, we conducted a search for any splittings attributable to a $\sim$ 0.8-day rotation period.

The results of this search are depicted in Figure 4.12. The plots corresponds to simplified versions of the model spectrum illustrated in Figure 4.4 (without the contribution of the window function), and identify the rotationally split components of a given (k,l) mode by colour. The l-values inferred from the frequency spacing are indicated next to what is thought to be the central periodicity (i.e., that with $m = 0$). Peaks with amplitudes below four times the mean noise level are denoted by dashed lines. Unfortunately, the abundance of peaks in the 135−170 μHz range means that we cannot exclude the possibility that some of the frequencies identified as split components are in fact independent modes. This is highlighted

by our difficulties in assigning a given mode a unique set of evenly spaced components. For instance, the high amplitude peak at 158.8 μHz could be regarded as an $l = 3$ mode with a lower amplitude component at 146.3 μ Hz, but may just as well constitute the central frequency of the $l = 1$ triplet at 151.1/158.8/165.2 μHz. It was in order to allow for this ambiguity that Figure 4.12 includes two different sets of solutions. The top panel illustrates a possible scenario involving modes with $l = 1$, while the lower graphic is based on the splitting of modes with $l = 2$ and 3 only. We find the upper plot to be more convincing as it identifies two beautiful triplets as well as two doublets compared to the lower panel's odd selection of $m \neq 0$ components. Moreover, many of the splittings in the latter are based on the lowest amplitude peaks extracted from the frequency spectrum, which are the least reliable. Adopting the $l = 1$ scenario partly alleviates the fine structure problematic as a lot of the closely spaced peaks can then be explained by rotational splitting. Nevertheless, some of the close frequencies, such as the 217.6/218.0/218.3 μHz triplet and the 142.2/142.6 μHz doublet, remain unexplained and warrant further investigation.

One obvious approach is to determine the feasibility of the close splittings being a result of the pulsation mechanism itself. Since the close spacings between adjacent periodicities are relatively monotonous, it initially seemed possible that the two or three evenly spaced components of any frequency cluster may correspond to modes with the same degree index l and consecutive values of k. Comparing the 8−20 s period spacings observed to those predicted for adjacent modes in our PG 1627+017 model (see Figure 4.11), we find that the theoretical values are significantly larger for all degree indices. If however we decrease the mass of the model and thicken the hydrogen shell the spacings diminish. We thus constructed a model with the lowest plausible overall mass for a subdwarf of PG 1627+017's atmospheric parameters, $M_* = 0.4\ M_\odot$, and thickest reasonable hydrogen shell at $\log q(\mathrm{H}) = -1.0$ and calculated the adiabatic periods for modes with $l = 3$ and 4, those with the closest period spacing. For the case of $l = 3$, the average difference between consecutive periods was quantified at around 30 s, and at $\sim$ 20 s for $l = 4$. As these values are still too large to explain all the fine frequency structure observed, we concluded that the close frequency splittings cannot be accounted for in terms of adjacent modes of the same degree index. Thus, the modes making up the doublets

by our difficulties in assigning a given mode a unique set of evenly spaced components. For instance, the high amplitude peak at 158.8 μHz could be regarded as an $l = 3$ mode with a lower amplitude component at 146.3 μ Hz, but may just as well constitute the central frequency of the $l = 1$ triplet at 151.1/158.8/165.2 μHz. It was in order to allow for this ambiguity that Figure 4.12 includes two different sets of solutions. The top panel illustrates a possible scenario involving modes with $l = 1$, while the lower graphic is based on the splitting of modes with $l = 2$ and 3 only. We find the upper plot to be more convincing as it identifies two beautiful triplets as well as two doublets compared to the lower panel's odd selection of $m \neq 0$ components. Moreover, many of the splittings in the latter are based on the lowest amplitude peaks extracted from the frequency spectrum, which are the least reliable. Adopting the $l = 1$ scenario partly alleviates the fine structure problematic as a lot of the closely spaced peaks can then be explained by rotational splitting. Nevertheless, some of the close frequencies, such as the 217.6/218.0/218.3 μHz triplet and the 142.2/142.6 μHz doublet, remain unexplained and warrant further investigation.

One obvious approach is to determine the feasibility of the close splittings being a result of the pulsation mechanism itself. Since the close spacings between adjacent periodicities are relatively monotonic, it initially seemed possible that the two or three evenly spaced components of any frequency cluster may correspond to modes with the same degree index l and consecutive values of k. Comparing the 8−20 s period spacings observed to those predicted for adjacent modes in our PG 1627+017 model (see Figure 4.11), we find that the theoretical values are significantly larger for all degree indices. If however we decrease the mass of the model and thicken the hydrogen shell the spacings diminish. We thus constructed a model with the lowest plausible overall mass for a subdwarf of PG 1627+017's atmospheric parameters, $M_* = 0.4\ M_\odot$, and thickest reasonable hydrogen shell at $\log q(\mathrm{H}) = -1.0$ and calculated the adiabatic periods for modes with $l = 3$ and 4, those with the closest period spacing. For the case of $l = 3$, the average difference between consecutive periods was quantified at around 30 s, and at ~ 20 s for $l = 4$. As these values are still too large to explain all the fine frequency structure observed, we concluded that the close frequency splittings cannot be accounted for in terms of adjacent modes of the same degree index. Thus, the modes making up the doublets

and triplets have at least two different l-values.

Is this feasible? In terms of the number of modes predicted and their density in frequency space, certainly. Invoking all periodicities with degree indices up to $l = 4$ in the 4500−9000 s range for the representative model renders of the order of 100 modes, compared to the 23 observed. Their distribution in period space compared to that of the observed oscillations is illustrated in Figure 4.13. The theoretical spectrum for all degree indices combined (second strip from the top) clearly shows that the measured frequency splittings could theoretically be explained in terms of modes with $l = 1$, 2, and 3 and/or 4, since dense frequency clustering does occur in the calculated distribution. However, if the fine structure is indeed caused by the random clustering of independent modes, it is hard to justify why pulsations should preferentially be observable in these narrow bandpasses rather than distributed uniformly throughout the unstable period range. Moreover, it is not apparent why the frequency splitting should be so similar (between 0.3 and 0.7 μHz) for all modes. In this context it is interesting to note the detection of closely spaced doublets with frequency separations of less than 0.7 μHz in several delta Scuti stars (Breger & Bischof 2002). Convincingly dismissing observational or data analysis artefacts and variable amplitudes as possible culprits, the authors conclude that the frequency pairs extracted are inherent to stellar pulsation for at least one of the extensively observed targets. Potential explanations for the phenomenon include an unknown mode selection mechanism in a dense theoretical period spectrum. It is tentatively suggested that mode selection could be due to trapping and the fact that low kinetic energies are often predicted for very closely spaced modes.

Another potential mechanism for generating the fine structure was that of some form of frequency modulation during the course of the observations, which could result in smearing or close splitting in the Fourier transform. In order to investigate this possibility, we divide the main campaign data into three (overlapping) two-week chunks and checked for variability in the 8 highest amplitude peaks, which were present in each of the datasets. The resolution achieved in any one dataset was ~ 0.8 μHz, corresponding to an estimated accuracy of about 0.1 μHz, or 5 s in the period range of interest. The only frequencies that showed a modulation on the same scale or greater than this were the three highest amplitude peaks lying

between 7027−7037 s, 6663−6678 s and 6624−6642 s respectively. While these periods are identified with split peaks, the variation observed does not seem large enough to account for the splittings, and other split peaks such as the triplet around 4588 s do not exhibit discernible modulation. Moreover, there is no immediately obvious reason why the pulsations detected in PG 1627+017 should be subject to frequency changes on the 0.35 μHz scale. While the Doppler shift resulting from the star's binary motion is expected to manifest itself in a systematic shift of frequency with respect to the rest value, the variation was determined to be an order of magnitude lower than the formal resolution and thus not observable.

Following the discovery of a small modulation in the radial velocities for PG 1627+017 (For et al. 2006) potentially due to a slight orbital eccentricity, we considered the possibility of this inducing the fine structure observed but were unsuccessful. Other explanations considered were differential rotation of the star, the case of an oblique pulsator and resonant excitation of stable modes by those driven nearby. However, it is well known that differential rotation of a pulsating star results in unequally spaced multiplets rather than discrete sets of split components and, that in the case of an oblique pulsator it is the amplitudes of the components split by rotation that are modulated rather than their frequencies (Kurtz 1990). Finally, if resonant excitation were effective and the reason behind the fine structure observed we would expect to detect oscillations not only in the period range predicted to be unstable for l = 2, 3 and 4 modes, but also at shorter periods where excited l = 5, 6, 7... modes, though themselves not visible, would resonantly drive l = 1, 2 and 3 modes. In fact, due to the much narrower spacing between adjacent higher degree modes we should see *more* oscillations at higher frequencies than in the instability range of low degree modes.

Throughout our investigation into possible reasons for the close frequency splitting we had kept in mind the possibility of a data treatment or analysis fault, particularly seeing as though the $\sim$ 0.35 μHz spacings observed correspond to approximately 30 days, the time baseline of the main campaign. As we found no other totally convincing explanation for the fine structure, we set about searching the photometry and the data analysis methods used for sources of fake peaks induced near high-amplitude periodicities. Examining the window function for the run revealed no closely spaced aliases which could have mistakenly been attributed to stellar

pulsation. Besides, the spacings remained unaffected by halving the baseline of the data, implying that the splittings are not directly associated with window effects. We also checked for timing problems between the different observing sites and experimented with photometry obtained at one site only. Finally, we generated synthetic data characteristic of the typical periods measured from the light curves and conducted exactly the same Fourier analysis as for the stellar data. While the technique used had been tested extensively for the more rapidly pulsating EC 14026 stars, it was possible that the longer periods and reduced number of cycles per run present in our photometry could have somehow affected the efficiency of the process and perhaps even induced fake peaks. However, the oscillations pre-whitened from the artificial data corresponded well to those generated, rendering a data treatment fault unlikely. According to Breger & Bischof (2002), close frequency splitting could nevertheless be an artefact caused by a single peak with a variable amplitude. In the case of the delta Scuti star studied, this possibility was eliminated by the observational detection of phase jumps as predicted to occur for two independent but very closely spaced beating modes. Unfortunately, the time baseline achieved for PG 1627+017 is not long enough to study the behaviour of the periodicities' phases or amplitudes in any detail. Breaking the data up into 10−15 day chunks does suggest some variability in the two parameters, but it is not clear whether this is due to measurement errors, the beating of close (unresolved) modes, or intrinsic amplitude changes of a single periodicity.

In conclusion, we must concede that the fine structure found in the Fourier Transform of PG 1627+017 remains somewhat mysterious. The splitting of $l = 1$ modes through binary synchronous rotation seems plausible and partly alleviates the problem, however the remaining closely spaced peaks cannot be convincingly explained. While the κ-mechanism is, in theory, able to drive close frequencies by invoking modes of multiple degree indices, it is incomprehensible why the distribution of observable periods should be quite so non-uniform. We can nevertheless not exclude this possibility, as our model predictions are based on linear calculations, which are incapable of predicting the intrinsic amplitudes of the excited modes computed. Other potential, but not entirely convincing, explanations include frequency/amplitude variations over time and effects induced by the close binary nature of the target. Of course,

we can never completely dismiss the possibility of observational or data analysis errors despite careful verification of the measurement timing and pre-whitening technique employed, especially considering the link between the frequency spacings and the campaign baseline. In this context it is interesting to note that the photometry obtained for the single long-period variable subdwarf PG 1338+481 (see Paper II of these series, Randall et al. in preparation) exhibits a comparable, if not as pronounced, fine structure signature. However, in this case the frequency spacing is far larger than the resolution of the observations, rendering a data analysis fault unlikely. It thus seems that the excitation of closely spaced peaks may be inherent to long-period subdwarf B pulsators, which would point towards an unknown mode selection mechanism preferentially exciting modes in certain bandpasses.

4.5.4 Search for an Optimal Model in Parameter Space

The ultimate goal when observing a pulsating star is to use the periods detected to asteroseismologically infer its fundamental properties. Since our models' oscillations are dependent on the five input parameters $T_{\rm eff}$, $\log g$, M_*, $\log q(\mathrm{H})$ and $\log q(\mathrm{He})$, it is in theory possible to assign PG 1627+017 values for these by determining the model whose period spectrum matches that observed most closely. Employing the so-called "forward" approach in asteroseismology then involves computing a 5-dimensional grid of models in parameter space and finding the best possible fit between the observed and predicted period spectrum at each grid point. The quality of the period match is quantified by the dimensionless goodness-of-fit merit function

$$\chi^2 = \sum_{i=1}^{n} \left(P^i_{obs} - P^i_{theo} \right)^2 , \tag{4.4}$$

where n is the number of periods to be fitted, P^i_{obs} is one of the n observed periods and P^i_{theo} is the theoretical value assigned to that observed period at a given grid point by our period matching algorithm (see Brassard et al. 2001 for details). Models allocated a smaller χ^2 value will provide a better match to the periods observed than those with a larger merit function.

This "forward" approach in asteroseismology has been used very successfully for the study of EC 14026 stars. In the first fruitful asteroseismological analysis of a subdwarf B star,

Brassard et al. (2001) fitted the 13 observed modes of PG 0014+067 to those calculated for an unambiguous optimal model with a relative average dispersion of only $\sim$ 0.8 %. As the theoretical periods matched corresponded to those predicted to be excited and the optimal model's atmospheric parameters were in line with those determined from spectroscopy, it was believed that a realistic model had been identified. Similar results have been achieved more recently for the fast pulsators PG 1047+003 (Charpinet et al. 2003), PG 1219+534 (Charpinet et al. 2005a), and Feige 48 (Charpinet et al. 2005b). In all cases the period matching algorithm yielded a small number of χ^2 minimum regions, which could be reduced to just one family of optimal solutions on the basis of spectroscopic parameters. Thus the fundamental parameters of the stars could be inferred with some accuracy.

The conditions under which we attempt a first asteroseismological interpretation of the period spectrum uncovered for PG 1627+017 differ markedly from those encountered for the fast oscillators and are subject to numerous difficulties. Most importantly, pulsation calculations applied to PG 1716 star models typically predict many more frequencies than are extracted from current photometry. Our representative model invokes of the order 100 periodicities in the appropriate period range compared to the 23 observed for PG 1627+017, implying that any frequency matching exercise will result in a multitude of "optimal" models that fit the observed period spectrum equally well. Naturally, the small values of χ^2 thus achieved are not a consequence of having found the optimal or even a good model, but are simply due to the overabundance of predicted frequencies compared to those observed. In order to obtain a meaningful match, mode identification of the input periodicities must be constrained from the outset. There are several ways of determining a mode's degree index l observationally, most notably through the exploitation of multi-colour photometry (e.g., Randall et al. 2005a), rotational splitting (e.g., Charpinet et al. 2005b), and line-profile variations (e.g., Schoenaers & Lynas-Gray, 2005). For the case of PG 1627+017, the U/R photometry obtained is of sufficient quality only to exclude a degree index of $l = 3$ for the periodicities at 7032 s and 6630 s, although the amplitude ratios measured fall closest to those predicted for $l = 1$. This ties in well with the more convincing rotational splitting scenario depicted in the top panel of Figure 4.12, which invokes $l = 1$ for the four harmonic oscillations at 7032 s, 6630 s,

6299 s and 4588 s assumed to be rotationally split. While the abundance of peaks found in the $\sim$ 6200−7100 s range and the mysterious fine frequency structure discussed in the previous section imply that we cannot be certain of this interpretation, we believe it constitutes the most likely option. Admittedly, the excitation of $l = 1$ modes in PG 1627+017 is in conflict with current non-adiabatic theory, which however was found to have important shortcomings from the observation of hotter PG 1716 stars and may well need substantial improvement. It is quite possible that models incorporating a more sophisticated treatment of the inner layers of subdwarf B stars will lead to the prediction of unstable g-modes with $l = 1$. This would make sense from a mode visibility point of view, given that the brightness variation caused by an oscillation of given intrinsic amplitude strongly decreases with increasing l-value when integrating over the visible disk of the star. Indeed, all main sequence g-mode pulsators with good empirical mode identification show $l = 1$ modes only (Conny Aerts, private communication). A similar scenario holds true for white dwarfs, which do exhibit the occasional $l = 2$ mode, but primarily excite dipole modes. Since subdwarf B stars lie in between the two regimes, it would be most surprising if they did not follow the same pattern. For the purpose of the optimal model search, we thus assume the high-amplitude periodicities detected at 4588 s, 6299 s, 6630 s and 7032 s to be identified with $l = 1$ modes. Comparing the relatively even period spacing between the latter three peaks ($331 < \Delta P < 402$) to that expected between dipole modes with adjacent values of k (see Figure 4.11) reveals them to be similar. It is thus likely that the three lower frequency oscillations are associated with consecutive k values, a notion that can be used to constrain the location of the optimal model in parameter space.

Another important difference between the slow oscillators and the EC 14026 stars is the length of the periods observed. The fact that the periods we are dealing with for PG 1627+017 are around 30 times longer than those encountered in previous asteroseismological exercises means that we must employ a much greater number of quadratic elements in the pulsation calculations to achieve a similar numerical accuracy (we found 800 elements to be sufficient for our purposes, compared to 140 for the rapid pulsators). Since this drastically increases the computing time required, the number of periodicities calculated must be limited in any way possible. This is done, on the one hand, by confining the modes computed to those with $l = 1$

lying in the 4400−7200 s range. Naturally, only the four strong oscillations believed to be dipole modes can then be used in the fit, which we believe is appropriate in any case considering the uncertainties associated with the interpretation of the period distribution. The second way of cutting down on computing time is to reduce the number of models calculated. Unfortunately, the adiabatic periods of g-modes depend very sensitively on all five input parameters (see Charpinet et al. 2001), implying that grid points have to be closely spaced if regions of minimum χ^2 are to be detected. This leaves no option but to severely restrict at least some of the values. The obvious choice is to keep the two spectroscopically constrained parameters $T_{\rm eff}$ and $\log g$ constant and explore the remaining 3-dimensional $M_* - \log q(H) - \log q(He)$ space in detail as follows:

1. The effective temperature and surface gravity are set to our best estimates from spectroscopy, these being the weighted mean of U. Heber's values and those obtained by G.F. from the MMT spectra (see Green, Fontaine, & Chayer, in preparation). We thus adopt $T_{\rm eff} = 22{,}900$ K and $\log g = 5.25$.

2. The fractional logarithmic depth of the transition between the hydrogen-rich envelope and the outer core, $\log q$(H), is thought to range from around -2.0 to -5.0 for the subdwarf B star population as a whole (Dorman et al. 1993; see also Charpinet et al. 2005a). However, evolutionary calculations predict the thickness of the envelope to increase with decreasing temperature and surface gravity (i.e., cooler stars have larger $\log q$(H)). And indeed, the values of $\log q$(H) derived from asteroseismological studies of EC 14026 all lie at the lower end of the possible range. As one of the coolest subdwarf B stars, PG 1627+017 should then be characterised by a relatively deep H/He transition zone, conservatively estimated to lie between $-1.5 < \log q(H) < -3.5$. Exploratory calculations varying $\log q$(H) over this range, while keeping the other model parameters constant at representative values result in the sequence of period spectra depicted in Figure 4.14a. The plot indicates the dipole modes predicted in the 4400−7200 s range for each model, modes with the same radial index k being connected in order to illustrate the evolution of the mode distribution more clearly. We can see that the periods of modes with a given k value increase strongly and systematically with decreasing $\log q$(H),

individual modes deviating slightly from the general trend due to mode bumping and avoided crossing (see Charpinet et al. 2002). Another feature that stands out is the rapid loss of mode density as the hydrogen shell thins. Assuming that the three observed peaks at 6299 s, 6630 s and 7032 s correspond to modes with adjacent values of k, $\log q(\mathrm{H})$ can then be constrained from the imprint it leaves on the mean period spacings computed. We find empirically that only models with $-2.0 \leq \log q(H) \leq -2.6$ can describe the three main observational peaks in terms of modes with adjacent values of k. Of course, the period spacing does not only depend on $\log q(\mathrm{H})$, but also on the other two variables M_* and $\log q(\mathrm{He})$. While the effect of increasing the stellar mass is similar to that observed in Figure 4.14, it is comparatively weak over the canonical range assumed (see below) and does not require us to widen the interval of $\log q(\mathrm{H})$ adopted. Meanwhile, $\log q(\mathrm{He})$ has virtually no impact on the mode density of the model in question. We will thus consider only H/He transition zones in the narrower range during the period matching procedure. In addition to drastically reducing the computing time, this also renders the χ^2 hypersurface more meaningful as the very dense period spectra associated with thicker hydrogen shells are eliminated from the outset. Figure 4.14b shows the change in period distribution within the smaller $\log q(\mathrm{H})$ range at a resolution of $\Delta \log q(H) = 0.005$. The period of a mode with given k typically changes by less than 20–30 s from one model to the next, which is deemed sufficient for detecting regions of small χ^2. Once identified, these can then be explored using a finer grid.

3. The total stellar mass M_* is taken to lie in the canonically predicted range $\sim 0.44 < M_*/M_\odot < 0.53$ (Dorman et al. 1993). While more recent calculations (Han et al. 2003) have derived a somewhat larger distribution of masses resulting from binary evolution scenarios involving Roche lobe overflow and the merger channel (yielding $\sim 0.30 < M_*/M_\odot < 0.70$ but still strongly peaked on $\sim 0.5\ M_\odot$), all EC 14026 stars for which asteroseismology has been achieved are associated with masses near the predicted distribution peak of $\sim 0.47\ M_\odot$ (Charpinet et al. 2005c). Although this does not exclude the possibility of a wider mass distribution for other subdwarfs, it does indicate they are likely to fall into the canonical range, which we adopt in order to save computation time.

The spacing between grid points is set to $\Delta M_* = 0.001\ M_\odot$. Since the adiabatic period spectrum depends quite sensitively on the total mass of the star (see Figure 4.15), this is the minimum resolution needed to produce period changes of no more than 20–40 s from one model to the next.

4. The location of the transition between the carbon-oxygen nucleus and the outer helium-rich core lies at the edge of the star's convective core, believed to be located at a fractional logarithmic depth of between -0.11 and -0.27 during the core helium burning phase identified with subdwarf B star evolution (see Charpinet et al. 2000 for details). We thus conservatively consider values of $\log q(\mathrm{He})$ in the -0.10 to -0.30 range, and illustrate their effect on the predicted period spectrum in Figure 4.16. It can be seen that $\log q(\mathrm{He})$ leaves a much weaker overall trace on the frequency distribution than either $\log q(\mathrm{H})$ or M_*, although the effects are relatively pronounced for $-0.10 < \log q(\mathrm{He}) < -0.16$. We initially adopt a spacing between grid points of $\Delta \log q(\mathrm{He}) = 0.01$, which is certainly sufficient for $\log q(\mathrm{He}) < -0.16$, but may have to be modified if larger values are found to be involved.

First results of our search for a model capable of reproducing the four main peaks observed in the lightcurve of PG 1627+017 are depicted in Figure 4.17. We show a slice of the χ^2 hypersurface in the $M_* - \log q(\mathrm{H})$ plane, where we choose the value of $\log q(\mathrm{He})$ that provides the best fit at each grid point. The transitions between different shadings correspond to contours of equal χ^2, values of which are colour-coded according to the scale provided. Considering the systematic variation of the theoretical period spectrum with both M_* and $\log q(\mathrm{H})$ (see Figures 4.14 and 4.15), it comes as no surprise that the regions of minimum χ^2 are concentrated in several valleys that are inclined towards the axes. Evidently, an increase in total mass is compensated for by thickening the hydrogen shell in terms of the frequency spectrum predicted, giving rise to an equivalent fit. Note that a similar effect was found for the effective temperature and $\log q(H)$ or M_* in the case of the EC 14026 stars (see, e.g., Charpinet et al. 2005a). Conversely, the position of the CO/He boundary affects the fit to a lesser extent. This can be seen from Figure 4.18, which shows the $M_* - \log q(\mathrm{H})$ hypersurface with $\log q(\mathrm{He})$ fixed to a value of -0.15. Instead of altering the structure of the contour plot

completely, a change in $\log q$(He) simply narrows and/or smoothes the χ^2 valleys previously uncovered. Thus, the decision which of the valleys in Figure 4.17 provides the best solution lies with the choice of $\log q$(He).

From Figure 4.17 we identify three regions of parameter space associated with similarly small values of χ^2 (recognisable by their pink/purple centres). The first is centred at $M_* = 0.452\ M_\odot$, $\log q(\mathrm{H}) = -2.220$ and $\log q(\mathrm{He}) = -0.15$ and includes the absolute minimum of $\chi^2 = 149$. In terms of a match between the theoretical and observed periods, the fit sports an average dispersion of only 5 s, which is similar to the frequency resolution achieved from photometry. All periods predicted in the 4400−7200 s range for this "optimal" model are listed together with those fitted and their period dispersion in Table 4.6. The second, distinctly shallower, valley ($\chi^2_{\mathrm{min}} = 502$) is located around $M_* = 0.440\ M_\odot$, $\log q(\mathrm{H}) = -2.505$ and $\log q(\mathrm{He}) = -0.17$. Note that we have verified, by extending the mass range to $0.420\ M_\odot$, that the true minimum of the region really does lie at $M_*/M_\odot = 0.440$ rather than at a lower mass off the edge of the plot. Since the period match from this second region is nearly as good as for the first family of models, we cannot really discriminate between the two. This also holds true for the third valley centred at $M_*/M_\odot = 0.445$, $\log q(\mathrm{H}) = -2.050$ and $\log q(\mathrm{He}) = -0.15$ ($\chi^2 = 531$). In contrast, the next deepest minimum ($M_*/M_\odot = 0.494$, $\log q(\mathrm{H}) = -2.410$, $\log q(\mathrm{He}) = -0.30$) is associated with $\chi^2 = 1097$ and results in fits that are less acceptable, with average period dispersions of 15−20 s.

Bearing in mind that the search for an optimal model was based on a number of a priori assumptions, it would be extremely optimistic to believe that either of the minimum χ^2 valleys detected harbours the true "optimal" model. Consequently, we make no attempt to explore the valleys uncovered further (e.g., by constructing a finer grid around the χ^2 minima) and find the absolute minimum in χ^2 hyperspace. Instead, we would like to draw attention to the quality of fit achieved and the small number of minimum χ^2 regions found. It was not clear from the outset that we would be able to find a model with physically viable parameters that could describe the four prominent periodicities observed in terms of near-consecutive dipole modes with such accuracy. Equally, the fact that only three families of models present good matches to the observed peaks is something of a surprise considering the initial overabundance

of theoretical periods compared to those detected. Of course, this is a result of the assumptions made concerning the degree indices of the modes and the atmospheric parameters of the target. Nevertheless, our results imply that, given high quality spectroscopy, a moderate number of reliable periods, and some constraint on the degree indices involved, asteroseismology remains a viable option for long-period variable subdwarf B stars.

4.6 CONCLUSION

The work presented in this Paper constitutes the first serious attempt at quantitatively extracting and interpreting the observed period spectrum of a long-period variable subdwarf B star. To this end we organised the most extensive multi-site campaign conducted for a slowly oscillating sdB to date and secured over 300 hours of high-quality R-band differential photometry for PG 1627+017. The baseline and duty cycle achieved proved adequate for the extraction of 23 frequencies present in the lightcurve down to an amplitude of ~ 0.05 % of the mean brightness. Periodicities extracted range from 4500 to 9000 s, with the highest amplitude oscillations clustering between 6300 and 7050 s. Interestingly, we find several groups of peaks spaced very closely together in frequency, the reason for which is not obvious. While some of the components can be explained in terms of binary synchronous rotational splitting, others remain unaccounted for. After conducting various tests we find it unlikely that the close multiplets are due to problems with the data processing. Instead we tend towards an explanation in terms of an unknown mode selection mechanism (see below), the amplitude variation of a single oscillation, or effects associated with the binary nature of the target.

Employing a sequence of newly updated models, we find that the period range observed for PG 1627+017 and the instability band predicted are in qualitative agreement if the star's atmospheric parameters are pushed to the lower end of the spectroscopic uncertainties. The periodicities detected then correspond to modes with degree indices $l = 2$, 3 and/or 4 as dipole modes cannot be driven. However, due to some uncertainty as to the atmospheric parameters of the target it is not clear that the observed period spectrum falls entirely into the unstable band computed. Assuming a mean value of the atmospheric parameters derived, the longest periods measured cannot be driven from non-adiabatic calculations. This may

indicate problems with the theoretical blue edge, a hypothesis that is also supported by the fact that we have detected slow pulsations in a number of much hotter subdwarfs which models predict to oscillate only with modes of $l = 7$ or 8 and upwards. Clearly, our models can be improved upon further in this respect. Since current computations simplify the composition of the envelope by taking into account only traces of iron in a pure hydrogen background, one possible way forward would be to include the small quantities of helium and metals known to be present in these stars' envelopes. However, this is well beyond the scope of the current paper.

Comparing the observed and theoretical period spectra quantitatively, the difference in the number of oscillations present in a given range is striking. While from photometry we detect 23 periods between 4588 s and 8901 s, some of which are most likely rotationally split components rather than independent modes, a representative PG 1627+017 model will yield around 100 low-degree (i.e., $l \leq 4$) modes. Although the abundance of predicted periods means that the fine structure found in the observed power spectrum can in theory be explained by invoking modes with two or more degree indices, it is hard to understand why we should detect dense accumulations of oscillations in such narrow bandpasses when the rest of the observed period spectrum is so sparsely populated compared to that computed. One idea that springs to mind is that, for some unknown reason, the energy generated by the κ-mechanism is preferentially transferred into the excitation of modes in certain frequency ranges, boosting their amplitudes and thus rendering them observable. While modes outside these ranges could nevertheless be driven, their amplitudes would be too feeble for us to detect. Unfortunately, linear non-adiabatic pulsation calculations cannot predict the amplitudes of excited modes, leaving us with no direct means of testing the hypothesis. It may however prove interesting to re-observe PG 1627+017 at a later time and investigate whether the observed frequencies have changed as a result of a shift in energy towards different modes. This would strongly support the notion of selective energy concentration, particularly if the oscillations measured were once again heavily clustered in narrow bandpasses.

The overabundance of computed compared to observed frequencies implies that mode identification must be restricted from the outset if any kind of meaningful period match is to

be achieved. It was to this end that we secured ~50 hours of simultaneous U/R band data in addition to the R-band data discussed above. A quick comparison of the U and R band power spectra revealed that the U band amplitudes are systematically higher than those in the R, as was to be expected from theory. Quantitative frequency extraction however was less successful due to the low temporal resolution and duty cycle of the photometry, recovering only the two highest amplitude oscillations present in the R-band data. The U/R amplitude ratios derived exclude degree indices of $l = 3$ for the two highest amplitude peaks, and tentatively point to the detection of dipole modes. This is in line with the most convincing rotational splitting scenario, in which four of the main periodicities are assigned $l = 1$ on the basis of the frequency spacing between components of different azimuthal index m. Comparing the mean spacing between the periods at 6299 s, 6630 s and 7032 s to that predicted for dipole modes then suggests that they should be associated with adjacent values of the radial index k. This makes sense from a mode excitation point of view, as the relatively small changes in growth rate from one mode to the next suggest that all modes in a given band of instability should be driven. The question that then remains is why there is such a large gap between the three consecutive modes and other high amplitude peaks such as those at 4588 s or 8261 s. We can provide no conclusive answer to this, but would hazard a guess that it is related to the selective energy concentration of the driving mechanism postulated above. The idea is supported by the fact that we detect weak pulsations at, e.g. 6053 s, 5760 s, 5162 s and 4681 s. Judging from their period distribution, these could well correspond to (near) consecutive dipole modes that happen to have less energy available to them than the more prominent oscillations. Other lower amplitude pulsations, in particularly those lying close to the main peaks, would then be associated with modes of higher degree indices that happen to to be driven to appreciable amplitudes because of their location in that specific frequency range. Of course, this is pure speculation in an attempt to make sense of the period spectrum observed, and should be treated as such.

Consequently, we based our search for an optimal PG 1627+017 model on the main oscillations at 4588 s, 6299 s, 6630 s, and 7032 s only, albeit under the assumption that they all correspond to dipole modes. By fixing the effective temperature and surface gravity to

the mean values deduced from spectroscopy, we were able to locate a small number of model families in $M_* - \log q(\mathrm{H}) - \log q(\mathrm{He})$ space that provide good matches to the periodicities observed. While this constitutes a promising result that was not guaranteed from the outset, the fact that a number of a priori assumptions had to be made renders the parameters inferred from the χ^2 minima unreliable. Fortunately, this does not exclude the possibility of finding meaningful and unique optimal models for other long-period variables. In retrospect, PG 1627+017 as part of a short-period binary system and the coolest subdwarf known was perhaps not the ideal target for our first campaign. Of course, we are now in a position to argue from a theoretical point of view rather than from the purely observational standpoint from which the star was chosen. Since we have shown cooler models to drive denser period spectra than those with higher effective temperatures, future campaigns should focus on hotter targets for an easier interpretation of the period spectrum. Moreover, choosing a slowly rotating single star would offer the advantage of an undistorted frequency distribution. Finally, it would be highly advantageous for asteroseismology if individual modes' degree indices could be constrained more convincingly than was the case for this study. From the results obtained it seems plausible that we could determine the degree indices of most modes detected if given two-colour data covering a sufficient number of pulsation cycles. It could thus prove extremely worthwhile to gather simultaneous U/R photometry for the entire duration of any future campaign on a long-period variable subdwarf B star.

We would like to thank Pierre Chayer for providing us with an extension of his iron abundance profiles to models with lower temperatures. Further thanks go to Uli Heber for his spectroscopic estimates of PG 1627+017's atmospheric parameters. We also acknowledge the help of Etienne Artigau with the SSO data reduction. This work was financed in part by the Natural Sciences and Engineering Research Council of Canada and by the Fonds de la recherche sur la nature et les technologies (Québec). G.F. also acknowledges the contribution of the Canada Research Chair Program. The contribution of E.M.G. was made possible by NSF grant AST-0098699. L.L.K., A.P.J. and T.R.B. are supported by the Australian Research Council. Many thanks also to the Steward Observatory staff, especially Jim Grantham, Bob Peterson, and Gary Rosenbaum.

4.7 TABLES

TABLE 4.1 – 2003 Campaign involvement

Dates (LT)	Telescope	Type of Observation
9 May-11 June +	1.55-m, Mt. Bigelow, Arizona	R band photometry
17-23 May	1.52-m, Mt. Lemmon, Arizona	U band photometry
13-20 May	2.3-m, Kitt Peak, Arizona	spectroscopy
13-19 May	1.9-m, SAAO, South Africa	spectroscopy
13-22 May	2.3-m, Siding Spring, Australia	R photomety + spectroscopy
20 May-3 June	1.0-m, SAAO, South Africa	R band photometry
9-13 June	2.3-m, Kitt Peak, Arizona	spectroscopy
2-7 July	2.4-m, Kitt Peak, Arizona	U/R band photometry

TABLE 4.2 – R band photometry data obtained 2003

Date (UT)	Start (UT)	Telescope	Length (h:m)	No. of images
30 March	07:55:09	MB	4:39	194
05 April	08:08:10	MB	4:12	171
06 April	08:20:25	MB	4:00	166
07 April	06:57:52	MB	5:24	223
08 April	06:53:06	MB	5:29	229
29 April	05:23:56	MB	5:38	249
30 April	05:28:44	MB	6:21	265
01 May	05:17:38	MB	6:31	272
03 May	08:01:56	MB	2:12	87
10 May	04:19:56	MB	7:20	309
11 May	05:10:17	MB	6:40	274
12 May	04:05:03	MB	7:37	317
13 May	06:32:29	MB	5:10	213
16 May	03:44:18	MB	7:57	329
17 May	03:34:03	MB	7:55	319
18 May	07:07:56	MB	4:32	188
19 May	03:23:57	MB	8:20	346
19 May	12:11:38	SSO	4:11	179
20 May	03:20:13	MB	8:20	349
20 May	21:16:51	SAAO	5:33	225
21 May	03:29:50	MB	8:05	339
21 May	20:43:06	SAAO	6:07	272
22 May	03:25:02	MB	8:12	342
22 May	11:23:17	SSO	6:52	276
23 May	05:46:14	MB	5:45	243
23 May	20:06:23	SAAO	5:50	211
24 May	21:08:03	SAAO	5:32	236
25 May	03:44:32	MB	5:39	238
26 May	03:17:46	MB	8:10	345
27 May	03:08:42	MB	8:23	349
27 May	20:22:37	SAAO	3:03	127
28 May	03:46:39	MB	7:45	319
28 May	19:53:04	SAAO	4:19	116
29 May	03:28:37	MB	8:15	342
29 May	19:35:44	SAAO	5:04	135
30 May	03:57:01	MB	5:20	231
30 May	19:21:27	SAAO	6:29	168
31 May	20:07:26	SAAO	6:30	179
02 June	03:38:59	MB	7:51	327
03 June	03:09:33	MB	8:17	346
04 June	03:22:35	MB	8:03	343
05 June	03:13:21	MB	8:13	342
06 June	03:10:02	MB	8:20	346
08 June	03:15:39	MB	8:19	346
09 June	05:35:30	MB	4:07	158
10 June	03:12:52	MB	8:18	348
12 June	03:15:28	MB	8:05	333

TABLE 4.3 – Simultaneous U/R band data obtained 2003

Date (UT)	Start (UT)	Telescope	Length (h:m)
17 May	06:02:37	ML/MB	2:51
19 May	05:31:31	ML/MB	5:30
20 May	04:10:04	ML/MB	7:17
21 May	05:00:51	ML/MB	2:40
22 May	04:00:47	ML/MB	6:24
02 July	05:37:05	MDM	4:02
03 July	04:18:23	MDM	5:27
04 July	04:27:31	MDM	4:37
05 July	03:55:38	MDM	5:25
06 July	04:31:07	MDM	4:31
07 July	04:54:04	MDM	4:14

TABLE 4.4 – Oscillations Detected in the Light Curve of PG 1627+017

No.	Frequency (μHz)	Period (s)	1 σ Error (s)	Amplitude (%)	1 σ Error (%)	Phase (s)	1 σ Error (s)
1	112.3	8901	0.4	0.182	0.011	3825	86
2	121.1	8261	0.4	0.181	0.011	4280	80
3	137.2	7291	1.1	0.047:	0.011	4355	271
4	142.2	7032	0.1	0.414	0.011	4097	30
5	142.6	7012	0.5	0.092	0.011	1325	133
6	143.0	6992	0.3	0.186	0.011	6803	66
7	146.3	6833	0.9	0.050:	0.011	3601	239
8	150.1	6663	0.1	0.380	0.011	3339	31
9	150.8	6630	0.1	0.479	0.011	2166	24
10	151.1	6619	0.7	0.060	0.011	307	193
11	153.3	6523	0.3	0.124	0.011	2475	92
12	158.3	6315	0.3	0.120	0.011	2006	92
13	158.8	6299	0.1	0.321	0.011	4526	34
14	162.8	6142	0.8	0.046:	0.011	1466	234
15	165.2	6053	0.6	0.060	0.011	3084	177
16	173.6	5760	0.5	0.059	0.011	5087	171
17	193.7	5162	0.4	0.065	0.011	4546	139
18	210.3	4756	0.5	0.043:	0.011	4605	194
19	213.6	4681	0.3	0.069	0.011	1499	119
20	215.5	4640	0.3	0.068	0.011	2904	119
21	217.6	4596	0.4	0.051:	0.011	2913	158
22	218.0	4588	0.1	0.156	0.011	3420	51
23	218.3	4580	0.2	0.083	0.011	3152	97

TABLE 4.5 – Properties of the Equilibrium Models

Model	$T_{\rm eff}(K)$	$\log g$	$M/M\odot$	$\log q$(H)
1	19,000	4.95	0.48	−1.15
2	20,000	5.01	0.48	−1.32
3	21,000	5.07	0.48	−1.48
4	22,000	5.13	0.48	−1.64
5	23,000	5.19	0.48	−1.81
6	24,000	5.25	0.48	−1.97

TABLE 4.6 – Fit of the four prominent periodicities detected to an "optimal" model at $T_{\rm eff}$ = 22,900 K, $\log g = 5.25$, $M_* = 0.452\ M_\odot$, $\log q$(H) = −2.220 and $\log q$(He) = −0.15.

l	k	$P_{\rm theo}$	$P_{\rm obs}$	ΔP	$(\Delta P)/P(\%)$
1	13	4431	...	...	...
1	14	4598	4588	10	0.22
1	15	4943	...	...	...
1	16	5241	...	...	...
1	17	5435	...	...	...
1	18	5739	...	...	...
1	19	6089	...	...	...
1	20	6302	6299	3	0.05
1	21	6625	6630	5	0.08
1	22	7029	7032	3	0.04

4.8 REFERENCES

Allard, F., Wesemael, F., Fontaine, G., Bergeron, P., & Lamontagne, R. 1994, AJ, 107, 1565

Bergeron, P., Wesemael, F., Beauchamp, A., Wood, M.A., Lamontagne, R., Fontaine, G., & Liebert, J. 1994, ApJ, 432, 305

Billères, M., Fontaine, G., Brassard, P., & Liebert, J. 2002, ApJ, 578, 515

Billères, M., Fontaine, G., Brassard, P., Charpinet, S., Liebert, J., & Saffer, R.A. 2000, ApJ, 530, 441

Brassard, P., Fontaine, G., Billères, M., Charpinet, S., Liebert, J., & Saffer, R.A. 2001, ApJ, 563, 1013

Brassard, P., Pelletier, C., Fontaine, G., & Wesemael, F. 1992, ApJS, 80, 725

Breger, M. & Bischof, K.M. 2002, A&A, 385, 537

Charpinet, S. et al, 2005c, Baltic Astronomy, 14, in press

Charpinet, S., Fontaine, G., Brassard, P., Billères, M., Green, E.M., & Chayer, P. 2005b, A&A, in press

Charpinet, S., Fontaine, G., Brassard, P., Green, E.M., & Chayer, P. 2005a, A&A, 437, 575

Charpinet, S., Fontaine, G., & Brassard, P., 2003, in White Dwarfs, eds. D. de Martino, R. Silvotti, J.-E. Solheim, & R. Kalytis, Kluwer Academic Publishers, NATO Science Series II - Mathematics, Physics, and Chemistry, 105, 69

Charpinet, S., Fontaine, G., Brassard, P., & Dorman, B. 2002, ApJS, 139, 487

Charpinet, S., Fontaine, G., & Brassard, P. 2001, PASP, 113, 775

Charpinet, S., Fontaine, G., Brassard, P., & Dorman, B. 2000, ApJS, 131, 223

Charpinet, S., Fontaine, G., Brassard, P., Chayer, P., Rogers, F.J., Iglesias, C.A., & Dorman, B. 1997, ApJ, 483, L123

Charpinet, S., Fontaine, G., Brassard, P.,, & Dorman, B. 1996, ApJ, 471, L103

Dorman, B. Rood, R.T., & O'Connell, R.W., 1993, ApJ, 419, 596

Dreizler, S. 1993, in NATO ASI series 403, White Dwarfs: Advances in Observations and Theory, ed. M.A. Barstow (Dordretch: Kluwer), 287

Fontaine, G., Green, E.M., Chayer, P., Brassard, P., Charpinet, S., Randall, S.K 2005, Baltic Astronomy, 14, in press

Fontaine, G., Brassard, P., & Charpinet, S. 2003b, Ap&SS, 284, 257

Fontaine, G., Brassard, P., Charpinet, S., Green, E.M., Chayer, P., Billères, M., & Randall, S.K. 2003a, ApJ, 597, 518

Fontaine, G., Charpinet, S., Brassard, P., Chayer, P., Rogers, F.J., Iglesias, C.A., & Dorman, B. 1998, in IAU Symp. 185, New Eyes inside the Sun, & Stars, ed. F. Deubner, D.W. Kurtz, Kluwer Academic Publishers, 367

Fontaine, G., Brassard, P., Wesemael, F., Tassoul, M. 1994, ApJ, 428, L61

For, B.-Q., Green, E.M., O'Donoghue, D., Kiss, L.L., Randall, S.K., Fontaine, G., Jacob, A., O'Toole, S.J., Hyde, E.A., & Bedding, T.R. 2006, ApJ, submitted

Green, E.M., Callerame, K., Seitenzahl, I.R., White, B.A., Hyde, E.A., Giovanni, M., Reed, M., Fontaine, G., & Østensen, R. 2003a, Ap&SS, 284, 64G

Green, E.M., Fontaine, G., Reed, M.D., Callerame, K., Seitenzahl, I.R., White, B.A., Hyde, E.A., Østensen, R., Cordes, O., Brassard, P., Falter, S., Jeffery, E.J., Dreizler, S., Schuh, S.L., Giovanni, M., Edelmann, H., J. Rigby, & Bronowska, A. 2003b, ApJ, 583, L31

Han, Z., Podsiadlowski, P., Maxted, P.F.L., & Marsh, T.R., 2003, MNRAS, 341, 669

Heber, U. 1986, A&A, 155, 33

Kilkenny, D., Koen, C., O'Donoghue, D., & Stobie, R.S. 1997, MNRAS, 285, 640

Kurtz, D.W. 1990 ARA&A, 28, 607

Maxted, P.F.L., Heber, U., Marsh, T.R., & North, R.C. 2001, MNRAS, 326, 1391

Montgomery, M.H., & O'Donoghue, D. 1999, in Delta Scuti Star Newsletter, No. 13

Morales-Rueda, L., Maxted, P.F.L., Marsh, T.R., North, R.C., & Heber, U. 2003, MNRAS, 338, 752

Randall, S.K., Fontaine, G., Brassard, P., & Bergeron, P. 2005a, ApJS, in press

Randall, S.K., Matthews, J.M., Fontaine, G., Rowe, J., Kuschnig, R., Green, E.M., Brassard, P., Chayer, P., Guenther, D.B., Moffat, A.F.J., Rucinski, S., Sasselov, D., Walker, G.A.H., & Weiss, W.W. 2005b, ApJ, 633, 460

Randall, S.K., Fontaine, G., Green, E.M., Kilkenny, D., Crause, L., Cordes, O., O'Toole, S., Kiss, L., For, B.-Q., & Quirion, P.-O. 2004a, Ap&SS, 291, 465

Randall, S.K., Fontaine, G., Green, E.M., Brassard, P., & Terndrup, D.M. 2004b, Proceedings of the SOHO 14/GONG 2004 Workshop (ESA SP-559). "Helio- and Asteroseismology: Towards a Golden Future", ed. D. Danesy, 119

Reed, M.D., Green, E.M., Callerame, K., Seitenzahl, I.R., White, B.A., Hyde, E. A., Giovanni, M. K., Ostensen, R., Bronowska, A., Jeffery, E.J., Cordes, O., Falter, S., Edelmann, H., Dreizler, S., & Schuh, S.L. 2004, ApJ, 607, 445

Saffer, R., Bergeron, P., Koester, D., & Liebert, J. 1994, ApJ, 432, 351

Schechter, P.L., Mateo, M., & Saha, A. 1993, PASP, 105, 1342

Schoenaers, C., & Lynas-Gray, A.E. 2005 , Baltic Astronomy, 14, in press

4.9 FIGURES

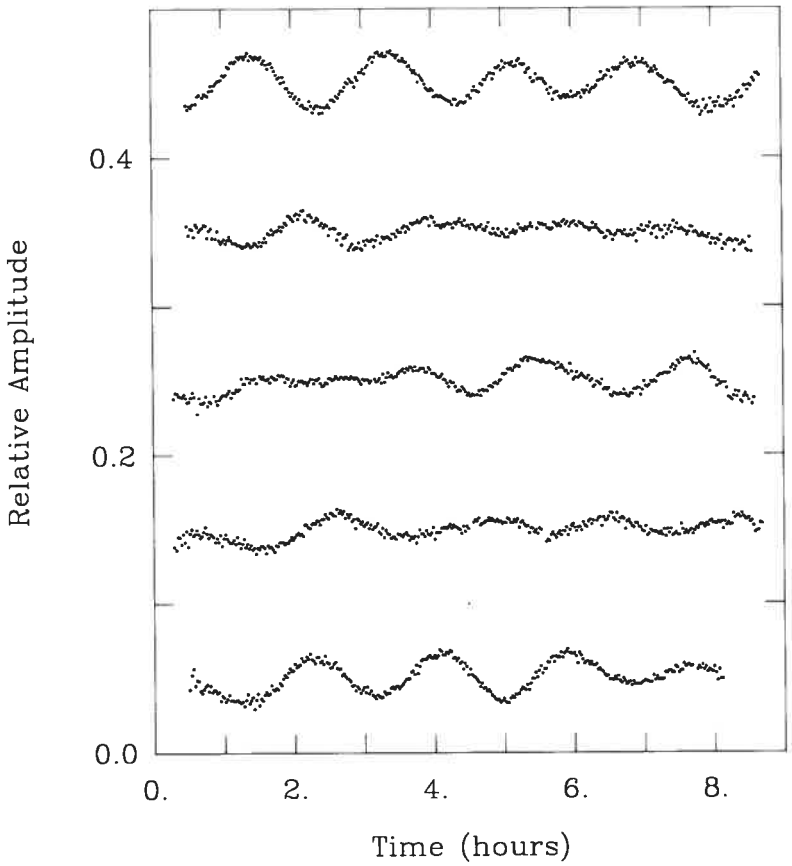

FIGURE 4.1 – Typical light curves of PG 1627+017, as obtained at Steward Observatory's 1.55-m telescope on Mt. Bigelow. The plots show the variation of the fractional intensity (the residual amplitude of the pulsation relative to the mean brightness of the star) as a function of time, and are shifted with respect to the y-axis in order to facilitate viewing. Each curve spans roughly 8 hours, which is typical of the length of data chunks obtained at Mt. Bigelow during the campaign. The change in pulsational amplitude from one curve to another is due to the beating between different modes of pulsation. Note that the maximum peak-to-peak amplitude resulting from constructive interference (e.g. top curve) is around a factor of 10 higher than the amplitudes of the strongest individual modes (c.f. Figure 4.3).

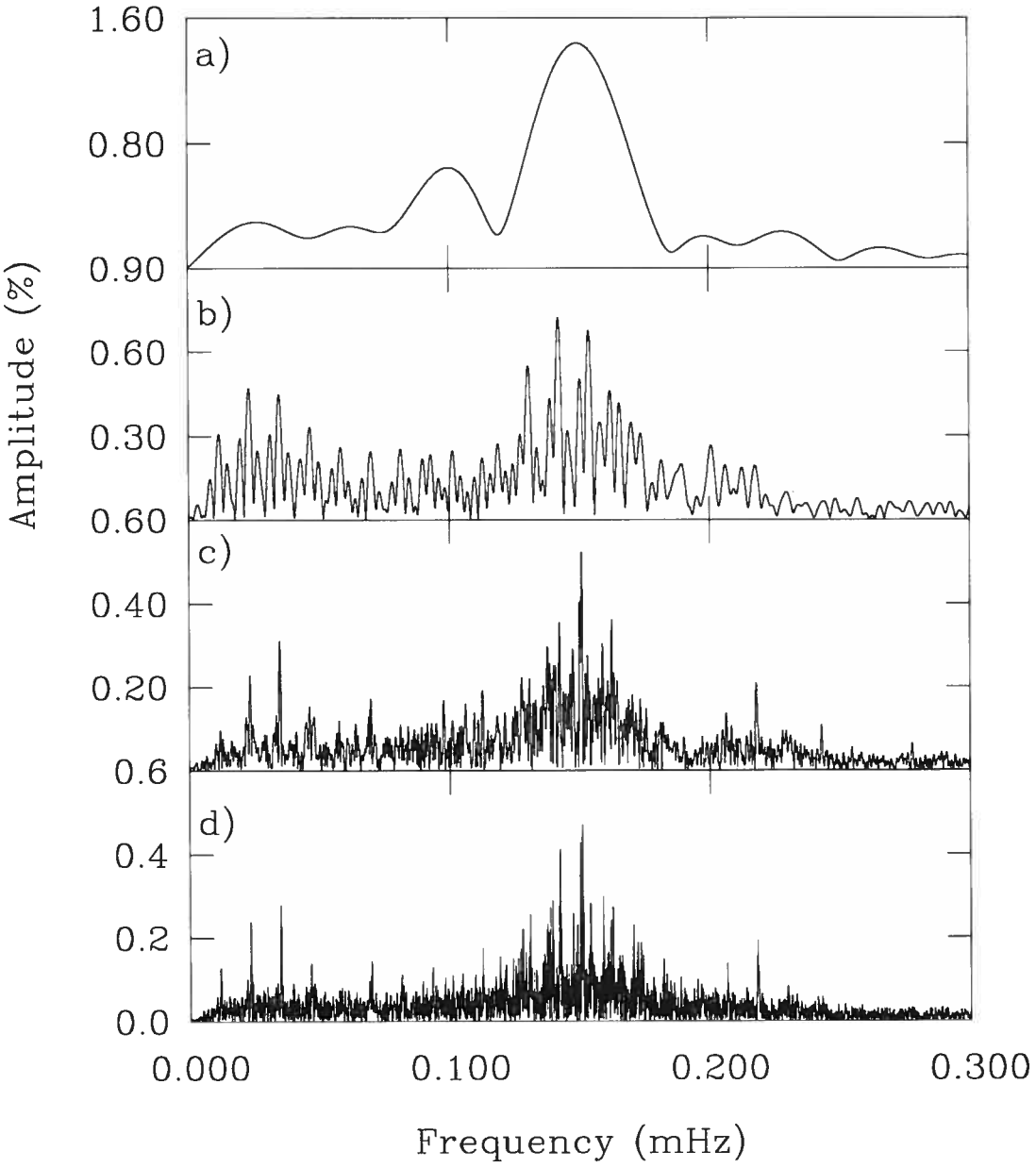

FIGURE 4.2 – Demonstration of the temporal baseline's drastic effect on the FT of PG 1627+017. Panel a) shows the FT of just one single lightcurve, the spectrum in panel b) was derived from five consecutive nights of observation, and FT c) is a result of the combination of 15 nights of data. The lowest panel displays the final Fourier spectrum computed using all the data listed in Table 4.2.

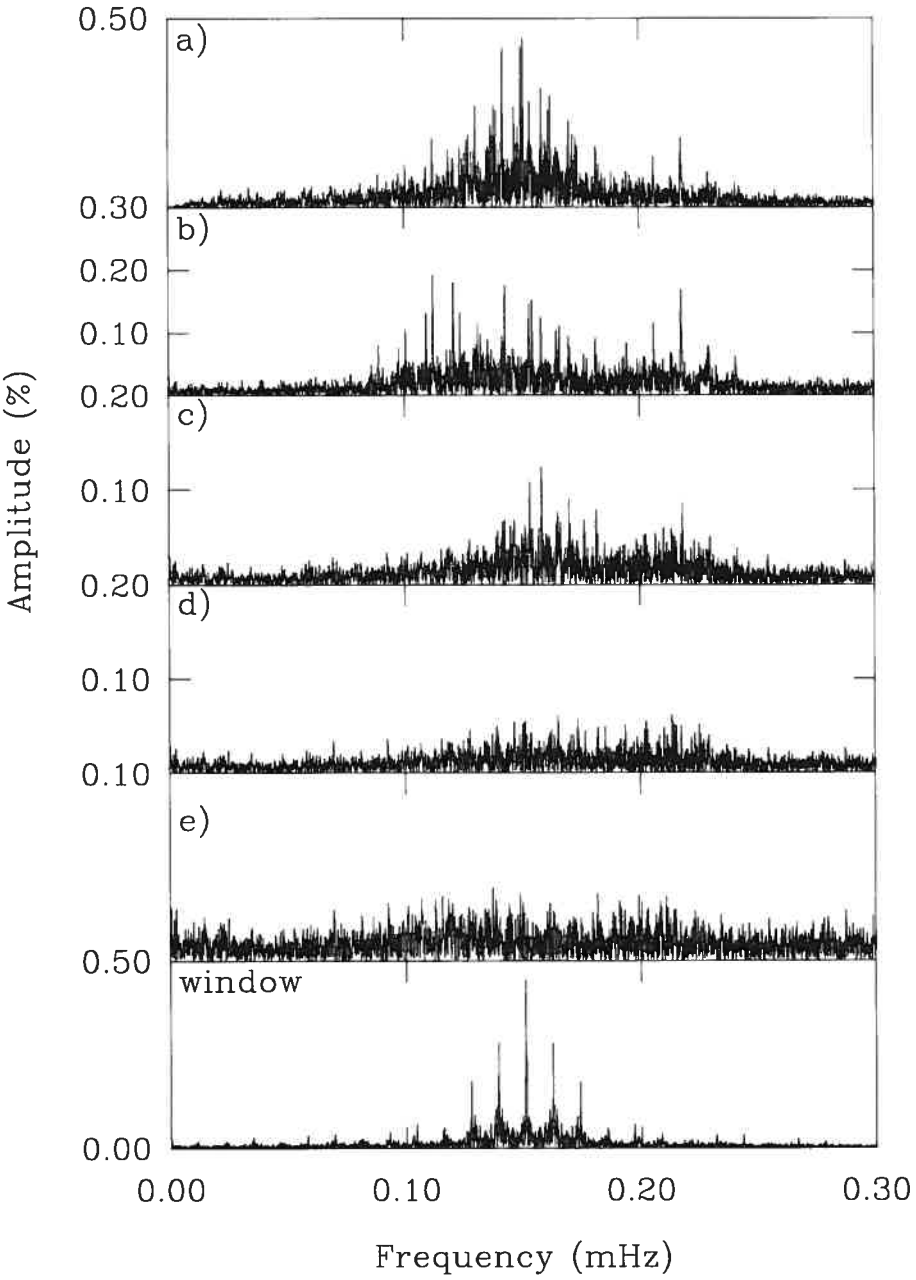

FIGURE 4.3 – Visualisation of the pre-whitening procedure the total Fourier Transform was subjected to. From top to bottom the panels picture a) the original Fourier spectrum, b) the FT pre-whitened by the 4 dominant periods, c) the transform with 8 convincing periods taken out, d) the spectrum after extracting 12 frequencies, and e) the residual spectrum after the pre-whitening by 23 periods. Note the change in the ordinate axes. The window function of the data sampling is illustrated in the bottom panel.

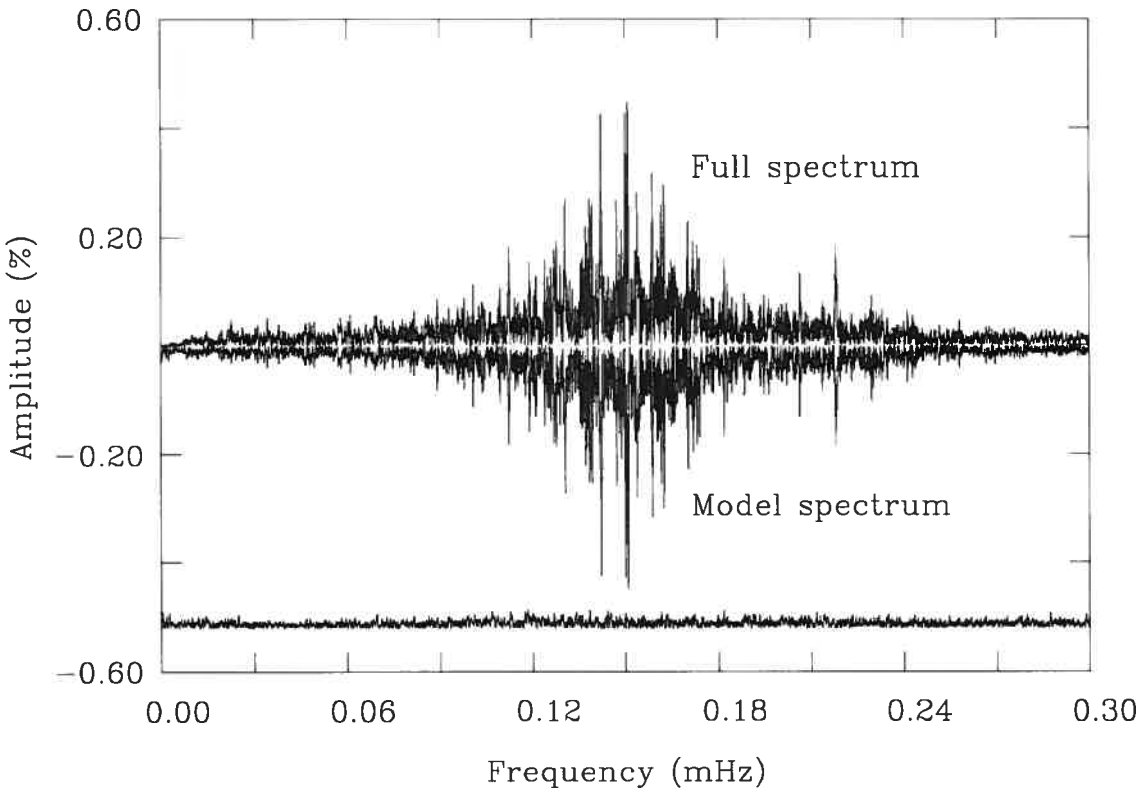

FIGURE 4.4 – Illustration of the quality of the frequency extraction. The top curve shows the Fourier amplitude spectrum of the complete lightcurve of PG 1627+017 in the 0-0.3 mHz bandpass. Some 200,000 frequency points were used in its calculation. The lower half of the Figure shows the Fourier amplitude spectrum (plotted upside down) calculated from the noiseless lightcurve reconstructed on the basis of the 23 extracted periods listed in Table 4.4. Plotted beneath this, and shifted downwards by 0.52% for clarity is the residual spectrum.

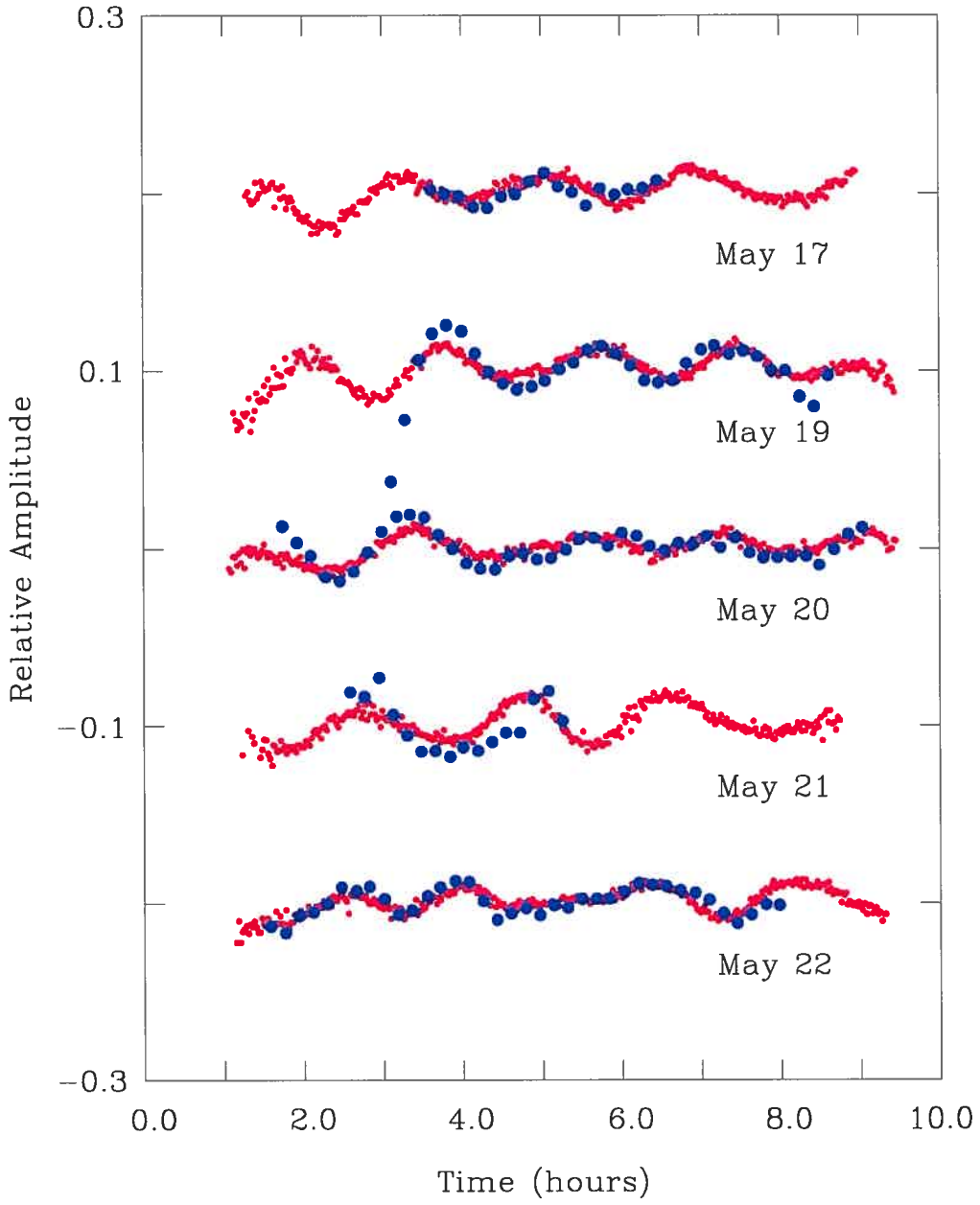

FIGURE 4.5 – The five simultaneous U/R light curves obtained at Mt. Lemmon (U), and Mt. Bigelow (R). The U band photometry is represented by blue points while the R band data is indicated by red points. The curves have been shifted by an arbitrary zero-point, and relative amplitude for illustration purposes. Whereas the R band curves correspond to actual data points measured, the U band data has been binned by a factor of 64 to reduce scatter.

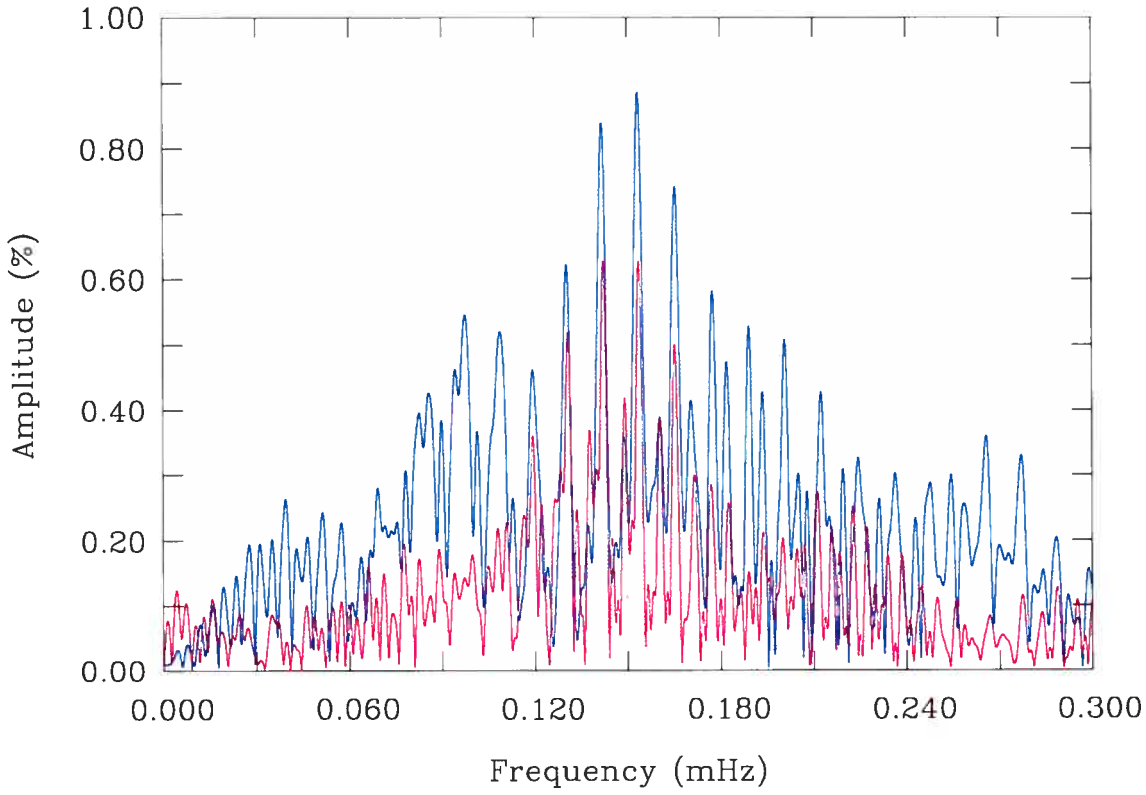

FIGURE 4.6 – The U and R band Fourier transforms of the simultaneous photometry obtained at Mt. Lemmon, and Mt. Bigelow in the 0−0.3 mHz bandpass. The blue spectrum refers to the U data, while the red spectrum indicates the R data. Both of the transforms were calculated on the basis of some 100,000 frequency points.

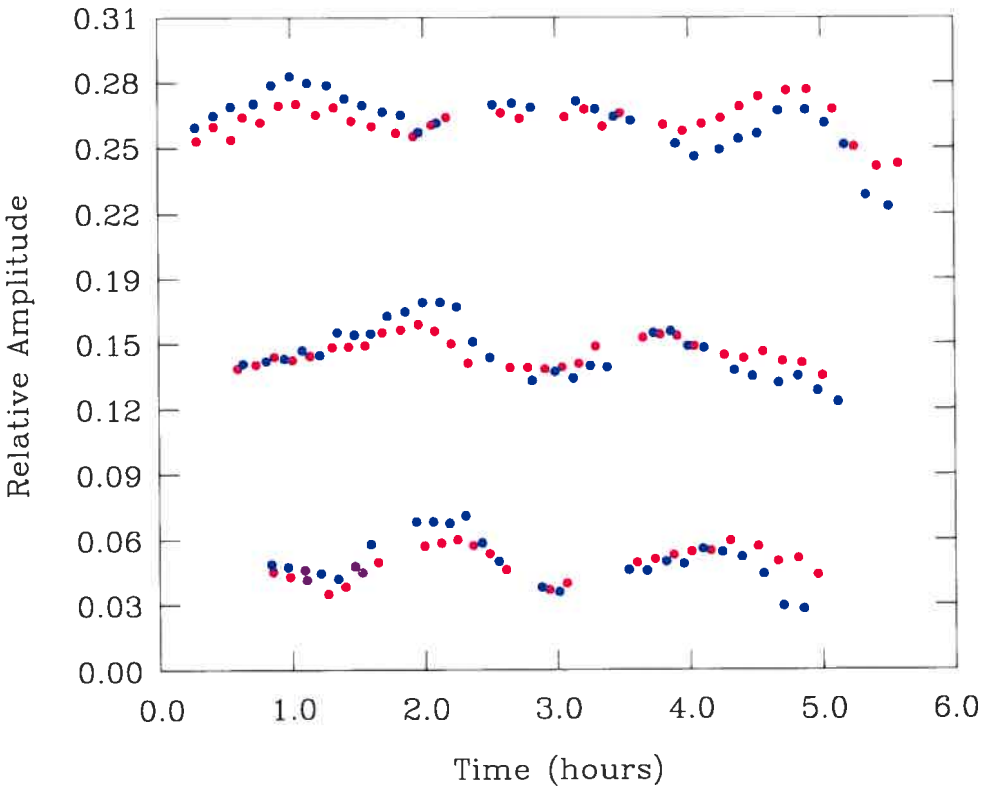

FIGURE 4.7 – The best three U/R band light curves obtained at MDM. As before, blue points denote U band data while red points refer to R band data. The curves have been shifted by an arbitrary zero-point, and amplitude for illustration purposes. The data has been binned by a factor of three to reduce scatter.

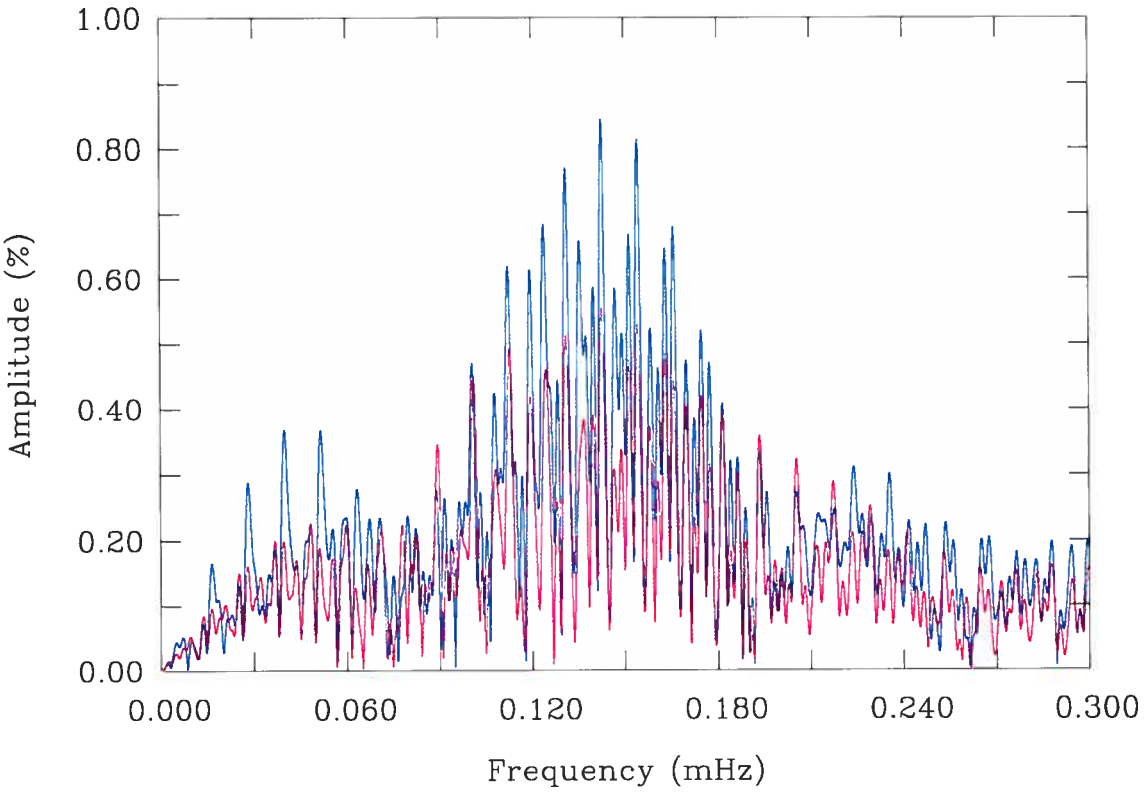

FIGURE 4.8 – The U and R band Fourier transforms of the MDM multi-colour photometry. For further details, please see Figure 4.6.

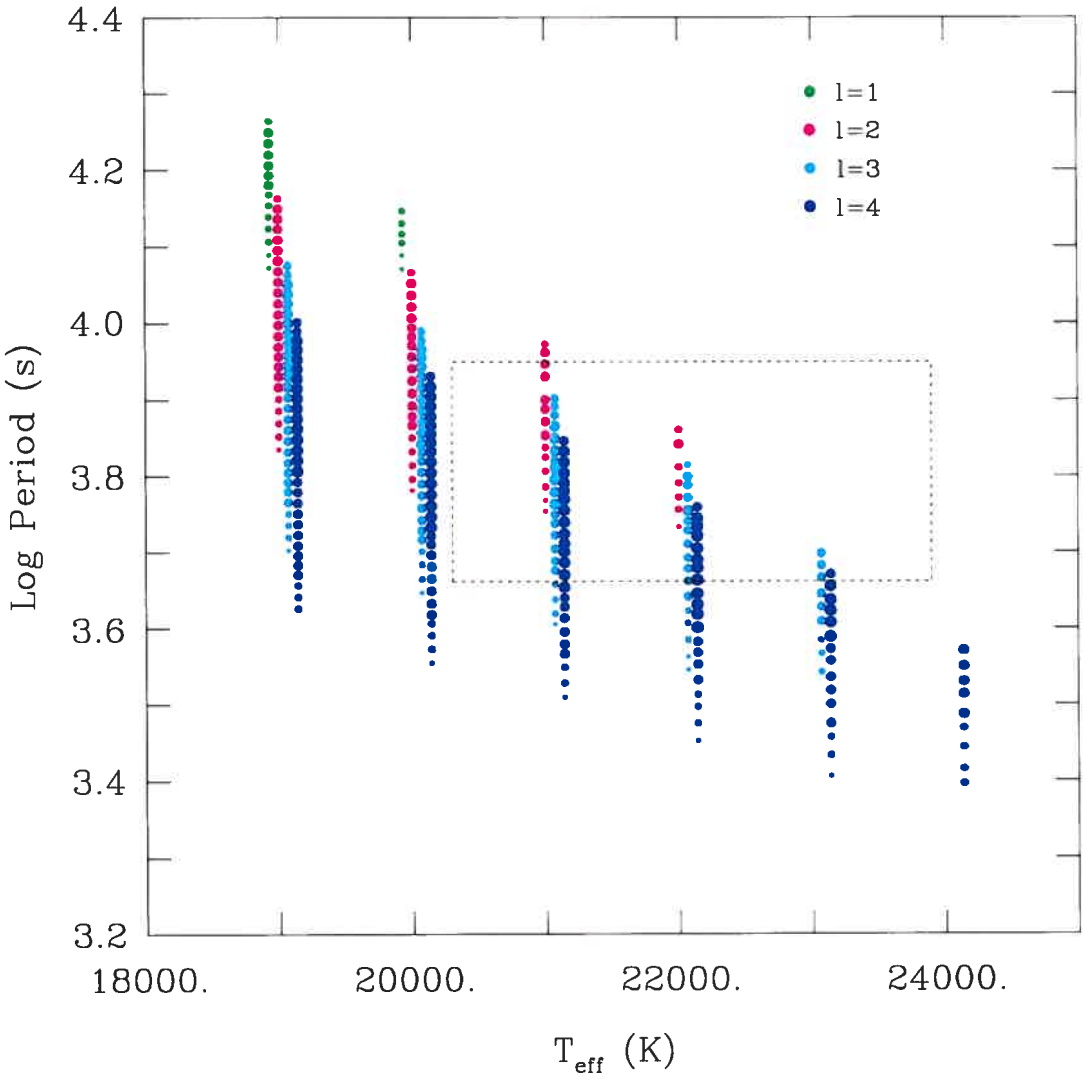

FIGURE 4.9 – Bands of excited g-modes found in long-period variable sdBs as a function of effective temperature. The sizes of the symbols provide a logarithmic measure of the modulus of the imaginary part of the complex eigenfrequency. Excited modes with $l \leq 4$ are depicted using the following colour code: green for $l = 1$ modes, magenta for l=2 modes, cyan for $l = 3$ modes, and dark blue for $l = 4$ modes. The columns of points for a given model are slightly offset in $T_{\rm eff}$ according to their l-index to facilitate viewing. The superposed black box represents the temperature uncertainty on PG 1627+017 in the horizontal direction, and the range of periods observed in the vertical.

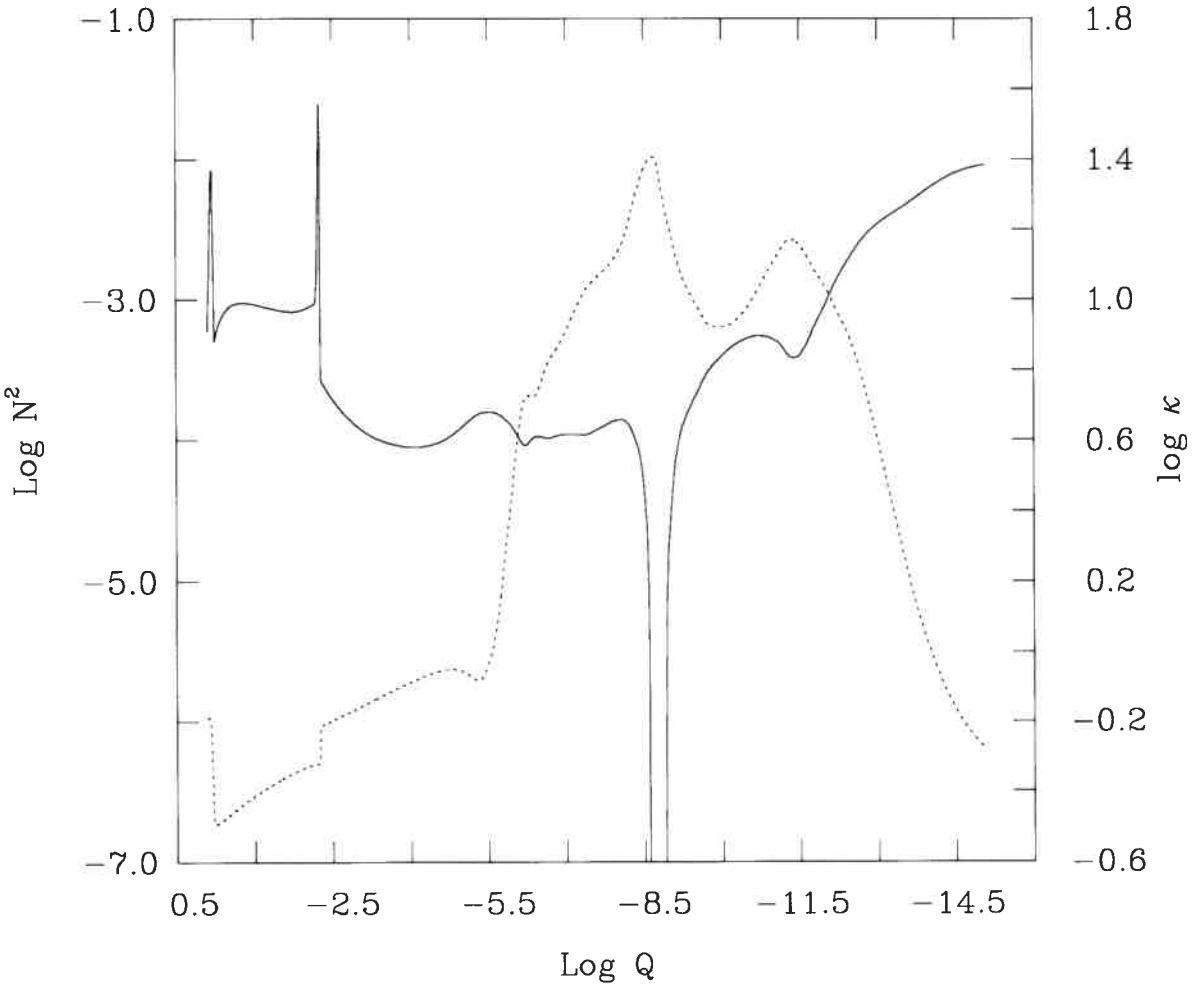

FIGURE 4.10 – Details of a model with $T_{\rm eff}$ = 24,000, $\log g$ = 5.25, M = 0.48 $M_{\odot}$, $\log q$(H) = −1.97, and $\log q$(He) = −0.24. The solid curve depicts the run of the square of the Brunt-Väisälä frequency (N^2) from the centre at $\log q$ = 0.0 to the surface at $\log q$ = −15.0. Also shown is the profile of the Rosseland mean opacity, represented by the dotted line.

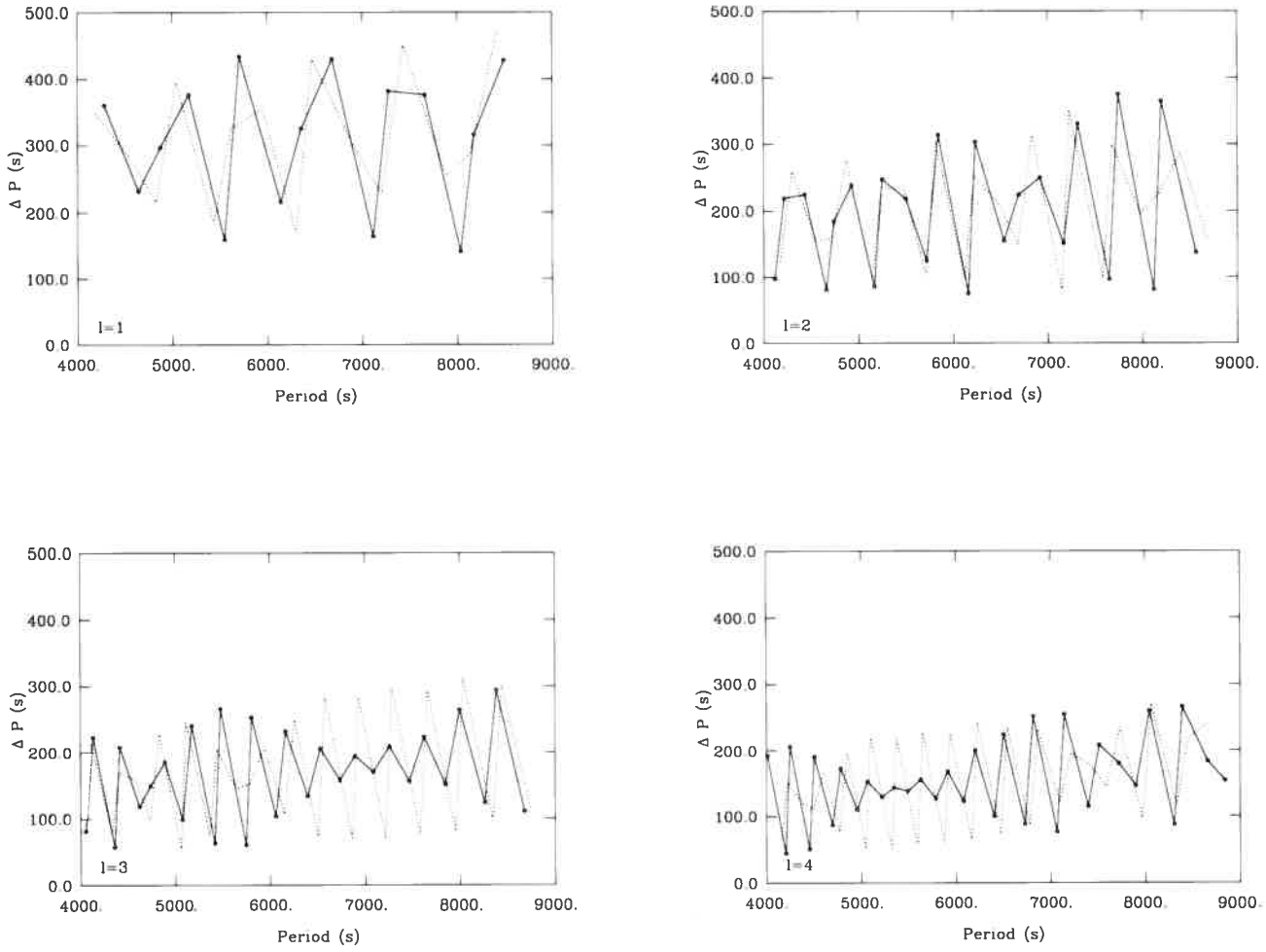

FIGURE 4.11 – Period spacing of modes with consecutive k-values for degree indices $l = 1$, 2, 3, and 4 calculated for a representative PG 1627+017 model (see text for details).

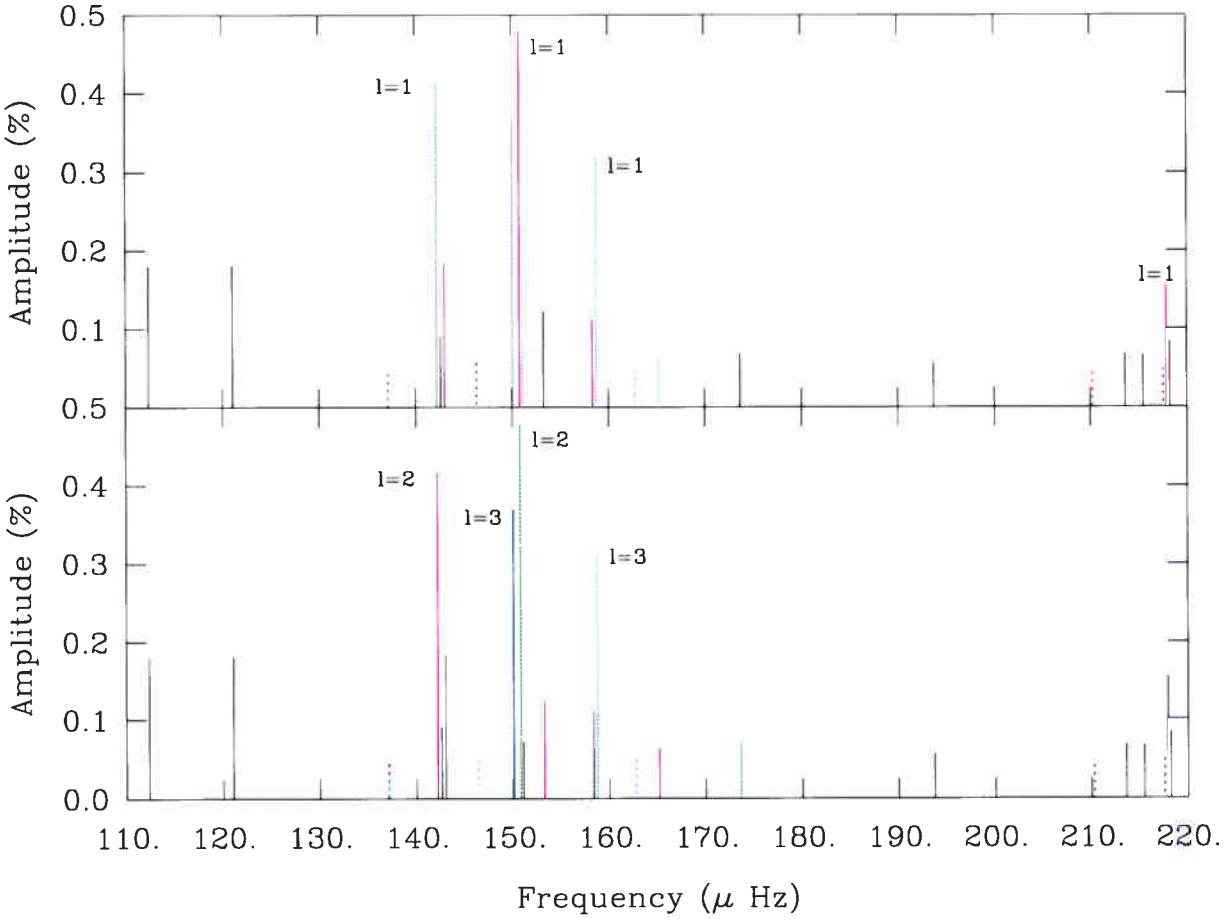

FIGURE 4.12 – Possible manifestations of binary synchronous rotational splitting on the basis of the periodicities listed in Table 4.4. In both panels, peaks of the same colour refer to split components of a mode with given k, l indices, while the vertical black lines show peaks for which no binary synchronous splitting was found. The l-index inferred from the spacing between the discrete components is indicated where applicable. Dashed line segments refer to periodicities with amplitudes of less than four times the noise level.

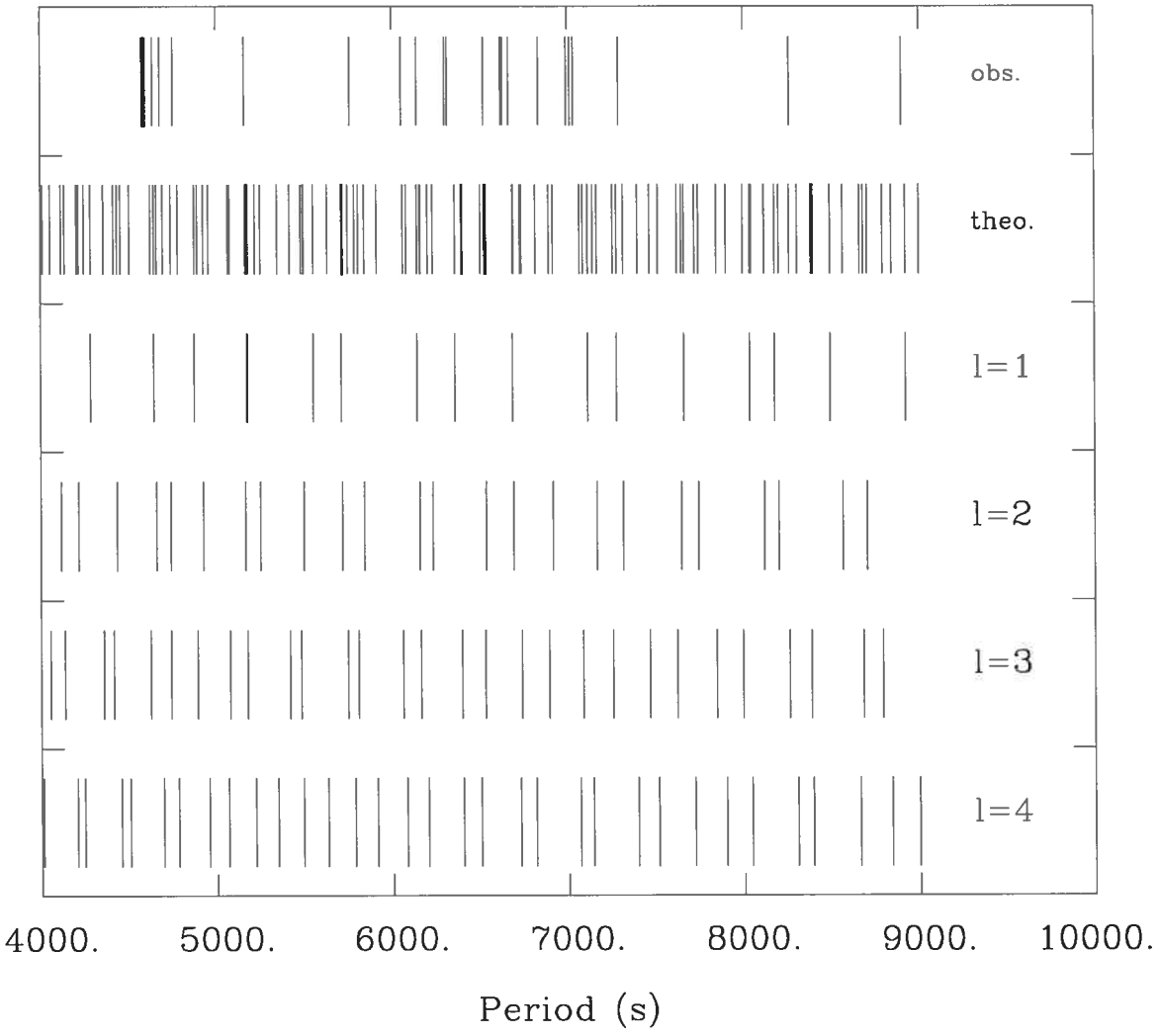

FIGURE 4.13 – Comparison of the periodicities observed in PG 1627+017, and those predicted for a representative model (see text for details). From top to bottom the rows show the periods extracted from the data, the superposition of theoretical modes with $l = 1$, 2, 3 and 4, and separate spectra for each of the degree indices separately as indicated.

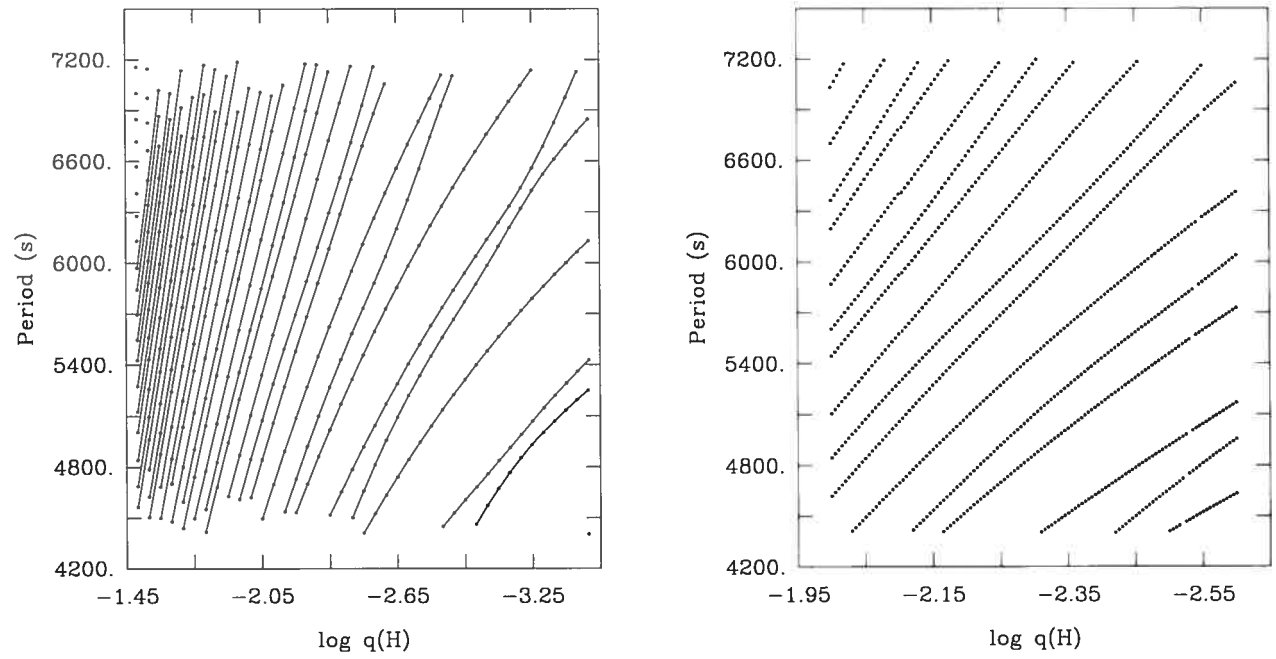

FIGURE 4.14 – Theoretical adiabatic period spectra ($l = 1$) for a sequence of models with $T_{\rm eff}$ = 22,900 K, $\log g = 5.25$, $M_*/M_\odot = 0.48$, $\log q$(He) = −0.25 and $\log q$(H) varying a) from −1.50 to −3.50 in steps of 0.05, and b) from −2.000 to −2.600 in steps of 0.005. In plot a), modes with the same value of k are connected for clarity. Note that isolated points correspond to modes that lie outside the period range illustrated in the adjacent model. The radial orders invoked range from 30−48 for the model on the left to 6−10 on the right. In panel b), the evolution of a given mode's period is more obvious thanks to the increased resolution. Values of k are between 15 (bottom) and 24 (top) on the left, and between 9 and 15 on the right.

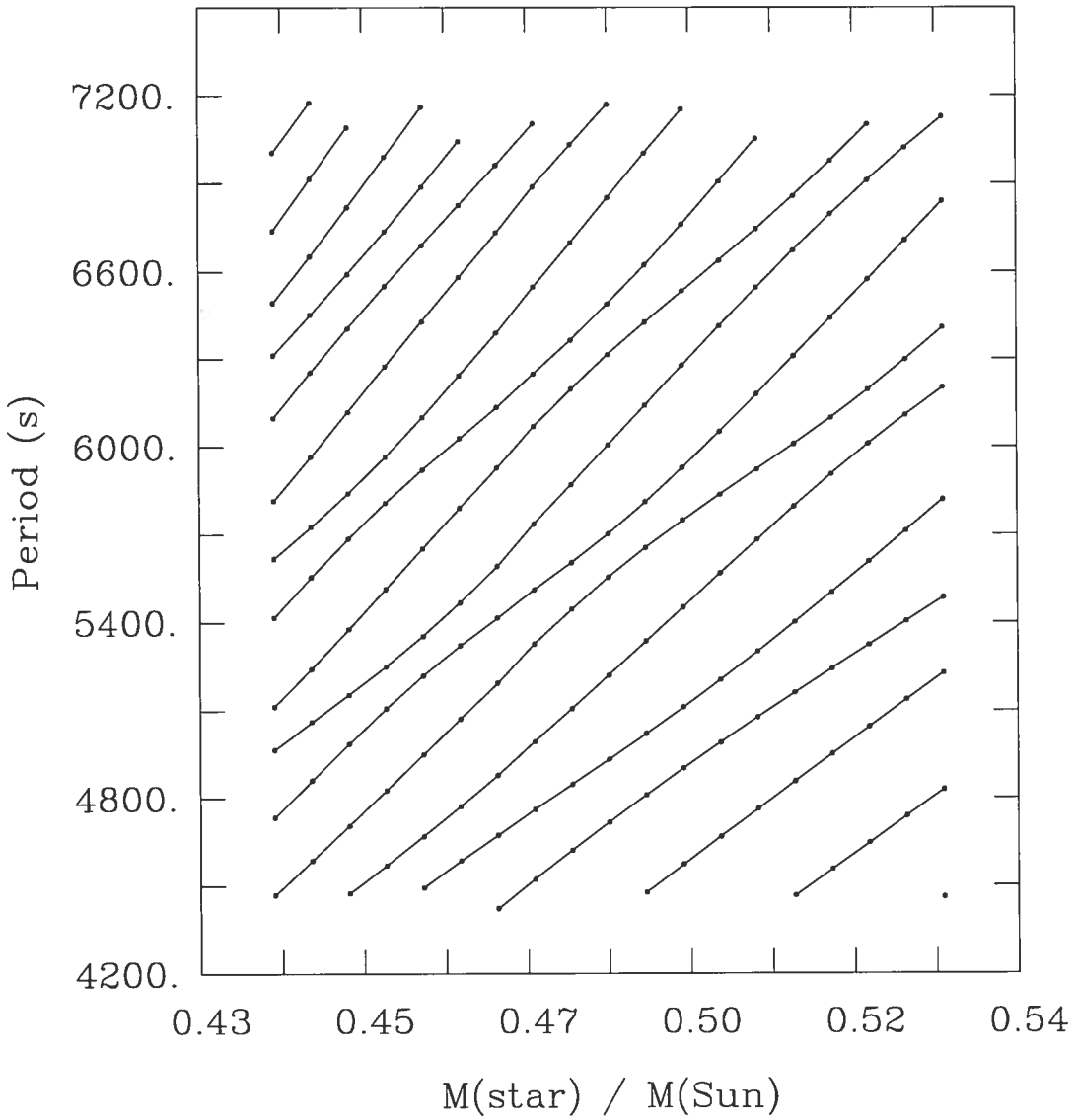

FIGURE 4.15 – Theoretical adiabatic period spectra ($l = 1$) for a sequence of models with $T_{\rm eff}$ = 22,900 K, $\log g = 5.25$, $\log q(\mathrm{H}) = -2.000$, $\log q(\mathrm{He}) = -0.25$ and $M_*/M_\odot$ varying from 0.44 to 0.53. Modes with the same value of k are connected for clarity. From the bottom on the left hand side the branches indicate radial indices between 18 and 29.

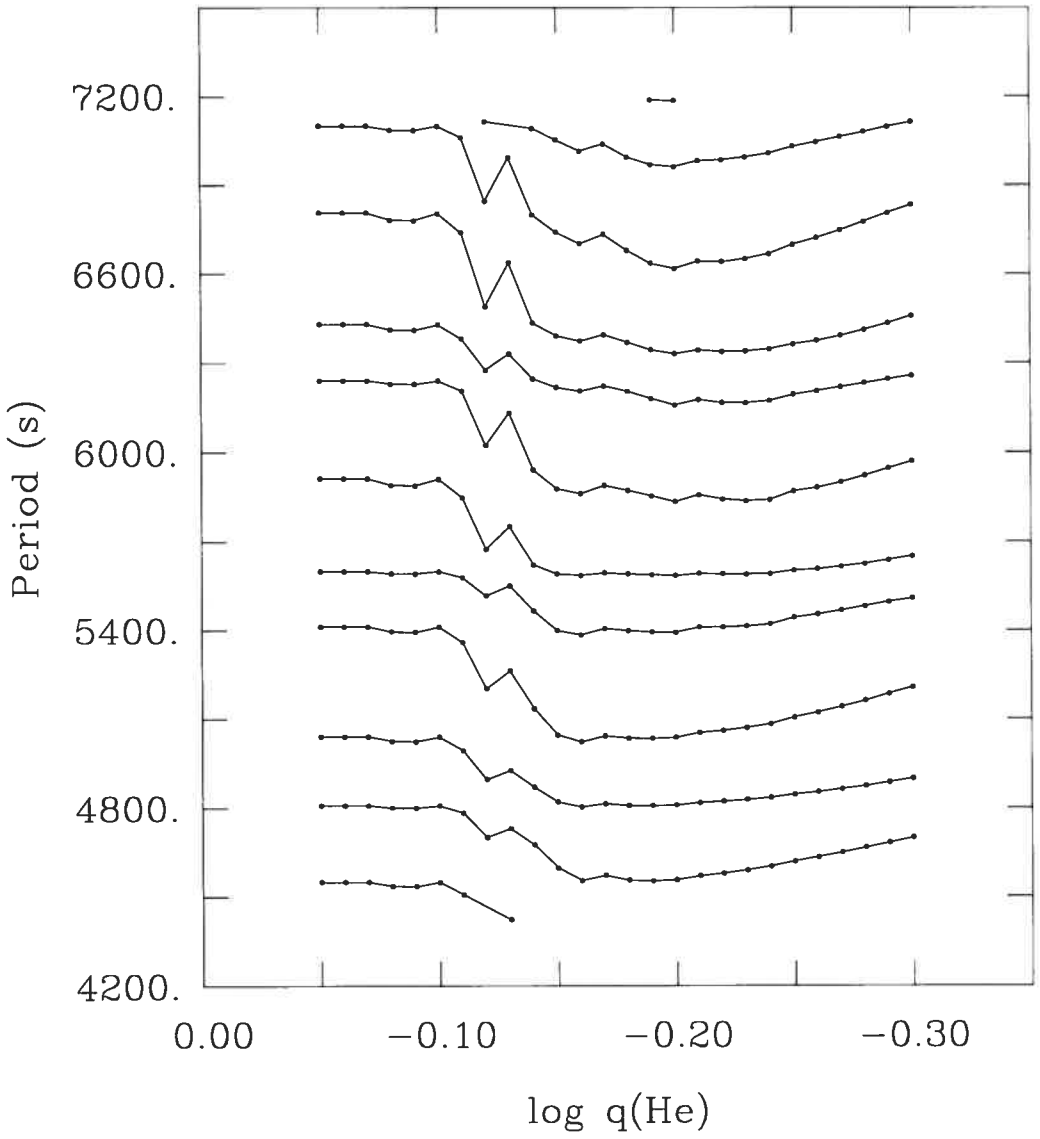

FIGURE 4.16 – Theoretical adiabatic period spectra ($l = 1$) for a sequence of models with $T_{\rm eff}$ = 22,900 K, $\log g = 5.25$, $M_*/M_\odot$=0.48, $\log q$(H) = −2.000 and $\log q$(He) varying from −0.05 to −0.30. Modes with the same value of k are connected for clarity. From the bottom on the left hand side the branches indicate radial indices between 14 and 23.

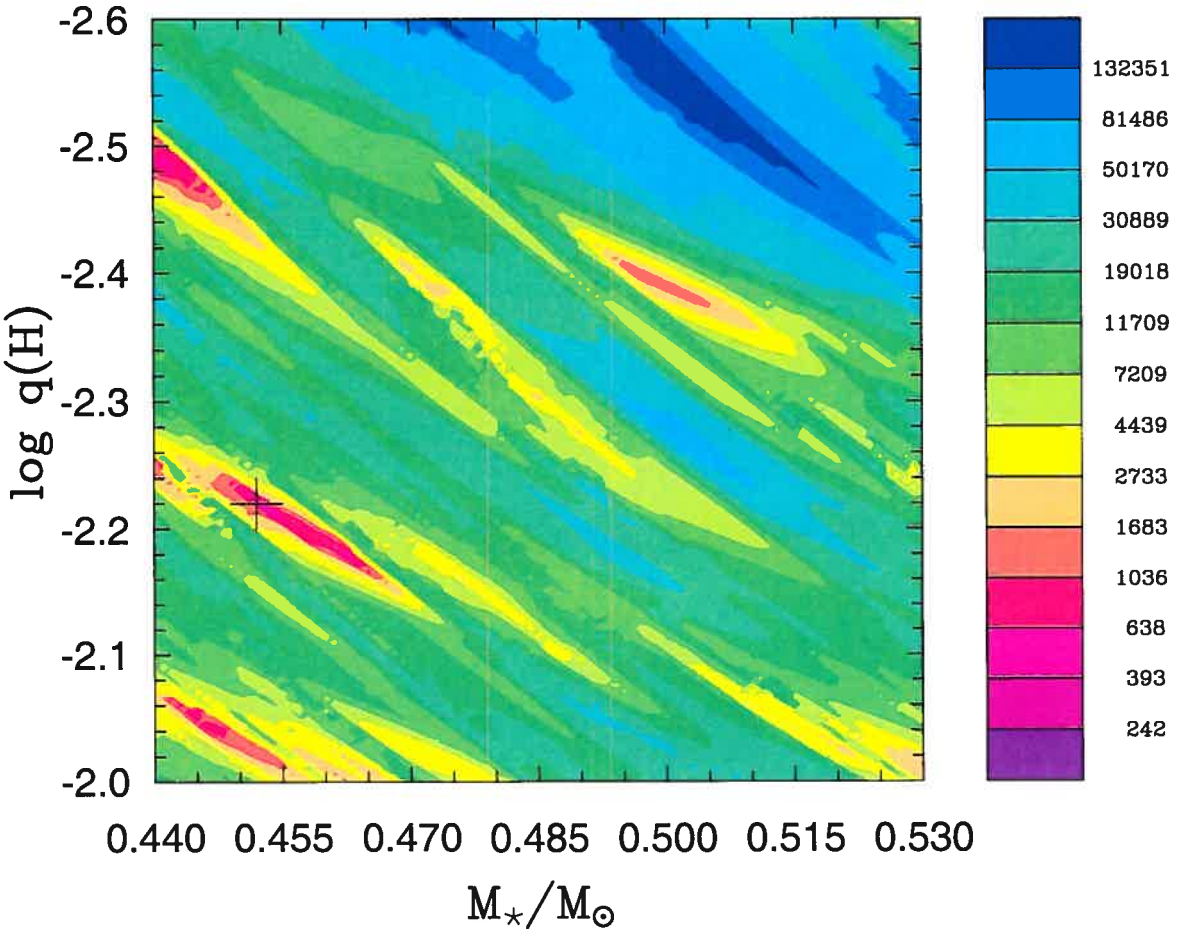

FIGURE 4.17 – Slice of the χ^2 hypersurface in the $M_*-\log q(\mathrm{H})$ plane. The third free parameter, $\log q(\mathrm{He})$, is set to the value that minimises χ^2 at each grid point. Some 231,230 models were computed to generate this plot. The scale depicted to the right of the figure refers to the value of χ^2 indicated by a given colour. The black cross indicates the location of the χ^2 minimum ($\chi^2 = 149$) at $M_*/M_\odot = 0.452$, $\log q(\mathrm{H}) = -2.220$ and $\log q(\mathrm{He}) = -0.15$.

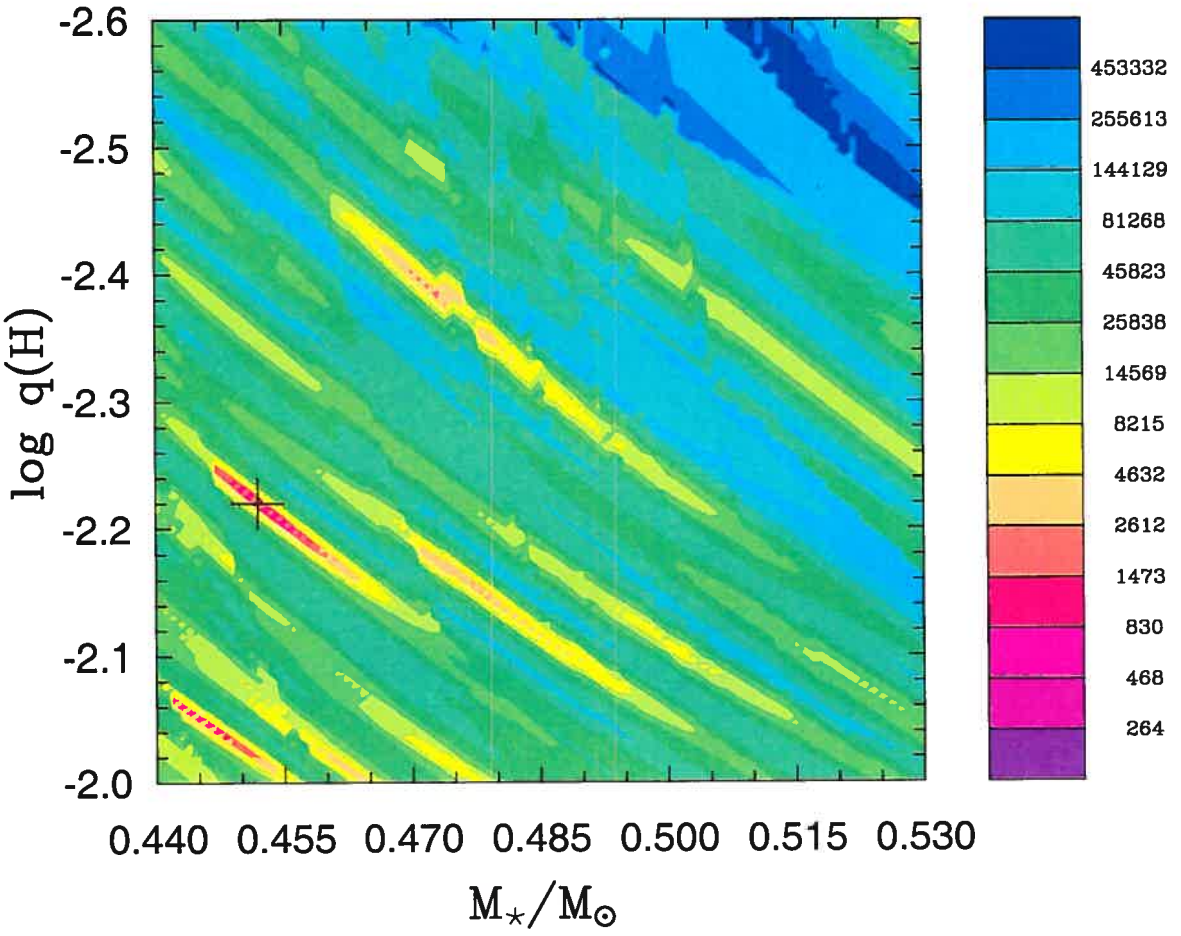

FIGURE 4.18 – Slice of the χ^2 hypersurface in the $M_*-\log q(\mathrm{H})$ plane. The third free parameter, $\log q(\mathrm{He})$, is set to -0.15, the value yielding the absolute χ^2 minimum in the previous figure. Here, 11,010 models were required to generate the plot. The scale depicted to the right of the figure refers to the value of χ^2 indicated by a given colour. The black cross indicates the location of the χ^2 minimum ($\chi^2 = 149$) at $M_*/M_\odot = 0.452$, $\log q(\mathrm{H}) = -2.220$.

Chapter 5

ASTEROSEISMOLOGICAL STUDIES OF LONG-PERIOD VARIABLE SUBDWARF B STARS - II. TWO-COLOUR PHOTOMETRY OF PG 1338+481[1]

S.K. Randall[2] , G. Fontaine[2], E.M. Green[3] , P. Brassard[2], D.M. Terndrup[4] , N. Brown[4], M. Fontaine[2], and P. Zacharias[2,5]

Submitted to *The Astrophysical Journal*

[1]Some of the observations reported here were obtained at the MMT Observatory, a joint facility of the University of Arizona and the Smithsonian Institution.

[2]Département de Physique, Université de Montréal, C.P. 6128, Succ. Centre-Ville, Montréal, Québec, Canada H3C 3J7; randall@astro.umontreal.ca, fontaine@astro.umontreal.ca, brassard@astro.umontreal.ca, mfontaine@astro.umontreal.ca

[3]Steward Observatory, University of Arizona, Tucson, AZ 85721; bgreen@as.arizona.edu

[4]Department of Astronomy, The Ohio State University, 140 West 18th Avenue, Columbus, OH 43210, USA; terndrup@astronomy.ohio-state.edu

[5]Kiepenheuer-Institut für Sonnenphysik, Schöneckstr. 6, 79104 Freiburg, Germany; pia@kis.uni-freiburg.de

5.1 ABSTRACT

We present the results of an ambitious observational campaign for the long-period variable subdwarf B star PG 1338+481. Seven continuous weeks of observing time at the Steward Observatory 1.55-m Kuiper telescope on Mt. Bigelow, Arizona, and the 1.3-m MDM telescope at Kitt Peak rendered $\sim$ 250 hours of simultaneous U/R time-series photometry, as well as an extra $\sim$ 70 hours of R-band only data. The analysis of the combined lightcurves resulted in the extraction of 13 convincing periodicities in the 2100−7200 s range, with amplitudes up to $\sim$ 0.3 % and $\sim$ 0.2 % in the U and R respectively. Comparing the ratios of amplitudes in the two wavebands to those predicted from theory suggests the presence of dipole modes, a notion that is further supported by the period spacing between the highest amplitude peaks. If confirmed, this would point to a significant discrepancy between the blue edge of the theoretical instability strip and that observed. At the quantitative level, we find that the distribution of the observed period spectrum is highly non-uniform and much sparser than that predicted from a representative model. One possible interpretation is that the available pulsational energy is preferentially channelled into certain period ranges through an unknown mode selection mechanism, and that oscillations outside these ranges are not excited to detectable amplitudes. The asteroseismological analysis attempted for PG 1338+481 on the basis of 6 observed periodicities believed to constitute consecutive dipole modes renders encouraging results. Fixing the effective temperature and surface gravity to the spectroscopic estimates, we successfully isolate just one family of optimal models that can reproduce the measured periods to better than 1 %. While the stellar parameters thus inferred must be regarded as preliminary, the achieved fit bodes well for future asteroseismic analyses of long-period variable subdwarf B stars.

5.2 INTRODUCTION

Subdwarf B (sdB) stars are evolved objects that populate the extreme horizontal branch and have atmospheric parameters in the ranges 20,000 K $\lesssim T_{\rm eff} \lesssim$ 40,000 K and 5.0 $\lesssim \log g \lesssim$ 6.2 (see Saffer et al. 1994). They are characterised by a helium-burning core surrounded by

a thin hydrogen-rich envelope that is chemically peculiar, with average atmospheric helium under-abundances of more than one order of magnitude. Their masses are typically constrained to about 0.5 $M_{\odot}$ as a result of the stars' direct descent from the first red giant tip. At some point during red giant evolution, the sdB progenitors undergo substantial mass loss, which all but strips them of their hydrogen-burning envelopes. They are thus unable to ascend the asymptotic giant branch after helium core exhaustion (Heber 1986). Instead, they evolve along the extreme horizontal branch, spending $\sim 10^8$ years in the sdB phase before becoming subdwarf O stars (with $T_{\rm eff} \sim 45{,}000$ K and $\log g \sim 5.5$ according to Dreizler 1993) and finally joining the white dwarf cooling track at $\sim 80{,}000$ K (Bergeron et al. 1994). They ultimately collapse as low-mass white dwarfs.

We distinguish two classes of variable subdwarf B stars, the fast and the slow pulsators. Members of the former group, named EC 14026 stars after the prototype, were first discovered at the South African Astronomical Observatory a few years ago (Kilkenny et al. 1997; Koen et al. 1997; O'Donoghue et al. 1997; Stobie et al. 1997). Their short-period variations on timescales of 100−200 s are interpreted in terms of low-order, low-degree pressure modes (see, e.g., Charpinet et al. 1996, 1997). The acoustic modes observed are well accounted for through the action of a classical κ-mechanism associated with an opacity bump due to the ionization of iron. In order for the mechanism to be effective, a local overabundance of iron is required in the driving region. This is achieved by the competition of gravitational settling and radiative levitation, two processes dependent on the star's surface gravity and effective temperature respectively. An iron distribution suitable for mode excitation is thus created only for certain combinations of $\log g$ and $T_{\rm eff}$, giving rise to a broad instability strip on the Hertzsprung-Russell (H-R) diagram, within which all stars should pulsate. Fast p-mode variations are predicted to occur in stars with effective temperatures between 28,000 and 38,000 K and surface gravities in the $5.5 \lesssim \log g \lesssim 6.2$ range, which is consistent with the atmospheric parameters derived from spectroscopic studies of EC 14026 stars. Moreover, the ranges of periods predicted to be excited by the models are in accordance with those observed, implying that a good qualitative understanding of the driving mechanism has been reached. In addition, unique quantitative matches between period spectra observed and those predicted

from a model with plausible atmospheric parameters have been possible in several instances (Brassard et al. 2001; Charpinet et al. 2003; Charpinet et al. 2005a; Charpinet et al. 2005b), allowing the tools of asteroseismology to be applied.

The second class of variable subdwarf B stars is made up of cooler objects (20,000 K $\lesssim T_{\rm eff} \lesssim$ 29,000 K) exhibiting slower, lower amplitude luminosity variations on timescales of one to two hours. Discovered a few years after the EC 14026 stars (Green et al. 2003), the so-called PG 1716 stars have not yet been observed and studied to the same extent. We do however believe to have identified the driving mechanism to be the same κ-mechanism that accounts so well for the EC 14026 phenomenon (Fontaine et al. 2003). The major difference to the case of the fast pulsators is that the theoretically excited periods correspond to gravity rather than pressure modes and that only high radial order modes with degree indices of $l \geq 3$ are successfully driven in the majority of models. While the coolest realistic PG 1716 star models at $T_{\rm eff} \sim$ 22,000 K are also capable of exciting $l = 2$ modes, the unstable modes' minimum degree index increases with effective temperature, implying that the very hottest slow oscillators at $T_{\rm eff} \sim$ 28,000 should exhibit modes of $l \geq 8$ only. The fact these would most likely not be observable due to cancellation effects when integrating over the visible disk of the star indicates some disparity between the instability strip observed and that predicted, a problem which is not yet clearly defined due to current difficulties in pinning down an absolute temperature scale for the cooler subdwarfs from spectroscopy. Nevertheless, it now seems clear that the blue edge of long-period variables observed lies at significantly higher temperatures than that predicted for low-degree modes.

Time-series photometry observations have so far uncovered 32 slowly oscillating subdwarfs (Green et al. 2006, in preparation; Kilkenny 2005), only four of which have been monitored in any detail. The first of these is the prototype, PG 1716+426, which was observed for $\sim$ 81 hours during a multi-site campaign conducted between April and June 2001 (Green et al. 2003; Reed et al. 2004). While the periods of oscillation were found to lie between 0.8 and 1.4 hours with amplitudes less than 0.2% of the mean brightness, the number of cycles secured was not sufficient for accurate frequency extraction. We thus launched a more ambitious multi-site campaign for one of the coolest slow pulsators, PG 1627+017, between April and

June 2003 and obtained over 300 hours of high quality photometry (see Randall et al. 2006, hereafter Paper I). Thanks to the relatively elevated duty cycle and long baseline we were able to isolate 23 frequencies in the 4500-8900 s range, however it was not entirely clear which of these were independent modes and which were caused by rotational splitting associated with the target's close binary status. A comparison between the number of periodicities observed and those predicted for low-degree modes (those with $l \leq 4$) revealed a strong overabundance of the latter, implying that mode identification would have to be constrained from the outset if asteroseismology was to be possible. From the exploitation of multi-colour photometry and rotational splitting we found that four of the highest amplitude peaks detected probably correspond to dipole modes, and based an exploratory search for an "optimal" model on that assumption. While our computations yielded a small number of model families that were able to reproduce the four observed periodicities surprisingly well, the fact that a number of assumptions were made concerning the fundamental parameters of the target and the probable nature of the periodicities rendered the results unreliable from an asteroseismology point of view. The conclusion reached was that any future campaign should concentrate on a slowly rotating single star, expected to show a simpler period spectrum than that detected for PG 1627+017. In addition, it was believed that the mode identification of individual periodicities could be more stringently constrained by obtaining multi-colour photometry throughout that campaign. Since it had previously been found that the degree index l of a mode leaves a detectable trace on the ratio of amplitudes measured in different wavebands (Randall et al. 2005a), an attempt was made to obtain some simultaneous U/R photometry during the PG 1627+017 observing run. Unfortunately, the low number of cycles accumulated in the U band for that star meant that precise colour-amplitude ratio determinations were not possible for most of the peaks detected, however it was gratifying to note an agreement with theory at the qualitative level. It thus seemed feasible that, given a sufficient baseline and duty cycle of simultaneous photometry in two wavebands, individual modes' l values could be determined, paving the way for asteroseismology.

It was in this context that we embarked on a two-site campaign for the long-period variable subdwarf B star PG 1338+481. Note that we have since then monitored a fourth slow

oscillator, PG 0101+039 (Randall et al. 2005b), and will draw upon results from that study in the present Paper. In the next chapters we will first describe the observations, subsequently detail the period extraction process and discuss the results obtained, and finally attempt an asteroseismological comparison with theory. We end with a discussion and conclusion of the results.

5.3 OBSERVATIONS

5.3.1 PG 1338+481

PG 1338+481 was chosen as a target for our second multi-site campaign for two main reasons. Firstly, it is typical of long-period variable subdwarf B stars in terms of atmospheric parameters and therefore more representative of the class as a whole than PG 1627+017. Secondly, radial velocities obtained at various epochs with the MMT Blue Spectrograph as part of a long-term sdB radial velocity/atmospheric parameters survey exhibit a standard deviation completely consistent with the observational errors, strongly suggesting that PG 1338+481 is a single star. Consequently, we expect this target to be a slow rotator ideally suited to an asteroseismological interpretation, since its period spectrum should be less complicated without the line splitting caused by a fast rotation rate. From an observational point of view PG 1338+481 presents more of a challenge than the previous target as it is substantially fainter at a V-band magnitude of V=13.61. Moreover, preliminary observations suggested average pulsational amplitudes to be less than half those detected for PG 1627+017. This may be outweighed in part by the fact that typical periods of PG 1338+481 are also shorter, meaning that the same length of observation renders more pulsational cycles than for the previous target.

While it is clear that PG 1338+481 is significantly hotter than PG 1627+017, the precise values of its atmospheric parameters are still under debate as a result of current difficulties in establishing a temperature scale for the cooler subdwarfs. Unlike for the EC 14026 stars, where the surface gravity and effective temperature can often be pinned down to within a couple of hundred degrees, the atmospheric parameters determined from spectroscopy for the

slow pulsators vary strongly depending on the type of model used in the fit. The inclusion of metals in the right proportions seems vital, as does a comprehensive treatment of non-LTE effects. Unfortunately, it is difficult and extremely time-consuming to incorporate both at the same time, leaving an important choice to be made in terms of the precision of the model. We opted for the non-LTE treatment, ignoring the effect of metals known to be present in the chemically peculiar atmospheres of subdwarf B stars, and found $T_{\rm eff} = 28{,}179 \pm 264$ and $\log g = 5.375 \pm 0.035$ based on high-resolution spectra obtained at the MMT (see Green, Fontaine & Chayer, in preparation, hereafter GFC). The inclusion of metals lowers both these values significantly. Assuming a uniform solar metallicity under the LTE approximation, Uli Heber (private communication, hereafter UH) determined the atmospheric parameters to be $T_{\rm eff} = 24{,}197 \pm 235$ and $\log g = 5.11 \pm 0.03$. Since metals are generally under-abundant in the outer layers of sdB stars compared to the case of the Sun, the values inferred are probably underestimated and the atmospheric parameters most likely lie in between the two determinations. For the remainder of this Paper we adopt the estimates of GFC as representative of PG 1338+481, while always keeping in mind that the possible values range from $\sim$ 24,000 K $\lesssim T_{\rm eff} \lesssim$ 28,500 K and $\sim 5.10 \lesssim \log g \lesssim 5.40$ respectively.

5.3.2 Campaign Organisation and Outcome

The observational requirements of the PG 1338+481 campaign were largely based on the experience gained from the previous year's PG 1627+017 run and as such were readily quantifiable. We estimated that the faintness of the star and the low pulsation amplitudes would be outweighed by the shorter oscillations, implying that the $\sim$ 300 hours of photometry secured for PG 1627+017 would produce a Fourier transform of similar quality for PG 1338+481. Thus, it seemed appropriate to apply for roughly the same amount of observing time at telescopes of equivalent sizes as for the first run. The main difference to the PG 1627+017 campaign was the intention of securing two-colour photometry throughout the run with the aim of using the ratio between the pulsational amplitudes in different wavebands to restrict the degree index of the mode in question. It was deemed that simultaneous U/R data would best achieve this, since the two wavebands are well separated in frequency space and both result

slow pulsators vary strongly depending on the type of model used in the fit. The inclusion of metals in the right proportions seems vital, as does a comprehensive treatment of non-LTE effects. Unfortunately, it is difficult and extremely time-consuming to incorporate both at the same time, leaving an important choice to be made in terms of the precision of the model. We opted for the non-LTE treatment, ignoring the effect of metals known to be present in the chemically peculiar atmospheres of subdwarf B stars, and found $T_{\rm eff} = 28{,}179 \pm 264$ and $\log g = 5.375 \pm 0.035$ based on high-resolution spectra obtained at the MMT (see Green, Fontaine & Chayer, in preparation, hereafter GFC). The inclusion of metals lowers both these values significantly. Assuming a uniform solar metallicity under the LTE approximation, Uli Heber (private communication, hereafter UH) determined the atmospheric parameters to be $T_{\rm eff} = 24{,}197 \pm 235$ and $\log g = 5.11 \pm 0.03$. Since metals are generally under-abundant in the outer layers of sdB stars compared to the case of the Sun, the values inferred are probably underestimated and the atmospheric parameters most likely lie in between the two determinations. For the remainder of this Paper we adopt the estimates of GFC as representative of PG 1338+481, while always keeping in mind that the possible values range from $\sim 24{,}000$ K $\lesssim T_{\rm eff} \lesssim 28{,}500$ K and $\sim 5.10 \lesssim \log g \lesssim 5.40$ respectively.

5.3.2 Campaign Organisation and Outcome

The observational requirements of the PG 1338+481 campaign were largely based on the experience gained from the previous year's PG 1627+017 run and as such were readily quantifiable. We estimated that the faintness of the star and the low pulsation amplitudes would be outweighed by the shorter period oscillations, implying that the $\sim$ 300 hours of photometry secured for PG 1627+017 would produce a Fourier transform of similar quality for PG 1338+481. Thus, it seemed appropriate to apply for roughly the same amount of observing time at telescopes of equivalent sizes as for the first run. The main difference from the PG 1627+017 campaign was the intention of securing two-colour photometry throughout the run with the aim of using the ratio between the pulsational amplitudes in different wavebands to restrict the degree index of the mode in question. It was deemed that simultaneous U/R data would best achieve this, since the two wavebands are well separated in frequency space and

both result in light curves of adequate quality. The latter was tested during the PG 1627+017 campaign, where simultaneous U/R photometry, while inadequate for quantitative statements due to the low number of cycles acquired, yielded qualitative results in line with theoretical predictions.

We were allocated 49 near consecutive nights between 15 March and 3 May 2004, split between the McGraw-Hill 1.3-m telescope of the MDM observatory at Kitt Peak, Arizona (11 nights) and Steward Observatory's 1.55-m Kuiper telescope on Mt. Bigelow, Arizona (38 nights). While we had planned on gathering simultaneous U/R photometry for the duration of the entire campaign, this was restricted to 39 of the 49 nights due to instrument availability. For the remaining 10 nights we gathered simple R-band data in the hope of improving on the period accuracy and detection limit of the two-colour photometry. Despite bad weather during a full two weeks of our observing time, we were able to accumulate about the same amount of data as for the PG 1627+017 campaign, clocking in at $\sim$ 250 hours of simultaneous U/R photometry and an extra $\sim$ 70 hours of R band only data. This corresponds to a duty cycle of $\sim$ 21% for the simultaneous data (compared to $\sim$ 27% in the R alone), and a frequency resolution of 0.26 μHz (0.23 μHz). For details of all useful observations obtained, see Table 5.1.

The MDM Kitt Peak data were obtained with the "Templeton" CCD, a thinned SITe device with 24 micron pixels. The field of view was such that 4 comparison stars could be used for both the Johnson U and the Cousins R filter, although the stars themselves varied. Images alternated between the two wavebands, one complete cycle generally lasting 279 s with adjustments being made for variable observing conditions. The average U band exposure time was 150 s and the R and images were integrated for 60 s, leaving an overhead time of 69 s. Standard IRAF[6] routines were used to perform bias-subtraction, flat-fielding, and cosmic ray removal, followed by aperture photometry of the target star and a predefined set of nearby reference stars in each image. The photometry of PG 1338+481 was then corrected for atmospheric variations using the weighted mean of the comparison stars and normalised

[6]The Image Reduction and Analysis Facility, a general purpose software package for astronomical data, is written and supported by the IRAF programming group of the National Optical Astronomy Observatories (NOAO) in Tucson, AZ.

to the mean intensity.

At Mt. Bigelow two different CCDs were used. The simultaneous U/R photometry was acquired on the blue-sensitive 2048×2048 pixel ccd21 loaned from the 90" telescope at Kitt Peak. A field-of-view of $5' \times 5'$ meant that 3 comparison stars could be imaged besides PG 1338+481 itself for both the Johnson U and the Cousins R filter. As at the MDM observatory, images were alternated between the two bands, with typical exposures of 30 s in the R and 120 s in the U. The overhead time was 70 s, resulting in U/R cycles every 220 s. On nights when ccd21 was unavailable, R band data were obtained with an older frontside-illuminated red-sensitive chip, ccd32, which is very similar to ccd21 except for a much lower quantum efficiency. R band exposures of similar quality to those achieved with ccd21 were obtained with ccd32 on the basis of 60 s integrations and 27 s overhead time; U band imagery was not possible due to the lack of blue sensitivity. Data processing and reduction were equivalent to those performed for the MDM photometry.

One evident problem with the nightly stellar light curves is that they are affected by differential extinction, particularly those obtained in the U band. This is not surprising considering the fact that differential photometry of the blue subdwarf was carried out on the basis of much redder comparison stars. The U band (and, to a lesser extent, the R band) light curves of PG 1338+481 thus exhibit a change in brightness as the star rises and sets in the sky. Since this variation occurs on a similar timescale as the intrinsic stellar pulsations, it must be corrected for in order to avoid confusion. Initially, we thought this correction could be quantified by monitoring 2MASS 1325+4008, a constant subdwarf of similar effective temperature as PG 1338+481 every hour or so, obtaining differential photometry on the basis of the other stars in the field-of-view, and from this deriving the differential extinction as a function of airmass. The reasoning was that, since 2MASS 1325+4008 is a hot subdwarf and its comparison stars are in all likelihood much redder, the luminosity variation due to differential extinction should be equivalent to that of another sdB of similar temperature. And indeed, in the case of PG 1627+017 this method proved very effective for flattening the U band light curves of long-term variations atmospheric in nature. Unfortunately, the only comparison star available for 2MASS 1325+4008 in the U band proved to be relatively blue compared to the comparison

stars in PG 1338+481's field-of-view, rendering a differential extinction correction too small to flatten the pulsator's nightly brightness variation with airmass.

Instead, we used a technique calibrated on the reduced PG 1338+481 light curves themselves. For each filter, we over-plotted all light curves of sufficient length and quality as a function of airmass and fit a second-order polynomial, thus estimating the average brightness variation of PG 1338+481 due to changes in airmass. We then corrected the original light curves for this variation, which resulted in nicely flattened U and R light curves such as those depicted in Figure 5.1. Each pair of curves shows the variation in relative brightness of PG 1338+481 in the U (blue) and the R (red) band over the course of a typical 9-hour night. The amplitudes of the curves change from night to night as a result of the beating between modes. From comparing the blue and red light curves of any one night it can be seen that, while the oscillations are clearly phase- and frequency-locked, the amplitudes of pulsation are significantly larger in the U than in the R as was to be expected from theory.

Since the telescope scheduling was such that the time granted on the two telescopes overlapped by 1.5 nights, we used the opportunity to perform an important consistency check between the two sites. The results of this are depicted in Figure 5.2, where the MDM (black) and Mt. Bigelow (magenta) R band light curves of PG 1338+481 from March 29 have been superposed. Despite having been acquired, reduced and flattened completely independently, the two curves are in remarkable agreement. While not unexpected, this provides a beautiful illustration of the accuracy and objectivity of the differential photometry gathered.

5.4 FREQUENCY ANALYSIS

5.4.1 The R-band data

The frequency analysis of the photometry gathered for PG 1338+481 was split into two parts in order to maximise the potential of the observations. While the first step concentrates on unambiguously identifying the oscillations present in the data, the second focuses on determining their colour-amplitude ratios. Since the frequency resolution and duty cycle achieved are superior for the R band data compared to that obtained in the U, the initial frequency

extraction is based on the R filter photometry. We thus combine all R band data available and analyse the resulting lightcurve in a standard fashion, employing Fourier analysis, least-squares fits to the lightcurve and pre-whitening techniques. This process has been described in detail by Billères et al. (2000), and we refer the interested reader to their work for more information.

Figure 5.3 shows, in the top panel, the Fourier transform of all useful R band data up to 0.6 mHz, beyond which it was found to be consistent with noise. We can distinguish two main regions of excess power. The first of these contains the most prominent periodicities with amplitudes up to ~ 0.2 % in the $\sim 0.20-0.35$ mHz range while the second covers lower amplitude oscillations up to about 0.1 % between ~ 0.08 and 0.17 mHz. In order to quantify the oscillations present in terms of their period, amplitude and phase, the peaks are extracted one by one through pre-whitening, which removes sidelobes due to window aliases as well as the actual pulsation peaks. The resulting, successively pre-whitened spectra are illustrated in the remaining panels of Figure 5.3. Plot b) shows the original spectrum pre-whitened by four dominant peaks with amplitudes between ~ 0.1 and 0.2 % and periods in the 3500–4500 s range. Moving down, this is followed by the additional extraction of another two periodicities above 0.09 %, and finally, in panel d) by the subtraction of all 11 peaks above the imposed threshold of three times the global noise level, in this case 0.06 %. It is evident from the last Fourier transform that the noise level varies significantly in the frequency range plotted in the sense that it is higher at lower frequencies, no doubt due to atmospheric effects. We thus divided the spectrum into two portions, below and above 0.3 mHz respectively, and computed the noise level for the two parts separately. Re-scanning the Fourier transform for convincing peaks, we found another three higher frequency oscillations that had been below the global threshold but rose to more than three times the local noise level. After extracting these also, we were left with the residual spectrum shown in panel e), from which no more plausible periodicities can be derived. Finally, the bottom panel shows the spectral window of the entire R band data obtained.

The frequencies extracted from the R band data are listed in Table 5.2 together with their period, amplitude and relative phase with respect to an arbitrary point in time (which,

in practice, is identified with the beginning of the first R band run listed in Table 5.1). All uncertainties quoted were estimated from the recipes proposed by Montgomery & O'Donoghue (1999). This method yields amplitude and phase uncertainty estimates that are typically a factor of 3 higher than the formal errors of the least-square fits used in the process. We also note that the error on the period is, on average, about 0.5 s, which corresponds to $\sim 1/9$ of the formal resolution at 4500 s. While all periodicities with amplitudes of more than three times the local noise level are included in Table 5.2, we have highlighted those that lie above the 4 sigma limit, a more conservative threshold sometimes employed for the extraction of periodicities.

To summarise our results from the first part of the frequency analysis, we have identified 14 periods between 2000 and 9500 s in the R band lightcurve of PG 1338+481, the most prominent of which reach amplitudes of up to $\sim$0.2 % and lie between 3500 and 4350 s. Despite these oscillations being present in the flattened and cleaned lightcurve obtained, we cannot be absolutely sure that they are identified with stellar pulsations as atmospheric origins cannot be ruled out, especially at lower frequencies. In this context the relatively high-amplitude peak at 9509.7 s, by far the longest period detected, is particularly dubious and should be regarded with caution.

5.4.2 The simultaneous U/R data

The second part of the frequency analysis is based on the simultaneous U/R photometry and has the objective of verifying the oscillations extracted from the R band data as well as determining the ratio of pulsational amplitudes monitored in the two bandpasses. We first combined all useful U band data and the U simultaneous parts of the R-band data to yield equivalent total light curves in the U and R respectively. Then, we followed the same procedure as outlined in the previous section, calculating the U and R band Fourier transforms and successively pre-whitening them of oscillations. The process is visualised in Figure 5.4, where spectra computed for the U and R photometry are over-plotted in blue and red for easy comparison. As before, the top panel contains the original spectra, which show a remarkable resemblance in the two wavebands. Apart from the U band amplitudes being appreciably

larger than those in the R, the transforms are virtually identical, with all significant peaks located at the same frequency in the two colours. The spectra differ most markedly at low frequencies ($\lesssim 0.1$ mHz), where the U band data is more noisy due to its greater dependence on atmospheric variations. Despite lying above the global amplitude threshold in the blue, very low frequency peaks are hence ignored during pre-whitening. Moving downwards in the figure, the spectra in panel b) have been pre-whitened by the 5 dominant periodicities, which include the 4 oscillations between 3500 and 4500 s extracted in panel b) of Figure 5.3 as well as the low-frequency period at $\sim$ 9500 s. Note that in the case of these dominant peaks the independent extraction of the U and R data rendered the frequencies in the same order of amplitude, i.e., the dominant peak was the same in both spectra after each extraction. This changed for subsequent steps of pre-whitening, where the strongest oscillation found in one colour often corresponded to the second or third highest peak or even a daily alias sidelobe in the other. When in doubt as to which oscillation to proceed with, we used the frequencies extracted from the R band data discussed in the previous section as a guideline. In this way, we extracted an additional two periodicities above 0.12/0.08 % in the U/R respectively in panel c), followed by all 12 oscillations above the global amplitude threshold of 0.08/0.05 % in the U/R in panel d). Finally, we determined the local threshold in the 0.3–0.6 mHz range for both colours and extracted an additional 3 higher frequency periodicities above 0.04 % (U) and 0.03 % (R) respectively. As for the previous data set, we show the window function in the bottom panel.

An overview of the oscillations extracted from the two-colour data is presented in Table 5.3. The format is similar to that of the previous table, apart from the fact that we have included the ratio of the U and R amplitudes as well as the $R - U$ phase differences. We believe that the errors given on the U/R amplitude ratios and phase differences roughly correspond to, or slightly overestimate the true errors, since the uncertainty recipes of Montgomery & O'Donogue (1999) remain rather conservative. For the amplitude ratios, the errors typically constitute 30–40 % of the values themselves and rise to $\sim$ 100 % for the lowest amplitude oscillations found. Clearly, the latter ratios do not hold much value, and so for the detailed colour-amplitude analysis discussed later we focus primarily on those ratios where the error is

less than 30% of the actual value (highlighted in bold in Table 5.3). For now, let us summarise that the average U/R amplitude ratio is 1.48, with individual values ranging from 1.28 to 1.73. Considering the $R-U$ phase differences, we find them to be relatively small and to be essentially consistent with 0 within the uncertainties quoted.

Comparing the frequencies extracted from the R band data with those of the two-colour photometry we find that they are generally in excellent agreement, with one exception: the simultaneous data's periodicity at $\sim$ 4159 s appears only below the amplitude threshold in the R band data. Since it corresponds to the lowest amplitude oscillation uncovered in the noisier 0−0.3 mHz regime and was included in Table 5.3 mostly because of its relatively high amplitude in the U, this is not surprising and no cause for concern. Nevertheless, we regard its signal as unproven and have placed it in brackets in Table 5.3. The other periodicity that is not totally convincing is the very low frequency peak at 9506 s discussed previously. While it is clearly present in both the U and the R lightcurve and does not constitute an artefact of the flattening procedure employed, we feel that its isolation and location in frequency space point to atmospheric effects rather than pulsational origins. Additionally, its (well-constrained) U/R amplitude ratio is significantly higher than the other convincing amplitude ratios listed in Table 5.3. Whereas this could of course be due to the measurement error or the associated mode having a degree index different from the other pulsations, there is no reason for this particular oscillation to fall out of line in terms of pulsational characteristics. On the other hand, low-frequency atmospheric variations leave a much more significant imprint in the U than in the R, as can be determined from the relative amplitudes of the spurious low-frequency peaks in Figure 5.4. We thus ignore the 9506 s oscillation during our interpretation of the pulsational period spectrum, and consider the pulsational periodicities observed for PG 1338+481 to lie in the 2100−7200 s range only.

5.5 INTERPRETATION OF THE PERIOD SPECTRUM

5.5.1 Comparison with Non-Adiabatic Theory

In order to qualitatively compare the range of periods observed for PG 1338+481 and those excited in models of appropriate atmospheric parameters, we constructed a sequence of the static envelope structures discussed at length in Paper I. These constitute an extended version of the computations employed to infer the driving mechanism operating in long-period variable subdwarf B stars (Fontaine et al. 2003) and correspond to the same numerical tools as the "second generation" models of Charpinet et al. (1997; see also Fontaine et al. 1998 and Charpinet et al. 2001) used to explain the EC 14026 phenomenon. Each model is now characterised by five free parameters: the effective temperature $T_{\rm eff}$, the logarithm of the surface gravity $\log g$, the total mass $M_*/M_\odot$, the logarithmic depth of the transition zone between the helium core and the thin hydrogen envelope $\log q({\rm H}) \equiv \log[M({\rm H})/{\rm M}_*]$, and the depth of the carbon-oxygen/helium core boundary $\log q({\rm He}) \equiv \log[M({\rm H+He})/{\rm M}_*]$. The fact that each input parameter can be specified independently of the others means that we can construct a model at any point in 5-dimensional parameter space, and determine its adiabatic periods by solving the 4 differential equations describing adiabatic oscillations (see, e.g., Unno et al. 1989). This is achieved with the aid of an updated version of the adiabatic finite-element pulsation code described in Brassard et al. (1992). The question of whether or not the modes are stable is answered by a more complicated algorithm solving the 6 complex differential equations describing non-adiabatic oscillations (Unno et al. 1989). In this study, the calculations are carried out using an upgraded version of the nonadiabatic pulsation code briefly described in Fontaine et al. (1994).

Modes in subdwarf B stars can be unstable only if iron is locally overabundant in the driving region, an effect achieved by the competing actions of gravitational settling and radiative levitation. In our models we include the non-uniform iron abundance profile based on diffusion calculations taking into account the levitation of iron in a pure hydrogen background. This is thought to be a relatively good approximation since iron is the main contributor to the opacity bump which drives the oscillations, and the atmospheres of subdwarf B stars

are dominated by hydrogen, with helium and metals being underabundant by typically more than one order of magnitude. However, it is possible that the inclusion of heavier elements, in particular helium, in the hydrogen envelope and the diffusion calculations would yield more accurate instability estimates. While it will be interesting to investigate this possibility in the future, the detailed computations required are far beyond the scope of the present study, and will be reported elsewhere.

We computed the non-adiabatic periods for a small set of 9 equilibrium models (spaced $\Delta T_{\rm eff} = 1000$ K apart), designed to represent the 21,000 K $\lesssim T_{\rm eff} \lesssim$ 29,000 K range of temperatures where long-period pulsating sdBs are found. Values of $\log g$ and $\log q$(H) were chosen such that the sequence would be somewhat above and parallel to the zero-age extreme horizontal branch, while the stellar mass was kept constant at 0.48 $M_{\odot}$. The CO/He transition zone was neglected since it has no impact on the instability calculations. Exact values of $\log g$ and $\log q$(H) are listed in Table 5.4. Figure 5.5 shows the bands of logarithmic periods predicted to be unstable for these models as a function of effective temperature. Each point denotes an excited mode and is colour-coded according to degree index l in magenta (l=2), blue (l=3), cyan (l=4), green (l=5), yellow (l=6), red (l=7) or black (l=8). Note that the columns for individual degree indices have been shifted slightly in the horizontal direction to facilitate viewing. As was discussed by Fontaine et al. (2003), we find that the range of unstable periods decreases with increasing effective temperature and surface gravity, and that the minimum degree index of the modes excited becomes larger.

Upon this sequence of unstable period bands we have superposed the range of periods observed for PG 1338+481 together with those extracted for the three other extensively observed long-period variables PG 1716+426 (Green et al. 2003; Reed et al. 2004), PG 1627+017 (Paper I of these series) and PG 0101+039 (Randall et al. 2005b). For each target, the horizontal component of the continuous box indicates the effective temperature uncertainty derived by GFC, while the dotted extension allows for the shift to lower atmospheric parameters on the basis of LTE model atmospheres including metals at solar abundances as calculated by UH. For details on the two estimates of $T_{\rm eff}$ and $\log g$, as well as the ranges of periods and amplitudes measured for the four stars, please see Table 5.5. Note that for PG 1716+426 the frequency

and amplitude ranges are approximate and may respectively under- and overestimate the true limits due to the poor baseline and duty cycle achieved during the observations. Comparing the predicted instability strip to that observed we find that the resemblance is quite striking at the qualitative level, particularly at the cooler end of the subdwarf distribution. Indeed, for the case of PG 1627+017, the entire range of periodicities detected can be reproduced in terms of modes with $l = 2$, 3 and 4 if the atmospheric parameters are pushed to the lower limits of the uncertainty estimates. However, the match is less good for the hotter targets, particularly PG 0101+039, where any overlap between theoretical and observed periodicities can be excluded thanks to the more stringently constrained temperature uncertainty. Moreover, the only modes predicted to be excited in the majority of models have degree indices $l \geq 3$ (rising to $l \geq 6$ for the hotter targets), which should not be observable due to cancellation effects when integrating over the visible disk of the star. Finally, even the driving of $l = 2$ modes in the coolest models seems insufficient to account for the oscillations detected for PG 1627+017, since these are believed to be associated with dipole modes. It is thus clear that our instability calculations are subject to some deficiencies that need to be addressed and rectified.

Despite these difficulties, we believe that the basic physical mechanism proposed by Fontaine et al. (2003) to excite high-order g-mode pulsations in cool sdB stars is fundamentally sound and that the discrepancies between the empirical and theoretical blue edges of the PG 1716 instability strip can likely be alleviated using more realistic evolutionary models incorporating helium and other absorbers of radiation. This is based on two convincing arguments. Firstly, the period spectra predicted from non-adiabatic theory show the same relative behaviour with atmospheric parameters as those observed, the periods excited decreasing with increasing temperature and surface gravity in both cases. Also, the amplitudes of pulsation measured systematically decrease with increasing surface gravity of the star, as can be seen from Figure 5.6 (see also Table 5.5). This inverse dependence of mode driving strength on $\log g$ is analogous to that observed for the EC 14026 stars and can be explained in terms of the iron bump underlying the efficiency of the κ-mechanism. Since the surface gravity directly influences the strength of the gravitational settling process, a higher value of $\log g$ implies that

smaller amounts of iron can levitate in the envelope of the star, leading to a lower and broader Z-bump. This in turn results in a flatter opacity peak and the decrease in the driving efficiency observed for more compact subdwarfs (see Charpinet et al. 2001 for details). The second argument supporting the validity of the κ-mechanism is the strong qualitative resemblance that exists between the two classes of subdwarf B pulsator and the SPB / β Cep stars on the main sequence (see Fontaine et al. 2003 and references therein). In both cases, the κ-mechanism drives short-period, low-order p- and g-modes in the hotter stars, while the cooler stars excite long-period, high-order g-modes. The major difference between the two types of sdB pulsator and their main-sequence counterparts is that the models of the latter long-period variables are able to drive g-modes with low degree indices of $l = 1$ and 2, which our PG 1716 models, for the most part, cannot. Since subdwarfs are generally chemically peculiar, this shortcoming may well be related to structural deficiencies of the models. In contrast to the SPB / β Cep scenario, models of sdB stars already require radiative levitation to drive oscillations, and it is possible that we are missing an aspect related to this. In particular, the inclusion of other levitating metals in competition with iron may improve our quantitative description of the blue edge of the PG 1716 strip. This problem is however well beyond the scope of this paper.

5.5.2 Constraining Mode Identification from Multi-Colour Photometry

The modelling presented in this section closely follows the theory developed by Randall et al. (2005a), and we refer interested individuals to that Paper for more information. Nevertheless, we include a brief recap of the most relevant aspects here for the convenience of the reader. The technique employed is based on the fact that the observed frequency dependence of an oscillation's amplitude and phase bears the signature of the mode's degree index l, as well as the star's atmospheric parameters, the intrinsic amplitude of the periodicity and its viewing aspect. The influence of the latter two parameters can be eliminated by computing the ratio of pulsational amplitudes (and the difference between phases) as measured in two or more bandpasses. Given a target's effective temperature and surface gravity, the observed mode's degree index can thus be inferred from multi-colour photometry.

For each value of l, the brightness variation expected across the visible disk during a

pulsational cycle can be expressed in terms of temperature, radius, and surface gravity perturbations to the emergent flux. These in turn are dependent on quantities obtainable from model atmospheres and non-adiabatic pulsation theory, as well as on the period of the mode in question (see equations 34 – 38 of Randall et al. 2005a). The model atmosphere parameters are made up of the logarithmic derivative of the emergent flux with respect to the effective temperature / surface gravity and the weighted limb darkening integral together with its derivatives. Initially computed as monochromatic quantities from specially modified sdB atmosphere codes, they are subsequently integrated over the bandpasses of interest to allow for comparison with observations. The second set of parameters includes the non-adiabatic quantities R and Ψ_T, which are related to an oscillation's departure from adiabacity in amplitude and phase respectively. Together with the adiabatic gradient, ∇_{ad}, they are computed on the basis of the static envelope models described in the previous sections. These are submitted to adiabatic and non-adiabatic pulsation calculations that yield the relative behaviour of the radius and temperature perturbations in the stellar atmosphere for each mode. Integrated over the atmospheric layers contributing most to the emergent flux (taken to lie at optical depths $\tau = 0.1-10$), the ratio of the two perturbations' moduli and their phase lag yield the atmosphere-averaged values of R and ψ_T describing the departure from adiabacity of the observed brightness variations.

In our quest to determine the l-values of the modes extracted from the photometry of PG 1338+481 we calculated the predicted U/R amplitude ratios and phase differences for low degree indices from $l = 1$ to $l = 5$ in the 2000–7500 s period range. The monochromatic model atmosphere quantities were obtained under the assumption of $T_{\rm eff} = 28{,}200$ K and $\log g = 5.38$ (i.e., the spectroscopic estimates of GFC), and were integrated over wavebands corresponding to the convolution of the standard Johnson U and Cousins R bandpasses with the response curve of ccd21 (the detector used at Mt. Bigelow) and the atmospheric transparency curve of a representative medium altitude site (in this case, Kitt Peak National Observatory). Note that we also carried out test calculations with the response curve of the Templeton CCD used for the MDM observations and the atmospheric transparency of a higher and lower altitude site but obtained very similar results. In contrast, lowering the spectroscopic parameters to the

values suggested by U. Heber resulted in a slight increase in the final amplitude ratios, however the changes were not significant enough to affect the implications for mode identification.

Figures 5.7 and 5.8 respectively illustrate the predicted U/R amplitude ratios and the $R-U$ phase shifts for modes with $l = 1$ (magenta), $l = 2$ (blue), $l = 3$ (cyan), $l = 4$ (green) and $l = 5$ (black) in the 2000−7500 s range. Superposed on the theoretical quantities are the well-constrained values obtained for the four highest amplitude oscillations (black points). For completeness, we also indicate periodicities whose amplitude ratio error is less than 50 % of the actual value (green points), however these are deemed too uncertain to be used in the determination of the degree index. Looking at the amplitude ratio plot (Figure 5.7), it is clear that we can exclude modes with $l = 3$ and probably $l = 5$ for all peaks extracted, but are not necessarily able to discriminate between those with $l = 1$, 2 and 4. While degree indices of 1 and 4 provide closer matches to the convincing amplitude ratios observed, the error bars of three of the four periods reach into the curve for $l = 2$. If we assume for a moment that the four high amplitude oscillations are associated with the same degree index (see the following section for a justification), we can derive a more meaningful estimate of the goodness-of-fit for different l-values using the merit function

$$\chi^2 = \sum_{i=1}^{4} \left(\frac{a^i_{theo} - a^i_{obs}}{\sigma^i} \right)^2, \tag{5.1}$$

where a^i_{theo} is the theoretical amplitude ratio for one of the i periodicities, a^i_{obs} is that observed, and σ^i is the measurement error. By definition, the quality of the fit improves with decreasing χ^2. We then find that the predictions for $l = 1$ match the observed amplitude ratios best at $\chi^2 = 0.555$, followed closely by those for $l = 4$ ($\chi^2 = 0.653$). The fit for $l = 2$ is certainly inferior ($\chi^2 = 2.33$), but not to the point of being unacceptable. Finally, it is unlikely that the peaks observed correspond to $l = 5$ ($\chi^2 = 6.09$) or $l = 3$ ($\chi^2 = 61.9$).

Considering the phase difference plot (Figure 5.8), we find that the predicted values lie close to zero in the period range where oscillations are observed. This is in line with the notion that non-adiabatic effects become undetectable at very long periods. Unfortunately, it also means that the phase differences hold virtually no information on a mode's degree index for PG 1716 stars. It is thus clear that the analysis of the phase shifts is futile from a mode

identification point of view and that all the discriminative power lies with the amplitude ratios discussed above.

5.5.3 Quantitative Analysis of the Adiabatic Period Spectrum

In order to give the reader a better overview of the pulsation spectrum observed we have illustrated, in the top panel of Figure 5.9, the periodicities extracted from the R band lightcurve of PG 1338+481 (see Table 5.2 for details). These seem to be concentrated in three distinct period ranges, with the highest amplitude peaks accumulating between $\sim$ 3000 and 5000 s, and a few lower amplitude oscillations occurring around 2200 s and between 6300 and 7300 s. Within the main period cluster we uncover two pairs of doublets with an equal period spacing of 34 s, which in turn is similar to that found between the two closely spaced peaks at longer periods (46 s). The oscillation spectrum of PG 1338+481 should be compared to that observed for PG 1627+017, the only other long-period variable for which a similar number of frequencies has so far been uncovered (see Paper I of this series for details). Illustrated in the bottom panel of Figure 5.9, its period distribution shows a similar structure in terms of the clustering of peaks in three bandpasses. However, for PG 1627+017 the entire distribution is shifted to longer periods, with the highest amplitude peaks lying between $\sim$ 6000 and 7500 s. In addition, the (R band) amplitudes are significantly higher than those detected for PG 1338+481. As discussed in section 5.4.1, these two effects are almost certainly due to differences between the atmospheric parameters of the two targets and qualitatively tie in with non-adiabatic theory. The resemblance of the two stars' frequency distribution on the other hand is not so easily explained. If we for a moment assume that the period structures observed for our targets are typical of those excited in PG 1716 stars (which does not seem too far-fetched bearing in mind the similar, if much sparser and less well-defined periodicity spectra measured for PG 0101+039 and PG 1716+426 respectively), they would imply three distinct frequency ranges where pulsations are excited to appreciable amplitudes. Although this is seemingly in conflict with current non-adiabatic theory, which predicts a band of unstable periods, it perhaps could be explained by an unknown mode selection mechanism that preferentially transfers energy to modes in certain frequency ranges, thus boosting their

amplitudes.

Mode selection may also help explain the closely spaced doublets mentioned above. While the splitting found for PG 1338+481 is nowhere near as extreme as that uncovered for PG 1627+017 (see Paper I for a detailed account), it is nevertheless intriguing and warrants further investigation. In the case of the earlier target, some of the closely spaced components could be attributed to binary-synchronous rotational splitting, however others remained unaccounted for. Aside from energy channelling through mode selection, potential explanations included frequency or amplitude variations over time and effects induced by the close binary nature of the target. Matters were complicated by the fact that the (relatively even) frequency spacing between adjacent peaks roughly corresponded to the baseline of the campaign, indicating an observational or data analysis artefact. Thorough verification, re-analysis and experiments with synthetic data rendered this unlikely, but a nagging doubt remained. Fortunately, the situation is less complicated for PG 1338+481. The doublets observed are relatively evenly spaced in period rather than frequency, and the frequency differences between components are in no way linked to the campaign duration, being several times greater than the formal resolution. Moreover, there is no ambiguity as to the pulsational nature of the peaks, since PG 1338+481 is thought to be either single or in a very long-period binary system and no evidence for rotational splitting was found. We thus believe that the components of the three doublets correspond to independent harmonic oscillations that happen to lie close to each other. Considering the density of the representative[7] theoretical period spectrum illustrated in Figure 5.10, the small frequency spacings can easily be reconstructed in terms of the canonically expected modes with $l = 1$ and 2 only. In fact, our calculations predict many more low degree modes than those observed over the same period range, indicating that the energy available from the driving mechanism is preferentially channeled into modes with certain frequencies. It would then make sense if the lower amplitude components of the doublets are associated with higher degree indices than the other periodicities and are excited to observable amplitudes either through resonance or because they happen to lie in a period range that has

[7]The period spectrum shown in fact corresponds to that predicted for the optimal model identified below, however in the present context we simply wish to illustrate the overabundance of predicted compared to observed modes for PG 1338+481.

sufficient energy available. The higher amplitude peaks (at least those in the main frequency cluster) would then probably correspond to $l = 1$ (see below), while the weaker oscillations would have degree indices $l = 2$.

One potentially crucial characteristic of the period spectrum uncovered for PG 1338+481 is the near-equal spacing in period of six of the peaks uncovered (marked by arrows in Figure 5.9), including the four highest amplitude periodicities. Lying at 3252 s, 3530 s, 3828 s, 4090 s, 4348 s and 4625 s, these oscillations are separated by an average period spacing $\langle \Delta P \rangle = 275$ s, with individual values narrowly constrained in the $258 \leq \Delta P \leq 298$ s range. According to asymptotic theory, this is precisely what would be expected for modes with the same degree index l and consecutive values of the radial order k. Comparing the $\langle \Delta P \rangle$ observed to that predicted for modes with $l = 1$ and 2 (see Figure 5.10), we find that the dipole modes' distribution constitutes the better match. Modes with $l = 2$ (and consequently those with higher degree indices) are spaced much closer together and cannot recreate the observed spectrum in terms of adjacent periodicities. While the peaks extracted could be associated with intermittent $l = 2$ modes, the low variation in growth rate predicted from one mode to the next renders the excitation of only every other mode unlikely. We thus believe that these 6 pulsations correspond to dipole modes, which is in accordance with the amplitude ratios obtained. Furthermore, it is likely that they have consecutive values of k. This places significant constraints on mode identification, an invaluable asset to the attempt at asteroseismology presented in the next section.

5.6 ASTEROSEISMOLOGY

5.6.1 Background

The ultimate goal when analysing the frequency spectrum of a pulsating star is to infer its fundamental properties from asteroseismology. This can be achieved by unambiguously matching the periods observed to those predicted for a physically viable model. Since our PG 1716 star models are dependent on five free parameters, finding the "optimal" model first requires the computation of a 5-dimensional grid of models in parameter space. The best

possible fit between the adiabatic periodicities at each gridpoint and those observed is then quantified by the goodness-of-fit merit function

$$\chi^2 = \sum_{i=1}^{n} \left(P^i_{obs} - P^i_{theo} \right)^2 , \tag{5.2}$$

where P^i_{obs} is one of the n periodicities observed and P^i_{theo} is the theoretical period that matches it best. Models that result in a smaller value of χ^2 provide a superior match to the pulsations observed than those with a larger merit function, allowing the determination of an "optimal" model via the so-called "forward" approach in asteroseismology (see Brassard et al. 2001 for details). This method is being used with great success for the EC 14026 stars, where asteroseismology has so far been achieved for four targets (see Charpinet et al. 2005 for a summary). In each case, good fits to the measured period spectra were found for just one or two families of models in parameter space, one of which could be designated the preferred solution on the basis of independent spectroscopic estimates of $\log g$ and $T_{\rm eff}$. Hence, the targets' fundamental parameters could be inferred with some certainty and accuracy.

The asteroseismology of long-period variable subdwarf B stars is more challenging than that of the EC 14026 stars, as we realised when attempting to interpret the period spectrum of PG 1627+017 (see section 4.4.3). There are a number of reasons for this, linked to shortcomings at both the observational and the theoretical level as well as complications inherent to the slow oscillators themselves. First of all, owing to the relative overabundance of predicted compared to observed modes, some assumptions need to be made regarding the measured peaks' l-values if meaningful fits are to be achieved. Otherwise the majority of models computed will be associated with a small value of χ^2, irrespective of their characteristic parameters. Fortunately, in the case of PG 1338+481 we have reason to believe that the six evenly spaced periods discussed in the previous section correspond to consecutive dipole modes. Being able to place this constraint on mode identification from the outset is vital to the detection of well-defined minima and forms the basis of our asteroseismological exploration.

The second challenge faced in the study of the PG 1716 stars is related to the computation time required, which is far longer than that needed to accurately calculate the χ^2 hypersurface for the EC 14026 stars. One reason for this is that sampling parameter space to a similar

relative period accuracy entails the construction of a larger number of models for the slow oscillators. This is partly a result of the g-modes excited in PG 1716 stars being dependent on 5 free parameters rather than the 4 that are of interest for the p-modes found in EC 14026 stars. While the latter constitute shallow envelope modes and are as such practically independent of the CO/He boundary, the periods of g-modes are influenced by both the CO/He and the He/H transition zone. In addition, the fact that the slow oscillators have lower surface gravities and effective temperatures than the rapid pulsators manifests itself in an increased sensitivity to changes in the two quantities (see Figures 9, 10, 13 and 14 of Charpinet et al. 2002). Unlike pressure modes, the periods of gravity modes depend strongly on the temperature of the model invoked, while their variation with $\log g$, M_* and $\log q(\mathrm{H})$ remains comparable. Consequently, the spacing between adjacent gridpoints in $T_{\rm eff} - \log g - M_* - \log q(\mathrm{H}) - \log q(\mathrm{He})$ hyperspace needs to be small in all five dimensions if χ^2 minima are to be detected, requiring the construction of a large number of models. The length of the computations is drawn out further by the long periods involved. While modes with periods typical of the EC 14026 stars can be determined to higher than observational accuracy using relatively few quadratic elements in the pulsation calculations based on our finite-element codes (generally set to 140 when calculating a grid of models), oscillations on the timescale of a few thousand seconds demand a substantially higher number of elements (we empirically find 800 to be sufficient). Even if the range of periods estimated is severely limited, in this case to the 3100−4900 s range where the six dipole modes are found, the computation time for each model increases drastically. Therefore, we need to reduce the number of models calculated in any way possible.

The final, and perhaps most serious, problem associated with the asteroseismology of long-period variable subdwarfs is the current lack of means to verify the authenticity of potential "optimal" models. A strong constraint used to verify the χ^2 minima for the fast pulsators is their compatibility with spectroscopic estimates of the targets' atmospheric parameters. Unfortunately, these are associated with large uncertainties for the PG 1716 stars, and only marginally constrain acceptable regions of $\log g - T_{\rm eff}$ space. In addition, it is possible to test the mode identification postulated for EC 14026 stars by inferring the degree index using an independent means such as the exploitation of multi-colour photometry. In contrast to

the case of the long-period variables, no a priori assumptions need to be made to obtain a meaningful fit between the observed and predicted period spectra, since they generally count a similar number of frequencies in a given range. Therefore, comparing individual modes' degree indices inferred from amplitude ratios to those assigned during the period matching process can provide an important consistency check. While most of the multi-colour measurements obtained to date are not sensitive enough to allow the discrimination between modes with $l =$ 0, 1 and 2, those with degree indices of $l = 3$ have been ruled out in a number of cases and the detection of an $l = 4$ mode has been postulated in two stars (Jeffery et al. 2004; Jeffery et al. 2005). It thus seems likely that, given more sensitive multi-colour photometry, we will be in a position to confirm or reject the mode identifications made on the basis of asteroseismology for the EC 14026 stars. In contrast, we currently have no means of verifying the accuracy of our optimal model search for the PG 1716 stars, implying that any results obtained must be regarded as preliminary.

5.6.2 Search in Parameter Space for an Optimal Model of PG 1338+481

Our search in parameter space for models that can optimally reproduce the main oscillations observed for PG 1338+481 is based on the adiabatic periods computed for a grid of the equilibrium models described in the previous section. In order to get a feel for the parameter space resolution required to identify regions of minimum χ^2, we carried out test calculations assessing the impact of changing each of the five input parameters on the predicted period spectrum. Having defined a representative PG 1338+481 model at $T_{\rm eff} = 28{,}200$ K, $\log g =$ 5.38 (the values from spectroscopy according to GFC), $M_*/M_\odot = 0.48$, $\log q({\rm H}) = -2.8$ and $\log q({\rm He}) = -0.24$, we constructed sequences of models around each of these points while fixing the remaining parameters at their representative values. The resulting behaviour of the dipole period spectrum in the 3000−5000 s range of interest is illustrated in Figures 5.11, 5.12, 5.13, 5.14, and 5.15 for variations in $T_{\rm eff}$, $\log g$, M_*, $\log q({\rm H})$ and $\log q({\rm He})$ respectively. It can be seen that, for the case of the first four input parameters, the periods associated with a given radial order k (connected to each other by continuous lines) change relatively monotonically, increasing with surface gravity and mass, and decreasing with effective temperature

and hydrogen shell thickness. The mode density over the range considered is also affected in that the number of predicted oscillations grows with hydrogen shell thickness and (to a lesser extent) effective temperature, and drops with the total mass and (to a lesser extent) surface gravity. Given this systematic dependence of the period spectrum on the model parameters, it is clear that it will be challenging, if not impossible, to isolate one model that can optimally recreate the frequencies observed. In particular, we expect degeneracies in the χ^2 hypersurface caused by the fact that a change in one parameter is compensated for by the variation of another in terms of the period spectrum predicted. An increase in $T_{\rm eff}$ for example can be counterbalanced by an increase in total mass or surface gravity, the thinning of the hydrogen shell, or a combination of all three. More confusingly, a very similar period spectrum may be achieved through, e.g., a strong increase in $\log g$ coupled with a decrease of mass. While an analogous effect was encountered in the asteroseismic modelling of certain EC 14026 stars (see Charpinet et al. 2005b; Randall et al. 2006b), the correlation was largely confined to $T_{\rm eff} - M_*$ and $T_{\rm eff} - \log q({\rm H})$. Fixing $T_{\rm eff}$ to the (tightly constrained) spectroscopic value therefore alleviated the problem to a great extent, and enabled the identification of well-defined χ^2 minima in $\log g - M_* - \log q({\rm H})$ space. In the case of the PG 1716 stars, the situation is more problematic due to the fact that we are dealing with high radial order modes of $k \gtrsim 10$, where the asymptotic regime gains in influence. Asymptotic theory of course predicts an approximately uniform period spacing between consecutive modes of the same degree index l, where most of the information regarding the interior structure of the star is lost. Although it is obvious, both from the systematic period dependence on the model parameters (Figures 5.11–5.15) and the detection of relatively evenly spaced periodicities in the data (Figure 5.9), that we are approaching this regime, some deviations due to the chemical inhomogeneities of the models remain. These manifest themselves in the mode bumping/avoided crossing phenomena clearly present in Figures 5.11–5.14. Since this non-linear behaviour of the period spectrum is very different for each of the input parameters, we remain hopeful that it will be useful in limiting the degeneracies in χ^2 hyperspace.

The effect of the remaining model input parameter, $\log q({\rm He})$, is less pronounced in terms of an absolute change in period over the range considered. In contrast to the other variables, its

influence on the theoretical period spectrum is not monotonic, even if the variations induced are systematic for the majority of modes. The only oscillations that exhibit more or less constant periods with $\log q(\mathrm{He})$ (such as the fourth and the seventh curve from the bottom in Figure 5.15, identified with $k = 12$ and $k = 15$ respectively) correspond to "trapped" modes. First predicted for sdB stars by Charpinet et al. (2000), they are associated with lower kinetic energies than the average ("normal") mode and are literally trapped above the H/He transition zone. Their amplitudes in the deeper layers of the star are extremely small; therefore it is not surprising that they show virtually no dependence on the location of the CO/He transition zone.

Having investigated the influence of the individual stellar parameters, we constructed a first grid of models designed to sandwich PG 1338+481 in 5-dimensional parameter space. The idea was to identify potential regions of minimum χ^2 using as coarse a grid as possible (in order to limit the computation time, which nevertheless came close to two weeks on a small cluster of 10 rapid PC's), and subsequently zoom in on them to determine the true "optimal" model. Unfortunately, this met with very limited success due to the model parameter degeneracies discussed above. Unlike in the case of the EC 14026 stars, where the χ^2 function generally exhibits minima only in localised areas of $T_{\mathrm{eff}} - \log g$ space regardless of the other input parameters, we found that virtually any combination of effective temperature and surface gravity could provide an acceptable fit to the observations if M_*, $\log q(\mathrm{H})$ and $\log q(\mathrm{He})$ were adjusted accordingly. Since it was clearly impossible to isolate an optimal model (or even a small number of families of optimal models) on the basis of five free parameters, we decided the only option would be to fix some of them at the outset. The obvious choice was to keep the atmospheric parameters constant at their spectroscopic values, assumed to be those of GFC at $T_{\mathrm{eff}} = 28{,}200$ K and $\log g = 5.38$. We then constructed a detailed model grid in three-dimensional $M_* - \log q(\mathrm{H}) - \log q(\mathrm{He})$ parameter space, exploring the following ranges: $0.40 \leq M_*/M_\odot \leq 0.65$ with a spacing of $\Delta M_* = 0.002\ M_\odot$, $-3.5 \leq \log q(\mathrm{H}) \leq -1.5$ ($\Delta \log q(\mathrm{H}) = 0.01$) and $-0.30 \leq \log q(\mathrm{He}) \leq -0.06$ ($\Delta \log q(\mathrm{He}) = 0.02$). The spacings between gridpoints were chosen in such a way that the theoretical periods changed by no more than $\sim 20{-}40$ s from one model to the next, which was deemed sufficient for any minima

in the χ^2 function to be resolved. Constraints on the parameter ranges explored were taken from stellar evolution theory. According to the evolutionary calculations of Dorman et al. (1993), subdwarf B stars are core helium burning stars on the Extreme Horizontal Branch that evolve as "AGB Manqué" objects. Since this requires a progenitor with a mass high enough for helium ignition but too low for AGB evolution, the masses of sdB stars should be confined to $0.40{-}0.43 \lesssim M_*/M_\odot \lesssim 0.53$. However, more recent predictions investigating various binary evolution scenarios for the formation of B subdwarfs (Han et al. 2002, 2003) indicate a somewhat larger range. While the mass distribution is still sharply peaked at the canonical value of $\sim 0.47\ M_\odot$, individual masses can be as low as $\sim 0.30\ M_\odot$ if the subdwarf is formed via Roche lobe overflow, or as high as $\sim 0.70\ M_\odot$ if the merger channel is invoked. The latter formation process is of particular interest for the case of PG 1338+481, as it provides a mechanism to produce single sdB stars. We therefore kept to a canonical lower limit of $0.44\ M_\odot$ in our exploration of parameter space and extended the upper limit to $0.70\ M_\odot$, beyond which very few sdB stars are predicted even from the merger channel. The range of $\log q(\mathrm{H})$ was chosen according to the work of Dorman et al. (1993) to fully map the region where PG 1716 stars are found. While subdwarf B stars in general are assumed to have hydrogen envelopes corresponding to $-5.0 \lesssim \log q(\mathrm{H}) \lesssim -2.0$, the long-period variables are thought to be associated with thicker shells than the hotter EC 14026 stars. Consequently, their values of $\log q(\mathrm{H})$ will lie towards the higher end, and perhaps even above the canonical range for sdB stars. We therefore consider the range $-1.5 \lesssim \log q(\mathrm{H}) \lesssim -3.5$, which as we will later see encompasses all appropriate models. Finally, possible values of the remaining parameter $\log q(\mathrm{He})$ are based on the evolutionary sequence considered by Charpinet et al. (2000) from Ben Dorman's models. In this sequence, the vast majority of models in the core helium burning phase (i.e., those identified with subdwarf B stars) have a convective core extending to a depth of between -0.10 and -0.28. Since the latter is intimately related, but not strictly equivalent to, the CO/He transition zone, we adopt a slightly more conservative range $-0.30 \leq \log q(\mathrm{He}) \leq -0.06$.

Figure 5.16 shows the behaviour of the χ^2 hypersurface in the $M_* - \log q(\mathrm{H})$ plane, with the effective temperature and surface gravity fixed at the spectroscopic values mentioned

above. The remaining free parameter, $\log q(\mathrm{He})$, has been optimised at each gridpoint, that is to say it has been chosen in such a way as to minimise χ^2 for every combination of M_* and $\log q(\mathrm{H})$. This gives a very good idea of which pairings of total stellar mass and hydrogen envelope thickness are able to reproduce the period spectrum observed, and how tightly they can be constrained. Regions defined by red, pink or purple shading indicate minima in the merit function, and correspond to values of $\chi^2 \lesssim 10{,}000$, while the global minimum ($\chi^2 = 3219$) is denoted by a black cross. Period fits successively decreasing in quality are represented in yellow, green and blue hues as indicated by the χ^2 scale to the right of the main figure. Blank regions are associated with theoretical period spectra that could not be matched to the oscillations observed, generally because the number of dipole modes predicted for the period range of interest was too low. We can see that all the better fits are concentrated in a broad diagonal strip traversing the $M_* - \log q(\mathrm{H})$ plane from the low-mass/thin envelope to the high-mass/thick envelope domain. According to the χ^2 function computed, low-mass/thick envelope or high-mass/thin envelope models present much poorer matches to the periodicities observed for PG 1338+481. The lowest values of χ^2 occur for $\sim 0.59 \lesssim M_*/M_\odot \lesssim 0.65$ and $\sim -2.0 \lesssim \log q(\mathrm{H}) \lesssim -1.8$, with the global minimum situated at $M_*/M_\odot = 0.616$ and $\log q(\mathrm{H}) = -1.91$ for $\log q(\mathrm{He}) = -0.30$.

The rather poor definition of the χ^2 minimum regions in Figure 5.16 is caused by the fact that we chose to optimise $\log q(\mathrm{He})$ at each gridpoint rather than keeping it constant at one particular value. While this was useful in order to give the reader an unbiased appreciation of the χ^2 function in 3-dimensional hyperspace and its discriminative power in M_* and $\log q(\mathrm{H})$, the plot should also be compared to the slice through $\log q(\mathrm{He})$ space illustrated in Figure 5.17. Here, $\log q(\mathrm{He})$ has been held fixed at its optimal value ($= -0.30$) over the 2-dimensional $M_* - \log q(\mathrm{H})$ space considered. As a result of this, the χ^2 minimum valleys are much more accurately defined, and the broad band of good fits discernable in Figure 5.16 is resolved as a series of narrow parallel strips, which are separated from each other by ridges corresponding to values of χ^2 at least a factor of 10 higher. Within a given valley, the absolute minimum is rather poorly defined due to the degeneracies in $M_* - \log q(\mathrm{H})$ discussed above. The three or four central valleys all provide decent period matches ($\chi^2 \lesssim 20{,}000$), although the one containing

the optimal model is certainly to be preferred over the rest. Note that the mode identification jumps from one band of χ^2 minima to the next, while remaining the same within a given valley. In particular, the valley containing the globally optimal model fits the observed periodicities in terms of consecutive dipole modes with radial indices $k = 12-17$, while the neighbouring band corresponding to a slightly thinner hydrogen shell infers $k = 11-16$. This trend whereby models with higher $\log q(\mathrm{H})$ invoke lower radial order modes continues throughout the range considered and is related to the decrease in mode density as the hydrogen shell thins (see Figure 5.14). It is the latter effect that allows us to limit the possible range of $\log q(\mathrm{H})$ by making use of the a priori assumption that the six observed periodicities used in the calculation of χ^2 are associated with consecutive dipole modes. We should stress at this point that, without said assumption, it would have been impossible to derive any meaningful minima whatsoever, since the match between the six measured periods and the over hundred low-degree modes predicted in the same range would have been satisfactory for any combination of model input parameters.

Notwithstanding the fact that the two atmospheric input parameters of a model had to be kept fixed during the period matching exercise in order to constrain regions of minimum χ^2, it is nevertheless instructive to visualise their effect on the merit function. To this end, we constructed a two-dimensional grid of models with effective temperatures in the 22,000–32,000 K range ($\Delta T_{\mathrm{eff}} = 100$ K) and surface gravities between $\log g = 5.0$ and 5.6 ($\Delta \log g = 0.01$). The remaining parameters were set to their optimal values of $M_* = 0.616\ M_\odot$, $\log q(\mathrm{H}) = -1.910$ and $\log q(\mathrm{He}) = -0.30$. We can see that the resulting χ^2 contours illustrated in Figure 5.18 behave very similarly to those shown in Figure 5.17 in that they are characterised by a broad band of parallel minimum χ^2 valleys. These are well-defined in T_{eff} but rather less so in $\log g$ due to the strong temperature dependence of the g-modes excited. Once again, they are separated by ridges where χ^2 is at least an order of magnitude higher due to the fact that mode identification jumps from one valley to the next. This time, it is an increase in T_{eff} coupled with a decrease in $\log g$ that causes the related boost in the number of modes over the period range considered. Note that, as for the case of $M_* - \log q(\mathrm{H})$, the change in mode density with T_{eff} and $\log g$ can be exploited to constrain the two parameters under the assumption

that the periodicities fit to the theoretical spectra correspond to consecutive dipole modes. However, owing to the qualitative resemblance of the χ^2 function in the $M_* - \log q(\mathrm{H})$ and the $\log g - T_{\mathrm{eff}}$ plane, this can only be achieved if the stellar mass and the thickness of the hydrogen shell are accurately known from the outset. Conversely, optimal values of M_* and $\log q(\mathrm{H})$ cannot be determined unless the effective temperature and surface gravity are fixed. As the latter are derived using well-established spectroscopic and model atmosphere fitting techniques rather than hypothetical evolutionary models, it is the second scenario that is the obvious choice. Unfortunately, for the PG 1716 stars even the atmospheric parameters are currently associated with significant uncertainties owing to systematic discrepancies in the temperature scale derived from different model atmospheres.

The slices through χ^2 hyperspace illustrated in Figures 5.17 and 5.18 for PG 1338+481 should be compared to those published for the EC 14026 stars studied to date (Brassard et al. 2001; Charpinet et al. 2003, 2005a, 2005b; Randall et al. 2006). While the relative contrast in χ^2 over the parameter space considered is similar to, e.g., that detected for PG 1219+534 (Charpinet et al. 2005a), the behaviour of the contour lines is markedly different. In particular, the plots for the EC 14026 stars all reveal just one or two well-separated χ^2 minimum regions, which can generally be discriminated between on the basis of spectroscopy. Consequently, potential optimal models are restricted to only one region in 4-dimensional parameter space (remembering that the p-modes excited in the rapid pulsators are insensitive to $\log q(\mathrm{He})$). Depending on the number of observational periodicities matched to the theoretical spectra, this region can be well-defined in all four dimensions (e.g., PG 1219+534; Charpinet et al. 2005a) or form an elongated valley that must subsequently be constrained using spectroscopic estimates of T_{eff} (e.g., Feige 48; Charpinet et al. 2005b). In any case, we are left with just one family of optimal models rather than a sequence of parallel valleys like those calculated for PG 1338+481. This is of course a result of the differing impact that the model input parameters have on the low-order p-modes observed in the EC 14026 stars and the high-order g-modes excited in the PG 1716 stars. Most importantly, the rapid pulsators are associated with a small number of non-uniformly distributed oscillations, whereas the slow variables are predicted to show an abundance of nearly equally spaced periodicities. Mode identification in

the case of the former will thus remain the same over a wide parameter range, with a slow degradation in the quality of fit taking place as we move away from the optimal solution. In contrast, the uniformity and density of the period spectrum calculated for the PG 1716 stars lend themselves to jumps in mode identification over a relatively close parameter range, giving rise to a small number of discrete minima corresponding to similarly good fits. Note however that the χ^2 minimum associated with the optimal model is more than a factor of 2 lower than that of the second deepest valley (the one located just above the family of optimal solutions in Figure 5.17), and more than a factor of 3 smaller than that found in any of the other χ^2 minimum regions. In terms of the quality-of-fit, this constitutes a significant difference. We therefore feel that, keeping in mind the assumptions made at the outset, we have identified a convincing minimum in χ^2 hyperspace and can infer the corresponding model parameters with some certainty.

5.6.3 Structural Parameters and Period Fit of the Optimal Model

The optimal model uncovered for PG 1338+481 lies at $T_{\rm eff} = 28{,}200$ (the value from spectroscopy), $\log g = 5.38$ (again, the spectroscopic value), $M_* = 0.616\ M_\odot$, $\log q({\rm H}) = -1.91$ and $\log q({\rm He}) = -0.30$. Comparing the values of M_* and $\log q({\rm H})$ inferred from asteroseismology to those determined for the EC 14026 stars analysed to date, we find that the mass of PG 1338+481 seems to be noticeably higher, and its hydrogen-rich shell significantly thicker than that of the other targets (see Charpinet et al. 2005c). The latter is not surprising, and ties in with predictions that cooler subdwarfs should be associated with more extensive envelopes than their hotter relatives. On the other hand, the mass inferred for PG 1338+481 seems uncharacteristically high. While the merger channel proposed by Han et al. (2002, 2003) does allow for the formation of subdwarfs with masses up to $\sim 0.7\ M_\odot$, the distribution is sharply peaked at $\sim 0.5\ M_\odot$ and objects beyond $\sim 0.6\ M_\odot$ should be few and far between. Indeed, three of the four EC 14026 pulsators for which asteroseismology has been most successful also appear to be single stars[8], and the derived masses of all three fall into the canonical 0.47−0.50

[8]Three to five radial velocities at varying epochs have been obtained for each of PG 0014+067, PG 1047+003, and PG 1219+534 as part of a long-term MMT radial velocities/atmospheric parameters study. The ~ 2 km/s scatter in each of the three velocity sets is completely consistent with the observational errors

$M_\odot$ range. The discrepant mass determined for PG 1338+481 might be the first evidence for a more massive merger product, or it may simply point to limitations in our asteroseismological analysis.

Considering that the calculation of the χ^2 hypersurface was based on two fundamental assumptions (namely that the six periods used in the fit correspond to consecutive dipole modes and that GFC's spectroscopic estimates of the star's atmospheric parameters are accurate), the values of the parameters inferred must be regarded as preliminary. In particular, we expect even relatively small changes in either $T_{\rm eff}$ or $\log g$ to affect the remaining structural variables substantially. Exploratory calculations indicate that a decrease in effective temperature of $\sim$ 1000 K lowers the total mass of the optimal model determined by about 0.02−0.03 $M_\odot$, while $\log q$(H) remains relatively constant. On the other hand, a decrease in $\log g$ of $\sim$ 0.05 dex would just about compensate for the change in temperature in terms of mass, but increase the value of $\log q$(H) by $\sim$ 0.1 dex. Considering that current spectroscopic estimates of $T_{\rm eff}$ and $\log g$ for PG 1338+481 differ by about 4000 K and 0.25 dex respectively depending on the model atmospheres employed (see Table 5.5), the star's true mass could be up to $\sim$ 0.1 $M_\odot$ lower and its value of $\log q$(H) up to $\sim$ 0.5 dex higher than that inferred from our asteroseismological study. Of course, a change in the atmospheric parameters assumed during the optimal model finding process could also result in a different χ^2 valley becoming the global minimum. Consequently, we should not give too much weight to the precise values of the structural parameters determined for PG 1338+481.

The quality of the period match between the observed oscillations and those predicted for the optimal model is illustrated in Figure 5.10 and also quantified in Table 5.6. For each periodicity computed we have listed the degree index l, the radial order k, the theoretical period P_{theo}, the equivalent observed period used for the fit P_{obs}, and the relative difference between the latter two $\Delta P/P$. We can see that the agreement between the two period spectra is excellent, the largest discrepancy being just over 1 % and the mean dispersion amounting to only 0.47%. This is comparable to the quality of fit achieved for the EC 14026 stars, where the mean dispersion ranges from 0.005 % (Feige 48; Charpinet et al. 2005b) to 1.1 % (PG 0014+067; Brassard et al. 2001). Note however that in the case of the fast pulsators all

observed oscillations were fitted to the theoretical spectra with no a priori assumptions made. In contrast, we needed to constrain mode identification from the outset in order to find a meaningful χ^2 minimum for PG 1338+481. While we were fortunate enough to be able to do this with some certainty for six of the modes, the remaining 7 convincing periods listed in Table 5.2 remained wild cards as far as their mode identification was concerned. Unfortunately, the method of global χ^2 minimisation employed does not currently allow the simultaneous matching of periodicities with fixed and unknown degree indices, leaving us with no option but to discard the latter in our exploration of parameter space. Consequently, the optimal model is designed to provide the best match possible only for the 6 dipole modes detected. Attempting to subsequently fit the remaining pulsations in terms of low-degree modes with $l = 1$ or $l = 2$ resulted in a slight deterioration in the goodness-of-fit and a mean period dispersion of 0.77 %. Although this still corresponds to an excellent fit by asteroseismological standards, the ease with which our optimal model can satisfactorily reproduce the extra periods is most likely due to the mode density predicted rather than the model being physically accurate (see Figure 5.10 for a comparison of the mode density computed for the optimal model and all the pulsations observed). Underlying this conclusion is the fact that the additional periodicities are assigned a random collection of theoretical modes, i.e., a complete mixture of $l = 1$ and $l = 2$ with no particular amplitude hierarchy and non-consecutive values of k. Given that the combined $l = 1$ and $l = 2$ spectrum predicts ~ 60 periodicities in the same $\sim 2200-7200$ s range as the 7 periodicities to be matched, we would statistically expect the average period dispersion to be about 20−25 s. Since this is in line with the quality of the fit, we conclude that the relatively accurate match of the additional frequencies to those predicted from the optimal model is meaningless from an asteroseismic point of view.

On the other hand, the simultaneous reproduction of six of the highest amplitude periodicities observed in terms of consecutive dipole modes to such a high accuracy constitutes a remarkable result that was by no means guaranteed from the outset. We take it to imply that the basic physics used in the construction of our sdB star models is correct, as is also suggested by the successful asteroseismology of several EC 14026 stars. Nevertheless, we should point out that the period dispersion of the fit achieved is nearly two orders of magnitude larger

than the observational uncertainty. This is slightly larger than that encountered during the analysis of the short-period variables, and most likely indicates missing physical ingredients in our models. It is of course one of the goals of future asteroseismic studies to address this issue and thus gain a deeper understanding of the interior physics of subdwarfs.

5.7 CONCLUSION

Our observational efforts for the long-period variable subdwarf B star PG 1338+481 yielded $\sim$ 250 hours of simultaneous U/R band photometry, as well as an extra $\sim$ 70 hours of simple R band data. From the combined U and R light curves we were able to extract 13 credible periodicities in the 2100−7200 s range, with the strongest pulsations clustering between $\sim$ 3000 and 5000 s. While the frequencies of the oscillations were found to be the same in the two wavebands, their amplitudes are significantly higher in the U than in the R, as was to be expected from model atmosphere theory. A detailed analysis of the amplitude ratios measured suggests that the dominant pulsations most closely correspond to modes with $l = 1$, although degree indices of $l = 2$ and 4 cannot be ruled out. This notion is supported by the fact that 6 of the highest amplitude peaks show a relatively uniform period distribution with a spacing characteristic of consecutive dipole modes in a representative PG 1338+481 model. They are interspersed by lower amplitude periodicities that fall very close to two of the dominant peaks and can be interpreted in terms of $l = 2$ modes. Interestingly, the frequency spectrum uncovered is extremely non-uniform and far sparser than that predicted for low degree modes from theory. Although the reason for this is still open to debate, we suggest that an unknown mode selection mechanism could cause the pulsational energy available to preferentially be channelled into certain period ranges. Modes falling into these frequency bands would then be excited to observable amplitudes, whereas those lying in energy-poor ranges would be too weak to detect, giving rise to the strongly clustered period spectrum observed. A similar selection effect was already postulated for δ Scuti stars (Breger & Bischof 2002) in order to explain the closely spaced multiplets observed for several of these objects, and could also help account for the frequency splittings detected in the Fourier transform of our first target PG 1627+017. Unfortunately, our models are based on linear pulsation equations and

as such cannot predict the amplitudes of individual oscillations, giving us no way of testing the theory.

Beyond this, current "second generation" models are unable to quantitatively reproduce the PG 1716 star instability strip. Unlike for the case of the fast pulsators, where the theoretical and observed excited frequency ranges completely overlap, the periods predicted to be unstable for the slow oscillators are significantly shorter than those measured. Moreover, the models can excite only relatively high degree ($l \geq 3$) modes over the vast majority of the temperature range where the PG 1716 stars are found. A typical PG 1338+481 model for example is able to drive only modes with l-indices greater than 5, which is in stark contrast to the dipole modes thought to have been detected. It is clear that our instability predictions are subject to a blue edge problem that could underestimate the observed blue edge by up to $\sim$ 8000 K. Nevertheless, we still believe that the driving mechanism identified previously by Fontaine et al. (2003) is fundamentally sound. Underlying this conclusion is an agreement between predictions and observations at the relative level, as well as the strong correlation that exists between the two types of subdwarf B pulsator and the SPB/β Cep phenomenon on the main sequence. Instead, it is likely that the models themselves are missing some complementary physical ingredients for g-mode pulsations. We are currently investigating possible improvements but this is far beyond the scope of this paper.

Our attempts at an asteroseismological analysis of PG 1338+481 on the basis of the 6 high amplitude oscillations believed to constitute dipole modes yielded mixed results. On the one hand, we found that it was impossible to derive a localised χ^2 minimum in hyperspace if all five parameters were treated as free variables. This is due to the compensating effects that variations in the different stellar parameters have on the theoretical period spectrum for g-modes. On the other hand, an exploration of 3-dimensional parameter space at fixed values of the spectroscopic parameters $T_{\rm eff}$ and $\log g$ rendered a relatively convincing, well constrained χ^2 minimum region. The corresponding optimal model was able to account for the observed periodicities surprisingly well, a result that was in no way guaranteed from the outset. We believe this confirms that the basic physical constitution of our subdwarf B star models is realistic, even if they are still subject to numerous inaccuracies. Of course, it is the

goal of asteroseismology to identify and rectify these deficiencies by refining the input physics until the observed oscillations can be reproduced perfectly.

It is obvious that, at present, asteroseismology is more limited for the slow pulsators than for the EC 14026 stars. Observational and computational difficulties aside, this is mostly due to the density and uniform structure of the high radial order g-mode spectrum compared to that of low-order p-modes. In order to derive any meaningful χ^2 minimum for PG 1338+481, we needed to assume that the observational pulsations used in the period fit correspond to dipole modes with consecutive values of k. Moreover, both the effective temperature and surface gravity had to be fixed at the spectroscopic values in order to constrain the remaining parameters with any accuracy. These approximations notwithstanding, the fact that we were able to isolate just one family of models that could account for the observed periodicities surprisingly well is encouraging. Nevertheless, numerous advances will have to be made in the study of long-period variable subdwarf B stars if their full asteroseismological potential is to be exploited. First of all, we will need to clarify the large discrepancies that still exist between estimates of the cooler sdB's atmospheric parameters. Considering the systematic effects of changes in $\log g$ and $T_{\rm eff}$ on the remaining parameters of the optimal model determined, it is vital to constrain these two parameters to a high accuracy at the outset of any asteroseismological exploration. Otherwise, the values of M_*, $\log q(\mathrm{H})$ and $\log q(\mathrm{He})$ inferred are not reliable and of limited use for restricting evolutionary scenarios.

Another factor critical to the asteroseismological exploitation of the long-period variables is the ability to constrain mode identification from the outset. While the 6 roughly equally spaced oscillations detected for PG 1338+481 were presumed to constitute consecutive dipole modes on the basis of their distribution and the indications of the colour-amplitude results, we have no solid proof of the validity of this assumption because the multi-colour photometry obtained is of insufficient quality to unambiguously discriminate between modes with degree indices of $l = 1$, 2 and 4. Future observational campaigns of long-period variable subdwarf B stars should thus aim to determine the degree indices of the modes observed more accurately. Achieving this on the basis of the colour-amplitude technique will require the sensitivity of larger telescopes, photometry obtained through a greater number of more widely spaced

bandpasses, or perhaps both. Since it is highly unlikely that an observing run of sufficient length ($\gtrsim$ 1 month) would be allocated on a medium-size telescope, a more promising option is to exploit the enhanced amplitude-wavelength dependence on l in the ultra-violet (UV) from space. Unfortunately, the only satellite currently dedicated to observations in the UV, *FUSE,* is slowly dying and there are currently no intentions of replacing it. Therefore, it seems worthwhile exploring alternative methods of determining the degree indices of modes observationally. One recent theoretical effort in this direction proposes the analysis of line-profile variations during a pulsation cycle (Schoenaers & Lynas-Gray 2005), but has yet to be tested. A much simpler way of deducing l from ordinary time-series photometry is the exploitation of rotational splitting, given that the frequency spacing between the individual m components of a (k,l) gravity mode depends strongly on its degree index. Of course, this method is applicable only to relatively fast rotators with known rotation periods, generally those located in short-period binaries. Even then, it is not necessarily trivial to distinguish between independent harmonic oscillations and rotationally split components, as we found during our analysis of PG 1627+017 (Paper I).

Considering the uncertainties involved in observationally determining the degree indices of oscillations detected in long-period variable subdwarf B stars, it is all the more important to extract as many periodicities as possible for a given target. The more frequencies that can be measured, the greater the chances will be of uncovering distributional particularities such as the equally spaced peaks found for PG 1338+481. As we demonstrated, these can be useful for mode identification, particularly when employed in conjunction with other observational constraints. Judging by our experience from the two ambitious multi-site campaigns described in this short series of papers, the asteroseismic future of long-period variable subdwarf B stars lies in space-based observations. One of their great advantages compared to ground-based campaigns is the high duty cycle attainable, which can reach over 95 % compared to the 30–40 % more typical even of multi-site collaborations. Given the slow oscillations involved, the length of individual light curves is critical to the clean extraction of frequencies, and a poor duty cycle can result in sampling aliases being mistaken for stellar pulsations. Another benefit of observing from space is the absence of atmospheric interference and extinction.

Both the PG 1627+017 and the PG 1338+481 photometry suffer from a high level of low-frequency noise, which makes it difficult to establish an upper limit on the period range of the stellar oscillations. Trial observations of the long-period variable subdwarf B star PG 0101+039 using the Canadian *MOST* satellite have already indicated the vast potential that space-based photometry holds for these objects (Randall et al. 2005b). After only two weeks (out of a possible 8) of observation, the 15-cm telescope had accumulated more hours of data than obtained during either of our ground-based campaigns, averaging a duty cycle of 96.5 %. The noise level achieved was about half that reported in this paper (although it should be kept in mind that the target was $\sim$ 1.5 magnitudes brighter), and could of course be further reduced during a longer run. From the quality of the data obtained, it is clear that space telescopes such as *MOST* and future missions *COROT* and *Kepler* will play a key role in the asteroseismology and eventual physical and evolutionary understanding of subdwarf B stars.

We would like to thank Uli Heber for providing us with his estimates of the atmospheric parameters of a number of subdwarf B stars. This work was financed in part by the Natural Sciences and Engineering Research Council of Canada and by the Fonds de la recherche sur la nature et les technologies (Québec). G.F. also acknowledges the contribution of the Canada Research Chair Program. The contribution of E.M.G. was made possible by NSF grant AST-0098699. Many thanks also to the Steward Observatory Staff, especially J. Grantham, R. Peterson, G. Rosenbaum, and B. Wood, for bringing ccd21 to Mt. Bigelow twice for this project.

5.8 TABLES

TABLE 5.1 – Observations of PG 1338+481, 2004

Date (UT)	Start (UT)	Telescope	Filter	Length (h:m)
16 March	05:28:06	MB	*R*	7:04
16 March	05:31:12	MB	*U*	7:00
17 March	03:54:10	MB	*R*	8:33
17 March	03:55:27	MB	*U*	8:33
18 March	03:42:15	MB	*R*	6:05
18 March	03:43:32	MB	*U*	6:01
19 March	04:38:26	MDM	*R*	5:17
20 March	04:00:05	MDM	*R*	4:41
20 March	04:06:08	MDM	*U*	4:36
21 March	05:01:06	MDM	*R*	6:20
21 March	05:02:41	MDM	*U*	6:20
23 March	04:16:56	MDM	*R*	6:29
23 March	04:18:31	MDM	*U*	6:29
24 March	04:39:30	MDM	*R*	7:42
24 March	04:40:55	MDM	*U*	7:17
26 March	03:48:42	MDM	*R*	8:30
26 March	03:50:16	MDM	*U*	8:30
27 March	03:28:53	MDM	*R*	8:38
27 March	03:24:02	MDM	*U*	8:56
28 March	03:39:38	MDM	*R*	8:51
28 March	03:41:13	MDM	*U*	8:51
28 March	07:37:58	MB	*R*	4:55
29 March	02:57:54	MB	*R*	9:31
29 March	03:40:33	MDM	*R*	8:38
29 March	03:42:08	MDM	*U*	8:12
30 March	03:19:27	MB	*R*	9:08
31 March	03:02:33	MB	*R*	7:46
31 March	03:03:51	MB	*U*	7:08
05 April	06:13:02	MB	*R*	4:20
05 April	06:14:04	MB	*U*	3:10
07 April	02:39:05	MB	*R*	5:58
07 April	02:40:06	MB	*U*	5:50
08 April	05:04:25	MB	*R*	3:14

TABLE 5.1 – *continued*

Date (UT)	Start (UT)	Telescope	Filter	Length (h:m)
08 April	05:05:27	MB	*U*	2:08
09 April	02:33:55	MB	*R*	8:49
09 April	02:34:57	MB	*U*	8:56
10 April	04:36:09	MB	*R*	5:46
10 April	04:37:11	MB	*U*	5:23
11 April	08:33:57	MB	*R*	2:47
11 April	08:34:58	MB	*U*	2:35
12 April	02:31:44	MB	*R*	9:27
12 April	02:32:46	MB	*U*	9:23
13 April	02:38:02	MB	*R*	9:35
13 April	02:39:04	MB	*U*	9:31
14 April	02:41:08	MB	*R*	9:27
14 April	02:42:10	MB	*U*	9:16
15 April	02:39:16	MB	*R*	9:31
15 April	02:40:19	MB	*U*	9:12
16 April	03:50:38	MB	*R*	8:14
16 April	03:51:40	MB	*U*	8:14
18 April	07:06:01	MB	*R*	4:59
18 April	07:07:02	MB	*U*	4:55
19 April	02:44:13	MB	*R*	9:20
19 April	02:45:20	MB	*U*	9:12
20 April	02:40:51	MB	*R*	9:20
20 April	02:41:54	MB	*U*	9:16
21 April	02:46:01	MB	*R*	9:12
21 April	02:47:07	MB	*U*	9:12
22 April	02:48:35	MB	*R*	8:56
22 April	02:49:37	MB	*U*	9:00
23 April	02:43:42	MB	*R*	9:04
23 April	02:44:44	MB	*U*	9:04
24 April	02:41:11	MB	*R*	9:20
24 April	02:42:13	MB	*U*	9:12
25 April	02:41:28	MB	*R*	9:16
25 April	02:42:30	MB	*U*	9:08
26 April	02:57:38	MB	*R*	8:33
26 April	02:58:40	MB	*U*	8:41
27 April	02:56:48	MB	*R*	7:42
27 April	02:57:53	MB	*U*	7:42
29 April	03:10:45	MB	*R*	7:50
30 April	02:48:58	MB	*R*	7:00
01 May	02:57:19	MB	*R*	8:45
03 May	03:13:05	MB	*R*	8:10
04 May	03:04:28	MB	*R*	8:17

TABLE 5.2 – PG 1338+481's oscillations as derived from all R band data available

No.	Frequency (μHz)	Period (s)	1 σ error (s)	Amplitude %	1 σ error %	Phase (s)	1 σ error (s)
(1	105.2	**9509.7**	1.9	0.094	0.016	8571	253)
2	138.9	7198.2	1.3	0.078	0.016	1473	231
3	155.4	**6437.0**	1.0	0.086	0.016	1754	187
4	156.4	6392.1	1.0	0.079	0.016	6227	202
5	216.2	**4625.0**	0.5	0.091	0.016	4533	127
6	230.0	**4347.5**	0.4	0.103	0.016	3905	106
7	231.8	4314.4	0.5	0.069	0.016	3662	156
8	244.5	**4090.2**	0.3	0.103	0.016	722	99
9	258.9	3862.9	0.4	0.070	0.016	3709	138
10	261.2	**3828.1**	0.2	0.193	0.016	1001	50
11	283.3	**3529.7**	0.2	0.138	0.016	1786	64
12	307.5	3252.1	0.5	0.042	0.016	2604	194
13	436.8	2289.3	0.3	0.035	0.016	1287	164
14	470.7	2124.5	0.3	0.034	0.016	139	156

TABLE 5.3 – Periodicities present in the simultaneous U and R band data, U/R amplitude ratios and phase lags

No.	U Period (s)	U Amplitude (%)	U phase (s)	R Period (s)	R Amplitude (%)	R phase (s)	U/R ratio	$\Phi_R - \Phi_U$ (deg)
(1	**9505.3±1.5**	0.175±0.032	9468±277	**9507.5±2.7**	0.104±0.021	8914±302	**1.68±0.46**	−21.0±15.5)
2	7196.9±2.3	0.103±0.032	1733±356	7196.9±2.1	0.075±0.021	1741±317	1.37±0.57	0.4±23.8
3	**6436.5±1.6**	0.122±0.032	1903±269	**6437.0±1.4**	0.090±0.021	1799±236	1.36±0.48	−5.8±20.0
4	6390.6±1.8	0.103±0.032	294±316	6391.8±1.8	0.070±0.021	6251±301	1.47±0.64	−24.4±24.6
5	**4624.7±0.8**	0.125±0.032	4458±189	**4625.3±0.8**	0.081±0.021	4386±188	1.54±0.56	−5.6±20.8
6	**4347.3±0.5**	0.171±0.032	3857±130	**4347.5±0.4**	0.134±0.021	3851±107	**1.28±0.31**	−0.5±13.9
7	4314.5±0.8	0.106±0.032	3548±208	4314.7±0.9	0.062±0.021	3612±230	1.71±0.78	5.3±25.9
(8	4159.6±0.8	0.102±0.032	3794±208	4159.4±0.9	0.059±0.021	4136±233	1.73±0.82	29.6±27.0)
9	**4090.4±0.5**	0.140±0.032	658±149	**4090.2±0.5**	0.102±0.021	768±132	**1.37±0.42**	9.7±17.5
10	3862.0±0.7	0.105±0.032	171±188	3862.3±0.6	0.072±0.021	103±177	1.46±0.62	−6.3±24.1
11	**3828.4±0.2**	0.272±0.032	822±72	**3828.2±0.2**	0.191±0.021	906±66	**1.42±0.23**	7.9±9.2
12	**3529.7±0.3**	0.215±0.032	1754±84	**3529.9±0.3**	0.145±0.021	1699±80	**1.48±0.31**	−5.6±11.8
13	3252.2±0.7	0.069±0.032	2484±240	3251.8±0.7	0.044±0.021	2819±244	1.57±1.04	37.1±37.9
14	2289.6±0.6	0.042±0.032	929±278	2289.2±0.6	0.029±0.021	1257±260	1.45±1.52	51.6±59.9
15	2124.6±0.4	0.046±0.032	1926±236	2125.9±0.4	0.036±0.021	136±195	1.28±1.16	56.7±51.9

TABLE 5.4 – Basic properties of equilibrium models with $M_*/M_\odot$=0.48

Model	$T_{\rm eff}$ (k)	$\log g$	$\log q$(H)
1	21,000	5.07	−1.48
2	22,000	5.13	−1.64
3	23,000	5.19	−1.81
4	24,000	5.25	−1.97
5	25,000	5.31	−2.13
6	26,000	5.37	−2.30
7	27,000	5.44	−2.46
8	28,000	5.50	−2.62
9	29,000	5.56	−2.79

TABLE 5.5 – Observational properties of the four well-studied PG 1716 stars. For each target, we have listed the atmospheric parameter estimates of Green, Fontaine, & Chayer (in preparation) and Uli Heber (private communication), as well as the range of observed periods and amplitudes taken from the references given. Since the amplitudes of pulsation are wavelength-dependent, we have indicated the filter used in the observations. Photometry of the first three targets was obtained with the Johnson R filter, while for PG 0101+039 a broadband filter was employed. The latter peaks in the V, which may lead to a slight overestimation of the pulsational amplitudes for PG 0101+039 compared to those of the other targets.

Star	$T_{\rm eff}$ (K) (GFC)	$\log g$ (GFC)	$T_{\rm eff}$ (K) (UH)	$\log g$ (UH)	$P_{\rm obs}$ (s)	$A_{\rm obs}$(%)	Reference
PG 1716+426	27,662±204	5.452±0.025	25,118±156	5.29±0.02	$\sim$ 2900−5000	$\lesssim$ 0.2 (R)	Reed et al. 2004
PG 1627+017	23,669±190	5.315±0.021	20,264±174	5.03±0.02	4588−8901	$<$ 0.48 (R)	Paper I
PG 1338+481	28,179±264	5.375±0.035	24,197±235	5.11±0.025	2100−7200	$<$ 0.27 (R)	this work
PG 0101+039	28,173±170	5.531±0.022	26,112±168	5.43±0.02	2650−7235	$<$ 0.06 (BB)	Randall et al. 2005b

TABLE 5.6 – Period match and mode identification for the optimal model

l	k	P_{theo} (s)	P_{obs} (s)	$\Delta P/P$ %
1	11	3122.18	...	...
1	12	3265.36	3252.1	0.40
1	13	3538.18	3529.7	0.23
1	14	3848.42	3828.1	0.52
1	15	4073.28	4090.2	0.42
1	16	4299.97	4347.5	1.08
1	17	4633.09	4625.0	0.17
1	18	4797.36	...	...

5.9 REFERENCES

Billères, M., Fontaine, G., Brassard, P., Charpinet, S., Liebert, J., & Saffer, R.A. 2000, ApJ, 530, 441

Bergeron, P., Wesemael, F., Beauchamp, A., Wood, M.A., Lamontagne, R., Fontaine, G., & Liebert, J. 1994, ApJ, 432, 305

Brassard, P., Fontaine, G., Billères, M., Charpinet, S., Liebert, J., & Saffer, R.A. 2001, ApJ, 563, 1013

Brassard, P., Pelletier, C., Fontaine, G., & Wesemael, F. 1992, ApJS, 80, 725

Breger, M., & Bischof, K.M. 2002, A&A, 385, 537

Charpinet, S., Fontaine, G., Brassard, P., Green, E.M., & Chayer, P. 2005a, A&A, 437, 575

Charpinet, S., Fontaine, G., Brassard, P., Billères, M., Green, E.M., & Chayer, P. 2005b, A&A, in press

Charpinet, S., Fontaine, G., Brassard, P., Chayer, P., & Green, E.M. 2005c, Baltic Astronomy, in press

Charpinet, S, Fontaine, G., & Brassard, P. 2003, in conf. proceedings, White Dwarfs, held in Naples, Italy, ed. D. de Martino, R. Silvotti, J.-E. Solheim and R. Kalytis, Kluwer Academic Publishers, NATO Science Series II - Mathematics, Physics and Chemistry, 105, 69

Charpinet, S., Fontaine, G., Brassard, P., & Dorman, B. 2002, ApJSS, 139, 487

Charpinet, S., Fontaine, G., & Brassard, P. 2001, PASP, 113, 775

Charpinet, S., Fontaine, G., Brassard, P., Chayer, P., Rogers, F.J., Iglesias, C.A., & Dorman, B. 1997, ApJ, 483, L123

Charpinet, S., Fontaine, G., Brassard, P., & Dorman, B. 1996, ApJ, 471, L103

Dorman, B., Rood, R.T., & O'Connell, R.W. 1993, ApJ, 419, 596

Dreizler, S. 1993, in NATO ASI series 403, White Dwarfs: Advances in Observations and Theory, ed. M.A. Barstow (Dordrecht: Kluwer). 287

Fontaine, G., Green, E.M., Chayer, P. Brassard, P., Charpinet, & Randall, S.K. 2005, Baltic Astronomy, in press

Fontaine, G., Brassard, P., Charpinet, S., Green, E.M., Chayer, P., Billères, M.,& Randall, S.K. 2003, ApJ, 597, 518

Fontaine, G., Brassard, P., Wesemael, F., & Tassoul, M. 1994, ApJ, 428, L61

Fontaine, G., Charpinet, S., Brassard, P., Chayer, P., Rogers, F.J., Iglesias, C.A., & Dorman, B. 1998, in IAU Symp. 185, New eyes inside the Sun and stars, ed. F. Deubner, D.W. Kurtz, Kluwer Academic Publishers, 367

Green, E.M., Fontaine, G., Reed, M.D., Callerame, K., Seitenzahl, I.R., White, B.A., Hyde, E.A., Østensen, R., Cordes, O., Brassard, P., Falter, S., Jeffery, E.J., Dreizler, S., Schuh, S.L., Giovanni, M., Edelmann, H., J. Rigby, & Bronowska, A. 2003, ApJ, 583, L31

Han, Z., Podsialowski, Ph., Maxted, P.F.L., & Marsh, T.R. 2003, MNRAS, 341, 669

Han, Z., Podsialowski, Ph., Maxted, P.F.L, Marsh, T.R., & Ivanova, N. 2002, MNRAS, 336, 449

Heber, U. 1986, A&A, 155, 33

Jeffery, C.S., Aerts, C., Dhillon, V.S., Marsh, T.R., & Gänsicke, B.T. 2005, MNRAS, 362, 66

Jeffery, C.S., Dhillon, V., Marsh, T., & Ramachandran, B. 2004, MNRAS, 352, 699

Kilkenny, D. 2005, Baltic Astronomy, in press

Kilkenny, D., Koen, C., O'Donoghue, D. and Stobie, R.S., 1997, MNRAS, 285, 640-644

Koen, C., Kilkenny, D., O'Donoghue, D., Van Wyk, F. and Stobie, R.S., 1997, MNRAS, 285, 645

Montgomery, M.H., & O'Donoghue, D. 1999, in Delta Scuti Star Newsletter, No. 13

O'Donoghue, D., Lynas-Gray, A.E., Kilkenny, D., Stobie, R.S. and Koen, C., 1997, MNRAS, 285, 657

Randall, S.K., Fontaine, G., Green, E.M., Brassard, P., Kilkenny, D., Crause, L., Terndrup, D.M., Daane, A., Kiss, L.L., Jacob, A.P., Bedding, T.R., For, B.-Q., & Quirion, P.-O. 2006, ApJ, submitted (Paper I)

Randall, S.K., Fontaine, G., Charpinet, S., Lynas-Gray, A.E., Lopes, I.P., O'Toole, S.J., & Brassard, P. 2006, in preparation

Randall, S.K., Fontaine, G., Brassard, P., & Bergeron, P. 2005a, ApJS, in press

Randall, S.K., Matthews, J.M., Fontaine, G., Rowe, J., Kuschnig, R., Green, E.M., Brassard, P., Chayer, P., Guenther, D.B., Moffat, A.F.J., Rucinski, S., Sasselov, D., Walker, G.A.H., & Weiss, W.W. 2005b, ApJ, 633, 460

Reed, M.D., Green, E.M., Callerame, K., Seitenzahl, I.R., White, B.A., Hyde, E. A., Giovanni, M. K., Østensen, R., Bronowska, A., Jeffery, E.J., Cordes, O., Falter, S., Edelmann, H., Dreizler, S. and Schuh, S.L., 2004, ApJ, 607, 445

Saffer, R., Bergeron, P., Koester, D. and Liebert, J., 1994, ApJ, 432, 351

Schoenaers, C. & Lynas-Gray, A.E. 2005, Baltic Astronomy, in press

Stobie, R.S., Kawaler, S.D., Kilkenny, D., O'Donoghue, D. and Koen, C., 1997, MNRAS, 285, 651

Unno, W., Osaki, Y., Ando, H., Saio, H., & Shibahashi, H. 1989, Nonradial Oscillations of Stars (2nd Edition), Tokyo: Univ. Tokyo Press

5.10 FIGURES

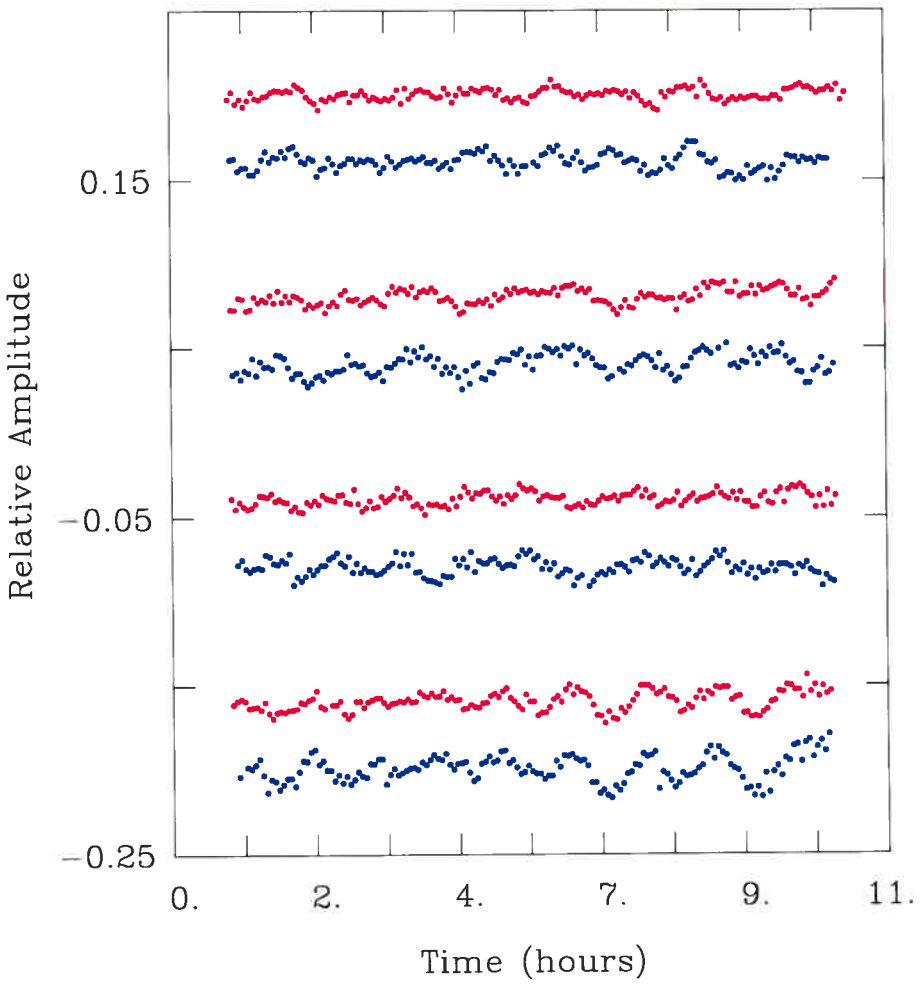

FIGURE 5.1 – Typical U (blue) and R (red) light curves of PG 1338+481, as obtained at the Steward Observatory's 1.55-m telescope on Mt. Bigelow. The brightness variations are expressed in terms of fractional intensity and are shifted arbitrarily to facilitate viewing.

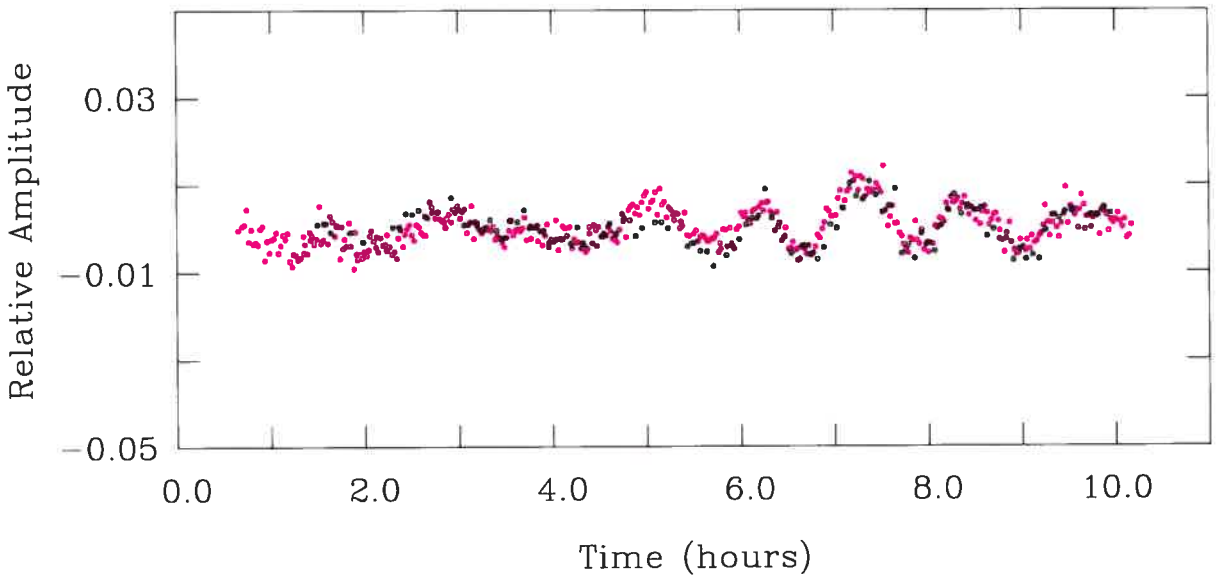

FIGURE 5.2 – *R* band light curves of PG 1338+481 from 29 March 2004, obtained at Mt. Bigelow (magenta) and MDM Kitt Peak (black) respectively.

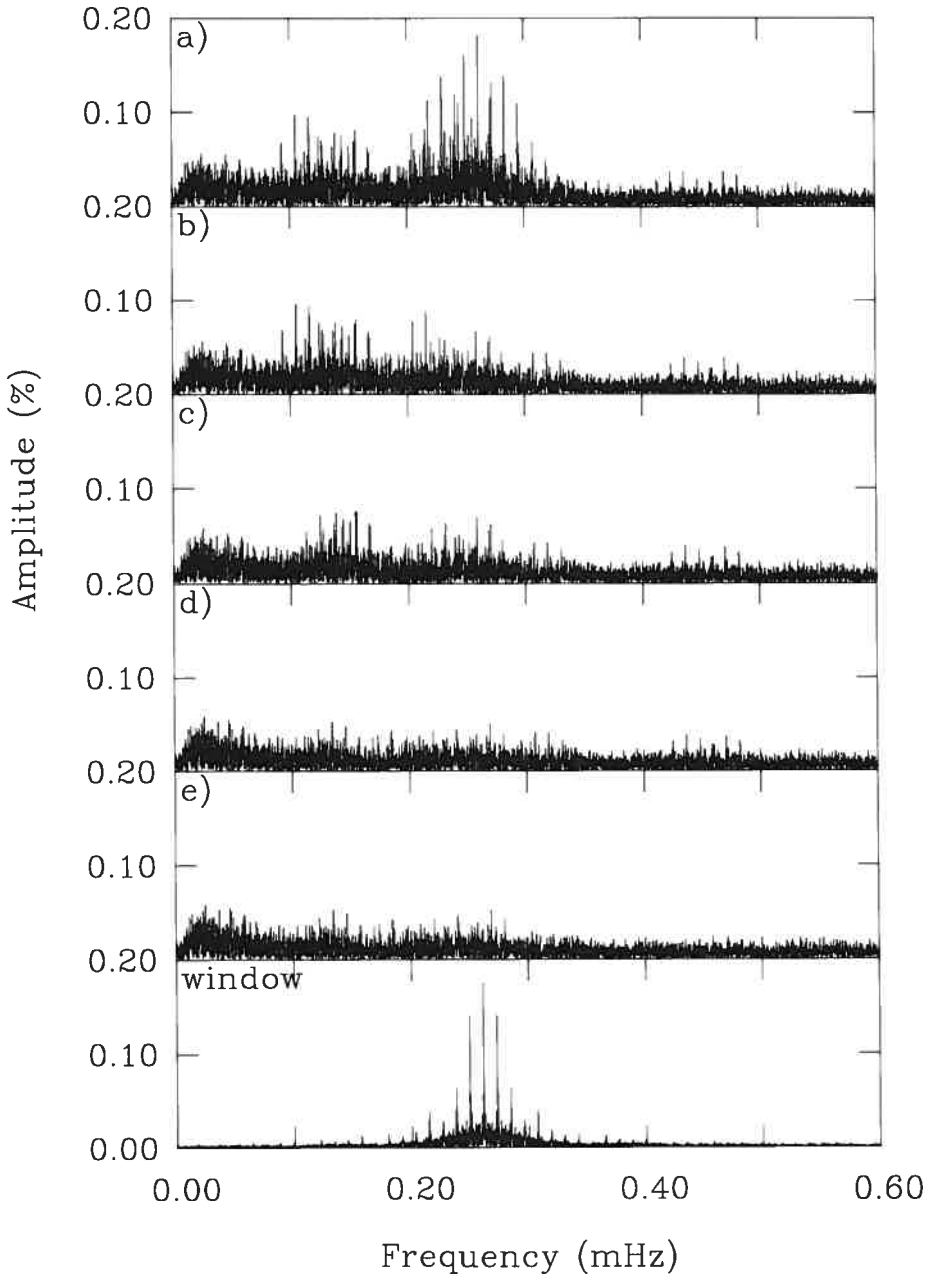

FIGURE 5.3 – Pre-whitening process of the Fourier transform constructed on the basis of all useful R band data and shown in the 0–0.6 mHz range. The spectrum from 0.6 mHz out to the Nyquist frequency is consistent with noise and hence of no interest. While the top panel a) depicts the original FT, the second panel b) illustrates the observed spectrum pre-whitened of the dominant 4 periodicities. Panels c) and d) represent the extraction of an extra two and all 11 periods down to an amplitude threshold of 0.06 % respectively. Finally, the spectrum shown in panel e) has been pre-whitened by another 3 lower-amplitude oscillations in the less noisy 0.3–0.6 mHz bandpass. The bottom panel shows the window function of all the combined R band data.

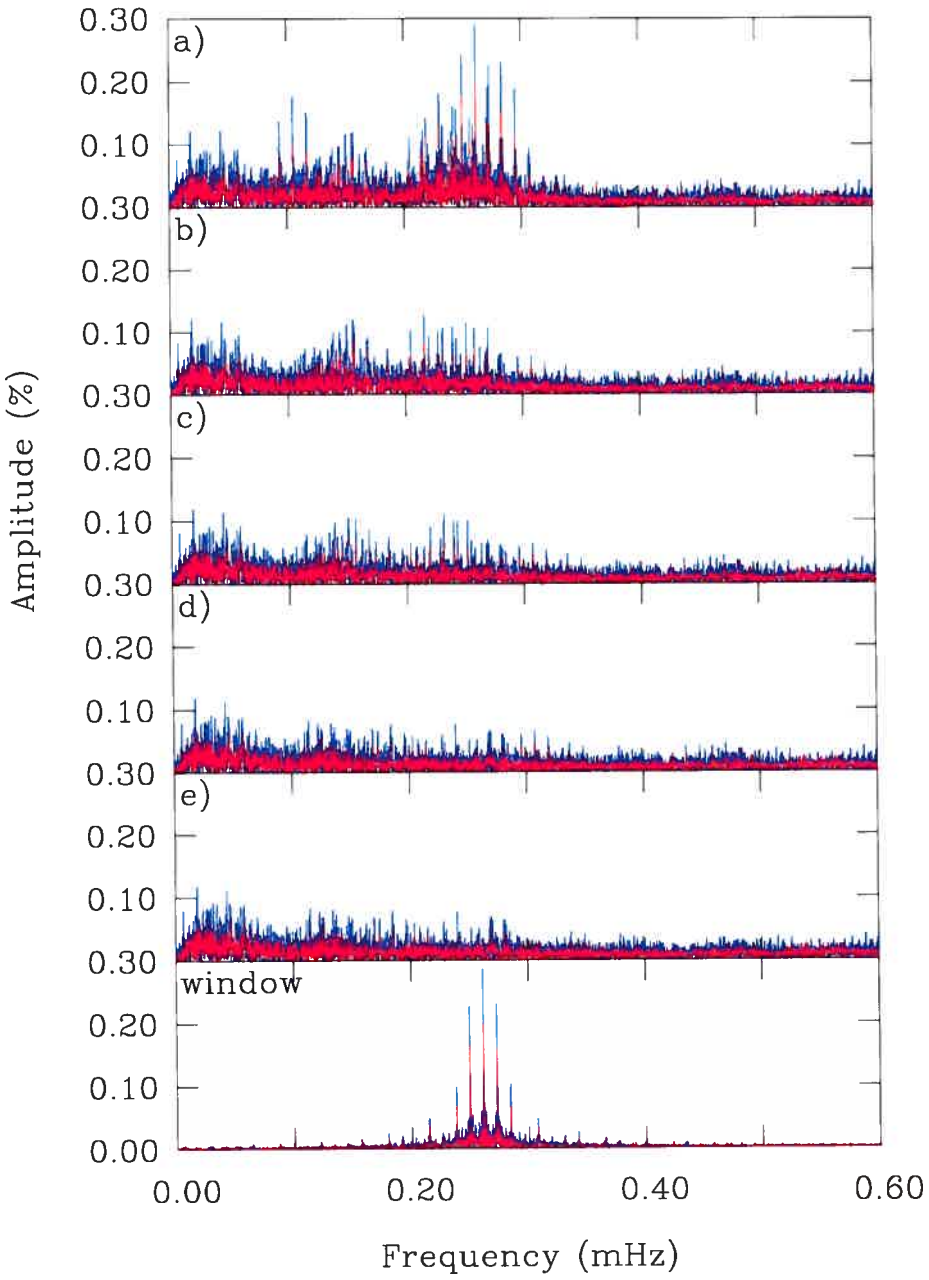

FIGURE 5.4 – Pre-whitening process of the Fourier transforms constructed on the basis of all useful simultaneous U and R data. We have overplotted the two spectra for visualisation and easy comparison purposes and depict them in the 0–0.6 mHz range. The top panel a) shows the original U (blue) and R (red) Fourier transforms, while the second plot b) illustrates the observed spectra pre-whitened of the 5 highest amplitude frequencies. Moving down, the subsequent spectra have been extracted first of another two (panel c), and then all 12 peaks above the amplitude threshold of 0.08 % (U) and 0.05 % (R) in panel d). Finally, the spectrum shown in the panel e) has been pre-whitened of an extra 3 lower-amplitude oscillations in the less noisy 0.3–0.6 mHz bandpass. The bottom panel shows the window function of the simultaneous U and R data.

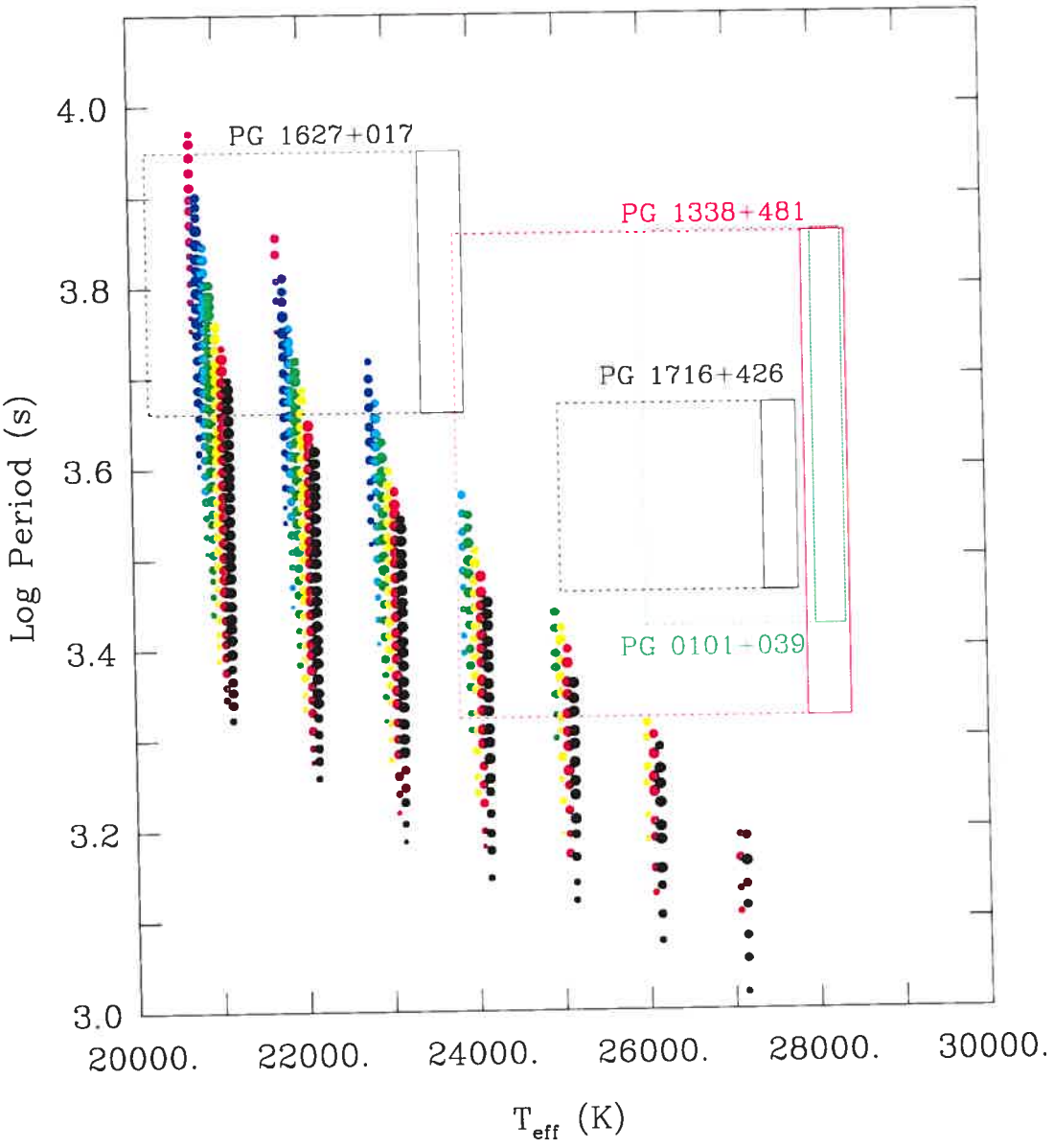

FIGURE 5.5 – Periods excited in a representative sequence of subdwarf B star models compared to those observed for PG 1338+481, PG 1627+017, PG 1716+426 and PG 0101+039. The coloured points refer to theoretical modes predicted to be unstable and are colour-coded according to degree index l as follows: magenta for l=2, blue for l=3, cyan for l=4, green for l=5, yellow for l=6, red for l=7 and black for l=8. The columns of circles have been shifted slightly in temperature to facilitate viewing. The superposed boxes give the temperature uncertainty of the targets indicated in the horizontal, and the logarithmic periods of the convincing oscillations observed in the vertical direction. The continuous boxes refer to the spectroscopic values obtained by GFC, while the dotted extensions are based on the lower temperatures derived by UH.

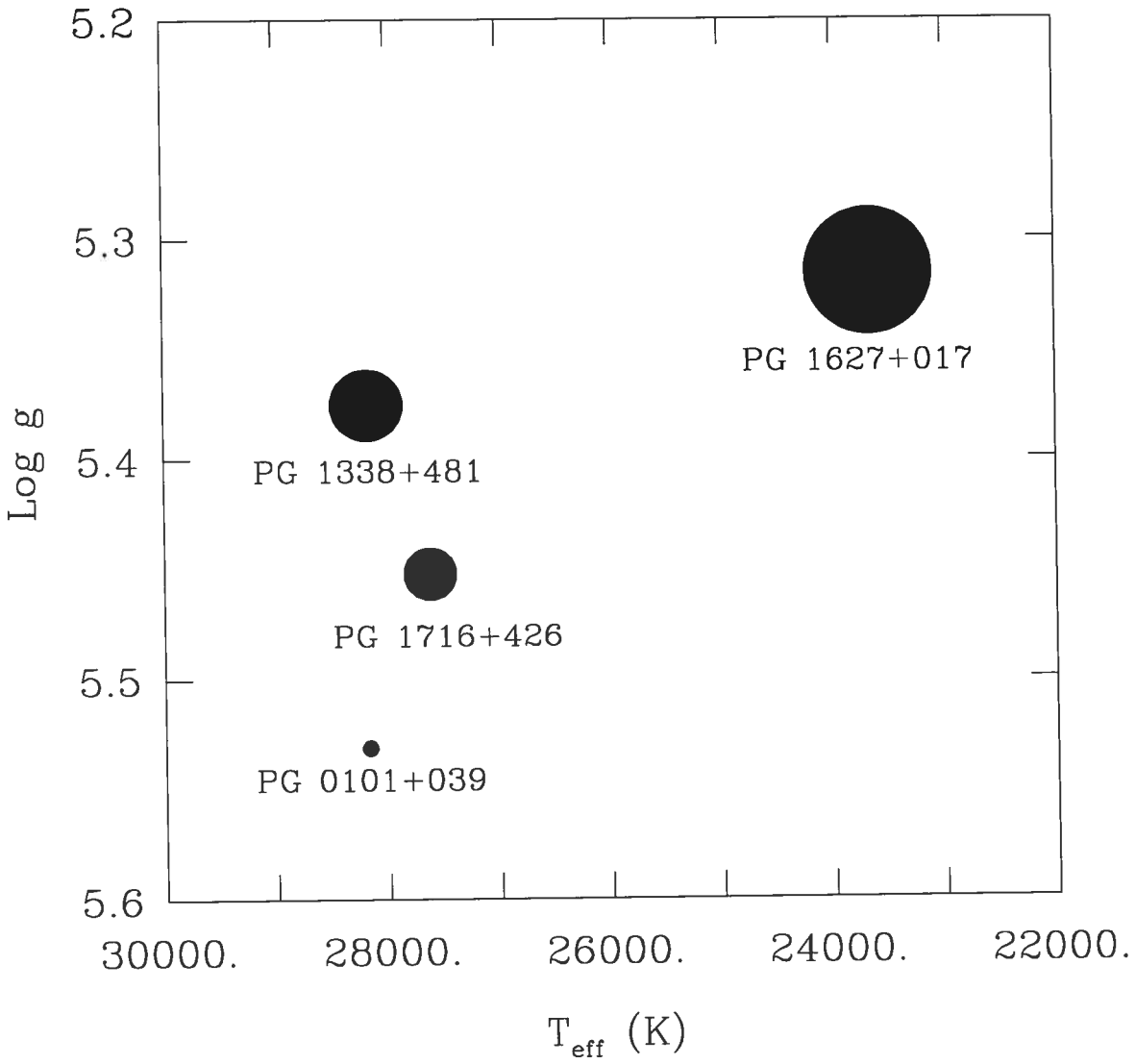

FIGURE 5.6 – Distribution of well-observed PG 1716 stars and their pulsational amplitudes in $\log g - T_{\rm eff}$ space based on the atmospheric parameters of GFC. The size of each point is correlated linearly with the pulsational amplitude measured for the dominant oscillation of each star.

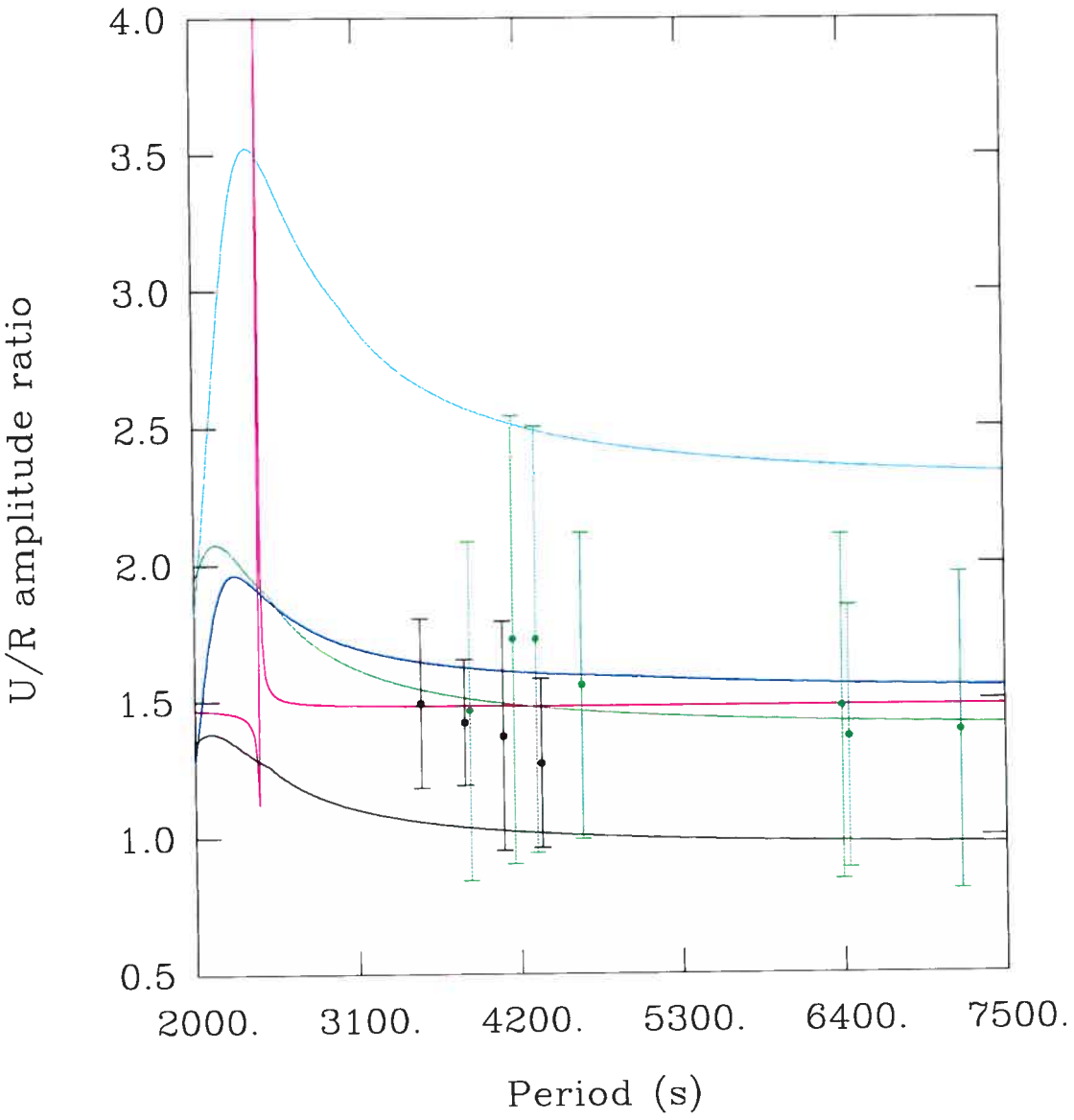

FIGURE 5.7 – Predicted U/R amplitude ratios for degree indices $l = 1$ (magenta), $l = 2$ (blue), $l = 3$ (cyan), $l = 4$ (green) and $l = 5$ (black) compared to those observed for PG 1338+481. The stellar model used in the computations has $T_{\rm eff} = 28{,}200$ K, $\log g = 5.38$, $M_*/M_\odot = 0.48$ and $\log q({\rm He}) = -2.8$. Black points indicate observed ratios with errors smaller than 30 % of their numerical value, i.e., those that are considered statistically significant (the bold entries in Table 5.3). Green points denote amplitude ratios with larger errors of up to 50 % of their numerical value for comparison.

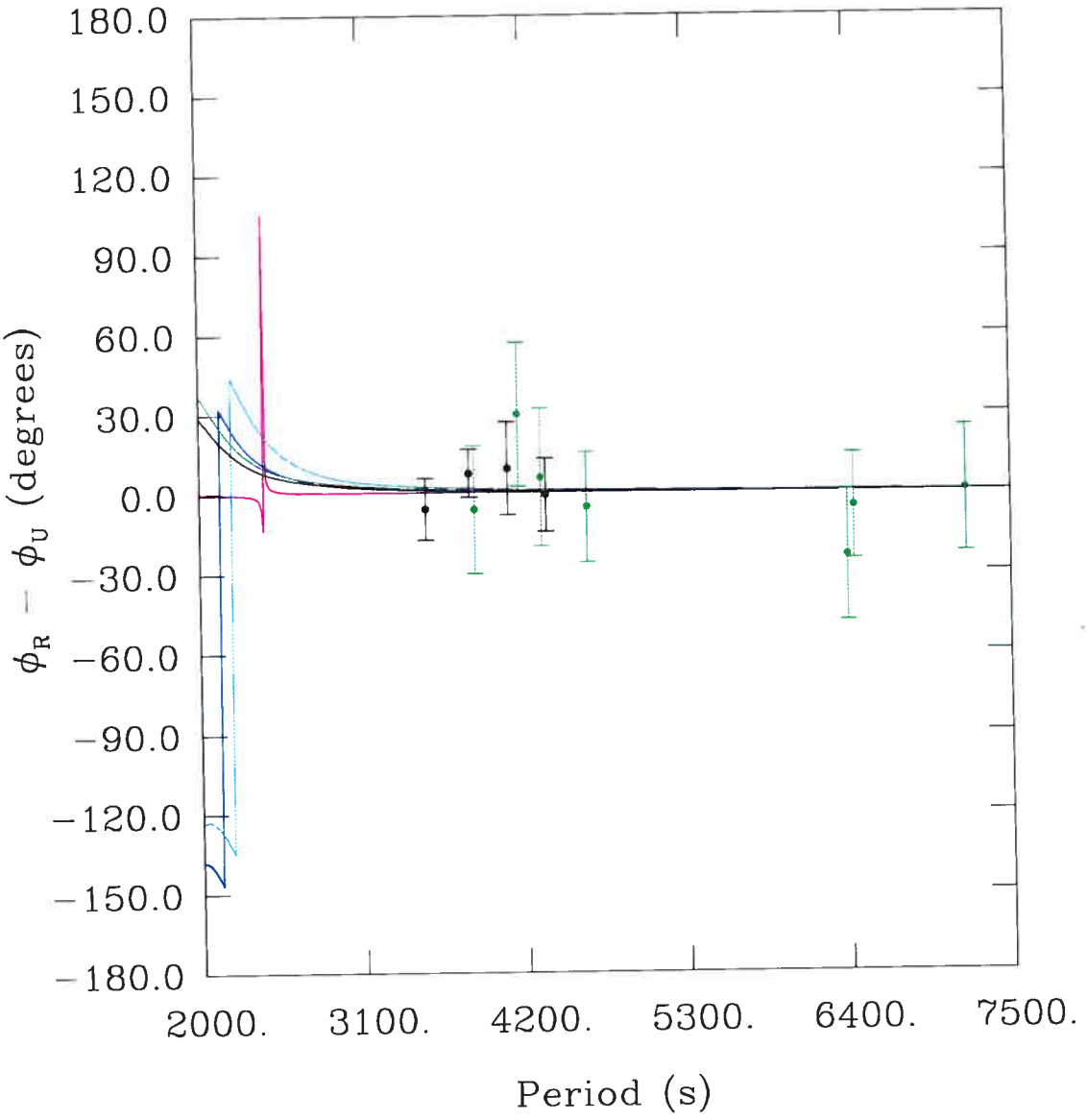

FIGURE 5.8 – Similar to Figure 5.7, but for $U - R$ phase differences.

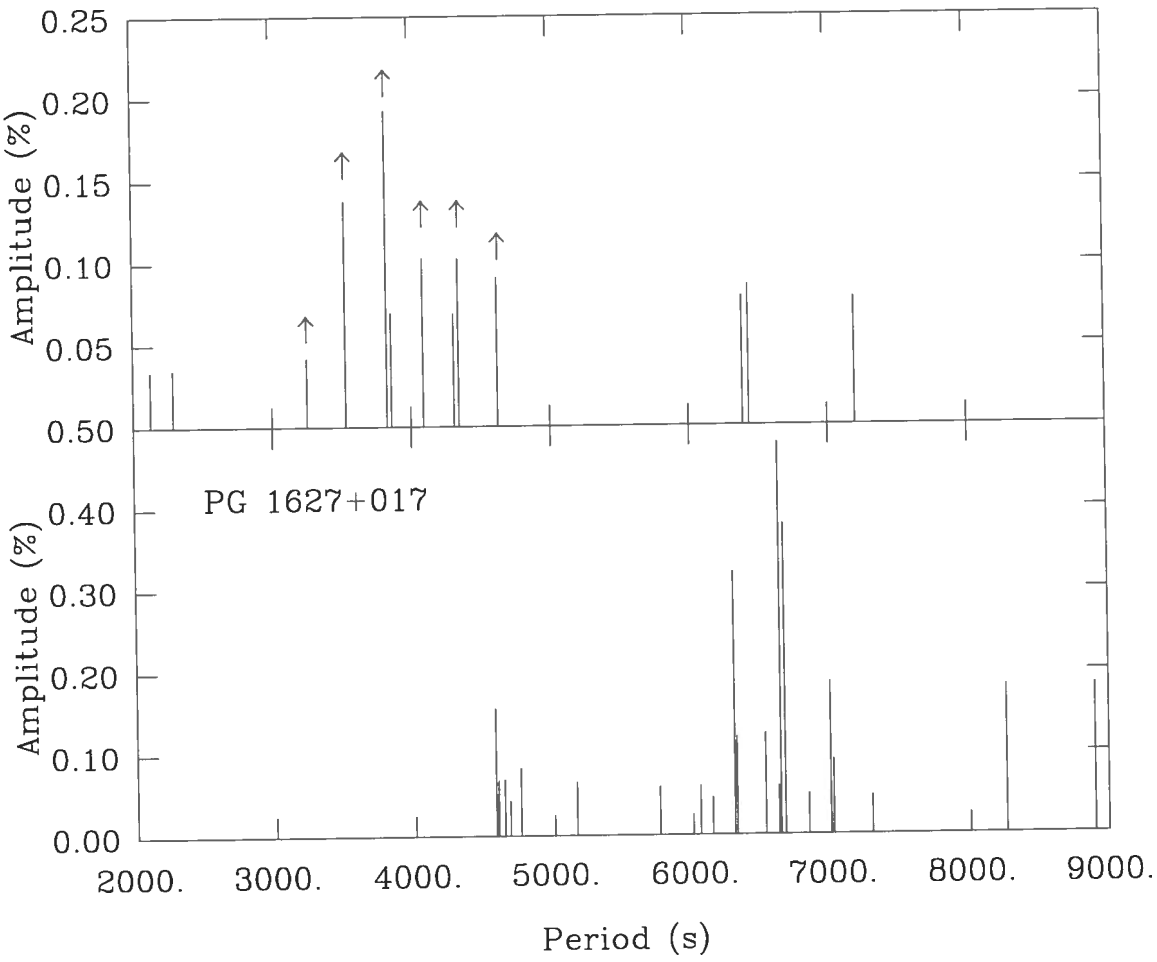

FIGURE 5.9 – Period spectrum uncovered for PG 1338+481 as detailed in Table 5.2 (top panel) compared to that measured for PG 1627+017 (bottom - see Paper I for details on the periodicities). Note the different ordinate axes.

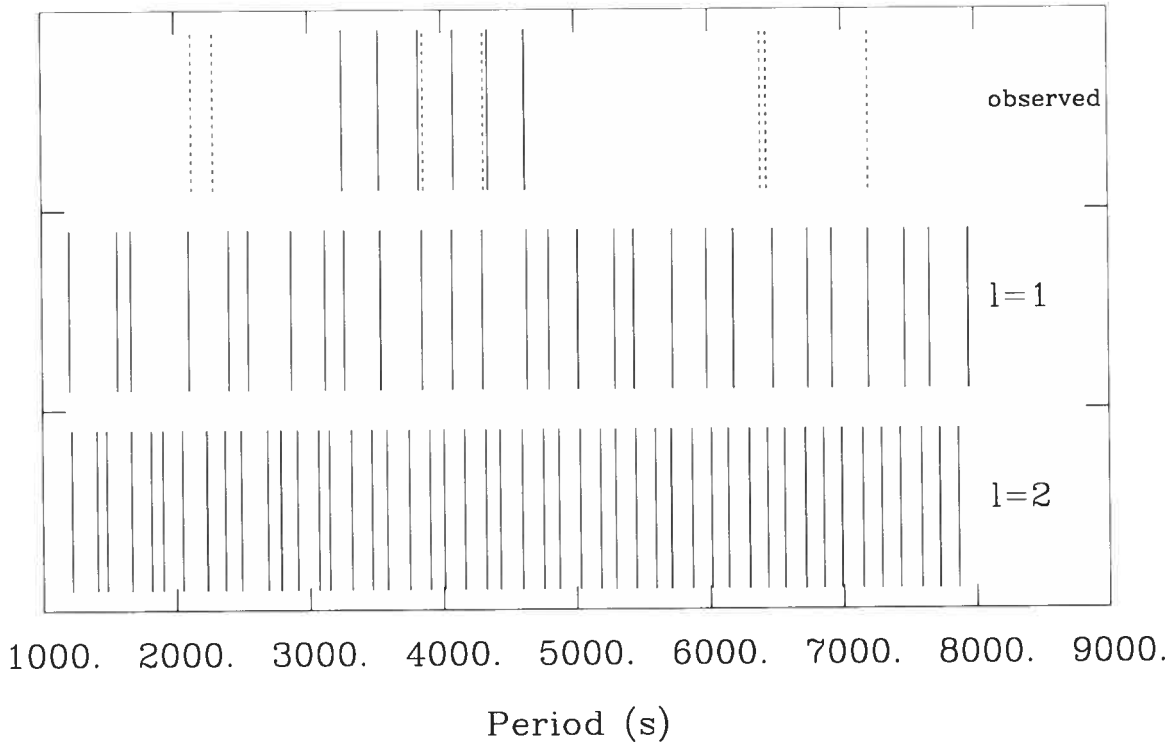

FIGURE 5.10 – Adiabatic periods predicted for a model with $T_{\rm eff}$ = 28,200, $\log g$ = 5.38, M_* = 0.616, $\log q$(H) = −1.91 and $\log q$(He) = −0.30 for degree indices l = 1 and 2 compared to those observed for PG 1338+481. The six observed periodicities assumed to correspond to consecutive dipole modes that are used in the optimal model finding exercise are indicated by continuous line segments, while the remaining oscillations detected are denoted by dotted line segments.

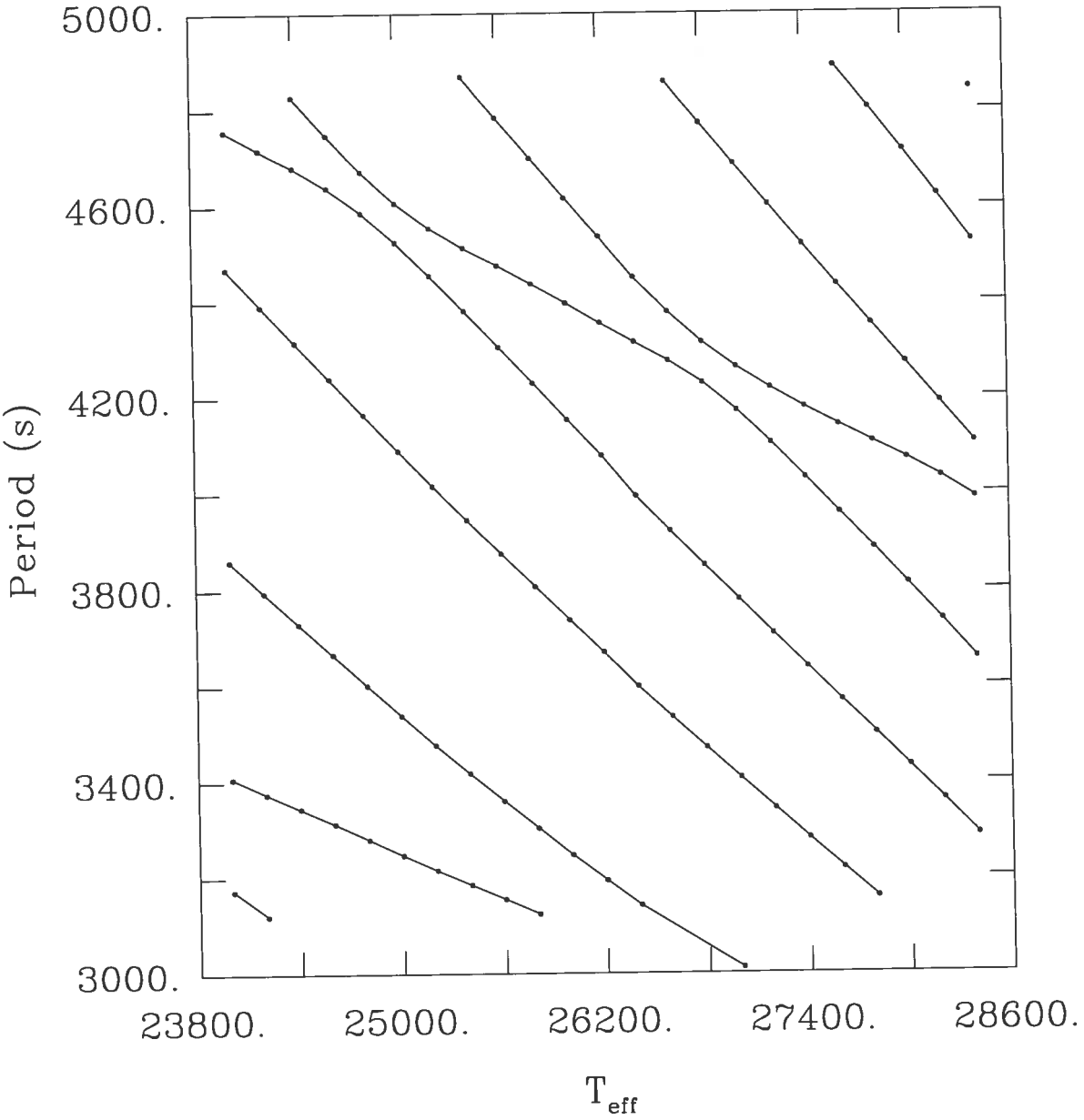

FIGURE 5.11 – Dependence of the theoretical periods for dipole modes in the 3000−5000 s range on $T_{\rm eff}$. The other model parameters have been kept constant at $\log g = 5.38$, $M_*/M_\odot = 0.48$, $\log q({\rm H}) = -2.8$ and $\log q({\rm He}) = -0.24$. Modes with the same radial index k are connected for clarity. From bottom to top, values of k range from 10 to 14 on the left and from 14 to 19 on the right.

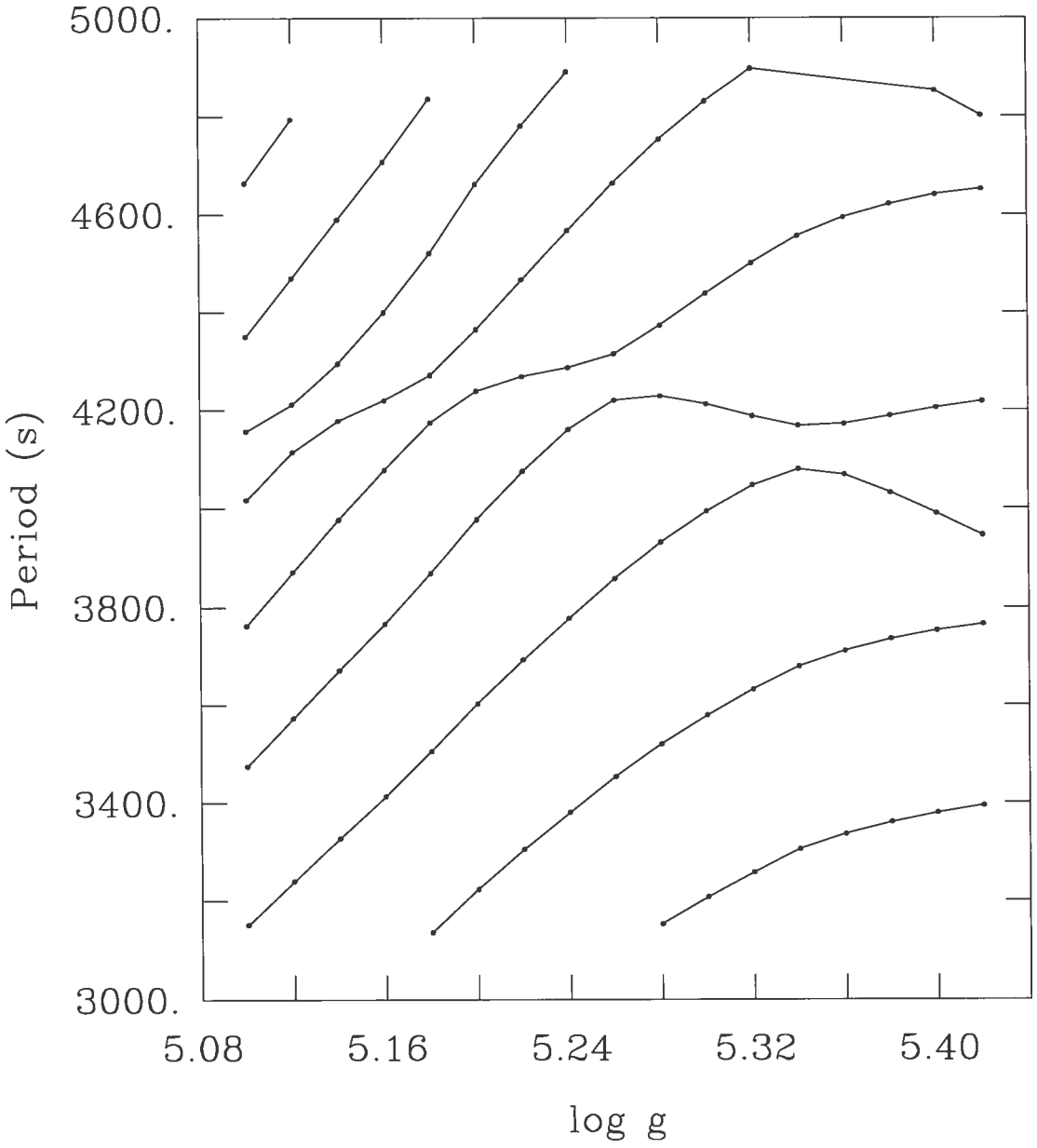

FIGURE 5.12 – Dependence of the theoretical periods for dipole modes in the 3000–5000 s range on $\log g$. The other model parameters have been kept constant at $T_{\rm eff}$ = 28,200 K, $M_*/M_\odot = 0.48$, $\log q({\rm H}) = -2.8$ and $\log q({\rm He}) = -0.24$. Modes with the same radial index k are connected for clarity. From bottom to top, values of k range from 8 to 14 on the left and from 6 to 11 on the right.

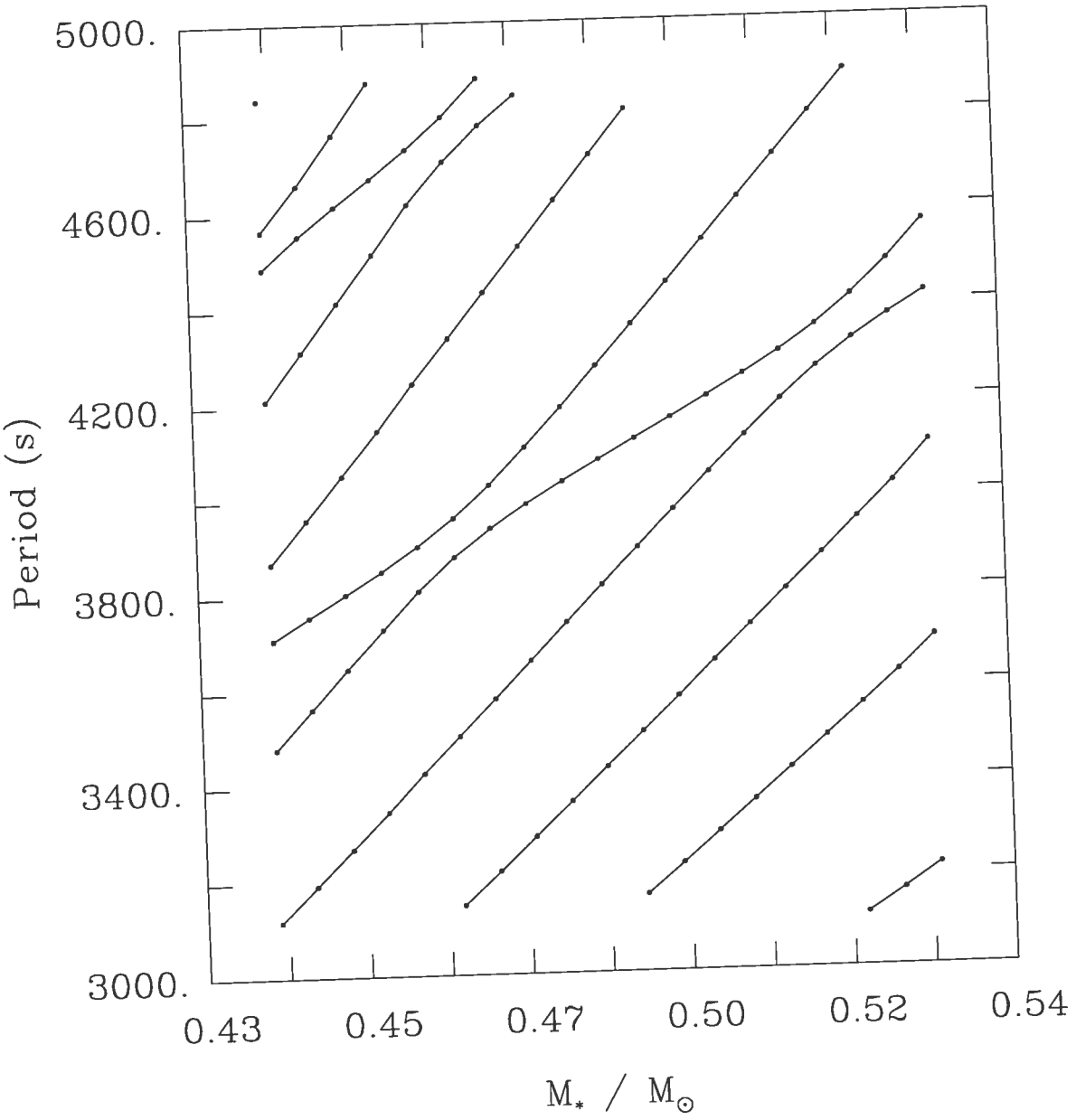

FIGURE 5.13 – Dependence of the theoretical periods for dipole modes in the 3000−5000 s range on M_*. The other model parameters have been kept constant at $T_{\rm eff}$ = 28,200 K, $\log g$ = 5.38, $\log q$(H) = −2.8 and $\log q$(He) = −0.24. Modes with the same radial index k are connected for clarity. From bottom to top, values of k range from 11 to 18 on the left and from 8 to 12 on the right.

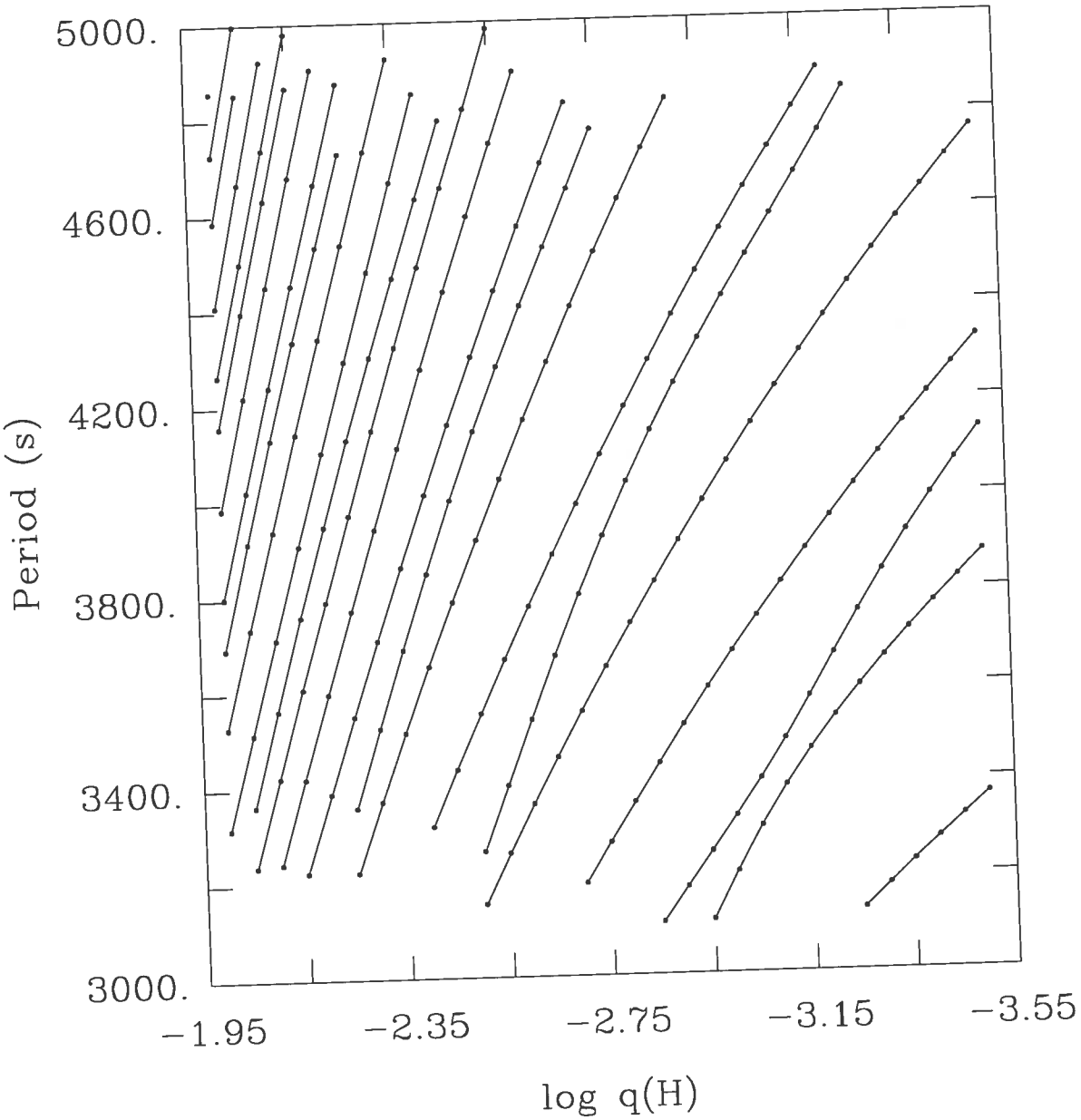

FIGURE 5.14 – Dependence of the theoretical periods for dipole modes in the 3000−5000 s range on $\log q(\mathrm{H})$. The other model parameters have been kept constant at $T_{\mathrm{eff}} = 28{,}200$ K, $\log g = 5.38$, $M_*/M_\odot = 0.48$ and $\log q(\mathrm{He}) = -0.24$. Modes with the same radial index k are connected for clarity. From bottom to top, values of k range from 20 to 30 on the left and from 7 to 11 on the right.

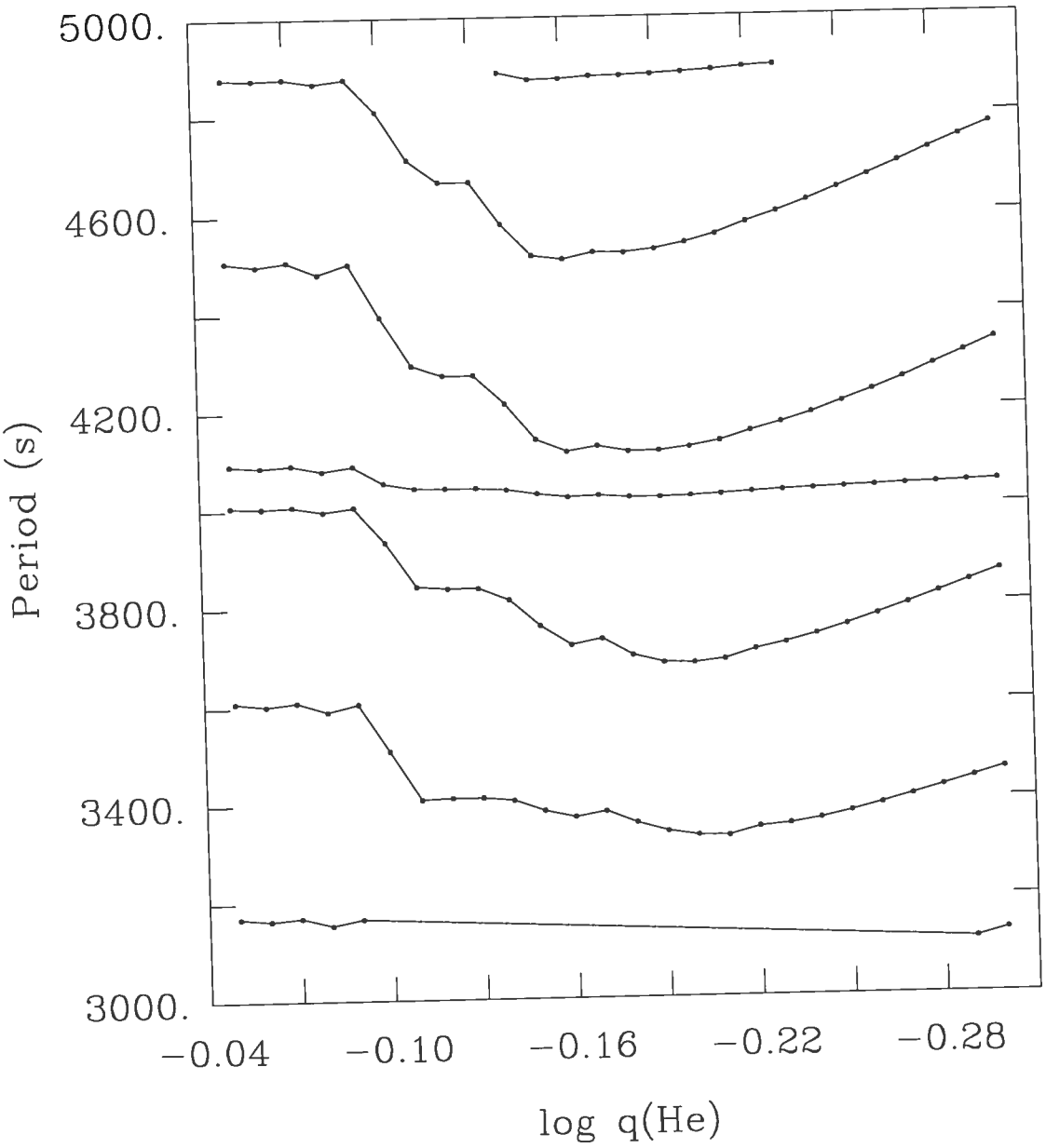

FIGURE 5.15 – Dependence of the theoretical periods for dipole modes in the 3000−5000 s range on $\log q$(He). The other model parameters have been kept constant at $T_{\rm eff}$ = 28,200 K, $\log g$ = 5.38, $M_*/M_\odot$ = 0.48 and $\log q$(H) = −2.8. Modes with the same radial index k are connected for clarity. From bottom to top, values of k range from 9 to 15.

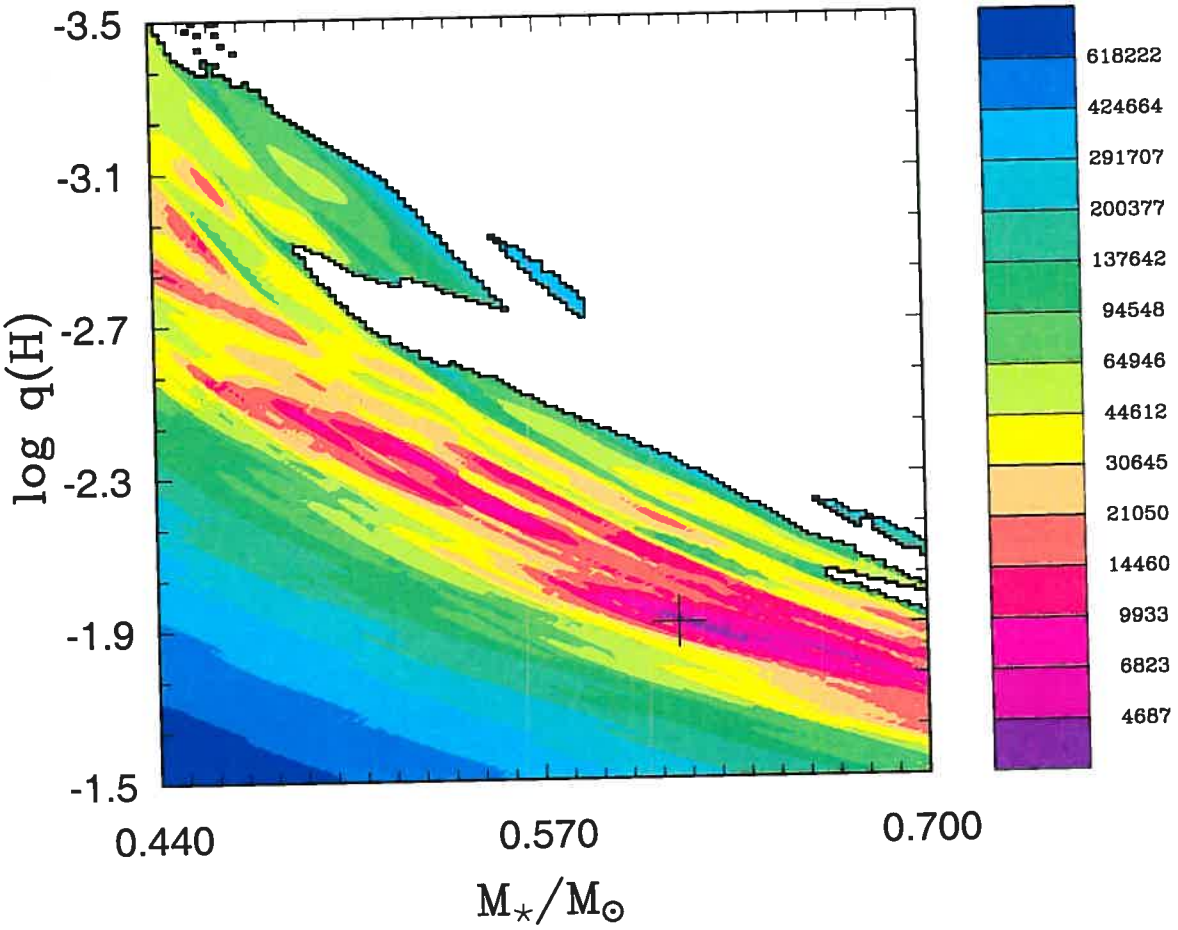

FIGURE 5.16 – χ^2 hypersurface in the $M_* - \log q(\mathrm{H})$ plane for fixed values of $T_{\rm eff}$ =28,200 K and $\log g = 5.38$. The remaining parameter $\log q(\mathrm{He})$ is set to its optimal value (i.e., the one that yields the lowest χ^2) at each gridpoint. Some 342,303 models were computed to generate this plot. The scale to the right of the main figure refers to the χ^2 value associated with a given colour. Blank areas correspond to models for which no fit was possible on the basis of the theoretical periods computed (i.e., the density of the predicted frequency spectrum was significantly lower than that observed over the period range considered). The location of the absolute minimum ($\chi^2 = 3219$) at $M_* = 0.616 M_\odot$, $\log q(\mathrm{H}) = -1.91$ and $\log q(\mathrm{He}) = -0.30$ is indicated by the black cross.

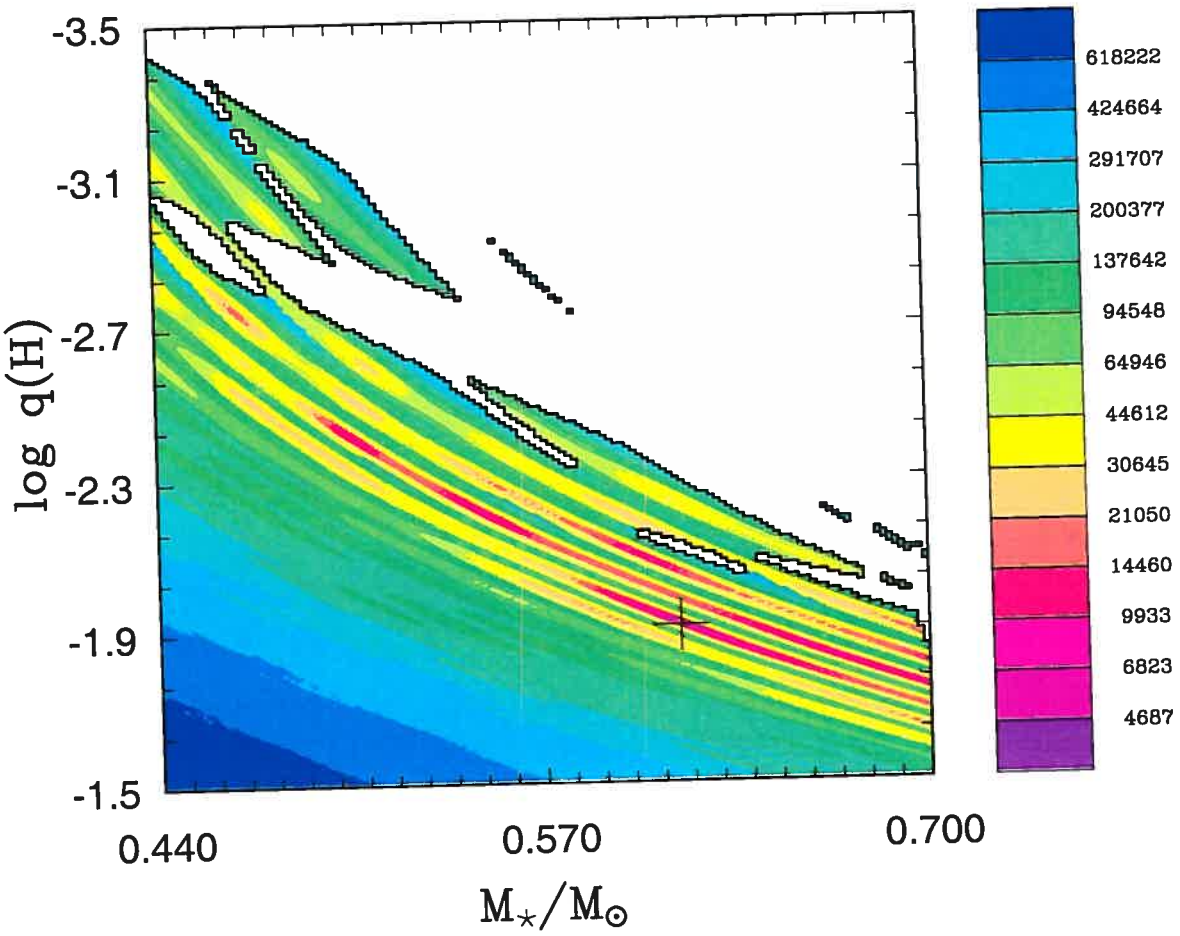

FIGURE 5.17 – Similar to Figure 5.16, except that $\log q(\mathrm{He})$ is held fixed at its global optimal value of -0.30. Here, 26,331 models were calculated to generate the plot.

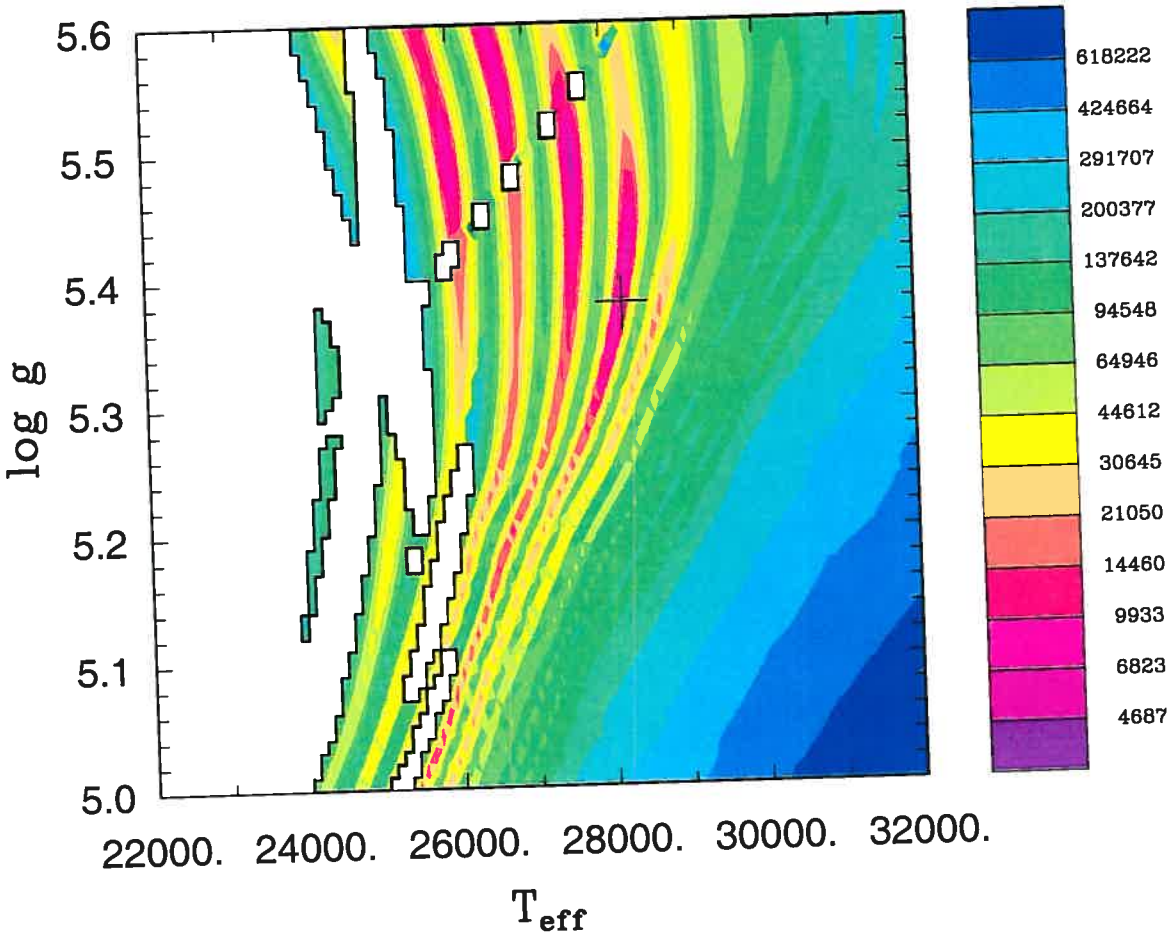

FIGURE 5.18 – Slice through χ^2 hypersurface in the $T_{\rm eff} - \log g$ plane with the other model parameters held fixed at the globally optimal values of $M_*/M_\odot = 0.616$, $\log q({\rm H}) = -1.910$, and $\log q({\rm He}) = -0.30$. For further details, see Figure 5.16. The generation of this plot required the computation of 6,161 models.

Chapter 6

DETECTION OF LONG-PERIOD VARIATIONS IN THE SUBDWARF B STAR PG 0101+039 ON THE BASIS OF PHOTOMETRY FROM THE MOST SATELLITE[1]

S.K. Randall[2] , J.M. Matthews[3] , G. Fontaine[3], J. Rowe[4], R. Kuschnig[4], E.M. Green[4] , P. Brassard[3], P. Chayer[5] , D.B. Guenther[6] , A.F.J. Moffat[3], S. Rucinski[7] , D. Sasselov[8] , G.A.H. Walker[4], and W.W. Weiss[9]

Received 2005 May 1; accepted 2005 July 14

Published in *The Astrophysical Journal*, November 1 2005, *Vol.* 633, *page* 460

---

[1]Based on data from MOST, a Canadian Space Agency mission operated jointly by Dynacon, Inc., the University of Toronto Institute of Aerospace Studies, and the University of British Columbia, with assistance from the University of Vienna. Spectroscopic observations reported here were obtained at the MMT Observatory, a joint facility of the University of Arizona and the Smithsonian Institution

[2]Département de Physique, Université de Montréal, C.P. 6128, Succ. Centre-Ville, Montréal, Québec H3C 3J7, Canada; [redacted]

[3]Department of Physics and Astronomy, University of British Columbia, 6224 Agricultural Road, Vancouver V6T 1Z1, Canada; [redacted]

[4]Steward Observatory, University of Arizona, Tucson, AZ 85721; bgreen@as.arizona.edu

[5]Bloomberg Center for Physics and Astronomy, Johns Hopkins University, Baltimore, MD 21218-2695; [redacted]

[6]Department of Astronomy and Physics, St. Mary's University, Halifax, NS B3H 3C3, Canada; [redacted]

[7]David Dunlap Observatory, University of Toronto, P.O. Box 360, Richmond Hill, ON L4C 4Y6, Canada; [redacted]

[8]Harvard-Smithsonian Center for Astrophysics, 60 Garden Street, Cambridge, MA 02138; [redacted]

[9]Institut für A[redacted]ronomie, Universität Wien, Türkenschanzstrasse 17, A-1180 Wien, Austria; [redacted]

6.1 ABSTRACT

We report the detection of three discrete pulsation frequencies in the long-period variable subdwarf B star PG 0101+039 on the basis of $\sim$ 400 hours of MOST wide-band photometry. The periodicities uncovered lie at 7235 s, 5227 s and 2650 s respectively and are associated with amplitudes between 0.03% and 0.06% of the mean brightness, lower than those measured in any other variable of this kind. We also find evidence for luminosity variations consistent with an ellipsoidal deformation of the subdwarf in the rotationally locked short-period binary system predicted from radial velocity measurements and evolutionary models. Our atmospheric modelling of two independent time-averaged optical spectra of PG 0101+039 yields $T_{\rm eff} \simeq 28,300$ K and $\log g \simeq 5.52$, making it one of the hottest long-period variable subdwarf B stars known. The fact that we nevertheless detect brightness variations in the data is in conflict with predictions from current models, which place the theoretical blue edge for observable long-period instabilities at a temperature around 4000 K cooler than that of PG 0101+039.

6.2 INTRODUCTION

Subdwarf B (sdB) stars are evolved extreme horizontal branch objects with atmospheric parameters in the range 20,000 K $\lesssim T_{\rm eff} \lesssim$ 40,000 K and 5.0 $\lesssim \log g \lesssim$ 6.2 (Saffer et al. 1994). They are composed of a helium-burning core surrounded by a hydrogen-rich shell and are characterised by masses of $\sim 0.5\ M_{\odot}$. SdB progenitors are thought to have lost a significant fraction of their hydrogen envelope near the red giant tip, leaving the remaining shell too thin for them to ascend the asymptotic giant branch after helium exhaustion (Heber 1986; Dorman 1995). Instead, they evolve off and along the horizontal branch and end their lives as low-mass white dwarfs (Bergeron et al. 1994). While their precise evolutionary path and the circumstances surrounding the mass loss are not yet fully understood, it is hoped that the asteroseismology of pulsating subdwarf B stars will help constrain potential evolutionary scenarios through the determination of key parameters such as the total mass and the thickness of the hydrogen shell.

We currently know of two types of subdwarf B pulsator: the rapidly oscillating EC 14026 stars (Kilkenny et al. 1997) and the more recently discovered long-period variable PG 1716 stars (Green et al. 2003). The former excite pressure (p-)modes with typical periods of 100−200 s and lie at effective temperatures between 28,000 K and 36,000 K, while the latter are noticeably cooler at 22,000 K $\lesssim T_{\rm eff} \lesssim$ 29,000 K and exhibit periodicities of around 1−2 hours corresponding to high radial order gravity (g-)modes. Oscillations are thought to be driven by a kappa-mechanism associated with a local overabundance of iron in the stellar envelope in both cases (see Charpinet et al. 1996, 1997 and Fontaine et al. 2003 for the two types of pulsator respectively). In the case of the rapid oscillators, the periodicities observed have been recovered by predictions not only to the extent where the ranges of unstable periods coincide, but also to the point where a quantitative interpretation of the detected period spectrum has been achieved in a few instances (Brassard et al. 2001; Charpinet et al. 2003, 2005). These asteroseismological analyses are based on the identification of low radial order p-modes with degree indices $l = 0$, 1, 2, and 3 and/or 4. Because there are not enough theoretical modes with $l = 0$, 1, and 2 to account for the mode density observed, the inclusion of the latter is necessary in the asteroseismological process.

For the PG 1617 stars, both observational and theoretical research is still in its infancy. To date, only three long-period variables have been monitored in any detail: the class prototype PG 1716+426 (Green et al. 2003; Reed et al. 2004), PG 1627+017 (Randall et al. 2004a), and PG 1338+481 (Randall et al. 2004b). While the periodicities observed for these stars occur on a similar timescale to those predicted from models, there seem to be systematic discrepancies between the two. In particular, current models are able to excite only modes with degree indices $l \geq 3$ for all but the coolest subdwarfs (see Figure 9 of Fontaine et al. 2003). The minimum degree index of unstable modes increases monotonically with temperature to the point where models corresponding to the very hottest PG 1716 stars can drive only modes with $l > 8$. Although this clearly indicates problems with the theoretical blue edge, these have been difficult to specify due to a lack of data. All previous observational campaigns have focussed on targets of low and intermediate temperatures, where the periods detected could qualitatively be explained by excited modes of $l = 2$, 3 and/or 4 if the star's effective tempe-

rature and surface gravity were pushed to the lower end of the spectroscopic estimates (which are less accurate for the cooler long-period variables). In order to quantify the discrepancies between modelled and experimental instabilities we thus deem it necessary to determine the periodicities exhibited by a hotter target for which no discernable brightness variations are expected.

It is with this in mind that we choose to monitor PG 0101+039, one of the hottest subdwarf B stars known to show long-period oscillations. Also known as Feige 11, PG 0101+039 is the second subdwarf B star for which long-period variability was detected, albeit at much lower amplitudes than for the prototype (Green et al. 2003). At an apparent magnitude of $V = 12.06$ it is one of the brightest subdwarf B stars and thus an obvious exploratory target. Radial velocity measurements have found it to form part of a binary system with a relatively short orbital period of $P_{\rm orb} \sim 0.569908 \pm 0.000007$ days (Moran et al. 1999), the companion most likely being a white dwarf (Maxted et al. 2002). Interestingly, the fit of the binary period to the radial velocity data of Moran et al. (1999) was associated with an unusually large χ^2 value, indicating either systematic measurement errors or an intrinsic brightness variation of the subdwarf on a timescale of $\sim$ 55 minutes. At the time, long-period variations in subdwarf B stars had not yet been discovered, and so the latter possibility was not further explored[10].

Since previous ground-based photometric campaigns have demonstrated that the detailed frequency analysis of long-period variable subdwarf B stars will in most cases require the high duty cycle and long time coverage of space-based observations (see, e.g. Randall et al. 2004b), the photometry of PG 0101+039 was obtained with the MOST ('Microvariability and Oscillations of STars') satellite (Walker et al. 2003) in a trial run for potential future missions. MOST houses a 15-cm optical telescope feeding a CCD photometer through a custom broadband filter (250−700 nm), and can monitor certain stars for up to 8 weeks without interruption from its Sun-synchronous polar orbit (altitude = 820 km). It was designed to perform rapid photometry of micromagnitude precision on Primary Target stars brighter than $V = 6$ through Fabry-lens projection of an extended pupil image of the telescope, however its

[10]In retrospect, the very low amplitudes of the pulsations detected in the PG 0101+039 photometry imply radial velocity variations of less than 1 km/s, below the typical measurement errors of ∼1.8 km/s reported by Moran et al. (1999). It is thus highly unlikely that the χ^2 excess reported in the radial velocity data is caused by the long-period pulsations detected.

Science CCD does have an open field where slightly defocussed images of Secondary Targets as faint as $V = 12-13$ can be obtained with reasonable signal-to-noise and time resolution of better than 1 minute. The preliminary results we present in this Paper confirm that MOST (and other future stellar photometry satellites such as COROT and Kepler) hold great promise for the identification and interpretation of long-period oscillations in subdwarf B stars.

6.3 OBSERVATIONS AND ANALYSIS

6.3.1 Spectra and Atmospheric Model Fit

We obtained optical spectroscopy of PG 0101+039 in the course of an ongoing program designed to provide homogeneous estimates of the atmospheric parameters of a large sample of subdwarf B stars. This program is based on low-resolution (9Å, $R \sim 500$) spectra from the 2.3-m Steward Observatory telescope at Kitt Peak and/or medium-resolution (1Å, $R \sim 4400$) spectroscopy obtained at the MMT. For PG 0101+039, high signal-to-noise-ratio (S/N $\sim 200 - 400$) time-averaged spectra from both telescopes were available, enabling two independent estimates of the atmospheric parameters on the basis of different sets of spectral lines. The model spectra are computed from non-LTE model atmospheres containing hydrogen and helium, but no metals (see Green, Fontaine, & Chayer, in preparation). Figure 6.1 shows our best fit to the hydrogen Balmer and helium lines available from the MMT spectrum, implying atmospheric parameters of $T_{\rm eff} = 28,175 \pm 170$ K, $\log g = 5.53 \pm 0.02$, and $\log N(He)/N(H) = -2.77 \pm 0.03$. The corresponding fit to the low-resolution spectrum gives $T_{\rm eff} = 28,430 \pm 170$ K, $\log g = 5.51 \pm 0.03$, and $\log N(He)/N(H) = -2.70 \pm 0.08$ in agreement with the previous values within the formal errors. Test calculations with non-LTE models including metals in solar proportions suggest that the effective temperature and the surface gravity of PG 0101+039 could perhaps be reduced by $\sim$ 1800 K and 0.15 dex respectively, but not much more. It is thus evident that both the effective temperature and the surface gravity of PG 0101+039 are substantially higher than the upper limit predicted for the excitation of modes with $l \leq 8$ from our models of long-period variable subdwarf B stars (see Figure 9 of Fontaine et al. 2003).

6.3.2 Photometry and Frequency Analysis

MOST photometry of PG 0101+039 was obtained over 16.9 days from 28 September to 15 October 2004 with an exposure time of 30 s and a sampling rate of once every 35 s. Observations were nearly continuous at this cadence except for one major gap of about 14 hours early in the run, when the MOST camera was shut off due to full Moonshine coming almost directly into the instrument. This implies a net duty cycle of 96.5%, and a formal frequency resolution of 0.68 μHz. The raw photometry obtained with MOST is subject to stray light variations caused by scattered Earthshine entering the focal plane at a well-specified range of phases in the satellite's 101.413-minute (6084.7 s/0.164 mHz) orbital period. This stray light background has been subtracted, and obvious outliers as well as very long-term trends have been removed from the data during the reduction process, resulting in the lightcurve illustrated in Figure 6.2. While there seems to be some evident structure in the curve, this is mostly due to the periodic increase in point-to-point scatter associated with the orbital phases of highest stray light. The field of the MOST Science CCD also included two comparison stars (GSC 00022-01077 and GSC 00022-01060) of similar brightness to PG 0101+039. Given that MOST was not designed for wide-field CCD photometry of stars near $V = 12$ (no onboard flat-fielding calibration, for example), differential photometry of PG 0101+039 relative to these comparison stars did not improve the scatter in the light curve and was decided against. Nevertheless, the independent photometry of these additional stars was useful when trying to gauge the reliability of periodicities uncovered in the target data.

The top panel of Figure 6.3 shows the Fourier transform of the entire PG 0101+039 dataset for the 0–0.6 mHz band pass of interest. Beyond this, the spectrum is consistent with noise out to the Nyquist frequency of 14.3 mHz. We subjected the data to our standard pre-whitening procedure (see Billères et al. 2000 for details), adopting a threshold of four times the noise level (indicated by the dotted horizontal line) above which peaks would be considered convincing. This value was derived from the Fourier transforms of the comparison star light curves depicted in the lower two panels of Figure 6.3, which exhibit peaks above the threshold only at periods longer than ~40,000 s. Since the amplitudes and periods of these peaks are similar to those of the low-frequency agglomeration of periodicities visible

in the Fourier spectrum for PG 0101+039, the latter are attributed to non-stellar noise and are not considered in the remainder of this Paper. In any case, it is not physically viable to find oscillations of this length in subdwarf B stars as they would be lost to space rather than reflected at the stellar surface[11]. The remaining three convincing peaks (marked by continuous vertical line segments) lie between 2600 and 7250 s, a range comparable to that found in other PG 1716 stars, and are associated with amplitudes between 0.03 % and 0.06% of the mean brightness. Probing slightly below our imposed threshold, but staying above the often assumed limit of three times the noise level, we uncover other potentially interesting periodicities (marked by dotted vertical line segments), most notably two peaks corresponding to (within 0.3 %) half the binary orbital period of PG 0101+039 ($P_{\rm orb}/2 = 24,620$ s) and its first harmonic respectively. Assuming the binary-synchronous stellar rotation rate expected in this type of system, these are likely caused by an ellipsoidal deformation of the subdwarf due to the gravitational pull of its companion. A similar effect was encountered for the short-period variable subdwarf B star KPD 1930+2752 (Billères et al. 2000), although in this case the deformation was much more extreme because of the greater proximity of the binary components.

6.4 MODELLING THE VARIATIONS OF PG 0101+039

The three convincing pulsational periods (f_1 to f_3) as well as the signature of the ellipsoidal variation and its first harmonic ($e1$ and $e2$) are listed in Table 6.1 in order of descending amplitude. While the amplitudes and phases of the oscillations are associated with formal errors due to the least-square fitting process to the lightcurve, the frequencies are derived directly from the Fourier transform, which provides no formal error estimates. The accuracy of the frequencies extracted should however be of the order of 1/10th of the resolution, i.e. about 0.1 μHz. Considering the periodicities arising from the ellipsoidal deformation of the subdwarf (e_1 and e_2) then yields a photometrically determined binary period of $P_{\rm orb} = 0.571 \pm 0.001$ days, marginally longer than, but still in accordance with that found from spectroscopy. While

[11] Following the theory developed by Hansen, Winget, & Kawaler (1985) for the case of white dwarfs and adapting it to our equilibrium model of PG 0101+039, we calculated that oscillations will be lost if their periods lie above the cut-off period for g-modes $P_g \sim 23,000/\sqrt{l(l+1)}$ s.

this strongly supports the assumed notion of a binary-synchronous rotation rate, the data show no convincing evidence for rotational splitting of the harmonic pulsation frequencies. Lifting the m-fold degeneracy of a mode with indices k and l by breaking spherical symmetry should result in a frequency multiplet whose components are separated by

$$\Delta f = \frac{(1 - C_{kl})}{P_{\rm rot}}, \tag{6.1}$$

where $P_{\rm rot}$ is the rotation period and

$$C_{kl} \sim \frac{1}{(l(l+1))} \tag{6.2}$$

in the limit where $k >> 1$ (see below for a justification of this assumption for PG 1716 stars). Apart from a peak at 2724 s (0.3671 mHz), which potentially constitutes the $m = -1$ component of the oscillation at 2650 s (f_2) and would imply an $l = 1$ mode, we find no indication of such splittings, which is probably due to their low amplitudes compared to the noise level. While this is disappointing from the point of view of constraining the modes' degree indices using the frequency spacing of a given multiplet, it does mean that the pulsation frequencies detected constitute independent harmonic oscillations and can be directly compared to the theoretical period spectrum.

We construct a model representative of PG 0101+039 with an effective temperature $T_{\rm eff} =$ 28,400 K, a surface gravity $\log g = 5.53$, a total mass $M_*/M_\odot = 0.48$ and the transition between the helium core and the hydrogen-rich envelope located at a logarithmic depth $\log q(H) = -2.70$. Based on the same numerical tools employed by Charpinet et al. (1997; see also Fontaine et al. 1998; Charpinet et al. 2001, and Fontaine et al. 2003) for the construction of their "second-generation" models, it features an opacity profile that largely depends on the non-uniform distribution of iron as a function of depth, computed by considering the competitive action of gravitational settling and radiative levitation on traces of iron in a pure hydrogen background. It is the precise shape of the resulting opacity profile that determines whether or not the kappa mechanism can operate effectively and thus generate the energy needed to drive oscillations. Since non-adiabatic calculations do not predict unstable modes with

degree indices $l \leq 8$ in our model, we focus on the theoretical period spectrum obtained from adiabatic oscillation computations. Figure 6.4 compares the periods detected in the lightcurve of PG 0101+039 to those calculated in the range 2000−8000 s on the basis of modes with degree indices $l = 1$−4. The predicted oscillations correspond to g-modes with high radial orders of $k \sim 10 - 55$. Although the precise values of the computed periods may vary with the atmospheric parameters of the model, the qualitative picture does not change noticeably within the spectroscopic uncertainties. It is immediately obvious that the observed periods are vastly outnumbered by those computed in the same range, even if only more readily visible modes with $l = 1$ and 2 are considered. The question is whether this is due to the observational constraints placed by the noise level of the data and could be overcome by more sensitive observations, or whether the excitation mechanism does simply not generate enough energy to drive all the modes in the period range. Even if a combination of the two is true, it is clear that unique mode identification in this star represents a major challenge and will require both additional observed periodicities and independent constraints on their degree indices, be it on the basis of multi-colour photometry (see e.g. Randall et al. 2005), time-series spectroscopy (see e.g. O'Toole et al. 2003), or the interpretation of rotational splitting (see e.g. Charpinet et al. 2005).

6.5 CONCLUSION

The analysis of ∼ 400 hours of MOST photometry for the long-period variable subdwarf B star PG 0101+039 uncovered 3 convincing stellar oscillations with periods in the 2650−7250 s range, as well as evidence for an ellipsoidal deformation of the subdwarf due to the gravitational pull of its binary companion. While the latter implies a binary-synchronous rotation rate as was to be expected from evolutionary scenarios, we were not able to detect the corresponding rotational splitting. The amplitudes of the pulsations extracted all lie below 0.06% of the star's mean brightness, significantly lower than those reported for the other three (cooler) PG 1716 stars monitored to date. According to current non-adiabatic theory, this observed trend of oscillation amplitudes decreasing with the effective temperature of the target can be explained by the fact that hotter models excite modes with a successively higher minimum

degree index l, and the brightness variations integrated over the visible disk thus diminish. Our models also recover the tendency for hotter PG 1716 stars to excite shorter periods than their cooler counterparts, albeit on a relative rather than an absolute scale. In particular, the theoretical range of instability consistently underestimates the range of periods observed for a given target.

The most serious shortcoming of our models is probably their inability to excite modes with "acceptable" degree indices (i.e., $l \leq 4$) over a substantial part of the atmospheric parameter range where real PG 1716 stars are found. The very fact that we detected long-period variations in a subdwarf B star as hot as PG 0101+039 is in conflict with predictions. According to theory, a model with the appropriate atmospheric parameters is able to excite only modes with degree indices $l \geq 9$, which we must concede would most likely not be observable even in the best of circumstances. Unlike for previous targets, where periods with $l \leq 3$ or 4 could be inferred by pushing the stars' atmospheric parameters to the lower end of the uncertainty on their estimates, the accuracy and high values of our spectroscopic determination of $\log g$ and $T_{\rm eff}$ for PG 0101+039 do not allow this. It is thus beyond doubt that our current PG 1716 models are subject to a real blue-edge problem, and will have to be refined if the oscillations detected in the lightcurve of PG 0101+039 are to be explained. One particularly promising idea that we are now investigating in Montréal is to include helium in the iron levitation calculations, which are currently effected assuming a pure hydrogen background. While preliminary computations indicate that this will significantly influence the iron abundance profile and hence have an impact on the opacity driving mechanism, it is not certain whether the instability strip will shift in the right direction. This can only be answered by detailed modelling, a discussion of which is beyond the scope of this Paper and will be presented elsewhere.

Beyond the implications for the study of long-period variable subdwarf B stars, the data obtained for PG 0101+039 have demonstrated that MOST can detect oscillations with $\sim$ 0.5 milli-magnitude amplitudes in a twelfth magnitude star from observations lasting just over two weeks. Considering that the satellite was primarily designed to monitor targets brighter than sixth magnitude, this is a considerable achievement and should constitute an

incentive for future MOST missions dedicated to subdwarf B stars. In particular, it would be extremely interesting to monitor a slightly cooler PG 1716 star with higher amplitude oscillations for the full 8 weeks that MOST can focus on a single target without interruption. It is almost certain that the resulting data would surpass anything obtainable from ground-based photometry as far as coverage and frequency resolution are concerned. Indeed, long-period variable subdwarf B stars make ideal targets for space-based observations as the data gaps and atmospheric brightness variations inherent to time-series photometry obtained at ground level often prevent the unambiguous identification of pulsation frequencies. Currently the only orbiting space telescope dedicated to asteroseismology, MOST may well hold the key to exploiting the period spectrum exhibited by these stars.

This work was supported in part by the Natural Sciences and Engineering Research Council of Canada and by the Fonds de recherche sur la nature et les technologies (Québec). G.F. also acknowledges the contribution of the Canada Research Chair Program. R.K.'s contributions are funded by the Canadian space agency.

6.6 TABLES

TABLE 6.1 – Oscillations Detected in the Lightcurve of PG 0101+039

	Frequency (mHz)	Period (s)	Amplitude (%)	Phase (rad)
f_1	0.1913	5227	0.054 ± 0.006	3917 ± 88
f_2	0.3774	2650	0.041 ± 0.006	707 ± 62
f_3	0.1382	7235	0.038 ± 0.006	4882 ± 182
e_1	0.0405	24,687	0.034 ± 0.006	10019 ± 665
e_2	0.0810	12,344	0.029 ± 0.006	1209 ± 405

6.7 REFERENCES

Bergeron, P., Wesemael, F., Beauchamp, A., Wood, M.A., Lamontagne, R., Fontaine, G., & Liebert, J. 1994, ApJ, 432, 305

Billères, M., Fontaine, G. Brassard, P., Charpinet, S., Liebert, J., and Saffer, R.A. 2000, ApJ, 530, 441

Brassard, P., Fontaine, G., Billères, M., Charpinet, S., Liebert, J., & Saffer, R.A. 2001, ApJ, 563, 1013

Charpinet, S., Fontaine, G., Brassard, P., Billères, M., Green, E.M., & Chayer, P. 2005, A&A, in press

Charpinet, S., Fontaine, G., Brassard, P., Green, E.M., and Chayer, P. 2005, A&A, 437, 575

Charpinet, S., Fontaine, G., & Brassard, P. 2003, in NATO ASIB Proc. 105: White Dwarfs, 69

Charpinet, S. Fontaine, G., & Brassard, P. 2001, PASP, 113, 785

Charpinet, S., Fontaine, G., Brassard, P., Chayer, P., Rogers, F.J., Iglesias, C.A., & Dorman, B. 1997, ApJ, 483, L123

Charpinet, S., Fontaine, G., Brassard, P., & Dorman, B. 1996, ApJ, 471, L103

Dorman, B. 1995, in Proc. 32d Liège Astrophys. Colloq., Stellar Evolution: What Should be Done?, ed. A. Noels, D. Fraipont-Caro, M. Gabriel, N. Grevesse, & P, Demarque (Liège: Institut d'Astrophysique), 291

Fontaine, G., Brassard, P., Charpinet, S., Green, E.M., Chayer, P., Billères, M., & Randall, S.K. 2003, ApJ, 597, 518

Fontaine, G., Charpinet, S., Brassard, P., Chayer, P., Rogers, F.J., Iglesias, C.A., & Dorman, B. 1998, in IAU Symposium No. 185, New Eyes to See Inside the Sun and Stars, ed. F.-L. Deubner, J. CHristensen-Dalsgaard and D. Kurtz, Kyoto, Japan, 18-22 August 1997, p. 367

Green, E.M., Fontaine, G., Reed, M.D., Callerame, K., Seitenzahl, I.R., White, B.A., Hyde, E.A., Østensen, R., Cordes, O., Brassard, P., Falter, S., Jeffery, E.J., Dreizler, S., Schuh, S.L., Giovanni, M., Edelmann, H., J. Rigby, & Bronowska, A. 2003, ApJ, 583, L31

Hansen, C.J., Winget, D.E., and Kawaler, S. 1985, ApJ, 297, 544

Heber, U. 1986, A&A, 155, 33

Kilkenny, D., Koen, C., O'Donoghue, D., & Stobie, R.S. 1997, MNRAS, 285, 640-644

Maxted, P.F.L., Marsh, T.R., Heber, U., Morales-Rueda, L., North, R.C., & Lawson, W.A. 2002, MNRAS, 333, 231

Moran, C., Maxted, P., Marsh, T.R., Saffer, R.A., & Livio, M. 1999, MNRAS, 304, 535

O'Toole, S.J., Jorgensen, M.S., Kjeldsen, H., Bedding, T.R., Dall, T.H., & Heber, U. 2003, MNRAS, 340, 856

Randall, S.K., Fontaine, G., Brassard, P., & Bergeron, P., 2005, ApJSS, in press

Randall, S., Fontaine, G., Green, E., Kilkenny, D., Crause, L., Cordes, O., O'Toole, S., Kiss, L., For, B.-Q. & Quirion, P.-O. 2004a, Ap&SS, 291, 465

Randall, S.K., Fontaine, G., Green, E.M., Brassard, P., & Terndrup, D.M. 2004b, Proceedings of the SOHO 14/GONG 2004 Workshop (ESA SP-559). "Helio- and Asteroseismology: Towards a Golden Future". 12-16 July 2004, New Haven, Connecticut, USA. Ed. D. Danesy, p. 119

Reed, M.D., Green, E.M., Callerame, K., Seitenzahl, I.R., White, B.A., Hyde, E. A., Giovanni, M. K., Østensen, R., Bronowska, A., Jeffery, E.J., Cordes, O., Falter, S., Edelmann, H., Dreizler, S. and Schuh, S.L., 2004, ApJ, 607, 445

Saffer, R., Bergeron, P., Koester, D. and Liebert, J., 1994, ApJ, 432, 351

Walker, G.A.H., Matthews, J.M., Kuschnig, R., Johnson, R., Rucinski, S., Pazder, J., Burley, G., Walker, A., Skaret, K., Zee, R., Grocott, S., Carroll, K., Sinclair, P., Sturgeon, D., Harron, J., 2003, PASP, 115, 1023

6.8 FIGURES

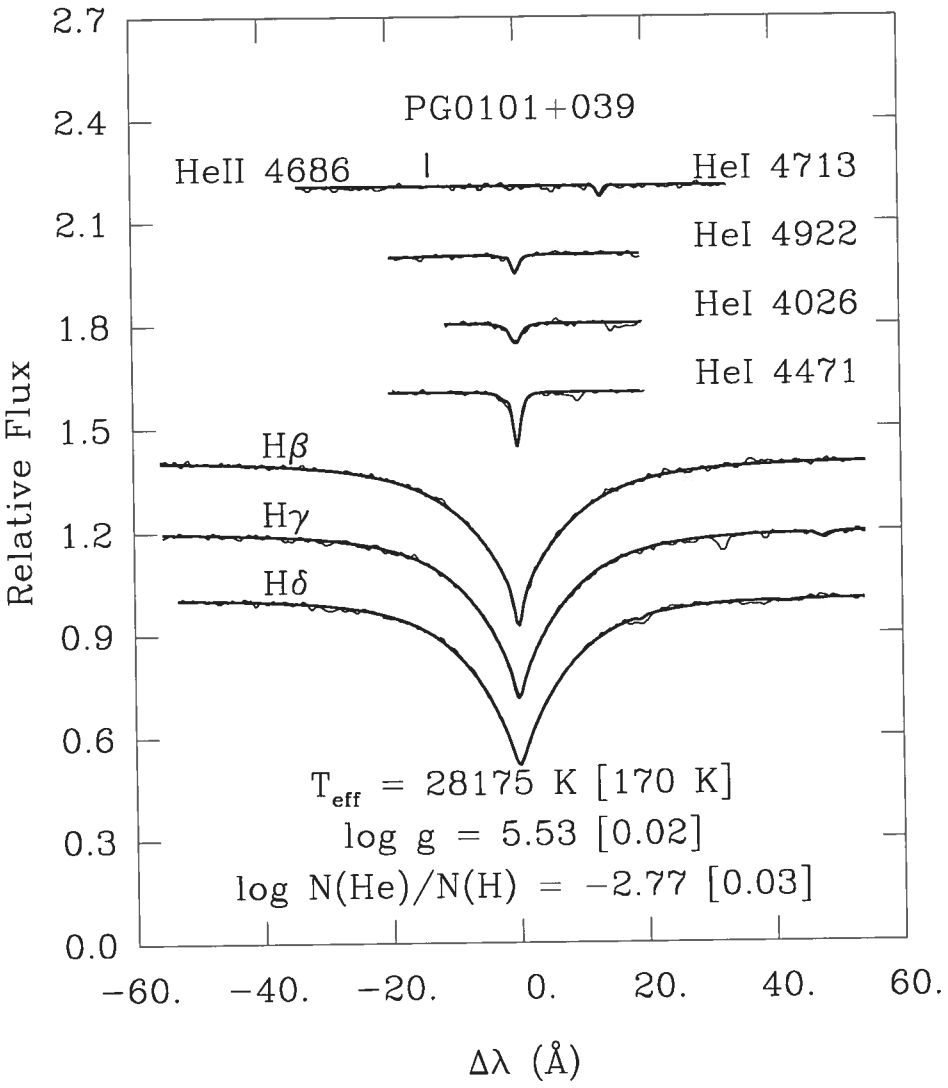

FIGURE 6.1 – Model fit (thick curve) to the available hydrogen Balmer and helium lines in our MMT spectrum of PG 0101+039.

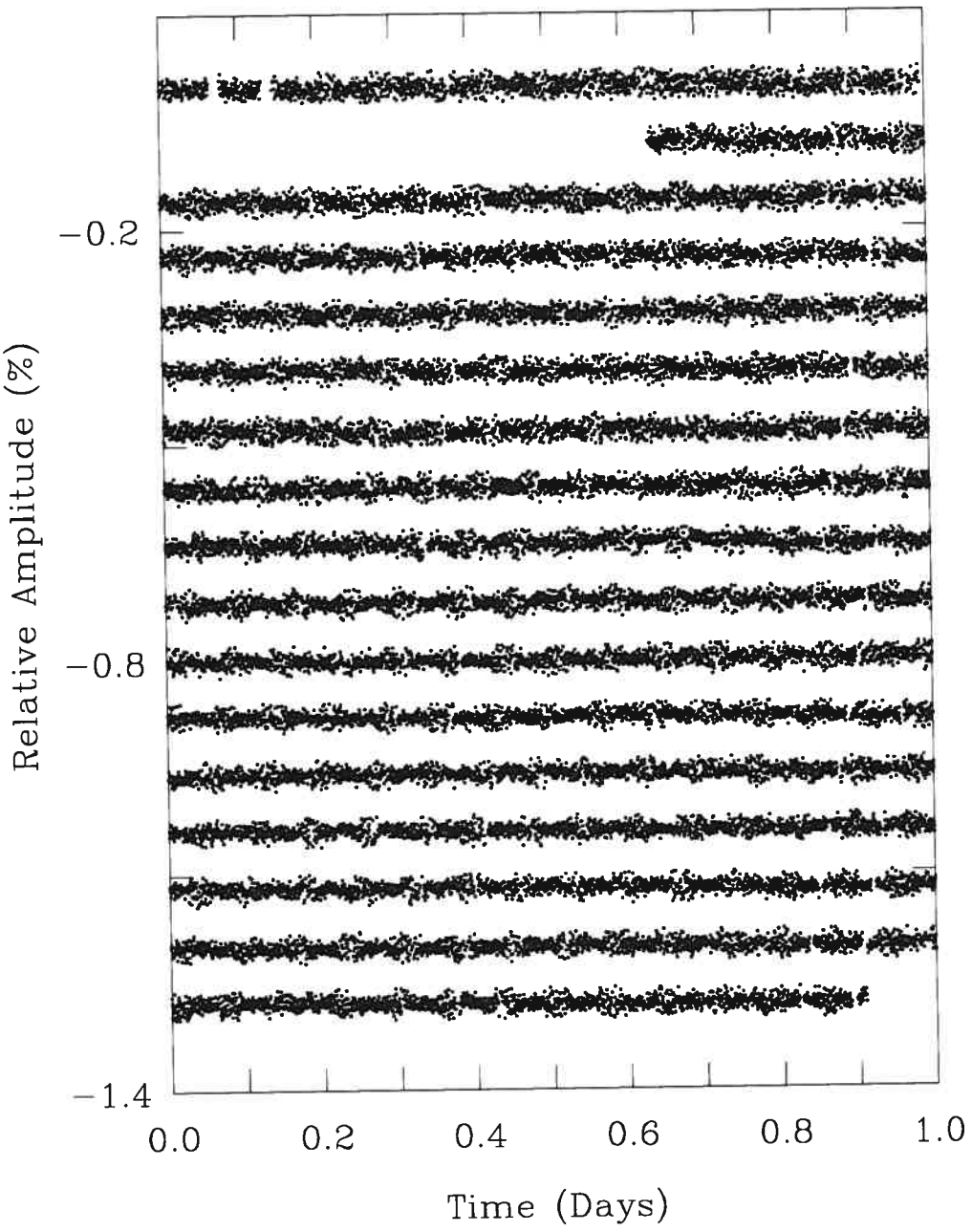

FIGURE 6.2 – MOST photometry of PG 0101+039 on an absolute timescale. The top row covers the first 24-hour period of the run, and the data for subsequent days have been shifted downwards arbitrarily for visualisation purposes. The lightcurve has been corrected for outliers, general long term trends and straylight variations due to the orbit of MOST. The latter produces a period of elevated scatter every 101.413 minutes, which is discernable from the lightcurve.

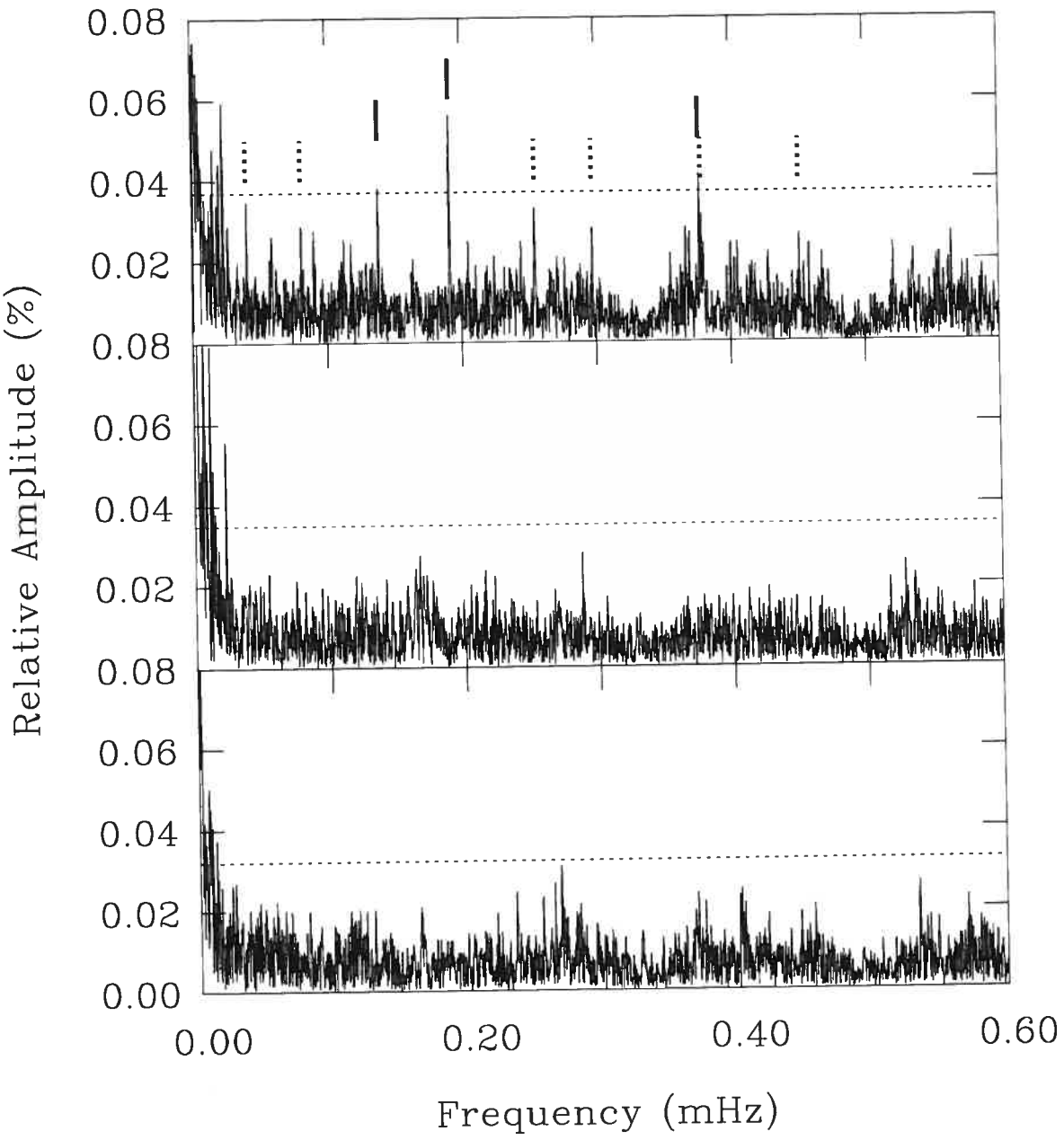

FIGURE 6.3 – Fourier amplitude spectra of PG 0101+039 (top panel) and the two comparison stars GSC 00022-01077 (middle panel) and GSC 00022-01060 (bottom panel) in the 0–0.6 mHz bandpass. The dotted horizontal line indicates the adopted threshold of four times the mean noise level for each dataset. In the plot for PG 0101+039 we have indicated the convincing periodicities detected (continuous vertical line segments) as well as other potential oscillations with amplitudes above three times the mean noise level (dotted vertical line segments).

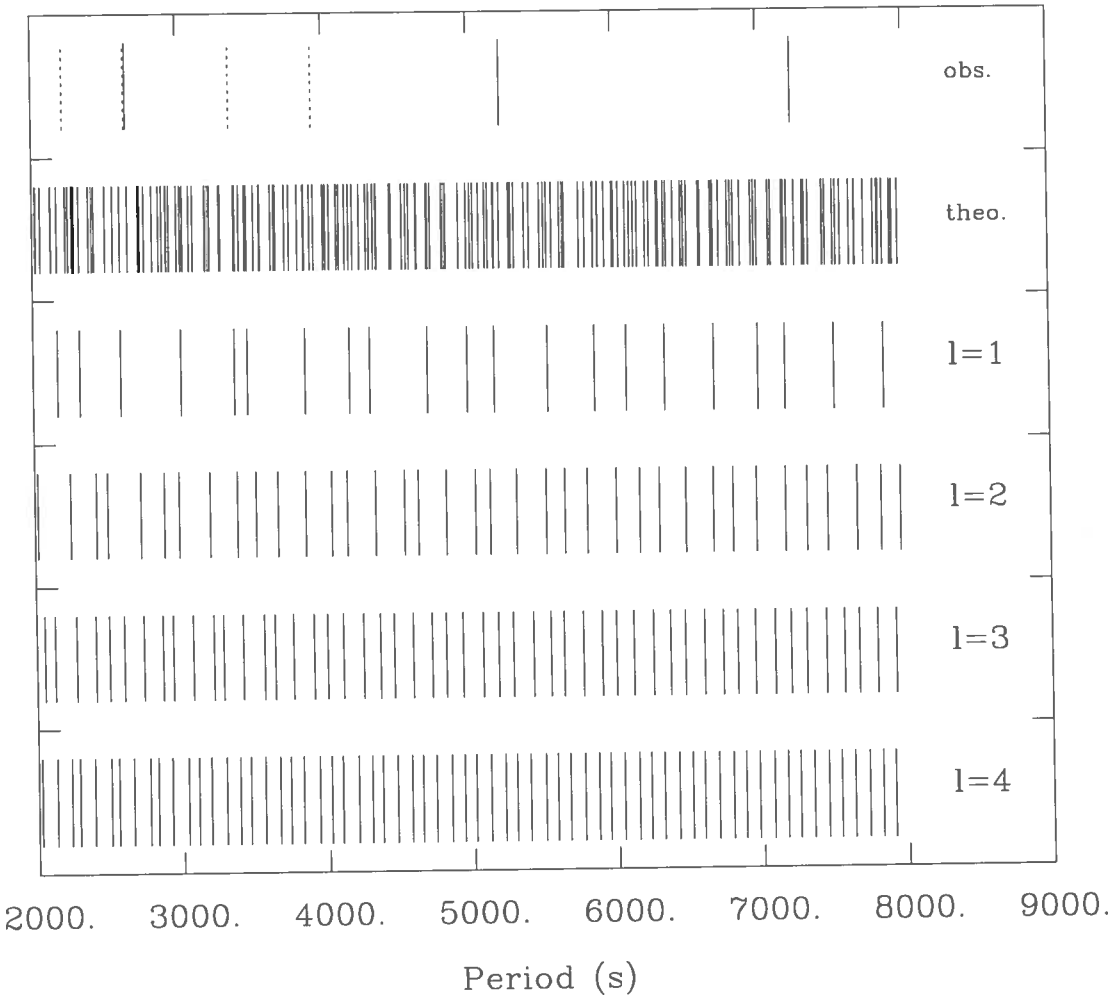

FIGURE 6.4 – Theoretical pulsation spectrum of a model representative of PG 0101+039 with $T_{\rm eff}$ = 28,400 K, $\log g$ = 5.53, $M_*/M_\odot$ = 0.48 and $\log q(H)$ = −2.70. All pulsation modes with l = 1, 2, 3 and 4 in the 2000−8000 s interval are indicated. Modes with different degree indices l are illustrated both separately and as part of the total theoretical spectrum. This is to be compared to the values of the stellar pulsation modes listed in Table 6.1 (continuous line segments) and the other potential oscillations indicated in Figure 6.3 (dotted line segments).

Chapter 7

CONCLUSION

The main aim of the thesis presented here was to establish an observational and theoretical basis for the asteroseismological interpretation of long-period variable subdwarf B stars. At the time I started my PhD, the class of Betsy stars had only just been discovered, whereas the first EC 14026 star had already been analysed quantitatively. Considering the success of asteroseismology for the rapid oscillators, it seemed feasible to apply the same technique to the slow variables and thus gain a deeper understanding of a larger proportion of subdwarf B stars. It was the objective of this thesis to assess the potential of such studies for the long-period variables.

After summarising the status quo on subdwarf B stars and introducing basic pulsation theory in Chapter 1, we first presented an asteroseismological analysis of the fast pulsator EC 20117−4014 on the basis of photometry acquired at the South African Astronomical Observatory (SAAO) and La Silla, Chile (Chapter 2). While we were not able to extract any oscillations beyond the three detected previously, the latter proved sufficient for the isolation of a well-defined family of optimal models in 3-dimensional $\log g - M_* - \log q(\mathrm{H})$ parameter space at the constant effective temperature provided by spectroscopy. The solution obtained was consistent with both non-adiabatic pulsation theory and spectroscopic estimates of the surface gravity, and reproduced the observed period spectrum to the measurement accuracy in terms of low radial order modes with degree indices of $l = 0$ and 1. Considering the fact that EC 20117−4014 constitutes the fifth rapidly pulsating subdwarf for which asteroseismology

has been successful, we conclude that the basic physics of our second generation models is sound, although there is certainly room for improvement at the quantitative level. Another implication of the result achieved is that, given reliable spectroscopic estimates of a target's atmospheric parameters, asteroseismology may well be possible on the basis of fewer observed periods than previously assumed. While EC 20117−4014 as a particularly compact subdwarf B star is in this sense an ideal target due to the comparatively low density of the theoretical period spectrum, it is conceivable that other EC 14026 stars can be exploited in a similar way without necessitating further observations. This could help provide more representative statistics on the structure of subdwarf B stars in the short term.

In Chapter 3 we investigated the dependence of a pulsation mode's amplitude-wavelength behaviour on its degree index l for both short- and long-period variable subdwarf B stars. The aim of this largely theoretical study was to assess the potential of multi-colour photometry for partial mode identification. It was hoped that for the EC 14026 stars the resulting constraints could be employed to cross-check the mode identification inferred from asteroseismology, while for the Betsy stars they would be used to place necessary limitations on the nature of the modes before attempting any quantitative analysis. Using state-of-the-art model atmospheres and considering non-adiabatic effects in detail, we developed a method of obtaining the theoretical relative pulsational amplitudes and phases to unprecedented accuracy for any sdB if provided with its atmospheric parameters. Test calculations for representative EC 14026 and Betsy star models showed that the phases hold virtually no discriminative power, and that the amplitude-wavelength behaviour is quite similar for the most visible modes with $l = 0$, 1 and 2, while differing substantially for higher degree oscillations. Consequently, the observational accuracy achieved from multi-colour photometry is rarely sufficient to discriminate between the lowest degree modes. Pulsations with $l = 3$ on the other hand have been ruled out for all the targets observed to date, and $l = 4$ modes have been inferred in two cases. The only low-degree mode whose l-index has been unambiguously identified within the formal measurement errors is the 182.4-s periodicity of KPD 2109+4401, which was observed on the 4.2-m William Herschel Telescope using *ULTRACAM* (Jeffery et al. 2004) and determined to be associated with $l = 0$ in the paper included here. However, if the uncertainty on the observational value is doubled

(which is feasible as the formal errors consistently underestimate the true errors), we can no longer exclude the possibility of the pulsation corresponding to $l = 1$. It is therefore clear that we will require more sensitive observations if the oscillatory amplitude-wavelength behaviour in subdwarf B stars is to be exploited fully for mode identification. Given that excellent UBV photometry of the rapid variable PG 1219+534 obtained at the 3.6-m Canada-France-Hawaii telescope yielded ambiguous results, we will most likely need to turn to 8-m class telescopes. One promising option is the VLT in conjunction with *ULTRACAM*, which currently enjoys visitor status at Paranal. Just one or two nights of observation time on a rapidly pulsating subdwarf could be enough to accurately determine the degree indices of at least the dominant modes, thus providing an invaluable consistency check for asteroseismology.

The remaining sections of this thesis (Chapters 4–6) were dedicated to the observation and subsequent analysis of long-period variable subdwarf B stars. In Chapter 4 we presented the first in-depth study of a Betsy star, in this case PG 1627+017. Around 300 hours of R band photometry proved sufficient for the extraction of 23 oscillations in the 4500–8900 s range, with amplitudes between 0.05 and 0.5 % of the star's mean brightness. However, it was not entirely clear which of these constituted independent harmonic oscillations and which were due to rotational splitting. One of the more convincing scenarios involved a binary-synchronous rotation rate and the splitting of the four highest amplitude peaks with frequency spacings characteristic of dipole modes. Using the assertion that the dominant oscillations correspond to $l = 1$ modes and that three of them have consecutive values of k (as indicated by their relatively even spacing in period), we attempted a quantitative exploration of $M_* - \log q(\mathrm{H}) - \log q(\mathrm{He})$ space at the constant values of T_{eff} and $\log g$ suggested from spectroscopy. This yielded a relatively small number of optimal model families that could reproduce the four high-amplitude period to within a few seconds. While the result achieved was deemed encouraging, it was obvious that a full asteroseismological analysis objectively inferring the fundamental parameters of PG 1627+017 was not possible on the basis of the observational information available. Most importantly, the number of periodicities used in the fit was too low to allow the isolation of just one optimal model. Due to difficulties in distinguishing independent harmonic oscillations from rotationally split components we had decided to use only the very

highest amplitude oscillations during the asteroseismological exercise. Moreover, we could not be certain that the a priori conditions imposed on the mode identification were justified, since they were based mostly on the assumption that the selected rotational splitting scenario was accurate. Therefore, it was decided that any further observational campaign on a Betsy star should focus on a slowly rotating single or long-period binary target and feature multi-colour photometry for much of its duration. In addition, we hoped to monitor a slow oscillator more representative of the class as a whole than the very cool PG 1627+017.

PG 1338+481, the long-period variable subdwarf discussed in Chapter 5, answered to the desired description perfectly. Around 250 hours of simultaneous U/R photometry, as well as an extra $\sim$ 70 hours of R band data allowed the detection of 13 periodicities thought to constitute independent harmonic oscillations. Relative amplitudes obtained from the two-colour photometry implied degree indices of $l = 1$ for the four dominant pulsations, although $l = 2$ and 4 could not be excluded within the measurement errors. The notion of dipole modes was further supported by the relatively even distribution of six high amplitude peaks with period spacings characteristic of those predicted for $l = 1$ modes with adjacent values of k from representative PG 1338+481 models. We thus launched a search in 5-dimensional parameter space for models that could reproduce these six periodicities in terms of consecutive dipole modes. However, due to strong degeneracies in the behaviour of the theoretical period spectrum with changes in different input parameters we were unable to constrain the regions of parameter space corresponding to potential solutions. It was only by fixing $T_{\rm eff}$ and $\log g$ to the values predicted from spectroscopy that we succeeded in isolating one well-constrained family of optimal models with any confidence. Consequently, the fundamental parameters inferred for PG 1338+481 are only as reliable as the spectroscopic estimates of its atmospheric parameters. The latter are unfortunately associated with significant uncertainties due to systematic problems in establishing a uniform temperature scale for long-period variable subdwarf B stars, particularly towards the cooler end of the distribution. It is clear that the issue will have to be resolved if the asteroseismic potential of the Betsy stars is to be exploited fully. In addition, it would be extremely beneficial if mode identification could be constrained more tightly from the outset than has been the case until now. Given that the 250 hours of simultaneous

U/R photometry obtained for PG 1338+481 did not bring about the accuracy necessary to unambiguously determine the degree index of even the highest amplitude modes, the latter will be challenging to achieve. One option would be to employ a significantly larger telescope, however it is very unlikely that an observing run of the length required (at least 1 month) would be allocated on a medium-size telescope. Another possibility is the exploitation of the greater amplitude-wavelength dependence on l in the UV using space-based observations in conjunction with those obtained from the ground. Unfortunately, this is again difficult from a logistical point of view since *FUSE*, the only satellite currently dedicated to the UV, is slowly dying and there are no plans for its replacement. It is therefore likely that we will have to explore other ways of constraining mode identification in the Betsy stars. Apart from the interpretation of rotationally split components as attempted for PG 1627+017, one potentially interesting method is the analysis of line-profile variations during a pulsation cycle. While this has been explored in recent theoretical efforts (Schoenaers & Lynas-Gray 2005), it is not yet clear whether the method is exploitable observationally.

In view of the difficulties associated with the determination of the l-indices using an independent means, the most promising avenue may well lie in the exploitation of the period spectrum itself. Characteristics such as the uniform spacing between six of the periods detected for PG 1338+481 could be used to impose new constraints, or complement those obtained from multi-colour photometry or rotational splitting. Of course, the detection of any interpretable structure in the period distribution is feasible only if a sufficient number of independent oscillations are extracted from the data, requiring the acquisition of high quality photometry. While our studies of PG 1627+017 and PG 1338+481 have shown that long-term ground based campaigns can yield interesting results, we believe that the future of Betsy star time-series photometry lies in space-based observations. These are more likely to produce the long baseline and high duty cycle required to resolve all frequencies present as well as not being subject to differential extinction. The possibility of monitoring long-period variations in subdwarf B stars using existing space-based facilities was explored in Chapter 6, where we described a 16.9 day trial run on the Betsy star PG 0101+039 with *MOST*, Canada's first space telescope. On the basis of the $\sim$ 400 hours of broadband photometry acquired, we were

able to extract 3 periodicities with amplitudes down to 0.04 % of the star's mean brightness. Although the number of oscillations extracted was too low to attempt any sort of quantitative analysis, this was due to their unusually small intrinsic amplitudes rather than a particularly high noise level in the data. In fact, the S/N achieved by *MOST* after a run lasting only a third of the time that the satellite can monitor well-positioned stars is slightly superior to that resulting from our multi-site campaign on PG 1627+017. While this is partly due to the fact that the latter target is fainter by $\sim$0.8 magnitudes, it is nevertheless clear that *MOST* photometry can rival that obtainable from the ground in terms of signal to noise, and easily surpass it as far as time coverage is concerned. Indeed, the *MOST* data boast a duty cycle of 96.5 % compared to the 33 % achieved for our ambitious multi-site campaign on PG 1627+017. We therefore think that every effort should be made to obtain more space-based photometry for long-period variable subdwarf B stars. At present, *MOST* is the only satellite dedicated to asteroseismology, however a slightly larger space telescope, *COROT*, is due to be launched in 2006. After negotiations with the *MOST* Science Team we believe the chances of further observing time being allocated to Betsy stars are good, and the sky fields monitored by *COROT* are currently set to include two long-period variables. Consequently, we feel that the prospects of successful asteroseismology for slowly oscillating subdwarf B stars are rosy from an observational point of view.

On the theoretical side numerous challenges remain. The work detailed in Chapters 4–6 has shown that our present models are subject to significant deficiencies, as is evidenced by the fact that the observed Betsy star instability strip and the range of periods detected are incompatible with those predicted from non-adiabatic pulsation calculations. Most disconcertingly, we are unable to excite low-degree modes for the hotter long-period variables such as PG 0101+039. Despite these shortcomings, we believe that the basic driving mechanism identified is correct. Certain observational trends, such as the shortening of pulsation periods with increasing effective temperature and the decrease in amplitude as the star becomes more compact are well understood, and recovered by our models. Moreover, the analogy between the EC 14026 / Betsy star phenomenon and the β Cep / SPB pulsators on the main sequence is so strong that significant differences between the operation of their excitation mechanisms

seem unlikely. Therefore, it is more probable that it is the models themselves that are missing certain ingredients. Taking into consideration the fact that the short-period pulsators are well described by the current structures, it seems that the inaccuracies affect the deeper regions of the envelope probed by the g-modes to a greater extent than the shallow layers where the p-modes reach appreciable amplitudes. They are thus in all likelihood related to the fact that our "second-generation" models are static envelope structures that do not include the inner core of the star. While the latter is convective and thus does not lend itself to mode propagation, it is surrounded by a thin semi-convective layer that may well influence gravity mode oscillations, but whose treatment is far from satisfactory in the current envelope models. In order to describe the deep stellar interior more realistically, we will need full evolutionary sequences that incorporate the radiative levitation calculations characteristic of our second generation models. A further improvement would be to calculate the latter not on the basis of iron in a pure hydrogen background as currently assumed, but taking into account traces of helium and other metals. These could significantly influence the number of photons available for the levitation of iron and alter the opacity profile, potentially enabling the excitation of low-degree g-mode oscillations.

Setting aside model deficiencies and observational difficulties, the fact remains that inferring the structural parameters through asteroseismology is more challenging for the Betsy stars than for the short-period variables. Since the high order g-modes observed approach the regime of asymptotic theory, their period distribution is relatively uniform and the traces left by the individual structural quantities are weak. Moreover, the stars observed to date only show us a fraction of the theoretically predicted modes, which further reduces our power of discrimination between different models. We have suggested that the detection of periodicities clustered in certain band passes is due to an unknown mode selection mechanism, which preferentially channels the available pulsation energy into oscillations falling into well-defined frequency ranges. While this cannot be verified by current pulsation calculations based on linear theory, the fact that a similar (if not as pronounced) effect is observed for most EC 14026 stars seems indicative. In this context, it would be interesting to re-observe some of the Betsy stars studied here at a later time to see whether the frequencies and/or ampli-

tudes of the pulsations have changed significantly. An affirmative result would confirm the mode selection hypothesis and also possibly yield more observational periodicities on which to base asteroseismological explorations. Changes in pulsational frequencies and amplitudes over time-scales of a few months or years have already been measured in certain EC 14026 stars (e.g. PG 1605+072, Falter et al. 2003; PG 0014+067, Charpinet et al. 2005c), suggesting a similar behaviour for the long-period variables. Mode selection could also help explain the groups of closely spaced peaks uncovered for both PG 1627+017 and PG 1338+481. The lower amplitude components of a given multiplet would then correspond to higher degree ($l > 1$) modes that are excited to observable amplitudes by virtue of their frequencies falling into a range selected by the energy channelling mechanism, or by resonance with the dipole modes measured at higher integrated amplitudes. Of course, we are working under the assumption that the fine frequency structure detected is inherent to the star rather than caused by observational artefacts. While this seems reasonable considering that the frequency spacing measured for PG 1338+481 is larger than that for PG 1627+017 (as would be expected for a hotter star with fewer theoretical periods), we will have to wait for other Betsy stars to be observed to a similar accuracy in order to be certain.

In conclusion, the thesis presented here has not so much exhaustively analysed long-period variable subdwarf B stars as opened up the field for both observational and theoretical research. At the beginning of my studies in September 2002, all that was known of the Betsy stars was that they showed luminosity variations of the order of one to two hours. Neither the driving mechanism, nor the observational pulsation properties or their potential for asteroseismology were understood. Thanks in part to the work detailed here, this has changed. We are now in a position where we can define observational requirements accurately, address the shortcomings of our models in detail, and begin to work on the asteroseismology of long-period variable subdwarf B stars in earnest. With current computational efforts directed at evolutionary sequences of realistic sdB star models, *MOST* going strong, and *COROT* to be launched next year, exciting times await...

BIBLIOGRAPHY

Aerts, C., Cuypers, J., De Cat, P., Dupret, M.-A., de Ridder, J., Eyer, L., Scuflaire, R., & Waelkens, C. 2004, A&A, 432, 1013

Allard, F., Wesemael, F., Fontaine, G., Bergeron, P., & Lamontagne, R. 1994, AJ, 107, 1565

Altmann, M., de Boer, K.S., Edelmann, H. 2001, AN, 322, 397

Balona, L.A., & Evers, E.A. 1999, MNRAS, 302, 349

Balona, L.A., & Stobie, R.S. 1979, MNRAS, 187, 217

Baran, A., Pigulski, A., Koziel, D., Ogloza, W., Silvotti, R., & Zola, S. 2005, MNRAS, 360, 737

Berger, J. 1963, PASP, 75, 393

Bergeron, P., Wesemael, F., Beauchamp, A., Wood, M.A., Lamontagne, R., Fontaine, G., & Liebert, J. 1994, ApJ, 432, 305

Bessel, M.S. 1990, PASP, 102, 1181

Billères, M., Fontaine, G., Brassard, P., & Liebert, J. 2002, ApJ, 578, 515

Billères, M., Fontaine, G., Brassard, P., Charpinet, S., Liebert, J., & Saffer, R.A. 2000, ApJ, 530, 441

Blanchette, J.-P., Chayer, P., Wesemael, F., Fontaine, G., Fontaine, M., Dupuis, J., Kruk, J.W., & Green, E.M. 2005, Baltic Astronomy, in press

Brassard, P., Fontaine, G., Billères, M., Charpinet, S., Liebert, J., & Saffer, R.A., 2001, ApJ, 563, 1013

Brassard, P., Fontaine, G., & Wesemael, F. 1995, ApJS, 96, 545

Brassard, P., & Fontaine, G. 1994, in IAU Colloq. 147, The Equation of state in Astrophysics, ed. G. Chabrier and E. Schatzman (Cambridge Univ. Press), 560

Brassard, P., Pelletier, C., Fontaine, G., & Wesemael, F. 1992, ApJS, 80, 725

Breger, M. & Bischof, K.M. 2002, A&A, 385, 537

Breger, M., Handler, G., Garrido, R., Audard, N., Beichbuchner, F., Zima, W., Paparo, M., Zhi-Ping, L., Shi-Yang, J., Zong-li, L., Ai-ying, Z., Pikall, H., Stankov, A., Guzik, J.A., Sperl, M., Krzesinski, J., Ogloza, W., Pajdosz, G., Zola, S., Serkowitsch, E., Reegen, P., Rumpf, T., & Schmalwieser, A. 1997, A&A, 324, 566

Buta, R.J., & Smith, M.A. 1979, ApJ, 232, 213

Castellani, V., Degl'Innocenti, S., & Pulone, L. 1995, ApJ, 446, 228

Charpinet, S., Fontaine, G., Brassard, P., Chayer, P., & Green, E.M. 2005, Baltic Astronomy, in press

Charpinet, S., Fontaine, G., Brassard, P., Green, E.M., & Chayer, P. 2005a, A&A, 437, 575

Charpinet, S., Fontaine, G., Brassard, P., Billères, M., Green, E.M., & Chayer, P. 2005b, A&A, in press

Charpinet, S., Fontaine, G., Brassard, P., Billères, M., Green, E.M., Chayer, P. 2005c, 14th European Workshop on White Dwarfs, ASP Conf. Series, Vol. 334. Proceedings of a meeting held at Kiel, July 19-23 2004, ed. D. Koester and S. Moehler. San Francisco: ASP 2005, p. 619

Charpinet, S., Fontaine, G., & Brassard, P. 2003, in White Dwarfs, proceedings of the conference held at the Astronomical Observatory of Capodimonte, Napoli, Italy. Ed. D. de Martino, R. Silvotti, J.-E. Solheim and R. Kalytis, Kluwer Academic Publishers. NATO Science Series II - Mathematics, Physics and Chemistry, Vol. 105, p. 69

Charpinet, S., Fontaine, G., Brassard, P., & Dorman, B., 2002, ApJS, 139, 487

Charpinet, S., Fontaine, G., Brassard, P., & Dorman, B., 2002b, ApJS, 140, 469

Charpinet, S., Fontaine, G., & Brassard, P. 2001, PASP, 113, 775

Charpinet, S., Fontaine, G., Brassard, P., & Dorman, B. 2000, ApJS, 131, 775

Charpinet, Stéphane 1998, PhD thesis, Universié de Montréal

Charpinet, S., Fontaine, G., Brassard, P., Chayer, P., Rogers, F.J., Iglesias, C.A., & Dorman, B. 1997, ApJ, 483, L123

Charpinet, S., Fontaine, G., Brassard, P., & Dorman, B. 1996, ApJ, 471, L103

Chayer, P., Fontaine, G., Fontaine, M., Lamontagne, R., Wesemael, F., Dupuis, J., Heber, U., Napiwotzki, R., & Moehler, S. 2004, Ap&SS, 291, 359

Chayer, P., Vennes, S., Pradhan, A.K., Thejll, P., Beauchamp, A., Fontaine, G., Wesemael, F. 1996, Astrophysics in the extreme ultraviolet. Proceedings of colloquium no. 152 of the International Astronomical Union; held in Berkeley; California; March 27-30; 1995; Dordrecht: Kluwer Academic Publ.; 1996; edited by Stuart Bowyer and Roger F. Malina, p.211

Chavira, E. 1958, Bol. Obs. Tonantzintla y Tacubaya, 17, 15

Cox, J.P. (1980). *"Theory of Stellar Pulsations"*. Princeton University Press.

Cugier, H., & Daszyńska, J. 2001, A&A, 377, 113

Cugier, H., Dziembowski, W., & Pamyatnykh, A.A. 1994, A&A, 291, 143

D'Cruz, N.L., Dorman, B., Rood, R.T., & O'Connell, R.W. 1996, ApJ, 466, 359

De Cat, P., Briquet, M., Daszyńska-Daskiewicz, J., Dupret, M.-A., de Ridder, J., Scuflaire, R., & Aerts, C. 2005, A&A, 432, 1013

Dorman, B. 1996, "Horizontal Branch Stellar Evolution", p. 291. 32nd Liège strophysical Colloquium. eds A. Noels, N. Grevesse, M. Gabriel, & P. Demarque.

Dorman, B. 1995, in Proc. 32d Liège Astrophys. Colloq., Stellar Evolution: What Should be Done?, ed. A. Noels, D. Fraipont-Caro, M. Gabriel, N. Grevesse, & P, Demarque (Liège: Institut d'Astrophysique), 291

Dorman, B., Rood, R.T., & O'Connell, R.W. 1993, ApJ, 419, 596

Dreizler, S., Schuh, S.L., Deetjen, J.L., Edelmann, H., & Heber, U., 2002, A&A, 386, 249

Dreizler, S. 1993, in NATO ASI series 403, White Dwarfs: Advances in Observations and Theory, ed. M.A. Barstow (Dordretch: Kluwer), 287

Dupret, M.-A. 2001, A&A, 366, 166

Dupret, M.-A., De Ridder, J., De Cat, P., Aerts, C., Scufflaire, R., Noels, A., & Thoul, A. 2003, A&A, 398, 677

Dziembowski, W.A., & Pamyatnykh, A.A. 1993, MNRAS, 262, 204

Dziembowski, W.A., Moskalik, P., & Pamyatnykh, A.A. 1993, MNRAS, 265, 588

Dziembowski, W., 1977, Acta Astron. 27, 203

Falter, S., Heber, U., Dreizler, S., Schuch, S.L., Cordes, O., & Edelmann, H. 2003, A&A, 401, 289

Faulkner, J. 1972, ApJ, 173, 401

Feige, J. 1958, ApJ, 128, 267

Fontaine, G., Green, E.M., Chayer, P., Brassard, P., Charpinet, S., & Randall, S.K. 2005, Baltic Astronomy, in press

Fontaine, G., Green, E.M., Brassard, P., Charpinet, S., Chayer, P., Billères, M., Randall, S.K., & Dorman, B. 2004, Ap&SS, 291, 379

Fontaine, G., Brassard, P., Charpinet, S., Green. E.M., Chayer, P., Billères, M., & Randall, S.K. 2003, ApJ, 597, 534

Fontaine, G., Brassard, P., Charpinet, S., Green, E.M., & Willems, B., 2003a, in Asteroseismology across the H-R diagram. Proceedings of the Asteroseismology Workshop, Porto, Portugal, 1-5 July, 2002. Ed. M.J. Thompson, M.S. Cunha, M.J.P.F.G. Monteiro. Reprinted from *Astrophysics and Space Science,* Vol. 284, No. 1, 2003, Kluwer Academic Publishers, Dordrecht, p. 517-520

Fontaine, G., Brassard, P., & Charpinet, S. 2003b, Ap&SS, 284, 257

Fontaine, G., Charpinet, S., Brassard, P., Chayer, P., Rogers, F.J., Iglesias, C.A., & Dorman, B. 1998, International Astronomical Union. Symposium no. 185. New Eyes to See Inside the Sun and Stars, edited by Franz-Ludwig Deubner, Joergen Christensen-Dalsgaard, and Don Kurtz. Kyoto, Japan, 18-22 August, 1997, p. 367.

Fontaine, G., & Chayer, P. 1997, The third conference on faint blue stars, edited by A.G.D. Philip, J. Liebert, R. Saffer and D.S. Hayes, published by L. Davis Press, p.169

Fontaine, G., Brassard, P., Bergeron, P., & Wesemael, F. 1996, ApJ, 469, 320

Fontaine, G., Brassard, P., Wesemael, F., & Tassoul, M., 1994, ApJ, 428, L61

For, B.-Q., Green, E.M., O'Donoghue, D., Kiss, L.L., Randall, S.K., Fontaine, G., Jacob, A., O'Toole, S.J., Hyde, E.A., & Bedding, T.R. 2006, ApJ, submitted

Gautschy, A., & Saio, H. 1993, MNRAS, 262, 213

Garrido, R., García-Lobo, E., & Rodriguez, E. 1990, A&A, 234, 262

Green, E.M., Callerame, K., Seitenzahl, I.R., White, B.A., Hyde, E.A., Giovanni, M., Reed, M., Fontaine, G., & Østensen, R. 2003, Ap&SS,284,65

Green, E. M., Fontaine, G., Reed, M. D., Callerame, K., Seitenzahl, I. R., White, B. A., Hyde, E. A., Østensen, R., Cordes, O., Brassard, P., Falter, S., Jeffery, E. J., Dreizler, S., Schuh, S. L., Giovanni, M., Edelmann, H., Rigby, J., & Bronowska, A. 2003b, ApJ, 583L, 31

Greenstein, J., & Sargent, A. 1974, ApJSS, 28, 157

Greenstein, J. L. 1960, "Stellar Atmospheres", University of Chicago Press. Ch. 19

Greenstein, J. L., 1966, ApJ, 144, 496

Greggio, L., & Renzini, A. 1990, ApJ, 364, 35

Han, Z., Podsialowski, Ph., Maxted, P.F.L., & Marsh, T.R. 2003, MNRAS, 341, 669

Han, Z., Podsialowski, Ph., Maxted, P.F.L, Marsh, T.R., & Ivanova, N. 2002, MNRAS, 336, 449

Han, Z. 1998, MNRAS, 296, 1019

Hansen, C.J., Winget, D.E., and Kawaler, S. 1985, ApJ, 297, 544

Heber, U. 1991, in IAU Symp. 145, Evolution of stars:The photospheric abundance connection, ed. G. Michaud and A. Tutokov, 363

Heber, U. 1986, A&A, 155, 33

Heynderickx, D., Waelkens, C., & Smeyers, P. 1994, A&A, 105, 447

Humason, M.L., & Zwicky, F. 1947, ApJ, 105, 85

Iben, I., Jr, & Tutukov, A.V. 1986, ApJ, 311, 753

Iriarte, B. & Chavira, E. 1957, Bol. Obs. Tonantzintla y Tacubaya, 16, 3

Jackson, J.D. 1975, Classical Electrodynamics, 2nd ed. (New York: Wiley & Sons)

Jeffery, C.S., Aerts, C., Dhillon, V.S., Marsh, T.R., & Gänsicke, B.T. 2005, MNRAS, 362, 66

Jeffery, C.S., Dhillon, V., Marsh, T., & Ramachandran, B. 2004, MNRAS, 352, 699

Kilkenny, D. 2005, Baltic Astronomy, in press

Kilkenny, D., Reed, M.D., O'Donoghue, D., Kawaler, S., Mukadam, A., Kleinman, S.J., Nitta, A., Metcalfe, T.S., Provencal, J.L., Watson, T.K., Sullivan, D.J., Sullivan, T., Shobbrook, R., Jiang, X.J., Joshi, S., Ashoka, B.N., Seetha, S., Leibowitz, E., Ibbetson, P., Mendelson, H., Meistas, E., Kalytis, R., Alisauskas, D., Martinez, P., van Wyk, F., Stobie, R.S., Marang, F., Zola, S., Kresinski, J., Ogloza, W., Moskalik, P., Silvotti, R., Piccioni, A., Vauclair, G., Dolez, N., Chevreton, M., Dreizler, S., Schuh, S., Deetjen, J.L., Solheim, J.-E., Gonzalez Perez, J.M., Ulla, A., Østensen, R., Manteiga, M., Suarez, O., Burleigh, M., Kepler, S.O., Kanaan, A., & Giovannini, O. 2003, MNRAS, 345, 834

Kilkenny, D. 2002, Radial and Nonradial Pulsations as Probes of Stellar Physics, ASP Conference Proceedings, Vol. 259. Edited by Conny Aerts, Timothy R. Bedding, and Jorgen Christensen-Dalsgaard. Also IAU Colloquium 185. San Francisco: Astronomical Society of the Pacific, 2002., p.356

Kilkenny, D., Billères, M., Stobie, R.S., Fontaine, G., Shobbrook, R.R., O'Donoghue, D., Brassard, P., Sullivan, D.J., Burleigh, M.R., & Barstow, M.A. 2002, MNRAS, 331, 399

Kilkenny, D., Koen, C., O'Donoghue, D., Van Wyk, F., Larson, K.A., Shobbrook, R., Sullivan, D.J., Burleigh, M.R., Dobbie, P.D. and Kawaler, S.D., 1999, MNRAS, 303, 525

Kilkenny, D., O'Donoghue, D., Koen, C., Lynas-Gray, A.E. and Van Wyk, F., 1998, MNRAS, 296, 329

Kilkenny, D., Koen, C., O'Donoghue, D. and Stobie, R., 1997, MNRAS, 285, 640

Kilkenny, D., O'Donoghue, D., Koen, C., Stobie, R.S., & Chen, A. 1997b, MNRAS,287, 867K

Kilkenny, D., Marang, F. and Menzies, J.W., 1994, MNRAS, 267, 535

Koen, C., O'Donoghue, D., Kilkenny, D., Lynas-Gray, A.E., Marang, F., & Van Wyk, F. 1998, MNRAS, 296, 317

Koen, C., 1998 MNRAS, 300, 567

Koen, C., Kilkenny, D., O'Donoghue, D., Van Wyk, F., & Stobie, R.S. 1997, MNRAS, 285, 645

de Kool, M., & Ritter, H. 1993, A&A, 267, 397

Kurucz, R.L. 1993, Atlas9 Stellar Atmosphere Programs, Kurucz CDROM No. 13

Kurtz, D.W. 1990 ARA&A, 28, 607

Lamontagne, R., Demers, S., Wesemael, F., Fontaine, G., & Irwin, M. 2000, AJ, 119, 241

Lasker, B, Sturch, C., McLean, B., Russel, J., Jenkner, H., & Shara, M. 1990, ApJ, 99, 2019

Maxted, P.F.L., Marsh, T.R., Heber, U., Morales-Rueda, L., North, R.C., & Lawson, W.A. 2002, MNRAS, 333, 231

Maxted, P.F.L, Heber, U., Marsh, T.R., & North, R.C. 2001, MNRAS, 326, 1391

Mengel, J.G., Norris, J., & Gross, P.G. 1976, ApJ, 204, 488

Michaud, G., Bergeron, P., Wesemael, F., & Fontaine, G. 1985, ApJ, 299, 741

Montgomery, M.H., & O'Donoghue, D. 1999, in Delta Scuti Star Newsletter, No. 13

Morales-Rueda, L., Maxted, P.F.L., Marsh, T.R., North, R.C., & Heber, U. 2003, MNRAS, 338, 752

Moran, C., Maxted, P., Marsh, T.R., Saffer, R.A., & Livio, M. 1999, MNRAS, 304, 535

O'Donoghue, D., Lynas-Gray, A.E., Kilkenny, D., Stobie, R.S., & Koen, C., 1997, MNRAS, 285, 657

Oreiro, R., Pérez Hernández, F., Ulla, A., Garrido, R., Østensen, R., & MacDonald, J. 2005, A&A, 438, 257

Osaki, Y., 1971, PASJ, 23, 485

O'Toole, S.J., Jorgensen, M.S., Kjeldsen, H., Bedding, T.R., Dall, T.H., & Heber, U. 2003, MNRAS, 340, 856

Press, W.H., Flannery, B.P., Teukolsky, S.A., & Vetterling, W.T. 1986, Numerical Recipes (Cambridge: Cambridge University Press)

Ramachandran, B., Jeffery, C.S., & Townsend, R.H.D. 2004, A&A, 428, 209

Randall, S.K., Fontaine, G., Charpinet, S., Lynas-Gray, A.E., Lopes, I.P., O'Toole, S.J., & Brassard, P. 2006, in preparation

Randall, S.K., Fontaine, G., Green, E.M., Brassard, P., Kilkenny, D., Crause, L., Terndrup, D.M., Daane, A., Kiss, L.L., Jacob, A.P., Bedding, T.R., For, B.-Q., & Quirion, P.-O. 2006, ApJ, submitted

Randall, S.K., Fontaine, G., Brassard, P., & Bergeron, P. 2005a, ApJS, in press

Randall, S.K., Matthews, J.M., Fontaine, G., Rowe, J., Kuschnig, R., Green, E.M., Brassard, P., Chayer, P., Guenther, D.B., Moffat, A.F.J., Rucinski, S., Sasselov, D., Walker, G.A.H., & Weiss, W.W. 2005b, ApJ, 633, 460

Randall, S.K., Fontaine, G., Green, E.M., Kilkenny, D., Crause, L., Cordes, O., O'Toole, S., Kiss, L., For, B.-Q., & Quirion, P.-O. 2004a, Ap&SS, 291, 465

Randall, S.K., Fontaine, G., Green, E.M., Brassard, P., & Terndrup, D.M. 2004b, Proceedings of the SOHO 14/GONG 2004 Workshop (ESA SP-559). "Helio- and Asteroseismology: Towards a Golden Future", ed. D. Danesy, 119

Reed, M.D., Green, E.M., Callerame, K., Seitenzahl, I.R., White, B.A., Hyde, E.A., Giovanni, M.K., Østensen, R., Bronowska, A., Jeffery, E.J., Cordes, O., Falter, S., Edelmann, H., Dreizler, S., & Schuh, S.L. 2004, ApJ, 607, 445

Robinson, E.L., Kepler, S.O., & Nather, R.E. 1982, ApJ, 259, 219

Saffer, R., Bergeron, P., Koester, D., & Liebert, J. 1994, ApJ, 432, 351

Schechter, P.L., Mateo, M., & Saha, A. 1993, PASP, 105, 1342

Schoenaers, C., & Lynas-Gray, A.E. 2005 , Baltic Astronomy, 14, in press

Schuh, S.L., Huber, J., Green, E.M., O'Toole, S.J., Dreizler, S., Heber, U., & Fontaine, G. 2005, in ASP Conf. Ser. 334, 14th European Workshop on White Dwarfs, ed. D. Koester & S. Moehler (San Francisco: ASP), 530

Schuh, S., Huber, J., Dreizler, S., Heber, U., O'Toole, S.J., Green, E.M., & Fontaine, G. 2005b, A&A, submitted

Schuh, S., Huber, J., Dreizler, S., Green, E.M., Stahn, T., Randall, S., Husser, T.-O., Heber, U., O'Toole, S., & Fontaine, G. 2006, Mem.S.A.It., in press

Silvotti, R., Østensen, R., Heber, U., Solheim, J.-E., Dreizler, S., & Altmann, M. 2002, A&A, 383, 239

Silvotti, R., Janulis, R., Schuh, S. L., Charpinet, S., Oswalt, T., Silvestri, N., Gonzalez Perez, J. M., Kalytis, R., Meistas, E., Alisauskas, D., Marinoni, S., Jiang, X. J., Reed, M. D., Riddle, R. L., Bernabei, S., Heber, U., Barnbantner, O., Cordes, O., Dreizler, S., Goehler, E., Østensen, R., Bochanski, J., Carlson, G. 2002, A&A, 389, 180

Stamford, P.A., & Watson, R.D. 1981, Ap&SS, 77, 131

Stobie, R.S., Kawaler, S.D., Kilkenny, D., O'Donoghue, D., & Koen, C. 1997, MNRAS, 285, 651

Stobie, R., Kilkenny, D., & O'Donoghue, D. 1995, ApJ, 230, 101

Stobie, R.S., Chen, A., O'Donoghue, D., & Kilkenny, D. 1992, in Warner B., ed., ASP Conference Series 30, Variable stars and Galaxies, Astron. Soc. Pac., San Francisco, p. 87

Sweigart, A.V. 1997, ApJ, 474, L74

Townsend, R.H.D. 2002, MNRAS, 330, 855

Townsend, R.H.D. 2003, MNRAS, 343, 125

Unno, W., Osaki, Y., Ando, H., Saio, H., & Shibahashi, H. (1989). *Non-radial Oscillations of Stars"*. University of Tokyo Press.

Villeneuve, B., Wesemael, F., Fontaine, G., Carignan, C., & Green, R. 1995, ApJ, 446, 646

Wade, R.A., & Rucinski, S.M. 1985, A&AS, 60, 471

Walker, G.A.H., Matthews, J.M., Kuschnig, R., Johnson, R., Rucinski, S., Pazder, J., Burley, G., Walker, A., Skaret, K., Zee, R., Grocott, S., Carroll, K., Sinclair, P., Sturgeon, D., Harron, J., 2003, PASP, 115, 1023

Watson, R.D. 1988, Ap&SS, 140, 255

Webbink, R.F. 1984, ApJ, 277, 355

Woolf, V. M., Jeffery, C.S., & Pollacco, D.L. 2002, MNRAS, 332, 34

Yi, S., Lee, Y.-W., Woo, J.-H., Park, J.-H., Demarque, P., & Oemler, A., Jr. 1999, ApJ, 513, 128

Yi, S., Demarque, P., & Oemler, A., Jr. 1997, ApJ, 486, 201

Appendix A

A MULTI-SITE CAMPAIGN ON THE LONG-PERIOD VARIABLE SUBDWARF B STAR PG 1627+017

S. Randall, G. Fontaine, E. Green, D. Kilkenny, L. Crause, O. Cordes, S. O'Toole, L. Kiss, B.-Q. For, and P.-O. Quirion

Proceedings of the first meeting on extreme horizontal branch stars and related objects, held in Keele, Staffordshire, England, from 16–20 June 2003

Published in *Astrophysics and Space Science*, Vol. 291, Nos 3-4, 2004

A MULTI-SITE CAMPAIGN ON THE LONG PERIOD VARIABLE SUBDWARF B STAR PG 1627+017

SUZANNA RANDALL[1], GILLES FONTAINE[1], ELIZABETH GREEN[2], DAVE KILKENNY[3], LISA CRAUSE[3], OLIVER CORDES[4], SIMON O'TOOLE[5], LÁZLÓ KISS[6], BI-QING FOR[2] and PIERRE-OLIVIER QUIRION[1]

[1]*Département de Physique, Université de Montréal, C.P. 6128, Succ. Centre-Ville, Montréal, Québec, Canada H3C 3J7;* [redacted]

[2]*Steward Observatory, University of Arizona, Tucson, AZ 8572[redacted] USA*

[3]*South African Astronomical Observatory, PO Box 9, Observatory 7935, Cape Town, South Africa*

[4]*Sternwarte der Universität Bonn, Auf dem Hügel 71, 53121 Bonn, Germany*

[5]*Dr. Remeis Sternwarte, Astronomisches Institut der Universität Erlangen-Nürnberg, Sternwartstr. 7, 96049 Bamberg, Germany*

[6]*School of Physics, University of Sydney, Sydney 2006, Australia*

Abstract. We report on the outcome of the first major multi-site campaign on a long-period variable subdwarf B star. The target PG 1627+017 was observed for a total of 334 h during April/May/June 2003 from the lynchpin observatory at Mt. Bigelow, Arizona, with important contributions coming from co-observations at SAAO, Calar Alto and Siding Spring. Preliminary analysis indicates the presence of 8–10 probable periods in the range ~4500 to ~8900 s with relative amplitudes between 0.1 and 0.5%. The range over which the periods are found is in qualitative agreement with theoretical predictions and the number of periods found shows potential for an in-depth asteroseismological analysis. Multi-colour observations show that the relative amplitudes of pulsation are larger in the U-band than in the R, which again is in agreement with theory. However, more multi-colour observations are needed to be able to make statements at the quantitative level.

Keywords: subdwarfs, pulsations

1. Introduction

Presently, all known pulsating subdwarf B (sdB) stars can be attributed to one of the two groups: the EC 14026 stars, whose pulsations are characterised by short periods, or the more recently discovered long-period pulsators, also known as PG 1716+426 stars. While the EC 14026 stars have been known since 1997 (Kilkenny et al., 1997), the PG 1716+426 stars were only discovered recently in the course of a binary sdB monitoring campaign (Green et al., 2003). These stars appear to be multimode pulsators with typical periods of the order of 1 h and amplitudes of ~1 mmag. They are distinctly cooler than the EC 14026 stars with effective temperatures between 22 000 and 29 000 K and log g between 5.2 and 5.7. Another noteworthy fact is that they are much more common than EC 14026 stars. They are surprisingly numerous among the cooler sdB's and it is indeed possible that all cool subdwarfs show long-period variations at some amplitude level.

Astrophysics and Space Science **291:** 465–471, 2004.

The long periods observed in PG 1716+426 stars automatically imply that we are looking at high radial order g-modes, rather than at p-modes as in the case of the short-period pulsators. It is thought that the excitation mechanism responsible for the long-period variations is the same kappa mechanism that explains the EC 14026 phenomenon (Fontaine et al., 2003). The major difference is that the modes we observe in EC 14026 stars are believed to be of low degree index ($l = 0, 1, 2, 3\ldots$), while only modes with $l = 3$ and upwards can be excited in current PG 1716+426 star models, except in the coolest ones where the excitation extends to modes with $l = 2$ and 1. This is in conflict with canonical wisdom, which suggests that modes with $l \geq 3$ should not be observed due to cancellation effects when integrating over the visible disk of the star.

Although the observed properties of the EC 14026 stars are well documented, the only long-period variable Subdwarf B star that has been monitored in any detail is the class prototype, PG 1716+426. The 81 h of photometry obtained for this star indicate the presence of at least 3–5 modes with periods in the range 0.8–1.4 h, however, the baseline and duty-cycle of the data are not sufficient for detailed analyses. It is clear that the successful observation of a PG 1716+426 star presents different challenges to that of an EC 14026 star. On one hand, significantly larger periods call for a longer baseline and a better duty cycle, making a multi-site campaign the obvious choice. Also, the fact that a typical night will yield only 8–10 cycles means that differential extinction plays an important role. Using an R-filter rather than the more conventional B-filter minimises this problem. On the other hand, exposure times can be longer than for EC 14026 stars, which enables the use of smaller telescopes in the campaign.

2. The Multi-Site Campaign

2.1. PG 1627+017

The target, PG1627+017, is the coolest subdwarf B star known, however estimates of its temperature vary, ranging from 21 600 K (Morales-Rueda et al., 2003) to 25 720 K (preliminary analysis of E.G.'s MMT spectra by G.F.). Similarly, estimates of $\log g$ range from 5.1 to 5.4. PG 1627+017 is part of a binary system with a short period of ~0.83 days (Morales-Rueda et al., 2003). This particular star was chosen for its large-amplitude pulsations, brightness ($V \sim 12.9$, Allard et al., 1994), equatorial location and the number of suitable comparison stars in the field of view.

2.2. Campaign objectives and organisation

The campaign was conducted with three main objectives in mind:

1. The primary goal of the campaign was to photometrically accumulate a sufficient number of cycles to extract the periods of pulsation, the ultimate idea being to

TABLE I

2003 Campaign involvement

Dates	Telescope	Type of observation
9 May–11 June	1.52-m, Mt. Bigelow, Arizona	R-band photometry
17–23 May	1.50-m, Mt. Lemmon, Arizona	U-band photometry
13–20 May	2.3-m, Kitt Peak, Arizona	Spectroscopy
12–19 May	2.2-m, Calar Alto, Spain	Multi-colour photometry
13–19 May	1.9-m, SAAO, South Africa	Spectroscopy
13–22 May	2.3-m, Siding Spring, Australia	R photomety + spectroscopy
20 May–3 June	1.0-m, SAAO, South Africa	R-band photometry
9–13 June	2.0-m, Kitt Peak, Arizona	Spectroscopy

use these in an asteroseismological analysis. Guided by previous campaigns on EC 14026 stars, around 300 h of photometry were deemed adequate for this purpose.

2. In addition to this, we hope to confirm the principal periods of pulsation by measuring the line shifts from simultaneous time-series spectroscopy. However, these results will be reported elsewhere.
3. Following theoretical work on the colour-amplitude relationship in PG 1716+426 stars and its potential for determining the modes' degree indices l, an effort was made to secure multi-colour photometry of PG 1627+017.

Table I shows details of the campaign involvement at different sites. Observational techniques varied from site to site and the data will have to be homogenised before final results can be presented. All results given in this paper refer to the preliminary analysis of the photometry obtained at Mt. Bigelow and Mt. Lemmon only.

3. Preliminary Results

The efforts of the campaign yielded a total of 334 h of R-band photometry, 286 of which lie in the main campaign period 9th May–11th June. This corresponds to a duty cycle of 38.5% over nearly 5 weeks. We achieved a frequency resolution of 0.1 μHz, which implies an error of around 4 s on the dominant periods of pulsation ($\sim$6600 s). In addition to the R data, we also obtained 54 h of multi-colour photometry, 26 of which were taken in the U-filter at Mt. Lemmon and will be discussed here (final multi-colour results will be published elsewhere).

3.1. The R-band photometry

Figure 1 shows two typical lightcurves of PG 1627+017, each spanning roughly 8 h. The change in pulsational amplitude between the two figures is a result of

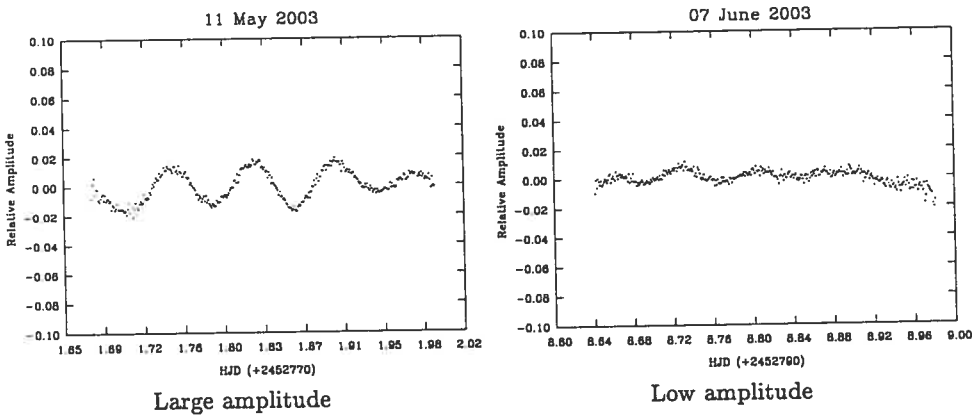

Figure 1. Typical lightcurves of PG 1627+017.

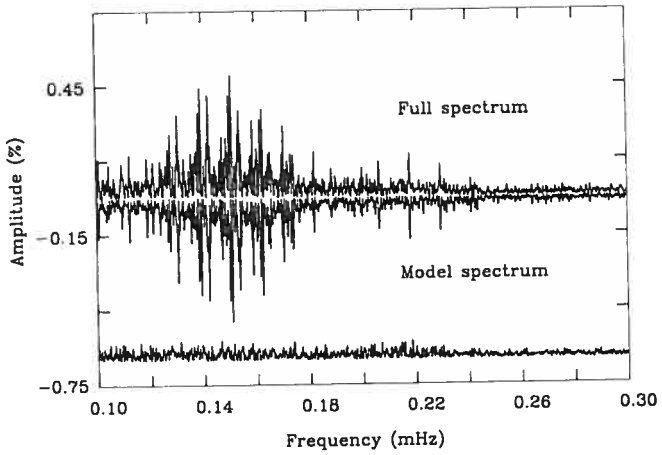

Figure 2. Pre-whitened Fourier transform.

the beating between different modes of pulsation. The Fourier Transform (FT) of all 27 Mt. Bigelow lightcurves combined is illustrated in Figure 2 (top curve). Standard pre-whitening techniques were used to calculate the model FT (middle curve, plotted upside down) and the difference between the observations and the model is given by the residual (bottom curve). The model FT was calculated using 10 preliminary periods, all of which fulfill the rule-of-thumb criterion that they have amplitudes of at least three times the noise level. It can be seen that the model FT shows a remarkable resemblance to that observed and the residual is generally small, even though there may be a few undetected low-amplitude peaks still present.

Table II shows the main periods extracted from the Mt. Bigelow data. We have tentatively identified another 4–6 periods, the nature of which will be verified after

TABLE II
Preliminary periods found for PG 1627+017

Number	Period (s)	Amplitude (%)
P1	6630	0.49
P2	6664	0.39
P3	7035	0.38
P4	6297	0.31

further analysis. All plausible periods found so far lie in the range 4500–8900 s and have amplitudes between 0.1 and 0.5%.

One surprising result is that there seems to be no evidence of rotational splitting, which was expected due to the star's short binary period (0.83 days, Morales-Rueda et al., 2003). Hence an interesting follow-up would be to obtain high-resolution spectroscopy of PG 1627+017 and determine the $v \sin i$ from line broadening. This would answer the question of whether the star is in fact rotating in phase with the binary motion or not.

A qualitative first comparison with theoretical predictions (Fontaine et al., 2003) is made in Figure 3b. The dots represent the theoretical period spectrum of *excited* modes in typical PG 1716+426 star models at different temperatures. They are colour-coded to distinguish modes with different degree indices l (yellow: $l = 2$; green: $l = 3$; red: $l = 4$; indigo: $l = 5$; cyan: $l = 6$; magenta: $l = 7$; black: $l = 8$). In the vertical direction, the superposed black box indicates the range of periods observed, and along the horizontal axis it shows PG 1627+017's temperature uncertainty. We see that a complete overlap of observed and predicted periods is found only if PG 1627+017 has $T_{\rm eff} \leq 22\,000$ K. In that case, the periods observed correspond to modes with $l = 2, 3$ and/or 4. Note that all but the shortest period ($\sim$4500 s) can be explained in terms of $l = 2$ modes (however, the shorter of these periods could just as well be $l = 3$ modes), but the shortest period *must* have $l \geq 3$ to agree with theory. As this goes against canonical wisdom, an independent test is called for. We have developed the theory necessary to carry out such a test, as will be discussed in the next section.

3.2. THE MULTI-COLOUR RESULTS

3.2.1. *Theoretical Considerations*

A theoretical study on the colour-amplitude dependence in PG 1716+426 stars (Randall et al., in preparation) found that the amplitude of the pulsation at a given wavelength shows a trace of the mode's degree index l, but also depends on the atmospheric parameters of the star and the viewing aspect. The latter parameter can be eliminated by taking the ratio of the amplitudes at two different wavelengths. This simplification was used in the creation of Figure 3a, which depicts the behaviour

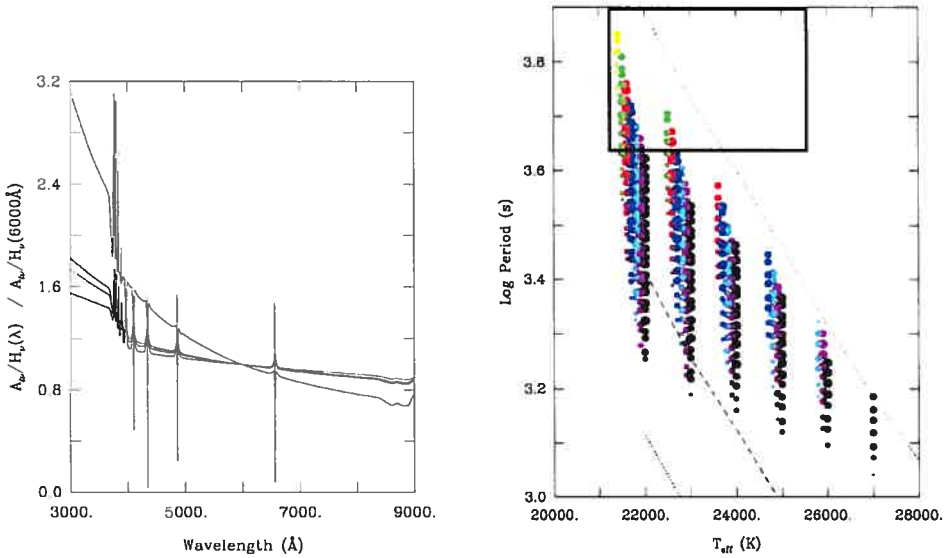

Figure 3. (a) The expected relative normalised flux A_{lv}/H_v for a PG 1716+426 star with $\log g = 5.5$ and $T_{\rm eff} = 25\,000$. From top to bottom at the left, the curves refer to a model with $l = 3,2,1$ and 4, respectively. (b) Comparison of theoretically predicted periods to those observed in PG 1627+017.

of the relative flux A_{lv}/H_v (where H_v is the Eddington flux) as a function of wavelength for a typical PG 1716+426 star. One can discern the Balmer jump, as well as the Balmer series in all the curves. The feature of interest to us is the fact that the l index of the mode of pulsation in question leaves a distinct imprint on the flux-wavelength dependence, an effect that is particularly strong in the UV. This implies that applying Fourier techniques to high-quality multi-colour photometry can be used to determine the degree index of a given pulsation mode.

In order to be able to compare theoretical predictions with observations, the expected relative fluxes are integrated over different filter bandpasses, of which the ratios are then calculated. We find that, while the relative amplitude is larger at shorter wavelengths for all l, the ratio for $l = 1, 2$ and 4 is noticeably different from that for $l = 3$. This implies that, in theory, we should be able to tell a mode with $l = 1, 2$ or 4 from a mode with $l = 3$ by comparing its amplitudes over two different bandpasses in the Fourier domain.

3.2.2. *Multi-Colour Observations*

We obtained 26 h of simultaneous U and R-band photometry over the course of 6 nights, the FTs of both of which are illustrated in Figure 4. It is immediately obvious that the spectra have poor frequency resolution, as the number of cycles accumulated is simply not sufficient for the determination of periods. Hence, we are not able to make any quantitative statements about the amplitude ratios, however on the qualitative level it is encouraging to see that the amplitudes in the U-band

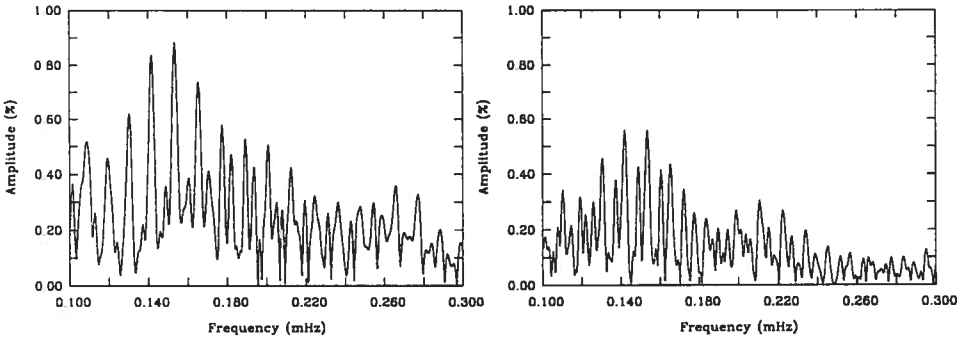

Figure 4. Multi-colour Fourier transforms.

are significantly larger than in the R. This makes us confident that, given a longer baseline and a higher duty-cycle, the theory developed could be applied to yield the degree indices of the PG 1716+426 stars' dominant modes of pulsation.

4. Conclusion

The preliminary results of this multi-site campaign are highly encouraging. The periods uncovered are in qualitative agreement with theory and we believe to have discovered a sufficient number to attempt a serious asteroseismological analysis. One puzzling aspect however is the apparent absence of any evidence for stellar rotation, which certainly warrants further investigation.

While we could not obtain enough multi-colour data to be able to identify different modes' colour-amplitude ratios, the observations agree with theoretical predictions at the qualitative level. This leaves us confident that, given the necessary data, we will solve the mystery of the degree indices of the modes excited in PG 1716+426 stars.

References

Allard, F., Wesemael, F., Fontaine, G., Bergeron, P. and Lamontagne, R.: 1994, *AJ* **107**, 1565.

Fontaine, G., Brassard, P., Charpinet, S., Green, E.M., Chayer, P., Billères, M. and Randall, S.K.: 2003, *ApJ* **597**, 518.

Green, E.M., Fontaine, G., Reed, M.D., Callerame, K., Seitenzahl, I.R., White, B.A., Hyde, E.A., Østensen, R., Cordes, O., Brassard, P. et al.: 2003, *ApJ* **583**, L31.

Kilkenny, D., Koen, C., O'Donoghue, D. and Stobie, R.S.: 1997, *MNRAS* **285**, 640–644.

Morales-Rueda, L., Maxted, P.F.L., Marsh, T.R., North, R.C. and Heber, U.: 2003, *MNRAS* **338**, 752.

Appendix B

RECENT DEVELOPMENTS IN THE STUDY OF LONG-PERIOD VARIABLE SUBDWARF B STARS

S.K. Randall, G. Fontaine, E.M. Green, P. Brassard, and D.M. Terndrup

Proceedings of the SOHO 14/GONG 2004 Workshop (ESA SP-559). "Helio- and Asteroseismology: Towards a Golden Future", held in New Haven, Connecticut, USA, from 12–16 July 2004. Ed. D. Danesy, p. 119

RECENT DEVELOPMENTS IN THE STUDY OF LONG-PERIOD VARIABLE SUBDWARF B STARS

Suzanna K. Randall[1], Gilles Fontaine[1], Elizabeth M. Green[2], Pierre Brassard[1], and Donald M. Terndrup[3]

[1]Département de Physique, Université de Montréal, C.P. 6128, Succ. Centre-Ville, Montréal, Québec, Canada H3C 3J7
[2]Steward Observatory, University of Arizona, Tucson, AZ 85721, USA
[3]Department of Astronomy, Ohio State University, 140 West 18th Avenue, Columbus, OH 43210, USA

ABSTRACT

We report on recent advances in the study of long-period variable subdwarf B stars. Two such objects, PG 1627+017 and PG 1338+481, were the targets of extensive multi-site campaigns conducted in 2003 and 2004 respectively. The photometry accumulated yielded up to 23 periodicities in the 4500-9000 s range for the former star and at least 4 convincing periods between 3500 and 4500 s for the latter. The band of periods observed is in qualititive agreement with theoretical predictions for both targets. In the case of PG 1338+481, we obtained multi-colour photometry of sufficient quality to constrain the observed modes' degree indices. Preliminary analysis suggests l=4 for all four modes, again in accordance with theory.

Key words: stars:oscillations; subdwarfs.

1. INTRODUCTION

Subdwarf B (sdB) stars are extreme horizontal branch (EHB) stars with effective temperatures between 20000 and 40000 K and high surface gravities ranging from log g=5.0-6.2 (Saffer et al. 1994). They are composed of a helium-burning core surrounded by a thin hydrogen-rich shell and are characterised by low masses of $\sim$0.5 M$\odot$. SdB progenitors are thought to have undergone substantial mass loss near the red giant tip, leaving the core stripped of all but a very thin hydrogen envelope. Thus unable to ascend the asymptotic giant branch these stars evolve along the EHB, spend around 10^8 years as subdwarf B stars, and end their lives as low-mass white dwarfs (Bergeron et al. 1994). Since the precise evolutionary path and the circumstances surrounding the mass loss are not fully understood, it is hoped that asteroseismology will succeed in determining key parameters such as the thickness of the hydrogen shell and thus help constrain evolutionary scenarios.

We currently know of two distinct types of multi-mode pulsators among subdwarf B stars: the rapidly oscillating EC 14026 stars (Kilkenny et al. 1997) and the more recently discovered long-period variable subdwarf B stars (Green et al. 2003). Lying at effective temperatures between 28000 and 38000 K, the rapid oscillators excite both radial and non-radial p-modes in the $\sim$80-500 s range with amplitudes between 0.4 and 25 % of their mean brightness. Distinctly cooler than the fast pulsators with $20000 \leq T_{eff} \leq 28000$ K, the slow variables typically oscillate on timescales of 1-2 hours with amplitudes less than 0.5%. In our current models the periods excited correspond to high radial order g-modes, generally associated with degree indices of $l \geq 3$, apart from in the coolest models where lower degree modes may also be driven.

While some of the rapid pulsators have now been observed and modelled extensively and very successfully, the study of the slow oscillators is still in its infancy. The potential of asteroseismology is immense in these objects, firstly because they are much more common than the EC 14026 stars and secondly because they are the only type of subdwarf to excite g-modes, thus offering the unique opportunity of probing deep into the stellar nucleus. Moreover, the prospects for applying asteroseismology are good. We recently uncovered the excitation mechanism operating in the slow variables to be the same Kappa-mechanism that accounts so well for the instabilities observed in the EC 14026 stars (Fontaine et al. 2003). Since full asteroseismological analyses have now been carried out successfully for a number of rapid pulsators (e.g. Brassard et al. 2001), it seems plausible that, given the necessary observational data, similar results could be achieved for the long-period variables. To this end, we organised multi-site campaigns for two slowly pulsating subdwarf B stars, PG 1627+017 and PG 1338+481 in May/June 2003 and March/April 2004 respectively. In the following paragraphs we report on the results from both campaigns and discuss the outcome of comparisons with theoretical predictions.

2. A MULTI-SITE CAMPAIGN ON PG 1627+017

For the purpose of our first campaign we were allocated 31 nights between 9 May and 11 June 2003 at Steward Observatory's 1.55-m telescope on Mt. Bigelow, Arizona. This was supplemented by simultaneous observing

time granted at the South African Astronomical Observatory's 1.0-m telescope (14 nights), the 2.2-m at Calar Alto, Spain (8 nights), and the 2.3-m Siding Spring Observatory in Australia (5 nights) as well as by weekend runs at Mt. Bigelow in the weeks leading up to and following the main campaign (20 nights total). The goal at all these locations was the accumulation of differential time-series photometry for the long-period variable PG 1627+017, a target chosen on purely observational grounds such as brightness, high-amplitude pulsations and location in the sky. Incidentally, PG 1627+017 is also one of the coolest subdwarf B stars at $T_{eff} \sim$ 20,700 K and $\log g \sim 5.04$ (U. Heber, private communication) and forms part of a short-period binary system with $P_{binary} \sim 0.8$ days (Morales-Rueda et al. 2003). All observations were taken in the R-band with the aim of minimising differential extinction.

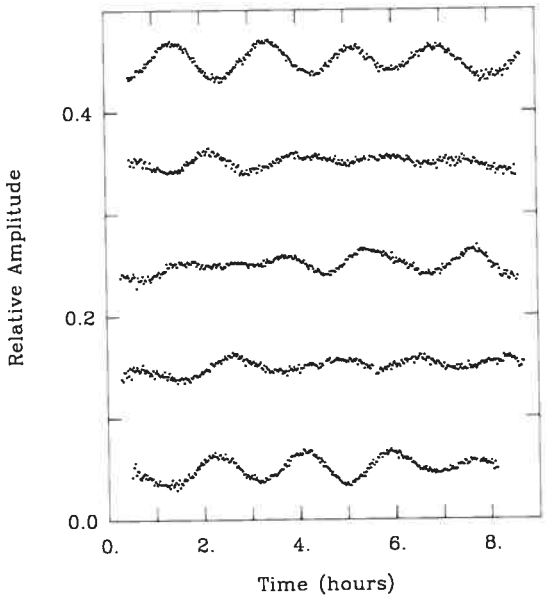

Figure 1. Typical R-band lightcurves obtained for PG 1627+017.

Our efforts yielded a total of 303 hours of useful data, achieving a duty cycle of 33% during the main part of the campaign. Typical lightcurves as obtained at Mt. Bigelow are illustrated in Figure 1, while the Fourier Transform of all nights combined is shown in Figure 2 (top curve). The model spectrum mirroring the observed spectrum was constructed on the basis of 23 extracted periodicities with amplitudes of at least three times the noise level, while the lower curve corresponds to the residual power, i.e. the difference between the observed and model spectra.

The periods detected lie in the 4500-9000 s range, with the highest amplitude peaks (A $\sim$ 0.3-0.5 %) found between $\sim$ 6300-7050 s (see Randall et al. 2004 for details). Whereas this is in good qualitative agreement with the theorerically predicted band of excited periods in a model with PG 1627+017's atmospheric parameters, the observed period spectrum is more difficult to understand at the quantitative level. In particular, the distribution of frequencies extracted is rather non-uniform, consisting in

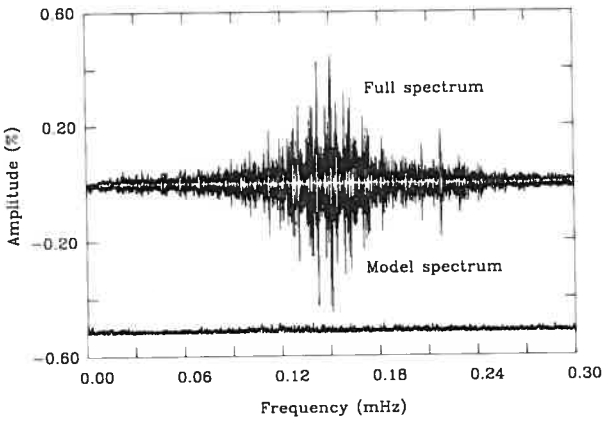

Figure 2. Fourier Transform of the combined PG 1627+017 data.

essence of the aforementioned dense clustering of dominant peaks between $\sim$ 6300-7050 s flanked by two much more sparsely populated low-amplitude groups between $\sim$ 8000-9000 s and around 4600 s respectively. Since according to asymptotic theory modes of the same degree index with consecutive values of k should be relatively evenly spaced in terms of period, it becomes clear that we are missing a substantial number of modes. Moreover, we cannot be certain that all the periodicities detected are intrinsic to the pulsation mechanism as stellar rotation is also expected to play a role, a possibility that we are still in the process of investigating.

In addition to collecting the R-band data as part of the main campaign we also made an effort to secure simultaneous U/R photometry and for this purpose were allocated 7 nights at Steward Observatory's 1.52-m telescope on Mt. Lemmon, Arizona during the main campaign, as well as a week at the MDM 2.3-m telescope, Kitt Peak, in early July 2003. The reason for obtaining multi-colour photometry was that a recent theoretical study on long-period variable subdwarf B stars had found the l-index of a mode to leave a significant trace on the wavelength dependence of its pulsational amplitude (Randall et al. in preparation). While the pulsational amplitude at any given wavelength also depends on a number of other factors such as the viewing angle and the intrinsic amplitude of the mode, these can be eliminated by taking the ratio of pulsational amplitudes measured at different wavelengths or, equivalently, integrated over well-separated bandpasses. This so-called colour-amplitude ratio is dependent only on the atmospheric parameters of the star and the degree index l of the mode in question. Figure 3 illustrates, for different values of l, the logarithm of the pulsational amplitudes calculated for the Johnson U,B,V and the Cousins R and I filters using a representative sdB model with $\log g$=5.5 and T_{eff}=25000 K. The curves have been arbitrarily normalised to the V-filter for clarity. It can be seen that, though the amplitudes fall off towards the red for all values of l, the effect is much more pronounced for modes with odd values of $l \geq 3$. Thus, given high quality simultaneous photometry in a minimum of two different bandpasses as well as reliable spec-

troscopic estimates of $\log g$ and T_{eff}, it should be possible to differentiate at least between modes with l=1,2,4 and those with l=3. Higher degree modes would most likely not be observable due to cancellation effects when integrating over the visible disk of the star.

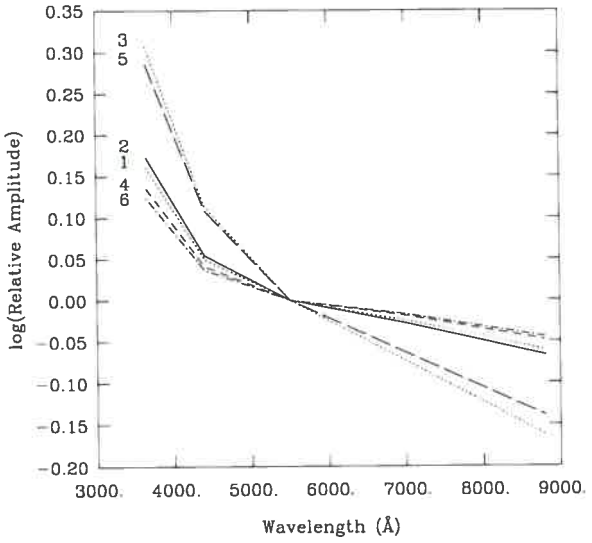

Figure 3. Dependence of pulsational amplitude on colour for different values of degree index l as calculated for a representative sdB model with $\log g$*=5.5 and* T_{eff}*=25000 K. The amplitudes have been scaled to unity in the V-band.*

Since in long-period variable subdwarfs the number of excited periods predicted by theory is much larger than that observed, being able to constrain observational periods' l-values is a crucial step towards successful asteroseismology. With this in mind, we obtained a total of 53 hours of simultaneous U/R photometry split into two ~25 hour sets separated by around 5 weeks. While the quality of the data was not sufficient for precise frequency, amplitude and hence colour-amplitude ratio determination, it was gratifying to find the average amplitudes in the U-band to be significantly larger than those in the R-band for both datasets. Thus encouraged, we concluded it would be worthwhile to attempt multi-colour photometry throughout future campaigns on long-period variable subdwarfs.

3. A TWO-SITE CAMPAIGN ON PG 1338+481

The target star of our second campaign was selected to be representative of the class of long-period variable subdwarf B stars in terms of atmospheric parameters. As such, PG 1338+481 is significantly hotter than the previous target at $T_{eff} \sim 24200$ K and has $\log g \sim 5.11$ (U. Heber, private communication). Preliminary observations showed that this manifests itself in pulsational periods shorter than, and maximum amplitudes about half of those measured in PG 1627+017. An additional factor in selecting PG 1338+481 was the fact that radial velocity measurements determined it to be a single star, leading us to expect fewer complications due to fast rotation, ellipsoidal deformations and the like. However, with a visible magnitude $V \sim 13.7$ it is also nearly one magnitude fainter than PG 1627+017, rendering the acquisition of high-quality lightcurves more challenging.

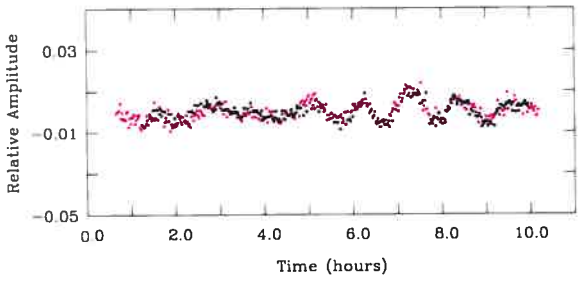

Figure 4. R-band lightcurves of PG 1338+481 from 28 March 2003, obtained at Mt. Bigelow (magenta) and MDM Kitt Peak (black) respectively.

We were allocated a total of 49 near consecutive nights of observing time between 15 March and 3 May 2004, split between the MDM 1.3-m telescope at Kitt Peak (11 nights) and Steward Observatory's 1.55-m telescope on Mt. Bigelow, Arizona (38 nights). Since the telescope scheduling was such that we had one night's overlap from the two sites, we used the opportunity to perform an important consistency check. The results of this are depicted in Figure 4, where we have overplotted the independently reduced R-band photometry from Mt. Bigelow (magenta) and MDM Kitt Peak (black). Both lightcurves are in remarkable agreement, which, while not unexpected, provides a beautiful illustration of the accuracy and objectivity of the differential photometry gathered.

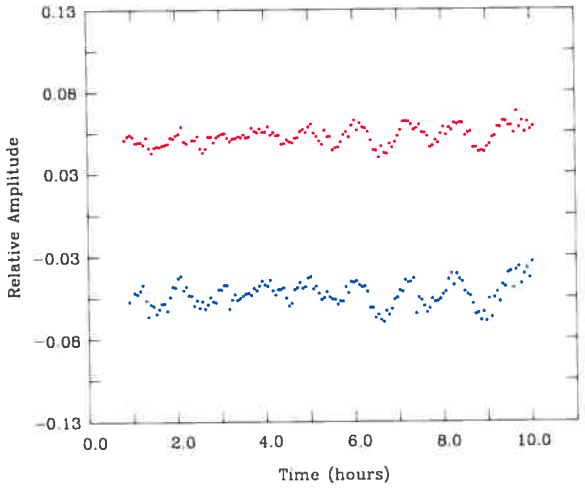

Figure 5. Typical U (lower) and R (upper) lightcurves of PG 1338+481.

As discussed in the previous section, we were hoping to secure simultaneous U/R differential photometry throughout the entire campaign, but for organisational reasons this was possible on only 39 of the 49 nights. For the remaining 10 nights we gathered simple R-band

data in the hope of improving on the period accuracy and detection limit of the two-colour photometry. Despite bad weather during a full 2 weeks of our observing time we were able to accumulate around the same amount of data as for the previous campaign, clocking in at $\sim$ 250 hours of simultaneous U/R photometry and an extra $\sim$ 70 hours of R-band data. A typical night's U (blue) and R (red) lightcurves are illustrated in Figure 5. It can be seen that while the oscillations are clearly phase- and frequency locked, the amplitudes of pulsation are significantly larger in the U than in the R as was to be expected from theory. The dominance of the U-band pulsations becomes even more discernable when comparing the two Fourier Transforms calculated from all simultaneous U (blue) and R (red) band data (see Figure 6).

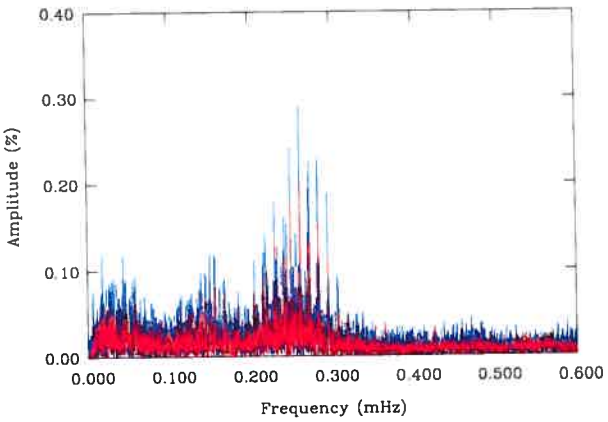

Figure 6. Fourier Transform of all simultaneous U (blue) and R (red) band data for PG 1338+481.

In terms of frequencies present, both the U and R-band Fourier Transforms illustrated in Figure 6 show a cluster of high-amplitude peaks between $\sim$ 0.2 and $\sim$ 0.3 mHz as well as some secondary power at lower frequencies up to $\sim$ 0.18 mHz. While the dominant group of periodicites is in rough qualitative agreement with the theoretically predicted band of unstable modes and is hence almost certainly intrinsic to the pulsation mechanism, the low-frequency peaks cannot be recreated with our current PG 1338+481 models and thus warrant closer inspection. The very shortest frequencies ($<$ 0.1 mHz) are probably caused by atmospheric effects. Although all the lightcurves were flattened using a second order polynomial to account for differential extinction changing with airmass as the target rises and sets in the sky, we are nevertheless bound to see residual low-frequency variations since observing conditions change slightly from night to night. Unfortunately the situation is not as clear-cut for the higher frequency peaks between $\sim$0.1 and $\sim$0.18 mHz. Whereas we would like to believe that they too are associated with differential extinction, the fact that their periods overlap with the range of periods excited in PG 1627+017 means that they cannot be discarded without further investigation. For the purpose of our present preliminary study we treat them as potential, but unproven stellar pulsations.

A first extraction of the Fourier spectra reveals of order 15

Table 1. Dominant periodicities found for PG 1338+481.

Period(s)	U_{amp} (%)	R_{amp} (%)	U/R
3828	0.274±0.011	0.193±0.008	1.42±0.1
3530	0.217±0.011	0.146±0.008	1.49±0.1
4347	0.173±0.011	0.136±0.008	1.27±0.1
4090	0.136±0.011	0.098±0.008	1.39±0.1

periods in the 3500-8000 s range, the most convincing of which lie between 3500 and 4500 s (0.22-0.28 mHz) and have R-band amplitudes $R_{amp} < 0.2$. As expected, the observed periods and amplitudes are significantly smaller than those found for PG 1627+017. The four highest peaks, common to both the U and the R-band data, are listed in Table 1 together with their respective amplitudes and the resulting U/R amplitude ratio. Since the periods are derived directly from the Fourier Transform, they are not associated with any formal error, but we estimate the probable accuracy to be $\sim$1/10 of the frequency resolution (0.24 μHz), i.e. around 0.5 s for the periods in question. By contrast, the pulsational amplitudes result from a least-squares fitting procedure to the lightcurve and are hence assigned formal errors, which however almost always underestimate the true uncertainties. Taking this into account, we find the U/R amplitude ratios for the four prominent modes to be the same within the probable errors, which suggests that they all have the same degree index l.

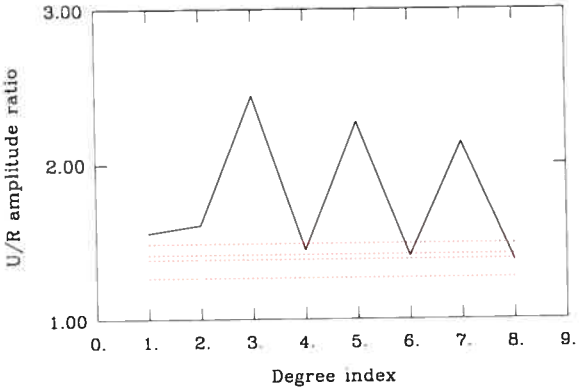

Figure 7. Comparison between observed U/R amplitude ratios (horizontal dashed lines) and those calculated for a PG 1338+481 model with T_{eff}=24200 K and log *g=5.11 (continuous line) as a function of degree index l.*

Figure 7 compares the U/R amplitude ratios observed (horizontal dashed lines) to those calculated for different degree indices l for a model adopting PG 1338+481's atmospheric parameters T_{eff}=24200 and log g=5.11 (continuous line). Assuming that modes with l=6 and 8 cannot be detected due to cancellation effects when integrating over the visible disk of the star, the ratios observed lie closest to the calculated value for l=4 at 1.45 and are in

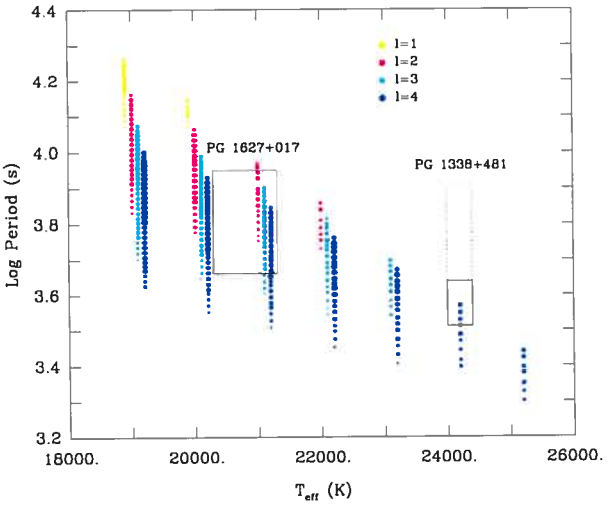

Figure 8. Comparison between the range of periods predicted from a sequence of sdB star models (colour-coded dots) and those observed for PG 1627+017 and PG 1338+481 (superposed boxes). See text for further details.

fact consistent with this number within the experimental errors. The relative proximity of the predicted U/R ratios for l=1 (1.56) and l=2 (1.61) to the l=4 value together with observational uncertainties means that we cannot exclude the idea of our observed periods corresponding to the lowest degree modes. Modes with odd degree indices of $l > 3$ on the other hand can be ruled out completely.

4. COMPARISON WITH THEORY

In order to compare our observational results to theoretical predictions, we constructed a small grid of sdB star models designed to be representative of both PG 1627+017 and PG 1338+481 in terms of atmospheric parameters. Based on the same numerical tools as used by Charpinet el al. (1997) for their "second-generation" models of EC 14026 stars, our sequence of models constitutes an extended version of that calculated by Fontaine et al. (2003) as part of their study on the excitation mechanism operating in long-period variable subdwarfs. The models are characterised by four free parameters: effective temperature T_{eff}, surface gravity $\log g$, stellar mass M_* and depth of the transition between the helium-core and the hydrogen-rich envelope $\log q(H)$. They include an opacity profile that depends largely on the nonuniform distribution of iron with depth, a crucial feature since it is precisely the local overabundance of iron in the driving region that enables the Kappa mechanism to excite oscillations.

We computed 7 equilibrium models with effective temperatures ranging from 19000 K to 25000 K in steps of 1000 K. For each value of T_{eff}, the corresponding $\log g$ was picked in such a way that the sequence of models would be above, and parallel to, the zero-age EHB, the coolest model being associated with the lowest surface gravity. Although this means that our grid does not specifically focus on the two observed stars in terms of $\log g$, the sequence stays more representative of the class as a whole and is perfectly adequate for the qualitative comparison we are aiming for here. We then calculated each model's adiabatic periods before determining whether or not these are excited using a non-adiabatic approach. The results of the latter calculation are shown in Figure 8, which illustrates the logarithm of the periods excited in each model as a function of effective temperature. The dots representing the discrete periods are colour-coded to differentiate between degree indices and shifted slightly in temperature for clarity. Yellow points indicate l=1, magenta l=2, cyan l=3 and blue l=4. Higher degree modes were omitted since they are most likely not observable and hence of no practical interest here.

The sequence of models pictured throws light on some key characteristics of the pulsation spectra of long-period variables. Firstly, the band of periods excited is broadest and counts the largest number of discrete modes for the coolest model, while the period spectra become simpler for hotter structures. Secondly, the periods systematically shorten with growing temperature, lying between $\sim$ 4000-18000 s for the first and between $\sim$ 2000-3000 s for the last model in T_{eff} space. Finally, the minimum degree index of the modes excited increases with temperature. For instance, the T_{eff}=21000 structure excites modes with l=2,3,4... while the model at T_{eff}=25000 can drive only modes with degree indices of 4 or higher. This may well translate to hotter stars exhibiting lower amplitude pulsations than cooler objects when integrating over the stellar disk.

To draw a qualitative comparison between the pulsational properties predicted and those observed for PG 1627+017 and PG 1338+481, we superposed two black boxes onto the model sequence computed. They indicate, in the horizontal direction, the uncertainty on the relevant star's spectroscopic temperature estimate and, in the vertical, the range of periods observed. In the case of PG 1627+017, the band of unstable periods detected falls completely within that predicted by theory. The periodicities observed would thus correspond to modes with l=2,3 and perhaps 4.

For PG 1338+481, the results are not quite as conclusive. Even if, for the time being, we ignore the questionable longer periods represented by the dotted extension to the box, the convincing periods observed tend to be slightly longer than those predicted. This discrepancy could very well be due to inaccuracies in the models regarding the composition of the hydrogen-rich envelope. In our simplified treatment, we calculate the abundance profile of iron assuming a pure hydrogen background and ignore the potentially important effects of other metals and traces of helium. While we need to undertake extensive calculations to make any definite statements, it is certainly possible that the inclusion of helium and other metals could alleviate the disparity between observed and calculated bands of excitation. Nevertheless, the fact that the two domains overlap considerably is very encouraging and points to an agreement at the qualitative level. Moreover, the theoretical modes predicted for a star such as PG 1338+481 are all associated with degree indices

l=4, which ties in very nicely with the U/R amplitude ratios discussed in the previous section.

5. CONCLUSION

The first two major multi-site campaigns on long-period variable subdwarf B stars discussed in this article have provided us with the observational tools to test the validity of the driving mechanism and the basic pulsational properties recently proposed by Fontaine et al. (2003). At the qualitative level we find the range of periods observed to be consistent with those predicted, which is very encouraging since there was no guarantee for this at the outset. In addition, preliminary analysis of the simultaneous U- and R-band photometry obtained for PG 1338+481 suggests the higher amplitude modes to be associated with degree indices l=4, which, if confirmed, would back one of the most controversial claims associated with the driving mechanism, namely that the majority of long-period variables pulsate in modes with $l \geq 3$.

Despite these encouraging results, numerous challenges remain. Firstly, it is obvious, both from the slight discrepancy between the ranges of periods observed and calculated for PG 1338+481 and the fact that we observe slow oscillations in Subdwarfs hotter than 25000 K (which, according to theory, excite only modes with $l \geq 5$), that the models do not account for the instabilities found in hotter long-period variables very well. Secondly, quantitative interpretations of the observed period spectra and subsequent asteroseismological analyses are still in the exploratory stages. In the case of PG 1627+017 we will most likely have to acknowledge that the band of periods observed is simply too complex, and that the corresponding models predict too many excited modes for us to find a unique solution. For PG 1338+481 prospects look more promising, as the period spectrum is simpler and we can place additional constraints on the modes' degree indices from the multi-colour data. Finally, it is evident that despite highly ambitious multi-site campaigns our data leave much to be desired in terms of coverage and atmospheric interference, making space-based observations the obvious choice for future campaigns.

ACKNOWLEDGMENTS

We would like to thank for their contribution to the observations: Tim Bedding, Naomi Brown, Oliver Cordes, Lisa Crause, Abby Daane, Mathieu Fontaine, Bi-Qing For, Andrew Jacob, Dave Kilkenny, Lazlo Kiss, Simon O'Toole, Pierre-Olivier Quirion and Pia Zacharias. We are also grateful to Uli Heber for providing us with his estimates of the two targets' atmospheric parameters.

REFERENCES

Bergeron, P., Wesemael, F., Beauchamp, A., Wood, M.A., Lamontagne, R., Fontaine, G. and Liebert, J., 1994, *ApJ*, 432, 305

Brassard, P., Fontaine, G., Billères, M., Charpinet, S., Liebert, J. and Saffer, R.A., 2001, *ApJ*, 563, 1013

Charpinet, S., Fontaine, G., Brassard, P., Chayer, P., Rogers, F.J., Iglesias, C.A. and Dorman, B., 1997, *ApJ*, 483, L123

Fontaine, G., Brassard, P., Charpinet, S., Green, E.M., Chayer, P., Billères, M. and Randall, S.K., 2003, *ApJ*, 597, 518

Green, E.M., Fontaine, G., Reed, M.D., Callerame, K., Seitenzahl, I.R., White, B.A., Hyde, E.A., Ostensen, R., Cordes, O., Brassard, P. et al, 2003, *ApJ*, 583, L31

Kilkenny, D., Koen, C., O'Donoghue, D. and Stobie, R.S., 1997, *MNRAS*, 285, 640-644

Morales-Rueda, L., Maxted, P.F.L., Marsh, T.R., North, R.C. and Heber, U., 2003, *MNRAS*, 338, 752

Randall, S.K., Fontaine, G., Green, E.M., Kilkenny, D., Crause, L., Cordes, O., O'Toole, S., Kiss, L., For, B.-Q. and Quirion, P.-O., 2004, *A&SS*, in press

Saffer, R., Bergeron, P., Koester, D. and Liebert, J., 1994, *ApJ*, 432, 351

Appendix C

LONG-PERIOD VARIABLE SUBDWARF B STARS: PROSPECTS FOR ASTEROSEISMOLOGY

S.K. Randall, G. Fontaine, E.M. Green, P. Brassard, and D. Terndrup

Proceedings of the second meeting on extreme horizontal branch stars and related objects, held on the island of La Palma, Canary Islands, Spain, from 6−10 June 2005

To be published in *Baltic Astronomy*

Baltic Astronomy, vol. 14, XXX–XXX, 2005.

LONG-PERIOD VARIABLE SUBDWARF B STARS: PROSPECTS FOR ASTEROSEISMOLOGY

Suzanna K. Randall[1], Gilles Fontaine[1], Elizabeth M. Green[2], Pierre Brassard[1], and Donald M. Terndrup[3]

[1] *Département de Physique, Université de Montréal, C.P. 6128, Succ. Centre-Ville, Montréal, Québec, Canada H3C 3J7*

[2] *Steward Observatory, University of Arizona, Tucson, AZ 85721, USA*

[3] *Department of Astronomy, The Ohio State University, 140 West 18th Avenue, Columbus, OH 43210, USA*

Received 2005 August 1

Abstract. We summarise the results of an extensive study aimed at quantitatively interpreting the oscillations detected in long-period variable subdwarf B stars. Our analysis is based on between 300 and 400 hours of time-series photometry obtained for each of three representative targets: PG 1627+017, PG 1338+481 and PG 0101+039. The former two were the subjects of extensive multi-site campaigns led from the 1.52-m Steward Observatory telescope on Mt. Bigelow, Arizona, while the latter was observed with the 0.15-m Canadian space telescope MOST . We find that, unlike for the short-period oscillators, where asteroseismology has been successful in some instances, our understanding of the slow pulsators is somewhat limited due to both observational and conceptual challenges. In particular, the period spectra measured to date are much sparser than those anticipated from models, implying that the indices of the modes observed must be constrained from the outset if asteroseismology is to be achieved. One promising idea is the exploitation of a mode's colour-amplitude dependence on its degree index ℓ through multi-colour photometry. Applying that method to the PG 1338+481 data together with other constraints suggests the excitation of $\ell = 1$ modes. If confirmed, this would point to a discrepancy between the observed and predicted long-period variable subdwarf B star instability strips of around 7000 K on the blue side, although some of it could be due to incorrect spectroscopic determinations of the effective temperatures of cool sdB stars.

Key words: stars: EHB and post-EHB, variable: general – stars: individual (subdwarfs)

1. INTRODUCTION

Pulsating subdwarf B (sdB) stars can be divided into two groups: the rapidly oscillating EC 14026 stars (Kilkenny et al. 1997) and the long-period variable PG 1716 stars (Green et al. 2003). At effective temperatures between 29,000 K and 36,000 K, the rapid oscillators correspond to the hotter of the two classes and excite both radial and low-degree non-radial pressure modes with typical periods

in the 80-500 s range. Their instabilities are thought to be driven by a classical kappa mechanism associated with a local overabundance of iron, which in turn depends on the competitive actions of gravitational settling and radiative levitation (Charpinet et al. 1996). Indeed, models taking into account diffusion processes and the resulting non-uniform iron abundance profile have been very successful at predicting the observed EC 14026 instability strip on the Hertzsprung-Russell diagram as well as the range of periods excited for a given object (see Fontaine et al. in these proceedings for details). Beyond this, quantitative period matches leading to mode identification and asteroseismological estimates of key stellar parameters have been possible in a few instances (see Charpinet et al. in these proceedings for details).

In comparison, the study of the long-period variables is still in its infancy. Found at cooler temperatures in the 22,000 K to 29,000 K range, these stars exhibit brightness variations on a typical timescale of 1−2 hours, immediately implying high radial order gravity modes. While the driving mechanism is believed to be the same as for the EC 14026 stars (Fontaine et al. 2003), the vast majority of current PG 1716 models can excite only modes with degree indices $\ell \geq 3$, the observability of which is controversial due to cancellation effects when integrating over the visible disk of the star. However, discrepancies between the observed and predicted instability strips have been difficult to quantify due to a lack of data. Unlike the EC 14026 stars, where just a few nights of photometry can be sufficient to identify enough periods for asteroseismology, the long-period variables need to be monitored over the course of weeks or even months to yield a comparable number of periodicities. Extracting the observed frequency spectrum is further complicated by severe aliasing effects and the fact that atmospheric variations occur on a similar timescale as the stellar oscillations. These observational challenges notwithstanding, the detailed study of long-period variable subdwarf B stars could prove invaluable to our understanding of post-main sequence stellar evolution. In contrast to the shallow pressure modes observed in the EC 14026 pulsators, the slow oscillators' gravity modes probe deep within the star and are sensitive to the exact composition of the CO/He core. Successful asteroseismology of the latter would thus hold implications for the core helium burning phase not only of subdwarfs, but of other evolved stars as well.

In what follows, we present the results of an ambitious observational campaign aimed at measuring and quantitatively interpreting the period spectra of three representative slowly oscillating subdwarf B stars. We begin with an account of the observing runs and the frequencies extracted before comparing our findings to qualitative non-adiabatic and quantitative adiabatic predictions. We then outline the steps taken towards asteroseismic modelling and note the implications of our preliminary results.

2. OBSERVATIONAL PROGRAMME

2.1. PG 1627+017

At atmospheric parameters $T_{\rm eff} \sim 23{,}700$ K and $\log g \sim 5.32$ (Green, Fontaine, and Chayer, in preparation), PG 1627+017 is one of the coolest subdwarf B stars known. It was chosen as a first observational target because of its brightness

($V \sim 12.9$), relatively high-amplitude pulsations, and an equatorial location vital to the success of our multi-site collaboration. While the majority of the data were gathered at the 1.52-m Steward Observatory telescope on Mt. Bigelow, Arizona, between 9 May and 11 June 2003, the time coverage and baseline were improved by simultaneous observing time granted at the South African Astronomical Observatory's 1-m telescope and the 2.3-m Siding Spring Observatory (Australia), as well as by weekend runs at Mt. Bigelow in the weeks leading up to the main campaign. Our efforts yielded a total of 303 hours of useful R-band photometry with a duty cycle of 33% over the five week period. Some spectroscopy was also obtained with the aim of recovering the main peaks from radial velocity shifts (see For et al. in these proceedings for details). The Fourier Transform of the entire photometry lightcurve is shown in Figure 1, mirrored by a model spectrum (upside down) constructed on the basis of 23 extracted periodicities with amplitudes of at least three times the noise level. The residual between the observed and modelled spectra is displayed at the bottom of the figure.

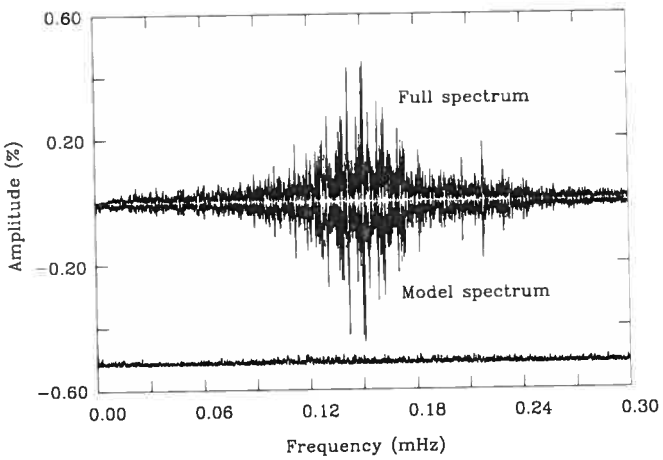

Fig. 1. Fourier Transform for PG 1627+017.

All 23 periods detected in the lightcurve of PG 1627+017 lie in the 4500-9000 s range and have R-band amplitudes between 0.3 and 0.5 % of the star's mean brightness. Note that their distribution in frequency space is non-uniform, with the most powerful oscillations clustering between $\sim$ 6300−7050 s and several very closely spaced doublets and triplets occurring throughout the period spectrum. The latter may partially be explained by rotational splitting. PG 1627+017 forms part of a close binary system and, assuming a binary-synchronous rotation rate, spins on its axis with a period of $P_{\rm rot} = P_{\rm bin} \sim 0.83$ days (Morales-Rueda et al. 2003). The resulting break in spherical symmetry lifts the $(2\ell + 1)$-fold degeneracy of a mode with given radial order k and degree index ℓ, introducing a dependence on the azimuthal index m. To first order, the components of a (k, l) mode with adjacent values of m are then separated by a frequency spacing $\Delta f = (1 - C_{k\ell})/P_{\rm rot}$, where for the high radial order gravity modes encountered in PG 1716 stars $C_{k\ell} \sim 1/(\ell(\ell + 1))$. These equations imply that, in theory, ro-

tational splitting can be exploited to determine the degree indices of the modes observed. However, in the case of PG 1627+017 the frequency spectrum uncovered is too dense to allow the unambiguous identification of a given peak, as is shown in Figure 2. While the scenario invoking modes with $\ell = 1$ (upper panel) seems more convincing, the possibility of explaining the observed period distribution in terms of $\ell = 2$ and $\ell = 3$ modes (lower panel) cannot be ruled out. It is thus unclear not only what degree indices the modes observed are associated with, but also which of the peaks detected are independent stellar pulsations, and which are rotational in nature. This makes asteroseismology and mode identification challenging, if not impossible.

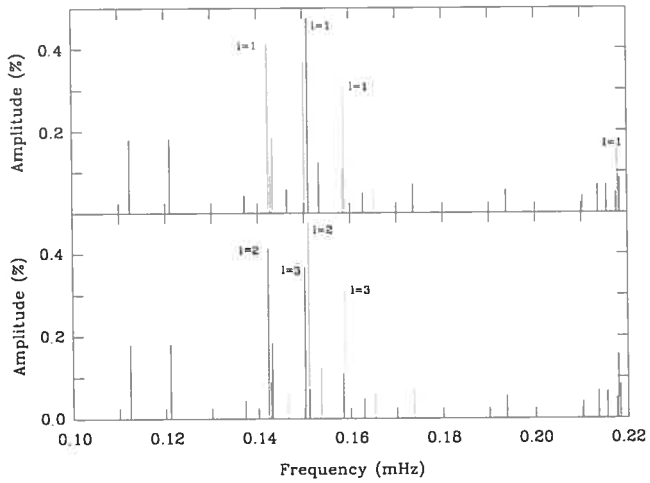

Fig. 2. Two possible manifestations of rotational splitting for PG 1627+017, depending on the degree indices invoked. Peaks illustrated in the same colour refer to modes with the same values of ℓ and k but different m. The values of ℓ shown are derived from the frequency spacing between split components.

2.2. PG 1338+481

Our second target, PG 1338+481 ($V \sim 13.6$), is a much more typical long-period variable in terms of atmospheric parameters at $T_{\rm eff} \sim 28{,}400$ K and $\log g \sim 5.40$ (Green, Fontaine, and Chayer, in preparation). It was chosen for its representative qualities as well as the fact that it is a single, and thus probably slowly rotating, star. Observational efforts were conducted between 15 March and 3 May 2004 and focussed on just two sites: the 1.52-m Steward Observatory telescope employed during the previous campaign, and the 1.3-m MDM telescope at Kitt Peak. In total, we obtained $\sim$ 250 hours of simultaneous U- and R-band photometry, as well as an additional $\sim$ 70 hours of R-band data. The resulting Fourier Transforms are displayed in Figure 3 for both the U (blue) and the R (red) lightcurves. It is evident that, while the amplitudes in the U are significantly higher than those in the R, the oscillations are locked in frequency and phase. This is confirmed during the pre-whitening process, where the periods determined in the two colours are

generally found to lie within 0.5 s of each other. Adopting a threshold of three times the local noise level, we were able to extract 13 periods in the 2100 s to 7200 s range with amplitudes up to 0.3 % and 0.2 % of the mean brightness in the U- and R-band respectively.

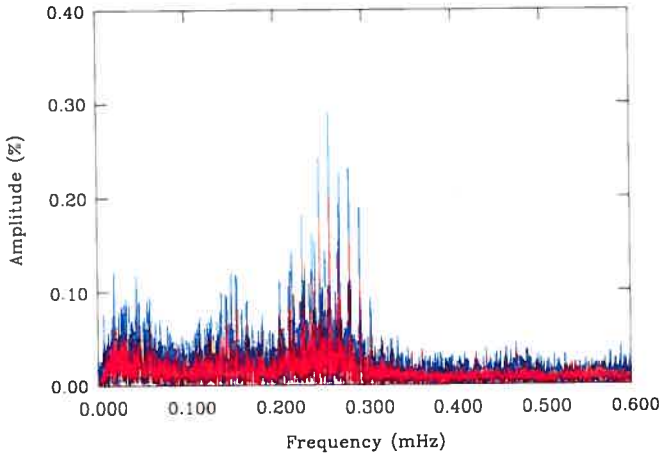

Fig. 3. U (blue) and R (red)-band Fourier transforms for PG 1338+481.

The decision to observe PG 1338+481 in two wavebands was based on a theoretical study exploiting the dependence of a mode's colour-amplitude behaviour on its degree index ℓ (Randall et al. 2005). Put simply, the ratio of a pulsation peak's amplitudes as measured in two well-separated bandpasses can be used to directly infer the associated mode's degree index provided the star's atmospheric parameters are known. We list, in Table 1, the U/R amplitude ratios for the five most convincing periodicities extracted from the data. Note that these all correspond to peaks with amplitudes of at least four times the local noise level. It is obvious from the table that the amplitude ratios of all five peaks are consistent within the error margins, which may imply that the corresponding modes have the same degree index. That possibility is supported by the fact that the oscillations are relatively evenly spaced in period, neighbouring peaks being separated by 257 s $\leq \Delta P \leq$ 298 s. According to asymptotic theory, this is precisely what would be expected for high radial order modes with consecutive values of k and constant degree index ℓ. While the matter remains to be investigated in more detail, the resulting constraint on mode identification makes PG 1338+481 a prime target for asteroseismological studies.

Table 1. U/R amplitude ratios for the five dominant peaks detected in the lightcurves of PG 1338+481

Period (s)	U/R amplitude
3530	1.49±0.29
3828	1.42±0.22
4090	1.39±0.40
4347	1.27±0.30
4625	1.55±0.51

2.3. PG 0101+039

PG 0101+039 was observed with the Canadian space telescope MOST (Walker et al. 2003) from 28 September to 15 October 2004 in a trial run for potential future missions. Since the effects of daily aliasing and atmospheric variation had undermined the extraction of periodicities for both of the previously studied targets, we had concluded that the successful asteroseismology of long-period variable subdwarf B stars would be facilitated by space-based observations. However, it was not clear from the outset whether the 15-cm aperture MOST telescope, currently the only satellite dedicated to asteroseismology, would be able to achieve sufficient precision for detecting pulsations in the relatively faint subdwarfs. It was therefore imperative to select a bright target like PG 0101+039 ($V \sim 12.1$), regardless of its other characteristics such as atmospheric parameters ($T_{\rm eff} \sim 28{,}300$ K and $\log g \sim 5.52$ according to Green, Fontaine, and Chayer, in preparation), or the fact that it forms part of a short-period binary system ($P_{\rm bin} \sim 0.57$ days from Moran et al. 1999).

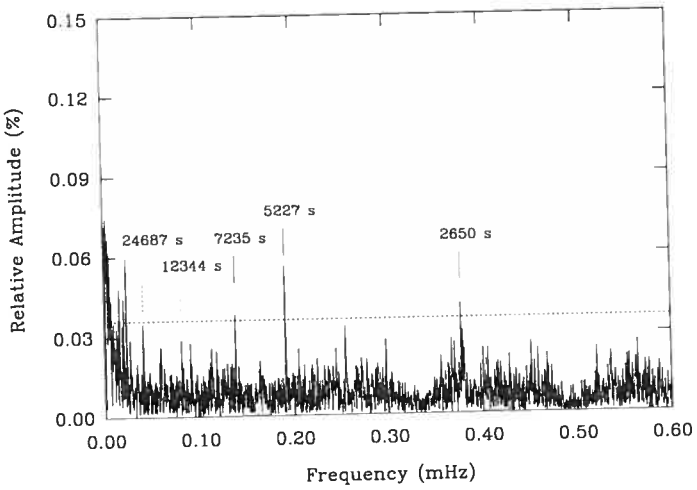

Fig. 4. Fourier transform for PG 0101+039.

The $\sim$ 400 hours of broadband photometry gathered by MOST boast a duty cycle of 96.5 % and a noise level similar to that achieved for PG 1338+481 after seven weeks of ground-based observations. It is thus beyond doubt that, given the appropriate observing time, data from MOST can surpass anything obtainable from the ground in terms of time coverage. And indeed, the Fourier transform illustrated in Figure 4 shows no visible signs of aliasing. Adopting a threshold of four times the mean noise level, we were able to extract three convincing periodicities attributed to stellar oscillation (continuous line segments). Note that their amplitudes are significantly lower than those detected for either of the previous targets, which could well be due to PG 0101+039's higher surface gravity. In addition, we found two lower amplitude peaks (dotted line segments) that are probably caused by an ellipsoidal deformation of the subdwarf due to the gravita-

tional pull of its companion, and would imply a binary-synchronous rotation rate. Unfortunately, the fact that only three pulsations were identified makes this star unsuitable for asteroseismology for the time being.

3. QUALITATIVE COMPARISON WITH NON-ADIABATIC THEORY

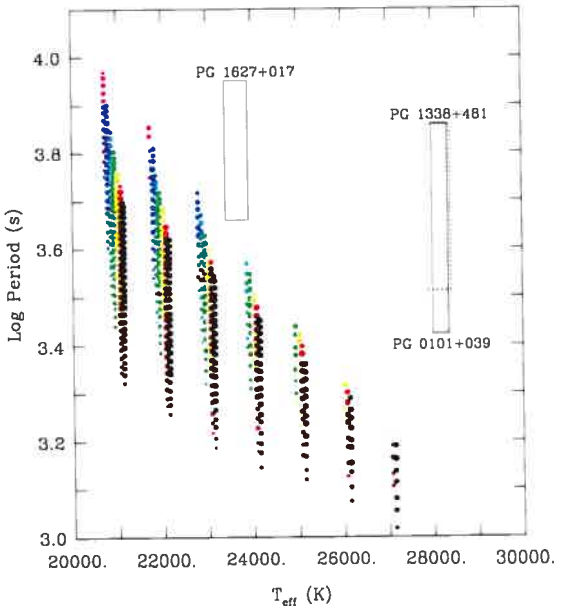

Fig. 5. Comparison between the range of periods predicted from a sequence of PG 1716 models (colour-coded dots) and those observed for PG 1627+017, PG 1338+481 and PG 0101+039 (boxes). See text for further details.

In order to compare the ranges of periods observed for PG 1627+017, PG 1338+481 and PG 0101+019 to those predicted by non-adiabatic theory, we computed a short sequence of sdB models in the appropriate temperature range. Constituting an updated version of the numerical tools employed by Charpinet et al. (1996) to explain the EC 14026 phenomenon, these models incorporate radiative levitation and are characterised by five free parameters: effective temperature $T_{\rm eff}$, surface gravity $\log g$, total stellar mass M_*, logarithmic depth of the transition between the hydrogen-rich envelope and the helium core $\log q$(H), and logarithmic depth of the extent of the inner carbon-oxygen core $\log q$(He). Note that, while M_* and $\log q$(He) were kept at constant representative values over the entire sequence, $\log q$(H) and $\log g$ were changed with $T_{\rm eff}$ so as to keep all of the structures parallel to the zero-age extreme horizontal branch (for precise values see Randall et al. in preparation). Each model was then subjected to adiabatic and non-adiabatic pulsation calculations, the former estimating the periods of modes present, and the latter computing their stability. Figure 5 illustrates the periodicities predicted to

be excited over the sequence for modes with $\ell = 2$ (magenta), $\ell = 3$ (blue), $\ell = 4$ (cyan), $\ell = 5$ (green), $\ell = 6$ (yellow), $\ell = 7$ (red) and $\ell = 8$ (black). Superposed on this theoretical instability strip are the ranges of periods observed for our three targets. It can be seen that the general trend of the unstable period range decreasing with increasing temperature is recovered by the models, however on an absolute scale the periods observed are longer than those predicted. Moreover, the modes excited by models hotter than 23,000 K are associated with degree indices $\ell \geq 4$, and the structure representative of PG 1338+481 and PG 0101+039 at $T_{\rm eff} = 28{,}000$ K drives no modes with $\ell \leq 8$ whatsoever. It is thus clear that our models are subject to important deficiencies that have yet to be determined and addressed. Given the similarities that exist between the theoretical instability strip and that observed, we nevertheless believe that the driving mechanism identified for the long-period variable subdwarfs lies at the origin of the oscillations detected and will be able to account for them quantitatively when more realistic models become available.

4. QUANTITATIVE COMPARISON WITH ADIABATIC THEORY

In a first attempt to quantitatively explain the period spectra uncovered in long-period variable subdwarf B stars we focus primarily on PG 1338+481, the most promising object observed so far. One thing that the photometry for all our targets have in common is a strong deficiency in periodicities observed compared to those predicted in the same range. While this could be partly alleviated by more sensitive measurements, it is obvious that asteroseismology will only be achieved if there is some constraint on mode identification from the outset. Possible methods of determining the degree index ℓ of a mode observed include the exploitation of rotational splitting (e.g., Charpinet et al. 2005), line-profile variations from time-series spectroscopy (see Schoenaers & Lynas-Gray, these proceedings) and multi-colour photometry (e.g., Randall et al. 2005). Since our observations do not include high-resolution spectroscopy and rotational splitting was found to yield ambiguous results when it was detected (see section 2.1), the simultaneous U/R photometry of PG 1338+481 is our best option. Figure 6 illustrates the period-dependent U/R

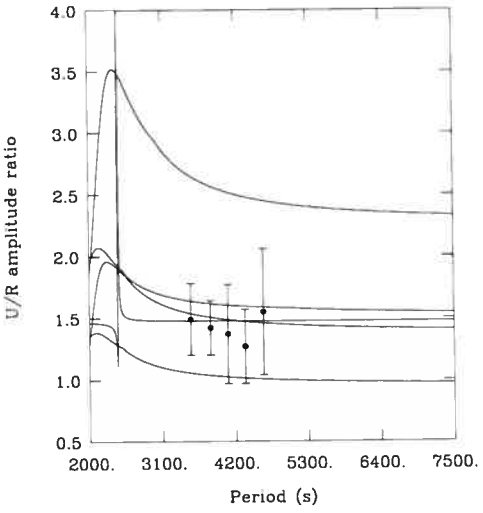

Fig. 6. U/R amplitude ratios predicted for a representative PG 1338+481 model for degree indices $\ell = 3$, 2, 1, 4 and 5 from top to bottom on the right hand side. The amplitude ratios measured for PG 1338+481 are also indicated.

amplitude ratios calculated from a model with $T_{\rm eff}$ = 28,200 K and $\log g$ = 5.38 for degree indices ℓ = 3, 2, 1, 4 and 5 (from top to bottom on the right hand side). Superposed on this are the amplitude ratios observed for the five dominant pulsations of PG 1338+481 (see Table 1). Considering the measurement errors, only modes with $\ell = 3$ and $\ell = 5$ can be excluded with any confidence, although the $\ell = 1$ and $\ell = 4$ curves do represent better matches to the data than that for $\ell = 2$.

Another feature that makes the PG 1338+481 data stand out is the nearly equal period spacing of the five highest amplitude pulsations. As discussed in section 2.2, this could well imply that they are all associated with the same degree index, which in light of the multi-colour findings would correspond to ℓ = 1, 4 or possibly 2. Since the brightness variation caused by an oscillation of given intrinsic amplitude strongly decreases with increasing ℓ-value when integrating over the visible disk of a star, the detection of ℓ = 1 or 2 modes is naturally favoured compared to that of ℓ = 4 modes. Indeed, all main sequence g-mode pulsators with good empirical mode identification show ℓ = 1 modes only. A similar scenario holds true for white dwarfs, which do exhibit the occasional ℓ = 2 mode, but primarily excite dipole modes. As subdwarf B stars lie in between the two regimes, we would expect their case to be no different. In addition to this, the average period spacing between the five peaks ($\langle \Delta P \rangle \simeq 274$ s) is very close to that expected for ℓ = 1 modes in a representative PG 1338+481 model, as can be seen in Figure 7. $\langle \Delta P \rangle$ decreases significantly with increasing degree index, implying that the observed period spectrum could be matched to that predicted for ℓ = 2 or higher only if a significant fraction of the theoretical periodicities were not excited to appreciable amplitudes. Since we find no convincing reason why this should be the case, we believe these modes to have degree indices of ℓ = 1.

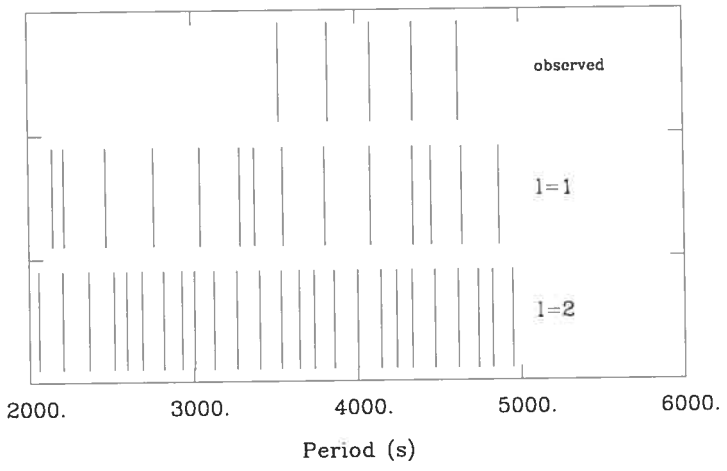

Fig. 7. Period spectrum predicted for a model with $T_{\rm eff}$ = 28,600 K, $\log g$ = 5.22, M_* = 0.45 $M_\odot$, $\log q$(H) = -2.68 and $\log q$(He) = -0.24. The five highest amplitude periodicities observed for PG 1338+481 are also illustrated.

5. CONCLUSION

The observational campaign described in these Proceedings constitutes the first serious attempt at quantitatively interpreting the period spectra excited in long-period variable subdwarf B stars. It has revealed that even the most sensitive measurements available yield an observed period spectrum far sparser than that expected from theory. Consequently, mode identification must be constrained from the outset if asteroseismology is to be possible. One way of doing this is the exploitation of multi-colour photometry, which we attempted for the case of PG 1338+481. Together with mode visibility and period spacing considerations, the results point to the excitation of $\ell = 1$ modes in that star. If confirmed, this would aggravate the discrepancy between the computed and the observed instability strip compared to the detection of $\ell = 3$ or 4 modes. Indeed, none of the models shown in Figure 5 are able to excite dipole modes. These are predicted only for models cooler than 21,000 K, implying a difference of 7,000 K between the theoretical and observed blue edge. While this clearly indicates shortcomings in our models that have yet to be addressed (the spectroscopic determinations may also be partly at fault), qualitative similarities between the observed and predicted instability strips nevertheless point to the identification of the correct driving mechanism. Beyond this, we feel that the constraints placed on the mode identification for PG 1338+481 have opened this star up to asteroseismology, a possibility we are still in the process of investigating.

ACKNOWLEDGMENTS. We would like to thank for their contribution to the observations: T. Bedding, N. Brown, O. Cordes, L. Crause, A. Daane, M. Fontaine, B.-Q. For, A. Jacob, D. Kilkenny, L. Kiss, R. Kuschnig, J. Matthews, S. O'Toole, P.-O. Quirion, J. Rowe and P. Zacharias.

REFERENCES

Charpinet S., Fontaine G., Brassard P., Billères M., Green E. M., Chayer P. 2005, A&A, in press

Charpinet S., Fontaine G., Brassard P., Dorman B. 1996, ApJ, 471, L103

Fontaine G., Brassard P., Charpinet S., Green E. M., Chayer P., Billères M., Randall S. K. 2003, ApJ, 597, 518

Green E. M., Fontaine G., Reed M. D., Callerame K., Seitenzahl I. R., White B. A., Hyde E. A., Ostensen R., Cordes O., Brassard P., Falter S., Jeffery E. J., Dreizler S., Schuh S. L., Giovanni M., Edelmann H., Rigby J., Bronowska A. 2003, ApJ, 583, L31

Kilkenny D., Koen C., O'Donoghue D., Stobie R. S. 1997, MNRAS, 285, 640

Morales-Rueda L., Maxted P. F. L, Marsh T. R., North R.C., Heber U. 2003, MNRAS, 338, 752

Moran C., Maxted P., Marsh T. R., Saffer R. A., Livio M. 1999, MNRAS, 304, 535

Randall S. K., Fontaine G., Brassard P., Bergeron P. 2005, ApJS, in press

Walker G. A. H., Matthews J. M., Kuschnig R., Johnson R., Rucinski S., Pazder J., Burley G., Walker A., Skaret K., Zee R., Grocott S., Carroll K., Sinclair P., Sturgeon D., Harron J. 2003, PASP, 115, 1023

Appendix D

DETECTION OF LONG-PERIOD VARIATIONS IN THE SUBDWARF B STAR PG 0101+039 ON THE BASIS OF MOST PHOTOMETRY

S.K. Randall, J.M. Matthews, G. Fontaine, P. Brassard, J. Rowe, and R. Kuschnig

Proceedings of the stellar pulsation and evolution meeting, held at Villa Mondragone, Monte Porzio Catone, Italy, from 19−24 June 2005

To be published in *Memorie della Societa Astronomica Italiana*

Mem. S.A.It. Vol. 75, 282

Memorie della

Detection of Long-Period Variations in the Subdwarf B Star PG 0101+039 on the Basis of MOST Photometry

S.K. Randall[1], J.M. Matthews[2], G. Fontaine[1], P. Brassard[1], J. Rowe[2], and R. Kuschnig[2]

[1] Département de Physique, Université de Montréal, C.P. 6128, Succ. Centre-Ville, Montréal, Québec, Canada H3C 3J7
[2] Department of Physics and Astronomy, University of British Columbia, 6224 Agricultural Road, Vancouver, British [redacted]olumbia, Canada V6T 1Z1
[redacted]

Abstract. We present the results of ∼ 400 hours of optical wide-band photometry for the long-period variable subdwarf B (sdB) star PG 0101+039 obtained by MOST, Canada's first orbiting space telescope, in September/October 2004. Despite the relative faintness of the target, the observations uncovered three low-amplitude periodicities between 2600 and 7250 s attributed to intrinsic stellar pulsations, as well as an ellipsoidal deformation of the subdwarf due to its close binary status. The fact that slow pulsations were detected in a target as hot as PG 0101+039 is in conflict with current non-adiabatic theory, which only predicts the excitation of more rapid oscillations that have amplitudes too small to be observable when integrating over the visible disk of the star. In light of our findings we will thus have to reconsider our models and refine their construction.

Key words. Stars: interiors – Stars: oscillations – Stars: subdwarfs

1. Introduction

Subdwarf B (sdB) stars are evolved extreme horizontal branch (EHB) objects with effective temperatures in the 20,000−40,000 K range and high surface gravities of $5.0 \leq \log g \leq 6.2$ (Saffer et al. 1994). Their progenitors are thought to have undergone substantial mass loss near the red giant tip, leaving the helium core surrounded by a hydrogen shell too thin for the stars to ascend the asymptotic giant branch. Instead, they settle on the EHB, spend around 10^8 years burning core helium as subdwarf B stars, and end their lives as low-mass white dwarfs (Bergeron et al. 1994). As a result of their evolutionary history, the masses of sdB's are believed to be tightly constrained, canonically predicted values lying in the 0.44−0.53 $M_\odot$ range (Dorman et al. 1993). However, more recent developmentary hypotheses including the merging of two white dwarfs and Roche lobe overflow in a close binary system predict a somewhat larger range of pos-

Send offprint requests to: S.K. Randall

sible masses (Han et al. 2003). The thickness of the hydrogen shell depends on the exact temperature at which the star settles on the zero-age EHB and thus contains valuable information on pre-EHB conditions. Since usually neither the mass nor the exact composition of a star can be observed directly, it is their determination through asteroseismology that holds the key to a more mature understanding of these stars' evolution.

Fortunately, we know of two distinct types of oscillator among subdwarfs, each probing a different part of the stellar interior. The hotter EC 14026 stars (Kilkenny et al. 1997) exhibit rapid pulsations on a typical time scale of 100−200 s, which can be accounted for surprisingly well by a classical kappa mechanism in the presence of an iron opacity bump achieved through radiative levitation (Charpinet et al. 1997). Asteroseismological analyses invoking low-degree, low radial order pressure modes have been possible in several instances, yielding accurate estimates of the targets' masses and the thickness of their envelopes (see Charpinet et al. these proceedings for details). While these are becoming statistically significant for restricting evolutionary scenarios, the fact that pressure modes propagate primarily in the outer layers of a star means that they contain virtually no information on its inner regions. To obtain that, we need to turn to the PG 1716 stars, a second class of subdwarf B pulsator discovered only recently (Green et al. 2003). Distinctly cooler than the rapid variables, these stars exhibit periodicities between 1000 and 9000 s, which automatically implies high radial order gravity modes. The driving mechanism is believed to be the same as for the EC 14026 stars, however current models have been able to excite only modes with degree indices $\ell \geq 3$ for the majority of the spectroscopic temperature range, and modes with $\ell > 8$ for the very hottest PG 1716 stars detected (Fontaine et al. 2003). According to canonical wisdom, high degree modes should not be observable due to cancellation effects when integrating over the visible disk of the star. It thus seems that the instability strip predicted by our models is subject to some uncertainties, although these have been difficult to quantify due to a lack of data. In the present study, we address the issue by obtaining high quality photometry for one of the hottest long-period variables known, and compare the ensuing results to theoretical predictions.

2. Observations and Analysis

The slow oscillator PG 0101+039 has atmospheric parameters $T_{\rm eff} \sim 28{,}300$ K and $\log g \sim 5.52$ (Green, Fontaine, & Chayer, in preparation) and forms one half of a short-period binary system with $P_{\rm bin} \sim 0.57$ d (Moran et al. 1999). As one of the brightest subdwarfs at $V = 12.06$, it was considered an ideal exploratory target for the Canadian space telescope MOST ('Microvariability and Oscillations of STars; see Matthews et al. in these proceedings). After encountering severe problems with daily aliasing and atmospheric extinction during ground-based campaigns on PG 1716 stars, we had come to the conclusion that a detailed frequency analysis would be greatly facilitated by observa-

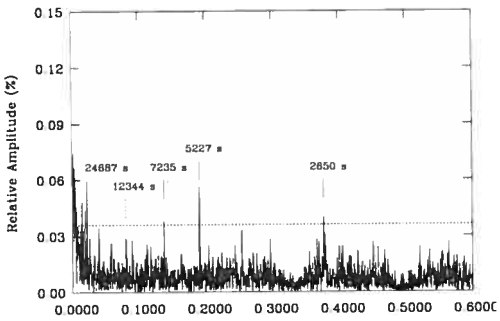

Fig. 1. Fourier transform of the entire light curve obtained for PG 0101+039 with MOST. Continuous line segments indicate periodicities believed to constitute stellar oscillations, while peaks associated with the ellipsoidal variation of the subdwarf during its binary orbit are marked by dotted lines.

tions from space. Currently the only satellite dedicated to asteroseismology, MOST was the obvious choice. However, it was not clear from the outset whether the 15-cm aperture telescope, primarily designed to monitor targets brighter than $V = 6$, would be able to achieve sufficient precision to detect low-amplitude oscillations in the relatively faint long-period variable subdwarfs. Besides constituting a scientific study in its own right, the trial run reported here was therefore intended to assess the feasibility of observing slowly oscillating subdwarfs with MOST.

Broadband photometry of PG 0101+039 was gathered nearly continuously from 28 September to 15 October 2004, with only one major gap of about 14 hours occuring near the beginning of the run. This implies around 400 hours of data with a net duty cycle of 96.5 %, significantly higher than anything achievable from the ground. The Fourier transform (FT) of the entire reduced light curve is illustrated in Figure 1. Note that it shows no visible signs of aliasing and boasts a noise level similar to that achieved for other PG 1716 stars after 3−5 weeks of observation from ground-based telescopes in the 1−2-m class. Adopting a threshold of four times the mean noise level (indicated by the horizontal dotted line), we were able to extract three frequencies attributed to stellar oscillation, indicated by continuous line segments. They are asociated with periods of 2650 s, 5227 s and 7235 s and have relatively low amplitudes of less than 0.06 % of the star's mean brightness. In addition, we found two weaker peaks corresponding to half the binary frequency and its first harmonic, probably indicating an ellipsoidal deformation of the subdwarf due to the gravitational pull of its companion. While interesting from the point of view of binary studies, the latter periodicities are not related to an intrinsic pulsation mechanism and will not be discussed in the what follows.

3. Comparison with non-adiabatic theory

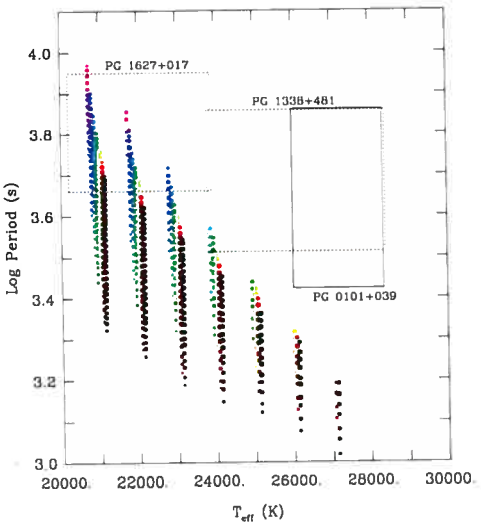

Fig. 2. Periodicities predicted to be excited from a sequence of PG 1716 star models. Individual modes are colour-coded in magenta ($\ell = 2$), blue ($\ell = 3$), cyan ($\ell = 4$), green ($\ell = 5$), yellow ($\ell = 6$), red ($\ell = 7$) and black ($\ell = 8$). The superposed boxes refer to the period range observed in the vertical direction and the temperature uncertainty from spectroscopy in the horizontal direction. Values for PG 0101+039 are indicated together with those for previous targets PG 1627+017 (Randall et al. 2006) and PG 1338+481 (Randall et al. in preparation).

We qualitatively compare the pulsational periods extracted to those predicted from theory with the aid of a short sequence of PG 1716 star models (see Charpinet et al. 1997 and Fontaine et al. 2003 for details on these models). Designed so as to lie parallel to the zero-age EHB, the sequence covers the entire temperature range where long-period variables are observed. Figure 2 illustrates the periodicities predicted to be unstable on the basis of the kappa mechanism for each model. The points are colour-coded according to the degree index of the mode in question (see figure caption for de-

tails). Superposed on the period sequence are the ranges of periods extracted for PG 0101+039 as well as two previously observed slow oscillators as a function of their effective temperature. Note that, for each target, the widths of the boxes give the temperature uncertainties based on two different sources (U. Heber, private communication, and Green, Fontaine & Chayer, in preparation) rather than the formal errors obtained from one spectral fit. As such, they are indicative of the significant discrepancies that still exist for cool sdB stars between atmospheric parameters derived from different sets of model atmospheres. In all likelyhood, the true values lie somewhere in between, however we belive it is safest to adopt conservative uncertainty estimates until the issue has been resolved.

Figure 2 clearly shows that, while the tendency for hotter stars to exhibit shorter periods is recovered by the models, there are discrepancies at the quantitative level. This is particularly obvious for the two hotter targets, where the periods observed are significantly longer than those predicted. Moreover, the frequencies predicted to be excited correspond to modes with relatively high degree indices, particularly in the models representative of PG 0101+039 (which, for the most part, are not able to drive modes with $\ell < 6$). Whereas there is some overlap between the theoretical and experimental instability regions for the other two stars, the more stringent constraints on the effective temperature of PG 0101+039 eliminate any hope of recreating the observed period spectrum with current models. It is thus clear that the latter are subject to deficiencies, at least at the non-adiabatic level, that have not yet been identified. Since it is probable that structural improvements made to the models would quantitatively affect the adiabatic period spectrum as well as the instability calculations, the inaccuracies will have to be addressed if meaningful asteroseismological fits are to be achieved for long-period variable subdwarf B stars.

4. Conclusion

The quality of the photometry obtained for PG 0101+039 conclusively shows that MOST is ideally suited to the monitoring of long-period variable subdwarf B stars. Indeed, the data obtained are far superior to anything achievable from the ground as far as time coverage is concerned, making space-based observations the obvious choice for future missions. While the number of periodicities detected for PG 0101+039 is too small to contemplate asteroseismology, we are hopeful that a MOST observing run of longer duration could uncover many more oscillations for other long-period variables, particularly those exhibiting higher amplitude pulsations. However, the successful use of these observed frequencies to infer the structural parameters of long-period variable subdwarfs depends on the identification and correction of deficiencies in our current models. We are in the process of addressing this issue and hope to solve the problem in the near future.

References

Bergeron, P., Wesemael, F., Beauchamp, A. et al. 1994, ApJ, 432, 305
Charpinet, S., Fontaine, G., Brassard, P. et al. 1997, ApJ, 483, L123
Dorman, B., Rood, R. T., & O'Connell, R. W. ApJ, 419, 596
Fontaine, G., Brassard, P., Charpinet, S. et al. 2003, ApJ, 597, 518
Green, E. M. , Fontaine, G., Reed, M. D. et al. 2003, ApJ, 583, L31
Han, Z., Podsialowski, P., Maxted, P. F. L., & Marsh, T. R. 2003, MNRAS, 341, 669
Kilkenny, D., Koen, C., O'Donogue, D., & Stobie, R. S. 1997, MNRAS, 285, 640
Moran, C., Maxted, P., Marsh, T. R. et al. 1999, MNRAS, 304, 535
Randall, S.K., Fontaine, G., Green, E.M. et al. 2006, ApJ, submitted
Saffer, R., Bergeron, P., Koester, D., & Liebert, J. 1994, ApJ, 432, 351